

DEVOLATILIZATION OF PULVERIZED COAL
AT HIGH TEMPERATURES

by

HISASHI KOBAYASHI

B.E., University of Tokyo
(1970)

S.M., Massachusetts Institute of Technology
(1972)

E.M., Massachusetts Institute of Technology
(1975)

SUBMITTED IN PARTIAL FULFILLMENT
OF THE REQUIREMENTS FOR THE
DEGREE OF
DOCTOR OF PHILOSOPHY

at the

MASSACHUSETTS INSTITUTE OF TECHNOLOGY

June, 1976

Signature of Author

Hisashi Kobayashi
Department of Mechanical Engineering, April, 1976

Certified by

James W. Labadie
Thesis Supervisor

Certified by

James W. Labadie
Thesis Supervisor

Accepted by

James W. Labadie
Chairman, Department Committee on Graduate Students

ARCHIVES



DEVOLATILIZATION OF PULVERIZED COAL
AT HIGH TEMPERATURES

by

HISASHI KOBAYASHI

Submitted to the Department of Mechanical Engineering in May 1976, in partial fulfillment of the requirement for the degree of Doctor of Philosophy.

ABSTRACT

Weight losses and changes in the elemental composition in char during devolatilization of pulverized coal were measured for a wide range of experimental conditions, thus extending existing information on the kinetics of devolatilization from a previous upper temperature of 1700°K to 2100°K.

Data on the devolatilization kinetics were obtained in a laminar flow furnace for a lignite and a bituminous coal, under rapid heating (10^4 - 2×10^5 °K/sec), at high temperatures (1000-2100°K), short residence times (0-200 msec) and rapid quenching ($\sim 10^6$ °K/sec) conditions with time resolutions down to 3 msec. Weight losses of both coals increased significantly with temperature (about 30% at 1250°K and 200 msec to about 65% at 2100°K and 25 msec on d.a.f. basis) and reached different final values at different temperatures within residence times between 30 and 250 msec.

Devolatilization in crucibles under slow heating (1-10°K/sec), but with the same peak temperature, showed that weight loss reaches an asymptotic value close to that of the ASTM proximate test at around 1200°K and further heating to 2100°K resulted in only a slight increase in weight loss. The effect on the weight loss of changing the bed depth of coal in the crucible from 1 to 200 layers was shown to be negligible under the present conditions.

Use of ash as a tracer in determining the weight loss was critically assessed and the range of its applicability was determined.

From the ultimate analysis of char it was found that more carbon, less hydrogen and less oxygen are retained in chars from the crucible experiment than in those from the flow experiment at the same weight loss.

Kinetic parameters based on a single first order reaction (about 25 Kcal for activation energy and $6.6 \times 10^4 \text{ sec}^{-1}$ for frequency factor) was in general agreement with the extrapolation of available data at lower temperatures.

A model based on two competing overall reactions was found to provide an adequate empirical correlation of the present data and that previously reported at lower temperatures for the same coal.

A possible mechanism for increases in volatile yield under rapid heating and high temperature conditions was proposed.

Thesis Supervisors: Jack B. Howard
Professor of
Chemical Engineering

Adel F. Sarofim
Professor of
Chemical Engineering

ACKNOWLEDGMENTS

The author is glad to have the opportunity to express his sincere appreciation to his thesis supervisors for their guidance throughout the course of this research. Professor A. F. Sarofim's enthusiasm and understanding of the problem, and many discussions late at night have provided valuable educational experience and encouragement. Constructive criticism and patience of Professor J. B. Howard helped improve the understanding of the problem. Thanks are due to Professor J. B. Heywood and Professor J. F. Louis who served on the committee and provided useful suggestions. Special mention is due to Dr. D. B. Stickler of AVCO Everett Research Laboratory, who initiated the topic for my Master's thesis and provided valuable comments since then.

The author is very grateful to John H. Pohl for his cooperation in the later stage of the experiment and suggestions through his experience in the field of reaction kinetics. Some of the results and figures are made through the joint efforts and Appendix I is prepared by him.

Thanks are also due to Dr. Jerzy Chomiak of Instytut Lotnictwa for building a two-color pyrometer system to measure particle temperatures.

Dr. Ashok S. Padia, as my former colleague, provided much assistance in building the experimental apparatus. His cooperation is highly acknowledged. Thanks are extended to Jerry Mandel for his experimental help and to Lisa Chan for preparing SEM pictures.

Gerrard F. Power is to be thanked for his assistance in many aspects of the experiment and for reading some part of the manuscript.

Stanley R. Mitchell prepared superb drawings for many figures.

James Waletzko, of Thermo Systems Inc., offered a laser doppler anemometer system which made it possible to measure particle velocities. Thanks are also due to Mrs. Gabriele Ivey for her excellent typing.

Personal financial support from the Murata Scholarship Foundation of Kyoto is gratefully acknowledged. This research was funded by ERDA Contract No. E(49-18)-2215.

Finally, I am deeply indebted to my wife, Miyako. Her understanding, help and patience in the rather limited life of a student's wife provided the best encouragement.

TABLE OF CONTENTS

<u>Chapter No.</u>		<u>Page No.</u>
1	INTRODUCTION	17
	1.1 Background	17
	1.2 Literature Review	19
	1.2.1 Enhanced Volatile Yields and Experimental Techniques	19
	1.2.2 Devolatilization Mechanism	27
	1.2.3 Devolatilization Models	36
	1.3 Objectives	46
	1.4 Scope of the Study	48
2	EXPERIMENTAL APPARATUS AND PROCEDURES	51
	2.1 Selection of Apparatus	51
	2.1.1 Shock Tube	51
	2.1.2 Irradiation Heating	51
	2.1.3 Flow Furnace	52
	2.2 Laminar Flow Experiment	53
	2.2.1 Coal Feeder	55
	2.2.2 Particle Collector	57
	2.2.3 Gas Preheater	59
	2.2.4 Suction System	59
	2.2.5 Experimental Procedure	59
	2.3 Free Fall Experiment with Bronze Collector	61
	2.3.1 Experimental Procedure	64
	2.4 Free Fall Experiment with Alumina Collector	65
	2.4.1 Experimental Procedure	65
	2.5 Crucible Experiment	68
	2.5.1 Experimental Procedure	70
	2.6 ASTM Proximate Analysis Equipment	70
	2.7 Coal Characterization	72
	2.7.1 Electron Micrographs	72
	2.7.2 Particle Size Distribution	77
	2.7.3 Ultimate and Proximate Analyses	82

<u>Chapter No.</u>		<u>Page No.</u>
3	ANALYSIS OF EXPERIMENTAL SYSTEM AND DATA REDUCTION	87
	3.1 Velocities of Coal Particles Measured by a Laser Doppler Anemometer	89
	3.1.1 Initial Velocities of Coal Particles	93
	3.1.2 Acceleration of Particles in Laminar Flow Experiment	95
	3.1.3 Particle Velocities in Free Fall Experiments	95
	3.2 Analysis of Temperature and Velocity Fields	98
	3.3 Determination of Weight Loss	118
4	RESULTS	127
	4.1 Weight Loss	127
	4.1.1 Weight Loss of Coals	127
	4.1.2 Weight Losses Determined by Using Ash as a Tracer and Ash Losses	142
	4.1.3 Effects of Sample Size on Weight Loss in Crucible Experiment	155
	4.2 Loss of Major Elements	162
5	DISCUSSIONS	181
	5.1 Temperature-Time History of Coal Particles and Effects of Heating Rates on Volatile Yields	181
	5.1.1 Temperature-Time Histories of Coal Particles in Laminar Flow Experiment	181
	5.1.2 Heating Rates and Average Reaction Temperature	187
	5.2 Secondary Char Forming Reactions in the Gas Phase and on the External Surface of Coal	195
	5.2.1 Parameters Affecting the Secondary Reactions	195
	5.2.2 Implications from Crucible Experiments with Different Bed Depth	199
	5.3 Changes in Elemental Composition of Char and their Implications to the Devolatilization Mechanism	201
	5.3.1 Comparison with Previous Observations	202
	5.3.2 Possible Mechanisms of the Rapid Devolatilization	206

<u>Chapter No.</u>		<u>Page No.</u>
	5.4 Effects of the Transport Process of Volatile Matter in the Pores of Coal on Secondary Char Forming Reactions	216
	5.5 Problems in Weight Loss Measurements Using Ash as a Tracer	225
	5.6 Comparison of the Enhanced Volatile Yields with Those Reported in Previous Studies	230
	5.7 Concluding Remarks	236
6	KINETICS OF DEVOLATILIZATION	239
	6.1 First Order Arrhenius Parameters	239
	6.2 Comparison with Previous Results	241
	6.3 Comparison with the Rates of Decomposition of Pure Hydrocarbons	251
7	DEVOLATILIZATION MODELS	261
8	CONCLUSIONS	277
 <u>Appendices</u>		
A	Characteristic Heat Transfer Times of Particles	280
B	Results of Laminar Flow Experiment	285
C	Results of Free Fall Experiments	295
D	Results of Crucible Experiments	304
E	Results of Ultimate Analysis of Char	312
F	Particle Velocities Measured by a Laser Doppler Anemometer	334
G	Physical Changes of Coal During Devolatilization	338
H	Enhanced Volatile Yield under Rapid Heating Conditions	346
I	Coal Characterization	357
J	Listings of Computer Programs and Data Cards	379
	REFERENCES	412
	BIOGRAPHICAL NOTE	424

LIST OF FIGURES

<u>Figure No.</u>		<u>Page No.</u>
1.1	Enhanced Volatile Yields Observed by Different Investigators	24
1.2	Variation of Q with Temperature	25
1.3	Comparison of Devolatilization Rate Constants	38
2.1	Laminar Flow Furnace System	55
2.2	Coal Feeder	57
2.3	Water Cooled Collector	59
2.4	Free Fall Experiment with Bronze Collector	64
2.5	Free Fall Experiment with Alumina Collector and Crucible Experiment	67
2.6	Axial Temperature Profiles in Free Fall and Crucible Experiments	68
2.7	Typical Temperature Time Histories in Crucible Experiment	70
2.8	Proximate Analysis Equipment and a Typical Temperature Distribution	72
2.9	Raw Montana Lignite	74
2.10	Polished Montana Lignite	75
2.11	Raw Pittsburgh Seam #8 Bituminous Coal	76
2.12	Polished Pittsburgh Seam #8 Bituminous Coal	77
2.13	Raw Lignite Rosin-Rammler Distribution	79
2.14	Raw Lignite Frequency Distribution	80
2.15	Raw Bituminous Coal Rosin-Rammler Distribution	81
2.16	Raw Bituminous Frequency Distribution	82
3.1	Conceptual Diagram of Main Flow Development in Laminar Flow Furnace	89
3.2	Laser Doppler Anemometer System for Velocity Measurement of Coal Particles	91
3.3	Typical Velocity Distributions of Coal Particles in Laminar Flow Furnace	93
3.4	Average Particle Velocities at Injector Tip	95
3.5	Average Coal Particle Velocities in Laminar Flow Furnace at Different Locations	97

<u>Figure No.</u>		<u>Page No.</u>
3.6	Average Coal Particle Velocities under "Free Fall" Conditions	98
3.7	Conceptual Diagram of Thermal Boundary Layer at Injector Tip	101
3.8	Schematic Diagram of Boundary Layers and Approximated Velocity Profile	103
3.9	Calculated Temperatures and Velocities	114
3.10	Calculated Temperatures and Velocities	115
3.11	Calculated Particle Temperatures and Residence Times	117
3.12	Flow Diagram of Devolatilization Experiments	120
4.1	Results of Laminar Flow Experiment, Montana Lignite	128
4.2	Results of Laminar Flow Experiment, Pittsburgh Seam Bituminous Coal	129
4.3	Weight Loss at Different Temperatures, Lignite	132
4.4	Weight Loss at Different Temperatures, Bituminous	133
4.5	Maximum Weight Losses Observed under Different Experiments, Lignite	138
4.6	Maximum Weight Losses Observed under Different Experiments, Bituminous Coal	139
4.7	Comparison of Directly Measured Weight Loss with Weight Loss Measured by Using Ash as a Tracer in Free Fall and Crucible Experiments, Montana Lignite	143
4.8	Comparison of Directly Measured Weight Loss with Weight Loss Measured by Using Ash as a Tracer in Free Fall and Crucible Experiments, Pittsburgh Seam Bituminous Coal	144
4.9	Ash Loss in Crucible Experiments, Lignite	147
4.10	Ash Loss in Crucible Experiments, Bituminous Coal	148
4.11	Comparison of Directly Measured Weight Loss with Weight Loss Measured by Using Ash as a Tracer in Laminar Flow Experiment, Montana Lignite	149
4.12	Comparison of Directly Measured Weight Loss with Weight Loss Measured by Using Ash as a Tracer in Laminar Flow Experiment, Pittsburgh Seam Bituminous Coal	150
4.13	Comparison of Directly Measured Weight Loss with Weight Loss Measured by Using Ash as a Tracer in Laminar Flow Experiment, Montana Lignite	153

<u>Figure No.</u>		<u>Page No.</u>
4.14	Comparison of Directly Measured Weight Loss with Weight Loss Measured by Using Ash as a Tracer in Laminar Flow Experiment, Pittsburgh Seam Bituminous Coal	154
4.15	Weight Loss of Different Sample Sizes in Crucible Experiments, Lignite	157
4.16	Weight Loss of Different Sample Sizes in Crucible Experiments, Bituminous Coal	158
4.17	Weight Loss of Different Sample Sizes in Crucible Experiments, Bituminous Coal	159
4.18	Percent of Element Retained in Char, Montana Lignite	163
4.19	Percent of Element Retained in Char, Pittsburgh Seam #8 Bituminous Coal	164
4.20	Elements Retained in Char in Crucible Experiment, Montana Lignite	166
4.21	Element Retained in Char in Crucible Experiment, Pittsburgh Seam Bituminous Coal	167
4.22	Elements Retained in Char at Different Weight Losses, Montana Lignite	169
4.23	Elements Retained in Char at Different Weight Losses, Pittsburgh Seam Bituminous Coal	170
4.24	Changes in Elemental Ratios in Char with Time, Montana Lignite	172
4.25	Changes in Elemental Ratios in Char with Time, Pittsburgh Seam Bituminous Coal	173
4.26	Changes in Elemental Ratios in Volatile Matter with Time, Montana Lignite	175
4.27	Changes in Elemental Ratios in Volatile Matter with Time, Pittsburgh Seam Bituminous Coal	176
4.28	Changes in Elemental Ratios in Char with Weight Loss Montana Lignite	177
4.29	Changes in Elemental Ratios in Char with Weight Loss Pittsburgh Seam Bituminous Coal	178
4.30	Changes in Elemental Ratios in Volatile Matter with Weight Loss, Montana Lignite	179
4.31	Changes in Elemental Ratios in Volatile Matter with Weight Loss, Pittsburgh Seam Bituminous Coal	180
5.1	Weight Loss Versus Calculated Particle Temperature Montana Lignite	183

<u>Figure No.</u>		<u>Page No.</u>
5.2	Weight Loss Versus Calculated Particle Temperature Pittsburgh Seam Bituminous Coal	184
5.3	Schematic Diagrams of Weight Loss-Temperature Curves under Different Conditions	186
5.4	Effects of Heating Rate on the Average Devolatilization Temperature	192
5.5	Estimated Weight Loss-Temperature Histories Montana Lignite	194
5.6	Weight Loss Versus Initial Weight of Coal in Crucible (Portal and Tan, 1974; Gray, et al.1974)	200
5.7	Loss of Elements During Carbonization (Van Krevelen, 1961)	204
5.8	H/C Versus O/C Diagrams for Coalification and Carbonization (Van Krevelen 1961)	207
5.9	Change with Coal Devolatilization	208
5.10	Behavior of Hydrogen During Devolatilization, Montana Lignite	213
5.11	Behavior of Hydrogen During Devolatilization, Pittsburgh Seam Bituminous Coal	214
5.12	Comparison of Enhancement in Volatile Yield	231
5.13	Different Coals and Enhancement in Volatile Yield	234
6.1	First Order Arrhenius Plot for Weight Loss, Montana Lignite	241
6.2	First Order Arrhenius Plot for Weight Loss, Pittsburgh Seam Bituminous Coal	242
6.3	First Order Arrhenius Plot for Retention of C, H, O. Montana Lignite	244
6.4	First Order Arrhenius Plot for Retention of C, H, O. Pittsburgh Seam Bituminous Coal	245
6.5	Comparison of Devolatilization Rate Constants	246
6.6	Variation of Devolatilization Rate Constants for Different Coals	248
6.7	Variation of Devolatilization Rate Constants for Different Stages of Devolatilization	250
6.8	Comparison of Devolatilization rate Constants	252
6.9	Comparison of Devolatilization Rate Constants for Pittsburgh Seam HVB bituminous Coal	253

<u>Figure No.</u>		<u>Page No.</u>
6.10	Comparison of First Order Devolatilization Rates with Those for Decomposition of Pure Hydrocarbons	254
6.11	Apparent First Order Rates Approximated for Hypothetical Three First Order Parallel Reactions	256
6.12	First Order Arrhenius Rates Evaluated at Same Weight Loss Levels. Montana Lignite	258
6.13	First Order Arrhenius Rates Evaluated at Same Weight Loss Levels. Pittsburgh Seam Bituminous Coal	259
7.1	Comparison of Model Curve Fit with Experimental Data for Montana Lignite	270
7.2	Comparison of Model Curve Fit with Experimental Data for Pittsburgh Seam Bituminous Coal	271
7.3	Comparison of a Single Overall Reaction Model with Experimental Results	273
7.4	Comparison of Model Curve Fit with Experimental Data for Pittsburgh Seam Bituminous Coal	274
7.5	Comparison of Calculation H/C and O/C Ratios with Experimental Data for Pittsburgh Seam Bituminous Coal	275

<u>Figure No.</u>		<u>Page No.</u>
A.1	Characteristic Heat Transfer Times to a Particle	284
B.1	Illustration for Residence Time Correction	286
C.1	Schematic Diagram of the Distribution of Char and Condensed Material in the Bronze Filter	300
E.1	Elements Retained in Char at Different Weight Losses Pittsburgh Seam Bituminous Coal	331
E.2	Changes in Elemental Ratios in Char with Weight Loss, Pittsburgh Seam Bituminous Coal	332
E.3	Changes in Elemental Ratios in Volatile Matter with Weight Loss, Pittsburgh Seam Bituminous Coal	333
G.1	Bubble Development, Pittsburgh Seam #8 Bituminous Coal	340
G.2	Void Development with the Pittsburgh Seam #8 Bituminous Coal	341
G.3	Electromicrograph of a Devolatilized Bituminous Coal Particle	342
G.4	Photomicrographs of a Devolatilized Coal: A Single Bituminous Coal Particle; A Collection of Lignite Particles	343
G.5	Void Development with Temperature, Pittsburgh Seam #8 Bituminous Coal, Free Fall to Cup	344
G.6	Agglomeration, Pittsburgh Seam #8 Bituminous Coal	345

LIST OF TABLES

<u>Table No.</u>		<u>Page No.</u>
1.1	Coal Types and the Sources of the Data Shown in Fig. 1.3	38
1.2	General Hypothetical Scheme for Coal Pyrolysis	45
2.1	Summary of Operating Conditions	62
2.2	Particle Size Distribution	82
2.3	Coal Characterizations	83
2.4	Characterization of Montana Lignite	84
2.5	Bituminous Coal	85
2.6	Results of Proximate Analyses	86
3.1	Calculated Heating Times of Particles	117
4.1	Measured Weight Loss of Different Sample Sizes in Crucible Experiments at 1220°K	160
5.1	Estimated Weight Loss of Coal by Loss of Functional Groups	210
7.1	Classification of Possible Kinetic Models for Devolatilization	262
B.1	Results of Laminar Flow Experiment, Montana Lignite	287
B.2	Results of Laminar Flow Experiment, Pittsburgh Seam Bituminous Coal	291
C.1	Results of Free Fall Experiment with Alumina Collector, Sample Predried at 105°C for 2-48 Hours	296
C.2	Results of Free Fall Experiment with Alumina Collector, Montana Lignite	297
C.3	Results of Free Fall Experiment with Alumina Collector, Pittsburgh Seam Bituminous Coal	298
C.4	Measured Weight Loss in Free Fall Experiment with Bronze Collector (d.a.f.)	302
D.1	Results of Crucible Experiment	305
D.2	Results of Crucible Experiment, Montana Lignite	306
D.3	Results of Crucible Experiment, Effects of Bed Depth, Montana Lignite	308
D.4	Results of Crucible Experiment, Pittsburgh Seam Bituminous Coal	309

<u>Table No.</u>		<u>Page No.</u>
D.5	Results of Crucible Experiment, Effects of Bed Depth, Pittsburgh Seam Bituminous Coal	311
E.1	Results of Ultimate Analysis of Char, Montana Lignite	313
E.2	Results of Ultimate Analysis of Char, Pittsburgh Seam Bituminous Coal	320
E.3	Results of Ultimate Analysis, Pittsburgh Seam Bituminous Coal	327
F.1	Results of Particle Velocity Measurements	335
H.1	Weight Loss of Various Coals in a Laminar Flow Furnace	347
H.2	Weight Loss of Coals at Different Temperatures in a Laminar Flow Furnace	348
H.3	Weight Loss of an Elkol Coal in a Transport Reactor	349
H.4	Weight Loss of a High-Volatile A Bituminous Coal in an Argon Plasma	350
H.5	Weight Loss of Various Coals in a Hydrogen Plasma	351
H.6	Weight Loss of a High-Volatile B Utah Coal in an Entrained Flow Reactor with Hydrogen-Oxygen Combustion Gases	352
H.7	Weight Loss of Various Coals by Pulse-Heating in a Wire-Screen Heating Element	353
H.8	Weight Loss by an Electrically Heated Wire Screen under Various Atmospheres	354
H.9	Weight Loss of Various Coals by Microsample Strip Furnace	355
H.10	Weight Loss of Various Coal in an Electrically Heated Wire Screen	356
I-1	ASTM Coal Rank	358
I-2	Ash Characterization	366
I-3	Functional Group Analysis of a Lignite	368
I-4	Functional Group Analysis of a High Volatile Bituminous Coal	375

CHAPTER I

INTRODUCTION1.1 Background

Coal is one of the only viable options for supplying increased energy requirements in the near future. Currently about 20 percent of the total energy supply in the United States comes from coal. Some studies (Nail, et al., 1975) project that a substantial portion of the total energy may be supplied by coal at the turn of the century. The dwindling reserves of oil and gas, difficulties in developing nondepletable and clean energy sources, and large capital investments required for new systems, make coal the most important source of energy in the middle range energy policy. Currently the main use of coal is the generation of high temperature high pressure steam in industrial boilers. The proposed uses of coal include gasification, liquefaction and advanced combustion systems such as coal-fired magnetohydrodynamic (MHD) power generation and fluidized bed combustors (Hottel and Howard, 1972). In most of the systems, coal is pulverized and injected into a hot environment. The volatile matter in coal particles comes out at a significant rate upon rapid heating. The total amount of volatile matter produced by devolatilization depends mainly on the type of coal, the temperature of the surrounding gas and the size of coal particles. Under conventional laboratory heating conditions such as those of the ASTM proximate analysis test, a typical high-volatile bituminous coal yield 30 to 40 percent by weight volatiles by thermal decomposition. In contrast to this behavior, volatile yields significantly larger than the proximate volatile matter obtained under

certain conditions. For example, some data of the British Coal Utilization Research Association (BCURA) (Kimber and Gray, 1967) indicate the volatile yield may be as high as 70 percent when finely ground coal particles are injected into hot combustion gases of 2000°K or more. Although the total burning time or gasification time of coal particles is dominated by the relatively slow char gasification, the amount of char to be consumed and therefore the residence time is determined by the devolatilization step. Any increase in volatile yield would shorten the overall burning time. This is particularly important for coal fired MHD combustors, where the attainment of high temperatures through efficient combustion and minimal heat loss to the wall is critically required. Also, the ignition mechanism of the coal particles is closely related to the devolatilization process (Howard and Essenhigh, 1967; Nettleton and Stirling, 1967). Therefore the informations on the rate of volatile yield under various conditions are indispensable for proper designs of combustion chambers.

Enhanced volatile yield could improve the efficiency of synthetic gas production from coal. The Garrett flash pyrolysis process (McMath, et al., 1973; Adam, et al., 1973) does indeed achieve increased volatile yields. The rapid reaction is achieved by mixing pulverized coal with hot recycled char, yielding both gas and char as products. The volatile field reported at 1700°F was about 41 percent (on a dry basis) of volatile yield, as compared to 30 percent proximate volatile matter. In Synthane (Bureau of Mines), Hydrane (Bureau of Mines), and Bigas (Bituminous Coal Research, Inc.) processes the initial steps are rapid devolatilization of coal in

dispersed phases by mixing with hot gases (Hottel and Howard, 1971). Larger yields in volatile matter, therefore, would reduce the amount of char which has to be gasified in the succeeding steps. Other applications of rapid devolatilization reactions include coal gasification in a chemical regenerative MHD cycle (Gannon, et al., 1974), where the thermal energy of the hot MHD exhaust gas is transformed into chemical energy of the fuel gas through gasification of coal.

In spite of these practical interests, little research has been carried out at high temperatures, and the mechanism of rapid devolatilization is still poorly understood. More extensive research is needed in order to confirm the observed enhanced volatile yield and to clarify the conditions required to achieve the effect in practice.

1.2 Literature Review

1.2.1 Enhanced Volatile Yields and Experimental Techniques

Augmentation in volatile yield under rapid heating conditions has been observed by different researchers using various experimental techniques. These include entrained flow reactors (Coates, et al., 1974; Stickler, et al., 1974; Badzioch and Hawksley, 1970; Kimber and Gray, 1967; Eddinger, et al., 1966) and electrical screen heating (Mentser, et al., 1974; Anthony, et al., 1974; Loison and Chauvin, 1964).

Badzioch and Hawksley (1970) measured the extent of thermal decomposition of size graded coal particles in the pulverized-fuel size range using a laminar flow vertical furnace for 11 different coals. Coal particles are injected with cold carrier gas along the axis of the preheated nitrogen stream in a cylindrical alumina tube. The ambient gas temperature ranged from 400°C to 1000°C and the particle residence time

from 30 to 100 milliseconds. They determined the weight loss and the change in volatile matter using ash as a tracer. The experimental data were correlated by the following empirical equations. (Symbols are changed to conform with the notation in this thesis.)

$$\Delta V = V_0(1-D) \left[1 - \exp\left(-Be^{-\frac{E}{RT}} t\right) \right] \quad (1.1)$$

$$\Delta W = Q \cdot \Delta V \quad (1.2)$$

$$D = \exp[-K_1(T-K_2)] \quad (1.3)$$

where V_0 is the proximate volatile matter of original coal, determined by the standard proximate analysis test, on a dry ash-free (d.a.f.) basis and ΔV , ΔW , T and t denote change in volatile matter (d.a.f.), weight loss (d.a.f.), temperature of a coal particle ($^{\circ}\text{K}$) and decomposition time (sec.) respectively. D is the fraction of volatile matter remaining in char and K_1 , K_2 , B and E are constants depending on the kind of coal. As a ratio of weight loss to the differences between proximate volatile matter in original coal and that in char they found a constant Q for each kind of coal ranging from 1.3 to 1.8. For weakly-swelling coals, D did not depend on temperature appreciably and could be set equal to 0.14.

Kimber and Gray (1967-a, 1967-b) measured weight loss and change in volatile matter using the same kind of vertical furnace. The reactor temperature ranged up to 2200°K . They found that for the low-rank coal (N.C.B. Coal Rank Code No. 902) Q varied between 1.3 to 1.95 for a single kind of coal depending on the furnace temperature. The maximum yield reached more than 70 percent (d.a.f.) at 2170°K .

Although the factor Q is a convenient tool to estimate weight loss under rapid heating conditions, by performing the proximate volatile test for char, it is not necessarily a good measure of the enhancement in volatile matter. The ratio of the asymptotic value of weight loss measured at very long reaction time at a particular set of devolatilization conditions to the proximate volatile matter may be defined as the enhancement factor, f_E .

$$f_E = \frac{\Delta W_\infty}{V_o} \quad (1.4)$$

where ΔW_∞ is the asymptotic weight loss. In practical cases, however, asymptotic values of weight loss may not be reached within the experimental reaction time. When this is the case, the proximate volatile matter of char may be added to the measured weight loss to give an approximate enhancement factor

$$f'_E = \frac{\Delta W + D}{V_o} \quad (1.5)$$

The true enhancement factor may or may not be greater than f'_E , depending on the specific conditions. It should be noted that the factor Q becomes equal to the true enhancement factor only when the same ratio of enhancement occurs to the remaining volatile matter in char (i.e., if yield of volatile matter from char, when the experimental reaction time is extended long enough, becomes $Q \cdot D$). The ratio of measured weight loss to the proximate volatile matter of coal may be used as an enhancement factor in the absence of the proximate volatile matter test of char.

$$R = \frac{\Delta W}{V_o} \quad (1.6)$$

In using R as a measure of enhancement, the remaining volatile matter in char has to be small compared to the original volatile matter. It should be noted that

$$Q \geq \frac{f'}{E} \geq R \quad (1.7)$$

holds in general.

In Appendix H, these enhancement factors are calculated for weight losses observed under various experimental conditions and summarized in Tables H.1 to H.10. Figure 1.1 shows R versus the proximate volatile matter of coal. Badzioch and Hawsley's results appear to indicate larger enhancement with smaller proximate volatile matter. But Mentser's results, which were measured using an electrically heated wire-screen in vacuum, do not exhibit such trend. Since the amount of volatile matter remaining in char is not known for Mentser's coals, any conclusion can not be drawn (see Tables H.1, H.7 and H.8 for details). Figure 1.2 shows the temperature dependence of the Q factor. Both Kimber and Gray (1967-a) and Eddinger, et al. (1916) used entrained flow reactors (see Tables H.2 and H.3). but Eddinger reported significant interactions between the volatile products and the reactor wall, which caused an apparent decrease in weight loss at higher temperature through the formation of solid carbon by thermal cracking of the volatile matter. If a 60 percent weight loss is used at 1570°K furnace temperature (as estimated by Eddinger), all the data points follow the dotted line. The rapid increase in Q with temperature should be noted.

Large volatile yields at high temperatures were also observed by the injection of coal particles into hot combustion gases. Coates, et al.,

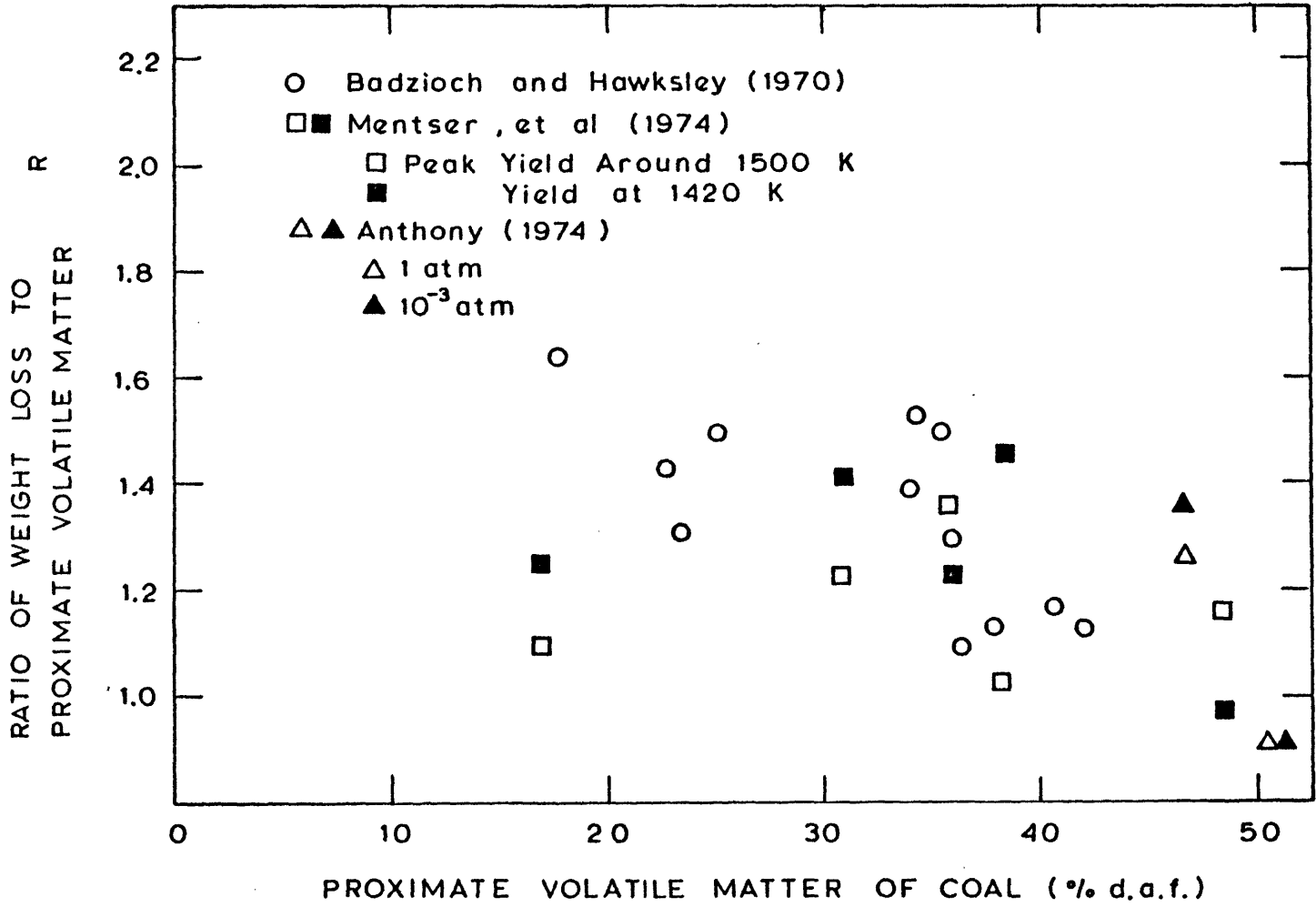


FIGURE 1.1 ENHANCED VOLATILE YIELDS OBSERVED BY DIFFERENT INVESTIGATORS.

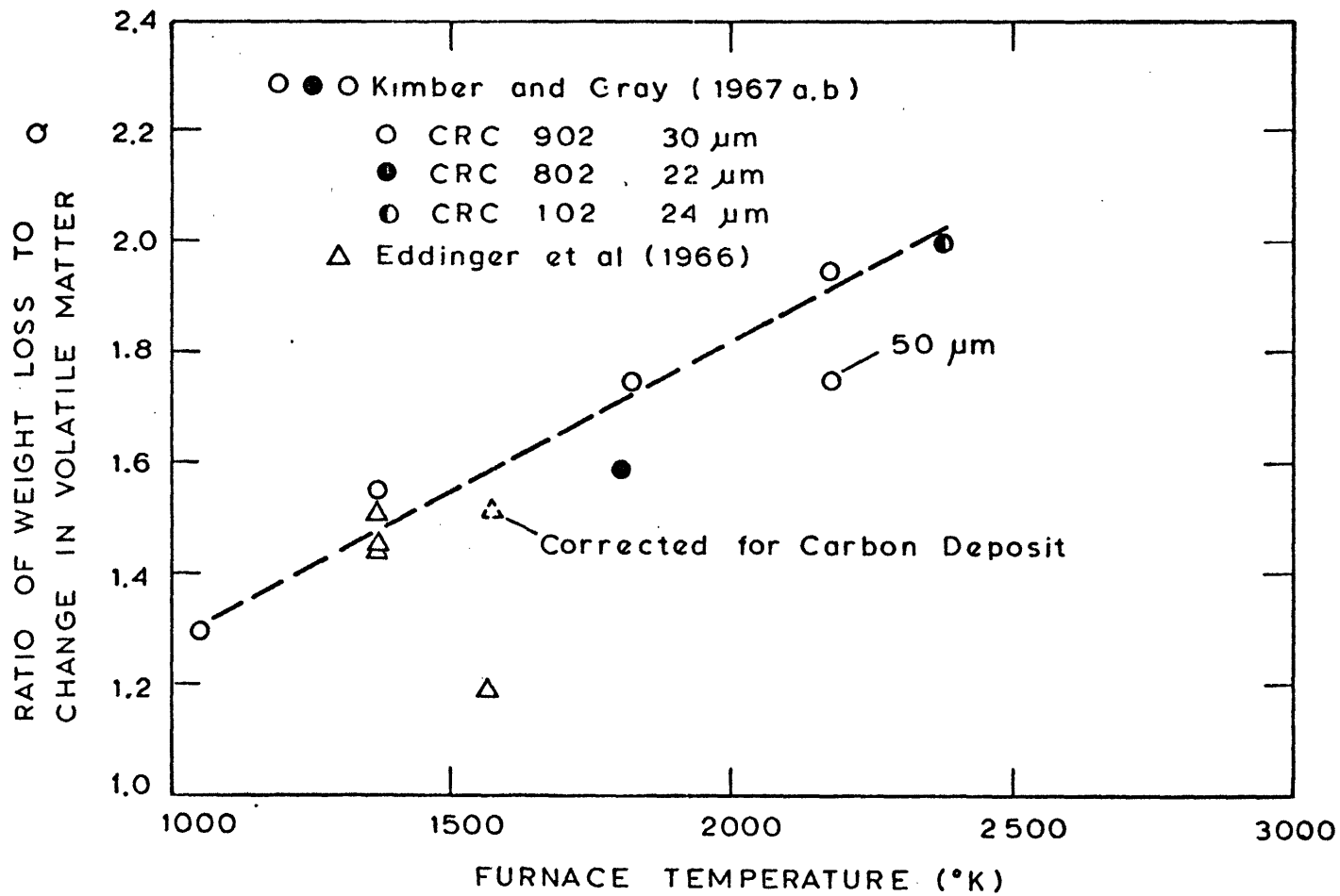


FIGURE 1.2 VARIATION OF Q WITH TEMPERATURE

1974, studied rapid devolatilization and product composition using a hydrogen-oxygen flame (Table H.6). Weight losses in excess of 60 percent were reported for a coal with 39 percent d.a.f. proximate volatile matter. Stickler, et al., 1974, reported more than 70 percent weight loss for a coal injected into the combustion products of a benzene/air mixture. In both cases contributions of heterogeneous reactions were estimated to be small. The trend in Fig. 1.2 indicates further increase in weight loss at higher temperatures. Graves, et al., 1966, injected pulverized coal into argon plasma in an attempt to achieve high yield of acetylene. Though the average plasma temperature ranged up to 9000°K, the particle temperature was much lower due to the heat transfer limitation and the maximum value of Q obtained was 1.73 (Table H.4). In a hydrogen arc, Stickler, et al., 1974, reported values as high as 2.22 (Table H.5). But the volatile matter in the char was high so that the corresponding value of R was only 1.34. The maximum amount of weight loss they obtained was 71.7 percent from a high volatile coal with 41.4 percent proximate matter.

Despite the fact that many researchers have observed enhanced volatile yields, only few of them were able to provide data on the kinetics of the rapid devolatilization. Experimental difficulties in achieving rapid quenching as well as rapid heating under the well controlled conditions made it very difficult to study the transient behavior of the rapid devolatilization. Among the experiments with flow reactors (Coates, et al., 1964; Badzioch and Hawksley, 1970; Kimber and Gray, 1967-A; and Eddinger, et al., 1966), only Badzioch and Hawksley measured

weight losses during transient periods of devolatilization. In their study, however, weight losses were calculated using ash as a tracer, because of the particle loss to the collector wall occurred as a consequence of the softening of coal under transient devolatilization stages. Since ash is neither a well defined material, nor is it a mixture of pure metal oxides, accuracy of the ash tracer method is somewhat questionable even at temperatures below 1000°C. The temperature of the coal particles was assumed to reach the main gas temperatures in 20 msec after the injection, which was estimated from a separate experiment measuring the "diffusion" time of carrier gas (O_2) into the main gas (N_2) in simulated experimental conditions. Such an estimation is open to doubt, since the exact similarity between the concentration and the temperature did not exist because of differences in boundary conditions (i.e., thermal boundary layer development on the insulation of the water cooled injector and effects of particles). Also, they did not account for the cooling period, which might have been as important as the heating period. Therefore the accuracy of the kinetic parameters derived from their results is somewhat questionable.

Fixed sample techniques such as electrically heated wire screens normally give better control in monitoring the temperature of coal particles during devolatilization. Anthony (1974) measured weight losses under transient stages of devolatilization by an electrically heated wire screen, and kinetic parameters were obtained by a nonisothermal technique using measured temperature-time histories of coal particles. Although the temperatures of coal particles are more

reliable than those of Badzioch and Hawksley, his system has its inherent problems. Heat and mass transfer mechanisms are quite different from actual systems, where particles are injected into hot gases, and interactions of coal particles and volatile matter with the hot screen is unavoidable. Thus, applications of the results to actual systems require special interpretations. Another problem was the slow quenching times (typically a few seconds), compared to the fairly high heating rates (up to $10,000^{\circ}\text{K}/\text{sec}$). The transient weight losses he obtained, therefore, were limited to those of low temperatures (below 700°C) and long reaction times (more than 1 sec).

In view of the limitations mentioned above, there is a need for experimental studies in weight loss of coal under well controlled atmosphere, in a temperature range applicable both to gasification and combustion systems with a good time resolution in order to provide the better understanding of the kinetics of rapid devolatilization.

1.2.2 Devolatilization Mechanism

Devolatilization of coal is a very complicated phenomenon involving numerous chemical reactions coupled with physical escape of volatile matter through the micropores in coal. One of the difficulties in studying coal is that the chemical structure of coal itself is not well defined, which tends to obscure the true mechanism of any physico-chemical phenomena associated with coal. Hence a brief review on the structure of coal may help understand the devolatilization mechanism.

The chemical structure of coal varies widely depending on the original plant structure and the geological conditions during the

coalification process. Because of its complexity and nonuniformity, efforts have been made to describe coal in terms of statistical average quantities such as the fraction of aromatic carbon (carbon aromaticity), the fraction of hydrogen bonded to aromatic carbon (hydrogen aromaticity) the size of the aromatic cluster and the average number of rings per structural unit (Van Krevelen, 1961). Various physical and chemical methods have been used to elucidate the structure, but completely satisfactory results have not yet been obtained. The general consensus (Tingey and Morrey, 1973) is: (1) that coal consists of an aromatic-aliphatic lamellar structure with only three to five condensed rings per lamella, (2) that sulfur and nitrogen are incorporated into heterocyclic rings, and (3) that oxygen exists mainly as hydroxyl and carbonyl groups. About 70-85 percent of total carbon in the bituminous range is reported to be aromatic, 10-25 percent is hydroaromatic, and 4-5 percent is aliphatic. Aromatic carbon increases with increase in rank, but the sum of the aromatic and hydroaromatic fractions is almost constant in coals of 80-90 percent carbon content (on a d.m.f. basis). (Mazumdar, et al., 1966.) More recently, Chakrabartty and Berkowitz (1974) proposed a structural model of coal as a modified bridged tricycloalkane system. The theory was based on oxidation studies of coal with sodium hypochlorite (Chakrabartty and Kretschmer, 1972, 1974), which indicated that coal is largely made up of nonaromatic structures. The authors claimed that such a model is not inconsistent with the experimental evidence now regarded as pointing to aromatic structure, since data are generally interpreted on the assumption that a high degree of aromaticity is likely.

Although the possibility of the predominant non-aromatic structure of coal may not be excluded, the evidence for it is not strong. The claim that sodium hypochlorite oxidation is exclusively restricted to non-aromatic carbon structures has been seriously questioned by other investigators. (Ghosh, et.al., 1975; Landolt, 1975) In the present study coal will be viewed as a predominantly aromatic substance in interpreting the experimental results.

Much of the past studies on devolatilization mechanism were done in relation to industrial coking operations, where heating rates were slow (less than $10^{\circ}\text{C}/\text{min}$) and final temperatures were relatively low (mostly below 1000°C). Although quantitative extrapolations of these results to rapid heating conditions encountered, for instance, in pulverized coal flames may lead to significant deviations from observed behavior unless a proper model is employed in the extrapolation, fundamental mechanisms found under the low temperature slow heating conditions may still play important roles under high temperature rapid heating conditions. A brief summary of the slow devolatilization studies may be worthwhile. More extensive reviews may be found elsewhere. (Badzioch, 1967, Yellow, 1965, Jones, 1964, and Howard, 1963.)

Van Krevelen et al. (1951) observed two different stages of devolatilization by heating coals at $2^{\circ}\text{C}/\text{min}$, 'primary' reactions which took place between 400 and 500°C producing mainly tar and 'secondary' reactions (above 500°C) producing gases rich in hydrogen. For caking coals, the primary stage is coupled with physical softening of the coal.

Through extensive studies of coal model compounds, Van Krevelen (1961) concluded that the two stages are governed by the numerical content of aliphatic and aromatic hydrogen in coal. The primary devolatilization is a depolymerization process in which aliphatic bridges are ruptured with simultaneous transmission of hydrogen (disproportionation). The structural units to which this hydrogen is transmitted evaporate as tar, or recondense and yield semi-coke. The formation of tar terminates completely when the original aliphatic hydrogen atoms in the reaction mixture have been used up. Reactive oxygen groups such as OH groups, which are richer in low rank coals, decrease tar yield by consuming available hydrogen through dehydration thus promoting condensation of aromatic nuclei. Low tar yields of high rank coals are explained by physical limitation of the structural units being too large to evaporate. This mechanism agreed well with other studies. Den Hertog and Berkowitz (1960) concluded from their data on coal carbonization in the presence of nitric oxide that free radical mechanisms occur during the primary devolatilization. Depp, et. al. (1956), through studies of coal model compounds, concluded that free radical rupture of weak carbon-carbon linkage such as methylene bridge linking aromatic units is an important step in pyrolysis of coal at low temperatures. Importance of physical factors during carbonization was stressed by many researchers. Carbonization under reduced pressure typically yields larger amount of tar containing high molecular weight products, while the reverse is true under high pressures (Howard, 1963). Such phenomenon was interpreted as the result that rapid escape of the primary tar under reduced pressure diminish the chance of secondary reactions such as

condensation or polymerization of the tar within the coal (Jones, 1964). Different explanations exist on the origin of the high molecular weight volatile matter. Orning and Greifer (1956) suggested distillation of some portion of coal without changing the original structure, based on the close resemblance of the infra-red spectra of the primary tar obtained under high vacuum and those of the parent coal. The other possibility is that small fragments, such as the smaller free radicals and unsaturated compounds broken off from larger molecules by pyrolysis, polymerize to form large molecule weight products. (Billington, et. al. 1952). Berkowitz (1960) concluded that pore diffusion of the volatile matter is the rate controlling factor, from thermogravimetric measurements of about 600 to 2000 μ size coal at temperatures between 253°C and 524°C. Deviations of measured weight loss curves from a first order reaction model were explained in terms of internal pressure build-up (as high as 200 atm) of volatile matter. Peters (1963) suggested that the heat transfer limitation caused by the latent heat of evaporation of volatile matter is the controlling factor for 1.5 mm coal particles devolatilized with heated sand.

Evolution of gases during pyrolysis has been studied to elucidate the mechanism of devolatilization in relation to the structure of the coal. Fitzgerald and Van Krevelen (1959) measured the rates of evolution of hydrogen, methane, hydrocarbons up to C_4 , and the oxides of carbon, from samples of coal heated from 300°C to 700°C at a constant rate (1.8°C/min) in a static bed under reduced pressure. Assuming a first order reaction for each gas, Arrhenius plots were derived, which indicated more than one reaction contributed to the formation of some of

gases. From the analyses of the Arrhenius plots the authors linked the evolution of the gases to the structure of the coal as follows.

"Hydrogen -- Each hydrogen molecule originates from two peripheral sites, upon breaking of a C-H bond, followed by hydrogen molecule formation. The molecule formation is assumed to be faster than the bond breaking process.

Hydrocarbons -- Each hydrocarbon molecule originates from two peripheral sites, upon breaking of the appropriate carbon-radical bond, and the breaking of a C-H bond, followed by molecule formation. A portion of the methane is formed by autohydrogenation, for which the necessary hydrogen comes from four peripheral sites.

Carbon monoxide -- The carbon monoxide appearing below 500°C is thought to be derived from oxygen replacing carbon in the periphery of lamellae, so that no peripheral sites are vacated.

Carbon dioxide -- Carbon dioxide comes from a carboxyl group, without vacating a peripheral site.

Water -- Water comes from hydroxyl groups and hydrogen, thus vacating two peripheral sites."

Berkowitz and den Hertog (1962) investigated the kinetics of hydrogen evolution in some depth. In order to avoid the formation of hydrogen by secondary reactions, the tar was removed by preheating the coal prior to the measurement of hydrogen. The reaction was assumed to be first order with respect to the remaining hydrogen, and activation energies around 8-15 Kcal/mol were obtained. The observed low activation energies led the authors to conclude that hydrogen forms in

a bimolecular process which occurs whenever two contiguous carbon lamellae move into an appropriate configuration.

Jüntgen, Van Heek and their coworkers (Jüntgen and Van Heek, 1970, 1969, 1968; Hanbaba et al., 1968) investigated gas release from coal and other substances at constant heating rates between 10^{-2} and 10^5 °C/min. From the detailed analyses of gas evolution rates - temperature curves combined with mathematical techniques, they suggested that hydrogen evolution can be interpreted as a combination of numerous overlapping first-order reactions with statistical distribution of the activation energy. The shape of the methane release curve was characteristic of a mixture of different reactions. Higher hydrocarbons mostly had simple curves which could be explained by a first-order reaction. (Jüntgen and Van Heek, 1968). However, in the later publications the apparently simple curves are shown to be results of many overlapping reactions. Importance of pore diffusion and nonisothermality for large particles was stressed as it could influence the gas release significantly.

The mechanism of rapid devolatilization in a dispersed phase was first investigated by Russian researchers. (Chukhanov, 1954; Shapatina et al., 1960). Finely ground particles were dropped in a vertical furnace tube in an inert atmosphere collected in a dish and kept at a known temperature (about 250-550°C) for a certain duration (0.15-2 hours), followed by rapid quenching by water. Shapatina divided the rapid devolatilization into three stages:

- (1) Rapid carbonization proceeding at a very high rate in the initial 0.1 sec (1-2 order of magnitude greater than the 2nd stage).

- (2) Principal thermal decomposition proceeding at a relatively low rate during 2-3 min.
- (3) "Degassing" of coal proceeding at a long time (hours).

Interpretations of each step in relation to the structure of coal were not given. But it was noted that pyrogenic water was the main product in the initial 0.1 sec. Chukhanov, in modeling the devolatilization by five sets of independent reactions, assumed that the decomposition of oxygen groups in coal is responsible for the rapid stage, characterized by the evolution of carbon dioxide and water. The initial rapid evolution of volatile matter under rapid heating conditions was also observed by injecting coal particles into a fluidized sand bed. (Stone et al., 1954).

The enhanced volatile yields discussed in section 1.2.1 have been explained in several different ways.

- (1) Rapid escape of the initial volatile products minimizes further reactions inside the coal which could produce involatile residue.
- (2) Rapid heating to a high temperature causes rupture of the bonds in the coal structure, producing a considerable number of large radicals. (Chukhanov, 1954).
- (3) Under slow heating conditions, the structure of coal changes to a more ordered one through crosslinking, which binds a material that could escape under rapid heating. (Gray et al., 1974).
- (4) Secondary cracking of the volatile matter on the external surface of coal diminishes overall yields in a dense

packed bed of particles, which is a typical experimental condition for slow heating.

The first explanation was most commonly used (Badzioch, 1967, Yellow, 1965, Jones, 1964). Loison and Chanvin (1964) assumed that some of the initial products are too large to evaporate, which are ejected or escape in some other way from the coal before they can decompose. Van Krevelen and coworkers (1959) noted that some of the "metaplast" is carried away as a tar mist by gaseous products, which increases with the rate of gas evolution. Larger volatile yields observed under a reduced pressure (Dryden and Toy, 1961) also favors the explanation. More recently Anthony (1974) reached the same conclusion from an experimental study involving rapid heating of coal in an electrically heated wire screen under different atmospheres. For the hvA bituminous coal, volatile yields increased under reduced pressures and further increase was obtained under high pressure hydrogen atmosphere. Hydrogen was considered to interrupt the secondary reactions leading to char formations. For the lignite, however, no effect of pressure was observed in inert atmospheres. Although much experimental evidence appears to support the hypothesis, the effects of rapid heating on the secondary char forming reactions have been neglected almost completely. Rapid devolatilization requires rapid heating, which increases the effective devolatilization temperature and hence the rates of the secondary reactions. Rapid production of volatile matter could increase the partial pressure of reactive species inside the coal, which also could enhance the secondary reactions. In view of these facts the simple qualitative interpretation that "rapid devolatilization causes

rapid escape" requires a critical examination.

Hypotheses (2) and (3), although possible, lack experimental support. The external cracking of volatile matter, hypothesis (4), was observed by various investigators (Gregory and Littlejohn, 1965; Gray et al., 1974; Anthony, 1974). However, the extent of this external effect is not enough to explain the large enhancements.

In summary, the proposed mechanisms for the enhanced volatile yields contain several unresolved questions, especially the detailed analyses on the transport mechanism of the volatile matter through coal pores and the influences of rapid heatings on the secondary reactions. Both experimental and theoretical analyses are required to establish more satisfactory mechanisms.

1.2.3 Devolatilization Models

The simplest and the most commonly used model for correlating the kinetics of volatile yield is a first order overall reaction with Arrhenius rate constants. The rate of volatile yield was assumed to be proportional to the remaining volatile matter.

$$\frac{dV}{dt} = k(V_{\infty} - V) \quad (1.8)$$

$$k = B e^{-E/RT} \quad (1.9)$$

where V , V_{∞} , B and E denote volatile matter, total amount of volatile matter evolved at a long reaction time, frequency factor and activation energy. In Fig. 1.3 some of the Arrhenius parameters obtained under various experiments in the past are shown. The sources of the data are tabulated in Table 1.1. Wide discrepancies of several order of magnitude in rates are evident. Some of them may be attributed to the differences

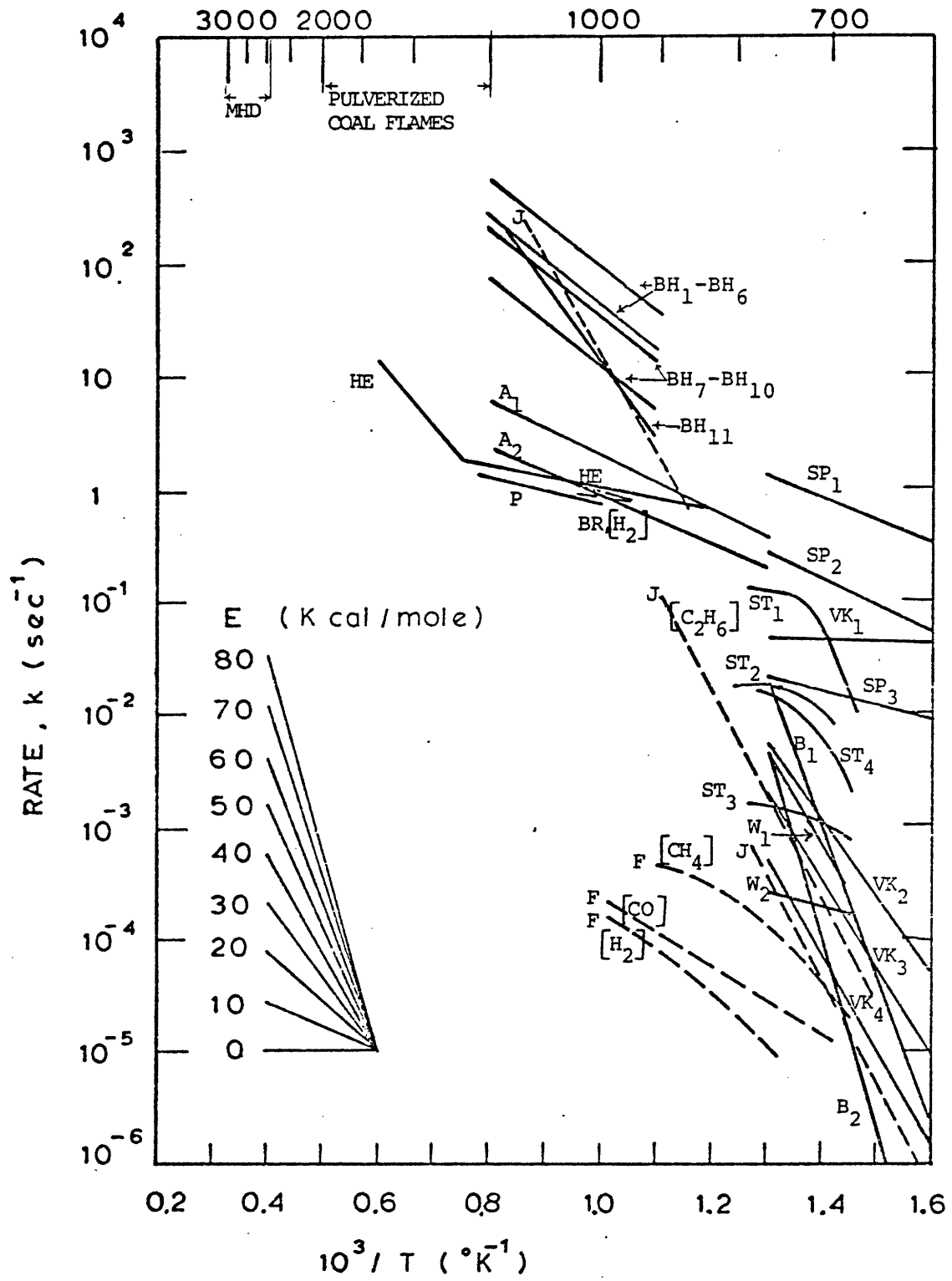
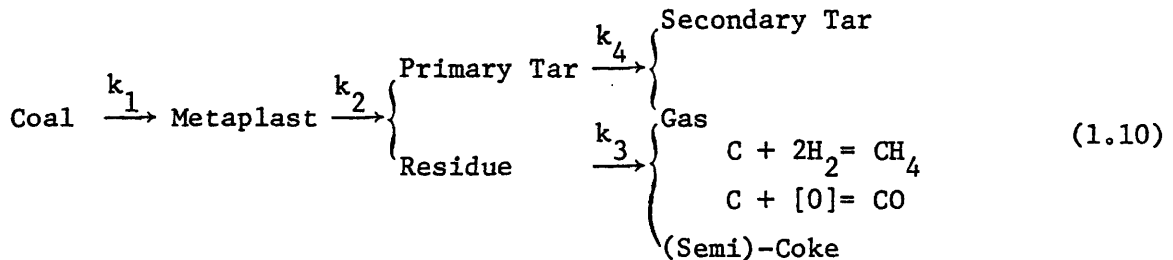


FIG. 1.3 COMPARISON OF DEVOLATILIZATION RATE CONSTANTS

P : Peters and Bertling (1965)	-
"From Fig. 8."	
SP ₁ -SP ₃ : Shapatina, et al. (1960)	50.2
Moscow District Brown Coal (Three different stages of devolatilization)	
ST ₁ - ST ₄ : Stone, et al. (1954)	
ST ₁ -ST ₃ : Pittsburgh Seam Bituminous Coal	42.2
ST ₄ : Colorado Coal	41.5
VK ₁ - VK ₄ : Van Krevelen, et al. (1951)	
VK ₁ : Brown Coal	51.0
VK ₂ : Bituminous Coal, low rank	39.5
VK ₃ : Bituminous Coal, high rank	18.8
VK ₄ : Semi-anthracite	14.2
W ₁ , W ₂ : Wiser, et al. (1967)	
Utah High Volatile Bituminous Coal	47.5 (% dry)
(W ₁ : first 60 min; W ₂ : 60-160 min)	

in the structure of coal and physical factors such as the particle size. However, the extent of the discrepancies both in rates and activation energies appeared to be too large to be explained solely by these factors. Above 1250°K the only kinetic data available are those of Howard and Essenghigh (1967), which was obtained from a pulverized coal flame. Since the devolatilization proceeded with simultaneously oxidation of char by heterogenous reactions, the reduction of the data required special assumptions on the nature of the heterogenous reaction. Hence the reliability of the parameters is open to question. Considering these facts, (1) close examination of the relatively low temperature data with an attempt to explain some of the discrepancies, and (2) dependable experimental measurements of rapid devolatilization above 1250°K appeared to be very important.

More complicated models involving more than one reaction have been developed in order to describe different aspects of devolatilization phenomena. Van Krevelen and his coworkers (Fitzgerald and Van Krevelen, 1959; Chermin and Van Krevelen, 1957; Van Krevelen et al., 1956; Fitzgerald, 1956; Van Krevelen et al., 1956, 1951) developed a model for carbonization describing both plasticity of coal and volatile yields by consecutive reactions (Fitzgerald and Van Krevelen, 1959).

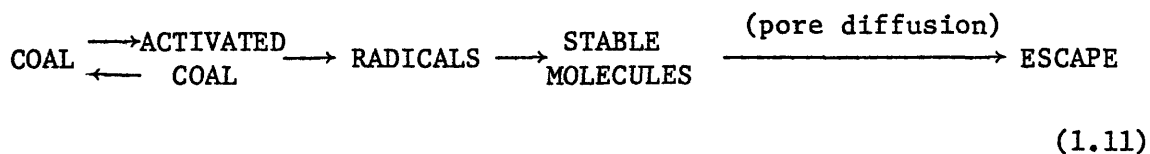


where "Metaplast" is an intermediate product responsible for the

fluidity of coal. Quantitative evaluation of the first three rate constants, k_1 , k_2 and k_3 were done for some coals assuming first order reactions (Chermin and Van Krevelen, 1957) and good agreements with the experimental results were obtained. For the gas evolution, k_3 , the activation energy was assumed to increase with the progress of "degassing," arguing that weaker bonds rupture initially leaving stronger bonds gradually. Although the model was developed for slow carbonization conditions, the authors noted that some of the metaplast was carried away as a tar mist, the amount of which was assumed to be proportional both to the amount of metaplast present and to the rate of degasification obtained at the moment (Chermin and Van Krevelen, 1957). In this model, the final yields differ by the amount of metaplast carried away under different conditions, predicting larger volatile yield under rapid heating conditions. However, such concept may not be valid in explaining the increased volatile yield observed for non-caking coals (Kimber and Gray, 1967; Eddinger et al., 1966).

Instead of the consecutive reactions, multiple parallel independent reactions have been used by several investigators. Chukhanov (1954) postulated five first order reactions with different activation energies and frequency factors, each representing a certain product of devolatilization. Recognition of numerous reactions associated with ruptures of various bonds with different energy levels led Pitt (1962) to employ a large number of independent reactions with a particular distribution of activation energies. His method involved a curve fit of the data by an empirical equation followed by construction of a

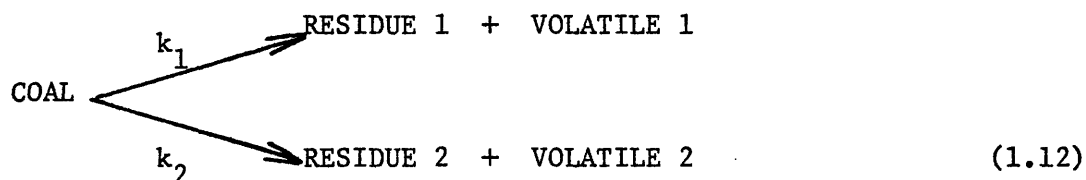
distribution curve assuming a constant frequency factor of 10^{15} min^{-1} . Jüntgen and Van Heek (1970, 1969, 1968) advanced a mathematical technique of analyzing reaction kinetics under non-isothermal conditions with applications to coal devolatilization at various heating rates. The proposed mechanism consists of four steps.



The "coal molecule" is thermally activated, ruptures of bonds produce many radicals which react inside the pores of coal to produce stable molecules. The stable molecules escape through the pores by diffusion. Although the overall scheme was not applied to any experiments, kinetics of gas evolution under slow to medium heating conditions (10^{-2} to 10^5 c/min) was studied in detail. Evolution of each gas (hydrocarbons, CH_4 to C_4) was modeled by many independent reactions having a Gaussian distribution of activation energies and a log-normal distribution of frequency factors (Hanbaba et al., 1968). Anthony (1974) also employed a Gaussian distribution of activation energies with a constant frequency factor to model the overall volatile yield under rapid heating conditions. One of the important aspects of the multiple reaction models with statistical distribution of rate constants is that these models could explain the low activation energies obtained using the single overall reaction (see Fig. 1.3). Jüntgen and Van Heek (1970) demonstrated that eight parallel first order reactions with a common frequency factor of 10^{15} min^{-1} and activation energies ranging from 48 to 62 Kcal/mol can be closely approximated by a single reaction with a frequency factor of

10^4 min^{-1} and an activation energy of 20 Kcal/mol. Although the fact that coal devolatilization involves numerous reactions may be better represented by statistical approaches, they require additional parameters and the parallel independent scheme, as it is, predict the same asymptotic yield under long reaction times.

Kobayashi (1972) tested several models consisting of two overall reactions against the data of Kimber and Gray (1967) and Badzioch and Hawksley (1970), in an effort to model the enhanced volatile yield under high temperature rapid heating conditions. He suggested that two bulk competing first order reactions of the type



best describe the observed volatile yields. One of the reactions is dominant at relatively low temperatures yielding small amount of volatile matter rich in hydrogen. At higher temperatures, the second reaction becomes competitive leading to higher volatile yields.

In spite of the fact that many researchers pointed out the importance of the secondary reactions in relation to the enhanced volatile yields observed under rapid heating conditions, very little theoretical analysis has been done. Anthony (1974) modeled the secondary char forming reaction to be competing with diffusional escape of the reactive volatile matter, the flow rate of which was assumed to be proportional to the product of the concentration of the volatile matter

inside the pore and the overall mass transfer coefficient. He obtained a limited solution for the volatile yield under a steady-state isothermal condition and explained that the higher yields under reduced pressures occur through an increase in the overall mass transfer coefficient which was assumed to be inversely proportional to the total pressure. Although the model predicted the observed effect of the ambient pressure on the volatile yield well, the detailed transport mechanism is concealed in the assumed mass transfer coefficient. More realistic models on the volatile evolution, based on the bubble transport process through plasticized coal, have been developed recently (Lewellen, 1975, and Miller et al., 1975). These models allow parametric studies on the effects of the heating rate, the particle size and others. However, lack of experimental data on the physical change of coal particles and large uncertainty in the fundamental physico-chemical properties such as viscosity and surface tension prevented the drawing of any quantitative conclusions.

Reidelbach and Summerfield (1975) extended the existing coal models by incorporating a competing chemical scheme leading to tar or gases and other reactions. Table 1-2 shows the proposed general scheme. Numerical calculations were performed for the first five reactions, and the results agreed with some of the experimental data such as changes of relative amount of tar and gases with temperature. However, the number of parameters used in the model (e.g., five reaction rates) compared with limited amount of existing data makes the model of little practical use. Models with large numbers of reactions should be more closely related

TABLE 1-2

GENERAL HYPOTHETICAL SCHEME FOR COAL PYROLYSIS

(Reidelbach and Summerfield, 1975)

C	k_1	AC	Activation Step (high E)
AC	k_2	$x_2 PT_L + (1 - x_2) S_1$	low E
AC	k_3	$x_3 PG_2 + (1 - x_3) S_2$	medium E
S_1	k_4	$x_4 PG_2 + (1 - x_4) S_3$	Primary Decomposition high E
S_2	k_5	$x_5 PG_3 + (1 - x_5) S_4$	high E
AC	k_6	DAC	Deactivation Step (DAC \neq C)
PT_L	k_7	$x_7 SG_1 + Y_7 S_5$	Polymerization in the liquid phase inside the particle
PT_L	k_8	PT_G	Vaporization (depending on heat and mass diffusion)
PT_G	k_9	$x_9 SG_2 + Y_9 S_6$	Polymerization in the gas phase
PT_G	k_{10}	$x_{10} SG_3 + Y_{10} S_7$	Cracking in the gas phase

where

- C = Initial coal
- AC = Activated coal
- PT_L = Liquid primary tar
- PT_G = Gaseous primary tar
- PG = Primary gas
- SG = Secondary gas
- S = Solid intermediate or residue
- x,y = Stoichiometric coefficients
- AE = Activation energy

to the actual chemical mechanisms, which could allow evaluations of the rate constants from the fundamental structure of coal. Cheong et al. (1975) analyzed devolatilization by assuming a certain chemical structure of coal and then postulating dominant reactions. In their analysis the rate constants are determined theoretically from the assumed structure of coal. Although such activities are important in the long run, the present lack of adequate knowledge of chemical structure and the uncertainties with which the theoretical values of the rate constants are known diminishes its value for engineering applications.

1.3 Objectives

There is a serious need for reliable data on the kinetics of rapid devolatilization of coals for purposes of improving the design of gasifiers and combustors and for testing models of coal pyrolysis. The short reaction times and rapid heating rates of interest impose severe experimental constraints particularly at high temperatures. The only data available are, under these conditions, those based on pulverized coal flames (Howard and Essenhig, 1968) and on flow experiments (Coates et al., 1974; Stickler et al., 1974; Badzioch and Hawksley, 1970; Kimber and Gray, 1967, and Eddinger et al., 1966). In the former, problems result from the need to separate contributions to weight loss of oxidation and pyrolysis. The data obtained from the flow experiments, although providing useful information, are questionable for the following reasons: (1) in the low temperature range (Badzioch & Hawksley, 1970), weight losses were derived using ash as a tracer, neglecting variations in the ash weight loss, an assumption which is not always valid as will be

shown, (2) the temperature-time history of the particles were not defined with precision, (3) at temperatures above 1250°K only asymptotic weight losses were obtained because of the inability to sample at short times. The detailed data are needed in order to evaluate existing models developed to explain the increases in volatile yield with increasing temperature under rapid heating conditions. In particular, models are needed that can be utilized to determine the conditions under which volatile yields are maximized. Additionally, the data may be used to evaluate various physico-chemical mechanisms proposed for coal pyrolysis.

In view of the above considerations, the following goals were selected for the present study:

1. The measurement of the overall weight losses and elemental losses of coal under well-controlled, high-temperature, rapid-heating conditions. The following variables are studied over the indicated ranges:

Coal Type	A high-volatile bituminous coal and a lignite
Particle Size	Narrowly size graded fraction below 100 micron
Temperature	1000 - 2200 °K
Reaction Time	1 - 200 msec
Time Resolution	1 - 10 msec
Heating Rate	$10^4 - 10^6$ °K/sec
2. The development of experimental techniques for rapid heating and for rapid quenching under high-temperature conditions.
3. The critical assessment of the validity of the use of ash as a tracer and the development of the methods for measuring weight

losses without using ash as a tracer.

4. The experimental testing of some of the mechanisms proposed for explaining increases in volatile yields under rapid heating conditions.
5. The development of a descriptive mathematical model of devolatilization through critical evaluations of the proposed mechanisms and experimental results.

1.4 Scope of the Study

In order to achieve the various goals of the study, four different types of devolatilization experiment were designed to cover a wide range of heating rates and heating times as indicated in the following tabulation.

	<u>Heating Rate</u>	<u>Reaction Time</u>
(1) Laminar Flow Experiment	$10^4 - 5 \times 10^5$ ($^{\circ}\text{K}/\text{sec}$)	1 - 200 msec
(2) Free Fall Experiment with Bronze Collector	$10^4 - 10^5$ ($^{\circ}\text{K}/\text{sec}$)	\sim 1 sec
(3) Free Fall Experiment with Alumina Collector	$10^4 - 10^5$ ($^{\circ}\text{K}/\text{sec}$)	\sim 10 min
(4) Crucible Experiment	$10^{-1} - 10$ ($^{\circ}\text{K}/\text{sec}$)	10 min - 10 hr

The majority of the experiments were carried out at high temperatures in the laminar flow system, i.e., with rapid heating and for short residence times. The free fall experiments supplement the laminar flow experiments by providing longer reaction times. The crucible experiments were used to study devolatilization mechanisms under slow heating but to the same peak temperatures.

The experimental systems and the characterization of the coals will be described in chapter 2. The data reduction methods are discussed in chapter 3, focussing on the estimation of the temperature-time histories of coal particles in the laminar flow system, and on the determination of weight losses by two independent methods - i.e., by differences in the weights of coal fed and char collected or by using ash as a tracer.

Results of the weight loss measurements are presented in the first half of chapter 4. The second half shows the results of changes in elemental composition in chars from different experimental conditions.

Discussions in chapter 5 aim to test some of the hypotheses previously proposed to explain the enhanced volatile yields observed under rapid heating conditions. The roles of the heating rates are first clarified in section 5.1. The contributions of secondary reactions in the gas phase on the overall weight loss are discussed in section 5.2, referring to a set of experiments designed to examine the effects (change in coal bed depth in the crucible). Implications from the ultimate analysis of char are discussed in relation to the possible chemical mechanisms of devolatilization in section 5.3. A hypothesis, that rapid escape of volatile matter from coal under rapid heating conditions diminishes the chance of secondary char forming reactions resulting in a larger overall volatile yield, is examined in section 5.4. The problems associated with the use of ash as a tracer in determining weight losses are presented in section 5.5. A possible mechanism which explains the various observations is presented in section 5.6.

First order kinetic parameters for devolatilization are derived from the result, based on a single overall reaction, and compared with other data in chapter 6. Some of the discrepancies among the previous data are also explained.

Chapter 7 presents a simplified model which provides an empirical description of the observed behavior of kinetics and yields.

CHAPTER II

EXPERIMENTAL APPARATUS AND PROCEDURES2.1 Selection of Apparatus

In selecting the apparatus, it is important to consider the applicability of the data to actual systems as well as the capability of the system to produce precisely controlled experimental conditions. Several alternatives are possible to achieve high temperatures.

2.1.1 Shock Tube

A shock tube has been used widely to study rapid reaction kinetics. It can provide very well defined temperatures and pressures almost instantaneously. Applications to coal particles have been done in ignition and combustion studies (Nettleton and Stirling, 1974, 1971, 1967) and in decomposition and hydrogenation behaviors (Woodburn, 1974). Major difficulties in applying such a system to weight loss measurement during devolatilization, however, are collection and quenching of char.

2.1.2 Irradiation Heating

Rapid heating of coal has been achieved in various atmospheres using lasers (Karn, et al., 1972, 1970, 1968, 1967; Sharkey, et al., 1966) or a xenon flash tube (Granger and Ladner, 1969). Although these methods provide convenient ways to attain high temperatures, it is very difficult to control the particle temperature and the reaction time. Also, direct applications of the results to actual systems are difficult, unless coal particles are suspended in gaseous atmosphere.

2.1.3 Flow Furnace

Flow reactors have been used widely by various researchers. Gray and Kimber (1967) applied such a system to coal studies at temperatures up to 2800°K. One of the main advantages of flow furnaces is its similarity to actual systems. By controlling both gas and wall temperatures, a wide range of simulation is possible, and the results may be readily applicable to real systems. A typical flow furnace system includes a temperature controlled furnace, a high temperature gas supply device, a coal feeder and a sampling probe. The relative complexity of the system and material problems at high temperatures are major detriments of such an apparatus.

For the present study a laminar flow furnace was chosen for its versatility. Similar systems were developed by BCURA researchers (Field, 1970; Badzioch and Hawksley, 1972), but some important improvements were made in system design and characterization. These improvements include a partially fluidized vibrating feeder, a water quenched collector with a bronze filter and particle velocity measurements by a laser doppler anemometer. In BCURA systems char particles were quenched by thermal conduction from water cooled collector walls and then separated by cyclone separators. Good recovery of particles was not achieved because of the adhesion of char particles to the collector wall. Thus they had to use ash as a tracer to determine weight loss. In our system this problem was solved by collecting char particles with a bronze filter at the mouth of the collector. Use of direct water jets provided faster quenching, thus giving better temperature-time history of coal particles.

2.2 Laminar Flow Experiment

A schematic of the laminar flow furnace system is shown in Fig. 2.1. The system is built around a modified ASTRO model 1000A graphite furnace (ASTRO Industries, Inc., Santa Barbara, California). A 3.5 in. I.D., 12 in. long graphite resistance heating element supplies necessary heat to maintain controlled furnace temperatures. A 4 in. I.D. graphite radiation shield and packed graphite powder provide thermal insulation. The outer shell is about 11 inches in diameter and water-cooled for easy access. The furnace is equipped with an automatic temperature controller and a programmer which allows temperature changes to be made at desired rates. This feature is especially important when ceramic muffle tubes are used, since they are susceptible to thermal shock. The temperature is controlled through a tungsten-rhenium thermocouple which is located just outside of the heating element in the center of the furnace. The maximum operating temperature of the furnace is about 3000°K with a graphite muffle tube. Three pairs of observation ports are located along the axis of the furnace at intervals of 1.5 inches. The ports have quartz windows which supply an observation area 0.5 in. in diameter. Optical instruments such as a radiation pyrometer or a laser doppler anemometer were used through these windows. Coal particles are injected axially at the center of the 2 in. I.D. graphite muffle tube through a 0.047 in. I.D., 3/16 in. O.D. water-cooled stainless steel injector. A 5/8 in. O.D. graphite tube is used as a heat insulator to minimize the heat loss to the water-cooled injector. Preheated gas is introduced horizontally to the axis of the furnace and straightened through a 1 inch thick graphite honeycomb. The honeycomb hole size is 0.067 in. in diameter

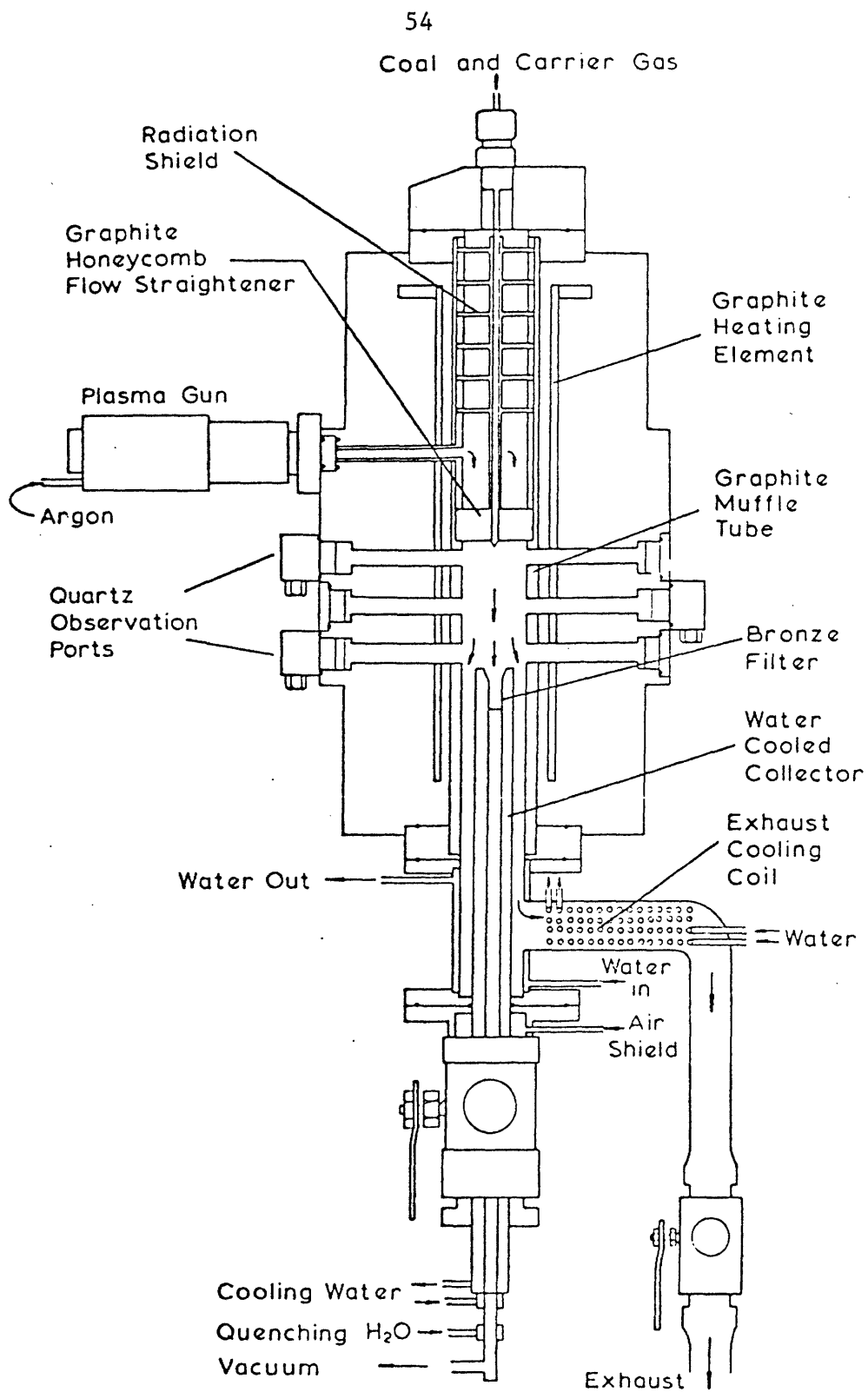


FIG. 2.1 LAMINAR FLOW FURNACE SYSTEM

and the distance between holes is 0.083 inches. The lower surface of the honeycomb is 0.5 in. above the center of the first observation port. Six 2-3/8 in. disks are placed 1 inch apart above the honeycomb to prevent radiation heat loss. The coal particles and the carrier gas are mixed with the preheated main gas. The char is collected at a water-cooled bronze filter after being quenched by water jets. The rest of the gas is cooled by water coils and exhausted. Since the muffle tube is graphite, atmospheric air has to be excluded at all times. Two ball valves provide a convenient way to close quickly the passages for the removal of collector or for shutting off the plasma gun. The graphite muffle tube and the honeycomb could be replaced by an alumina muffle tube and an alumina honeycomb to conduct experiments in oxidizing atmosphere. With the alumina muffle tube, however, sudden introduction of preheated gas by starting the plasma gun might cause severe thermal shock.

2.2.1 Coal Feeder

The coal feeder employs a mechanical vibrator and partial fluidization of coal particles to get uniform feed rates. Figure 2.2 shows the design. The main body is made of polished plexiglas to check the coal level and the feed rate visually. The I.D. of the plexiglas is 0.5 inches and the length 3 inches; about 5 gm of coal can be charged. The feed rate is controlled by the needle valve opening, the vibrator strength and the carrier gas flow rate. The carrier gas is introduced through the hollow needle valve and injected radially through four equally spaced, 0.010 in. holes at the tip of the needle valve. The gas fluidizes the coal particles locally, thus preventing packing and

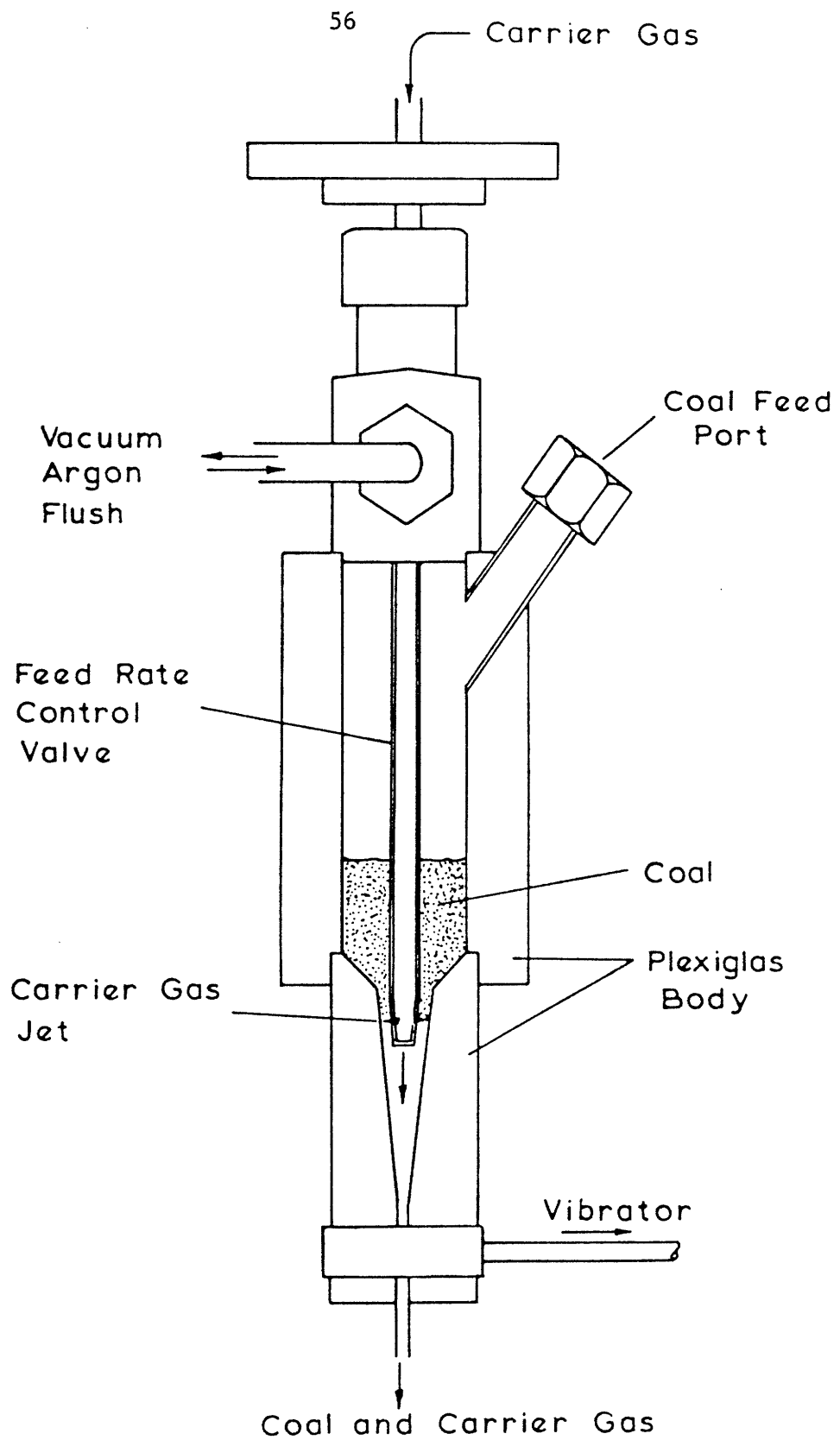


FIG. 2.2 COAL FEEDER

clogging in the narrow region. An external electric vibrator oscillates the entire feeder assembly. The exit of the feeder is connected to a 0.065 in. O.D. and 0.047 in. I.D. vertical stainless steel tube which enters the furnace. The vertical arrangement of the feeder-injector line allows the use of a fine tube with a very small amount of carrier gas flow (as small as 5 cc/min). Less carrier gas allows more rapid heating of the injected particles. Feed rates between 0.01 gm/min and 1.0 gm/min can be obtained with reasonable uniformity. In normal operations about 0.15 gm/min was used.

2.2.2 Particle Collector

The collector consists of three concentric copper tubes. Two passages are used for the external cooling water and one is used to withdraw the quenched gases and directly injected cooling water (see Fig. 2.3). Eight 1/8 in. O.D. copper tubes pass through the second water passage to carry the directly injected quenching water. Heat transfer analysis revealed that quenching by conduction to the water-cooled wall alone is insufficient to achieve char quenching because of the relatively large hot gas flow rate (up to 1 l/sec) and the necessarily large collector diameter. To overcome this problem quenching water is injected at the mouth of the collector through twelve holes located in the flared upper section of the sintered bronze filter. (The filters were manufactured specially by Thermet Inc., Gloucester, Mass.) This porous bronze filter allows some of the quenching water to pass through the whole area of the upper section of the filter, preventing coal particles from adhering and being exposed to intense radiation from the furnace wall. The bronze filter is 0.740 in. O.D. at the open

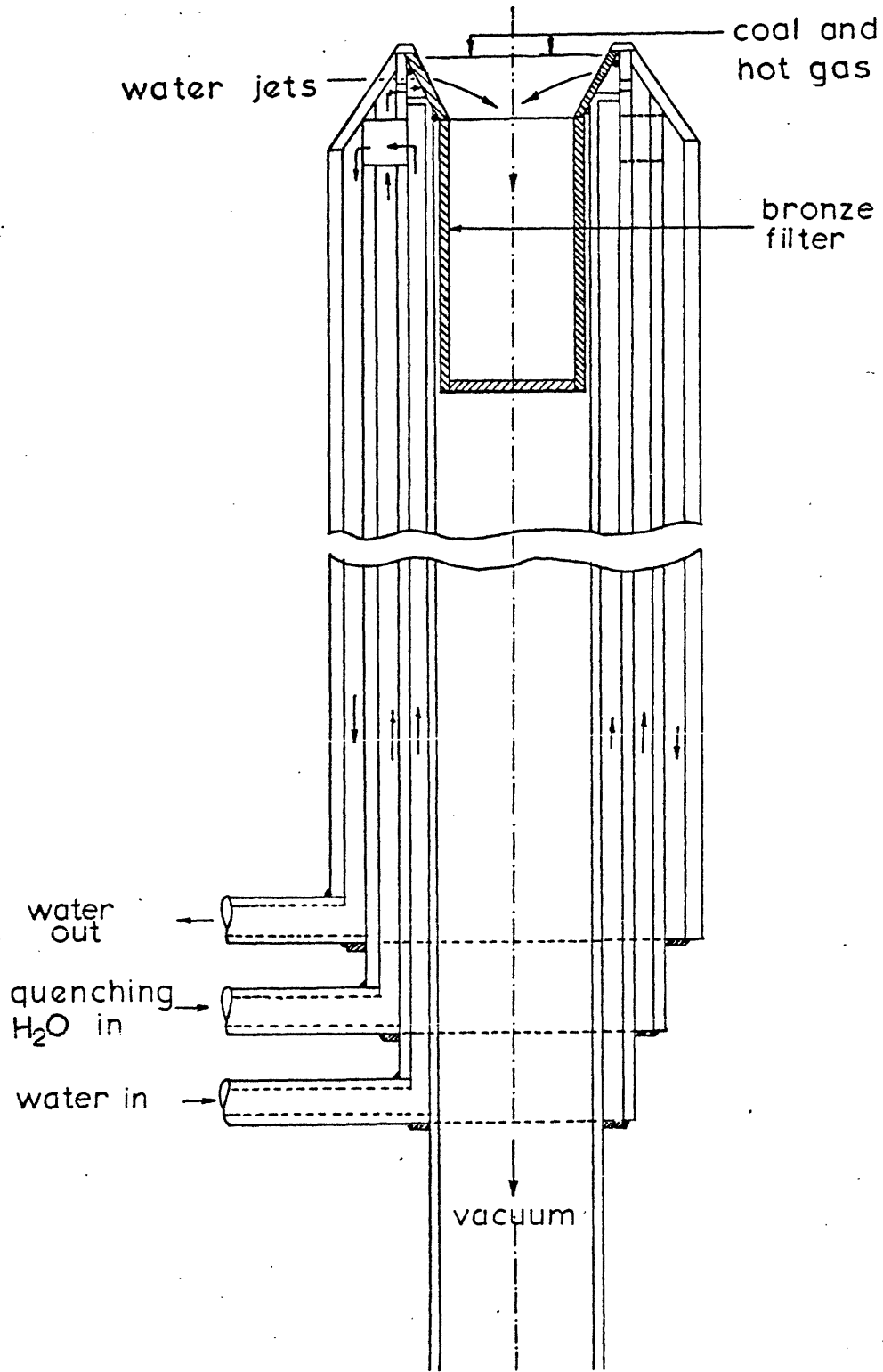


FIG.23 WATER COOLED COLLECTOR

end, 0.4 in. O.D. and 4 in. long at the straight section, and the wall thickness is 0.060 inches. The average particle size of bronze is about 15 micron, and coal particles larger than about 5 micron in diameter are retained in the filter.

2.2.3 Gas Preheater

An AVCO plasma gun model PG 040 is attached to the furnace to preheat the main gas stream. The plasma gun has a water-cooled tungsten cathode and an annular water-cooled copper anode. An AIRCO model 1500-C7 welding rectifier supplies D.C. power to the gun. The maximum power input to the plasma gun is 40 Kw with about 30 percent efficiency to heat the gas. The temperature of the preheated gas is controlled by changing the electric current and the gas flow rate. Argon, helium, nitrogen or hydrogen can be used as working gases. With a graphite muffle tube, however, only argon and helium are possible.

2.2.4 Suction System

A steam ejector supplies sufficient suction rates to withdraw both directly injected quenching water and quenched argon gas. Water is separated from the gas by a gravitational separation vessel. The quenched gas is dried through a packed bed of calcium sulfate and metered by a Fischer & Porter flowmeter.

2.2.5 Experimental Procedure

The furnace is heated to a desired temperature using the automatic temperature controller. Three tungsten-rhenium thermocouples, which were introduced through the observation ports, monitor the temperature inside the muffle tube. The temperature profile along the axis of the furnace is similar to that of "free-fall" furnace (see Fig. 2.6).

After steady-state is reached, the main gas is introduced and the plasma gun is started. The temperature of the main gas is controlled to the same temperature as the furnace wall temperature. This is done by matching the thermocouple readings before and after the introduction of the main gas. The main gas flow rate is controlled by a Fischer & Porter flowmeter to give desired main gas velocities. The pressure of the furnace is about 2 inches H_2O above atmospheric pressure.

A predried bronze filter is weighed and placed in the collector. Suction rates varied between 1/3 to 1/2 of the main gas flow rates depending on the temperatures. The flow rate of the quenching water jets was maintained at 0.7 l/min for most of the runs. After a desired suction rate and a water flow rate are obtained, the collector is raised into the furnace and positioned at a certain distance from the coal particle injector. About 0.05 to 0.5 gm of coal is weighed and charged into the feeder. Then, a carrier gas flow rate and a needle valve opening are set and the vibrator is turned on. The coal level in the feeder is continuously monitored and the end of the feeding is visually judged. As char particles accumulate in the bronze filter, the filter starts clogging. In order to maintain the same suction rate, the valve opening of the suction line has to be increased to compensate for a larger pressure drop across the filter. The maximum pressure drop allowed is about 20 in. Hg. Upon completion of the coal particle injection, the collector is removed from the furnace and a new bronze filter is placed. The collector is raised again to a different location and the next run is started. Normally about ten runs are repeated at the same conditions except for the location of the collector. A summary of

operating conditions is shown in Table 2.1. After all runs are finished, the filters are dried in a drying oven at 110°C for three hours in a nitrogen atmosphere. The filters are then cooled in a desiccator and weighed as soon as room temperature is reached. Some of the char samples are analyzed for ash content or sent to Galbraith Laboratories, Inc., Knoxville, Tennessee, for ultimate analysis. Weight loss of coal is determined by the difference of the weights between the coal fed and the collected char. The details of the weight loss calculations are discussed in section 3.3.

2.3 Free Fall Experiment with Bronze Collector

In order to obtain longer reaction times, an experiment was designed so that coal particles fall down through a preheated furnace by gravity. Figure 2.4 shows the schematic of the system. The main component of the system is an ASTRO model 100A graphite furnace. The same temperature control system, which is used for the laminar flow furnace, controls the furnace wall temperature. A 24 in. long, 3 in. O.D., 2 1/2 in. I.D. alumina muffle tube shields the graphite heating element from the reaction zone. A 15 in. long, 2 1/4 in. O.D., 2 in. I.D. alumina tube supports an alumina honeycomb flow straightener. The honeycomb, made by E. I. du Pont de Nemours, has a nominal pore diameter of 1/16 inch. The maximum temperatures of the alumina tubes and honeycomb are 2100°K and 1900°K respectively. A 9 in. long, 3 1/2 in. I.D. cooling section is attached to the bottom of the furnace. The coal feeder and the water-cooled injector are the same as the ones used in the laminar flow system, except the diameters of the tubes. The water-cooled injector has a 0.250 in. O.D. and a 0.101 I.D.

TABLE 2.1 SUMMARY OF OPERATING CONDITIONS

1. Laminar Flow Experiment

Furnace Temp. (°K)	Main Gas Flow Rate (ℓ/sec)	Suction Flow Rate (ℓ/sec)	Carrier Gas Flow Rate (cc/min)	Average Main Gas Velocity (m/sec)	Average Carrier Gas Velocity (m/sec)	Main Gas Reynolds No.
1000	0.49	0.25	40	0.81	0.60	420
1260	0.49	0.25	48	1.02	0.72	360
1510	1.16	0.50	15	2.88	0.22	760
1740 (LIG)	1.72	0.86	35	4.93	0.52	1040
1740 (BIT)	1.72	0.86	333	4.93	4.96	1040
1940 (LIG)	2.50	0.86	35	7.99	0.82	1410
1940 (BIT)	2.50	0.86	300	7.99	4.47	1410
2100	2.50	0.86	608	8.65	9.06	1290

2. Free Fall Experiment with Bronze Collector

Furnace Temperatures (°K): 1490 1830
 Main Gas Flow Rates (ℓ/sec): 0.048, 0.103, 0.158
 Carrier Gas Flow Rates (cc/min): 38

3. Free Fall Experiment with Alumina Collector

Furnace Temperatures (°K): 1040, 1240, 1490, 1830
 Main Gas Flow Rates (ℓ/sec): 0.0 ~ 0.05
 Carrier Gas Flow Rates (cc/min): 2.0 ~ 25.0

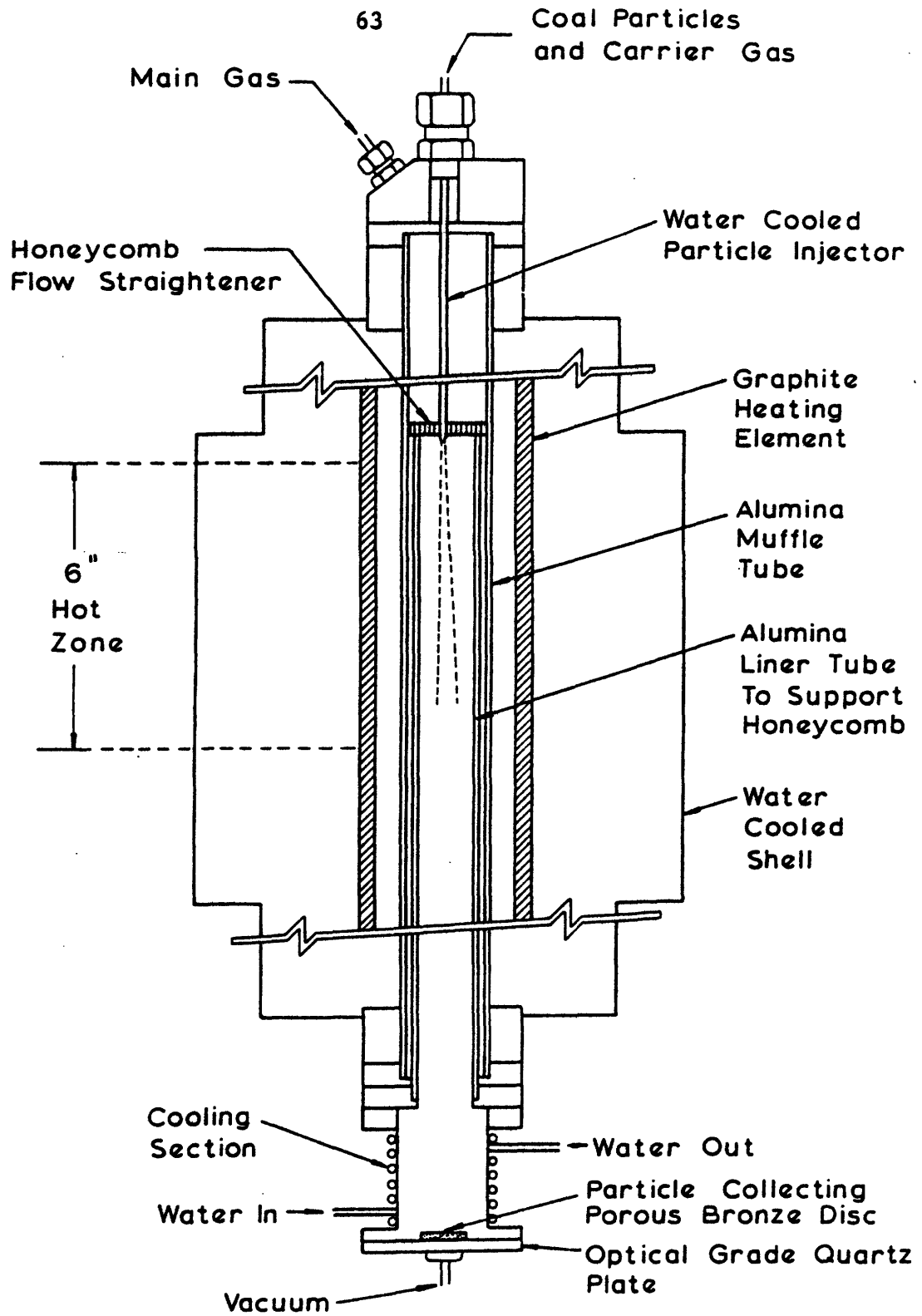


FIG. 2.4 FREE FALL EXPERIMENT WITH BRONZE COLLECTOR

Small amounts of main gas (about 0.05 l./sec) are introduced from the top of the furnace. The gas is heated by conduction from the muffle tube wall and honeycomb. The honeycomb induces uniform velocity and temperature profiles in the radial direction. The temperatures along the axis of the furnace were measured by a chromel-alumel thermocouple up to 1500°K and by a platinum-rhodium or an iridium-rhodium thermocouple above 1500°K. Typical temperature profiles are shown in Fig. 2.6. Since the main gas Reynolds number is small, the flow is practically fully developed for the entire region. Therefore the temperature of the main gas is considered to be close to the wall temperature of the muffle tube. Coal particles are introduced into the center line of the main flow through the water-cooled injector. Carrier gas flow rates between 2 cc/min and 25 cc/min were used. Char particles are collected in a 3 in. diameter, 1/8 in. thick sintered bronze disk at the bottom of the cooling section. The bronze disks were manufactured by Thermet, Inc., Gloucester, Mass. They have an average pore diameter of about 5 micron. The gas exits through a 1/4 in. pipe fitting under the center of the bronze disk.

2.3.1 Experimental Procedure

The furnace is heated to a desired temperature at a heating rate between 250°C/hr and 350°C/hr, using the temperature programmer. After a steady-state is reached, a preweighed bronze filter is placed on the bottom flange. Then the furnace is alternatively evacuated and filled with argon several times to eliminate atmospheric air. About 1 gram of coal is weighed and charged in the feeder. The suction rate is controlled so that the furnace pressure is maintained at atmospheric

pressure for fixed main gas and carrier gas flows. Then the vibrator is started and coal is fed in about 10 minutes, giving a feed rate of 0.1 gm/min. After all the particles are fed, the bronze disk is removed and quickly weighed to avoid adsorption of moisture. The collected char is transferred to a sample bottle for analyses, such as ash content, elemental composition, and particle size distribution.

2.4 Free Fall Experiment with Alumina Collector

Figure 2.5 shows char particles being collected in a cylindrical alumina collector which has been raised to the hot zone of the furnace. The object of the experiment is to obtain the asymptotic values of weight loss at very long reaction times. The furnace is the same as the one used in the free fall experiment with the bronze filters. A 40 mm O.D., 165 mm long cylindrical alumina crucible (Coors CN-170) is supported by a 1 7/8 in. O.D., 1/8 in. thick alumina disk, which is attached to a 1/2 in. O.D., 3/8 in. I.D. alumina tube. A thermocouple is placed between the support disk and the bottom of the collector to monitor the temperature during the experiment. The temperature is recorded continuously on a chart recorder. The collector is raised or lowered by a motor-driven linear actuator at a constant speed. This feature is especially important to protect the ceramic material from thermal shock caused by a sudden temperature change. At 1830°K it takes about 20 minutes to position or remove the alumina collector.

2.4.1 Experimental Procedure

After a desired temperature of the furnace is attained, a preweighed alumina collector is raised into the hot zone of the furnace by the linear actuator. The furnace is continuously purged by argon to

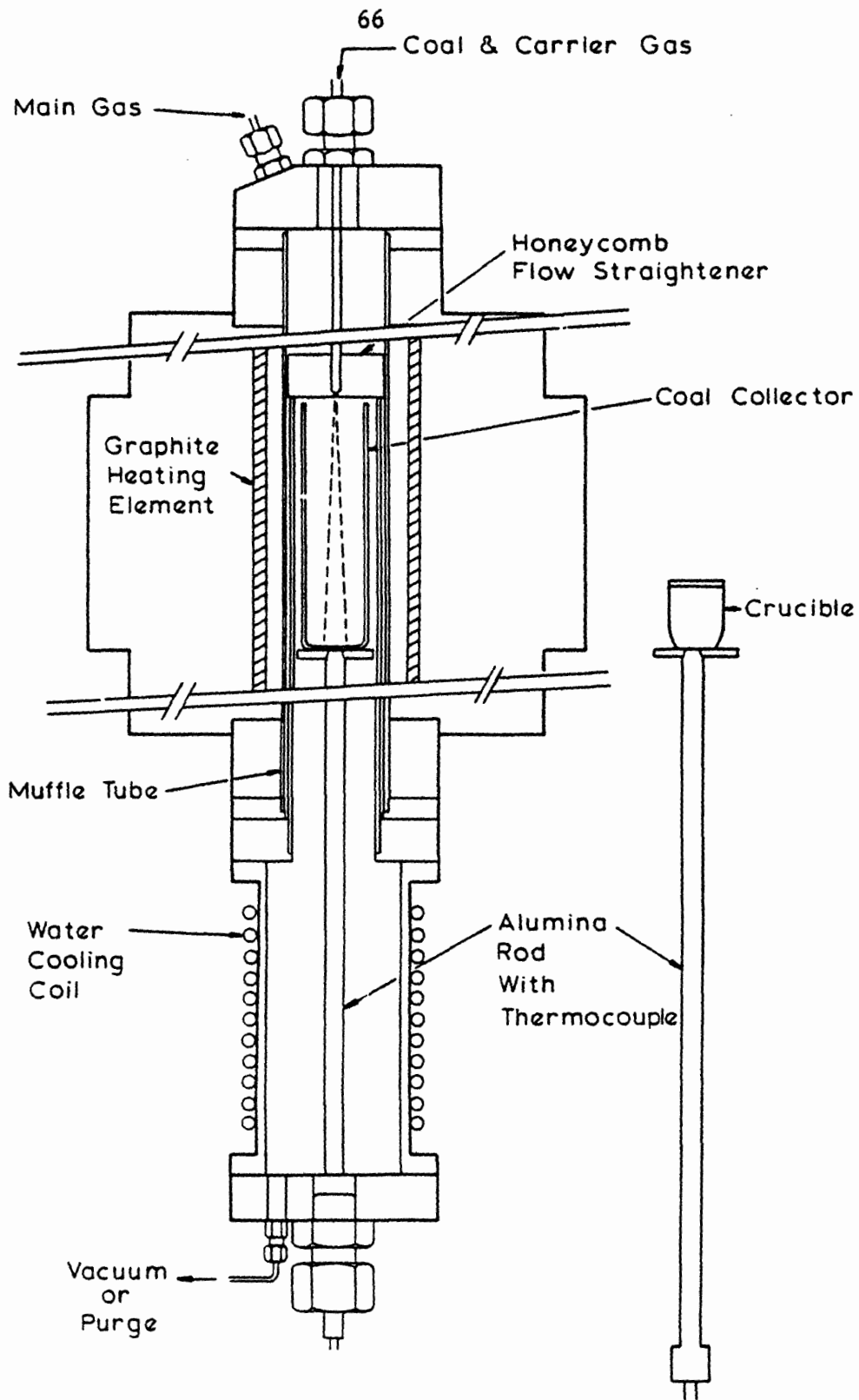


FIG. 2.5 FREE FALL EXPERIMENT WITH ALUMINA COLLECTOR AND CRUCIBLE EXPERIMENT

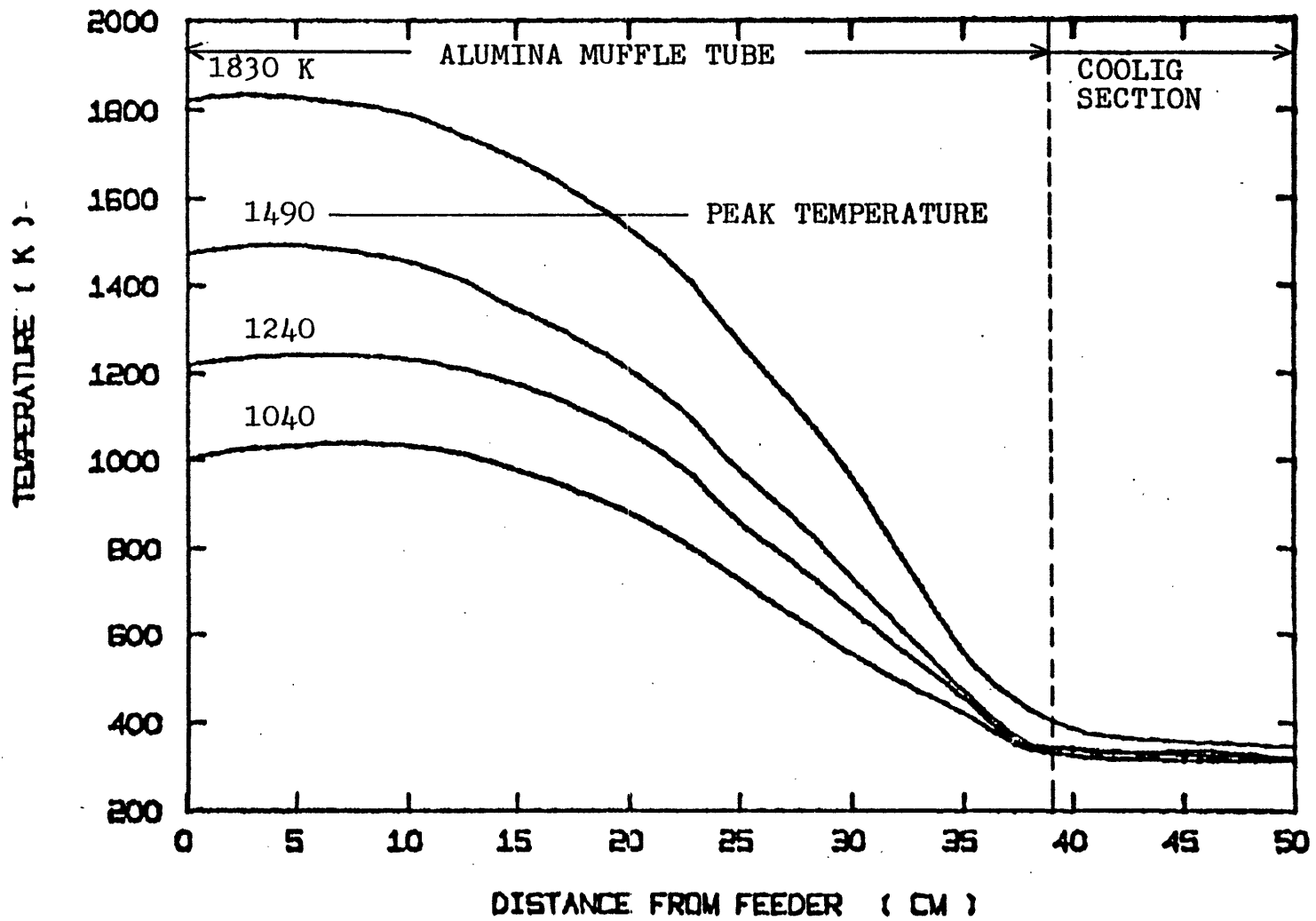


FIG. 2.6 AXIAL TEMPERATURE PROFILES IN FREE FALL AND CRUCIBLE EXPERIMENTS

prevent air inflow. The temperature at the bottom of the collector is recorded, and when a steady-state is reached, about 1 gram of coal is fed in approximately 10 minutes. Main gas flow rates between 0 and 0.05 l/sec and carrier gas flow rates between 2 cc/min and 25 cc/min were used. After all the particles are fed, the collector is kept for 10 minutes at the same position in order to assure sufficient reaction time for the particles fed last. The collector is then lowered into the cooling section and transferred to a desiccator. About half of the char sample and the material left in the crucible are analyzed for ash content. The details of the weight loss calculation are discussed in section 3.3.

2.5 Crucible Experiment

The object of the crucible experiments is to determine weight loss under slow heating conditions and extremely long residence times. Instead of feeding and collecting coal particles, as in the case of free fall and laminar flow experiments, about 1 gm of coal is weighed and placed in a 15 ml alumina crucible (Coors CH-16), then the crucible is raised into the hot zone of the furnace using the linear actuator discussed above. Figure 2.5 also shows a schematic of a 15 ml crucible supported by an alumina rod. The temperature between the crucible and the support disk is recorded by a thermocouple during the whole cycle of heating and cooling. Typical temperature-time histories are shown in Fig. 2.7. Heating rates between 0.5°K/sec and 5.0°K/sec can be obtained. It should be noted that this experiment is to a certain extent similar to the ASTM proximate volatile matter analysis, where one gram of coal is placed in a 15 ml platinum crucible and lowered into the heated

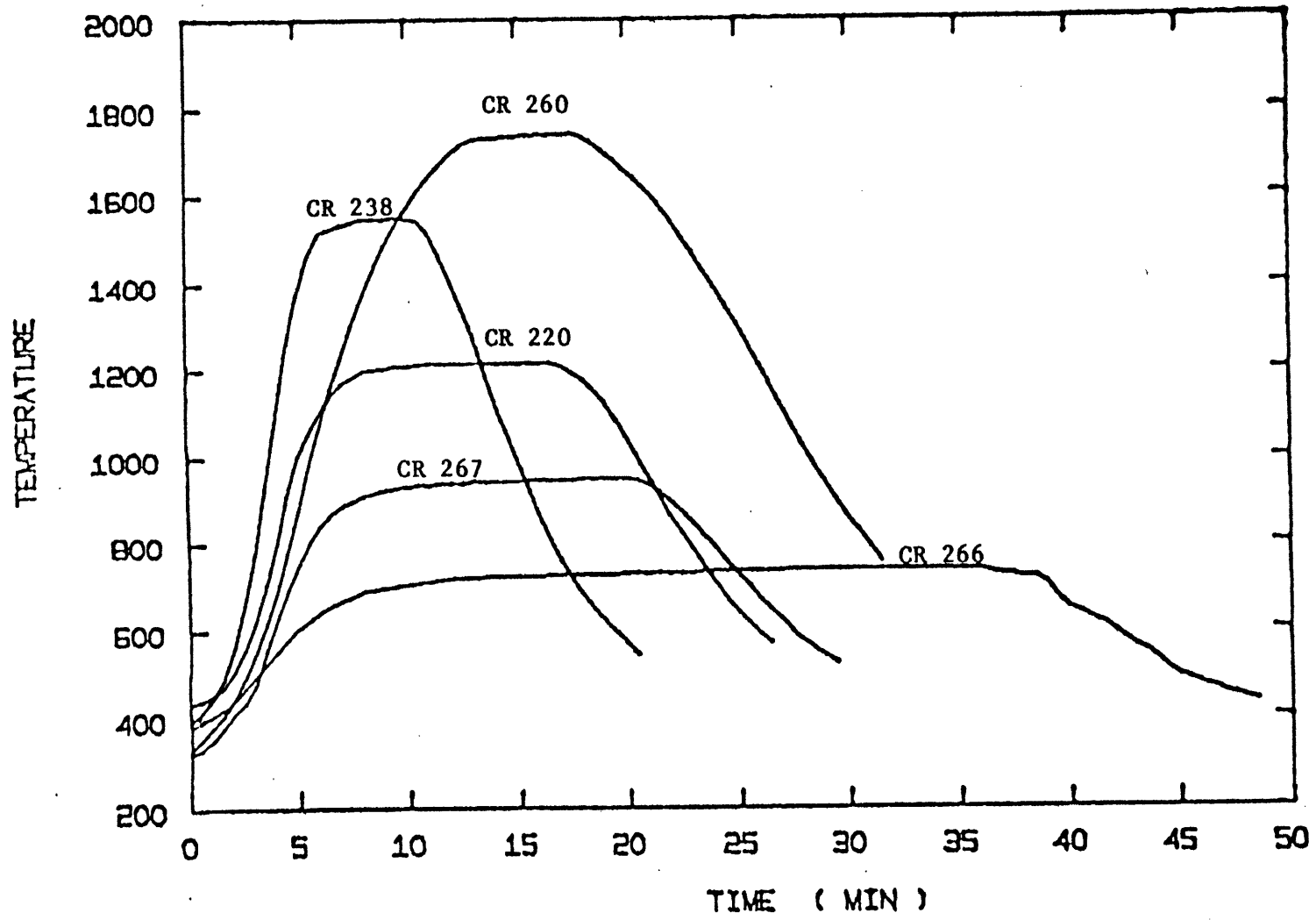


FIG. 2.7 TYPICAL TEMPERATURE TIME HISTORIES IN CRUCIBLE EXPERIMENTS

furnace at 950°C and held for 7 minutes.

2.5.1 Experimental Procedure

The procedure is essentially the same as that of the free fall experiment with alumina collector, except no coal is fed.

2.6 ASTM Proximate Analysis Equipment

A drying oven, a cylindrical furnace and a brick-insulated furnace were used to determine moisture, volatile matter and ash contents. ASTM standards (D3173-73, D3174-73 and D3175-73, 1972) were followed wherever possible. Some modifications were made, however, to accommodate smaller samples sizes. Figure 2.8 shows the equipment for determination of proximate volatile matter content. A Hoskin cylindrical furnace (Model 303 , 5.0 amps) is the main part of the system. The furnace is capable of a maximum of 1100°C temperature at full load. The heated cylindrical tube is 1.38 in. in diameter and 13 in. long. The equipment has a cooling section 15 in. long and 1.5 in. I.D. in order to provide adequate cooling for the devolatilized samples in an inert atmosphere, thus preventing the oxidation of the hot samples. The whole assembly is sealed with a high temperature alumina cement. The furnace is continuously purged with nitrogen when determining proximate volatile matter. A chromel-alumel thermocouple is centered in the heating zone 5.0 inches from the bottom. A procelain crucible (5 mL capacity) containing the samples to be analyzed is suspended in the hot zone of the furnace about 0.2 inches above the tip of the thermocouple. Figure 2.8 shows the furnace with the axial temperature of 1060°C. A reasonably steady hot zone (± 20 C) is maintained 4.3 inches to 8.6 inches from the bottom.

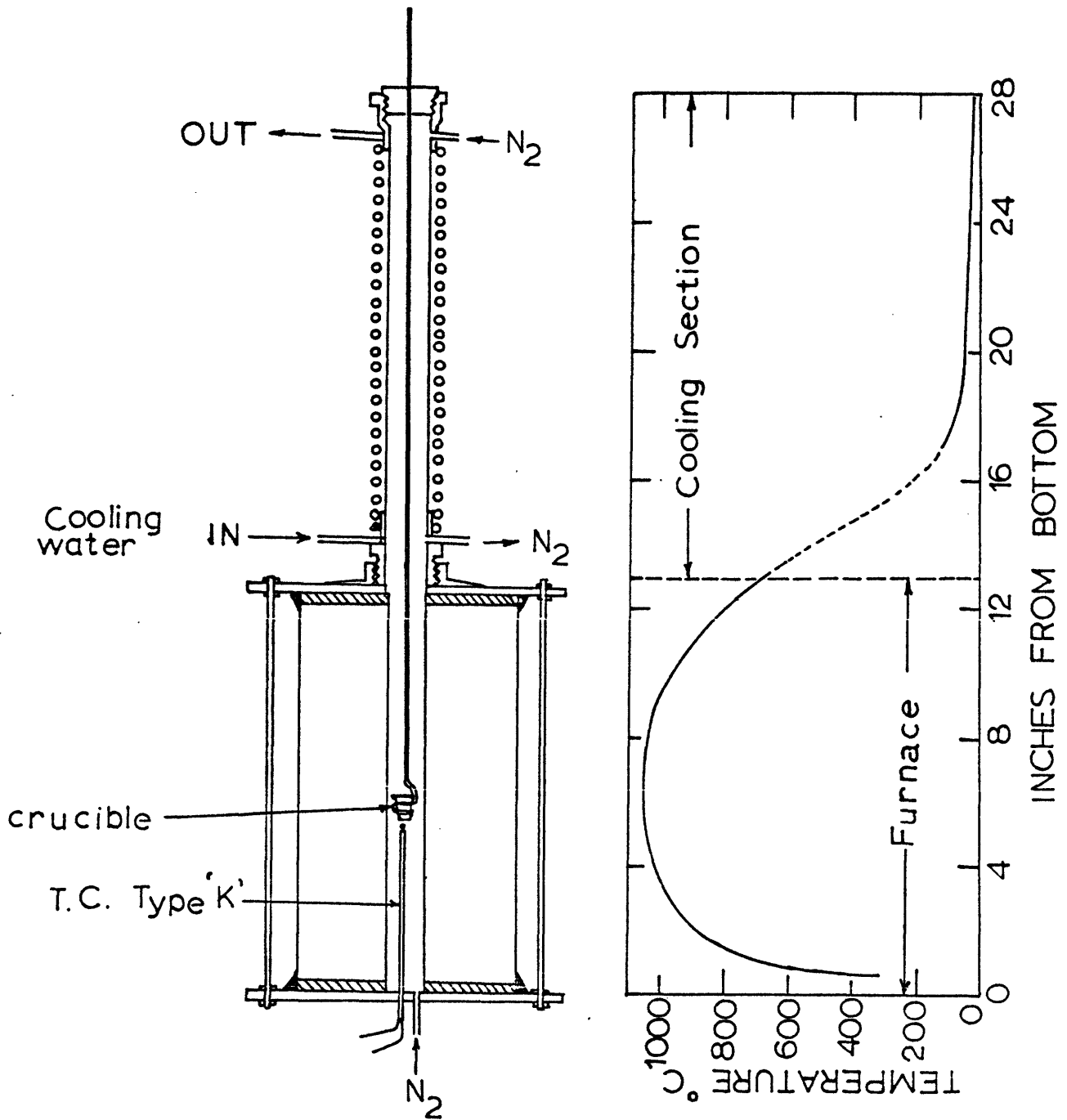


FIG. 2.8

PROXIMATE ANALYSIS EQUIPMENT and a typical TEMPERATURE DISTRIBUTION

Volatile matter determined by this system were compared with the results of two independent laboratories (Galbraith Labs., Inc., Knoxville, Tennessee, and M.I.T. Central Analytical Facility) which followed the ASTM specifications. Agreements to within 0.5 percent of the weights of original coals were obtained, which justified the present system.

For the determination of ash content a magnesium brick furnace was built. The inside dimensions of the furnace are a base 8.5 in. by 4 in. and a height of 9 inches. This furnace is large enough to accommodate the cylindrical alumina collector used in the free-fall experiment. Four silicon carbide heating elements (Norton XL 3/8 in. O.D. by 13 in. long) supply necessary heat to the furnace. Glazed porcelain crucibles were used to hold the samples. It was confirmed that the use of different crucible sizes has no effect on ash contents. ASTM standards were followed, other than the sizes of the crucibles and samples.

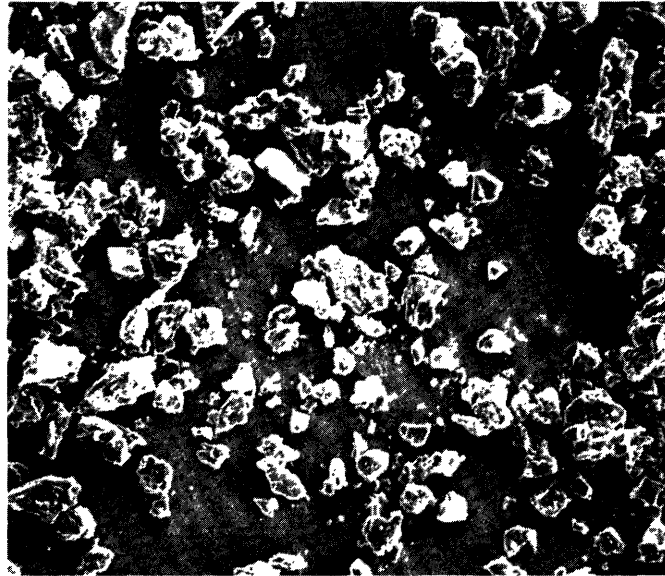
2.7 Coal Characterization

Two types of coals, supplied by the Institute of Gas Technology, were used in the present study. A Montana lignite from Savage Mine is an example of certain of the low rank, low sulfur, non-caking western coals. A Pittsburgh high volatile bituminous coal from Ireland Mine is an example of highly swelling and caking eastern coals. The detailed characterization of the two coals are discussed in Appendix I, and only a brief summary will be given in this section.

2.7.1 Electron Micrographs

Figure 2.9 and 2.11 are scanning electron micrographs of the Montana lignite and the Pittsburgh bituminous under different

RAW MONTANA LIGNITE, 38-45 μm



0 400 μm
100 X



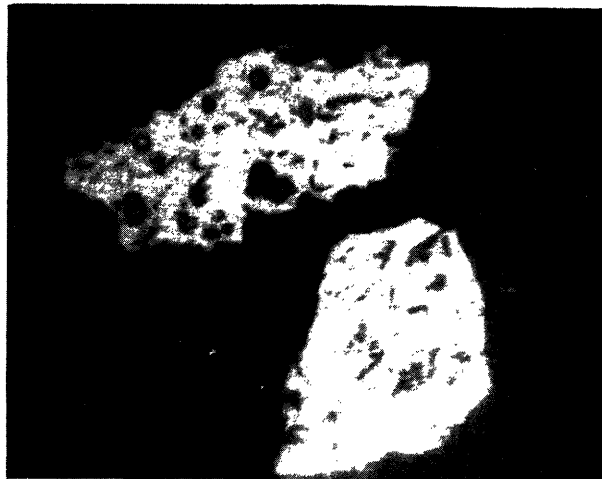
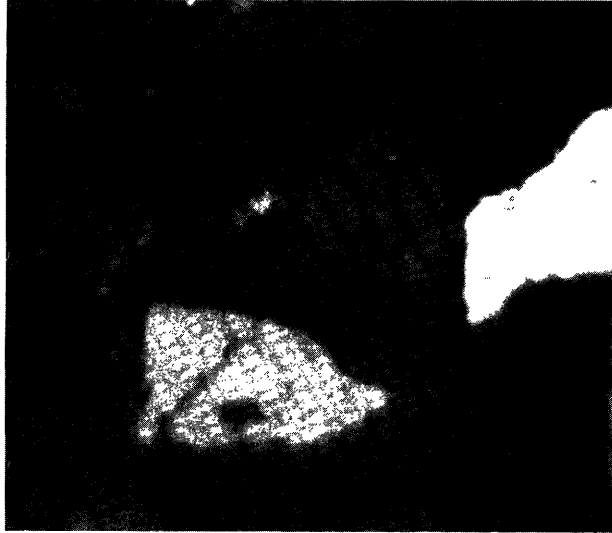
0 40 μm
1000 X



0 10 μm
3000 X

FIG. 2.9

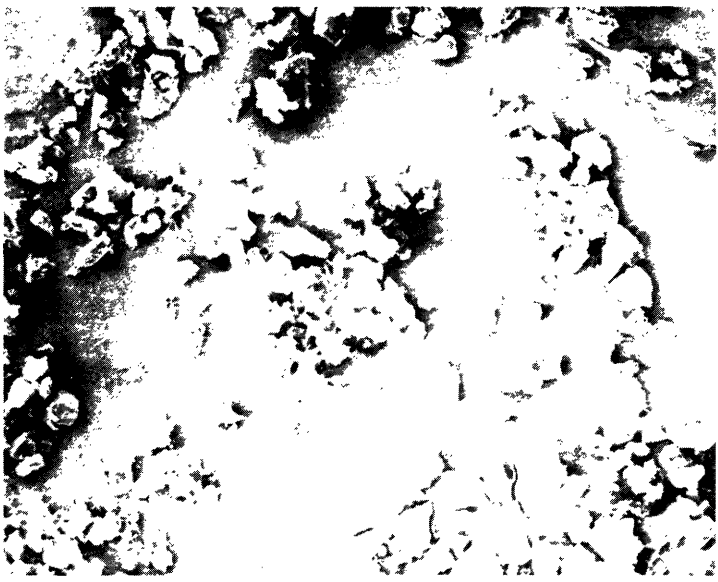
POLISHED MONTANA LIGNITE
under cedar oil 450X



50 um

FIG. 2.10

75
RAW PITTSBURGH SEAM # 8 BITUMINOUS COAL
38-45um



0 400um
100X



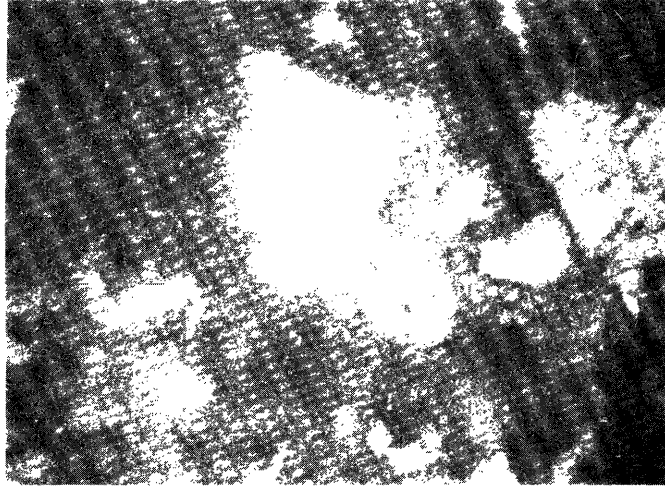
0 40um
1000X



0 10um
3000X

FIG. 2.11

POLISHED PITTSBURGH SEAM #8 BITUMINOUS COAL
under cedar oil 450 X



┌───┴───┐
50 um

FIG. 2.12

magnifications respectively. Though both coals were closely size graded by Tyler screens to +400, -325 meshes (nominal 38-45 micron), a number of undersized particles and a few oversized particles are evident in the micrograph. Figures 2.10 and 2.12 show the photomicrographs of polished section under oil immersion. Differences in brightness, which reflect different petrographic components, and an internal macropore area can be seen.

2.7.2 Particle Size Distribution

The particle size distributions of the two coals were obtained by counting different size particles in electron micrographs. Figures 13 to 16 show both cumulative and frequency distributions of the volume averaged particle size, fitted with the Rossin-Rammler distribution function.

$$f(x) = bsx^{s-1} \cdot \exp(-bx^s) \quad (2.1)$$

$$F(x) = 1 - \exp(-bx^s) \quad (2.2)$$

where

x = particle size

$f(x)$ = frequency distribution function

$F(x)$ = cumulative distribution function

b, s = Rossin-Rammler parameters

Parameters b and s are found through a least square fit of the particle frequency. Table 2.2 summarizes the results.

RAW LIGNITE
ROSIN-RAMMLER DISTRIBUTION

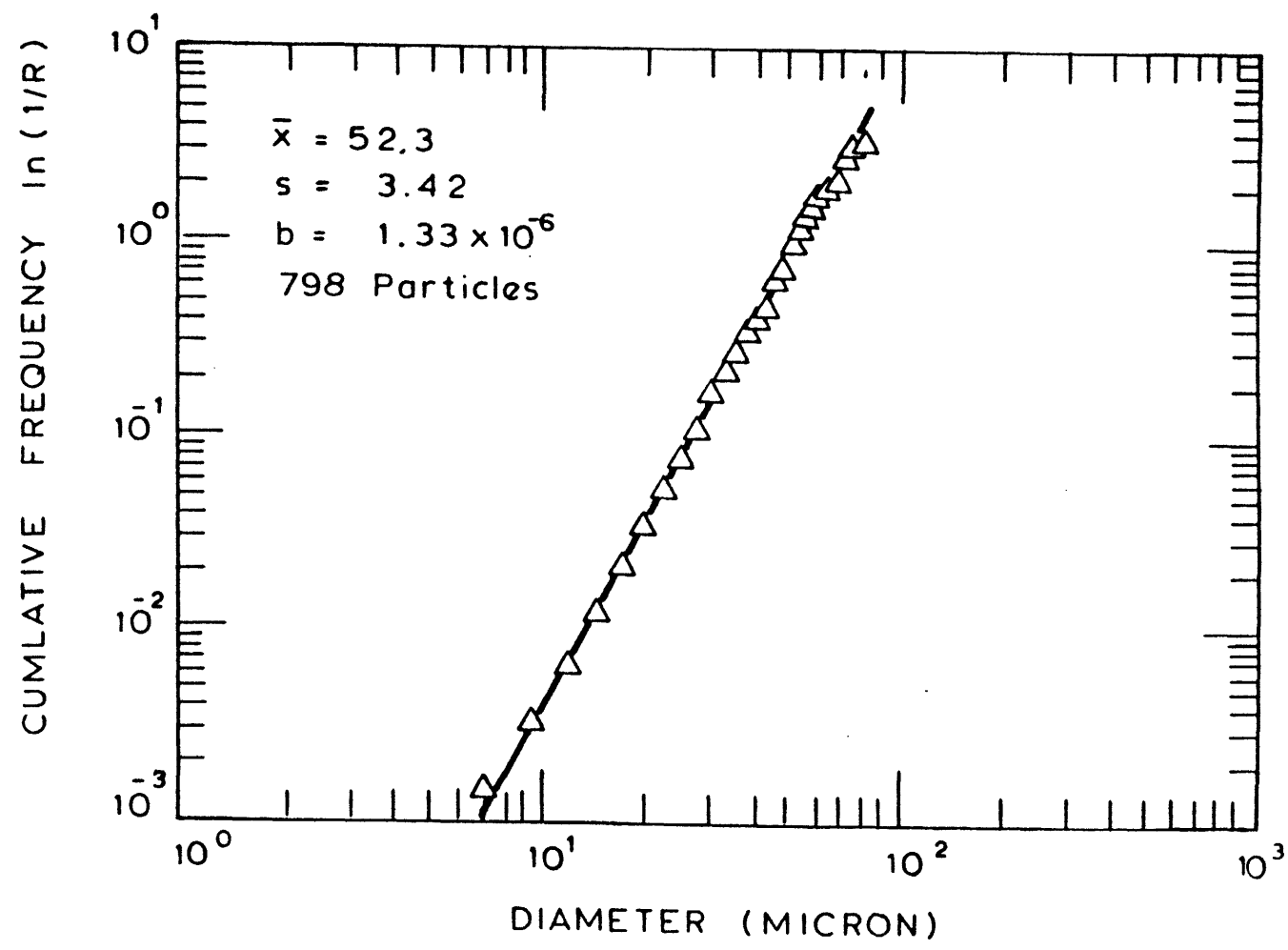


FIG. 2.13

RAW LIGNITE
FREQUENCY DISTRIBUTION

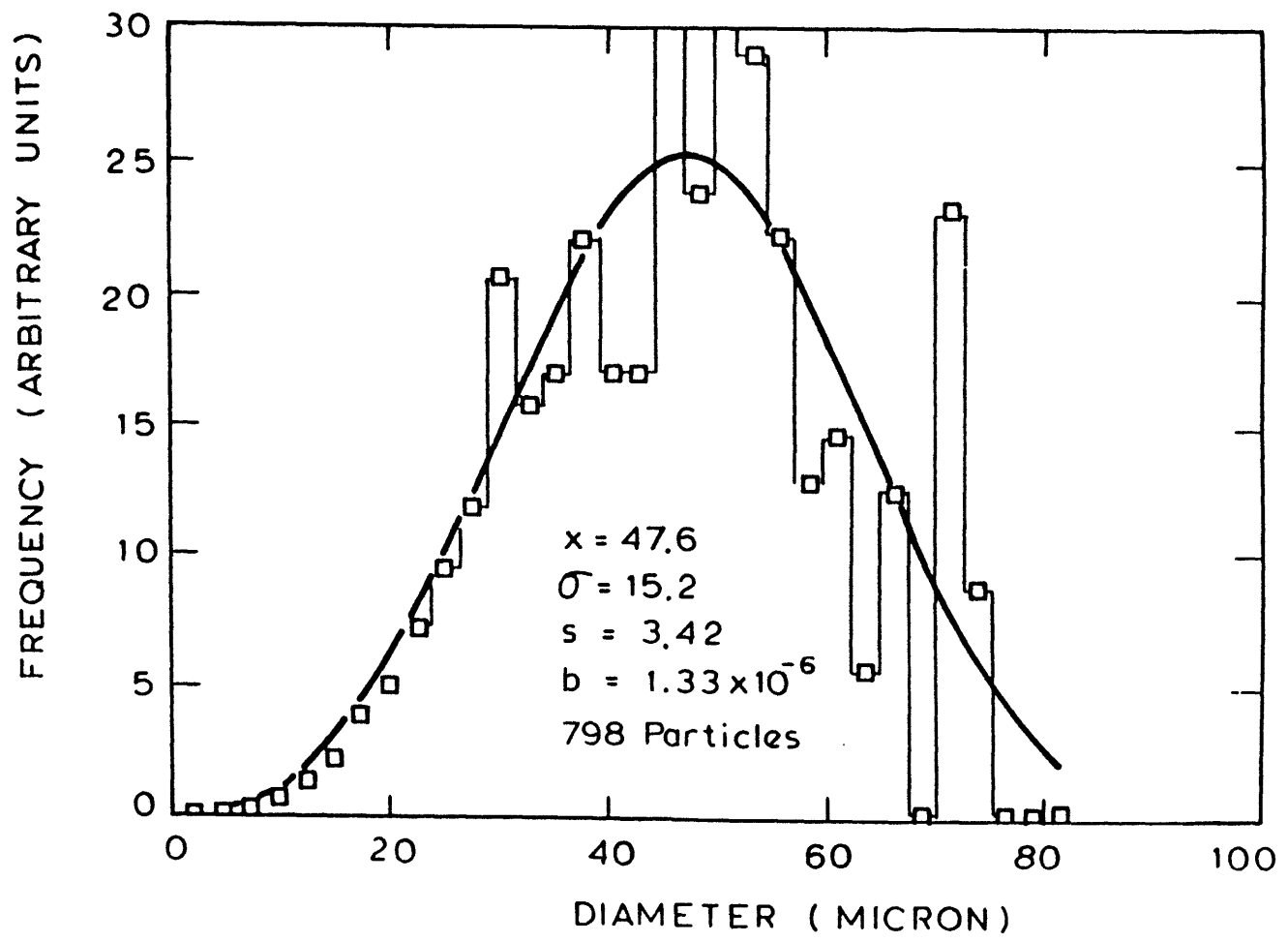


FIG. 2.14

RAW BITUMINOUS COAL
ROSIN - RAMMLER DISTRIBUTION

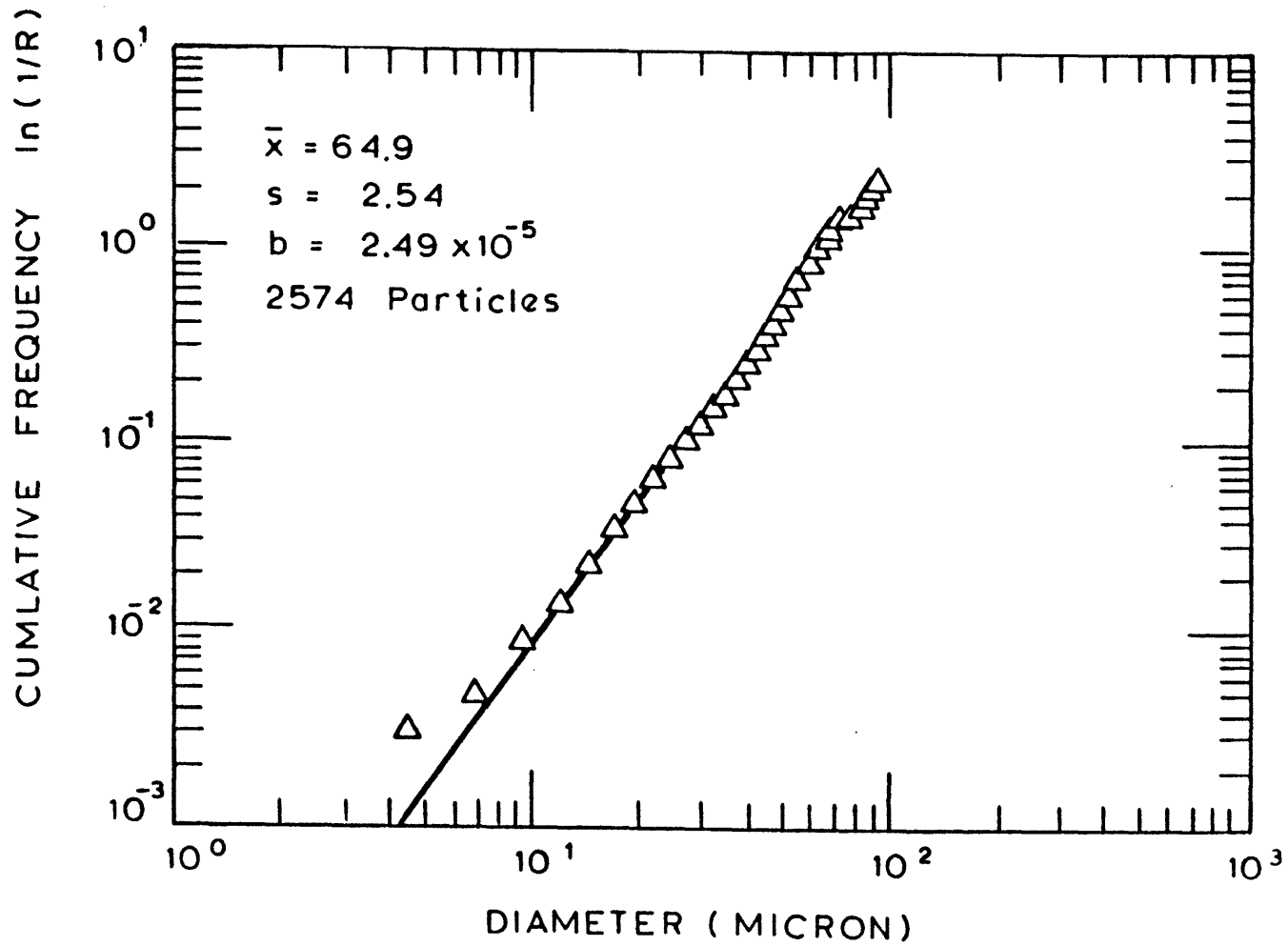


FIG. 2.15

RAW BITUMINOUS FREQUENCY DISTRIBUTION

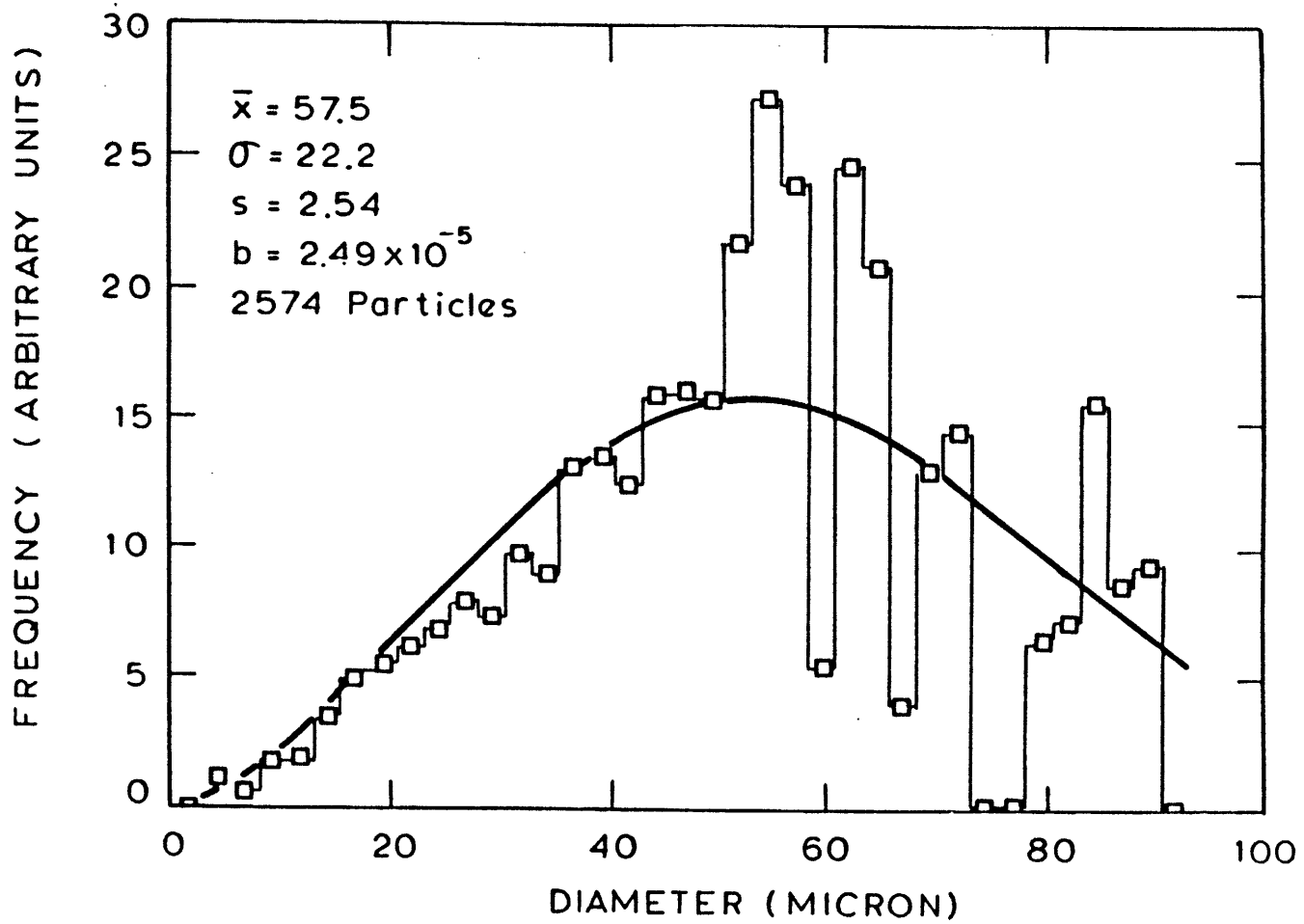


FIG. 2.16

TABLE 2.2
PARTICLE SIZE DISTRIBUTION

Coal	Volume Mean (m)	Cumulative		b	S
		10% (μm)	90% (μm)		
Lignite	47.6	27	67	1.33×10^{-6}	3.42
Bituminous	57.5	27	90	2.49×10^{-5}	2.54

2.7.3 Ultimate and Proximate Analyses

Tables 2.3 to 2.5 summarize the results of the ultimate and the proximate analyses of the coals used in this study. In Table 2.6 a summary of the results of the proximate analysis is shown on different weight bases.

TABLE 2.3
COAL CHARACTERIZATIONS

COAL	MINE	BTU/lb MOIST MM FREE*	PROXIMATE ANALYSIS A.R. Wt. %				ULTIMATE ANALYSIS A.R. Wt. %				SULFUR FORMS		
			H ₂ O	VM	ASH	C	H	N	S	By Diff. O	Pyr- itic S	SO ₂	Organic S
PITTSBURGH SEAM #8 hvA-b	IRELAND	14,377	2.2	40.7	10.8	67.81	5.03	1.05	4.83	8.55	2.50	0.69	1.62
MONTANA LIGNITE-A	SAVAGE	8,809	13.6	36.2	7.8	54.50	4.96	0.72	0.84	17.14	0.11	0.18	0.55

* HIGHER HEATING VALUES WERE CALCULATED ON THE BASIS OF EQUILIBRIUM MOISTURE WITH MINERAL MATTER, AS DETERMINED BY PADIA (1976) FROM LOW TEMPERATURE ASHING, REMOVED. THE MINE MOUTH MOISTURE CONTENT OF THE BITUMINOUS COAL WILL BE CLOSE TO ITS EQUILIBRIUM MOISTURE CONTENT SO THE HEATING VALUE WILL REMAIN UNCHANGED. LIGNITE FROM THE SAVAGE MINE HAS BEEN FOUND BY PAULSON ET AL. (1972) TO CONTAIN 28.2% MOISTURE; THE HEATING VALUE CALCULATED ON THIS BASIS WOULD BE 7346 BTU/lb.

TABLE 2.4LIGNITE

CHARACTERIZATION OF MONTANA LIGNITE
 FROM THE SAVAGE MINE IN RICHLAND COUNTY,
 GROUND AND CLASSIFIED TO 38-45 μ

COMPONENT	ULTIMATE AIR	ULTIMATE DRY	ULTIMATE daf	ULTIMATE dmf*	ULTIMATE C-H-O BASIS
H ₂ O	13.60	-	-	-	-
C	54.90	63.54	69.88	73.30	71.30
H	4.96	5.74	6.31	6.62	6.44
N	0.72	0.83	0.92	1.23	-
Pyritic S	0.11	0.13	-	-	-
SO ₄	0.18	0.21	-	-	-
ORGANIC S	0.55	0.64	0.73	0.73	-
TOTAL S	0.84	0.98	-	-	-
ASH	7.84	9.07	-	-	-
O(DIFF.)	17.14	19.84	22.16	18.12	22.26

* MINERAL MATTER FOUND FROM LOW TEMPERATURE ASHING BY PADIA (1976) TO
 BE 11.50% (WET BASIS)

TABLE 2.5BITUMINOUS COAL

CHARACTERIZATION OF PITTSBURGH SEAM #8

BITUMINOUS COAL FROM THE IRELAND MINE

GROUND AND CLASSIFIED TO 38-45 μ

COMPONENT	ULTIMATE A.R.	ULTIMATE DRY	ULTIMATE daf	ULTIMATE dmf*	ULTIMATE C-H-O BASIS
H ₂ O	2.20	-	-	-	-
C	67.90	69.46	77.80	82.27	83.31
H	4.91	5.01	5.62	5.95	6.01
N	1.04	1.06	1.19	1.26	-
Pyritic S	2.29	2.35	-	-	-
SO _x	0.68	0.65	-	-	-
Organic S	1.58	1.52	1.81	1.91	-
Total S	4.55	4.53	-	-	-
ASH	10.52	10.76	-	-	-
O(DIFF.)	8.88	9.19	13.58	8.61	10.87

* Mineral matter found from low temperature ashing by Padia (1976) to be 15.27% (wet basis).

TABLE 2.6

RESULTS OF PROXIMATE ANALYSES

Montana Lignite-A

	<u>As-Received</u>	<u>Dry</u>	<u>d.a.f.</u>
Moisture	2.2	-	-
Volatile Matter	40.7	41.6	46.7
Fixed Carbon	46.3	47.3	53.3
Ash	10.8	11.1	-

Pittsburgh Seam #8 HVA Bituminous Coal

	<u>As-Received</u>	<u>Dry</u>	<u>d.a.f.</u>
Moisture	13.6	-	-
Volatile Matter	36.2	41.9	46.0
Fixed Carbon	42.4	49.1	54.0
Ash	7.8	9.0	-

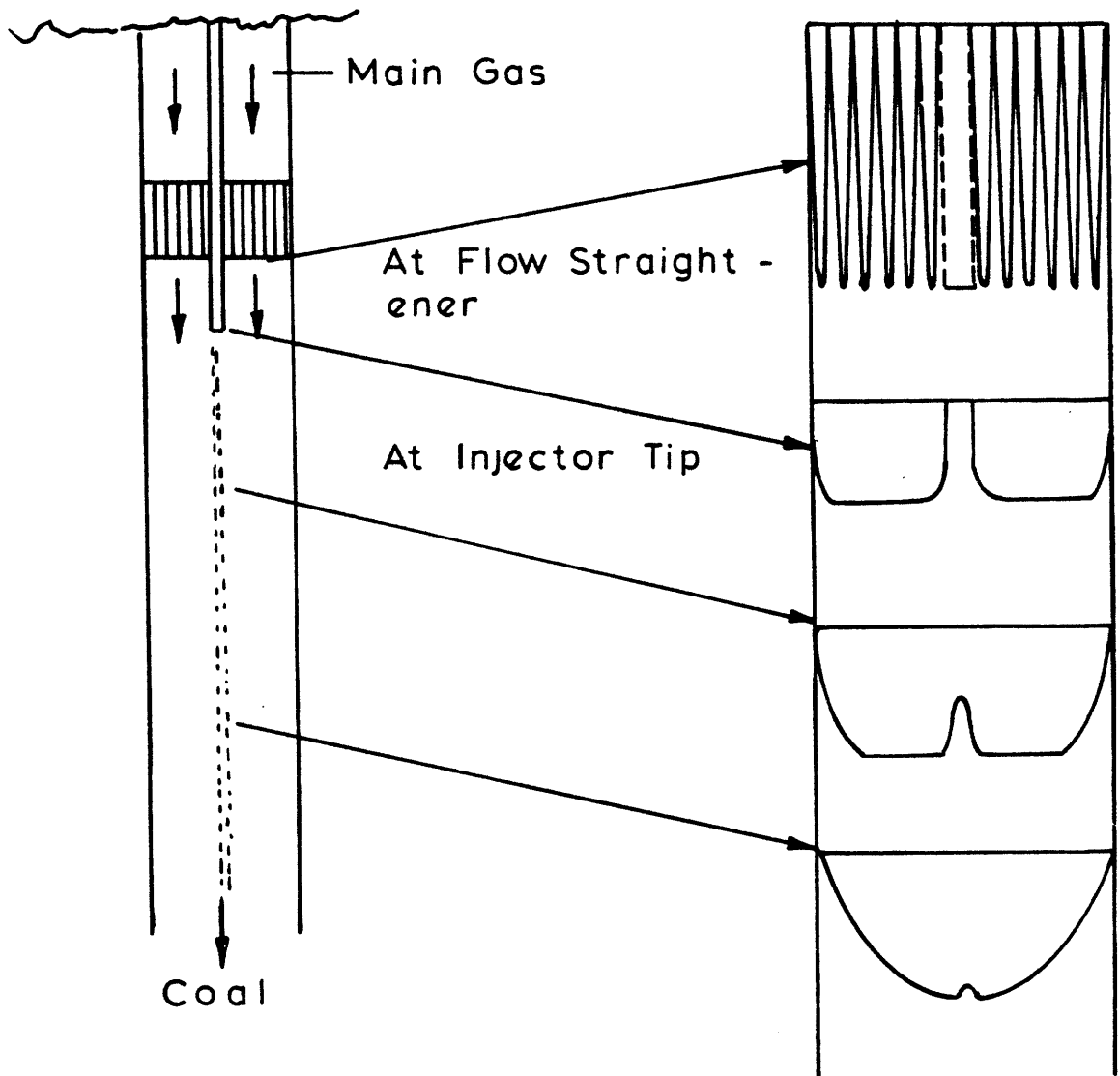
CHAPTER III

ANALYSIS OF EXPERIMENTAL SYSTEM AND DATA REDUCTION

In order to obtain kinetic information on the devolatilization reactions from the laminar flow experiment, temperature-time histories of the injected coal particles have to be known accurately. Though the experimental system (Fig. 2.1) was designed to give well defined wall and gas temperatures and a one-dimensional laminar flow field, introduction of coal particles through a water-cooled injector makes actual temperature and velocity fields fairly complicated. Figure 3.1 shows a conceptual diagram of the main flow development. The flow in each hole of the honeycomb straightener has a parabolic velocity profile, since the maximum Reynolds number in each hole for the experimental conditions (Table 2.1) is about 82. Since the voidage ratio of the honeycomb is 0.52, the maximum velocity of the parabolic flow is about four times as fast as the average main flow velocity. The characteristic decay time of the parabolic flows may be approximated by

$$t_{\text{decay}} \sim \frac{\ell^2}{\nu} \quad (3.1)$$

where ℓ is the spacing of the holes and ν is the kinematic viscosity. Substitution of the appropriate values at 1500°K in this equation yields 1 msec as an order of magnitude of the decay time. The injector tip was positioned 1.5 in. below the honeycomb to ensure flat velocity profiles under all the experimental conditions. Near the walls of the muffle tube and the injector, boundary layers grow, the thicknesses of which may be estimated using the analytical result of the flow over a flat plate



Laminar Flow
Furnace

Velocity
Profile

CONCEPTUAL DIAGRAM OF MAIN FLOW
DEVELOPMENT IN LAMINAR FLOW FURNACE

FIGURE 3.1

$$\frac{\delta}{x} = \frac{5}{\sqrt{Re_x}} \quad (3.2)$$

At 1500°K the boundary layer thickness, δ , at the injector tip ($x=3.8$ cm) is 0.8 cm and that of the muffle tube wall at 25.4 cm from the honeycomb is 2.1 cm (fully developed flow).

The temperature profile of the main flow is simpler than the velocity profile. Since the gas and the muffle tube wall temperatures are the same, the thermal boundary layer develops only along the injector. The thickness of the thermal boundary layer is considered to be about the same as that of the momentum boundary layer since the Prandtl number is close to one.

In view of these considerations the simple assumption that coal particles move at the same velocity as the average main flow velocity is inadequate. In the present study the velocities of the coal particles were measured directly using a laser doppler anemometer (sec. 3.1). The results were then used to evaluate a parameter in a mathematical model which describes the temperature and velocity of coal particles in the furnace (sec. 3.2).

Determination of weight loss requires accurate evaluation of particle loss, ash loss and other effects such as soot and tar formation. Different methods of weight loss calculations are shown in section 3.3.

3.1 Velocities of Coal Particles Measured by a Laser Doppler Anemometer

Velocities of coal particles were measured directly using a laser doppler anemometer as noted above. Figure 3.2 shows the schematic of

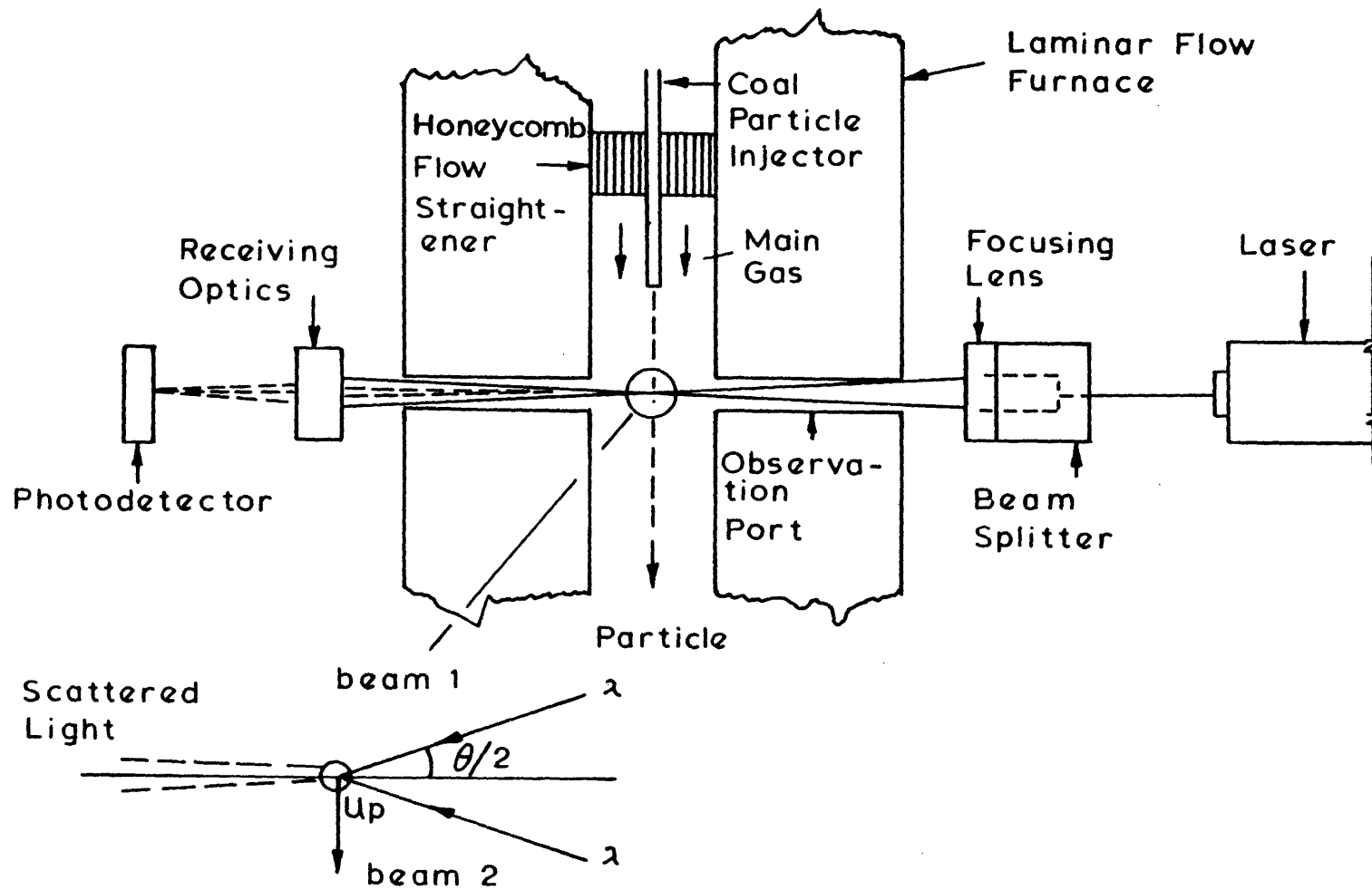


FIGURE 3.2

LASER DOPPLER ANEMOMER SYSTEM FOR VELOCITY MEASUREMENT OF COAL PARTICLES

the experimental system. The anemometer system* consisted of TSI Model 912 helium-neon laser, Model 910 transmitting optics, Model 930 receiving optics, Model 960 photomultiplier assembly, and Model 1090 signal processor. Since the optical axis is perpendicular to the flow, the frequencies of the light scattered from beams 1 and 2 are shifted by $(U_p/2) \sin(\theta/2)$ and $-(U_p/2) \sin(\theta/2)$, respectively.

Superposition of scattered light from these two sources, which is sensed by the photomultiplier, produces the following frequency:

$$f = \frac{U_p}{\lambda} \sin \frac{\theta}{2} \quad (3.3)$$

The particle velocity component in the direction of the flow can be calculated from measured value of f , using Eq. (3.3). Though the laser beams were fixed at the third observation port of the laminar flow furnace, velocities of the particles at different distances from the injector were measured by changing the position of the injector. It should be noted that this is not exactly the same as changing the position of the laser system fixing the injector. The growth of boundary layers from the honeycomb flow straightener makes some differences in the main flow development.

The results of the experiment are tabulated in Table F.1. Each particle velocity is the average of 50 to 200 particle velocities which were sampled randomly by the signal processor for a time span of several minutes. The velocity distributions were close to the Normal distributions. Typical distributions at 1500°K are shown in Fig. 3.3, approximated by the Normal distributions. The velocity distributions are

*The anemometer system was provided and set up by courtesy of Thermo-systems, Inc. (St. Paul, Minnesota) for demonstration purpose.

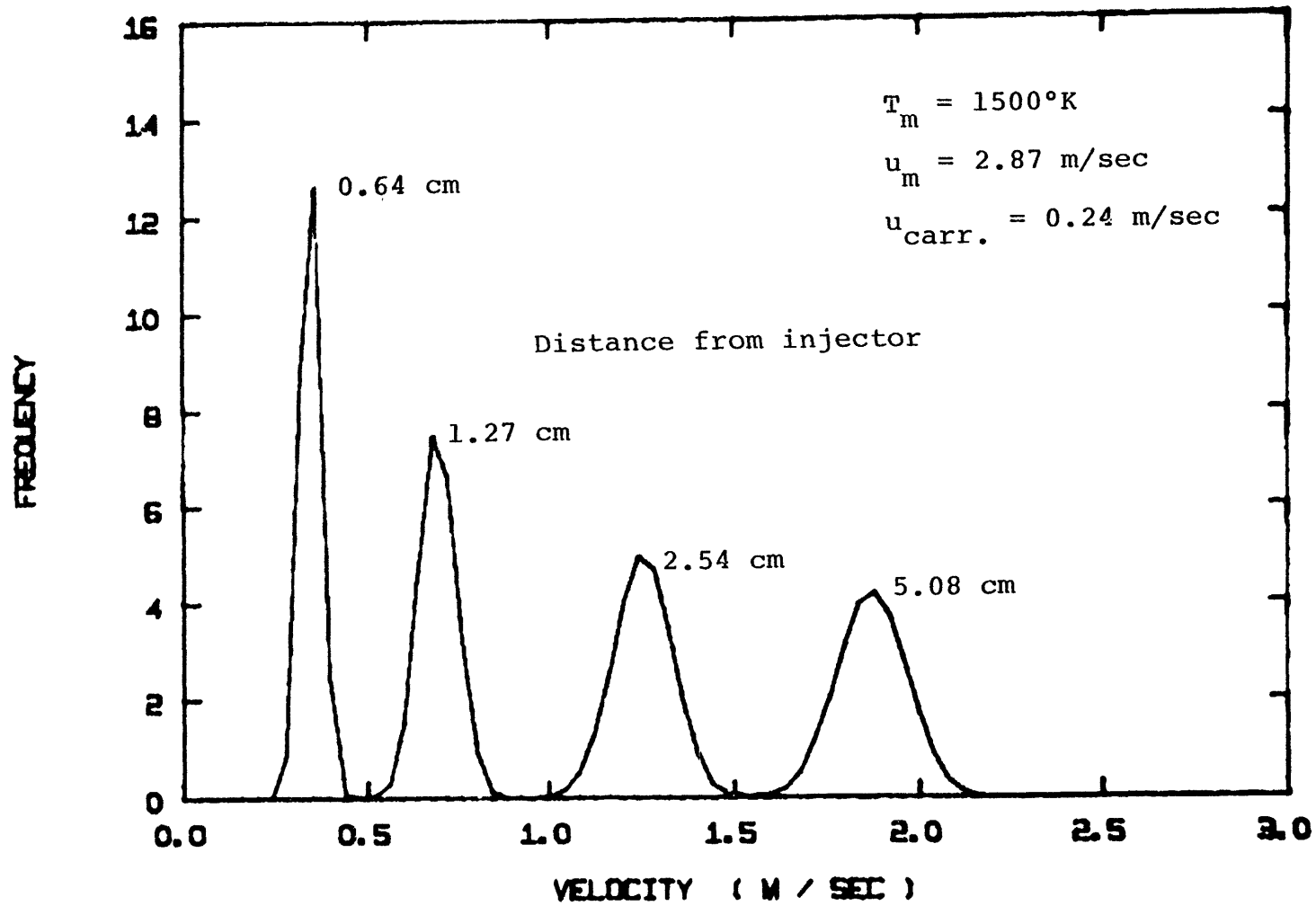


FIG. 3.3 TYPICAL VELOCITIES DISTRIBUTIONS OF COAL PARTICLES IN LAMINAR FLOW FURNACE

considered to be caused by the velocity gradient in the flow field, not by turbulence.

3.1.1 Initial Velocities of Coal Particles

Initial velocities were measured by positioning the injector tip right above the laser beams. Alignment of the injector tip and laser beams could be seen through the receiving optics. The beams could be centered within 1/50 of an inch. Since the diameter and the length of the intersection volume of the laser beams were about 2 mm and 1 cm respectively, the measuring space could cover the whole area of the particle stream (injector tubing I.D. 1.2 mm) if properly positioned. Figure 3.4 shows average initial particle velocities and standard deviations at various average carrier gas velocities. The velocity profile of the carrier gas in the injector tubing was considered to be parabolic, since Reynolds numbers were less than 100. If the particles were distributed uniformly in the injector tubing and the velocities of the particles were the same as the local velocities of the carrier gas, the initial velocities of the particles should have ranged from zero to twice the average velocity of the carrier gas. The measured average particle velocities were about 40 percent greater than the average carrier gas velocities. One of the possible reasons could be temperature rise in carrier gas at the injector tip by radiation. If the average temperature rises by 150°C, the average velocity increases by 50 percent. Approximate estimation of radiation, however, showed that the residence times of particles at the injector tip were too short to be heated sufficiently, especially at high carrier gas velocities. The other possible reason is nonuniform radial distribution of particles. The peak

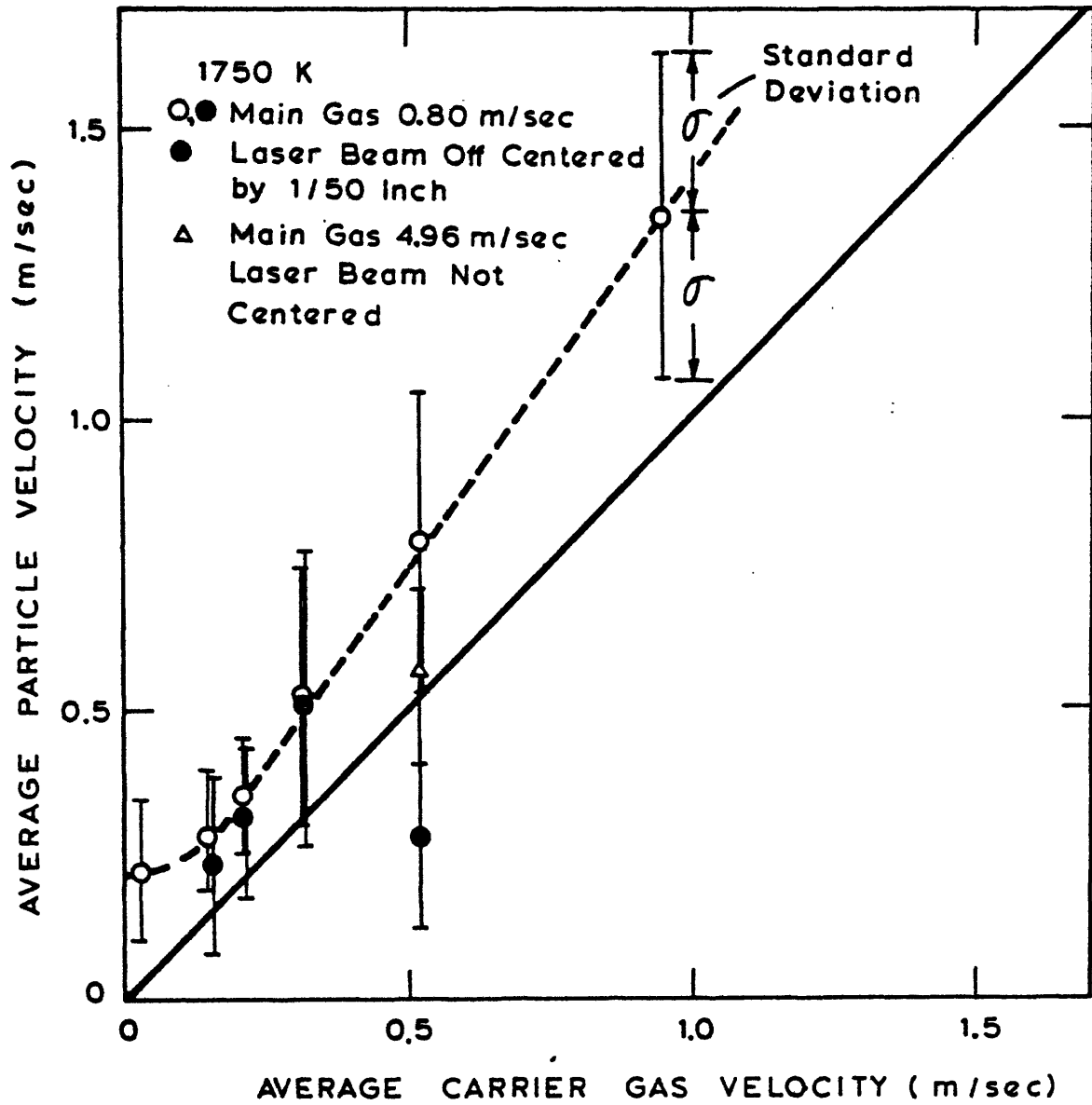


FIG. 3.4 AVERAGE PARTICLE VELOCITIES AT INJECTOR TIP

concentration of particles in suspension flow could be at a certain radial position in a tube (Soo, 1969). Particles near the wall receive aerodynamic lift toward the center of the tube because of the velocity gradient of the fluid. Thus the number density of the particles near the wall is generally smaller than the average. For the parabolic flow, if we assume that particles are distributed uniformly within 0.8 radius of the tube, the average particle velocity becomes about 40 percent larger than the average fluid velocity. Considering these effects, the observed particle velocities seem quite reasonable.

3.1.2 Acceleration of Particles in Laminar Flow Experiment

Average particle velocities under laminar flow conditions are plotted against distances from the injector in Fig. 3.5. Particles were accelerated by the faster main flow and approached the centerline velocity of the main flow. The reaction time of particles were calculated based on these values. Solid lines represent the results of a simulation based on a simplified model.

3.1.3 Particle Velocities in Free Fall Experiments

Conditions of the free fall experiment were reproduced in the laminar flow furnace to measure the particle velocities. Figure 3.6 shows the results. Since the initial velocities of the particles were larger than the main flow velocities, particles were decelerated in this case. For a wide range of experimental conditions, relative velocities of the particles were reasonably well correlated. Dotted lines indicate general trends at different initial particle velocities. It can be seen that the terminal velocity of the particle cloud is about 10 cm/sec for all free fall experiments. This value is considerably larger than the

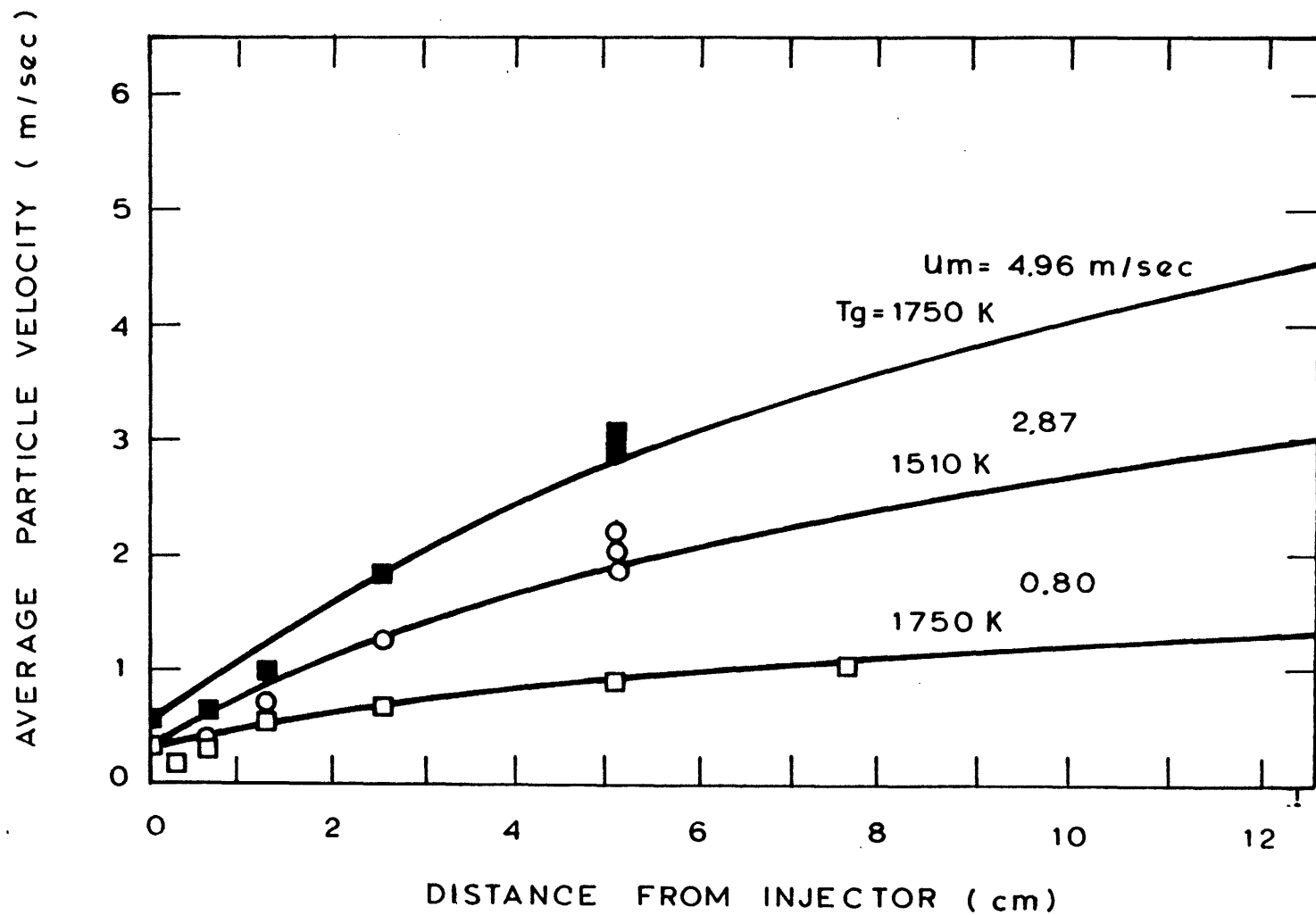


FIG. 3.5 AVERAGE COAL PARTICLE VELOCITIES IN LAMINAR FLOW FURNACE AT DIFFERENT LOCATIONS

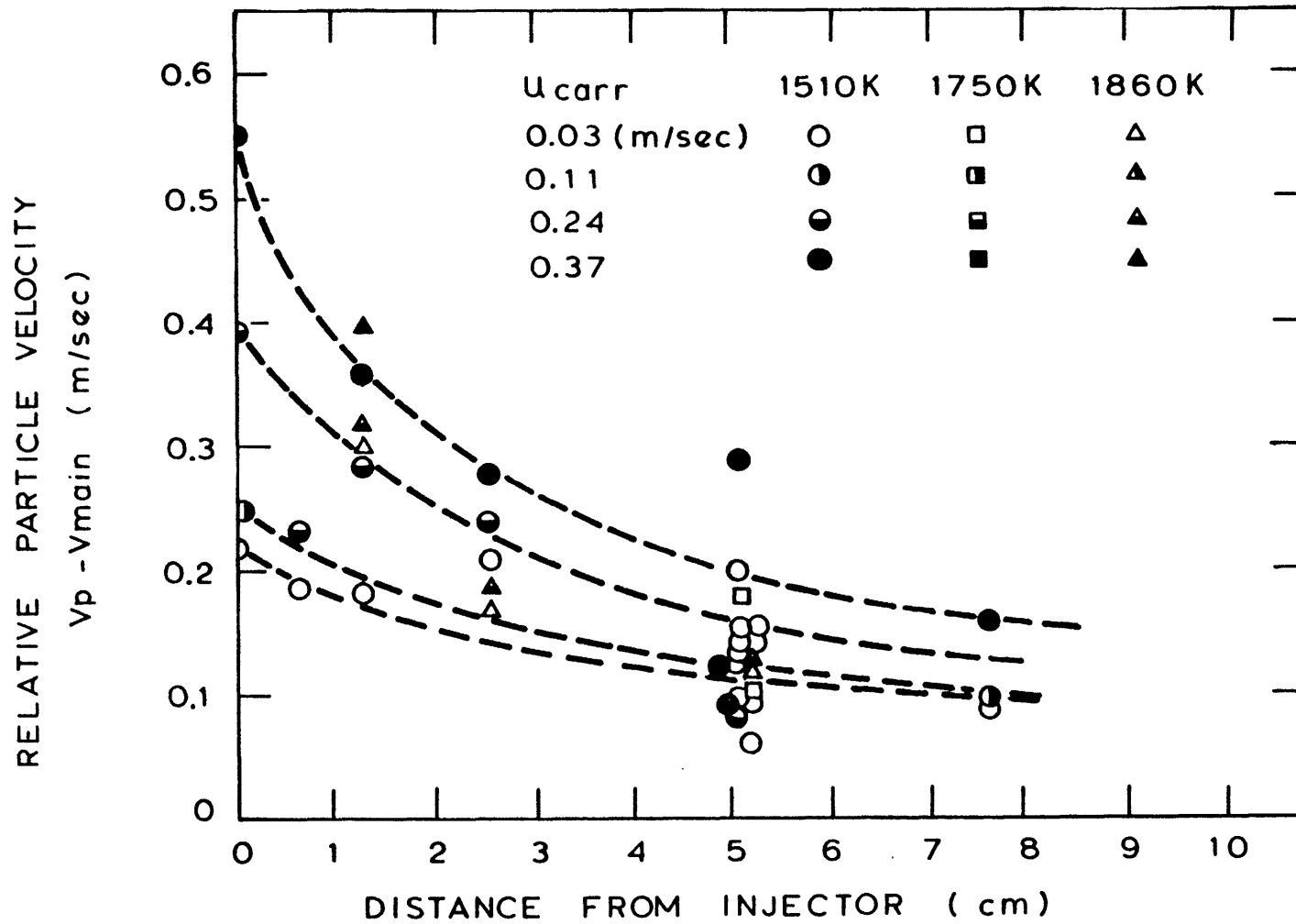


FIG. 3.6 AVERAGE COAL PARTICLE VELOCITIES UNDER "FREE FALL" CONDITIONS

terminal velocity of a single 40 micron particle in a stagnant argon atmosphere at 1500°K, which is about 1 cm/sec. The reason for the discrepancies between the terminal velocities appears to be the interactions between the particles, since the average inter-particle distance is not large enough to justify the single particle assumption.

3.2 Analysis of Temperature and Velocity Fields

Accurate prediction of the particle temperature and the velocity is very important in interpreting the devolatilization reactions. The injected coal particles are heated both by conduction from the hot main stream and by radiation from the furnace wall. The relative importance of these heat transfer processes is best understood in terms of characteristic heating times. In Fig. A.2 of Appendix A, characteristic gas phase conduction time, radiation time and internal conduction time inside a particle are plotted against particle diameter. For small particles ($\sim 10 \mu\text{m}$) gas phase conduction is dominant, while radiation becomes significant at high temperatures (above 2000°K) for larger particles ($\sim 100 \mu\text{m}$). Internal conduction is fast for pulverized coal sizes, hence the internal temperature of a coal particle is spatially uniform. It can also be seen that characteristic heating time of a 40 micron particle is about 4 msec. In the present system, however, coal particles are injected with cold carrier gas through a water-cooled tube. The gas temperature near the particles increases at a rate controlled by the mixing between the carrier gas and the hot main stream. Approximate mixing time can be estimated by assuming a uniform velocity field and neglecting the effect of radiation.

The governing equation is

$$U \frac{\partial T'}{\partial X} = D_T \cdot \left[\frac{\partial^2 T'}{\partial r^2} + \frac{1}{r} \frac{\partial T'}{\partial r} \right] \quad (3.4)$$

where the effects of the particles are neglected. T' is the nondimensional temperature defined by the following equation

$$T' = \frac{T_w - T}{T_w - T_o} \quad (3.5)$$

The temperature profile at the feeder tip could be approximated by the step change of temperature shown in Fig. 3.7. Since a cold boundary grows on the feeder surface, the radius of the cold region may be defined as the sum of the feeder radius and thermal displacement thickness, δ_T^* .

$$\delta_T^* \approx \frac{\delta^*}{1.03^3 \sqrt{Pr}} \quad (3.6)$$

where δ^* is the displacement thickness.

$$\delta^* = \frac{1.73 x}{\sqrt{Re_x}} \quad (3.7)$$

The boundary conditions for Eq. (3.4) become

$$\begin{aligned} x = 0, \quad 0 \leq r < r_F + \delta_T^*, \quad T' = 1 \\ r_F + \delta_T^* \leq r \leq R, \quad T' = 0 \\ x > 0, \quad r = R, \quad T' = 0 \end{aligned} \quad (3.8)$$

When U is constant, the solution of Eq. (3.4) with boundary conditions (3.8) is (Carslaw and Jaeger, 1959)

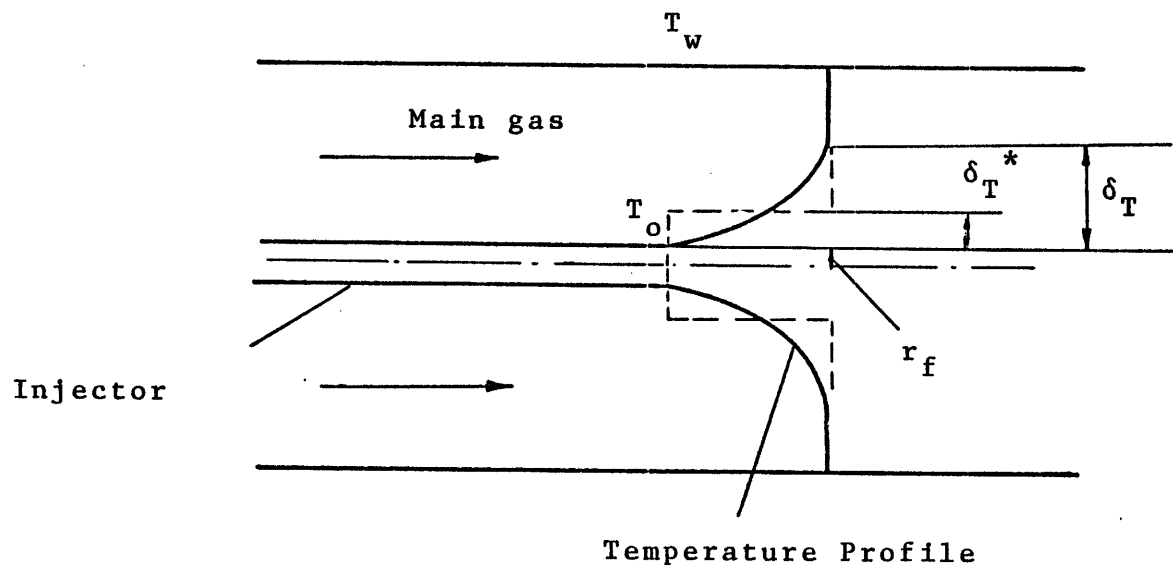


FIGURE 3.7 CONCEPTUAL DIAGRAM OF THERMAL BOUNDARY LAYER AT INJECTOR TIP

$$T' = 4 \cdot \sum_{n=1}^{\infty} \exp \left\{ - \frac{D_T \alpha_n^2 x}{U} \right\} \cdot \left\{ \frac{1}{R \alpha_n} \frac{J_1(a \alpha_n)}{J_1(R \alpha_n)} \right\} \quad (3.9)$$

where α_n is the n-th eigenvalue of

$$J_0(R \alpha) = 0 \quad (3.10)$$

J_0 and J_1 denote Bessel functions, and $a = r_F + \delta_T^*$.

Characteristic mixing distance under the experimental conditions at 1500°K (Table 2.1) was calculated from Eq. (3.9)

$$x_{T'} = 0.37 = 3.7 \text{ cm} \quad (3.11)$$

If we take U as the average of the velocities of the main flow and the carrier gas, the characteristic mixing time becomes

$$t_m = \frac{x_{T'}}{U} = 0.023 \text{ sec} \quad (3.12)$$

Since this value is much larger than the characteristic conduction time, heating of the real particles is mainly controlled by the mixing of the carrier gas and the main gas. This implies that detailed analysis of the temperature and velocity fields in the furnace is necessary in order to get accurate temperature-time history of the injected coal particles.

An approximate integral method is applied to simplify the analysis. Three concentric regions, center region, boundary region and main stream, were considered as shown schematically for the injector-tip position in Fig. 3.8. All the coal particles are assumed to remain in the center region, and the local velocities and temperatures of gas and particles are assumed to be the same, based on the foregoing arguments on the characteristic heating times and the relaxation time of the particle discussed in Appendix E. The boundary region is the annulus region

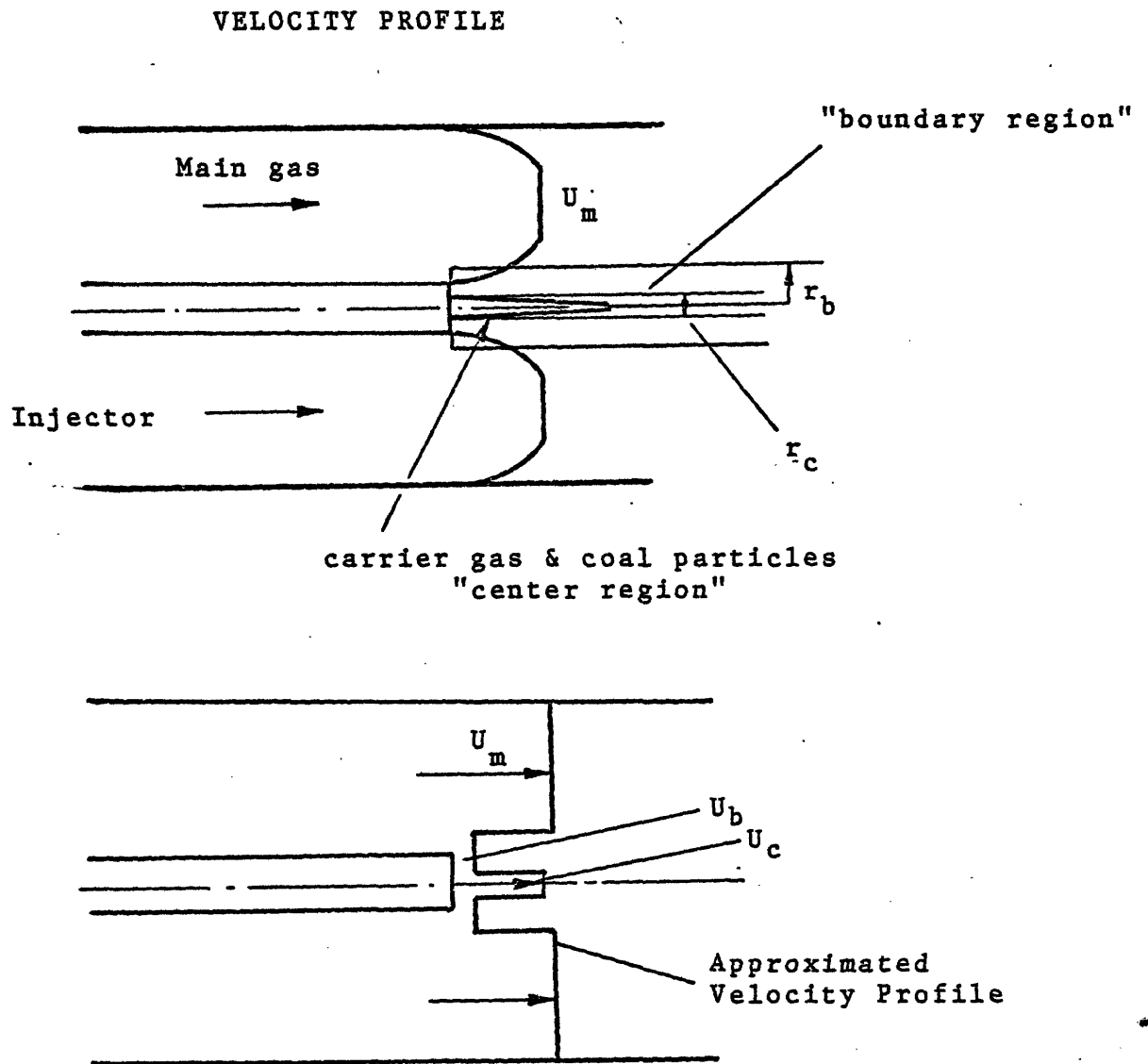


FIGURE 3.8 SCHEMATIC DIAGRAM OF BOUNDARY LAYERS AND APPROXIMATED VELOCITY PROFILE.

between the main flow and the center region, where the temperature and the velocity are considerably lower because of the boundary layer development on the cold injector surface. In the main flow region temperature is assumed to be constant, but the velocity near the center increases with the distance from the honeycomb (see Fig. 3.1). The basic equations for the center and the boundary regions can be expressed as follows.

Mass Conservation:

$$\frac{d}{dx} \left[\int_0^{r_c} (\dot{m}_p \cdot u_c + \rho_c u_c) 2\pi r dr \right] = \Delta \dot{M}_{bc} \quad (3.13)$$

$$\frac{d}{dx} \left(\int_{r_c}^{r_b} \rho_b u_b 2\pi r dr \right) = \Delta \dot{M}_{mb} - \Delta \dot{M}_{bc} \quad (3.14)$$

Momentum Conservation:

$$\begin{aligned} \frac{d}{dx} \left[\int_0^{r_c} (\dot{m}_p \cdot u_c + \rho_c u_c^2) 2\pi r dr \right] \\ = \Delta \dot{M}_{bc} \cdot u_{bc} + 2\pi r_c \cdot \mu \cdot \left(\frac{\partial u_c}{\partial r} \right)_{r=r_c} - \pi r_c^2 \cdot \frac{dp}{dx} \\ + \int_0^{r_c} (\dot{m}_p + \rho_c) 2\pi r dr \cdot g \end{aligned} \quad (3.15)$$

$$\begin{aligned} \frac{d}{dx} \left(\int_{r_c}^{r_b} \rho_b u_b^2 \cdot 2\pi r \cdot dr \right) = \Delta \dot{M}_{mb} \cdot u_{mb} - \Delta \dot{M}_{bc} \cdot u_{bc} \\ + 2\pi r_b \left(\mu \cdot \frac{\partial u_b}{\partial r} \right)_{r=r_b} - 2\pi r_c \left(\mu \cdot \frac{\partial u_c}{\partial r} \right)_{r=r_c} \\ - (\pi r_b^2 - \pi r_c^2) \cdot \frac{dP}{dx} + \rho_b 2\pi r dr \cdot g \end{aligned} \quad (3.16)$$

Energy Conservation:

$$\begin{aligned}
& \frac{d}{dx} \left[\int_0^{r_c} (n_p \cdot m_p \cdot u_c \cdot h_p + \rho_c u_c \cdot C_{p,g} \cdot T_c) \cdot 2\pi r \cdot dr \right] \\
&= \Delta \dot{M}_{bc} \cdot C_{p,g} \cdot T_{bc} + 2\pi r_c \left(\lambda \frac{\partial T}{\partial r} \right)_{r=r_c} \\
&\quad + \int_0^{r_c} n_p \cdot s_p \cdot \sigma \cdot \epsilon_p (T_w^4 - T_c^4) 2\pi r \, dr
\end{aligned} \tag{3.17}$$

$$\begin{aligned}
& \frac{d}{dx} \left(\int_{r_c}^{r_b} \rho_b u_b \cdot C_{p,g} T_b + 2\pi r \, dr \right) = \Delta \dot{M}_{mb} \cdot C_{p,g} T_{mb} \\
&\quad - \Delta \dot{M}_{bc} \cdot C_{p,g} T_{bc} + 2\pi r_b \left(\lambda \frac{\partial T}{\partial r} \right)_{r=r_b} - 2\pi r_c \left(\alpha \frac{\partial T}{\partial r} \right)_{r=r_c}
\end{aligned} \tag{3.18}$$

where

- n_p = Number density of particle
 m_p = Mass of a particle
 s_p = Surface area of a particle
 h_p = Specific enthalpy of a particle
 $\Delta \dot{M}_{bc}, (\Delta \dot{M}_{mb})$ = Mass flux from region b,(m) to region c,(b)
 $u_{bc}, T_{bc}, (u_{mc}, T_{mc})$ = Velocity and temperature of mass flux from region b,(m) to region c,(b)
 $C_{p,g}$ = Specific heat of gas
 p = Pressure (assumed to be uniform in radial direction)
 g = Acceleration of gravity

The integrated quantities can be rewritten in terms of the following average quantities.

$$\bar{\rho}_c = \int_0^{r_c} \rho_c 2\pi r dr / \pi r_c^2 \quad (3.19)$$

$$\bar{\rho}_b = \int_{r_b}^{r_c} \rho_b 2\pi r dr / (\pi r_b^2 - \pi r_c^2) \quad (3.20)$$

$$\bar{u}_c = \int_0^{r_c} \rho_c u_c 2\pi r dr / \bar{\rho}_c \cdot \pi r_c^2 \quad (3.21)$$

$$\bar{u}_b = \int_{r_c}^{r_b} \rho_b u_b 2\pi r dr / \bar{\rho}_b \cdot (\pi r_b^2 - \pi r_c^2) \quad (3.22)$$

$$\bar{n}_p = \int_0^{r_c} n_p u_c 2\pi r dr / \bar{u}_c \cdot \pi r_c^2 \quad (3.23)$$

Using the perfect gas law,

$$P = \rho RT (= 1 \text{ atm}) \quad (3.24)$$

Momentum and energy integrals are expressed as follows.

$$\int_0^{r_c} (n_p m_p u_c u_c + \rho_c u_c u_c) 2\pi r dr = (K_{PM} \bar{n}_p m_p + K_{cM} \bar{\rho}_c) \bar{u}_c^2 \pi r_c^2 \quad (3.25)$$

$$\int_{r_c}^{r_b} \rho_b u_b u_b 2\pi r dr = K_{bM} \bar{\rho}_b \bar{u}_b^2 (\pi r_b^2 - \pi r_c^2) \quad (3.26)$$

$$\begin{aligned} \int_0^{r_c} (n_p m_p u_c h_p + \rho_c u_c C_{p,g} T_c) 2\pi r dr \\ = (K_{pE} \bar{n}_p m_p \bar{u}_c \bar{h}_p + K_{cE} \bar{\rho}_c \bar{u}_c C_{p,g} \bar{T}_c) \pi r_c^2 \end{aligned} \quad (3.27)$$

$$\int_{r_c}^{r_b} \rho_b u_b C_{p,g} T_b 2\pi r dr = K_{bE} \bar{\rho}_b \bar{u}_b C_{p,g} \bar{T}_b (\pi r_b^2 - \pi r_c^2) \quad (3.28)$$

where K_{pM} , K_{cM} , K_{bM} , K_{pE} , K_{cE} and K_{bE} are shape factors, which can be calculated if appropriate radial profiles of velocity, temperature and number density are assumed. Since the main objective of the analysis is to obtain proper functional relations rather than the complete solution of the flow field, the following assumptions are made to simplify the problem.

A.1 Temperature and velocity profiles in each region are flat.

$$K_{pM} = K_{cM} = K_{bM} = K_{pE} = K_{cE} = K_{bE} = 1 \quad (3.29)$$

A.2 Effect of devolatilization is negligible.

$$\text{This implies } m_p = \text{const} \quad \text{and} \quad h_p = C(T - T_o)$$

A.3 Diameter of each region is constant.

A.4 Velocity and temperature gradients at the interfaces are approximated by the following equations with two adjustable parameters

$$K_\mu \quad \text{and} \quad K_\lambda$$

$$\left(\frac{\partial u}{\partial r}\right)_{r=r_c} = K_\mu \frac{u_b - u_c}{r_c} \quad (3.30)$$

$$\left(\frac{\partial u}{\partial r}\right)_{r=r_b} = K_\mu \frac{u_m - u_c}{r_b} \quad (3.31)$$

$$\left(\frac{\partial T}{\partial r}\right)_{r=r_c} = K_\lambda \frac{u_b - u_c}{r_c} \quad (3.32)$$

$$\left(\frac{\partial T}{\partial r}\right)_{r=r_b} = K_\mu \frac{u_m - u_b}{r_b} \quad (3.33)$$

A.5 Velocities and temperatures of the mass fluxes across the interfaces have the following values.

$$u_{bc} = u_c \quad (3.34)$$

$$u_{mb} = u_b \quad (3.35)$$

$$T_{bc} = \frac{T_b + T_c}{2} \quad (3.36)$$

$$T_{mb} = \frac{T_m + T_b}{2} \quad (3.37)$$

A.7 Pressure gradient and gravity effects are negligible.

A.8 Particles are spherical and have a constant diameter, r_p .

$$m_p = \frac{4}{3} \pi r_p^3 \cdot \rho_p, \quad s_p = 4\pi r_p^2 \quad (3.38)$$

Assumptions A.2 may need some explanations. Rapid devolatilization is probably endothermic, but such effect may be taken care of by increasing the average specific heat of coal. Since mass flow rate of coal particles is much smaller than that of the main gas cooled by the water-cooled injector, the enthalpy required to heat the particles is smaller than that to heat the gas in the cold boundary region. Hence, small change in the enthalpy requirement would not change the particle temperature.

Using Eqs. (3.19) - (3.38), the basic equations reduce to the following four equations.

$$(\dot{M}_p + \dot{M}_c) \frac{d\bar{u}_c}{dx} = 2\pi K_\mu \cdot \mu(\bar{u}_b - \bar{u}_c) \quad (3.39)$$

$$\begin{aligned}
& \dot{M}_p \left[\frac{\bar{T}_c + \bar{T}_b}{2\bar{T}_c} \cdot C_{p,g} \cdot \dot{M}_c \cdot \frac{d\bar{T}_c}{dx} + \frac{\bar{T}_c - \bar{T}_b}{2\bar{u}_c} \cdot C_{p,g} \cdot \dot{M}_c \cdot \frac{d\bar{u}_c}{dx} \right] \\
& = 2\pi K_\lambda \cdot \lambda \cdot (\bar{T}_b - \bar{T}_c) + \frac{3\dot{M}_p \cdot \sigma \cdot \epsilon_p}{\rho_p \cdot r_p} (\bar{T}_m^4 - \bar{T}_c^4)
\end{aligned} \tag{3.40}$$

$$\begin{aligned}
& \dot{M}_b \frac{d\bar{u}_b}{dx} - \frac{\bar{u}_b - \bar{u}_c}{\bar{u}_c} \dot{M}_c \frac{d\bar{u}_c}{dx} + \frac{\bar{u}_b - \bar{u}_c}{\bar{T}_c} \dot{M}_c \cdot \frac{d\bar{T}_c}{dx} \\
& = 2\pi K_\mu \cdot \mu \cdot (\bar{u}_m - \bar{u}_b) - 2\pi K_\mu \cdot \mu \cdot (\bar{u}_b - \bar{u}_c)
\end{aligned} \tag{3.41}$$

$$\begin{aligned}
& \frac{\bar{T}_b + \bar{T}_m}{2\bar{T}_b} C_{p,g} \dot{M}_b \frac{d\bar{T}_b}{dx} + \frac{\bar{T}_b - \bar{T}_m}{2\bar{u}_b} \dot{M}_b \frac{d\bar{u}_b}{dx} - \frac{\bar{T}_c - \bar{T}_m}{2\bar{T}_c} C_{p,g} \dot{M}_c \frac{d\bar{T}_c}{dx} \\
& + \frac{\bar{T}_c - \bar{T}_m}{2\bar{u}_c} C_{p,g} \dot{M}_c \frac{d\bar{u}_c}{dx} = 2\pi K_\lambda \lambda (\bar{T}_m - \bar{T}_b) - 2\pi K_\lambda \lambda (\bar{T}_b - \bar{T}_c)
\end{aligned} \tag{3.42}$$

where \dot{M}_b , \dot{M}_c and \dot{M}_p are mass fluxes defined by the following equations.

$$\dot{M}_c = \bar{\rho}_c \bar{u}_c \cdot \pi r_c^2 \tag{3.43}$$

$$\dot{M}_b = \bar{\rho}_b \bar{u}_b \cdot (\pi r_b^2 - \pi r_c^2) \tag{3.44}$$

$$\dot{M}_p = \bar{n}_p \bar{m}_p \bar{u}_c \cdot \pi r_c^2 \tag{3.45}$$

It should be noted that use of other temperature or velocity profiles, such as parabolic, changes the shape factors (assumption A.1), causing some differences in the relative importance of the terms in the basic equations. However, parameter K_μ in Eqs. (3.29) - (3.32) is determined

experimentally from the results of the laser velocity measurements. Hence use of different velocity profile may affect the value of K_μ , but the calculated velocities are considered to be insensitive to the choice of the profiles. The assumption on the velocities of the mass fluxes across the interfaces (A.5) can be understood in the same context. Use of the average velocity of two regions as the velocity of the mass flux across the interface might be thought more appropriate. However, such an assumption could result in physically unrealistic situations because of the inherent properties of the approximate integral method. For instance, an isothermal pipe flow of incompressible fluid with mass influx is considered. The average velocity is uniquely determined by the mass conservation equation, independent of the velocity of the mass influx. The momentum equation can be written as

$$\frac{d}{dx} (K_m \bar{\rho} \bar{u}^2 \pi r^2) = \frac{d}{dx} (\bar{\rho} \bar{u} \pi r^2) \cdot u_i + F \quad (3.46)$$

where K_m is a shape factor similar to the one defined in Eq. (3.26), F is the force term including shear, pressure and body forces, and u_i is the velocity of mass influx. For a self-preserving shape, K_m is a constant and Eq. (3.46) reduces to

$$\pi r^2 \bar{\rho} \left(2\bar{u} - \frac{u_i}{K_m} \right) \frac{d\bar{u}}{dx} = \frac{F}{K_m} \quad (3.47)$$

If F is positive (the boundary region defined before corresponds to this case), the velocity should increase from the physical reasoning. For any value of shape factor, one can always realize a case of high influx velocity such that

$$u_i > 2K_m \bar{u} \quad (3.48)$$

When this is the case, Eq. (3.47) predicts decreasing average velocity with high velocity of mass influx. Such an unrealistic situation is caused by the assumption of self-preserving profile. In other words, the shape factor is strongly dependent on the velocity of influx in real cases and always has to satisfy the following relation.

$$2\bar{u} - \frac{u_1}{K_m} > 0 \quad (3.49)$$

The assumption A.5 is equivalent to the hypothesis

$$\frac{u_1}{K_m} = \bar{u} \quad (3.50)$$

It should be stressed again that the model developed here is insensitive to the shape factors since the parameter K_μ is evaluated experimentally.

Equations (3.39) to (3.42) require evaluations of r_b , r_c and u_m . The main stream velocity, u_m , is approximated by the centerline velocity of the developing flow in a circular tube. Numerical results of Langhaar (1942) were curve-fitted by the following equations.

$$\frac{u_m}{\bar{u}_m} = 1 + 0.34 y^{0.45} \quad 0 \leq y \leq 6 \quad (3.51)$$

$$\frac{u_m}{\bar{u}_m} = 2 - 3.48 y^{-1.47} \quad y \geq 6 \quad (3.52)$$

where

$$y = 400 \frac{x}{D} \frac{1}{Re_D} \quad (3.53)$$

and D is the diameter of the muffle tube.

r_c is taken as the same diameter as the coal injector I.D. ($r_c = 1.2$ mm). Since the visual observations and the laser measurements confirmed that injected particles are narrowly centered, this assumption may be reasonable. The radius of the boundary region, r_b , depends on the boundary layer development on the water-cooled injector surface. The boundary layer thickness at the injector tip may be approximated by that of forced convection over a flat plate.

$$\delta = \frac{5 \cdot \ell}{\sqrt{Re_\ell}} \quad (3.54)$$

where ℓ is the length of the injector below the honeycomb. The thermal boundary layer thickness may be assumed to be the same as δ , since the Prandtl number is close to unity. In the boundary layer temperature and velocity profiles are approximated by the following equation.

$$\frac{u}{u_m} = \frac{T - T_o}{T_m - T_o} = \sin \frac{\pi}{2} \frac{r - r_i}{\delta} \quad (3.55)$$

where r_i is the outer radius of the injector. r_b is defined as the radius which balances overall energy and mass with the flat profile approximation.

$$\int_{r_c}^{r_b} \rho u C_{p,g} T 2\pi r dr = \rho_m u_m C_{p,g} T_m (\pi \delta^2 - \pi r_b^2) + \rho_o u_{b,o} C_{p,g} T_o (\pi r_b^2 - \pi r_c^2) \quad (3.56)$$

$$\int_{r_c}^{r_b} \rho u 2\pi r dr = \rho_m u_m (\pi \delta^2 - \pi r_b^2) + \rho_o u_{b,o} (\pi r_b^2 - \pi r_c^2) \quad (3.57)$$

where $T_o = 300^\circ\text{K}$
 $\rho_o = \rho (T = 300^\circ\text{K})$

Initial velocity of region b, $u_{b,0}$, is calculated together with r_b to satisfy the simultaneous equations (3.56) and (3.57). Differential equations (3.39) - (3.42) were solved numerically by the fourth order Runge-Kutta method for each experimental condition summarized in Table 2.1. By curve-fitting the observed velocities, parameter K_μ was found to be 4.5 regardless of the choice of K_λ . Figure 3.5 shows experimentally measured velocities and calculated velocities (solid lines). Good agreements were obtained. Figures 3.9 and 3.10 show results for typical simulations at 1510°K and 2100°K respectively. As expected, the temperature of the center region, T_c , rises faster than that of the boundary region because of the radiation from the furnace wall to the coal particles. The velocity of the center region (Fig. 3.11) decays quickly to that of the boundary region and after 5 cm from the injector both velocities are accelerated together by the faster main flow. Residence time of particles was obtained by numerically integrating the inverse of the center region velocity over the distance. Temperature-time history of particles depends on the choice of K_λ . As discussed earlier, K_μ and K_λ include the effects of the shape factors, which were assumed to be unity for simplicity. In reality, however, the shape factors could become much larger than unity when strong nonuniformity in temperature or velocity exists. To examine such effect the ratio of the momentum shape factor, K_M , to the energy shape factor, K_E , may be considered

$$\theta = \frac{K_M}{K_E} \quad (3.58)$$

K_M and K_E are defined by the equations similar to (3.26) and (3.28).

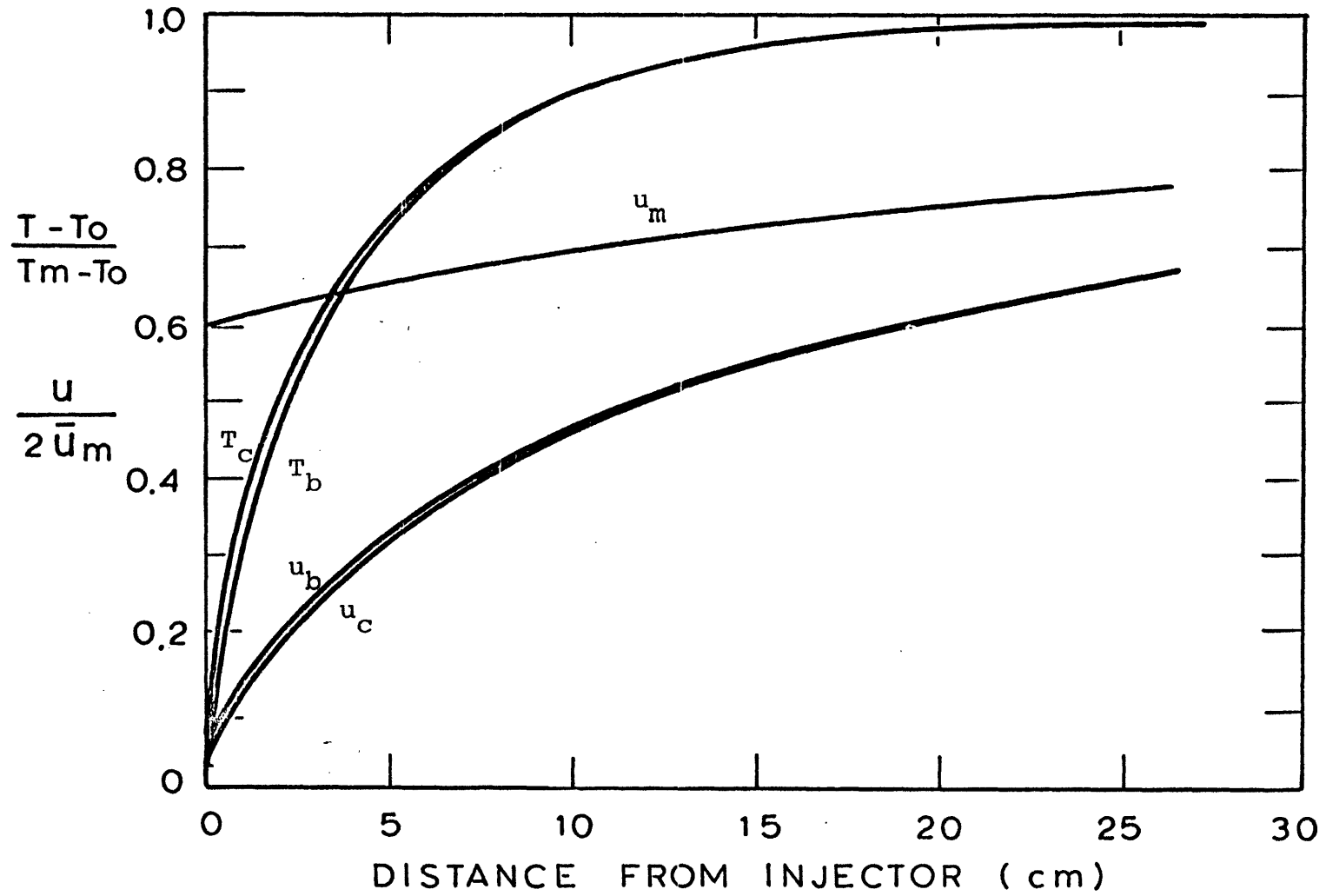


FIG. 3.9. CALCULATED TEMPERATURES AND VELOCITIES
 $T_m = 1510^\circ\text{K}$, $\bar{u}_m = 2.84$ m/sec, $u_{\text{carrier}} = 0.24$ m/sec

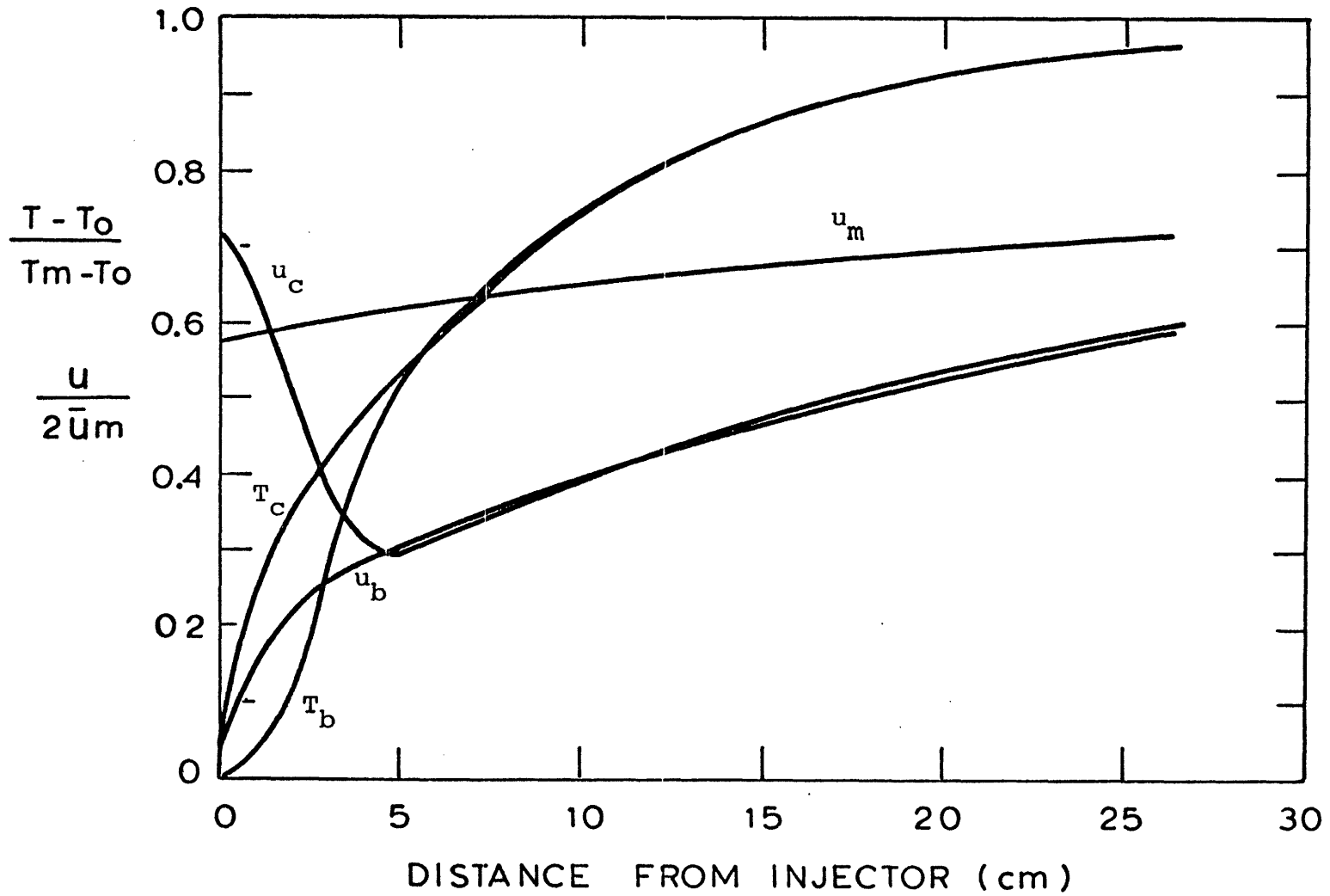


FIG. 3.10 CALCULATED TEMPERATURE AND VELOCITIES
 $T_m = 2100^\circ\text{K}$, $\bar{u}_m = 8.65 \text{ m/sec}$, $u_{\text{carrier}} = 9.1 \text{ m/sec}$

From the basic equations it can be seen that the two parameters, K_μ and K_λ , are related to θ approximately by

$$\frac{K_\mu}{K_\lambda} \propto \theta \quad (3.59)$$

For the experimental conditions θ is generally greater than unity, since the ratio of the main stream temperature to the average boundary region temperature is smaller than that of the main stream velocity to the average boundary region velocity. Assuming approximate temperature and velocity profiles in the boundary region, the shape factors were calculated for various cases, from which θ was estimated to be between 1 and 3 depending on the experimental conditions and locations from the injector tip. Temperature-time history of coal particles under each experimental condition was then calculated assuming $K_\lambda = \theta \cdot K_\mu$. Figure 3.11 shows calculated particle temperatures at main stream temperature of 2100°K for $\theta = 1, 2$ and 3. For practical purposes the temperature-time history of particles may be approximated by the following exponential curve with a characteristic heating time, t_H .

$$\frac{T - T_o}{T_m - T_o} = 1 - e^{-\frac{t}{t_H}} \quad (3.60)$$

In Table 3.1, calculated characteristic heating times are summarized for different values of θ .

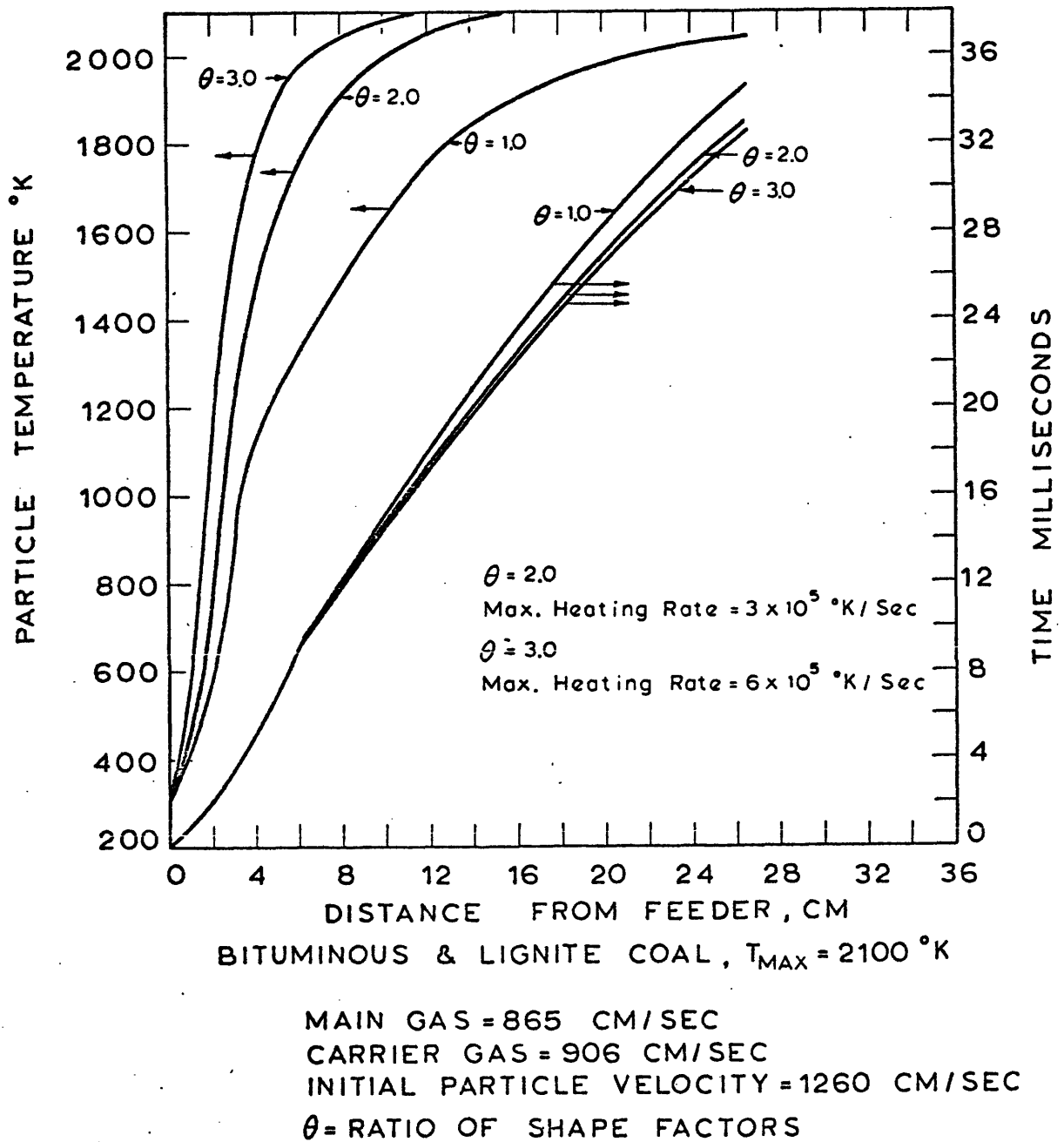


FIGURE 3.11 CALCULATED PARTICLE TEMPERATURES AND RESIDENCE TIMES

Table 3.1 - Calculated Heating Times of Particles

Furnace Temperature (°K)	Coal	Main Gas Velocity (m/sec)	Carrier Gas Velocity (m/sec)	Heating Times		
				$\theta=1$ (msec)	$\theta=2$ (msec)	$\theta=3$ (msec)
1000	LIG,BIT	0.8	0.64	53	31	21
1260	LIG,BIT	1.0	0.72	44	27	18
1510	LIG	0.7	0.24	43	35	29
1510	LIG,BIT	2.9	0.24	46	33	26
1740	LIG	0.8	0.21	32	30	26
1740	LIG	5.0	0.52	34	24	19
1740	BIT	5.0	5.0	16	8.0	4.7
1940	LIG	8.0	0.83	25	17	13
1940	BIT	8.0	4.5	15	8.0	5.1
2100	LIG,BIT	8.7	9.1	10	6.1	3.1

3.3 Determination of Weight Loss

A flow diagram of devolatilization experiments is shown in Fig. 3.12. Variables within the solid boxes are experimentally measured quantities. During a devolatilization experiment, moisture and some of the "volatile material" escape from coal particles, and some of coal particles and ash may be lost. Furthermore, soot and tar may be formed and may deposit on collector wall or on the surface of char particles. Fractional weight loss, f_V , is defined as the ratio of the volatile matter produced by devolatilization reaction to the original weight of coal, which is related to the experimentally measured residual material, x_R , by the following relation.

$$\begin{aligned}
 f_V &= \frac{x_V}{x_C - x_{PL}} = \frac{x_C - x_R - x_M - x_{PL} - x_{AL} + x_{ST}}{x_C - x_{PL}} \\
 &= 1 - f_M^O - \frac{x_R + x_{AL} - x_{ST}}{x_C - x_{PL}} \quad (3.61)
 \end{aligned}$$

where

$$f_M^O = \frac{x_M}{x_C - x_{PL}} \quad ; \quad \text{moisture fraction of coal}$$

It should be noted that x_R is the weight of the residual material including soot and tar, and that particle loss is assumed to have the same effect as starting with $x_C - x_{PL}$ gram of raw coal. In order to be able to calculate weight loss from Eq. (3.61), particle loss (x_{PL}), ash loss (x_{AL}), and soot and tar deposit (x_{ST}), must be known. Moisture content of coal can be obtained by an independent ASTM moisture determination test.

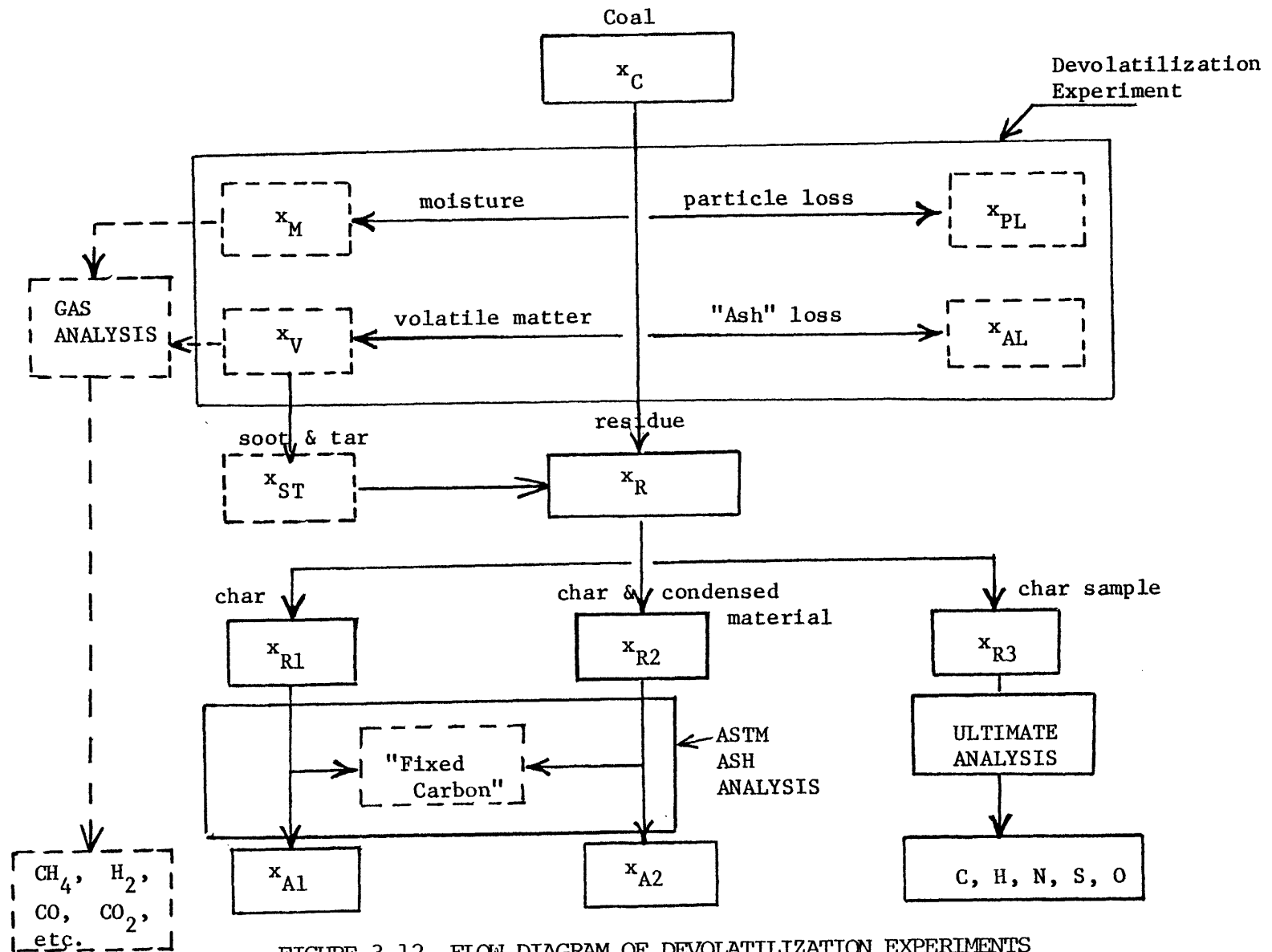


FIGURE 3.12 FLOW DIAGRAM OF DEVOLATILIZATION EXPERIMENTS

Particle Loss

Handling loss of coal or char particles can be practically eliminated by careful performance of the experiments. In flow experiments some of the particles remain in the feeder. However, the weight of the coal remaining is very small (about 1 mg), and also it is approximately constant between runs. Therefore this error is negligible. Particle loss associated with the flow field or devolatilization mechanism is more difficult to control. In fact, one of the major design efforts was to ensure good particle collection efficiencies. For this purpose, simulation of flow fields at room temperature and testing of various flow straighteners were conducted prior to the construction of the two furnaces. These results were utilized in the final design.

A narrow stream of coal particles was visually observed through the observation ports in the laminar flow furnace. The thermocouple, which monitors the main gas temperature, provided a reference length to measure the diameter of the particle cloud, and this diameter was found to be less than 1/16 inch up to the third observation port. This was confirmed by the laser velocity measurements. When the laser beam was off-centered by about 1/16 inch, no signal was obtained, indicating that no particle exists outside the center region. Quantitative measurements of collection efficiencies were obtained at room temperature using coal particles, and at experimental temperatures by using alumina particles. At room temperature, experimental conditions were simulated by matching the nondimensional parameters characterizing the flow field (see Appendix B). Collection efficiencies greater than 99 percent were obtained for all

cases in free fall conditions. Under laminar flow conditions, however, use of directly injected quenching water forced some of the fine bituminous particles to escape through the pores of the bronze filter. About 5 percent by weight of original coal was lost when a 50 mg sample was used. Relative particle loss decreased as the sample size increased, since some of the pores of the filter were closed by captured particles, thus preventing further particle loss. Another factor which tends to diminish the particle loss is the swelling of coal during devolatilization. Bituminous coal swells and agglomerates upon heating. Thus in the actual pyrolysis particle losses through filter is considered to be less. For lignite, recoveries were greater than 98 percent even under laminar flow conditions with water injection.

Ash Loss

Ash loss during devolatilization of coal can occur by vaporization, by decomposition and by reactions with coal. Quantitative measurement of ash loss is provided by the differences in the ASTM ash analysis for raw coal and char.

$$x_{AL} = f_A^0 (x_C - x_{PL}) - f_{A,R} \cdot x_R \quad (3.62)$$

where

f_A^0 : ash fraction of coal

$f_{A,R}$: ash fraction of residue

Ash loss determined by this method, however, is not necessarily the same as the weight change of the mineral matter during the devolatilization of coal. Ash is neither a well defined material, nor is it a mixture of pure

oxides. ASTM ash, which can be defined as the residual material remaining after burning coal in air at the maximum furnace temperature of 750°C, contains various sulfur compounds (Lowry, 1963). An extensive study on the behavior of the ashes of two coals used here during devolatilization and combustion was conducted in the laboratory using the same experimental apparatus. The details of the results will be reported elsewhere (Padie, 1976). Only a brief summary on ash loss during devolatilization is discussed in Appendix D. Since the weight of "mineral matter" in char is not known, use of the "ash loss" instead of the "weight change of mineral matter" is allowable. Error caused by such an approximation in calculating weight loss is quite small, since ash concentrations account for only about 10 percent by weight of the raw coals.

Soot and Tar Deposit

Volatile matter produced by thermal decomposition of coal could further undergo gas phase reactions. Soot may be formed by thermal cracking of volatile matter. Tar may recondense on external and internal surfaces of coal or on collector walls. It is desirable to correct the apparent weight loss for soot and tar deposit. Normally, separation of such materials is very difficult, if they deposit on coal surfaces. Soot and tar formed on the collector walls can be estimated through ash analyses. In a free fall experiment with alumina collector and in the crucible experiment the char is removed from the collector or from the crucible and about half of it, x_{R_1} , is used for ASTM ash analysis (see Fig. 3.12). The other half, x_{R_3} , is kept for further analyses, including ultimate analysis. The remaining residue, x_{R_2} , in the collector or in

the crucible is mainly soot and tar deposit, but still contains some char which could not be removed. The weight of this char can be estimated from the amount of ash produced from the residue, x_{A_2} , since the ash concentration in char is known from the independent ash analysis. Thus, the weight of soot and tar deposit on collector wall or on crucible wall is obtained by the following equation.

$$x_{ST} = x_{R_2} - x_{A_2} \cdot \frac{x_{R_1}}{x_{A_1}} \quad (3.63)$$

Such a method is not possible for laminar flow experiment nor for the free fall experiments with a bronze collector, since the weight of bronze filter is changed significantly by oxidation, if ASTM ash analysis is applied to the residual material in the bronze collectors. Estimation of soot and tar under these experimental conditions will be discussed in Chap. 4 together with the experimental results.

Ash Tracer Method

From Eqs. (3.59), (3.60) and (3.61) the following relation holds between weight loss and ash fractions.

$$f_v = 1 - f_M^\circ - \frac{f_A^\circ}{f_{A,R}} - f_{AL} \left(1 - \frac{1}{f_{A,R}}\right) + f_{ST} \quad (3.64)$$

where

$$f_{AL} = \frac{x_{AL}}{x_C - x_{PL}} \quad ; \quad \text{ash loss fraction}$$

$$f_{ST} = \frac{x_{ST}}{x_C - x_{PL}} \quad ; \quad \text{soot and tar fraction}$$

Equation (3.64) does not depend on particle loss, giving an independent method of determining weight loss from ash analysis. When ash loss, soot, and tar deposit are negligible, weight loss by ash tracer method, f_V^{AT} , is expressed as

$$f_V^{AT} = 1 - f_M^o - \frac{f_A^o}{f_{A,R}} \quad (3.65)$$

From Eqs. (3.62) and (3.63) the following relation holds.

$$f_V^{AT} (x_{AL} = 0) \leq f_V \leq f_V (x_{PL} = 0) \quad (3.66)$$

The importance of this relation is that ash tracer method assuming no ash loss and difference-of-the-weights method assuming no particle loss provide lower and upper limits of the true weight loss. In other words, if weight losses by these two independent methods agree, negligible particle loss and ash loss are confirmed.

The formula used for weight determination of free fall experiment with alumina collector and crucible experiment are summarized below. All the weight losses are expressed by dry-ash-free basis.

Apparent weight loss:

$$f_{V,APP} = [1 - \frac{x_R}{x_C(1-f_M^o)}] / (1 - f_{A,D}^o) \quad (3.67)$$

Apparent weight loss by ash tracer method:

$$f_V^{AT} = (1 - \frac{f_{A,D}^o}{f_{A,R}}) / (1 - f_{A,D}^o) \quad (3.68)$$

Weight loss, compensated for soot and tar:

$$f_{V,ST} = \left[1 - \frac{x_R - x_{ST}}{x_C(1-f_M^o)} \right] / (1 - f_{A,D}^o) \quad (3.69)$$

Weight loss by ash tracer method, compensated for soot and tar:

$$f_{V,ST}^{AT} = \left(1 - \frac{f_{A,D}^o}{f_{A,R_1}} \right) / (1 - f_A^o) \quad (3.70)$$

Weight loss, compensated for soot and tar and ash loss:

$$f_{V,ST,AL} = \left[1 - \frac{x_R - x_{ST} + x_{AL}}{x_C(1-f_M^o)} \right] / (1 - f_{A,D}^o) \quad (3.71)$$

where

$f_{A,D}^o$: ash fraction of raw coal on dry basis

$$f_{A,D}^o = \frac{f_A^o}{1 - f_M^o}$$

$f_{A,R}$: apparent ash fraction in char

$$f_{A,R} = \frac{1}{x_R} (x_{A_1} \cdot \frac{x_{R_1} + x_{R_3}}{x_{R_1}} + x_{A_2})$$

f_{A_1,R_1} : ash fraction in char R_1

$$f_{A_1,R_1} = \frac{x_{A_1}}{x_{R_1}}$$

Since soot and tar were not separated from the solid residue in laminar flow experiments or in free fall experiments with bronze collectors, only apparent weight loss and apparent weight loss by ash tracer method can be calculated.

CHAPTER IV

RESULTS4.1 Weight Loss4.1.1 Weight Loss of CoalsLaminar Flow Experiment

Figures 4.1 and 4.2 show results of the laminar flow experiment for lignite and bituminous coal, respectively. Weight losses were calculated based on dry-ash-free (d.a.f.) weights of the raw coals. Reaction times were determined through the simplified mathematical model of the particle behavior in the flow furnace as discussed in section 3.2, except for the small corrections made to account for the acceleration of the particles near the collector due to the high suction rates employed. The details of the calculations and the result of each run are shown in Appendix B. The experimental conditions and the calculated heating time at each furnace temperature are summarized in Tables 2.1 and 3.1, respectively.

From the figures the increase of weight loss with reaction time and the increase of rate of weight loss with furnace temperature are obvious for both coals. Also, weight loss clearly approaches an asymptotic value at each temperature (about 30 percent at 1260°K, 40 percent at 1510°K, 50 percent at 1740°K, and 60 percent at 1940°K for both coals) within the experimental reaction times. The marked change in the behavior of the bituminous coal between 1510°K and 1740°K was due to the different heating rates caused by a significant change in the flow rate of the carrier gas (see Tables 2.1 and 3.1).

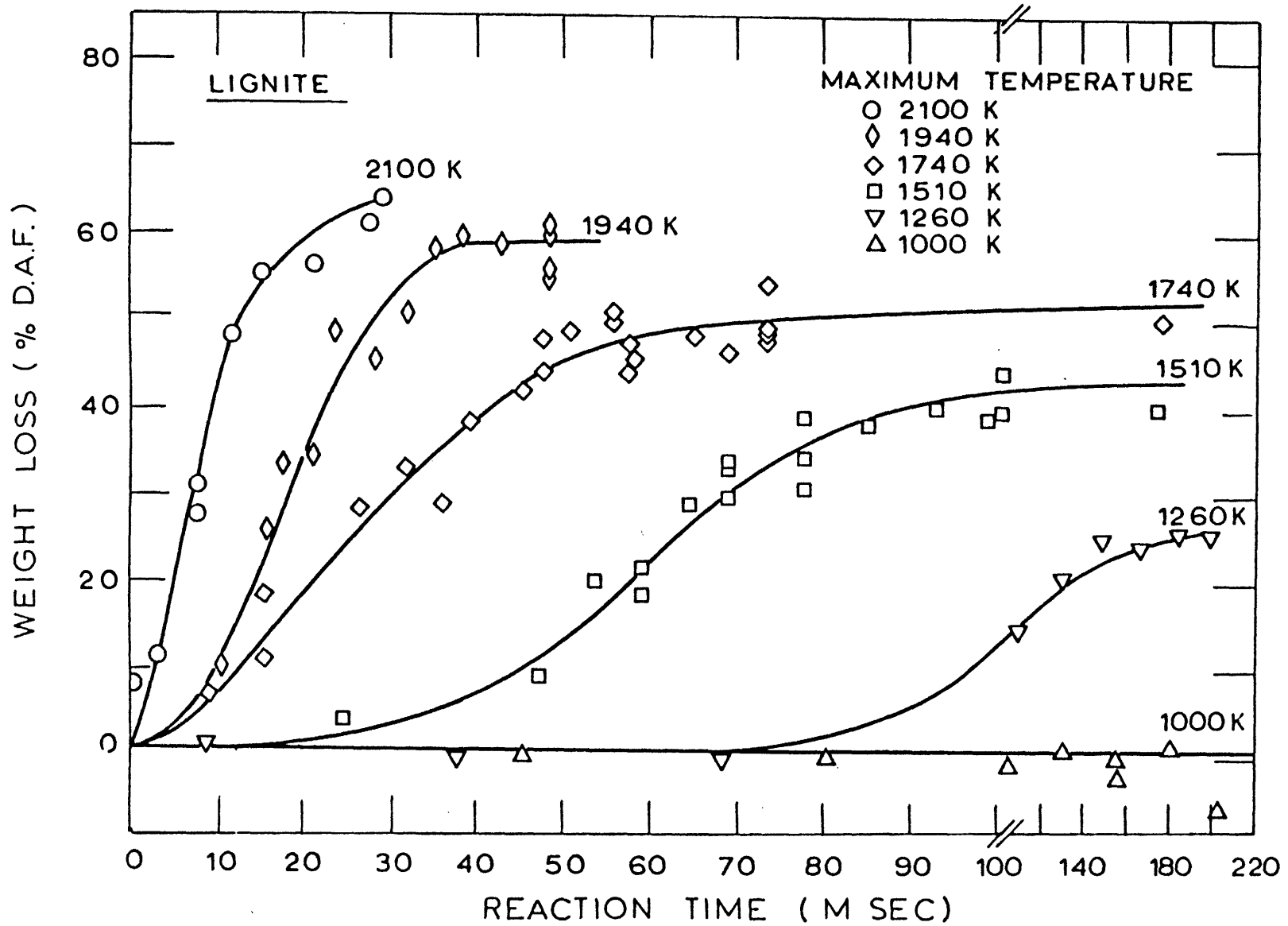


FIG. 4.1 RESULTS OF LAMINAR FLOW EXPERIMENT, MONTANA LIGNITE

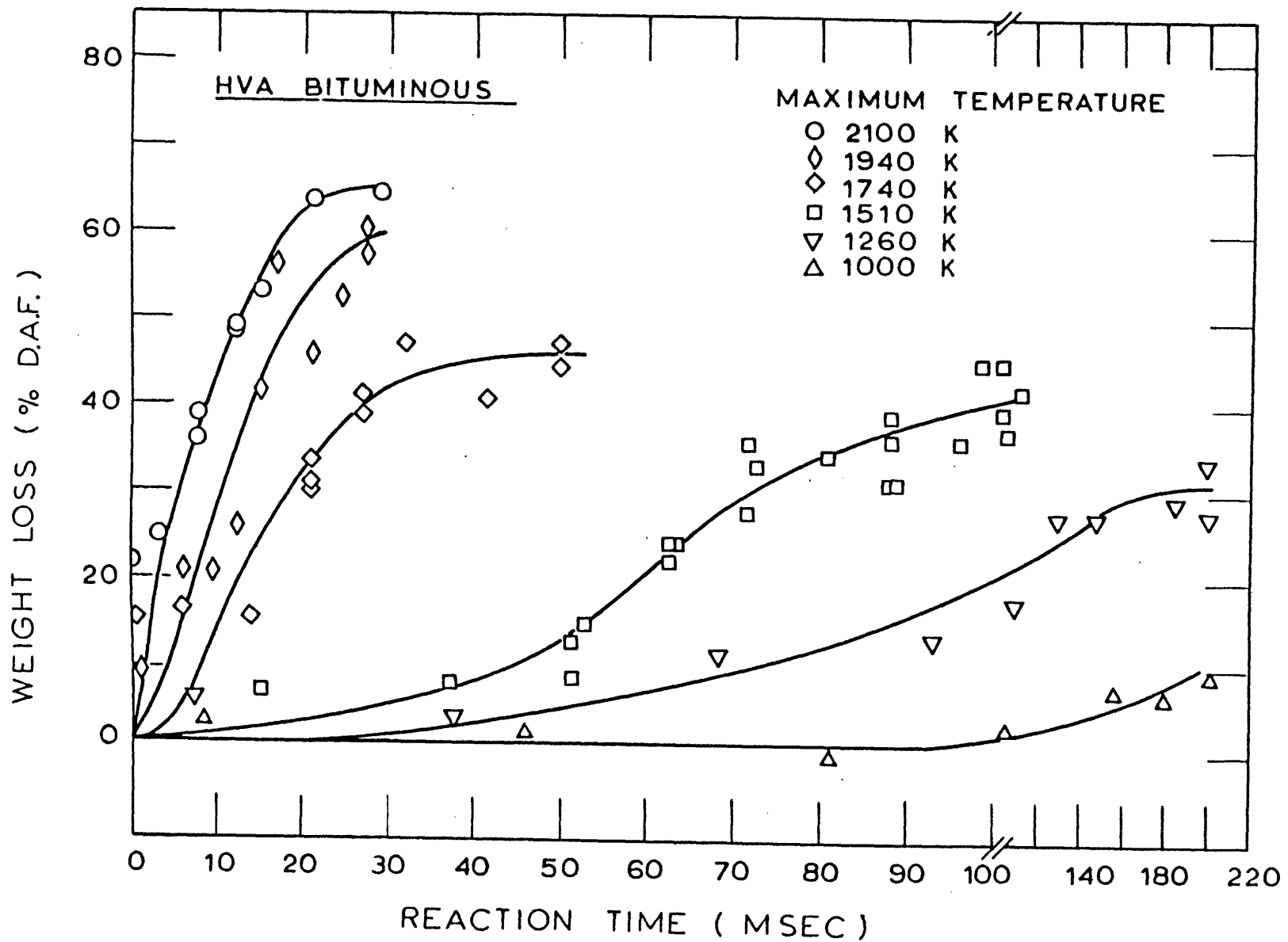


FIG. 4.2 RESULTS OF LAMINAR FLOW EXPERIMENT, PITTSBURGH SEAM BITUMINOUS COAL

Considering the differences in heating rates between the two coals at 1740°K and 1940°K, the observed weight losses are remarkably similar. It should be noted that the two coals differ widely both in chemical composition and in physical changes during devolatilization (The Pittsburgh seam bituminous coal is a highly swelling caking coal, while the Montana lignite is not.). The reproducibility of data is within about 5% of the d.a.t. weight of the raw coals. Several reasons are considered for the experimental scatter.

- 1) Weight changes of the bronze filters.
- 2) Changes in suction rate due to cloggings of the filters.
- 3) Variations in the particle collection efficiency.
- 4) Nonuniformities in the particle feed rate.

Prior to the main experiments, weight changes of the bronze filter were tested by soaking it in water for 10-20 minutes, drying it in an oven and reweighing. It was found that the weight stayed constant to within ± 0.5 mg. (weight of a filter is approximately 22 gm). It was later found that weight losses as high as 3 mg. could occur due to passage of water at high flow rates through the filter in the real experiment. Some impurities left in the porous matrix during the manufacturing process may be responsible for this loss. The quenching water was city water passed through a 0.3 micron filter before injection.

Clogging of the filter by the char particles was one of the serious problems encountered in the experiment. In some extreme cases, large pressure drops across the filter made it impossible to maintain a constant suction rates. To avoid this problem, the sample

size was varied depending on the experimental conditions. At temperatures below 1260°K, about 0.2 to 0.5 gm were used, while at higher temperatures 0.05 to 0.1 gm were typical sizes. More severe cloggings observed at higher temperatures may be due to soot and tar formation.

Variations in the particle collection efficiency are considered to be small, except for those due to particle loss through the filter. As discussed in section 2.3, particle losses outside the collector are unlikely, which is strongly supported by the weight losses of the lignite at 1000°K showing no appreciable loss of particle up to 9 inches from the injector (residence time 250 msec). Loss of the bituminous particles through the filter, which was measured to be about 5% of the raw coal under simulated experimental conditions at room temperature, remains as an uncertainty.

The coal feed rate was typically .15 gm/min, but varied between 0.1 and 0.2 gm/min. Preliminary tests showed negligible effect of the feed rate on weight loss when the feed rate was less than 0.2 gm/min. This is in agreement with the theoretical consideration (section 2.2) that enthalpy requirement to heat the coal particle is smaller than that to heat the cold carrier gas and the portion of the main gas cooled by the water-cooled injector.

Free Fall Experiments

Weight losses measured in the free fall experiments are plotted against the peak temperature of the each run in Figs.4.3 and 4.4. Weight losses with the alumina collector were corrected both for ash

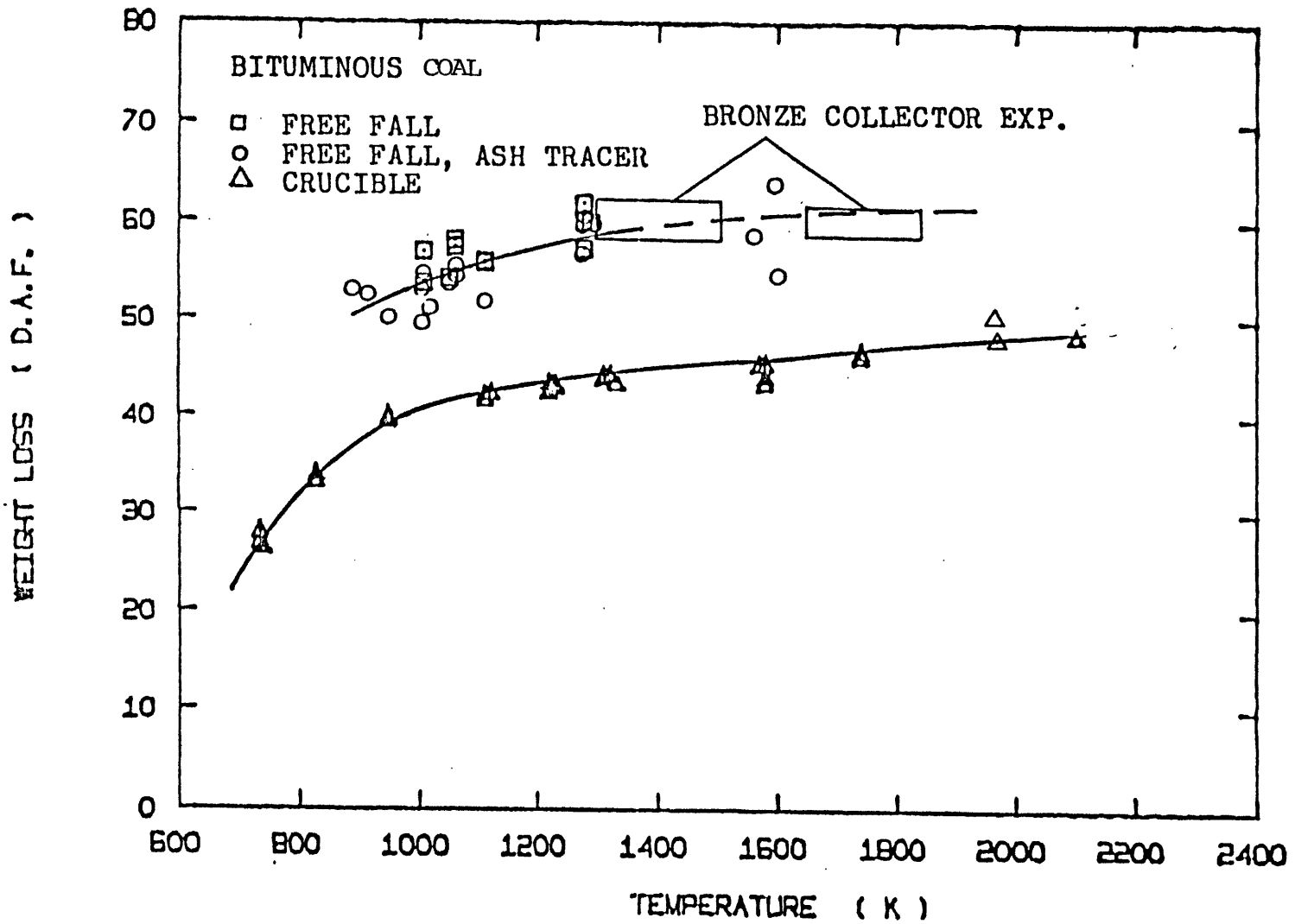


Figure 4.4 Weight Loss at Different Temperatures (Dry-ash-free basis, Compensated for thermal cracking and ash loss) Bituminous

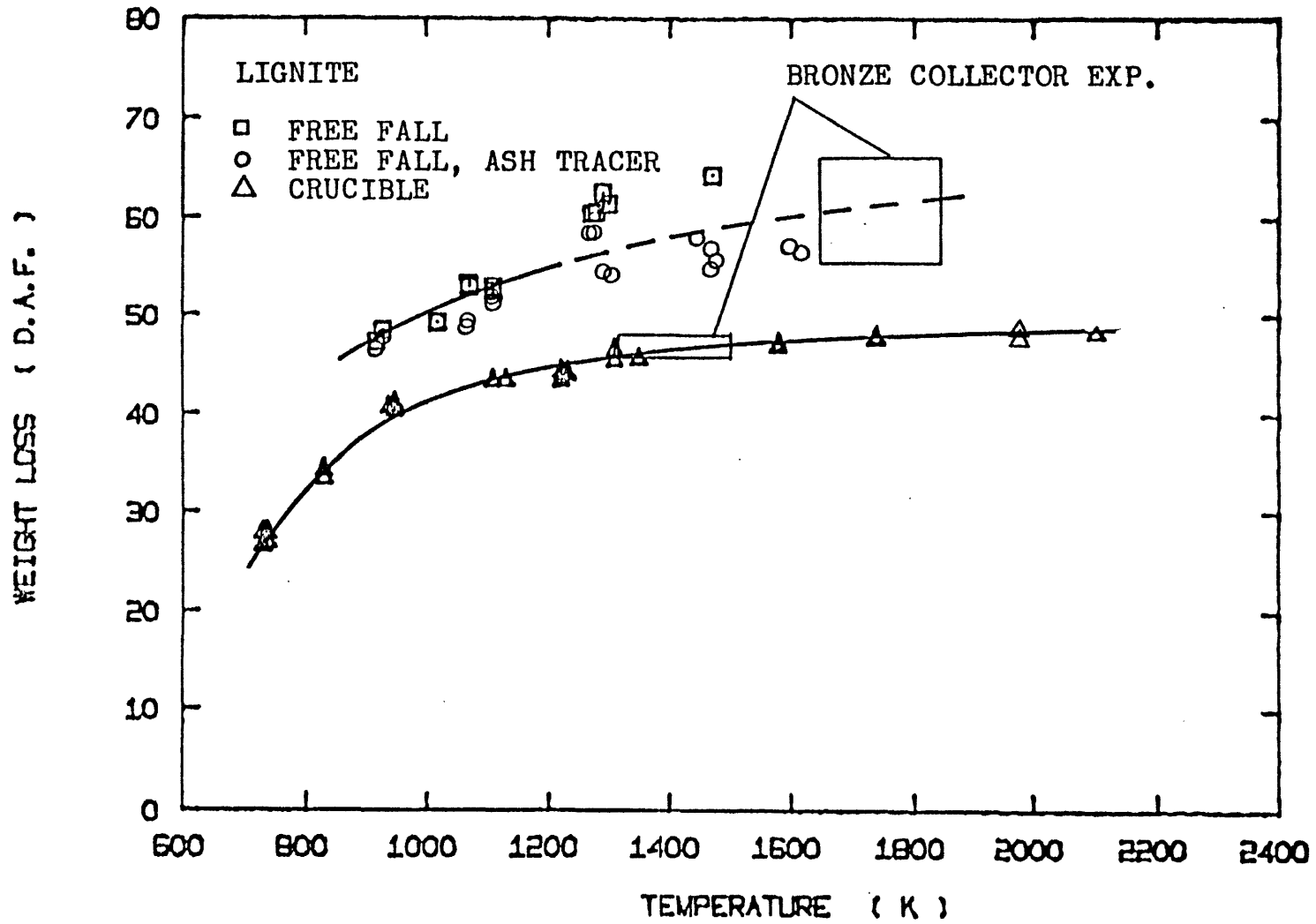


Figure 4.3 Weight Loss at Different Temperatures (Dry-ash-free basis, Compensated for thermal cracking and ash loss)
Lignite

loss and for soot and tar deposit on the collector wall. The details of each run are tabulated in Appendix C. In earlier runs (FF 500's and cancellable experiment CR 100's) coal particles were dried in air at 105°C for 2 hours to 24 hours before the runs. Later it was found that the drying caused oxidation of bituminous and reduced the weight loss significantly. Lignite showed no difference. Because of this, weight loss of dried bituminous should not be compared with those of undried coal. The temperatures reported for the alumina collector experiment are the values measured by a thermocouple which was placed between the collector and the support rod. Since the bottom of the collector was about 17 cm from the feeder, the temperature at this place was 50° to 200°K lower than the furnace peak temperature (Fig.2.6) without feeding coal particles. After the feeder was started, the thermocouple recorded a temperature drop of about 20°K. This was considered to be caused by the cooling effects of the coal fed. The cold stream of coal particles at the center caused strong downward natural convection reducing particle residence time. The particles were heated mainly by radiation from the collector wall instead of by conduction. This increased the heating time as compared with that of the flow experiment. When the particle landed at the bottom of the collector, the temperature of the particles were lower than that of the collector, which caused the temperature drop in the thermocouple reading. Therefore, the maximum temperature experienced by coal particles was assumed to be the peak temperature recorded by the thermocouple, rather than the peak temperature of the furnace. In the

free fall experiment with the bronze collector there was no direct measurement of the particle temperature. The maximum temperature of the coal particles was estimated to be within 200°K of the peak temperature of the furnace. The estimated weight losses are shown by rectangular areas in Figures 4.3 and 4.4. The experimental results are summarized in Table C.4.

The low apparent weight losses of bituminous coal appeared to be due to production of solids by secondary reactions of the volatile matter. In the bronze collector two visually different materials were collected. Relatively large grayish particles (char particles) were found in a deep black matrix of fine particles. The char particles were narrowly centered in the collector, while the black material covered the whole collector (see Fig.C.1 in Appendix C). This is probably because of the differences in particle densities. The lighter soot-like material could diffuse more widely than the heavier char particle. Ash analyses of the collector samples showed high ash concentrations for the material taken from the center of the collector dish and significantly lower ash concentrations for that from the periphery area, confirming the visual observation. An estimation of the true volatile yields could be done through the ash analysis of the materials taken from different radii of the bronze collector disk, by assuming certain statistical distributions of the materials. The details of the analysis are described in Appendix C. From table C.4, the amount of soot and tar formed can be calculated as the difference between the apparent weight loss and the estimated true weight loss.

More than 20% by d.a.t. weight of the raw coal is estimated to become soot and tar. For lignite no visual heterogeneity was detected in the collected sample, and the ash concentrations of the char at different radii in the collector disk were also uniform within the experimental variation.

In the experiment with the alumina collector, some particle loss was observed. Although the flow rate of the carrier gas was small (about 10cc/min), fine particles were considered to be carried away by the bulk upward flow of the volatile matter inside the cylindrical collector. For this reason, weight losses determined by using ash as a tracer were also plotted in the figures after compensating for ash loss (weight changes of ash will be discussed later). Reasonable agreement in the weight losses determined by these two methods were obtained.

Crucible Experiment

The results of the crucible experiment are also shown in figures 4.3 and 4.4. Weight losses are those corrected both for soot and tar deposit on crucible walls and for ash loss. The reported temperatures are the peak temperatures measured by a thermocouple placed between the bottom of the crucible and the support disk. Typical temperature-time histories at representative furnace temperatures are shown in Figure 2.7. The details of each run are tabulated in Appendix D. Most of the runs are made by alumina crucibles, but above 2000°K (Run No. CR 400's) graphite crucibles were used. A platinum crucible (ASTM specification for the proximate volatile matter test) was used

for some of the runs to test the effect of the crucible material on weight loss. (CR 226 and CR 234). With the platinum crucible, a negligible amount of soot and tar deposit was observed on the crucible wall. With alumina or porcelain crucibles, however, about 2.5% by weight of the bituminous coal (d.a.f.) was measured as soot and tar deposit under the same conditions. (CR 227 - CR 230). Hence the apparent weight loss with the platinum crucible was higher than that with alumina or porcelain crucible, but no appreciable difference exist in weight losses corrected for the deposit.

The overall trend of the weight losses of crucible runs shows marked differences from those of free fall runs for both coals. At about the ASTM volatile test temperature (1220°K), weight losses of the crucible experiment reach an asymptotic value, which is close to the ASTM volatile matter determined independently. The slight increases in weight losses above this temperature is considered to be caused mainly by the interactions of the mineral matter (ash) and the char. The ultimate analysis of char samples indicated that essentially no hydrogen and oxygen are left in the char above 1500°K, which supports the view that the added loss are due to changes in mineral matter. This will be discussed later in more detail.

Comparison Among the Different Experiments

Figures 4.5 and 4.6 show effects of the reaction time on weight loss under the dispersed phase experiments at different furnace temperatures. Although the experimental conditions, especially the heating rates, are not exactly the same among the different modes of

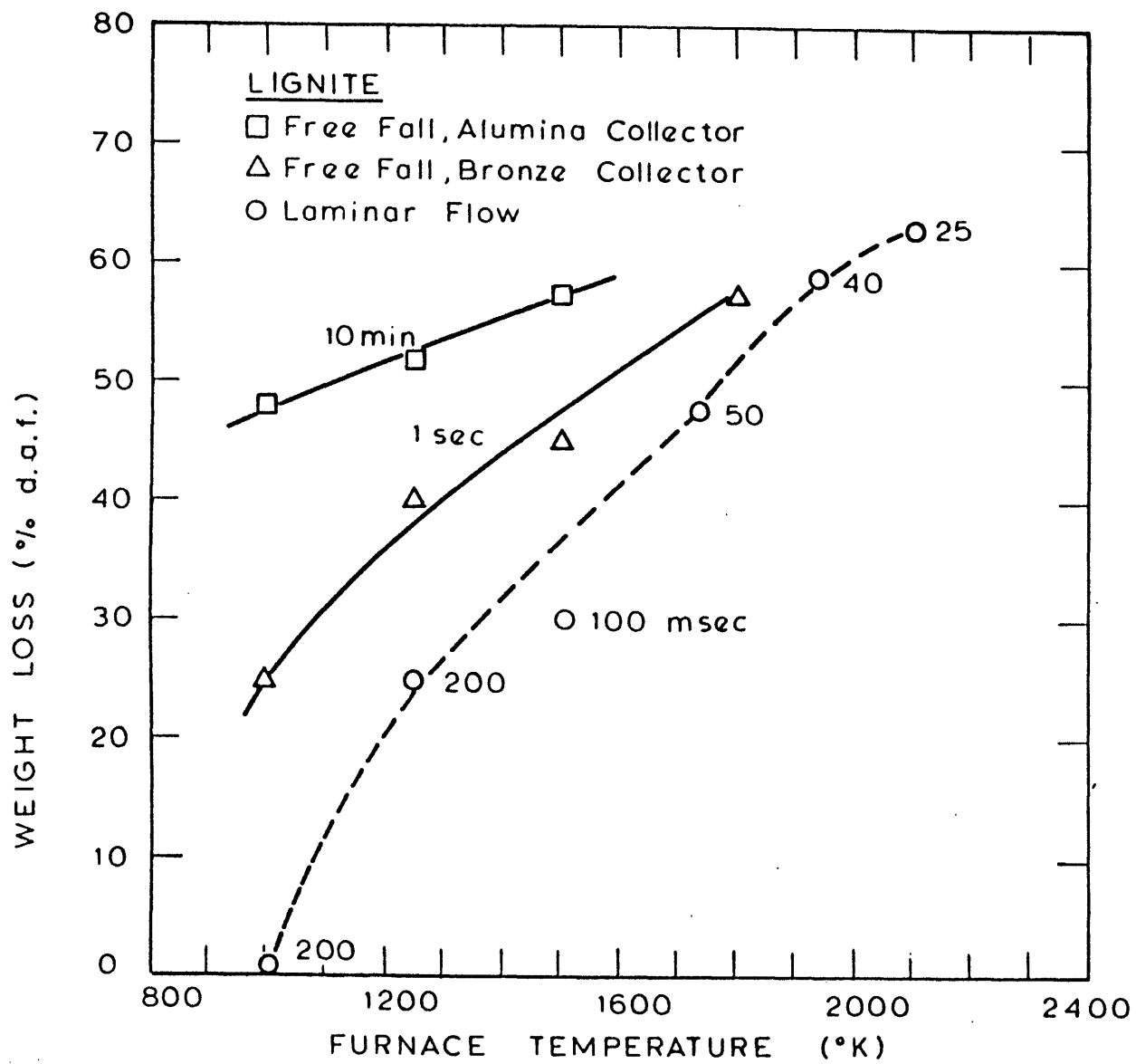


FIG. 4.5 MAXIMUM WEIGHT LOSSES OBSERVED UNDER DIFFERENT EXPERIMENTS, LIGNITE

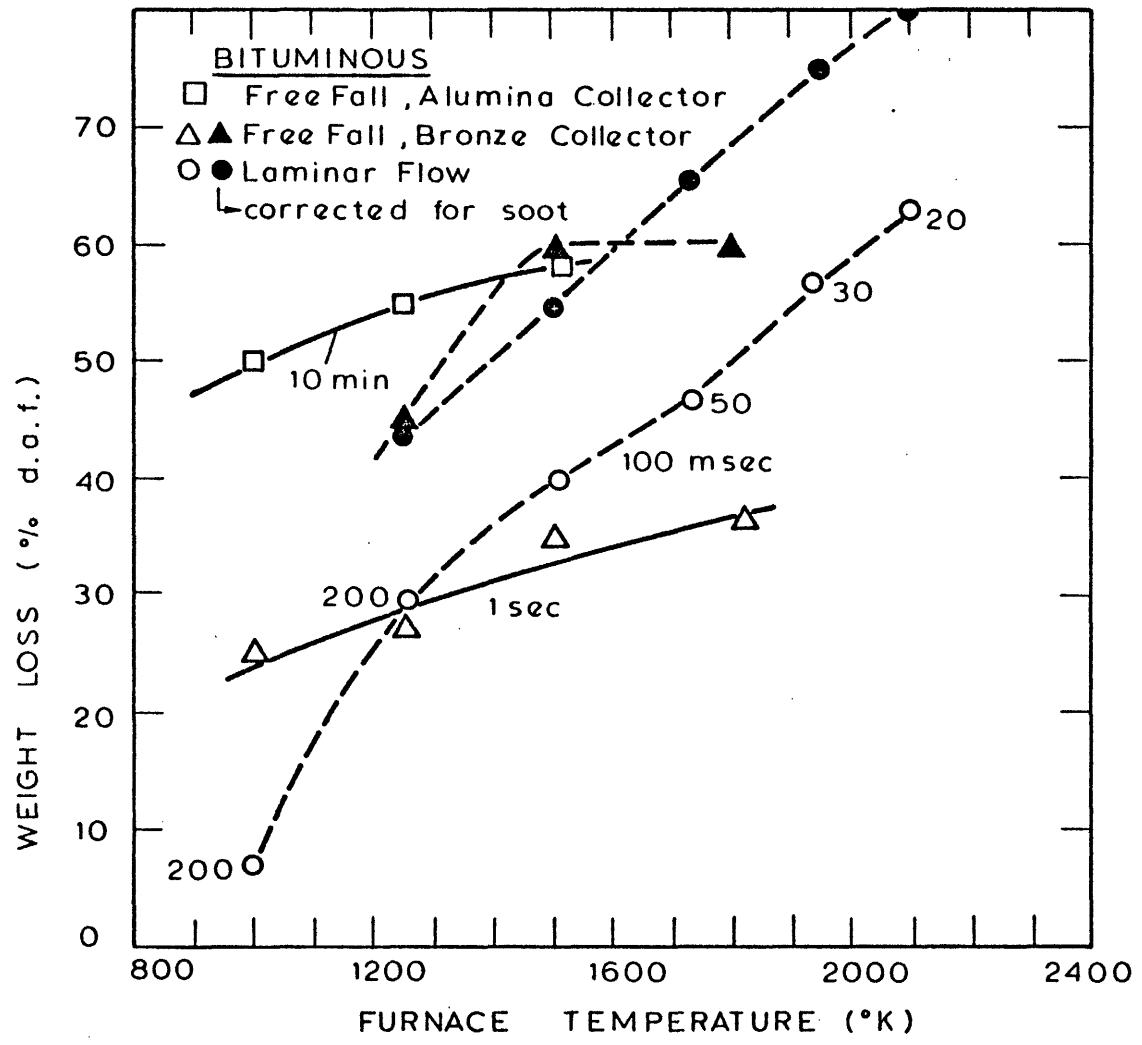


FIG. 4.6 MAXIMUM WEIGHT LOSSES OBSERVED UNDER DIFFERENT EXPERIMENTS, BITUMINOUS COAL.

runs, the results of the free fall runs may be interpreted as the approximate weight losses of the laminar flow experiment at longer reaction times. The apparent levelling-off's of weight loss curves observed under the laminar flow experiment (Figures 4.1 and 4.2) were found to be significantly lower than the asymptotic values of weight loss at long times. For lignite at 1510°K, about 30% was lost in 100 msec, 45% in 1 sec, and 57% in about 10 minutes. This implies that the rate of devolatilization during the first 100 msec is roughly 1 order of magnitude larger than that of the next 1 second period, and 3 orders of magnitude larger than that of the last 10 minute period. Such behavior is not peculiar to the present study, but observed by other groups at lower temperatures, (Shapatina, et al., 1960, Stone, et al., 1954). Elemental analysis of char from crucible experiments showed that less than 5% of original hydrogen and oxygen were retained in char after 10 minutes at temperatures above 1200°K. Hence, weight losses measured in the free fall experiment with alumina collector may be considered as approximate asymptotic values of weight loss at a very long reaction time.

The results for the bituminous coal are somewhat contradictory. Apparent weight losses in the free fall experiment in which the coal was collected on a bronze filter were lower than those obtained in a laminar flow experiment. This is considered to be caused by the extensive formation of soot and heavy tar. Since the gas flow rate in the free fall experiment was only a few liters per minute, practically all the soot formed during the devolatilization was trapped in the bronze collector. In the laminar flow experiment, however, large

amounts of gas (about 60 l/min STP) and quenching water (about 1 l/min) forced some of the soot and small particles through the pores of the filter. The amount of soot formed during the free fall experiment was estimated as mentioned before (Appendix C). Correction for soot in the laminar flow experiment was made by comparing the weight loss determined by ash-tracer method with that measured directly, which will be discussed in the next section. Weight losses corrected for soot are also shown in Figure 4.6. Reasonable agreement can be seen between the corrected weight losses obtained under the different experiments. It is noteworthy that about 80% of the d.a.t. bituminous coal was volatilized in about 25 msec at 2100°K. The trend indicates further weight losses at higher temperatures.

In contrast to this behavior, weight losses under slow heating conditions in the crucible experiment clearly reached asymptotic values close to those of ASTM proximate volatile test at around 1200°K for both coals (Figures 4.3 and 4.4). As the devolatilization reactions were considered to be completed in both cases, a conclusion that high temperatures alone can not enhance the volatile yield is drawn.

4.1.2. Weight Losses Determined by Using Ash as a Tracer and Ash Losses

In order to assure that losses of coal particles during the experiments are insignificant, char samples were analysed for ash content, following the ASTM specification, and weight losses calculated by using ash as a tracer were compared with the weight losses determined as the differences in weights of the coal fed and the char collected. The detailed results are tabulated in Appendices B, C and D.

Free Fall and Crucible Experiments

Figures 4.7 and 4.8 show the comparison of the two calculated weight losses under the free fall and the crucible experiments. The solid line in each figure represents perfect agreement of the two methods. Data points lower than the line generally indicate existence of either particle loss or ash loss, or both. Particle loss in the crucible experiment is very unlikely, as the coal is placed in a crucible and covered by a lid prior to heating. Good agreements of the bituminous coal below 1250°K confirmed negligible particle loss. At higher temperatures significant deviations resulted, indicating ash losses by decomposition and by vaporization of mineral matter. Results of free fall runs for the bituminous coal appeared to indicate small loss of particles (c.a. 3%), which is in agreement with the visual observation.

The results for lignite were somewhat different. About 5% discrepancy was found even at the lowest temperature. Since the furnace temperature of ASTM ash analysis is 750°C (particle temperature

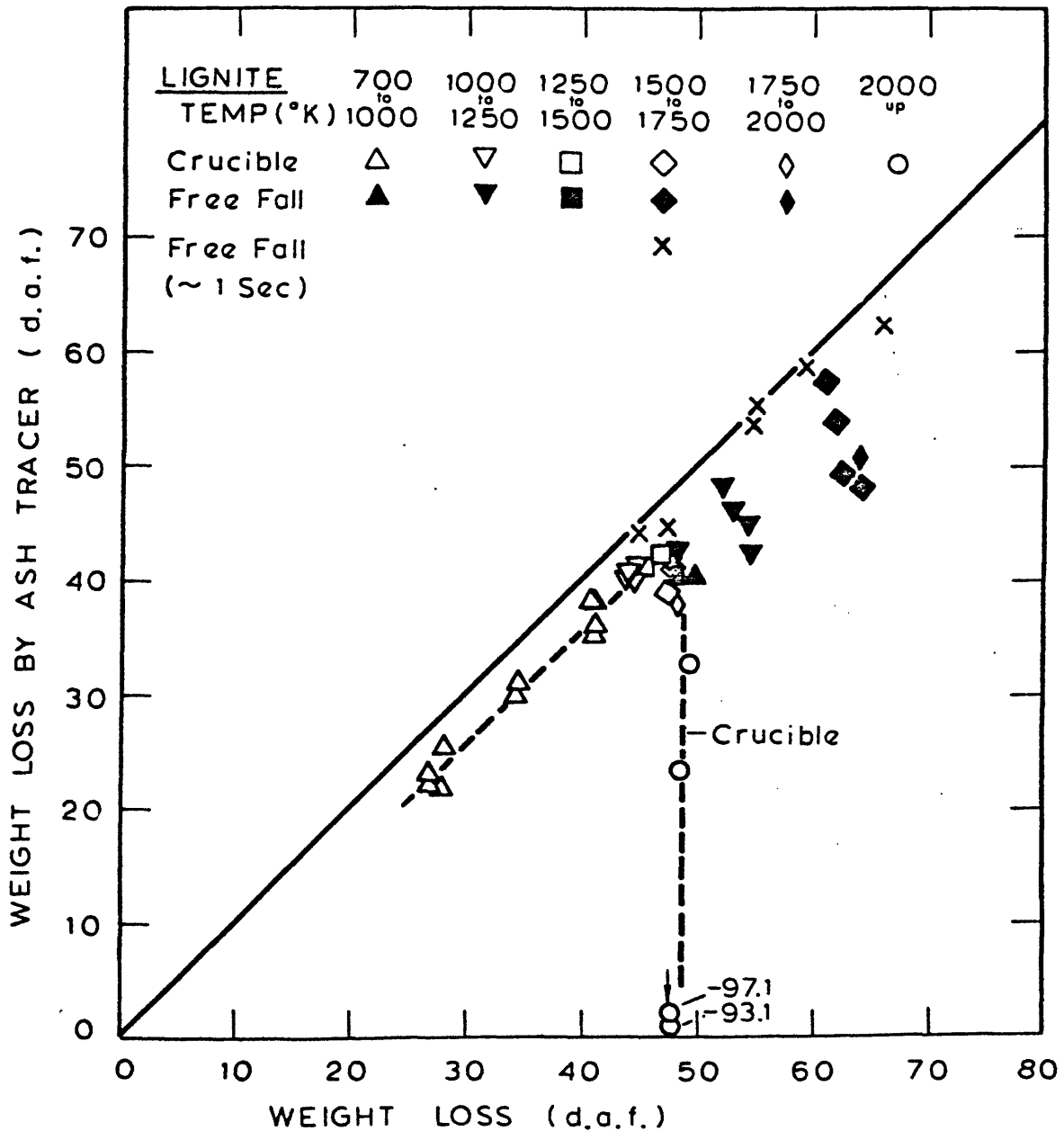


FIG. 4.7 COMPARISON OF DIRECTLY MEASURED WEIGHT LOSS WITH WEIGHT LOSS MEASURED BY USING ASH AS A TRACER IN FREE FALL AND CRUCIBLE EXPERIMENTS, MONTANA LIGNITE

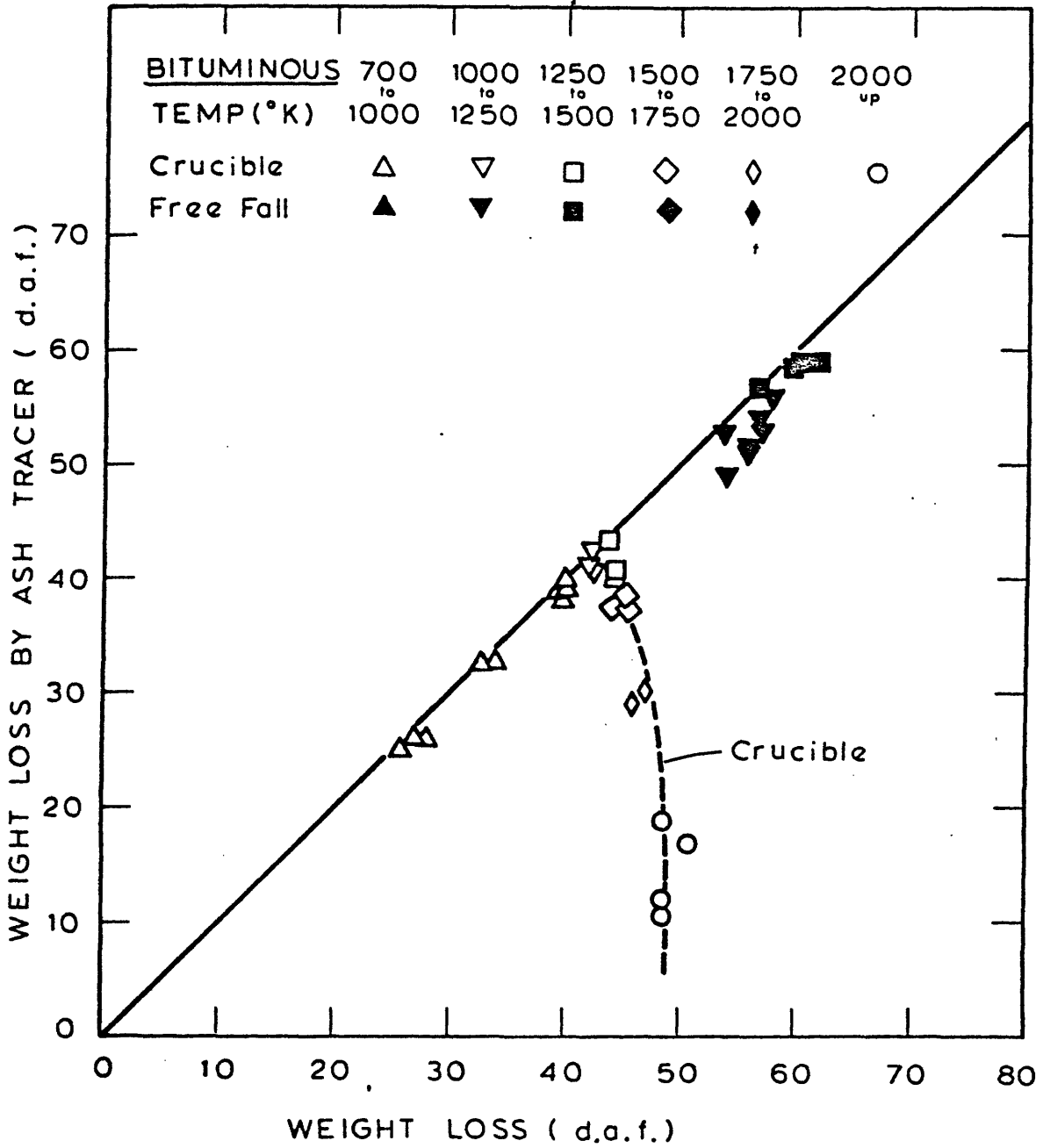


FIG. 4.8 COMPARISON OF DIRECTLY MEASURED WEIGHT LOSS WITH WEIGHT LOSS MEASURED BY USING ASH AS A TRACER IN FREE FALL AND CRUCIBLE EXPERIMENTS, PITTSBURGH SEAM BITUMINOUS COAL

are higher due to the heat of reaction), preheating of coal particles below that temperature was not considered, initially, to have caused ash loss by decomposition or by vaporization. The possibility of particle loss remained, as lignite is known to be a "sparking" coal. Since ASTM ash analysis requires heating of coal to 500°C in one hour and then to 750°C in two hours in an open crucible, devolatilization experiments at a lower heating rate should not cause any larger sparking than that which could occur during the ash analysis. To test this hypothesis, lignite coal was heated slowly to 740°K (467°C) in 1 1/2 hours and the char was analysed for ash content. (CR 264). The result showed 3.4% ash loss, which was similar to the other runs. This led to the conclusion that ash loss due to some chemical reactions, preferred in the inert atmosphere, occurred and made the discrepancy.

An extensive study of the ash behavior during combustion and devolatilization carried out using the same equipment supported the conclusion (Padia, 1976). This will be discussed in the next chapter.

The results of free fall runs with the bronze collector (about 1 sec residence time) for lignite show close agreements of the two methods, which may indicate that the decomposition reactions of ash are relatively slow in comparison with the devolatilization reactions. Larger discrepancies for free fall runs with the alumina collector are due both to ash loss and to particle loss. The contribution of ash loss could be estimated from crucible results at corresponding temperatures and reaction times. Weight losses plotted in figures 4.3

and 4.4 as "Free Fall, Ash Traces" were calculated through such procedures.

Ash Loss in Crucible Experiment

Assurance of negligible particle loss in the crucible experiment made it possible to evaluate the ash loss during devolatilization quantitatively. Figures 4.9 and 4.10 show the results. As indicated in Figures 4.7 and 4.8, ash losses increased rapidly above 1200°K, and reached to about 40% for bituminous and to about 80% for lignite at 2100°K. Average value of the ash losses below 1200°K for each coal is shown in each figure with the corresponding standard deviation. The measured ash losses were not the equilibrium values, as indicated by the increase with the reaction time. Therefore, evaluations of ash loss under pulverized coal flame conditions may require time resolved studies of ash loss.

Laminar Flow Experiment

Figures 4.11 and 4.12 show the comparison of the weight losses determined by the two independent methods. Larger scatter, compared with the results of the free fall and the crucible experiments (Figures 4.7 and 4.8) is evident, which is presumably caused by the smaller char samples of the laminar flow experiment used in the ash analysis (typically 10-50 mg, compared with 200-500 mg of free fall and crucible runs.). Deviations from the solid line increase with increasing temperature due to ash losses at higher temperatures. At first glance, deviations in the laminar flow experiment appeared to be significantly greater than those in the free fall experiment with the

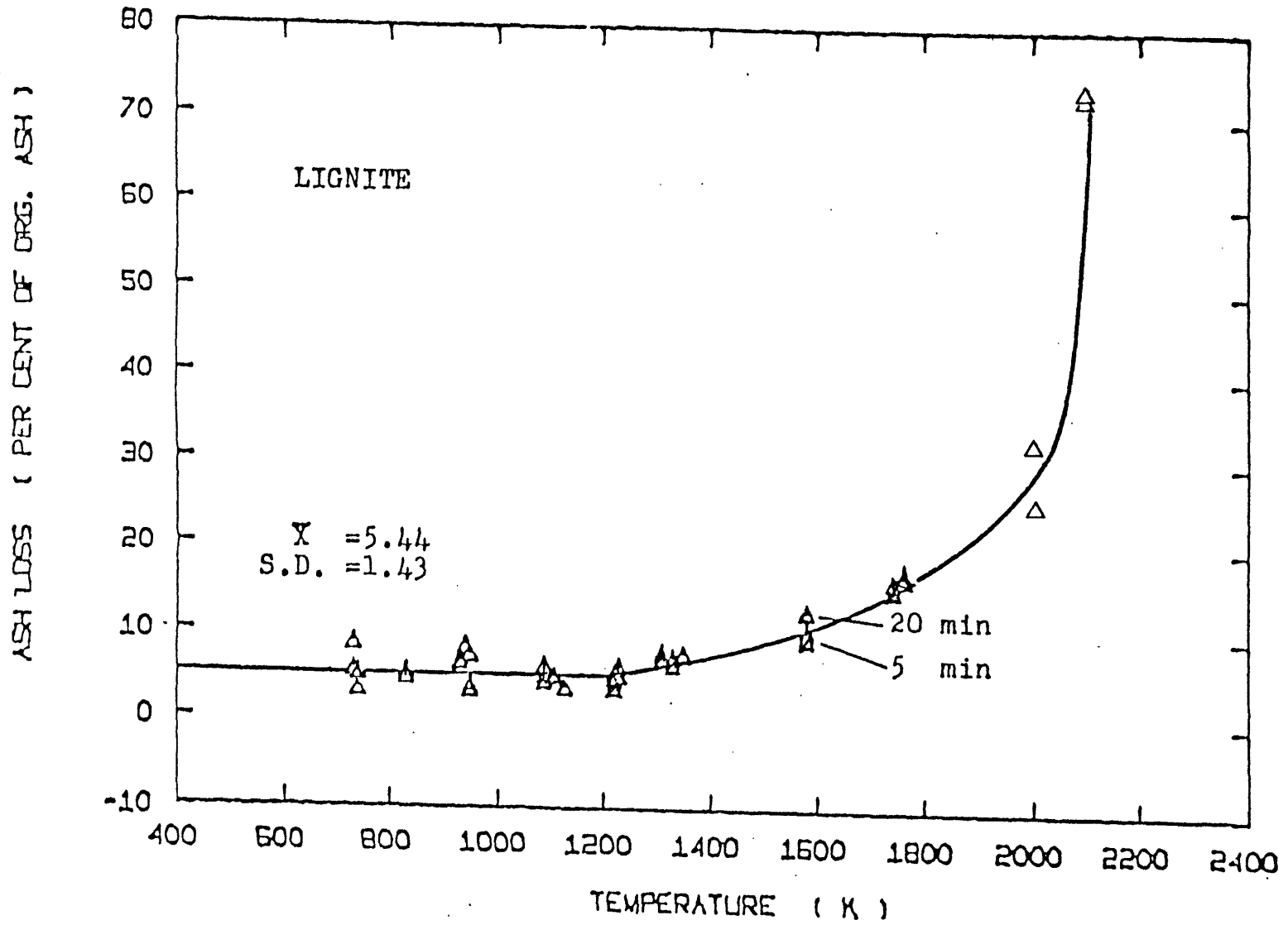


Figure 4.9 Ash Loss in Crucible Experiments (No Particle Loss Assumed)
Lignite

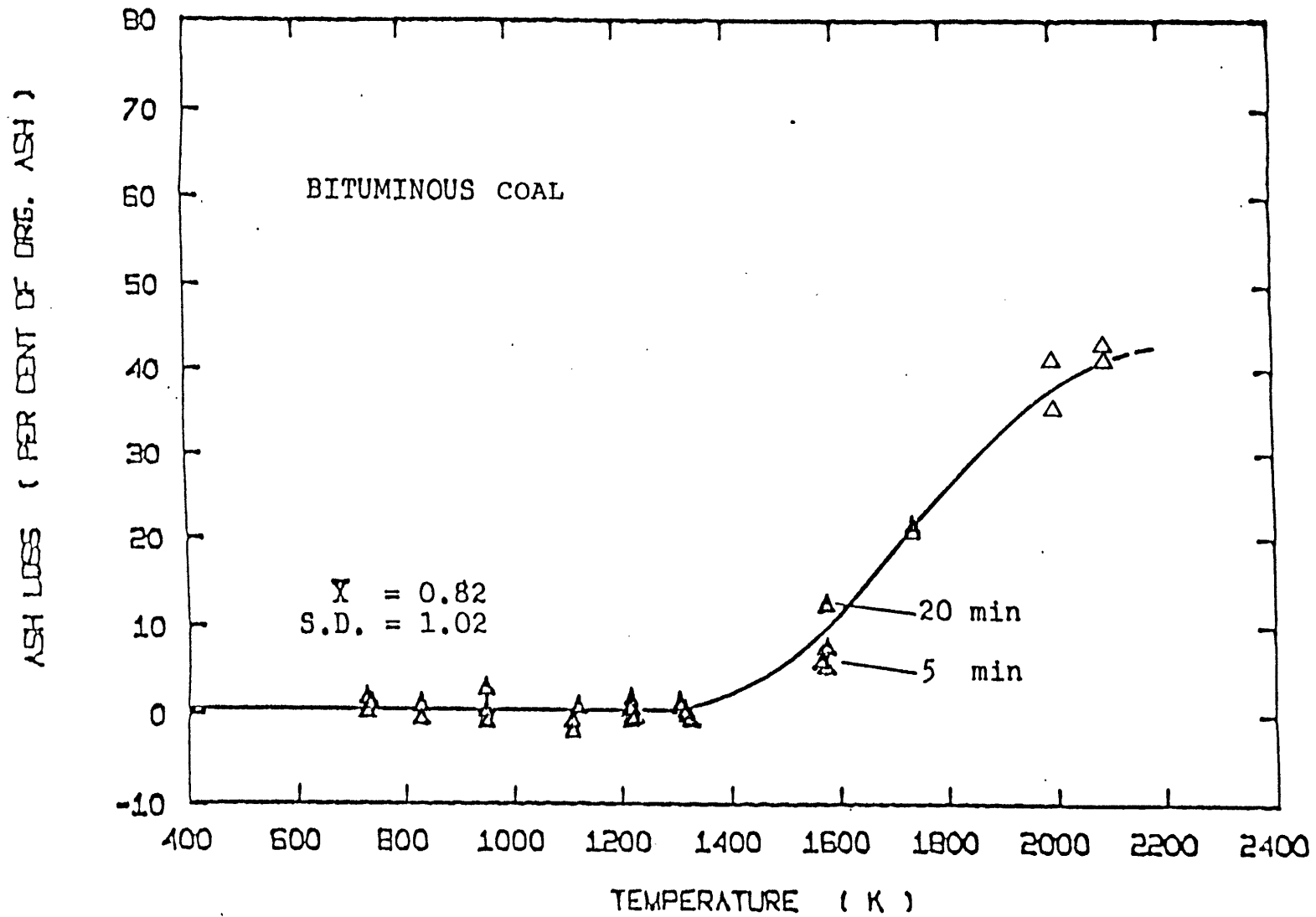


Figure 4.10 Ash Loss in Crucible Experiments (No Particle Loss Assumed) Bituminous Coal

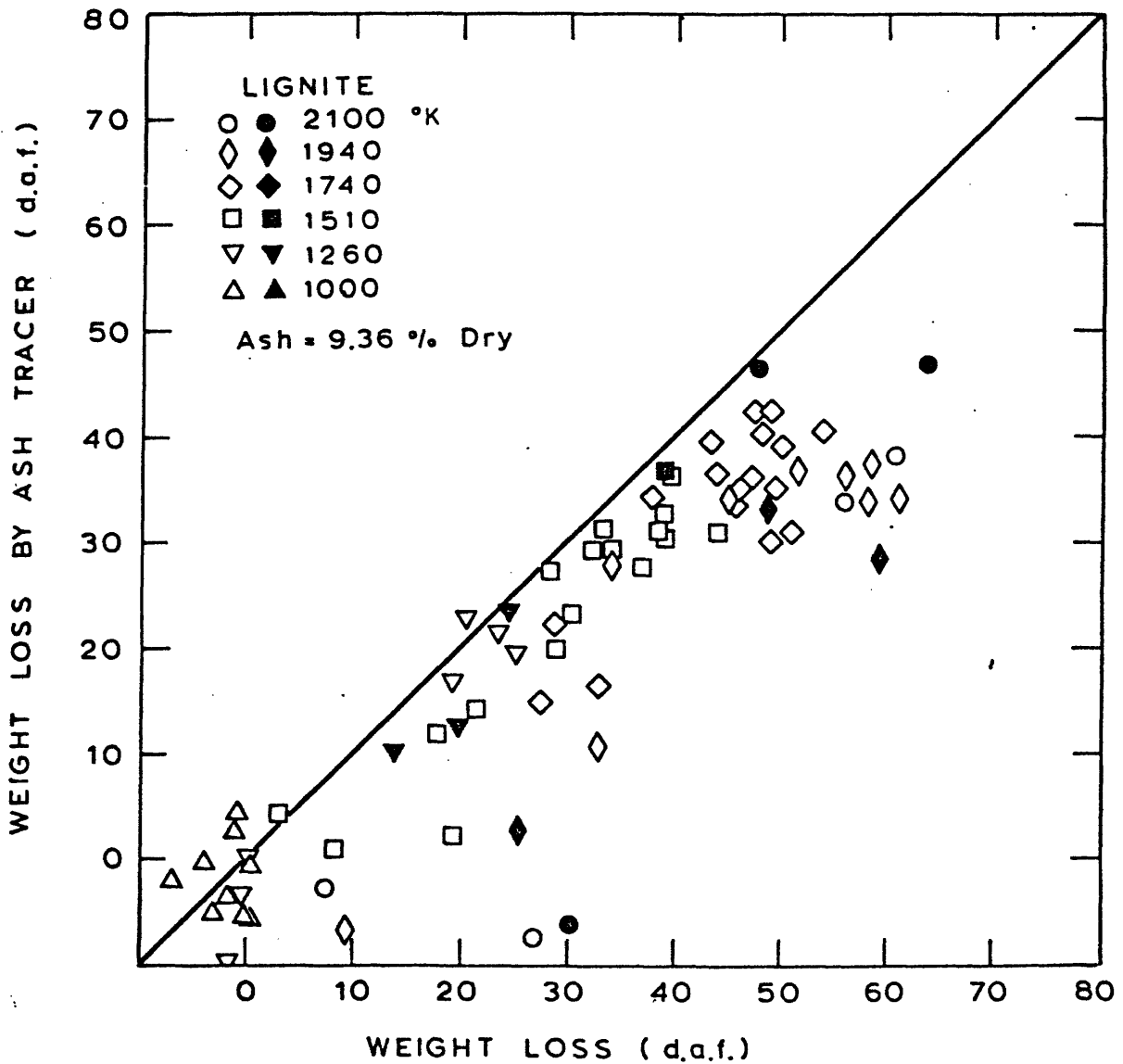


FIG. 4.11 COMPARISON OF DIRECTLY MEASURED WEIGHT LOSS WITH WEIGHT LOSS MEASURED BY USING ASH AS A TRACER IN LAMINAR FLOW EXPERIMENT, MONTANA LIGNITE.
 BLACK POINTS: ASH ANALYZED AT GALIBRAITH LAB. INC.
 KNOXVILLE, TENNESSEE
 WHITE POINTS: PRESENT STUDY

ASH CONTENT OF RAW COAL = 9.36% OF DRY COAL

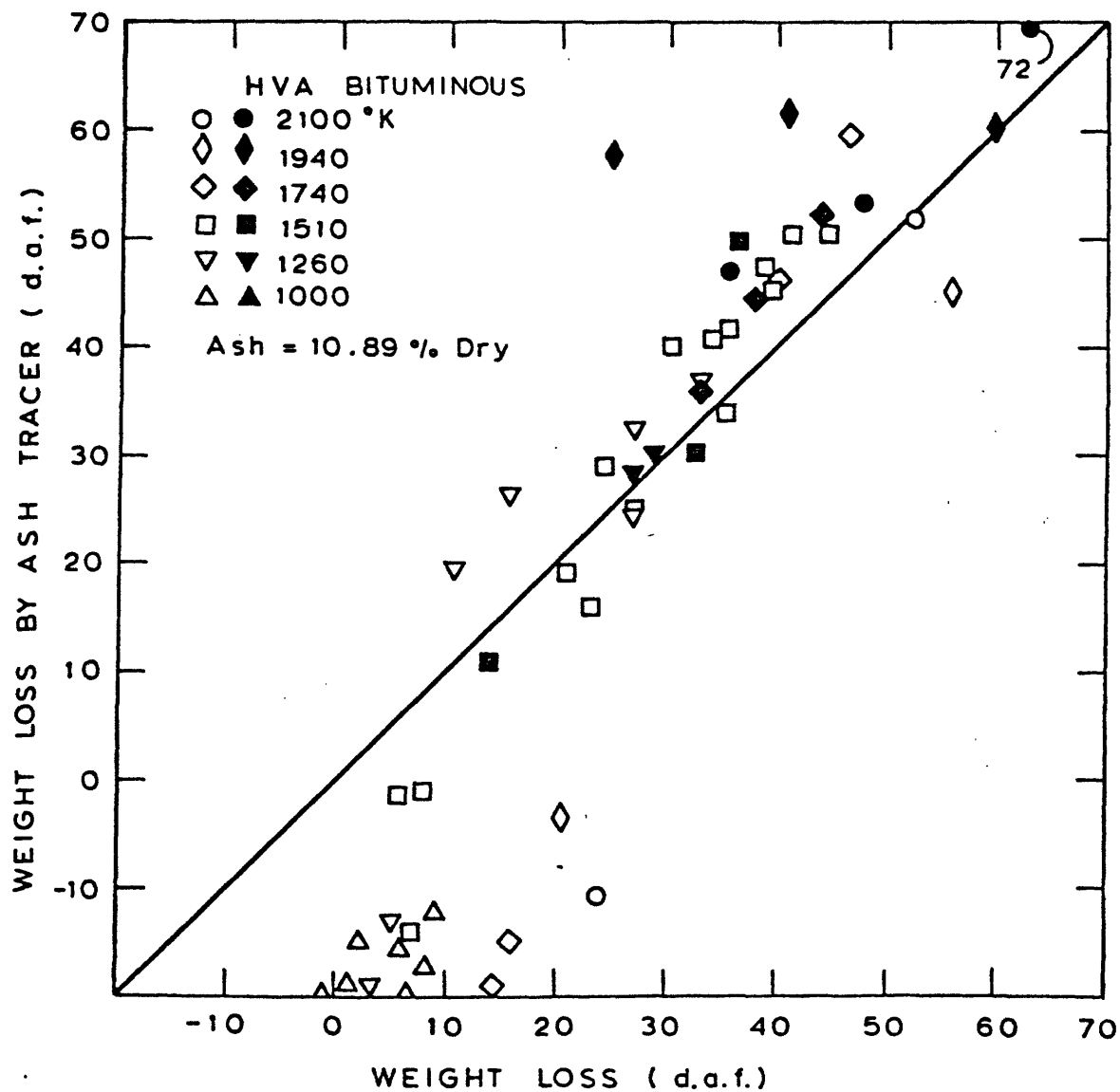


FIG. 4.12 COMPARISON OF DIRECTLY MEASURED WEIGHT LOSS WITH WEIGHT LOSS MEASURED BY USING ASH AS A TRACER IN LAMINAR FLOW EXPERIMENT, PITTSBURGH SEAM BITUMINOUS COAL. BLACK POINTS: ASH ANALYZED AT GALIBRAITH LAB. INC. KNOXVILLE, TENNESSEE
WHITE POINTS: PRESENT STUDY

ASH CONTENT OF RAW COAL = 10.89% OF DRY COAL

bronze collector (see Fig. 4.7 with symbol "x"). This is partly due to the fact that the temperatures of the coal particles in free fall runs are considerably lower than the peak furnace temperatures as discussed earlier. Another reason is the possible separation of ash particles under the laminar flow conditions. This will be discussed later.

The results for the bituminous coal show several distinct features: 1) Significant deviations at low weight losses; 2) deviations in the opposite direction at high weight losses; 3) no apparent differences in trend under different temperatures.

The lower (and negative) weight losses predicted by ash tracer could occur either by particle loss or by ash loss. Particle loss to account for the wide difference is unlikely, since the lignite coal did not show such effect. To examine the possible ash separation, several runs were performed for each coal under a simulated flow condition at room temperature. The collector was positioned directly below the injector tip to assure no particle loss outside the collector. The results showed about 5 percent particle losses for bituminous, about 2 percent particle losses for lignite, and ash concentrations of the coals removed from the filters were average 9.33 percent (dry basis) for bituminous and average 9.03 percent for lignite. This is interpreted as some of fine particles were "washed out" through the pores of the filter by the high flow of quenching water and the main gas. Scanning electron micrograph of the raw coals (Figs. 2.9 and 2.11) showed many fine particles of a few micron sizes especially for bituminous coal, some of which are considered to be separated ash particles. Although

the particle size distributions (Figs. 2.14 and 2.16) indicated negligible weight fractions below 5 micron in diameter, difficulties in counting fine particles from the pictures of coal particles and possible higher densities in fine particles seem to suggest the sizeable amount of fine particles. Littlejohn (1966) reported that considerable fraction of ash in coal exists as separate particles, not included inside the coal particles.

The larger weight losses predicted by ash tracer at high weight losses are considered to be caused by the preferential trapping of soot (and heavy tar) in the pores of the filter. Formation of large amount of soot for bituminous coal was discussed in section 4.1.3. Visual observations and rapid clogging of filters detected by rapid increases in the pressure drop across the filters under these conditions prove the hypothesis. The char samples removed from the filters necessarily have smaller amounts of soot, hence the weight losses determined by using the ash of the char removed from the filter as a tracer gives lower limits of "true" weight losses corrected for soot formation. If we assume that the same amount of ash particle separation as that observed in the simulated experimental conditions at room temperature occurs during the devolatilization experiment, the lower ash concentrations instead of the original ash concentrations should be used as the reference values in the ash tracer method. Figures 4.13 and 4.14 show the results with the lower ash values. About 75 percent weight loss is estimated from the ash tracer method as a corrected value for soot when apparent weight loss is about 60 percent. As the perfect separation of

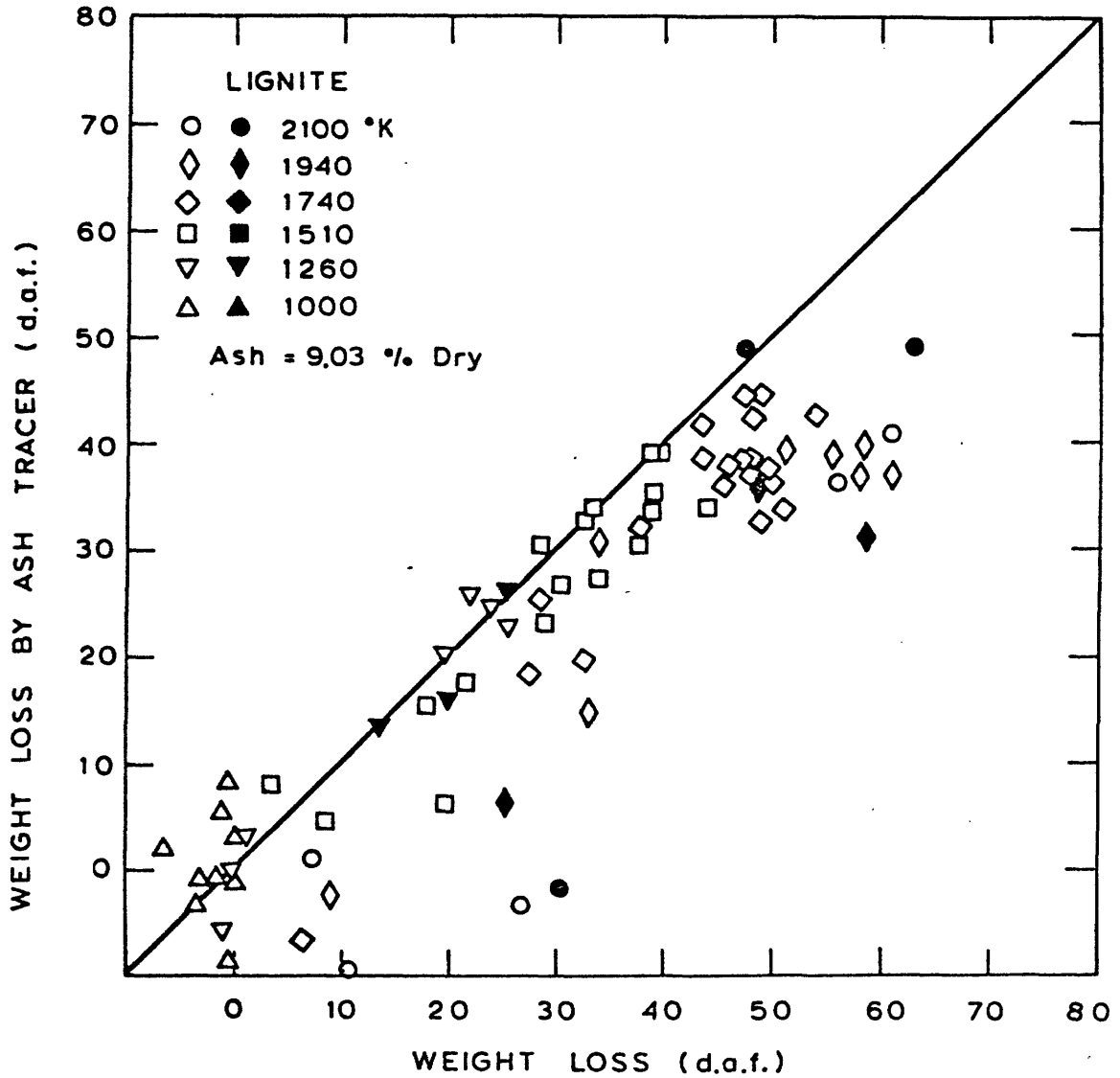


FIG. 4.13 COMPARISON OF DIRECTLY MEASURED WEIGHT LOSS WITH WEIGHT LOSS MEASURED BY USING ASH AS A TRACER IN LAMINAR FLOW EXPERIMENT, MONTANA LIGNITE.
 BLACK POINTS: ASH ANALYZED AT GALIBRAITH LAB. INC. KNOWVILLE, TENNESSEE
 WHITE POINTS: PRESENT STUDY
 ASH CONTENT OF RAW COAL = 9.03% OF DRY COAL

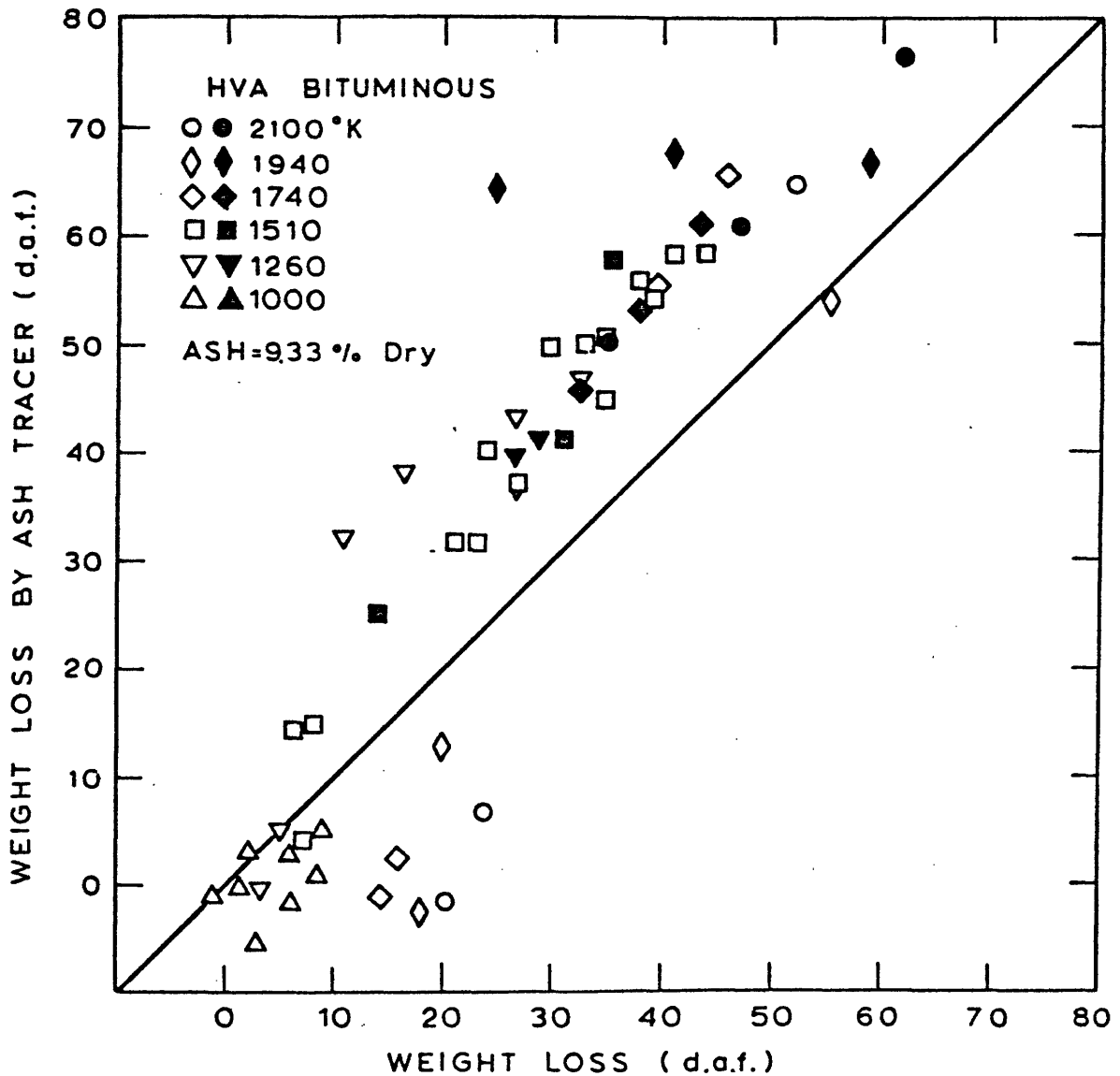


FIG. 4.14 COMPARISON OF DIRECTLY MEASURED WEIGHT LOSS WITH WEIGHT LOSS MEASURED BY USING ASH AS A TRACER IN LAMINAR FLOW EXPERIMENT, PITTSBURGH SEAM BITUMINOUS COAL. BLACK POINTS: ASH ANALYZED AT GALIBRAITH LAB. INC. KNOWVILLE, TENNESSEE
WHITE POINTS: PRESENT STUDY

ASH CONTENT OF RAW COAL = 9.33% OF DRY COAL

soot and char in the filter is unlikely, any allowance for the soot removed with char would increase the estimates, while possible agglomeration of fine particles would reduce ash separation, resulting in lower estimates of weight loss.

No apparent differences in trend under different temperatures seems to indicate that ash losses are small even at the high temperatures due to the short residence times. Hence, Fig. 4.14 may be used to estimate the approximate values of weight losses corrected for soot for the bituminous coal.

4.1.3 Effects of Sample Size on Weight Loss in Crucible Experiment

One of the mechanisms proposed for explaining the enhance volatile yields obtained under rapid heating conditions is that secondary reactions between the initial volatile matter and the char surfaces lead to additional char formation. Devolatilization in a packed bed at a slow heating rate could cause significant interactions of the volatile matters with the surfaces of the char particles and with the container walls, resulting in the formation of solid residue. The extent of formation of solid residue (presumably carbonaceous matter formed by thermal cracking of volatile matter) on the crucible walls or on the alumina collector walls was measured quantitatively in the free fall experiment with alumina collectors and in the crucible experiment. For lignite, the deposit formed in the crucible runs was negligible (Table D.1), but in some of the free fall runs (Table C.2) it amounted to 2 percent of the original coal weight. Larger yields of solid deposit were measured for bituminous coal. 2 ~ 3 percent of the weight

(d.a.f.) of the raw coal was converted into this solid residue in some of the crucible runs (Table C.2), and more than 5 percent in some of the free fall runs (Table C.3). These results imply formation of solid residue on the surface of the coal particle. In order to evaluate this effect, a set of experiments was conducted by changing the bed depth of coal particles in crucible at 1220°K. Three different types of crucibles were used: Alumina Highform (Coors CH-16, 15 ml), Alumina cylindrical (Coors CN-10, 40 mm O.D. x 10 mm H) and Glazed Porcelain (Coors Highform 15 ml, top dia. 35 mm, bottom dia. 18 mm, height 29 mm). The experimental procedures were the same as in the other crucible experiment (Section 2.5). The temperature-time history during devolatilization is represented by CR 220 in Fig. 2.7. The sample size ranged from about 2 gm to as little as 10 mg. Figures 4.15 to 4.17 show the results. The details of each run are shown in Tables D.4 and D.5. For small sample sizes the shallow cylindrical crucibles were used to get smaller bed depth. In Table 4.1 average weight losses and standard deviations for different size groups are shown. A 1-gram sample has about 120 particle layers and a 30 milligram sample in the shallow crucible has average 1 particle layer.* Lignite gave somewhat lower weight losses for smaller samples. Small samples, however, had larger scatter in weight losses because the experimental accuracy decreased, and the average value lay well within one standard deviation. Therefore, the

* An electrical vibrator was used to distribute the particles uniformly on the bottom surface of the shallow crucible.

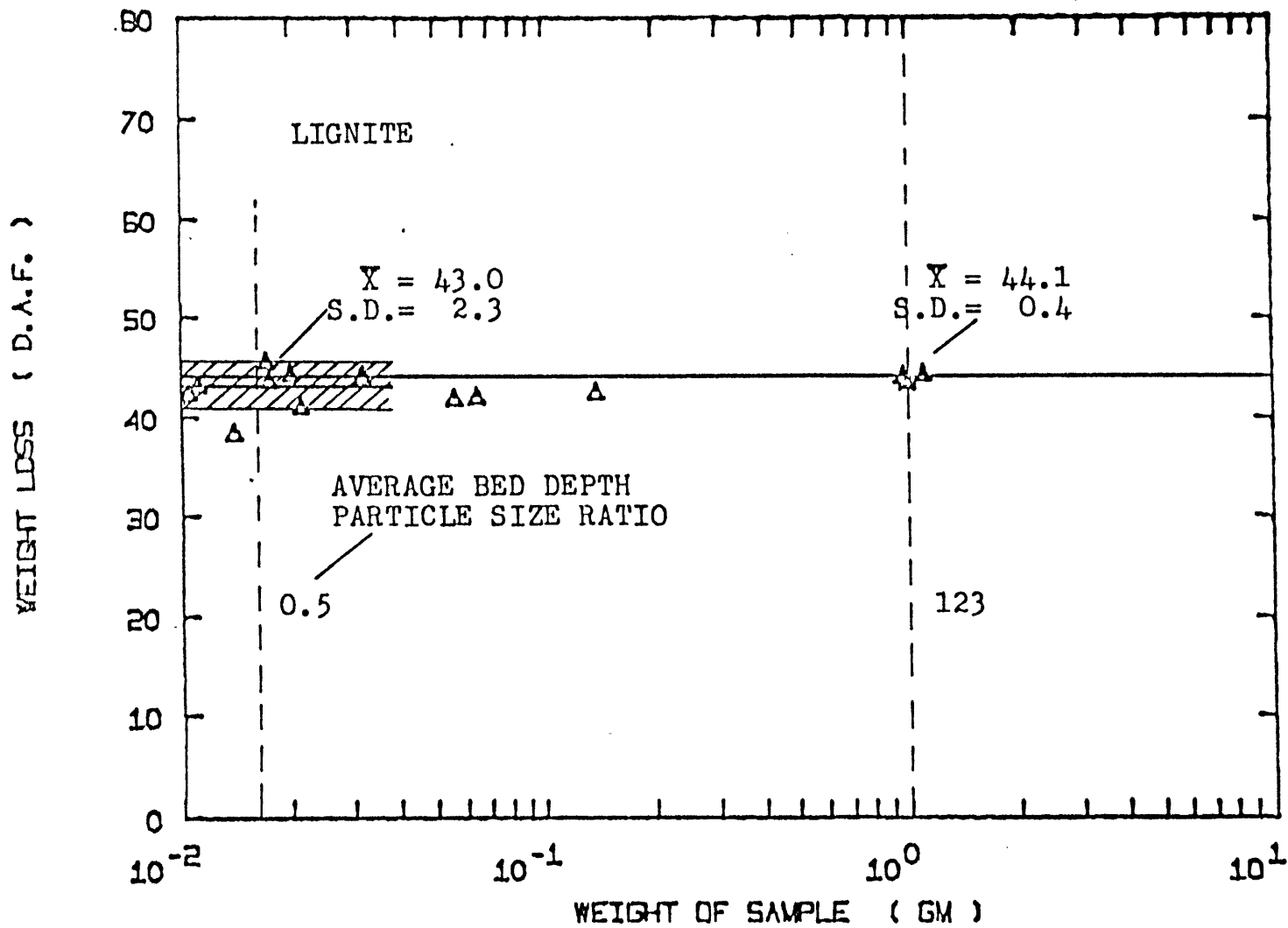


Figure 4.15 Weight Loss of Different Sample Sizes in Crucible Experiments
 Lignite Peak Temperature 1220 K
 (Weight Loss compensated for thermal cracking and ash loss)

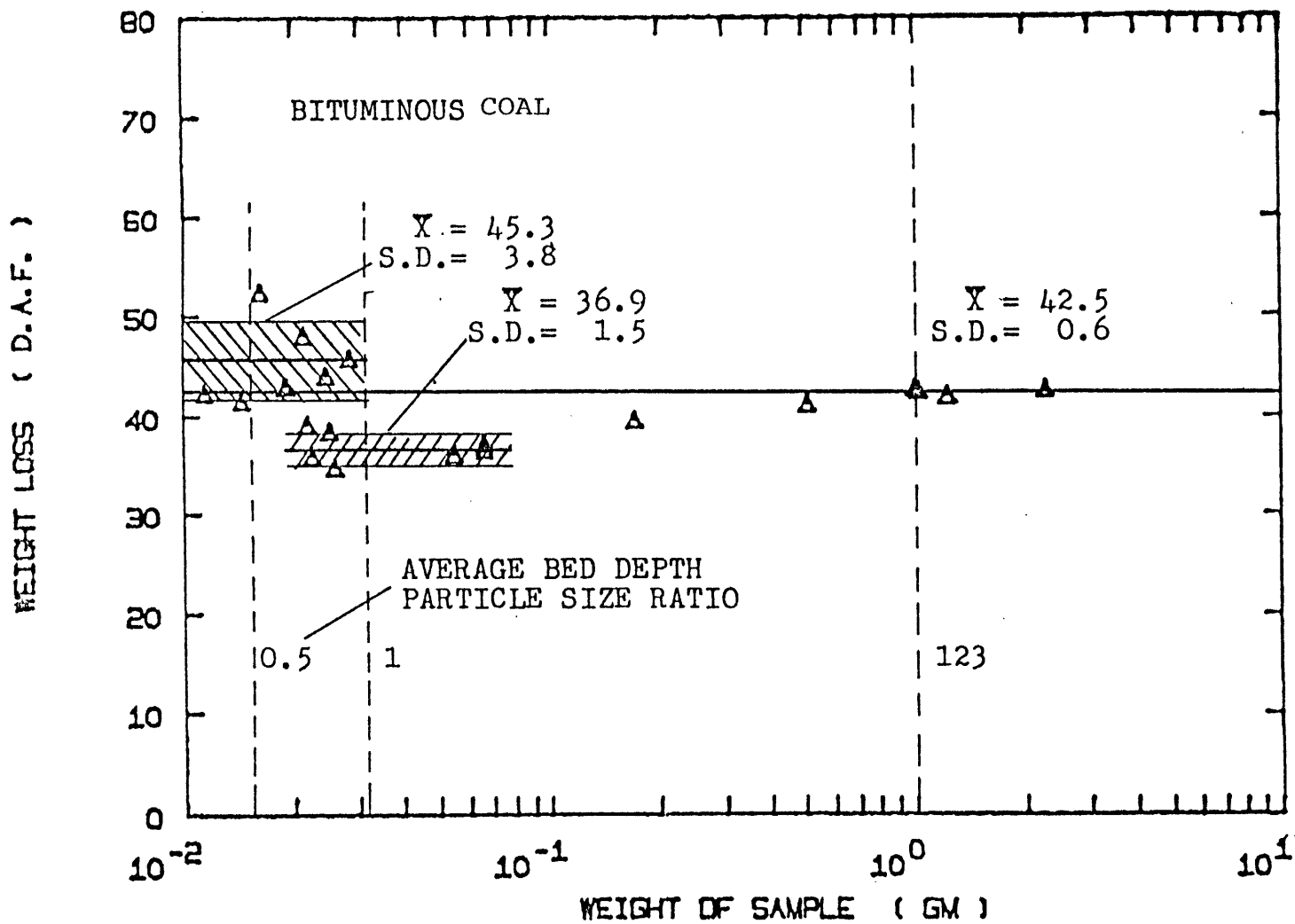


Figure 4.16 Weight Loss of Different Sample Sizes in Crucible Experiments
 Bituminous Coal Peak Temperature 1220 K
 (Apparent Weight Loss)

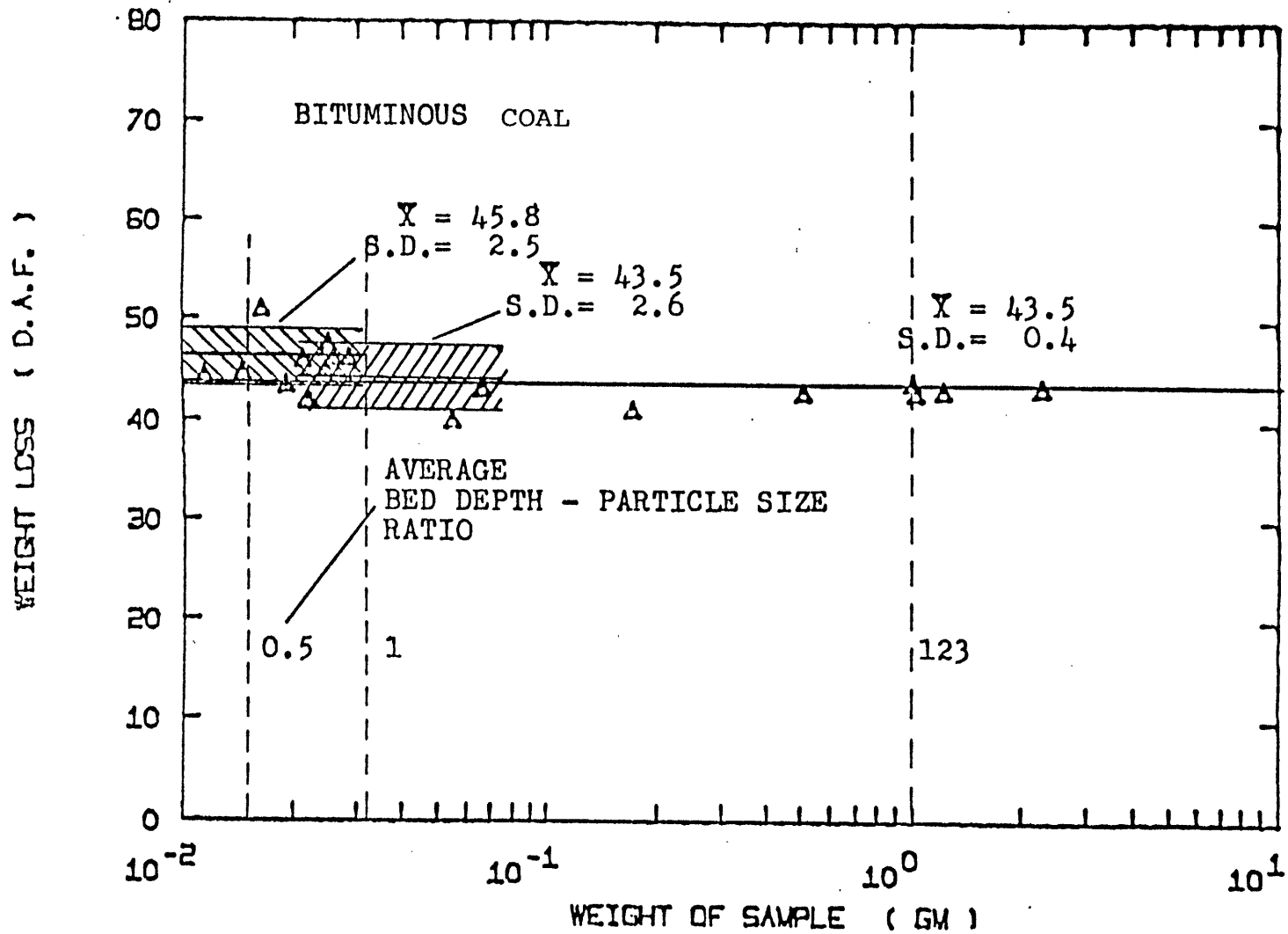


Figure 4.17 Weight Loss of Different Sample Sizes in Crucible Experiments
 Bituminous Coal Peak Temperature 1220 K
 (Weight Loss compensated for thermal cracking)

Table 4.1

Measured Weight Loss of Different Sample Sizes in Crucible Experiments at 1220 K

	Number of Runs	Apparent Weight Loss		Weight Loss T.C. (1)		Weight Loss T.C., A.L. (2)	
		Mean	S.D.	Mean	S.D.	Mean	S.D.
BIT. SMALL (A) (0.01 - 0.03 gm)	7	45.3	3.8	45.8	2.5	46.7	2.6
BIT. SMALL (B) (0.02 - 0.06 gm)	7	36.9	1.5	43.5	2.6	43.9	2.7
BIT. LARGE (1. - 2 gm)	4	42.5	0.6	43.4	0.4	43.4	0.3
LIG. SMALL (A) (0.01 - 0.03 gm)	8	44.1	4.4	42.9	2.3	43.0	2.3
LIG. LARGE (c.a. 1 gm)	4	44.6	0.4	44.6	0.5	44.1	0.4

160

(1) Weight loss compensated for thermal cracking

(2) Weight loss compensated for thermal cracking and ash loss

(A) Alumina cylindrical crucibles were used.
(Coors CN-10, 40 mm O.D., 10 mm Hight)

(B) Glazed Porcelain crucibles were used.
(Coors High form 15 ml, top dia. 35 mm, bottom dia. 18 mm, 29 mm hight)

S.D. Standard deviation evaluated by $N - 1$

difference is not statistically significant. Figure 4.16 shows apparent weight loss of bituminous. There was a distinct difference between the two different small size groups. Small size group (B) (sample size 20 to 60 milligram) were run by the glazed porcelain crucibles, and the other group (A) (sample size 10 to 30 milligram) by the alumina cylindrical crucibles. Both highform alumina and glazed porcelain crucibles are used for the large sample group, but no appreciable differences were observed. The apparent lower weight loss of the small size group (B) appeared to be caused by thermal cracking of the volatile matter on crucible surface. As the sample size becomes smaller, the ratio of the crucible surface to the volatile matter, which show potential for char formation, becomes large and therefore relatively more extensive cracking could occur. Visual observations supported this. Soot-like material coated both inside and outside of the crucible when large samples were used, indicating that some of the potential char producing volatiles escaped. As the sample size decreased, the coating on the outside wall diminished and almost no deposit was found for the small size group (B), indicating most of the potential char-producing volatiles cracked on the inside wall. The coating obtained with the small size group (A), however, was very thin and shiny. This could be due to the differences in catalytic effects of the walls. Weight loss values compensated for thermal cracking on the crucible wall are shown in Fig. 4.17. The method for measuring the deposits formed on the crucible walls is described in section 3.3. With the compensation the average weight loss of small size group (B) became almost the same as

the large size group. Small size group (A) gave about 2 percent increase in weight loss on the average, but the statistical significance is not so strong (about one standard deviation).

4.2 Loss of Major Elements

Representative char samples from different experiments were analyzed for their elemental compositions. All the ultimate analyses were performed by Galibraith Laboratories, Inc., Knoxville, Tennessee. Moisture, carbon, hydrogen, nitrogen, total sulfur and ash were measured. Organic, pyritic and sulfate sulfur were analyzed separately in some of the chars. Oxygen was determined by difference.

Figures 4.18 and 4.19 show the retention of each element in char as a function of time for all runs. The retentions were calculated from the original composition of the elements, the measured overall weight loss, and the composition of the elements in char. Since the temperature time histories and other conditions were significantly different between the crucible runs and the laminar flow runs, the results of the crucible runs should not be interpreted as the extension of corresponding laminar flow runs at long residence times. The results of the free fall experiment with bronze collector are plotted at 1 sec (10^3 milliseconds) residence time, which may be compared with the corresponding laminar flow runs. The residence time for the free fall runs is based on the particle velocities measured by the laser doppler anemometer (Figure 3.6), which showed that the particle velocity is about 20 cm/sec in the 20 cm "hot zone". The details of each run are tabulated in Appendix E. Although only limited number of samples were

PERCENT OF ELEMENT RETAINED IN CHAR
MONTANA LIGNITE

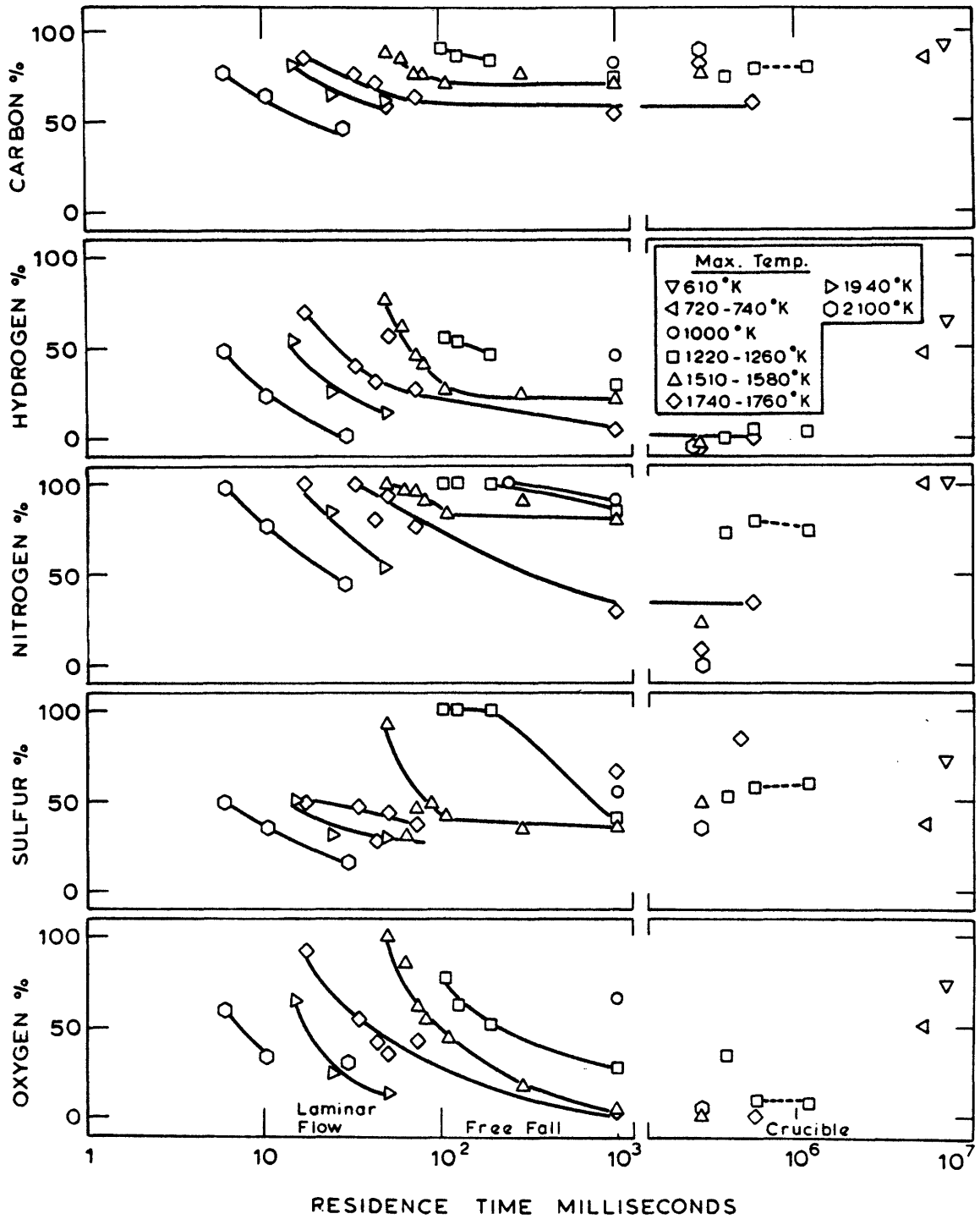


FIG. 4.18

PERCENT OF ELEMENT RETAINED IN CHAR
PITTSBURG SEAM # 8 BITUMINOUS COAL

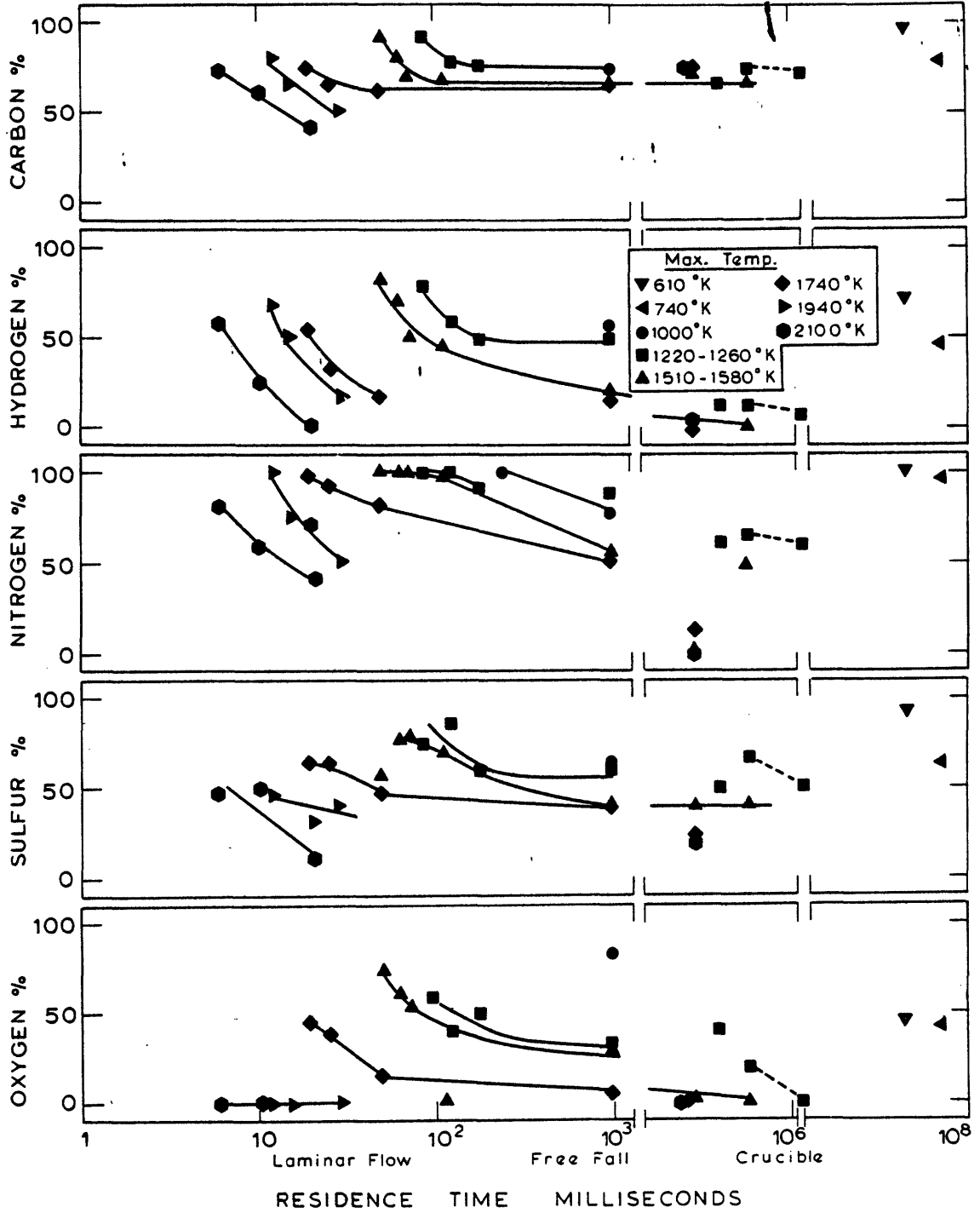


FIG. 4.19

analyzed at each furnace temperature, the overall trends of carbon, hydrogen, nitrogen and oxygen are clearly seen for the two coals. Both rates and final losses of elements increased with temperatures within the laminar flow range. The results for sulfur show more scatter than those for the other elements which might be due to some interactions of organic and inorganic sulfur. Among these elements, oxygen and hydrogen were most readily removed. At 2100°K, essentially all of oxygen and hydrogen were lost in about 20 msec, while about 50% of nitrogen was still retained. The asymptotic values for carbon retention decreased with increasing temperature, as would be expected from the increased volatile yields with increasing temperature.

In Figures 4.20 and 4.21, the retentions in the crucible experiment are plotted against the peak temperatures. The reaction times at the peak temperature ranged from about 5 min at 1750°K to 12 hours at 600°K. Weights of char (% d.a.f. weight of the raw coal) are also shown, providing a reference curve to which preferential losses or retentions of the elements may be compared. Char from the ASTM proximate analysis was also analysed for comparison, which essentially proved the earlier statement that the crucible runs at 1220°K provide a reasonable approximation to the standard ASTM proximate analysis. As was the case in the laminar flow runs, hydrogen and oxygen were preferentially lost. At 1200°K and about 10 minutes of reaction time, only about 10% of the hydrogen and oxygen were retained, which explains the observation that weight loss reached an asymptotic value at around 1200°K. Nitrogen exhibited a marked difference. At low temperatures no

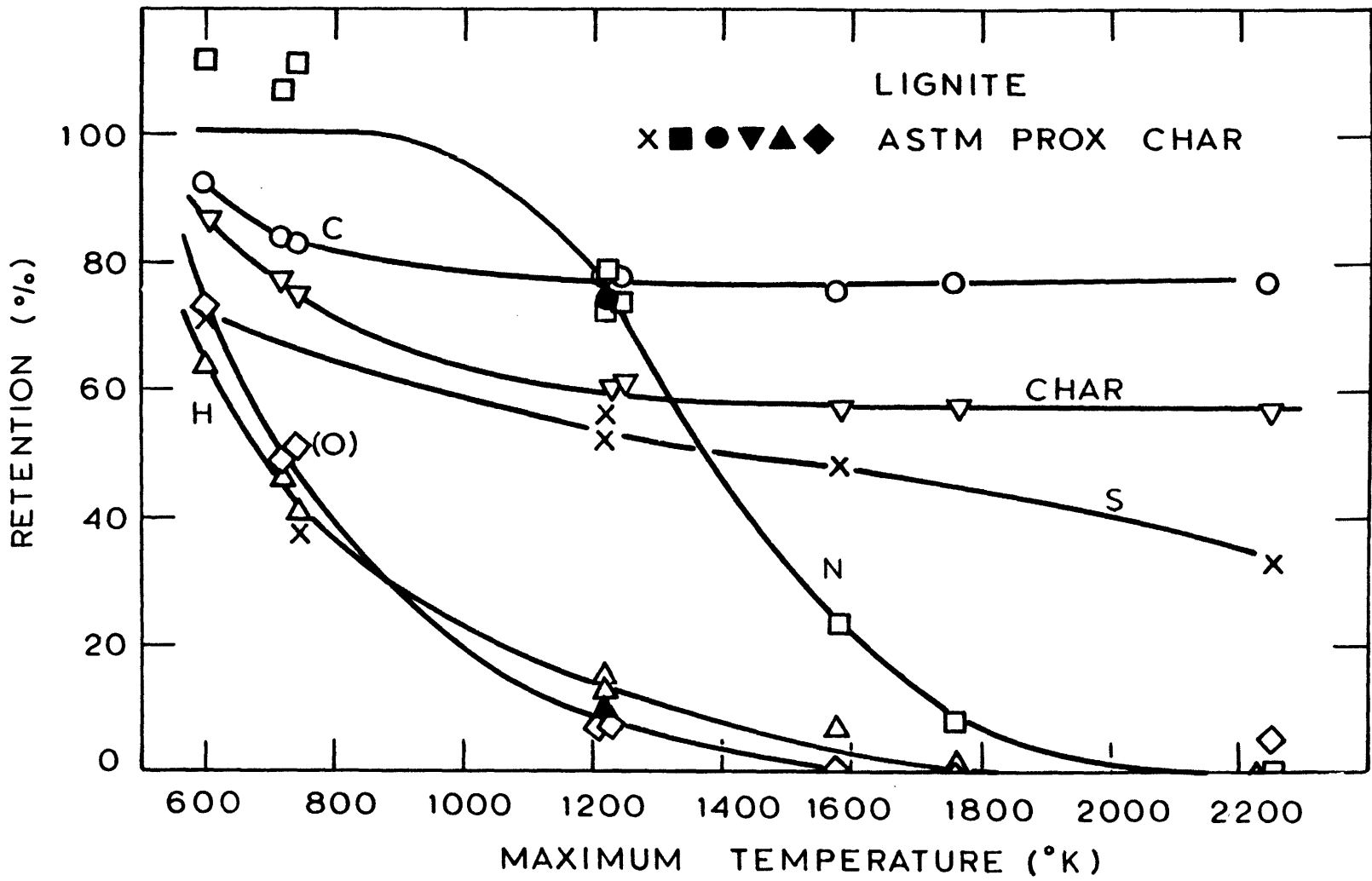


FIG. 4.20 ELEMENTS RETAINED IN CHAR IN CRUCIBLE EXPERIMENT, MONTANA LIGNITE

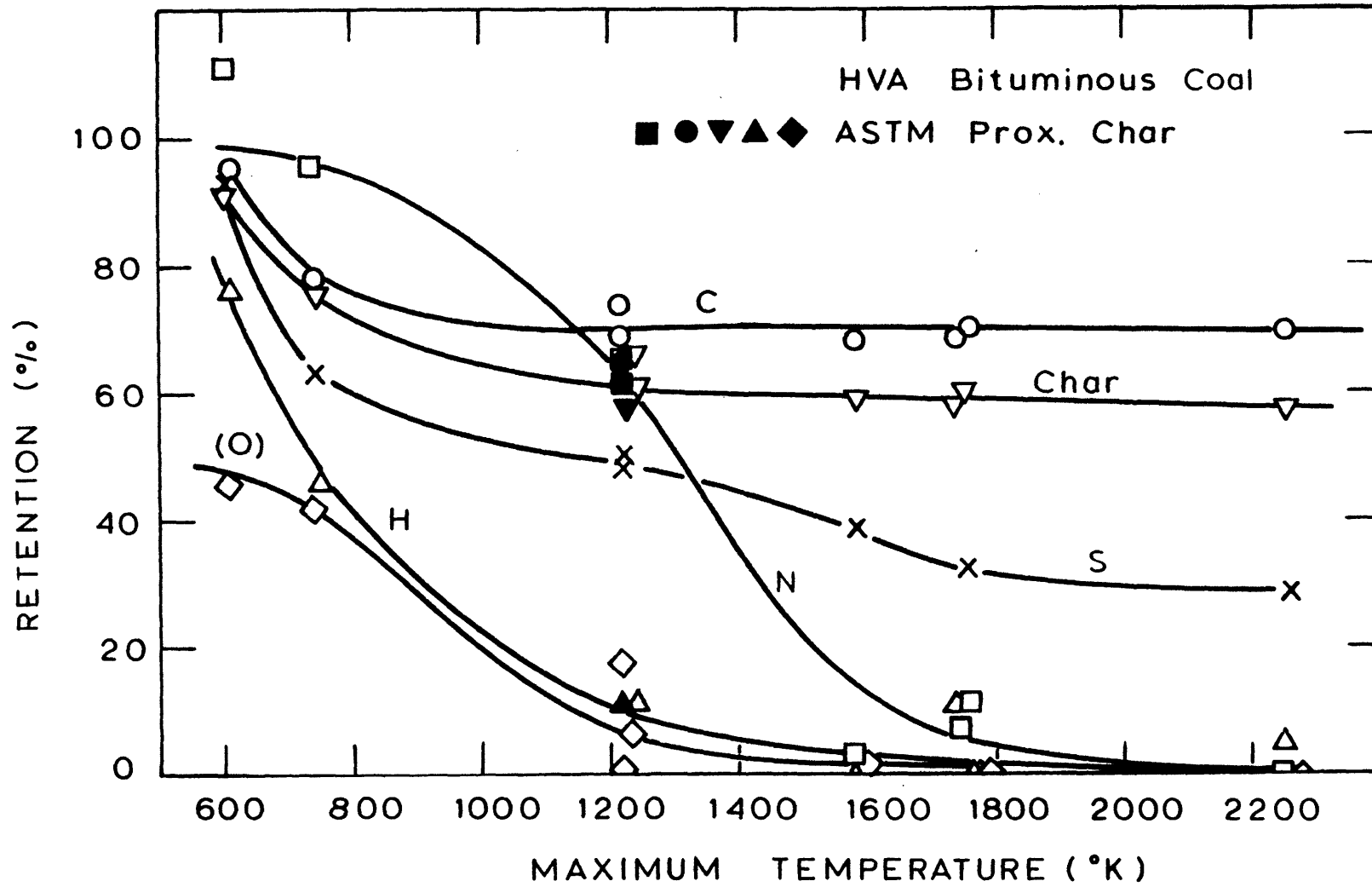


FIG. 4.21 ELEMENT RETAINED IN CHAR IN CRUCIBLE EXPERIMENT
PITTSBURGH SEAM BITUMINOUS COAL

nitrogen* was lost when about 20% of carbon was lost, while at high temperatures it was completely removed. About 40% of the sulfur was lost at about 800°K, but more than 30% was retained even at the highest temperature, which is in contrast to hydrogen, oxygen and nitrogen. Since both organic and inorganic sulfurs were included, the result requires special interpretations.

Comparisons of the elemental compositions of chars at a given level of devolatilization (i.e. at the same weight loss), but from different devolatilization conditions are of interest as they might provide insight on the mechanism of devolatilization. Figures 4.22 and 4.23 show the retention of the major elements plotted against weight losses (d.a.f.). For the bituminous coal, weight losses were corrected for soot using Figure 4.14. As mentioned in section 4.1.2, most of the soot formed during the devolatilization either escaped through or was captured in the pores of the filter. Hence the char samples taken out from the filters had little soot, whose weight losses are considered to be more representative by those determined by the ash tracer method. The corresponding figures based on the apparent weight losses are shown in Appendix E for comparison.

Both crucible runs and laminar flow runs are shown in the same figure. The solid diagonal shows nonpreferential retention

* Retentions greater than 100% might have resulted from the promotion of the digestion of coal in analysing coal by the Kjeldahl method after the mild "heat treatment" in the experiment.

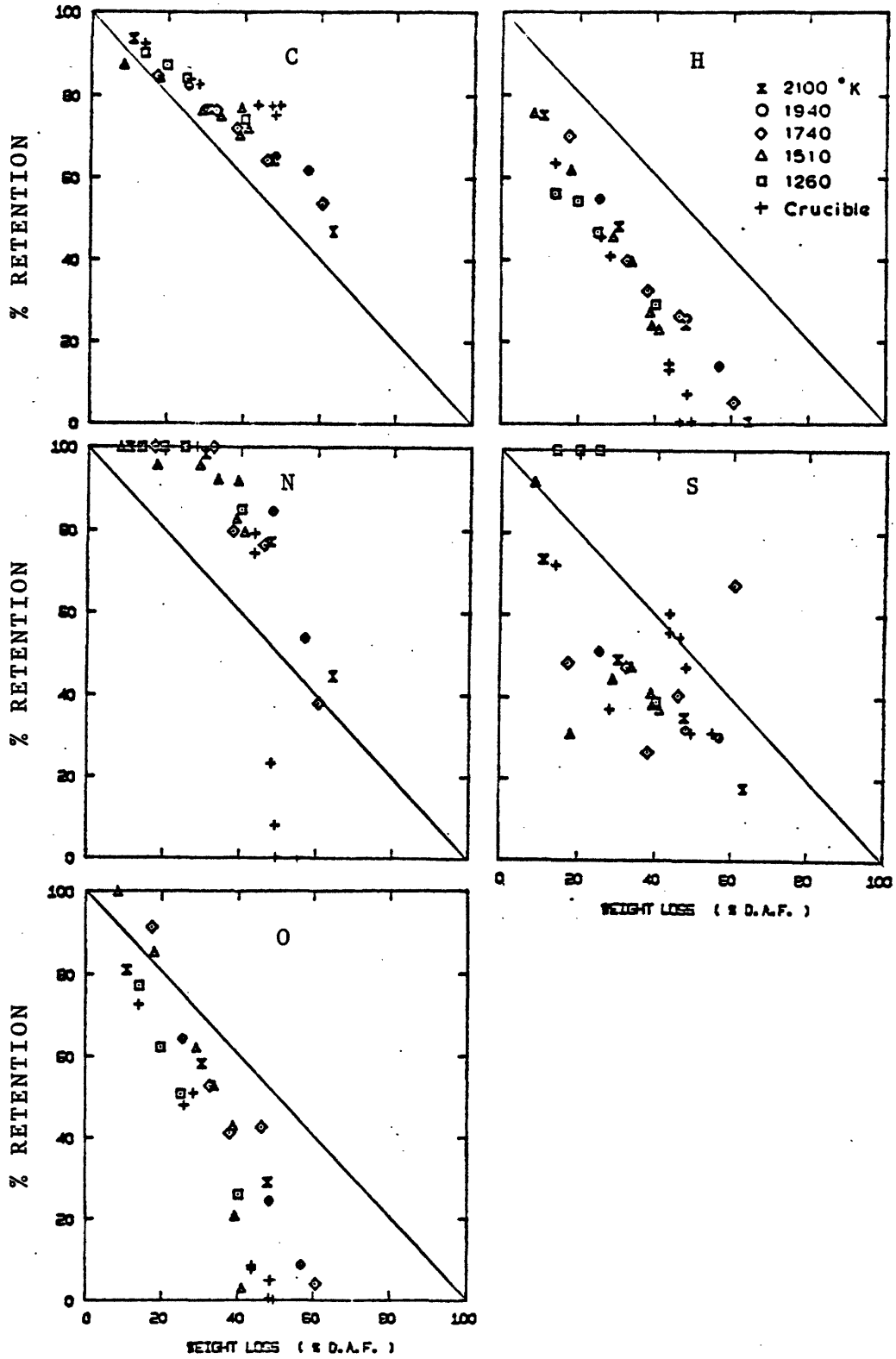


FIGURE 4.22 ELEMENTS RETAINED IN CHAR AT DIFFERENT WEIGHT LOSSES MONTANA LIGNITE COAL (APPARENT WEIGHT LOSS)

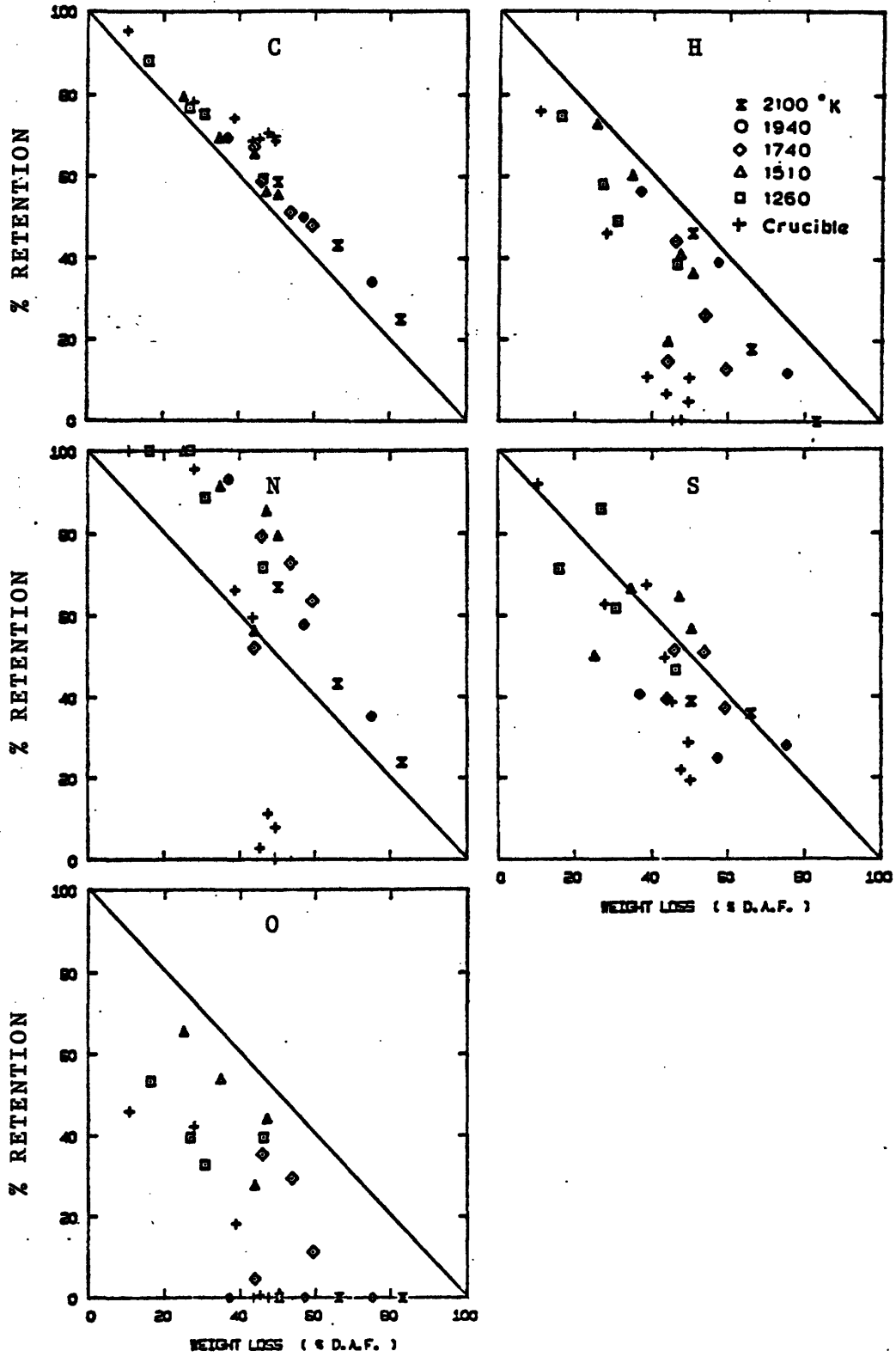


FIGURE 4.23. ELEMENTS RETAINED IN CHAR AT DIFFERENT WEIGHT LOSSES
PITTSBURGH SEAM BITUMINOUS COAL
(WEIGHT LOSS CORRECTED FOR SOOT)

of the elements. The broken line shows the apparent trends for the crucible runs. As can be seen from the figures, both lignite and bituminous coal showed similar trends. At a given weight loss, more carbon, less hydrogen and less oxygen were retained in chars from the crucible runs than in those from the laminar flow runs. Nitrogen did not show any loss until about 30% weight loss, and then the retention fell rapidly to zero in the crucible runs. For the laminar flow runs, the nitrogen retention above 50% weight loss appeared to be close to those of carbon. Sulfur data were somewhat scattered. For lignite, sulfur retentions in the crucible runs appeared to be higher on the average than those in laminar flow runs. The opposite trend was found for bituminous coal. Among the laminar flow runs at different temperatures, the data at 1260°K appeared to be closer to those from the crucible runs. Other runs did not show clear differences in trends, except that the higher temperature runs extended to larger weight losses.

Calculation of the elemental retentions requires information on weight losses during the devolatilization. Therefore the scatter in the data represents in part the errors associated with the weight loss measurements. Changes in the atomic ratio of elements in the char with time do not involve such errors. Figures 4.24 and 4.25 show H/C, N/C, S/C and O/C ratios in char plotted against the residence time. The broken lines represent the atomic ratios in the raw coals. The H/C and O/C ratios decreased sharply with time corresponding to the rapid losses of H and O compared to that of C. N/C ratios decreased slightly with time, but was generally higher than the ratio in the raw

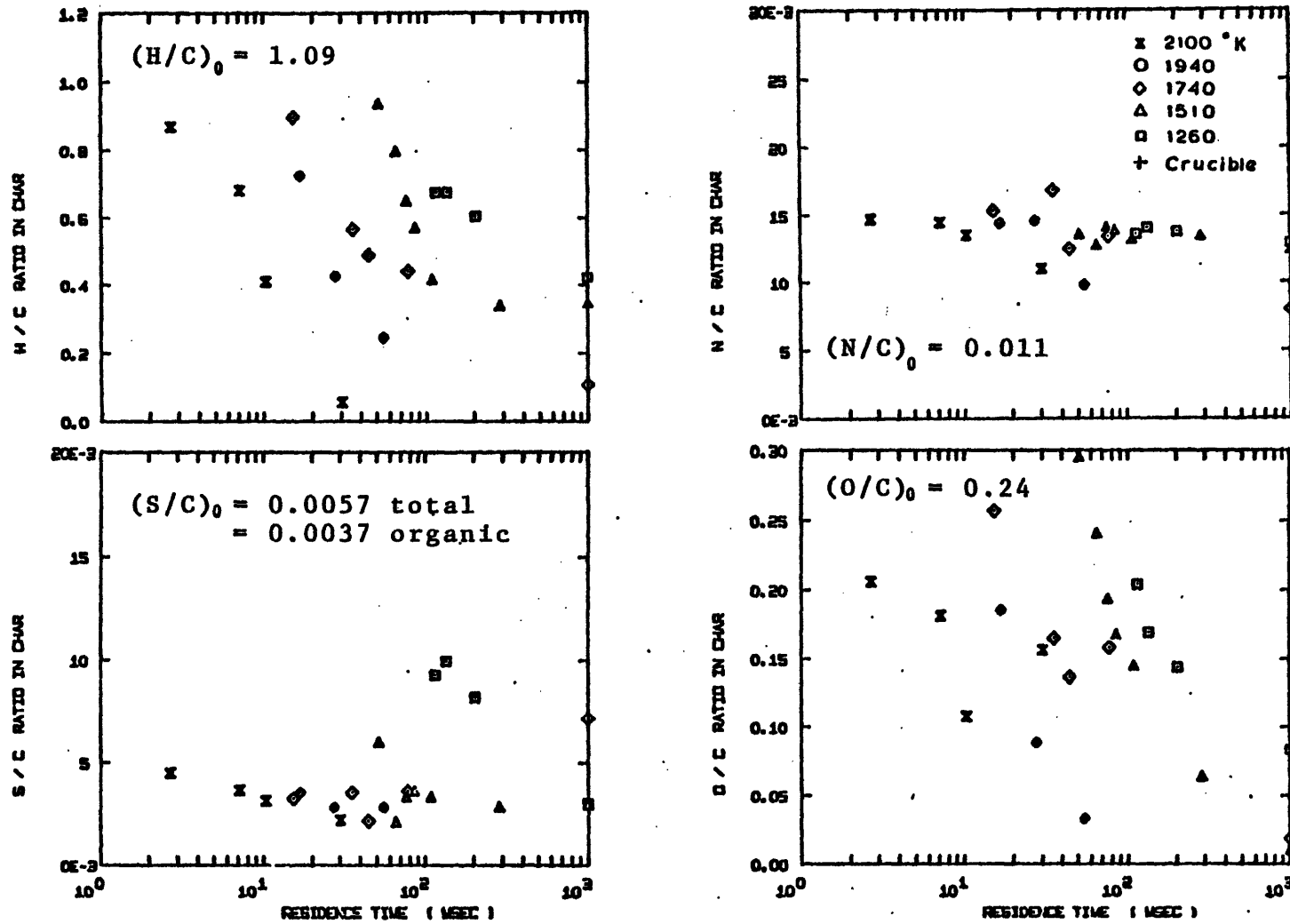


FIGURE 4.24. CHANGES IN ELEMENTAL RATIOS IN CHAR WITH TIME, MONTANA LIGNITE

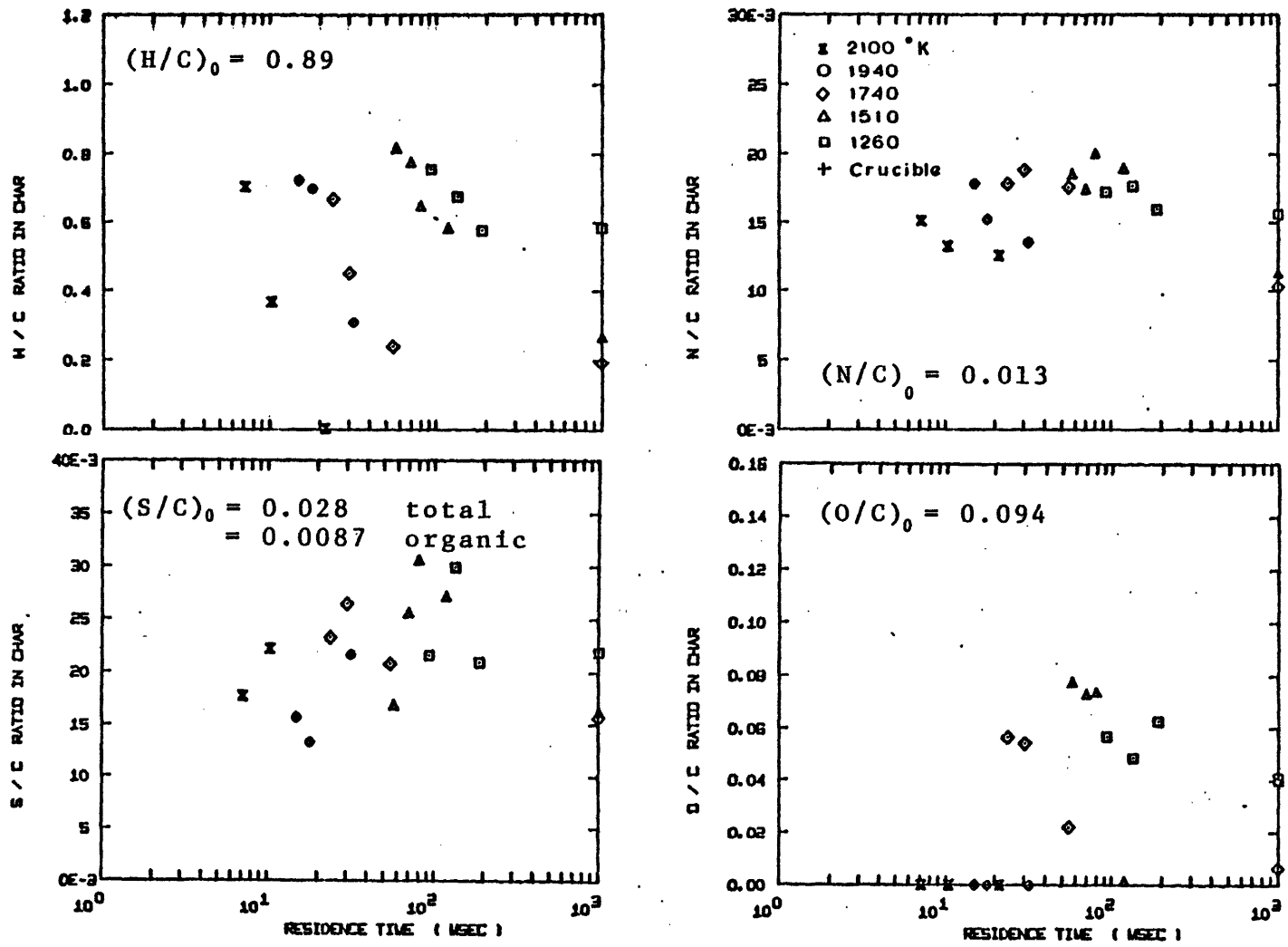


FIGURE 4.25. CHANGES IN ELEMENTAL RATIOS IN CHAR WITH TIME, PITTSBURGH SEAM BITUMINOUS COAL

coal. The S/C ratio in the lignite chars remained constant at a value about 40% lower than that in the raw coal, except those at 1260°K which were about twice as high as the other values. The S/C ratio for bituminous coal showed significant scatter, ranging from 50 to 100% of the ratio in the raw coal. No obvious trend was evident.

The atomic ratio in the volatile matter were calculated using the measured weight loss. The results are shown in figures 4.26 and 4.27. These figures are complementary to those in figures 4.24 and 4.25 which show the atomic ratio in the chars. The H/C ratio in the volatiles from bituminous coal were more or less constant except for the runs at 1260°K, where the ratios decreased with time. The results for lignite show decreases with time except for those at 1510°K. The N/C ratio increased with time, and the S/C ratio appeared to decrease rapidly with time. The behavior of the O/C ratio was similar to that of the H/C ratio, although the O/C data were more scattered.

Figures 4.28 and 4.29 show the atomic ratio in the chars as a function of total weight loss. For the same weight loss, all the ratio in the crucible runs except the S/C for lignite appeared to be smaller, on the average, than those for the laminar flow runs. Among the laminar flow runs, the data at 1260°K were closer to the crucible results except for the S/C ratio in the lignite, where systematically higher values were observed. The opposite trends occur in the volatile matter, as shown in figures 4.30 and 4.31.

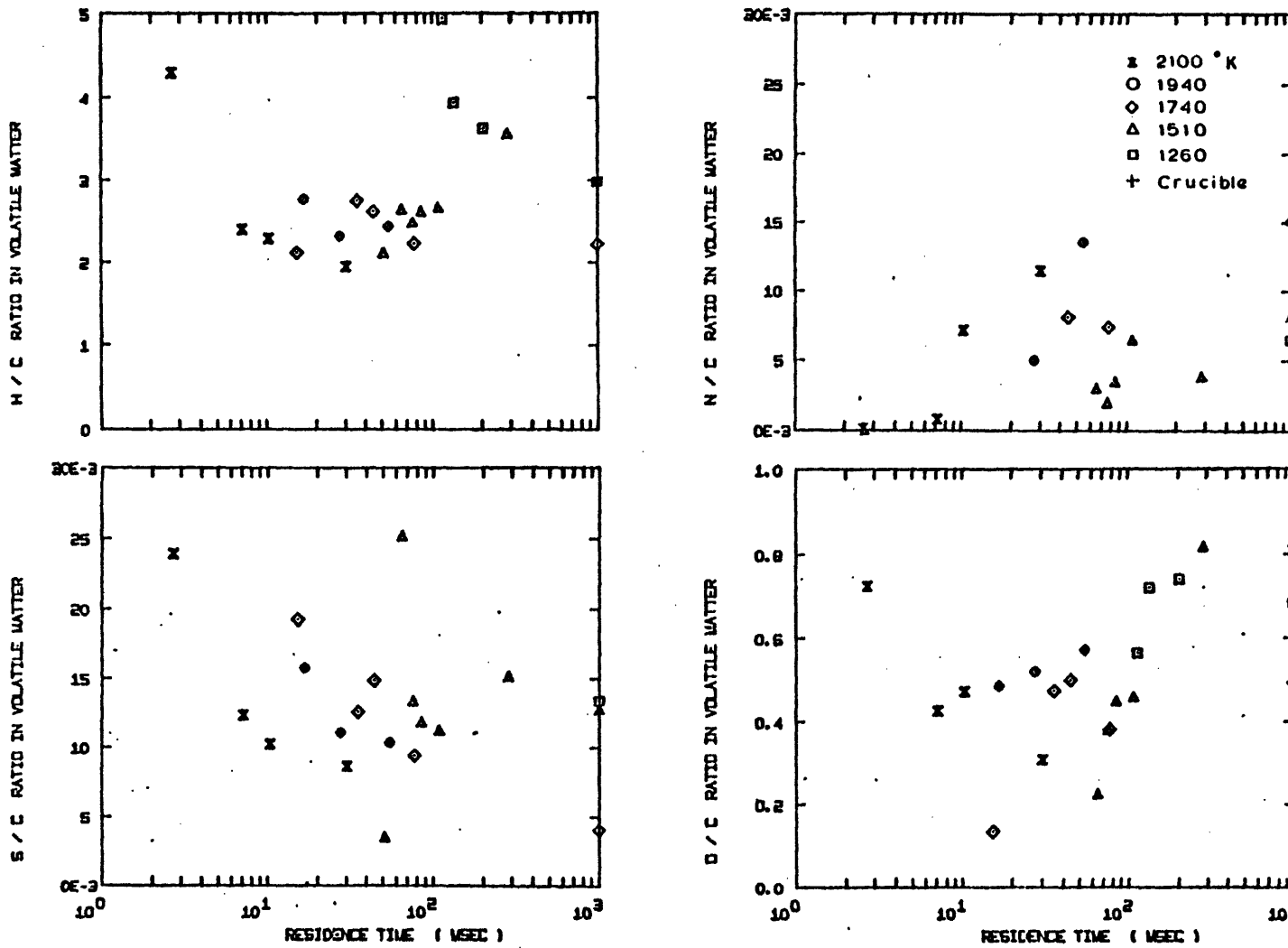


FIGURE 4.26 CHANGES IN ELEMENTAL RATIOS IN VOLATILE MATTER WITH TIME, MONTANA LIGNITE

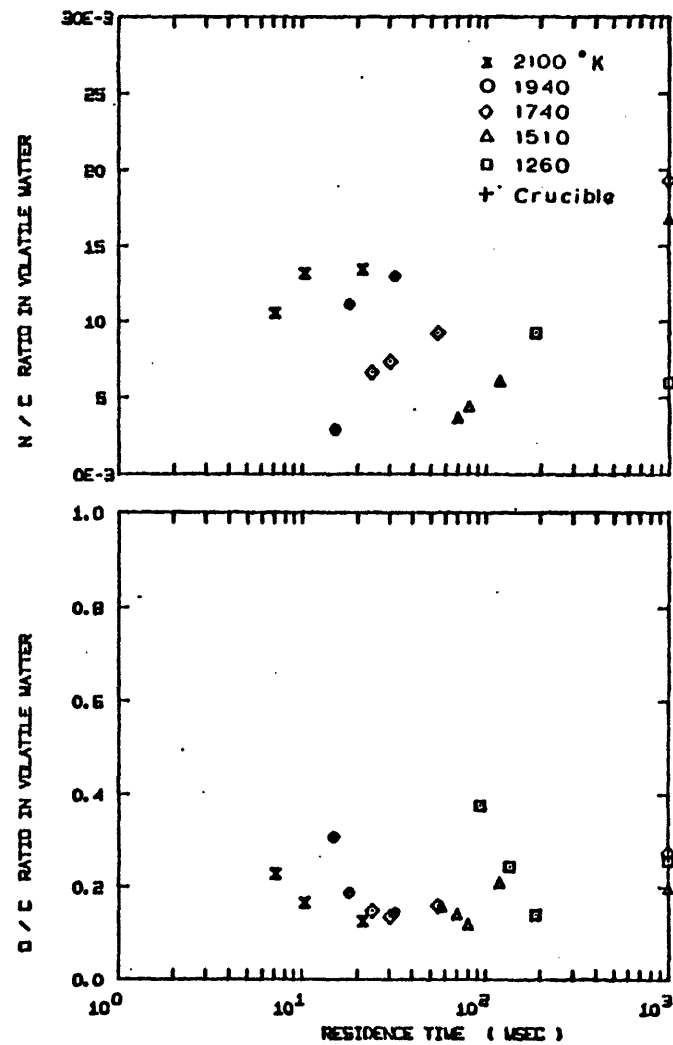
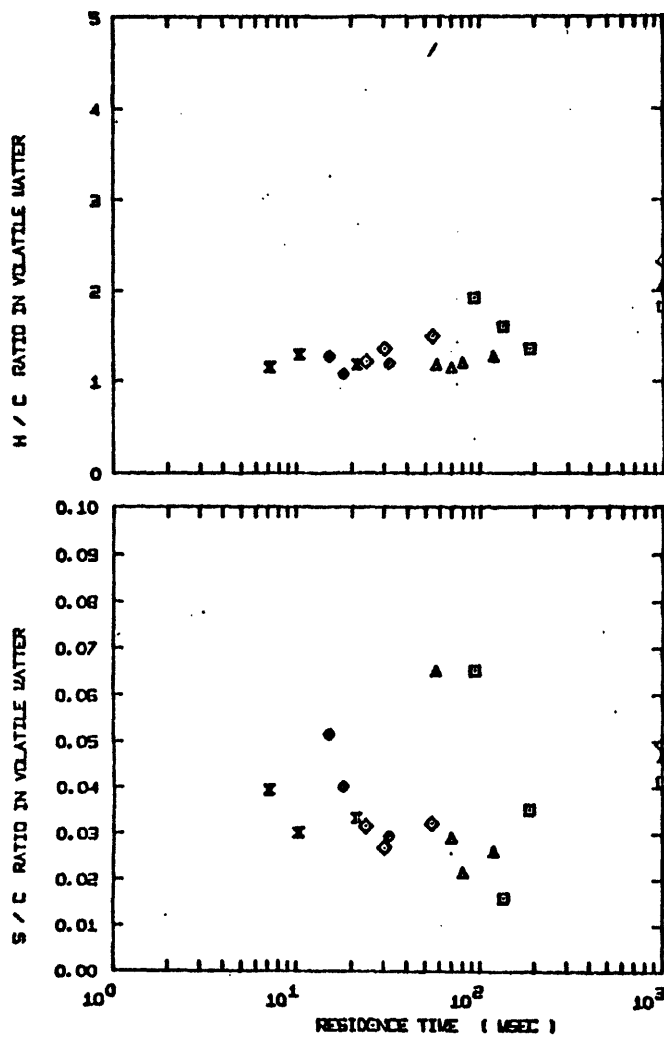


FIGURE 4.27 CHANGES IN ELEMENTAL RATIOS IN VOLATILE MATTER WITH TIME,
 PITTSBURGH SEAM BITUMINOUS COAL

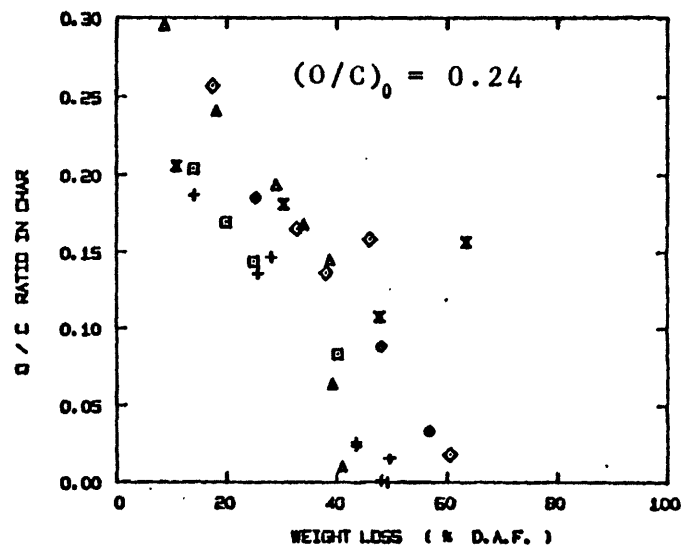
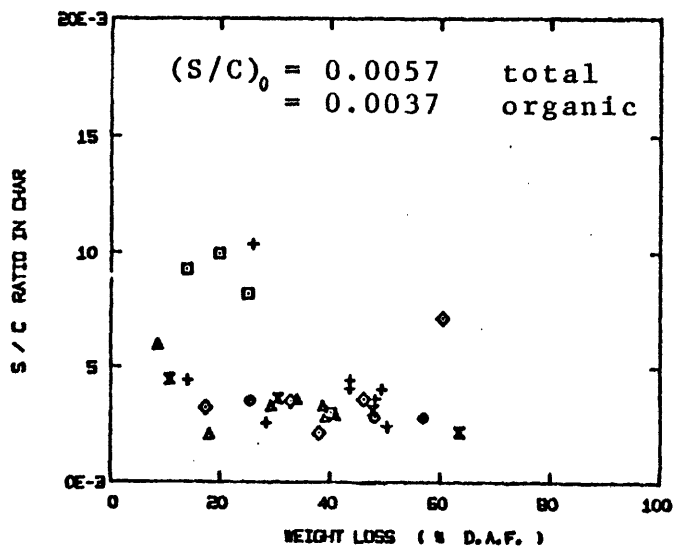
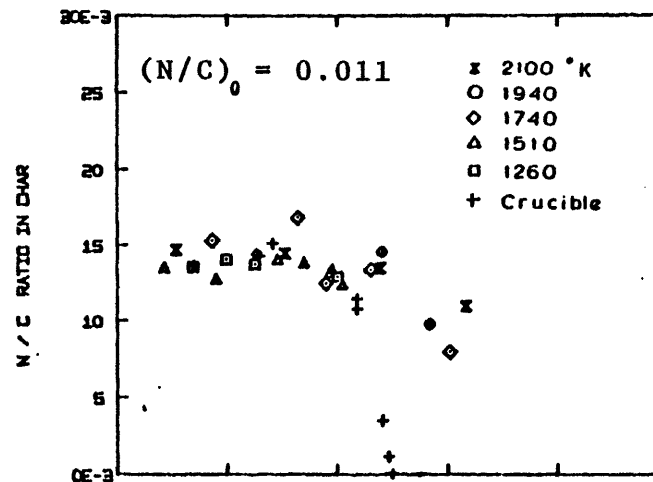
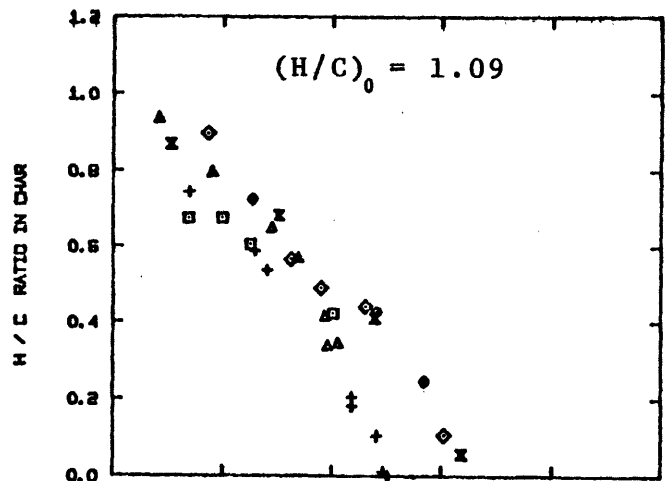


FIGURE 4.28 CHANGES IN ELEMENTAL RATIOS IN CHAR WITH WEIGHT LOSS, MONTANA LIGNITE

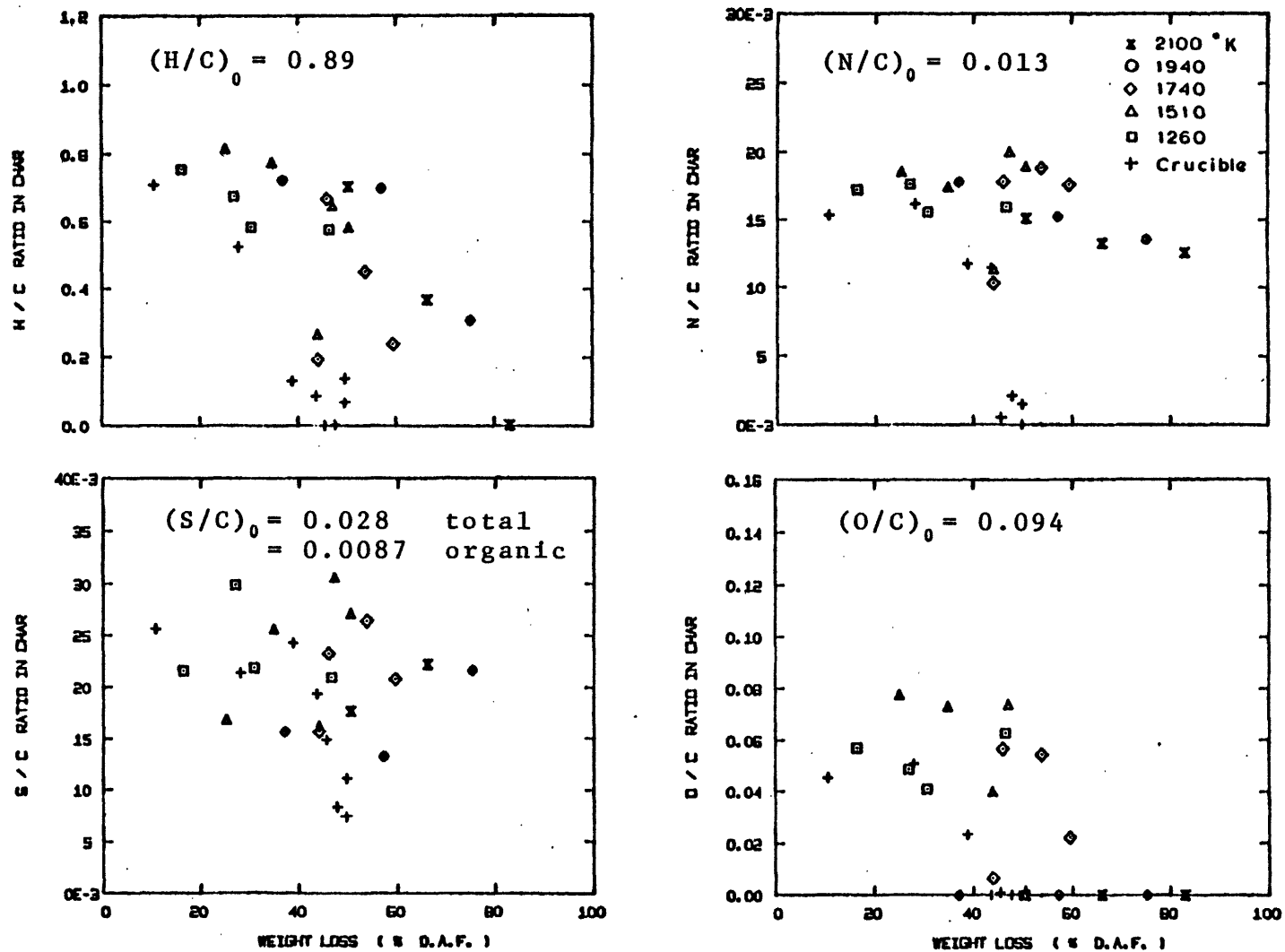


FIGURE 4.29 CHANGES IN ELEMENTAL RATIOS IN CHAR WITH WEIGHT LOSS, PITTSBURGH SEAM BITUMINOUS COAL (WEIGHT LOSS CORRECTED FOR SOOT)

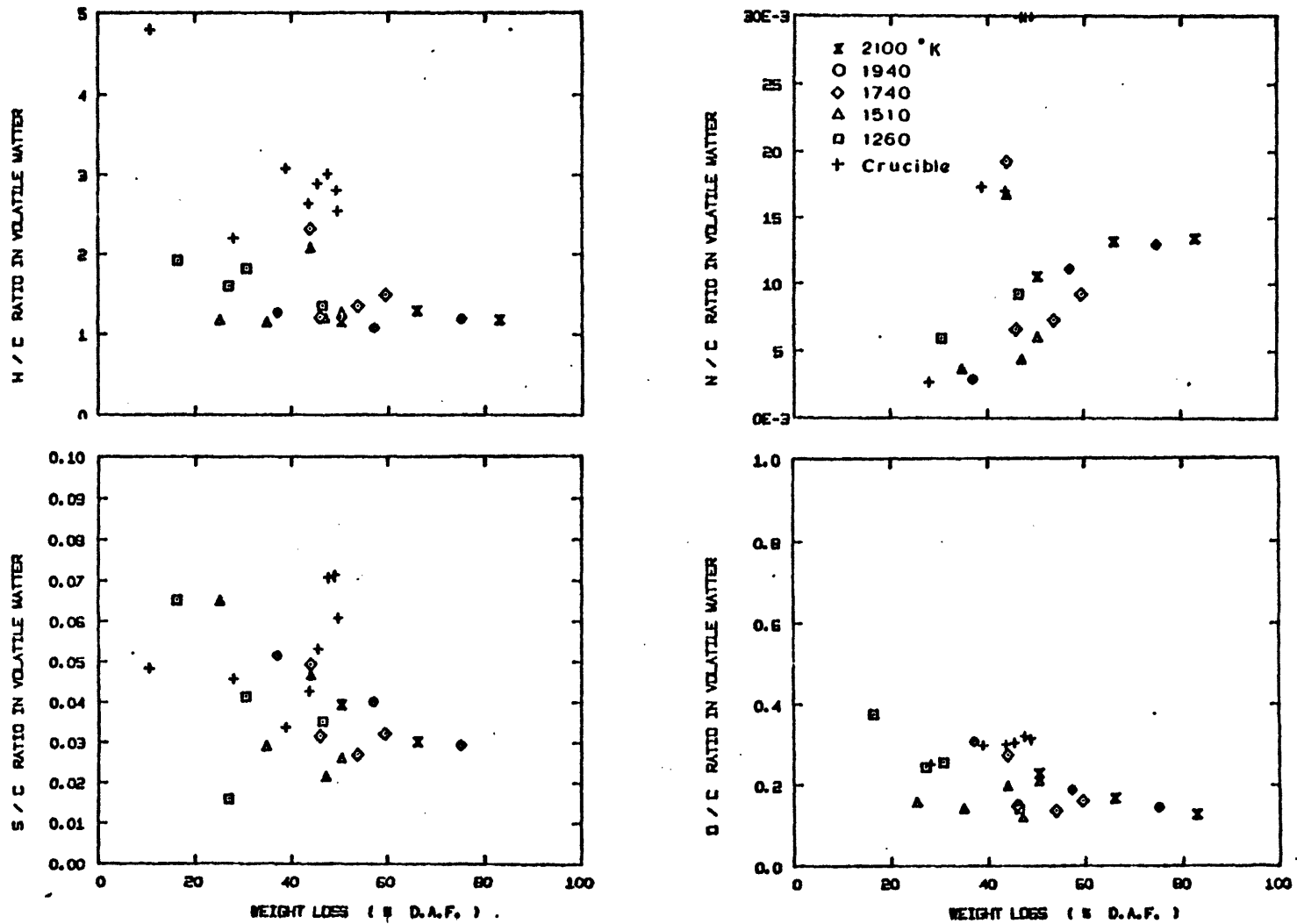


FIGURE 4.30 CHANGES IN ELEMENTAL RATIOS IN VOLATILE MATTER WITH WEIGHT LOSS PITTSBURGH SEAM BITUMINOUS COAL (WEIGHT LOSS CORRECTED FOR SOOT)

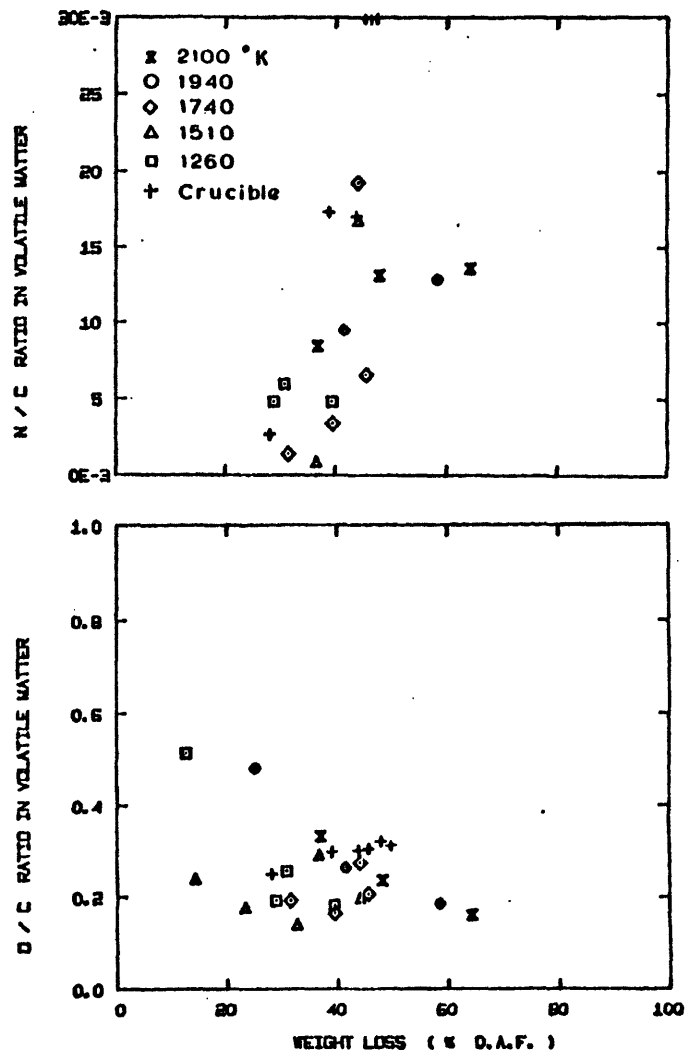
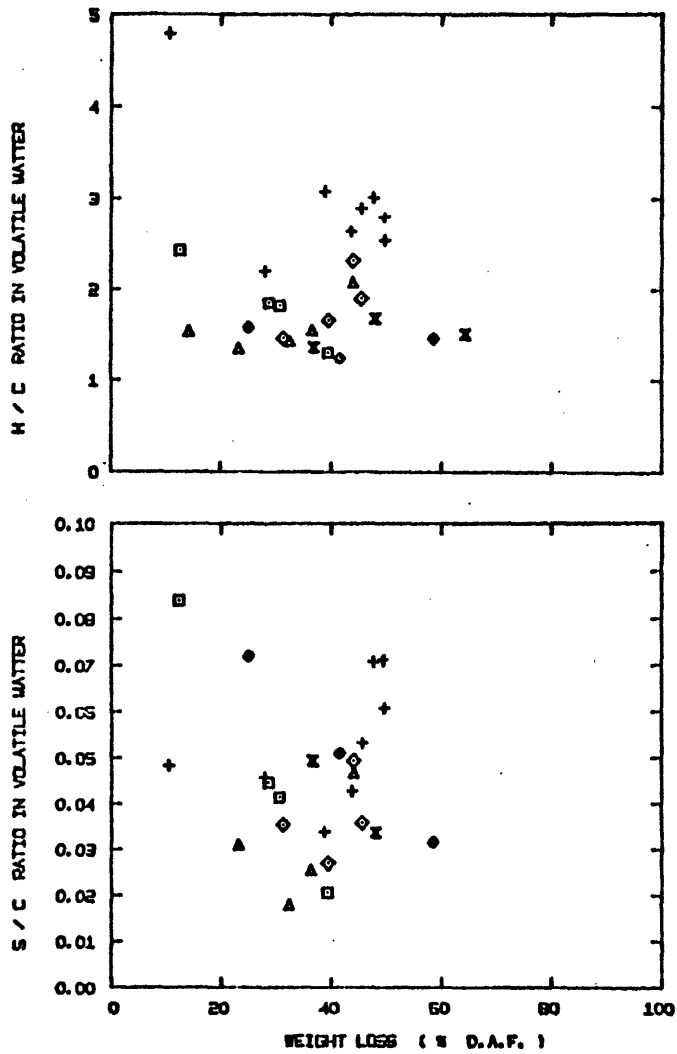


FIGURE 4.31 CHANGES IN ELEMENTAL RATIOS IN VOLATILE MATTER WITH WEIGHT LOSS MONTANA LIGNITE

CHAPTER V

DISCUSSIONS5.1 Temperature-time History of Coal Particles and Effects of Heating rates on volatile yields

Importance of heating rates has been emphasized by many investigators in relation to enhanced volatile yields. In the present study, particle temperatures were calculated from a simplified model described in chapter 3. Differences in the temperature-time histories of coal particles under the different experimental conditions and its implications on the observed differences in the asymptotic values of weight loss between the crucible experiment and the flow experiments will be discussed.

5.1.1 Temperature-time Histories of Coal Particles in Laminar flow experiment

Calculation of the particle temperature in chapter 3 involved a parameter θ , which is the ratio of the momentum shape factor to the energy shape factor. Calculated particle temperatures at an experimental temperature of 2100°K and calculated heating times at all the experimental temperatures for three different values of θ were shown in figure 3.11 and table 3.1 respectively. Although several attempts were made to measure the particle temperatures by a two color pyrometer and by the sodium D-line reversal method, the intense radiation from the hot furnace wall made it impossible to measure the particle temperature, when it is significantly lower than that of the wall. (Back ground radiation was eliminated, but reflection of wall radiation by the

particles could not be avoided). Therefore an indirect method was used to choose a proper value of θ . The method is based on the observed weight losses at different temperatures. From the weight loss-time curves (Figures 4.1), about 26% of the initial coal weight (d.a.f.) was lost at 1260°K in 200 msec. Since the reaction time is long, the particle temperature at this point may be safely assumed to be equal to that of the gas (i.e. 1260°K). At 1510°K, a 26% weight loss is observed at about 63 msec. Since this reaction time is much shorter than 200 msec, the temperature of the particles at this point must have reached at least 1260°K. By similar arguments, at the furnace temperature of 2100°K the particle temperature at 5 msec must be at least 1260°K. By extending the analysis to other temperatures, a value of θ of 3 was found to describe these data.

Figures 5.1 and 5.2 show the relation between the measured weight loss and the calculated peak temperature which the particles have attained during a run. For lignite for a furnace temperature of 1510°K, about 10% weight loss was observed during the transient time of heating, and the rest was lost at the peak furnace temperature. Weight losses in the transient time increased rapidly with increases in the furnace temperature. At 2100°K, the major fraction of the ultimate weight loss occurred before the particles reached the peak temperature. Since the time for a given amount of weight loss must decrease with increasing furnace temperature, the weight loss-temperature curve for a higher furnace temperature should lie below that for a lower temperature, i.e., at a given particle temperature, weight loss should decrease as

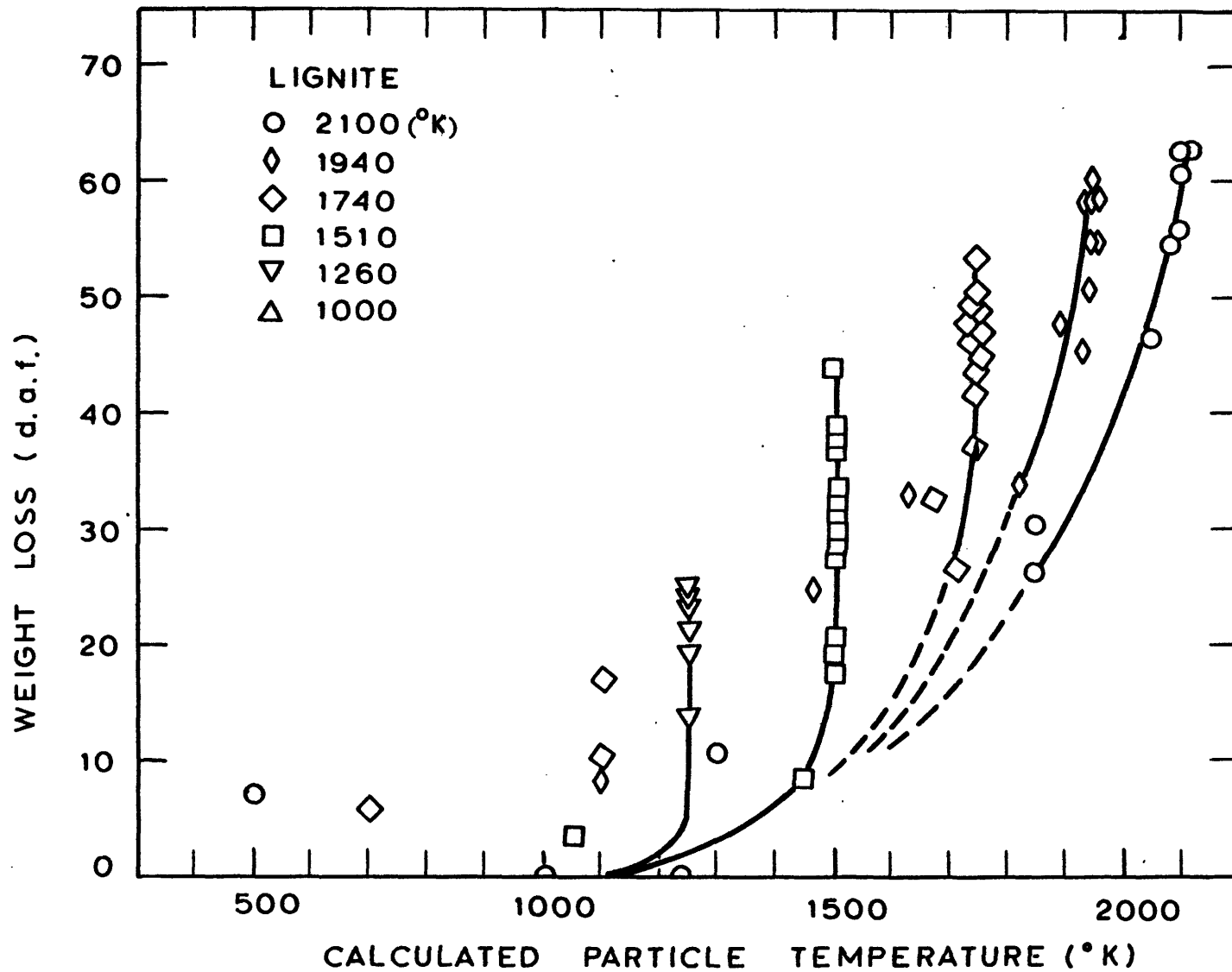


FIG. 5.1 WEIGHT LOSS VERSUS CALCULATED PARTICLE TEMPERATURE
MONTANA LIGNITE

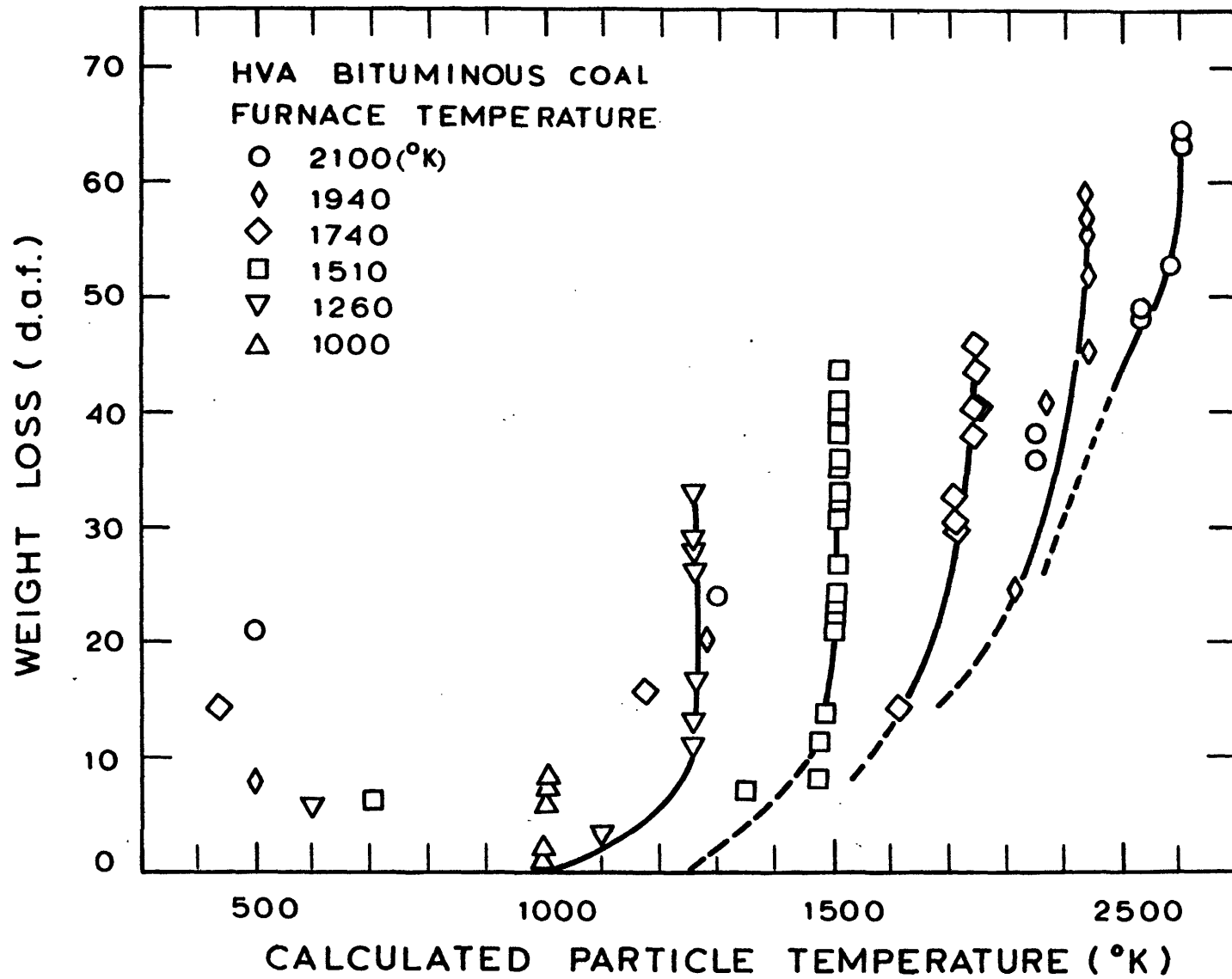


FIG. 5.2 WEIGHT LOSS VERSUS CALCULATED PARTICLE TEMPERATURE
PITTSBURGH SEAM BITUMINOUS COAL

furnace temperature decreases. However, some of the data at high furnace temperatures did not agree with the above statement.

Experimental variation, smaller samples and higher main gas flows at higher furnace temperatures, which increase particle loss through the filter, could be responsible for some of the discrepancies. More probable reason may be sought in the calculation of particle temperature by the simplified model. When the particle collector was positioned close to the injector, significant changes in the flow pattern could occur. More over the model did not account for the reaction during the quenching periods which would increase the effective reaction time, and hence the calculated particle temperature for a given weight loss. The minimum quenching time may be calculated by assuming that a coal particle is injected into water instantaneously. In appendix A, an analysis was made to estimate the heating time of a particle when it is introduced into a hot gas atmosphere instantaneously. The result is applicable in this case by replacing the thermal conductivity of the gas with that of water. Since the thermal conductivity of water (0.0016 cal/sec cm °C at 90°C) is about 15 times as large as the value used for argon, the gas phase conduction time, t_c , divided by 15 in figure A.1 will give an estimate for the minimum (fastest) quenching time. From the figure a 100 μ particle would require about 7 msec for quenching to 37% (e^{-1}) of the temperature difference between the particle and the water. This time may be negligible up to 1500°K, but may become significant at high temperatures because of the rapid reaction rates. Figure 5.3 illustrates a hypothetical devolatilization at a peak

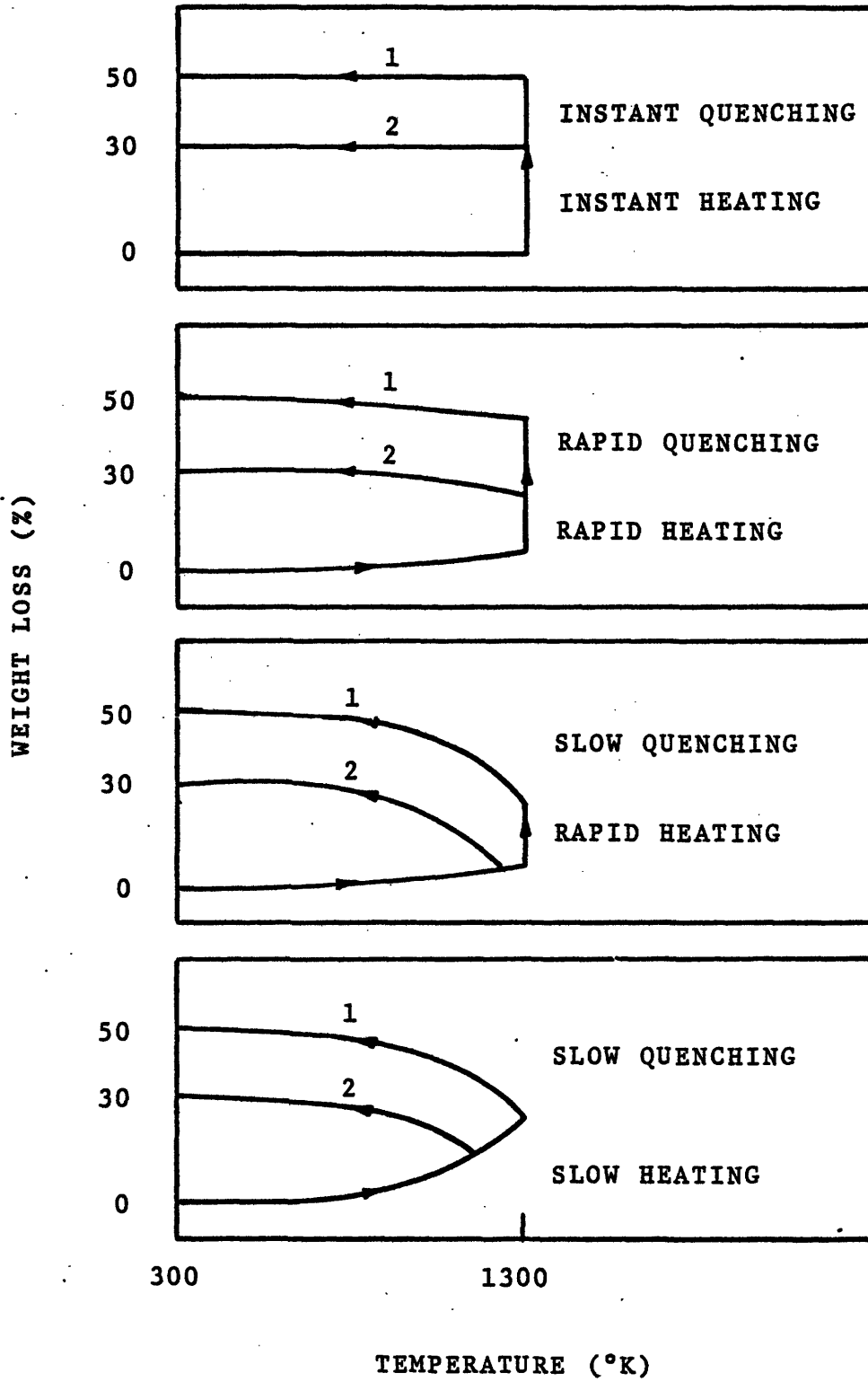


FIG. 5.3 SCHEMATIC DIAGRAMS OF WEIGHT LOSS-TEMPERATURE CURVES UNDER DIFFERENT CONDITIONS.

temperature of 1300°K. Different temperature-time histories leading to the same weight loss (50% or 30%) are shown schematically in order to illustrate the importance of the quenching time. The weight loss-temperature diagram has important implications in analysing the effects of heating on volatile yields.

5.1.2 Heating Rates and Average Reaction Temperature

As shown in chapter 4, rapid devolatilization of coal in the flow experiments resulted in much larger yields than slow devolatilization in the crucible experiment. Two major differences in the experimental conditions are (1) temperature-time histories during devolatilization and (2) the atmosphere surrounding the particles (i.e. dispersed phase versus packed bed). The latter will be discussed in the next section. Before discussing the detailed analysis of the temperature-time history of the two different experiments, some important aspects of the effects of heating rate must be stressed:

Devolatilization becomes rapid at higher temperatures, and variation of heating rate is a means for varying the temperature range, over which most of the devolatilization takes place. (Although rapid removal of volatile matter may be achieved by changing the mass transfer conditions, such as by reducing the system pressure.) In some cases, heating rates are not expected to make any differences in devolatilization behavior. For example, heating of coal particles to a certain final temperature may be considered. If the characteristic heating time is much shorter than the characteristic reaction time during the heating period, only negligible amount of reaction occurs during this period and the rest

proceeds isothermally at the final temperature. Changes in heating rates in this range, therefore, should not make any differences in the devolatilization behavior. If the devolatilization reactions are approximated by a first order overall reaction with an Arrhenius type rate constants (Eqs. 1.7 and 1.9), weight loss at time t is expressed as

$$\frac{\Delta W}{\Delta W_{\infty}} = 1 - \exp\left(-\int_0^t B e^{-\frac{E}{RT(t)}} dt\right) \quad (5.2)$$

The condition that only a small fraction $(1 - e^{-3})$ is lost during the heating time may be expressed as

$$\int_0^{t_H} B e^{-\frac{E}{RT(t)}} dt \geq 3 \quad (5.3)$$

where t_H is the heating time. For a constant heating rate of the form,

$$\frac{T - T_0}{T_{\infty} - T_0} = \frac{t}{t_H} \quad (5.4)$$

An explicit relation can be obtained by using an approximation (Jüntgen and Van Heek, 1970)

$$\int_0^T e^{-\frac{E}{RT}} dT = \frac{RT^2}{E} e^{-\frac{E}{RT}} \quad ; \quad \left(\frac{E}{RT} \gg 1\right) \quad (5.5)$$

After some mathematical manipulation, the critical heating time [value of t_H when equation (5.3) holds] is expressed as

$$t_{H_{cr}} = \frac{3}{B} \cdot \frac{E(T_{\infty} - T_0)}{R} \left(T_{\infty}' e^{-\frac{E}{RT_{\infty}}} - T_0^2 e^{-\frac{E}{RT_0}} \right)^{-1} \quad (5.6)$$

In most cases, the last term is negligible, hence

$$t_{H_{cr}} = 3 \cdot \frac{E}{RT_{\infty}} \cdot \frac{T_{\infty} - T_0}{T_{\infty}} \cdot t_R \quad (5.7)$$

where

$$t_R \equiv \frac{e^{E/RT_{\infty}}}{B} : \text{characteristic reaction time at } T = T_{\infty} \quad (5.8)$$

Equation (5.7) can be modified to define the critical heating rate,

$$\left(\frac{\Delta T}{\Delta t}\right)_{cr} \cdot \left(\frac{\Delta T}{\Delta t}\right)_{cr} \equiv \frac{T_{\infty} - T_0}{t_{H_{cr}}} = \frac{RT_{\infty}^2}{3E} \cdot \frac{1}{t_R} \quad (5.9)$$

For the case of exponential rise of temperature of the form

$$\frac{T - T_0}{T_{\infty} - T_0} = 1 - e^{-t/t_H'} \quad (5.10)$$

which may be a typical case in flow systems, $t_{H_{cr}} = 3t_H'$ may be used as an approximation.*

* Exact solution is (Badzioch and Hawksley, 1970)

$$t_H' = \frac{1}{B} \left[Ei \left(-\frac{E}{RT_{t=3t_H'}} \right) - Ei \left(-\frac{E}{RT_0} \right) - \exp \left(\frac{E}{RT_{\infty}} \right) \cdot \left\{ Ei \left[\frac{E}{R} \left(\frac{1}{T_{\infty}} - \frac{1}{T_{t=3t_H'}} \right) \right] - Ei \left[\frac{E}{R} \left(\frac{1}{T_{\infty}} - \frac{1}{T_0} \right) \right] \right\} \right]$$

where $Ei(x)$ is the exponential integral.

The concept of the critical heating time is important in interpreting the experimental results as well as in designing practical systems for devolatilization. Anthony (1974) observed no discernible effect of heating rate on the volatile yield for a lignite and only 2 percent increase in volatile yield for a bituminous coal when the heating rate was increased from 600 to 10,000°C/sec for a final temperature of 1000°C. In the publication based on this study (Anthony et al., 1974), it was suggested that changes in conditions such as particle size and differences in resistances to escape of volatile matter from the system, rather than changes in heating rate, may have been responsible for the observed differences in volatile yields reported in the literature under various heating conditions. However, the heating rates covered by Anthony were in the range where little effect would be expected,* and hence the experimental results should not be regarded as an evidence in evaluating the effects of heating rates in the general sense (i.e., higher heating rates generally imply that most of devolatilization occurs at higher temperatures).

* Using the reported rate parameters for the single overall reaction (values at a heating rate of 10,000°C/sec), the following criteria are obtained as critical heating rates.

Lignite ($E = 11,100$ Kcal/mole, $B = 283 \text{ sec}^{-1}$)

$$\left(\frac{\Delta T}{\Delta t}\right)_{\text{cr}} = \frac{RT_{\infty}^2}{3E} \cdot B e^{-E/RT} = 336^\circ\text{C/sec}$$

Bituminous coal ($E = 11,800$ Kcal/mole, $B = 706 \text{ sec}^{-1}$)

$$\left(\frac{\Delta T}{\Delta t}\right)_{\text{cr}} = 598^\circ\text{C/sec}$$

Of course, it is possible that the heating rate might have some other effects such as on the physical changes of coal, which in turn may affect the devolatilization process. Under these conditions the proper time scales with which the heating time is compared should be the characteristic times of the phenomena which influence devolatilization.

In summary, increases in heating rate result in increases in the effective temperature at which most of the devolatilization occurs, provided that a significant fraction of the devolatilization occurs during the heating stage. The criteria derived above can be used to determine the heating rate above which negligible devolatilization occurs during the heating stage and the major devolatilization reactions occur during the isothermal portion of the experiment. In this range of operation, it is obvious that further increases in heating rate will have negligible influence on the devolatilization process.

Figure 5.4 shows the weight loss-temperature history of a hypothetical devolatilization reaction expressed by a single first order reaction with $E = 25$ Kcal/mole and $B = 6.6 \times 10^4 \text{ sec}^{-1}$. Different heating rates to a final temperature of 2000°K are postulated. The temperature range where most of the reaction occurs shifts to higher temperatures as the heating rate increases.* The average reaction temperature for a

* Such a concept was also demonstrated by Jüntgen and Van Heek (1968) in a different manner. (They showed incremental weight loss versus temperature for heating at constant heating rate to a high temperature.)

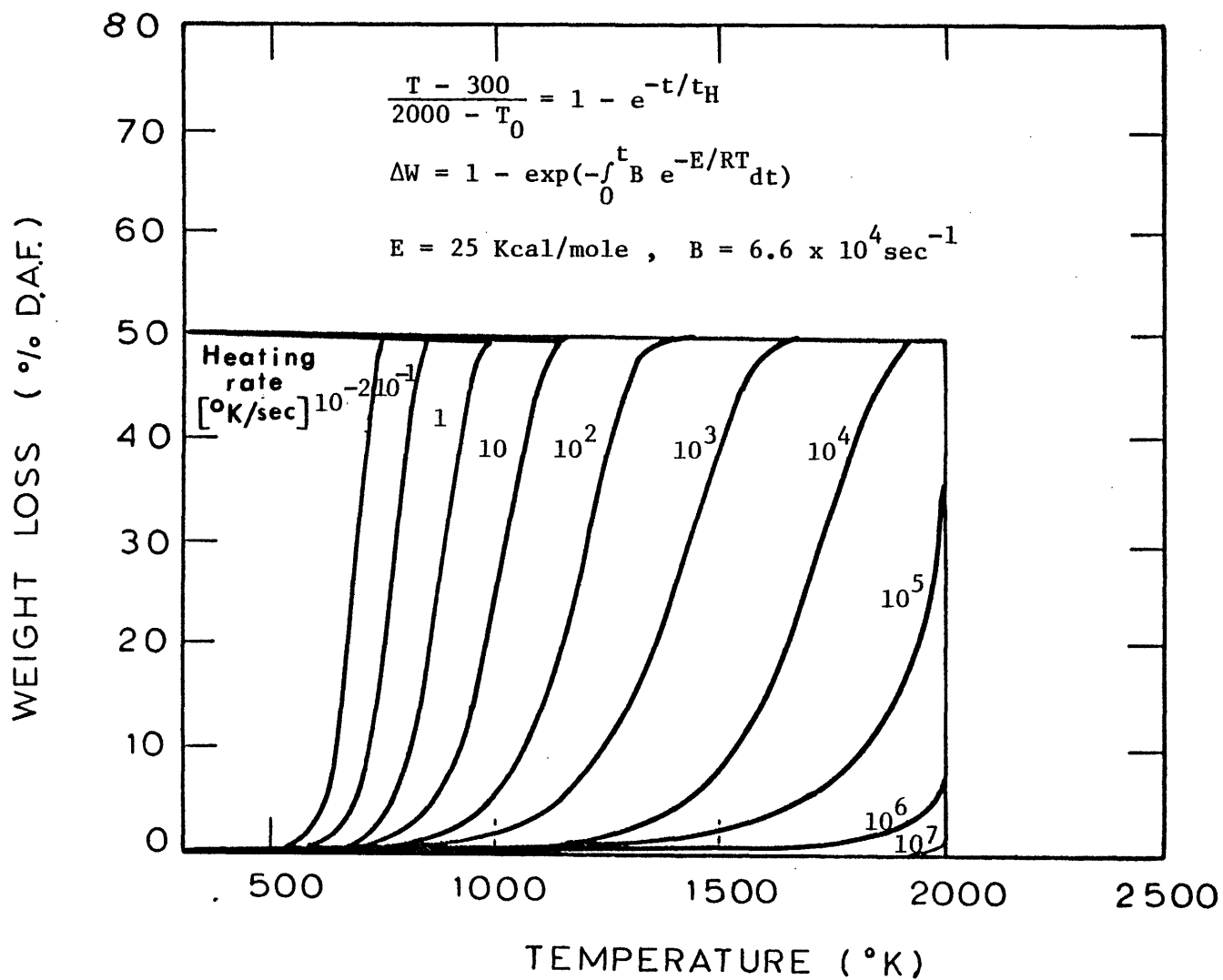


FIG. 5.4 EFFECTS OF HEATING RATE ON THE AVERAGE DEVOLATILIZATION TEMPERATURE.

non-isothermal case may be defined as

$$\bar{T} = - \frac{E}{R} \frac{t}{\ln \left\{ \int_0^t e^{-E/RT} dt \right\}} \quad (5.11)$$

where t is the overall reaction time including both heating and cooling periods. Close relation of the heating rate and the average reaction temperature can be seen from the figure. When the heating rate is greater than 10^6 °K/sec, the weight loss-temperature history becomes essentially the same as the isothermal case, as does the average reaction temperature. The average reaction temperature appeared to be important in analyzing the actual devolatilization reactions.

Figure 5.5 shows an estimate of weight loss-temperature histories under different experimental conditions for lignite. Weight losses of crucible runs during the heating periods were calculated from the first order rate constants obtained in this study. This will be discussed later. Marked differences between the crucible experiment and the flow experiments can be clearly seen. In the crucible runs with a high peak temperature, most of the reaction occurs before the peak temperature is reached, since the heating rate is relatively slow. High volatile yields are obtained with the fastest heating to peak temperature combined with sufficient residence time at peak temperature. to approach the asymptotic weight loss. It might be possible to define an area on the weight loss-temperature curve passage through which entails reduction in the maximum yield. For example, if weight loss-temperature for a pyrolysis experiment passes through the area bounded by the crucible run at 1220°K, a weight loss of, say, 60 percent might

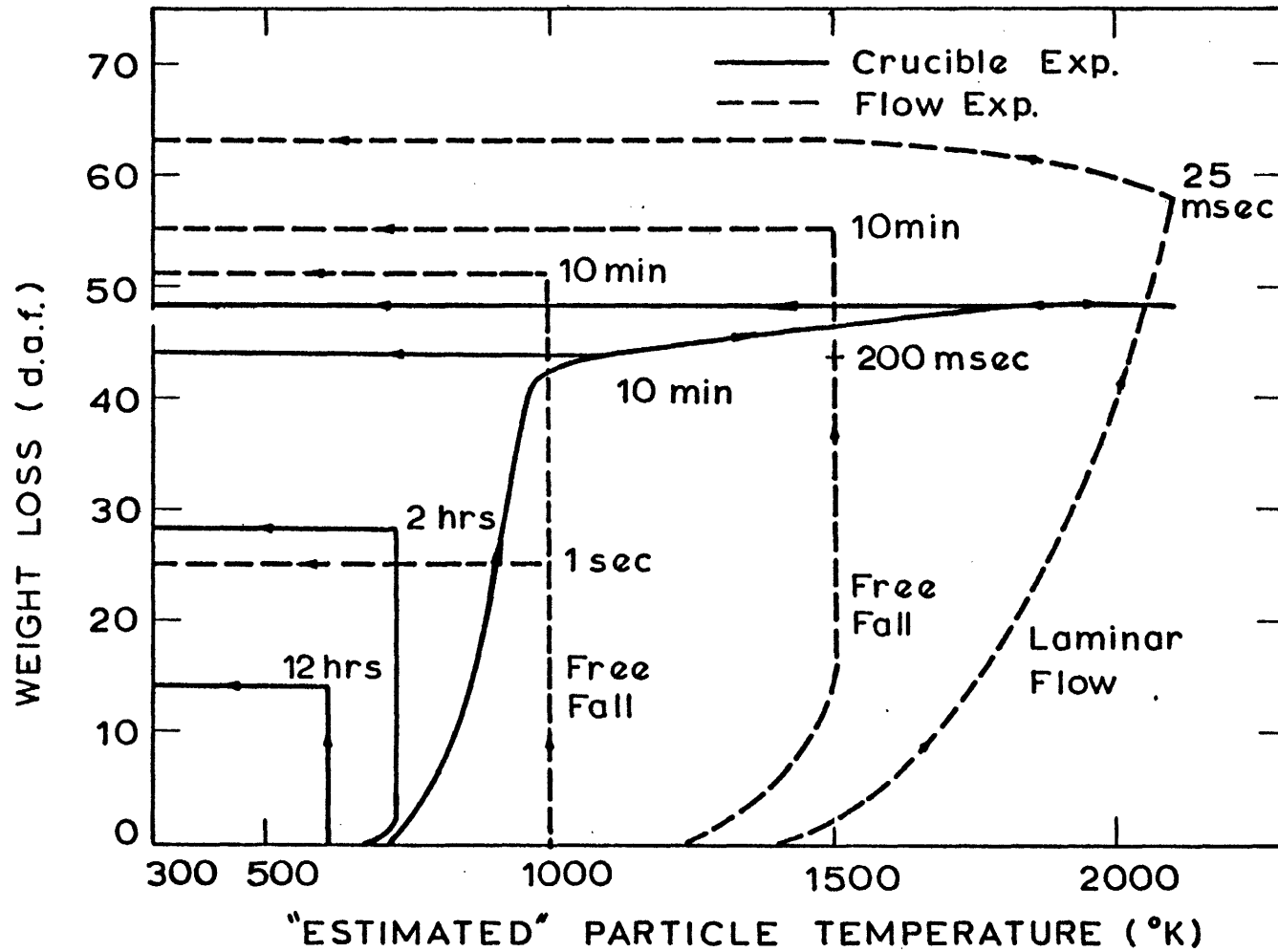


FIG. 5.5 ESTIMATED WEIGHT LOSS-TEMPERATURE HISTORIES, MONTANA LIGNITE.

not be attainable by subsequent exposure to extreme temperatures.

5.2 Secondary Char Forming Reactions in the Gas Phase and on the External Surface of Coal

Volatile matter that escapes from coal particles can undergo various secondary reactions in the gas phase with possible formation of solid products. The results of the present study indicated that such reactions under certain conditions could reduce the overall volatile yields substantially. In the free fall experiment with the bronze collector, the estimated weight of the soot-like material amounted to more than 20% of the original weight of the bituminous coal. Even under the short residence time conditions in the laminar flow experiment, it was estimated that 15 - 20% of the original coal was converted into the solid products (Figure 4.14). In contrast to this behavior, the lignite produced little discernible soot-like material in any of the present experiments. Yet the augmentation of the volatile yields at high temperatures closely resembled the results of the bituminous coal. (Figures 4.1 and 4.2). Whether or not the observed discrepancies in weight loss between the crucible runs and the flow experiments can be explained by the secondary reactions in the gas phase will be closely examined in this section.

5.2.1 Parameters Affecting the Secondary Reactions

Temperature, concentration of the volatile matter, external surface area of coal particles and physical resistance of the environment to the escape of volatiles from the sample are the major parameters determining the extent of the secondary reactions outside the

coal particles. As discussed in section 5.1, the temperature-time histories of the coal particles in the two different experiments are quite different, although the peak temperatures are the same. Since "the average reaction temperatures" for free fall runs are much larger than those for crucible runs, (see figure 5.5), given the same peak temperature the reaction rates for the secondary reactions are also higher for the free fall runs. If the secondary reactions are represented by thermal cracking of the volatile matter, more extensive "soot" formation is expected in free fall runs if the other conditions are kept constant. In fact, the large amount of soot observed in the free fall runs for the bituminous coal might have been due to such reactions. In crucible runs, the amount of solid deposit on the crucible wall increased with increases in the peak temperature for the bituminous coal. (Table D.2). Below 1000°K, only 0.0 to 0.5% of the weight of the original coal was converted into the deposit, while above 1300°K, 2 to 3% were the typical values. Furthermore, two stage heatings (first at a relatively low temperature and then reheating the char sample to a higher temperature) resulted in formation of very little deposit. (CR266 to CR278, CR268 to CR282). Evolution and escape of volatile matter at a relatively low temperatures where cracking is slow may be responsible for the observed decrease of deposition. Although the experimental evidence appeared to support thermal cracking as the mechanism for the formation of the solid residue, a contribution from equilibrium reactions, such as polymerization and depolymerization, cannot be excluded at this time. Such reactions tend to produce more

solid at relatively low temperatures.

The concentration of volatile matter near the coal particles depends on the production rate of volatile matter, the rate of destruction by secondary reactions, and mass transfer of the volatile matter from the crucible, or from the alumina collector in the free fall experiment. Since the coal feed rate in the free fall experiment was 0.1 gm/min, the production rate of volatile matter may be approximated by 0.05 gm/min, assuming a 50% volatile yield. In the crucible experiment at 1220°K, calculations based on the first order rate parameters (section 5.5) indicated that most of the devolatilization occurs between 700 and 1000°K in about 2 min. The approximate average mass production rates are, therefore, 0.25 gm/min with a 1gm sample, assuming a 50% volatile yield. Another factor which has to be considered is the difference in the capacity of the containers, i.e. 15 - 20 ml for the crucibles and 170 ml for the alumina collector used in the free fall experiment. Although the crucible runs were performed with covers, the range of concentrations of the volatile matter in the crucible when the smallest sample was used is probably about the same or even lower than that in the alumina collector. (Crucible; 10 mg sample in a 20 ml crucible with 0.0025 gm/min mass production rate of volatile matter versus Alumina collector; 1 gm sample in a 170 ml container with 0.05 gm/min mass production rate of volatile matter.)

The total external surface area of coal particles is initially proportional to the sample size. Since the particle size of the lignite did not change significantly in any experiments, the external

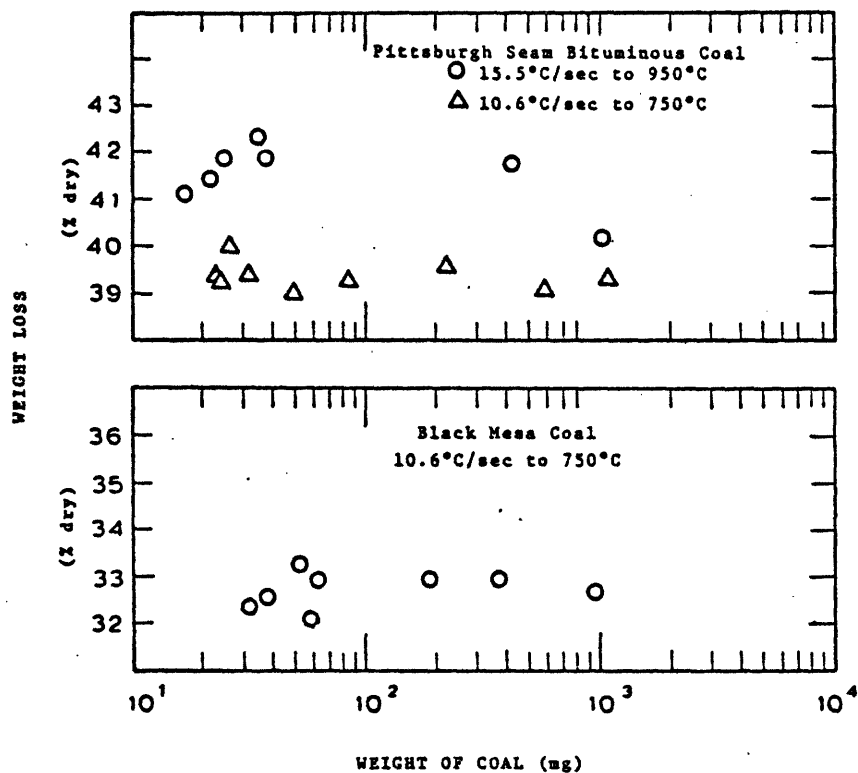
surface area per unit mass of coal particles available for secondary reactions is the same for the crucible experiment as for the free fall experiment, except that the reaction time of coal particles in the free fall experiment depend on when the particles are fed. For the bituminous coal, however, the particle size increased with the progress of devolatilization in the free fall experiment. In the crucible runs with bituminous coal, all the particles in the crucible fused together to form a single lump, which decreased the apparent external surface area. Evidently the volatile matter escaped through the lump as bubbles, but the extent of secondary reactions occurring in the bubbles is difficult to estimate.

The physical resistance of the environment to the escape of solid products of secondary reactions is quite different between the two experiments as stated above. In the free fall experiment, particles are injected into the mixture of volatile matter and argon gas, which induces a downward flow in the axial position by the cold particles. Near the inside wall of the alumina collector, a concentric upward flow is formed due to the evolution of the volatile matter. If solid material (soot) is formed in the gas phase, the upward flow can easily carry it away because of the very small particle sizes of such material. In fact, some soot-like material was observed in the bottom flange, which supports the alumina rod, of the free fall furnace. (See figure 2.5). In the crucible experiment, some of the solid products may be trapped in the particle bed, although some soot-like material was found in the bottom flange indicating that some of the material either escaped from the

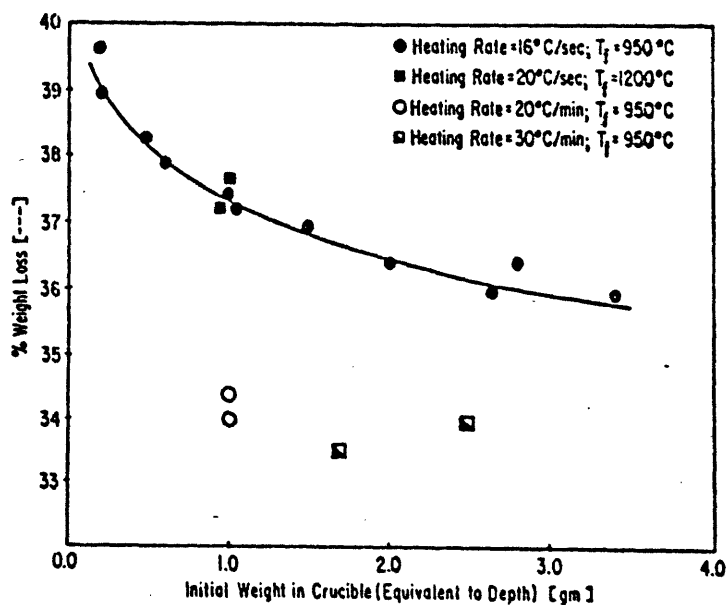
crucible or formed outside the crucible.

5.2.2 Implications from Crucible Experiments with Different Bed Depth

Effects of the bed depth on the volatile yield were investigated experimentally as discussed in section 4.1.3. The observed weight losses were not affected for the lignite and about 2% of the original coal weight for the bituminous coal when the average ratio of bed depth to particle size was decreased from about 100 (1 gm sample) to about 1 (10 mg sample). The statistical significance of the 2% increase was not strong because of the scatter of the data (see figure 4.17). The results of this study agreed very well with those of Portan and Tan (1974), who used a Pittsburgh seam bituminous coal from the same mine and a Black Mesa coal. Figure 5.6 (a,b) shows their results. The proximate analysis of these two coal are 1.96% moisture (as received basis), 40.48% volatile matter and 12.40% ash (dry basis) for the Pittsburgh seam bituminous coal, and 4.26% moisture (as received basis), 34.47% volatile matter and 27.05% ash (dry basis) for the Black Mesa coal. The experimental method was similar to that used in this study. The bituminous coal at 950°C appears to show a slight increase in yield of volatiles with decreases in size, but this apparent change could be within the scatter of the data. The Black Mesa coal and the bituminous coal at 750°C showed no effects of sample size. In contrast to these observations, Gray et al.(1974) reported considerable effects of sample size on the volatile yield. Figure 5.6c shows the result. About 4% increase was observed by changing the weight from 3 to 0.25 gram. Since



A, B: WEIGHT LOSS VS INITIAL WEIGHT OF COAL IN A CRUCIBLE.
PORTAL AND TAN (1974)



C: Per cent weight loss vs. initial weight of sample in crucible for different rates of heating and different final temperatures (T_f is final pyrolysis temperature achieved)
From Gray, et al. (1974)

neither the exact method of the experiment nor the kind of coal used in the experiment was reported, the cause of the difference is not clear. In any case, the present study demonstrated only small or no effects of sample size on the volatile yield. The observed differences in volatile yield between the crucible experiment and the free fall experiment (figures 4.3 and 4.4) are far greater than those observed by changing the bed depth. Since the bed depth affects both the concentrations of the volatile matter in the crucible and physical restrictions that can trap the solid products of the secondary reactions, the negligible observed effect of the bed depth on the volatile yield indicates that the secondary reactions outside the coal particles do not account for the larger observed yield differences between the two experiments. In particular, it should be noted that the conditions in the crucible experiment are not necessarily more favorable for the secondary reactions as compared with those in the alumina collector, although the solid products may be more easily captured in the crucible if they are formed.

5.3 Changes in Elemental Composition of Char and their

Implications to the Devolatilization Mechanism

The results of the ultimate analysis of char showed several distinct features:

- (1) The qualitative trends of the data for both the bituminous coal and the lignite were very similar.
- (2) At the same weight loss, more carbon, less hydrogen and less oxygen were retained in chars from the slow heating crucible runs than in those from the laminar flow runs.

- (3) No appreciable loss of nitrogen was observed until about 30% weight loss for both the crucible and the flow experiments.
- (4) Among the laminar flow runs at different temperatures, the data at 1260°K were closer to those from the crucible runs.

In this section, these observations are compared with those of previous workers, and their implications of these results to the mechanism of the devolatilization are discussed.

5.3.1 Comparison with Previous Observations

The available data on the changes in elemental composition of char are limited to those for slow heating conditions, typical of industrial coking operations. Dryden (1957) suggested the following empirical equations, based on the large amount of data reported by U.S. Bureau of Mine, for the amounts of carbon, hydrogen and oxygen carried out in the volatile matter under the standard test conditions at 900°C, for coals with 81 to 93% d.a.f. carbon content.

$$C_v = 988 \frac{H}{C} - 43.5 \left(\frac{183.5}{C} - 1 \right) \frac{O}{C} - 38.0 \quad (5.12)$$

$$H_v = 0.25 + 72 \frac{H}{C} \quad (5.13)$$

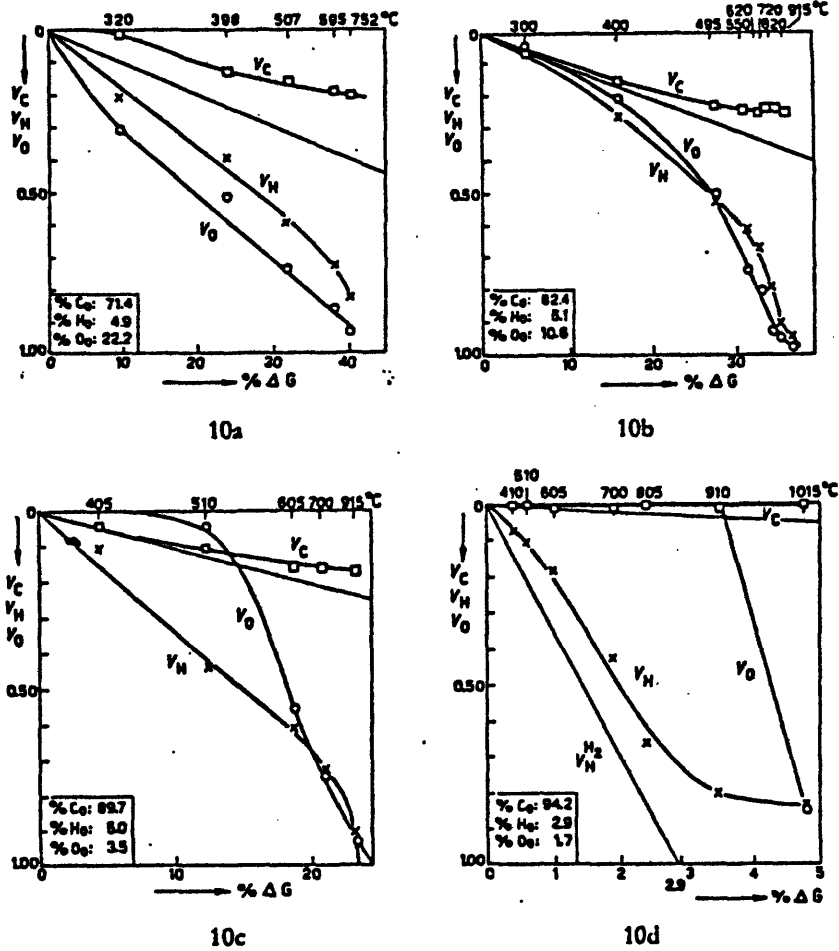
$$O_v = 83 \frac{O}{C} \quad (5.14)$$

Where C, H, O denote weight of each element in the original coal (% d.a.f.) and C_v , H_v , O_v denote weight percentages of the elements

in the volatile matter based on the original weight of each element.

Although the carbon content of the Pittsburgh seam bituminous coal (77.8 d.a.f., 82.3 d.m.f., Table 2.5) is slightly lower than the range used in the correlation, application of Eqs. (5.12) and (5.13) to the bituminous coal gives $C_v = 22.8$ and $H_v = 5.4\%$. These values are somewhat lower than the results of the crucible experiment at 1220°K ($C_v \sim 25$ to 30 and $H_v \sim 10\%$, Fig. 4.21), but still are reasonable as estimated values.

Van Krevelen (1961) reported loss of three elements (C, H, O) at different total weight losses for different coals, which is shown in Fig. 5.7. The marked change in the oxygen curves was noted. For lignite, oxygen was more easily removed than hydrogen. At a carbon content of 82%, more oxygen was retained compared to hydrogen at small weight losses, but rapid loss of oxygen at the higher weight losses exceeded the corresponding hydrogen losses. For coals above 90% carbon content, relatively more oxygen was retained at all values of weight losses, which was interpreted to mean that oxygen becomes more strongly bonded as the rank increases.



Analytical carbonisation diagrams. (a) Ligniet, (VAN KREVELEN¹¹). (b) Northumberland, (FRANKLIN¹²). (c) Wales, (FRANKLIN¹²). (d) Wales, (FRANKLIN¹²).

FIG. 5.7 LOSS OF ELEMENTS DURING CARBONIZATION. FROM VAN KREVELEN (1961).

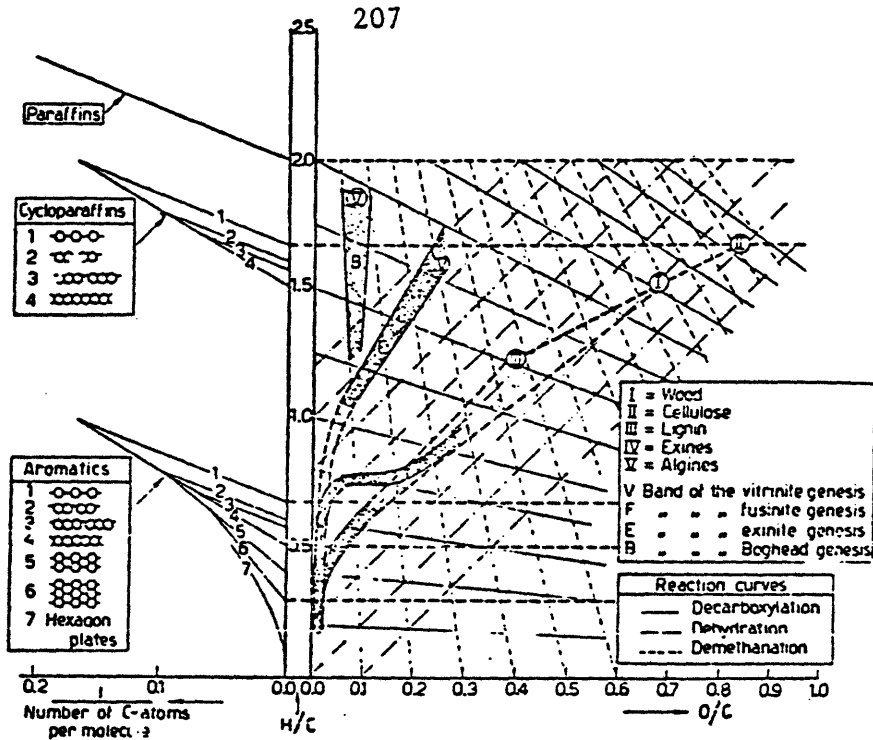
The results for the Montana lignite in the crucible experiment show good agreements in carbon and hydrogen with the data on lignite reported by Van Krevelen. At 40% weight loss, about 80% of the original carbon and 20% of the original hydrogen were retained. 20% retention of the oxygen in the present study appeared to be higher than that in Van Krevelen's study by 5 to 10 percentage points. Comparison of the Pittsburgh seam bituminous coal (Fig. 4.23) with the Northumberland coal (82.4% carbon) shows close resemblances. At 30% weight loss, both coals contain about 75% of the original carbon, about 40% of the original hydrogen and about 30% of the original oxygen. In the present study, however, the clear change in the relative position of the oxygen and the hydrogen curves were not observed.

The cross plot of atomic H/C ratio versus atomic O/C has been used in describing the natural coalification process as well as the carbonization process. Figure 5.8 shows the figures of Van Krevelen (1961). The difference between the coalification and the carbonization processes is that in the carbonization of a bituminous coal the path is close to the straight line between the original composition to the coal band at a value of H/C of about 0.28 ("carbonization pole"). Loss of hydrogen relative to that of oxygen in the carbonization process is faster than that in the coalification process. In Fig. 5.9 the results of the present study are shown. No obvious difference is seen between the data of the crucible experiment and those of the laminar flow experiment. Most of the scatter of the data is considered to be caused by the values of oxygen content, which were determined by taking the difference of the weight of char to that of the sum of carbon, hydrogen, sulfur, nitrogen and ash in char. The trend of the Pittsburgh bituminous coal agrees with the general trend of the carbonization curves in Fig. 5.8.

5.3.2 Possible Mechanisms of the

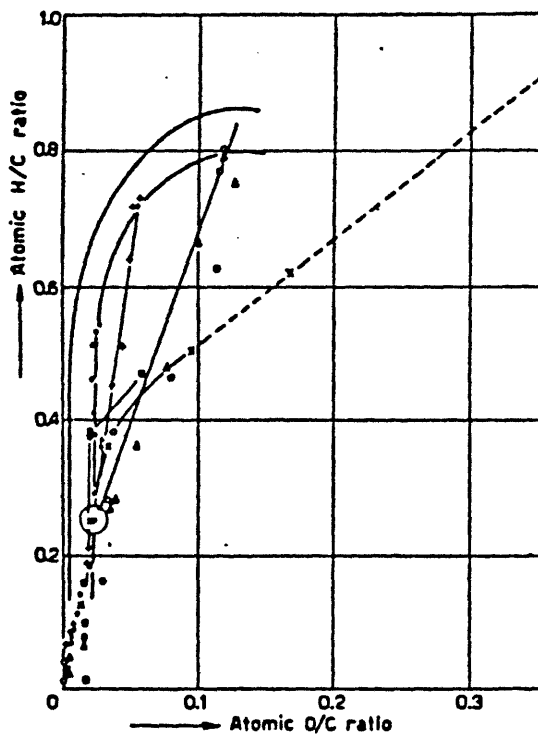
Rapid Devolatilization

In this section the observed changes in the elemental composition of char will be examined in relation to the generally agreed mechanism for the slow carbonization (see section 1.2.2). Then the observed differences between the results of the slow heating crucible experiment and those of the laminar flow experiment will be discussed.



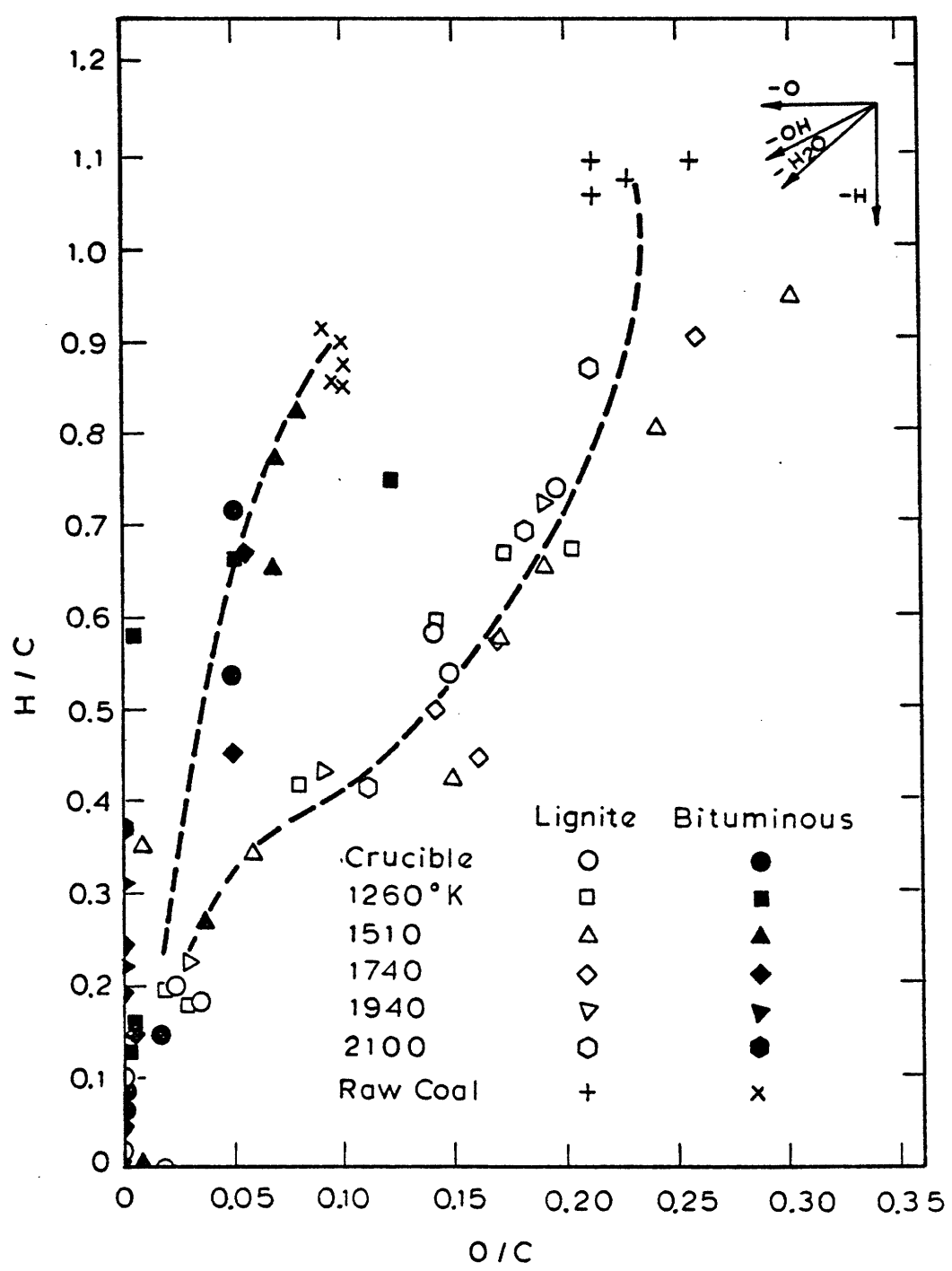
The H/C versus O/C diagram¹².

a. Coalification Diagram.



b. Carbonisation curves. x Cellulose; ● Limburg coal (semi-anthracite); + Limburg coal (medium rank); Δ Derbyshire coal; o Scottish coal.

FIG. 5.8 H/C VERSUS O/C DIAGRAMS FOR COALIFICATION AND CARBONIZATION. FROM VAN KREVELEN (1961).



ELEMENT CHANGE WITH COAL DEVOLATILIZATION

FIG. 5.9

The initial products of the pyrolysis of coal are considered to be related mainly to oxygen groups in coal. This view is supported by the high concentrations of water and carbon oxides in the initial volatile matter (Chukanov, 1954), and by the observed decreases in intensity of the hydrogen-bonded hydroxyl absorption band in infrared spectrometric measurements of char samples (Brown, 1955). In the retention versus weight loss diagrams (figures 4.22 and 4.23), rapid losses of hydrogen and oxygen associated with the first 10% weight loss appear to support the suggested mechanism. The average atomic C, H, O ratios in the crucible experiment at 610°K were $C_1 H_{5.3} O_{0.88}$ at 14% weight loss (d.a.f.) for the lignite (CR305 in Table E.1) and $C_1 H_{4.8} O_{1.15}$ at 10.7% weight loss (d.a.f.) for the bituminous coal (CR304 in Table E.2). The high concentrations of hydrogen in the volatile matter indicate loss of aliphatic groups. In fact, the close relationships between the volatile matter and the contents of aliphatic groups in coal has been discussed by Dryden (1957). For example, good agreement between the fraction of carbon in aliphatic form in the raw coal and the fraction of carbon lost in the volatile matter at 900°C was shown. However, Dryden stressed that the simple hypothesis that the aliphatic groups in coal solely contribute to the volatile matter is not acceptable. The remarkable resemblance of the volatile products of pyrolysis under high vacuum to the original coal (Orning and Greifer, 1956) suggested distillation of some portion of coal without changing the original structure. The extent of the loss of the aromatic structures is not well known, but Dryden (1957) suggested that 10 to 20% of the

original content of the aromatic structures may be lost.

For the two coals used in the present study, the following weight losses are estimated based on the functional group analysis of the similar coals. (Tables I.3 and I.4.)

Table 5.1

Estimated Weight Loss of Coal
by Loss of Functional Groups
(% d.a.f.)

	Aliphatic (1)*	Aliphatic Monoring (2)*	Aliphatic Peripheral (3)*
Lignite	44	64	82
HVA Bituminous	44	62	75

* Numbers refer to assumptions defined in text.

The assumptions employed in estimating the weight losses are (1) that all the oxygen, aliphatic carbon, and hydrogen are lost, (2) that all the oxygen, aliphatic carbon and hydrogen, and aromatic mono-rings are lost, and (3) that all the oxygen, aliphatic carbon and hydrogen, and aromatic carbon and hydrogen in the peripheral sites are lost. If the contributions of nitrogen and organic sulfur are included, the estimated values increase by a few percent. Although such estimations are very crude in view of the complicated mechanism of devolatilization, it is still of interest to compare these values with the

experimental results. The proximate volatile matter contents of both coals are close to the estimates based on the loss of the aliphatic groups. The highest weight loss observed for the lignite (63% at 2100°K) is comparable to the estimate based on the loss of the aliphatic groups and the mono-rings. The largest weight loss corrected for soot for the bituminous coal (about 80% at 2100°K) exceeds the estimated weight loss based on the loss of the aliphatic groups and peripheral groups. The differences between the two coals in the augmentation of the volatile yield could be due to the high oxygen content of the lignite coal. In extensive studies of model compounds of coal (Van Krevelen, 1961) oxygen groups such as hydroxyl were found to reduce the volatile yield by consuming available hydrogen thus promoting condensation of aromatic rings, or by providing oxygen cross linkings. The author noted the significant dependence of the volatile yield on the heating rate in the presence of oxygen groups, which was interpreted on the assumption that "depolymerization of the model substances is accompanied by a competing reaction in the form of a direct condensation proceeding via the polar groups." This mechanism implies that augmentation in the volatile yield for lignites is more difficult because of the larger fractions of the oxygen groups in lignites. In contrast to the effect of the oxygen groups, hydrogen is known to enhance the volatile yields, which was shown by the studies of model substances (Van Krevelen, 1961), and by devolatilization in hydrogen atmospheres (Anthony, 1974). In view of the importance of hydrogen in the mechanism of devolatilization, the observed behavior of hydrogen in the present experiments should be

closely examined.

Figures 5.10 and 5.11 show retention of hydrogen in char and H/C atomic ratio in volatile matter versus weight loss for each coal. The asymptotic values of H/C ratio in the volatile matter, $(H/C)_{\infty}$, were calculated assuming that all of the hydrogen, oxygen, sulfur and nitrogen are carried out in the volatile matter. The high H/C ratios in the crucible experiment at low weight losses were discussed before. The sharp rise of H/C ratio in the tail end of the crucible curve is considered to be mainly due to evolution of aromatic hydrogen, which is often termed secondary "degassing" in the carbonization of coal (Van Krevelen, 1961). Although the results of the laminar flow experiment show more scatter, clear difference exists between the results in the crucible experiment and those in the laminar flow experiment. It is evident that higher hydrogen retention for a given weight loss in the laminar flow runs resulted in a larger final weight loss. Several possible mechanisms can be proposed for the observed enhanced volatile yields under the laminar flow conditions.

- (1) More extensive break up of the particles or ejection of some of the "metaplast" for the case of the bituminous coal.
- (2) More rapid escape of the primary decomposition products, which have H/C ratios closer to those of the original coal, which decreases the secondary reactions forming char.
- (3) More rapid devolatilization at high temperatures which increases the rate of the decomposition reactions relative to that of the condensation reactions.

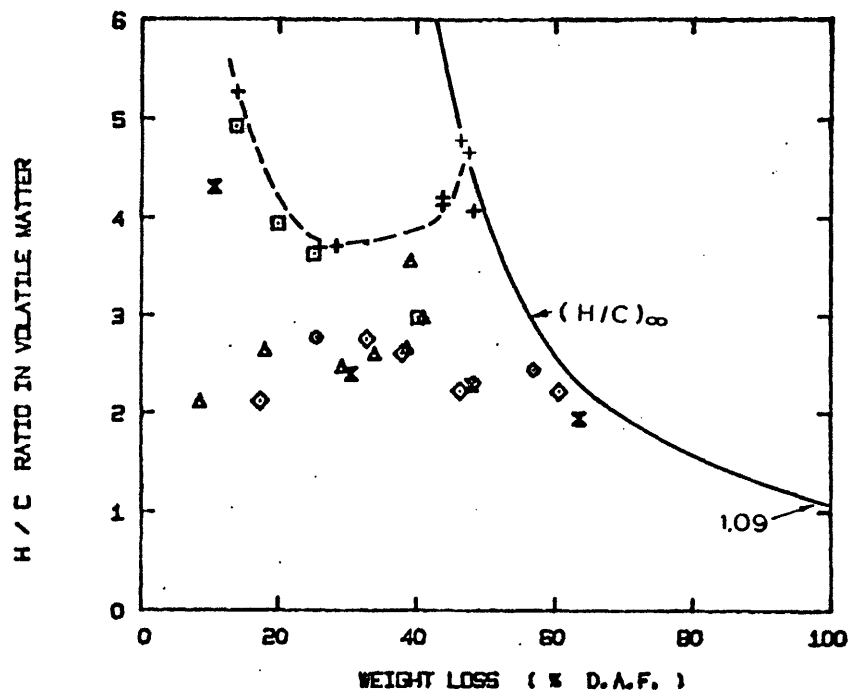
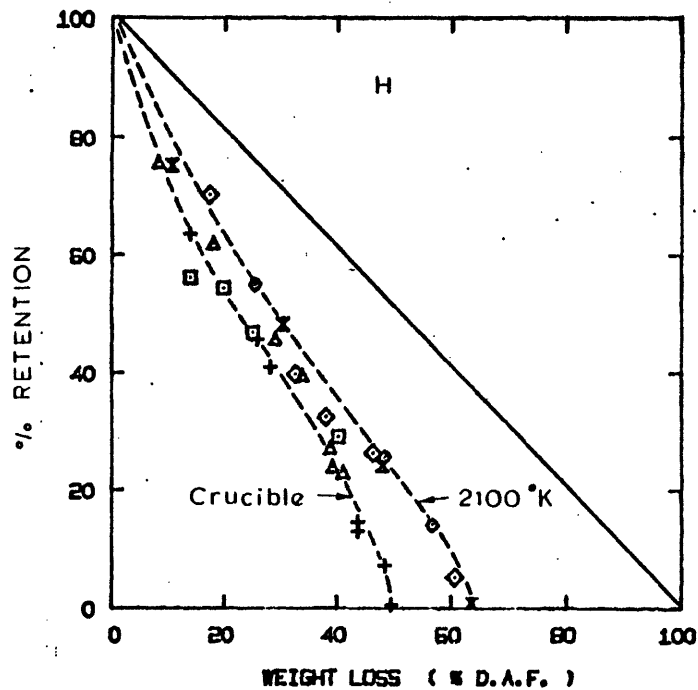


FIG. 5.10 BEHAVIOR OF HYDROGEN DURING DEVOLATILIZATION,
MONTANA LIGNITE.

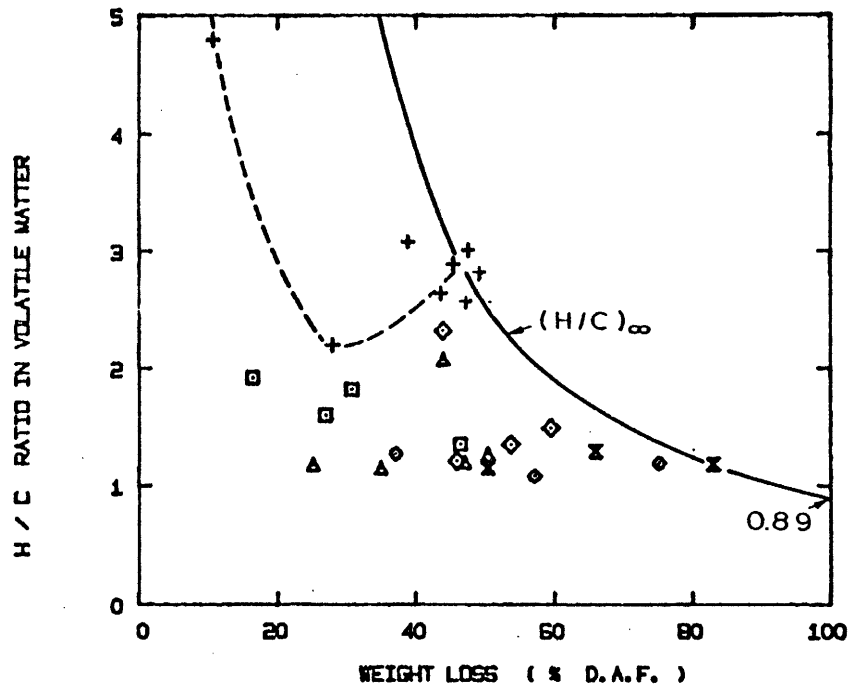
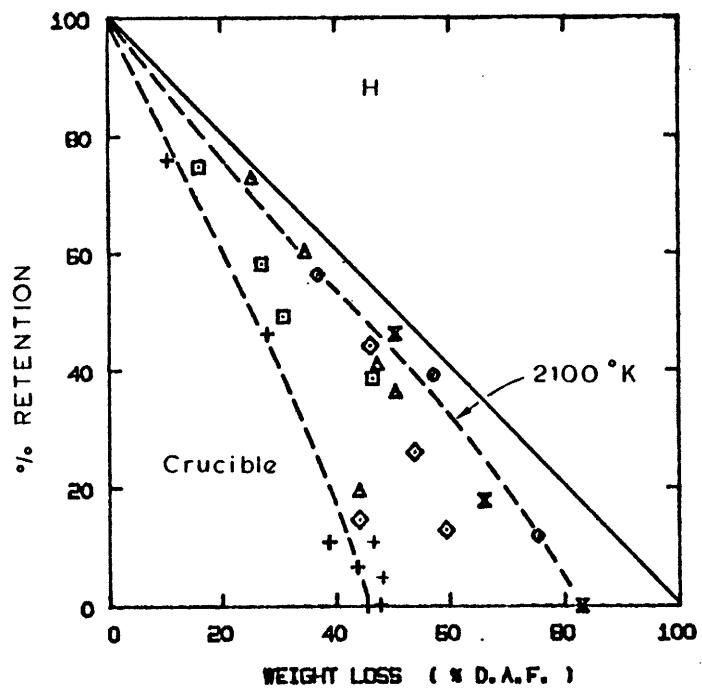


FIG. 5.11 BEHAVIOR OF HYDROGEN DURING DEVOLATILIZATION, PITTSBURGH SEAM BITUMINOUS COAL.

All of these hypotheses could explain the higher hydrogen retention in char from the laminar flow experiment. The behavior of nitrogen, i.e., no appreciable loss up to about 30% weight loss (Figs. 4.22 and 4.23) suggests that most of the volatile matter up to 30% weight loss is aliphatic, as nitrogen is mainly incorporated in the heterocyclic ring structures in the original coal (Pohl, 1976). The other possibility is that nitrogen is preferentially bonded in larger aromatic clusters and only small aromatic rings can escape in the initial volatile matter. If physical break-up is the mechanism, loss of nitrogen should be observed. Hence for the first hypothesis to be valid, physical break-up of the particles has to occur after 30% weight loss. The preliminary studies of the physical changes of the coals during the devolatilization by a scanning electron microscope (Appendix G) did not show any apparent increases in fine particles. Furthermore, the swelling of the bituminous coal appeared to be completed within the first 25% weight loss. Since ejection of "metaplas" is more likely during the rapid evolution of the volatile matter, no appreciable loss of nitrogen may suggest little chance of such mechanism. The negligible loss of ash, which is discussed in section 4.1.2, also provides a strong evidence against the physical break-up.

The second and the third hypotheses would explain the behavior of nitrogen by the mechanism mentioned before. The importance of the transport process of the volatile matter in the pores of coal will be discussed in the next section in relation to the second mechanism.

5.4 Effects of the Transport Process of Volatile Matter in the Pores of Coal on Secondary Char Forming Reactions

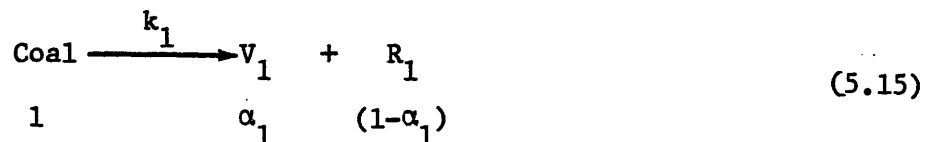
The volatile matter produced by the thermal decomposition of coal escapes through the small capillaries to the external surface of the coal for non-swelling coals or by a combination of bubbling through the plastic mass formed during heating and escape through capillaries for swelling coals. The apparent physical changes of coal particles such as swelling of coking coals are considered to be closely related to the transport mechanism of the volatile matter through capillaries or plastic coal mass. The internal surface area for coals with less than 85 percent carbon (d.m.f.) are in the range of $200 \text{ m}^2/\text{gm}$. Most of the surface area is accounted for by micropores with diameters less than about 12 \AA . Surface areas measured by adsorption of krypton at 77°K are typically $1\text{-}2 \text{ m}^2/\text{gm}$ for the coals used in this study (pores greater than about 12 \AA). The external surface area of monodispersed spherical coal particles, 40 micron in diameter, is about $0.1 \text{ m}^2/\text{gm}$ and is inversely proportioned to the diameter of the particles. (See Appendix I for more details.) The majority of the volatile matter is considered to be released into the micropores initially. Changes of the internal surface areas of coking coals under the carbonization conditions are not significant up to about 600°C . But above this temperature the larger pores which are accessible by large molecules such as krypton and argon decrease and almost completely vanish at temperatures about 1100°C , while the micropores remained approximately unchanged (Van Krevelen, 1961). Changes in the internal surface areas during devolatilization under rapid heating

conditions have not been extensively studied. Nsakada, et al. (1975) reported continuous increases of the surface area of a North Dakota lignite with the progress of devolatilization in an extrained flow reactor at a furnace temperature of about 800°C. The surface area of the 60 micron size particles measured by carbon dioxide absorption increased from 202 m²/gm for the raw coal to 321 m²/gm at 43 percent weight loss (d.a.f.). The surface area measured by nitrogen, which represents the larger pores, increased from less than 1 m²/gm for the raw coal to 35 m²/gm at 43 percent weight loss. The results of the surface area measurement under a slow heating condition in a fluidized bed for the same size coal showed 562 m²/gm with carbon dioxide and 165 m²/gm with nitrogen at 49 percent weight loss. These results indicate that most of the volatile matter pass through the micropores in any stages of devolatilization. The micropores may restrict the passage of some of the large molecules and may influence the composition of the volatile matter significantly. Experimental studies on the changes of the internal surface area and the pore sizes are not yet completed for the char samples obtained in the present study, and the detailed analysis of the mechanism of the transport process of the volatile matter through the micro-capillaries is beyond the scope of this work. However, one of the explanations proposed for the enhanced volatile yields under rapid heating conditions, that rapid escape of the volatile matter under rapid heating conditions diminishes the chance of the secondary reactions forming a solid residue, will be examined based on a simple model.

In spite of the fact that many researchers pointed out the importance of the secondary reactions in relation to the enhanced volatile yields observed under rapid heating conditions, very few theoretical models have been proposed. Anthony (1974) modeled the secondary char forming reaction to be competing with diffusional escape of the reactive volatile matter, the flow rate of which was assumed to be proportional to the product of the concentration of the volatile matter inside the pore and the overall mass transfer coefficient. He obtained a limited solution for the volatile yield under a steady-state isothermal condition and explained that the higher yields under reduced pressures occur through an increase in the overall mass transfer coefficient which was assumed to be inversely proportional to the total pressure. Although the model predicted the observed effects of the ambient pressure on the volatile yield well, the detailed transport mechanism is concealed in the assumed mass transfer coefficient. Of course such a model is simplistic, but it provides a convenient basis for qualitative studies of the complicated devolatilization mechanisms.

A more sophisticated model, but based on the same concept, is presented in this section and the effects of temperature and pressure on the volatile yields are discussed in order to test the model.

Two overall reactions of the following forms are assumed.



where V_1 denotes the volatile matter and R_1 and R_2 denote residue (char). The second reaction represents the (hypothesized) secondary char forming reactions. k_1 and k_2 are Arrhenius type rate constants and α_1 is the mass stoichiometric ratio. Assuming a first order rate for the decomposition of coal and a heterogeneous reaction, first order in the concentration of V_1 for the char forming step the following equations are obtained.

$$\frac{dm_C}{dt} = -k_1 m_C \quad (5.17)$$

$$\frac{dm_{V_1}}{dt} = \alpha_1 k_1 m_C - k_2 m_{V_1} S - \dot{m} \quad (5.18)$$

where m_C , m_{V_1} , \dot{m} and S denote d.a.f. mass of a coal particle, total mass of V_1 in the coal particle, total mass flux of the volatile matter (V_1) from the particle and internal surface area per unit volume of coal.

In Eq. (5.18) the first term is the production rate of V_1 by decomposition, the second term is the destruction rate by the char forming reaction and the third term represents the escape of the volatile matter from the coal particle. The average density of V_1 in the pores, ρ_{V_1} , and the total mass of V_1 in the coal, m_{V_1} , is related to the total pore volume, V_{pore} , by

$$m_{V_1} = \rho_{V_1} V_{\text{pore}} \quad (5.19)$$

The ratio of the average density of V_1 in the pores to that at the external surface of the particle is defined by ϕ .

$$\phi \equiv \rho_{V_1} / \rho_{V_1 S} \quad (5.20)$$

ϕ is always greater than unity and may be approximated by the ratio of the average internal pressure to the external pressure. Therefore, when the rate of evolution of the volatile matter is large, ϕ also becomes large. In the presence of both diffusion and convection, the mass flux of V_1 and the concentration of V_1 at the surface is related by the following equation assuming steady state, zero concentration of V_1 at infinity and spherical symmetry.

$$\dot{m} = -4\pi\rho_0 D r \cdot \ln\left(1 - \frac{\rho_{V_1,S}}{\rho_0}\right) \quad (5.21)$$

where ρ_0 , D and r denote total density of the gases, diffusion coefficient and the radius of the particle. To simplify the analysis, the following parameter is defined for Eq. (5.21).

$$\eta = -\frac{\rho_0}{\rho_{V_1,S}} \cdot \ln\left(1 - \frac{\rho_{V_1,S}}{\rho_0}\right) \quad (5.22)$$

It can be seen that η becomes unity when the convective effect is negligible ($\rho_{V_1,S}/\rho_0 \ll 1$), and it becomes much larger than unity when strong evolution of the gas exists ($\rho_{V_1,S}/\rho_0 \sim 1$). Equation (5.17) can be integrated to give

$$m_C = m_{C,0} e^{-\int_0^t k_1 dt} \quad (5.23)$$

where $m_{C,0}$ is the original d.a.f. mass of the coal particle. By using Eqs. (5.19), (5.20), (5.21), (5.22) and (5.23), Eq. (5.18) becomes

$$\frac{dm_{V_1}}{dt} = \alpha_1 m_{C,0} k_1 e^{-\int_0^t k_1 dt} - k_2 \cdot S \cdot m_{V_1} - \frac{4\pi D r \eta}{\phi V_{\text{pore}}} \cdot m_{V_1} \quad (5.24)$$

For the isothermal case (k_1, k_2 const.), Eq. (5.24) can be integrated to give the following solution, assuming that S, D, r, η, ϕ and V_{pore} are constant, expressed by certain average values.

$$m_{V_1} = \frac{\alpha_1 m_{C,0} k_1}{k_2 S - k_1 + \frac{4\pi r D \eta}{\phi V_{\text{pore}}}} \left[e^{-k_1 t} - e^{-(k_2 S + \frac{4\pi r D \eta}{\phi V_{\text{pore}}}) t} \right] \quad (5.25)$$

the total residue produced by the secondary reaction, m_{R_2} , is

$$m_{R_2} = \int_0^{\infty} V_{\text{pore}} \cdot k_2 \cdot \rho_{V_1} \cdot S dt = \frac{\alpha_1 m_{C,0}}{1+f(T,\rho,r)} \quad (5.26)$$

where

$$f(T,\rho,r) = \frac{4\pi r D \eta}{k_2 S V_{\text{pore}} \cdot \phi} \quad (5.27)$$

When $f(T,\rho,r)$ increases, the total residual matter decreases, and hence the overall volatile yield increases. An order of magnitude estimate of $f(T,\rho,r)$ is desirable to examine the effect of the changes in $f(T,\rho,r)$ on m_{R_2} , but the lack of knowledge on the exact nature of the rate of the assumed secondary reaction in relation to the actual physico-chemical process prevents such an attempt. Therefore the following arguments assume that the magnitude of $f(T,\rho,r)$ is comparable to or greater than 1, so that changes in $f(T,\rho,r)$ cause appreciable differences in m_{R_2} .

In order to examine the effect of temperature, pressure and the particle size on $f(T,\rho,r)$, the dependence of each parameter on the right hand side of Eq. (5.27) on these variables has to be known. The diffusion coefficient is usually proportional to temperature raised to 1.5 to 2.0th power and is inversely proportional to the pressure.

$$D \propto \frac{T^{1.5 \sim 2.0}}{P} \quad (5.28)$$

The temperature dependence of the reaction rate may be expressed as

$$k_2 \propto e^{-\frac{E_2}{RT}} \quad (5.29)$$

η can be reasonably estimated, given the average mass flux of the volatile matter. From Eq. (5.21)

$$\frac{\rho_{V1,S}}{\rho_0} = \left(1 - e^{-\frac{\dot{m}}{4\pi\rho_0 D} \cdot \frac{1}{r}} \right) \quad (5.30)$$

If we assume that half of the mass of a 40 micron coal particle is devolatilized in 1 millisecond, the following approximate value is obtained for the exponent in Eq. (5.30).

$$\frac{\dot{m}}{4\pi\rho_0 D} \cdot \frac{1}{r} \sim \frac{\rho_C r^2}{6 \rho_0 D t_{\text{reac}}} \sim \frac{1.3 \times (0.002)^2}{6 \times (4 \times 10^{-3}) \times (0.001)} \sim 0.2 \quad (5.31)$$

From Eqs. (5.22) and (5.30)

$$\eta \sim 1.1 \quad (5.32)$$

Since η is very close to 1 even under the extreme condition of rapid devolatilization, this implies that for small particles [note that Eq. (5.31) is proportional to the square of the diameter of the particle] diffusion is still the primary mode of mass transfer from the outer surface of the particle. Also it can be seen that Eq. (5.30) does not depend on the total pressure.

As mentioned before, ϕ is an approximate measure of the ratio of the internal pressure of the volatile matter to the pressure of the environment. If we assume the pressure difference is proportional to the mass flux of volatile matter as a first approximation, ϕ becomes a strong function of temperature since the rate of volatile production is proportional to $k_1 m_c$. Under this assumption

$$\phi \sim e^{-\frac{E_1}{RT}} \quad (5.33)$$

However, if the particle becomes plastic upon heating the internal pressure might not rise as much because of the swellings. The quantitative estimation of the internal pressure is quite difficult because of the lack of adequate knowledge on the physical structure of coal particles during devolatilization. Lewellen (1975) predicted a few hundreds atm of internal pressure, when a 70 micron particle is heated to 1000°C at 10,000°C/sec, in modeling the rapid devolatilization of coal based on a bubble transport mechanism. Although the calculated values may depend strongly on the assumptions employed, such as viscosity of the fluid coal, high internal pressures could be possible. Crude calculations by the author based on the experimentally measured gas flow rates through discs of coal and pressure drop at room temperature (Karn, et al. 1975) showed an internal pressure of 100 atm, which is not unreasonable under the high gas flow rates expected during the devolatilization.

The total pore volume, V_{pore} , is proportional to the cube of the particle size for raw coals.

$$V_{\text{pore}} \propto r^3 \quad (5.34)$$

When a cenosphere is formed during devolatilization, Eq. (5.34) predicts a large increase in the apparent pore volume. However, the surface area per unit volume, S , decreases approximately in inverse proportion to V_{pore} , if we assume the surface area per unit mass remains constant. [Such an assumption may be justified by the data on micropores under carbonization conditions (Van Krevelen, 1961) and under rapid heating conditions for a lignite (Nsakala, et al., 1975).] Hence, the product of S and V_{pore} might remain fairly constant.

By substituting Eqs. (5.28), (5.29), (5.31), (5.32) and (5.33) into Eq. (5.27), the following relation is obtained.

$$f(T, \rho, r) \sim \frac{T^{1.5 \sim 2.0}}{P} e^{\frac{E_1 + E_2}{T}} \cdot \frac{r}{S V_{\text{pore}}} \quad (5.35)$$

As Anthony (1974) explained, decreases in the pressure increases $f(T, \rho, r)$, and hence the volatile yield. However, increases in temperature appeared to predict lower overall volatile yield because of the strong temperature dependence of the reaction rate. It should be noted that a strong temperature dependence is predicted even if pressure effects are neglected [$E_1 = 0$ in Eq. (5.35)]. Although considerable uncertainty remains on the factor involving the physical change of coal (i.e., $r/S V_{\text{pore}}$), the experimental results of Nsakala suggest that they may not change markedly at least for lignites. Also it should be noted that a more complicated model based on the competition between a bubble transport mechanism and a

secondary char forming reaction predicted decreasing volatile yields with increasing heating rates (Lewellen, 1975), which was apparently due to the strong temperature dependence of the secondary reaction (an activation of 36.5 Kcal/mol was assumed)*.

In view of these facts, the commonly used hypothesis that rapid escape of volatile matter under rapid heating conditions diminishes the secondary char forming reactions does not appear to be supported. As discussed in section 5.1, rapid heating generally increases the effective devolatilization temperature and hence the rate of the assumed secondary reactions. Although the analysis presented in this section cannot exclude the possibility of such mechanism because of the insufficient knowledge on the physical changes of coal particles under different conditions, simplified models such as the one developed here cannot explain the enhanced volatile yields obtained at high temperatures.

5.5 Problems in Weight Loss Measurements Using Ash as a Tracer

Many investigators have used ash as a tracer in determining weight losses of pulverized coals (Nsakala et al., 1975; Stickler et al., 1974; Badzioch and Hawksley, 1970; Howard and Essenghigh, 1967). But the accuracy of the ash tracer method was not examined in depth in any of the works. In the present study, good particle recoveries

* Decrease in volatile yield was slight, but the heating rates examined were in the range in which little change in effective devolatilization temperature (see section 5.1) was expected. Therefore the qualitative trend is important. Lewellen explained the opposite trend in terms of more rapid bubble growth under high heating rates and suggested that the trend might be improved by modification in viscosity calculation. In the author's opinion the major factor is the increase in the rate of the secondary reaction due to the slight increase in the effective devolatilization temperature.

and an extensive study of the behavior of the ashes of the two coals under high temperature conditions (Padia, 1976) enabled a quantitative examination on the extent of the errors caused by the use of ash as a tracer. Possible problems associated with the method are first discussed and then these are reexamined in the light of the experimental results.

- (1) The percentage of ash in sized fractions of pulverized coals varies between size fractions in a manner that depends on the method of classification.
- (2) Some of the ash particles are not embedded in the coal particles, but exist as separate particles.
- (3) The original mineral matter undergoes different chemical reactions upon heating. Hence, pretreatments of coal at temperatures even lower than the standard ashing temperature could cause errors in estimating weight losses.
- (4) Significant loss of ash occurs at high temperatures due to vaporization and by decomposition. Furthermore, interactions between ash and carbon could contribute some of the weight losses of coal.

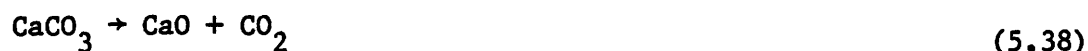
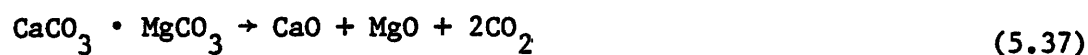
The first and the second points are important in relation to the sampling techniques used for char. Inertial separation methods such as a cyclone separation preferentially collect larger and heavier particles, which may have different ash contents compared to the average ash content of the original coal. Such a problem becomes more serious when a significant fraction of the ash exists as separate particles. In this study ash fractions of nominal 38-45 micron size group are 9.1 percent

for the lignite and 10.8 percent for the bituminous coal on a dry basis, and those of nominal 95-90 micron size group are 8.1 percent for the lignite and 11.8 percent for the bituminous coal. Although both coals were ground by the same ball mill and mechanically sieved by the same screens, the ash content is higher in smaller sized groups of the lignite and in the larger sized fraction of the bituminous coal. In the laminar flow experiment, use of the high flow rate of quenching water forced some of the fine particles through the bronze filter, which resulted in a significant underestimation of weight losses by the ash tracer method for the bituminous coal when the overall weight losses were below 20 percent (see Fig. 4.12). Separate tests under a simulated flow condition at room temperature reveals that the fraction of ash in the coal samples from the test experiment is about 15 percent lower than that of the original ash content. These observations are consistent with the work of Littlejohn (1966), in which he noted different ash fractions for different size groups and the existence of separate ash particles. Therefore it is recommended that the ash fraction of coal used in the ash tracer method should be that of coal particles which have experienced the same sampling process at room temperature as they would in the real experiment.

The third problem is related to the experimental observations that weight losses of the lignite by the ash tracer method were about 5 percent lower than those measured directly, even when the devolatilization temperatures were lower than the ashing temperature (Fig. 4.7). This was interpreted as a result of differences in CaSO_4 formation for ashes that are produced from coals preheated in the inert atmosphere to those

obtained without predevolatilization as described below (Padia, 1976).

"Analysis of the coal and ASTM ash shows that lignite ASTM ash contained more sulfate sulfur (about 0.38 percent by weight of coal) than the coal from which it was derived. This is probably due to transfer of some pyritic and organic sulfur to sulfate during ASTM ashing procedure by the following sequence of reactions:



SO_2 liberated due to oxidation of pyrites is picked up by CaO or MgO produced from decomposition of dolomite or calcite. Reactions (5.36) and (5.42) are favorable thermodynamically at ashing temperatures, ($\Delta G^\circ = -141.9$ Kcal/gmole, $\Delta G^\circ = -30.31$ Kcal/gmole). 0.38 percent of the weight of coal is equivalent to 4.75 percent by weight of ash (ASTM ash \approx 8 percent). In inert atmosphere FeS_2 decomposes first to FeS and then to Fe and sulfur is lost by sublimation. CaO produced by decomposition cannot form CaSO_4 due to absence of O_2 . Therefore the ash produced should weigh about 4.75 percent less than that produced by the ASTM method in

oxidizing atmosphere."

The extent of the above reactions depends both on temperature and time. When the reaction time is short enough, it may become insignificant. Hence, good agreement of the two methods of the determination of weight loss in the free fall experiment with the bronze collector (Fig. 4.7) could be understood in this context.

The fourth problem can be clearly seen in Figs. 4.9 and 4.10. Ash loss as high as 80 percent for the lignite and 50 percent for the bituminous coal were observed. Formation of silicon carbide from silica and carbon in char was discussed by Padia. It should be noted that reduction of metal oxides by carbon contributes to the weight loss of coal through formation of carbon oxides. The slight increases in weight losses in the crucible experiment above 1500°K are considered to be caused by such mechanisms, as only negligible amount of hydrogen and oxygen was left in char at 1500°K (Figs. 4.3 and 4.4).

In most of the cases the ash tracer method tend to underestimate the true weight loss as discussed here and in section 3.3. However in some cases, it could overestimate the apparent weight loss. Preferential loss of soot in the pores of the bronze filter in the laminar flow experiment presented such an example (Fig. 4.12), while at the same time it was used as a means for estimating the extent of soot formation. Another example of use of ash concentration in estimating the amount of soot in the free fall experiment is shown in Appendix C.

In summary, it has been shown that the ash tracer method alone could cause significant errors in determining the weight loss of coal. But the

combination of the two independent methods for the weight loss determination was clearly demonstrated to be valuable in analyzing the results of the different experiments.

5.6 Comparison of the Enhanced Volatile Yields with Those Reported in Previous Studies

With the high temperature rapid heating conditions achieved in the laminar flow furnace, apparent weight losses as high as 63 percent (d.a.f.) were obtained within 30 msec at 2100°K, and the weight losses determined using ash as a tracer for the bituminous coal, which was interpreted as the weight loss corrected for soot, was about 80 percent at 2100°K. These observations are consistent with the findings of Kimber and Gray (1967), who reported 72 percent (d.a.f.) weight loss for a low rank coal with 38 percent proximate volatile matter under the similar flow conditions at 2170°K (Table H.2). Figure 5.12 shows the comparison of the temperature dependence of the enhanced volatile yields. The estimated values of the asymptotic weight losses corrected for soot (Figs. 4.5 and 4.6) were used in calculating the ratio of the weight loss to the proximate volatile matter.* Since the Q factor assumes the same proportion of enhancement for the volatile matter remaining in char, it probably overestimates the asymptotic values of weight loss. (See section 1.1 for more details.) Therefore the ratio of the sum of weight loss and the volatile matter remaining in char to the proximate volatile matter of original coal, f'_E , is also shown. A large reduction in the ratio resulted for the data at 1050°K. As discussed in section 5.1, the effect of heating rate is

* Since char is assumed to contain no volatile matter, the ratio is equivalent to the ratio Q defined by Eq. (1.2).

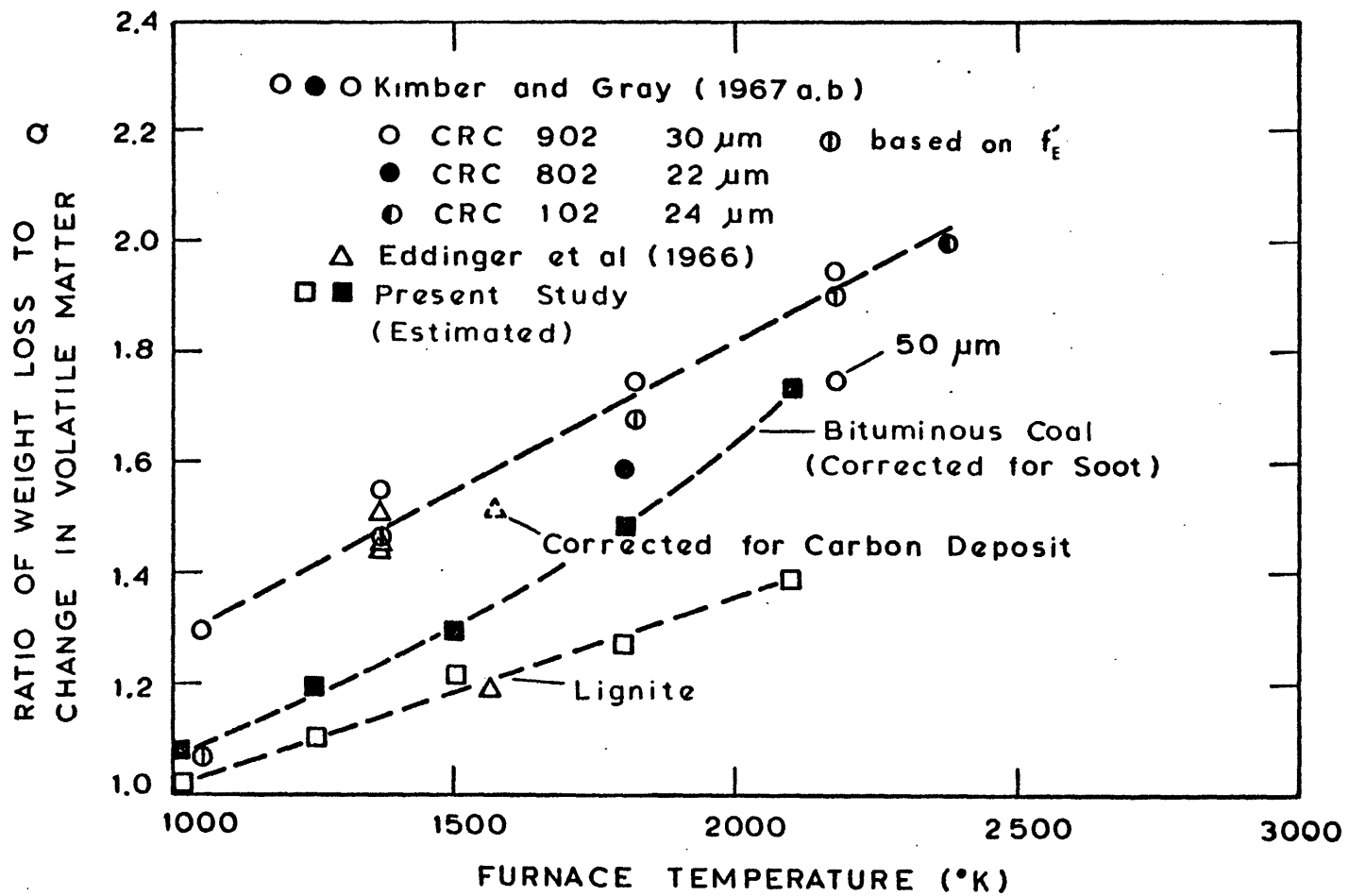


FIG. 5.12 COMPARISON OF ENHANCEMENT IN VOLATILE YIELD.

considered to be limited to the transient period of heating, and hence the asymptotic value of weight loss at an experimental temperature below that of the proximate test may be less than the sum of the weight loss measured in the experiment and the volatile matter remaining in char, which is determined by heating the sample to a temperature higher than the experimental temperature. Therefore the "Q factor" should not be considered as a reliable measure of the enhancement, especially at temperatures below that of the proximate test. In view of this, the small enhancements in volatile yields at around 1050°K agree with the expected small increases in effective temperature of devolatilization (section 5.1) which occur when the heating rate is increased. The estimated heat loss-temperature curves in Fig. 5.5 indicate that the average temperature of devolatilization for the crucible runs at 1220°K was about 900°K, and the rapid heating to 1000°K shifted the average temperature by 100°K resulting in the increase in weight loss from 44 percent to 51 percent. The expected heating rate of the proximate volatile test (a few minutes to 1220°K) is somewhat larger than that of the crucible run at 1220°K (several minutes to 1220°K), and so is the volatile yield (46 percent d.a.f.).

These results appeared to suggest that little increases in volatile yields could be expected by increasing the heating rate to the peak temperatures below about 1000°K, since the effective devolatilization temperature of the proximate test is considered to be close to 1000°K.

At high temperatures the results of Kimber and Gray show larger enhancements than observed in the present study, especially compared to those for the lignite. Since the experimental conditions in the present study and the Kimber and Gray reference were quite similar, the differences may be attributable to the differences in the coals studied. As discussed in section 5.3, there is some evidence that the hydrogen and oxygen contents in coal are also related to the enhancements in volatile yields observed at high temperatures. In order to examine the possible relation, the normalized enhancement factor, f , was compared with the H/C and O/C ratios of the parent coal using the experimental results of Badzioch and Hawksley (1967). f is defined as

$$f = \frac{\Delta W_{\infty} - V_0}{100 - V_0} \quad (5.36)$$

where V_0 and ΔW_{∞} denote the proximate volatile matter of original coal (% d.m.f.) and the asymptotic weight loss determined under specific experimental conditions. f can be interpreted as the fraction of the "fixed carbon" converted into volatile matter. Since the true asymptotic values are not available, ΔW_{∞} is approximated by the sum of weight loss and the volatile matter remaining in char (Table H.1). Figure 5.13 shows the results. Coals with high hydrogen contents and relatively low oxygen contents appear to show larger conversion of the "fixed carbon," which agrees with the previous statement that hydrogen promotes the volatile yield and oxygen tends to retard it. A separate experimental study on

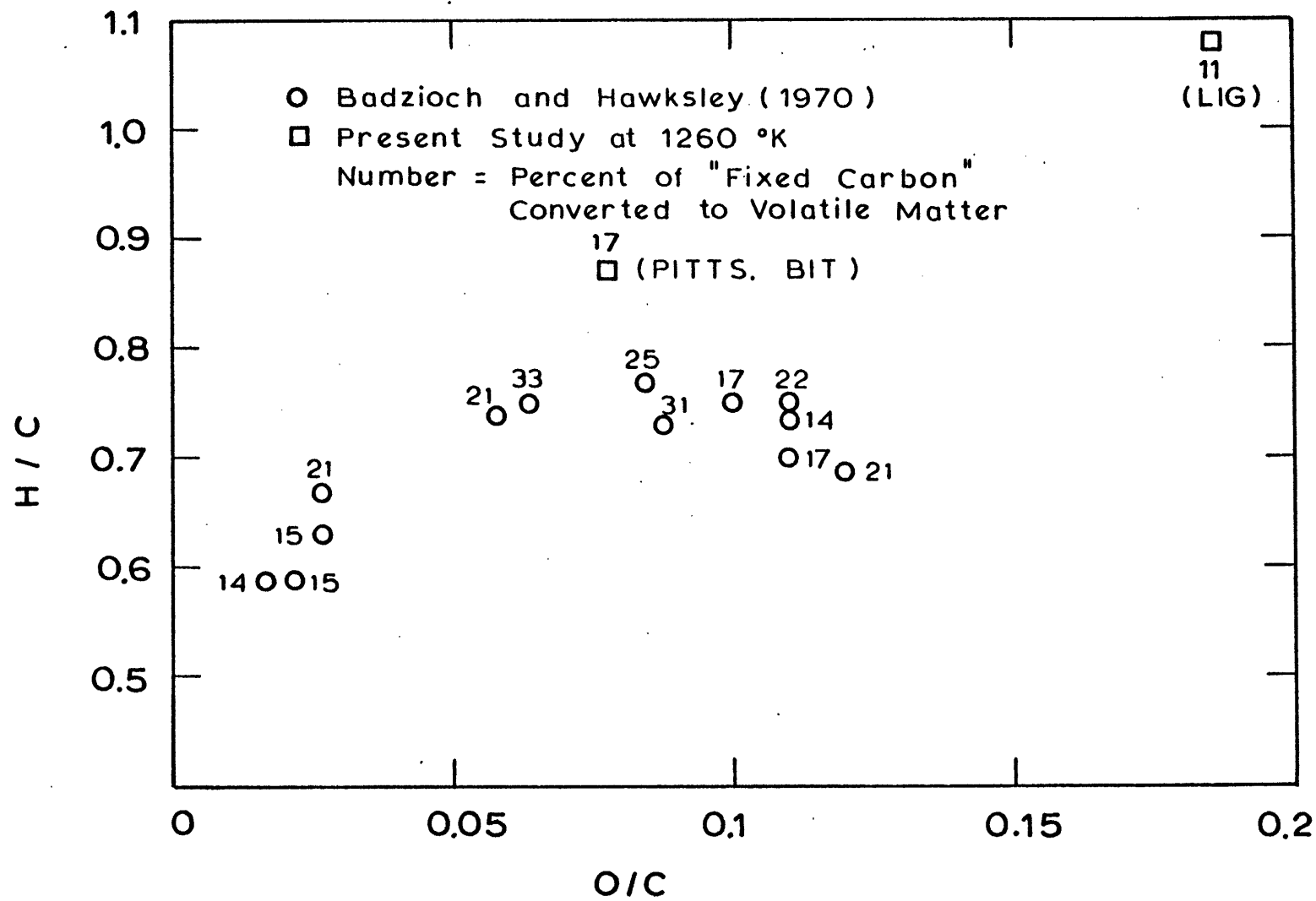


FIG. 5.13 DIFFERENT COALS AND ENHANCEMENT IN VOLATILE YIELD.

the oxidation of the bituminous coal showed as much as a 9 percent (d.a.f.) decreased in proximate volatile matter for coals kept in an oven at 105°C for 144 hours in air. The two coals used in this study are also plotted for comparison.

Anthony (1974) studied the devolatilization of a Montana lignite and a Pittsburgh seam HVA bituminous coal from the same mines as the two coals used in this study (see Table H.8). Since the proximate analyses between Anthony's coal and those of the present study are similar, it is of interest to compare the results obtained in the two studies. In some of Anthony's experiments a small amount of coal particles (5 to 10 mg) were heated in an electrical wire screen to 1000°C at heating rates between 600 and 1000°C/sec in various atmospheres. In a helium atmosphere, no effect of pressure was observed for the lignite, but the weight loss (d.a.f.) for the bituminous coal changed from 42 percent at 69 atm to 56 percent at 1 atm to 61 percent at 10^{-3} atm, as compared with a 46 percent (d.a.f.) proximate volatile matter. The value at 1 atm agrees well with the present data in the free fall experiment at 1260°K (about 58 percent). In a later publication Anthony et al. (1975) reported an additional loss of 4.5 percent to 7 percent of the weight of the original coal (as received basis) when the char sample was heated in a proximate apparatus for 420 sec. Since the extent of soot and tar trapped in the screen is not known, discrepancies of several percentages are possible in the absolute weight losses quoted. The results for lignite appeared to be quite different. The observed low

yield compared to the proximate volatile matter (46 percent d.a.f.) could be explained by the possible volatile content of the residual char. The volatile yield of the present lignite at 1260°K is higher than the value reported by Anthony by about 10 percent. There are, however, some indications from a recent examination that these differences are due to variation in the properties of the lignites, even though they are from the same mine.

5.7 Concluding Remarks

The importance of heating rates on the volatile yields was analyzed in terms of the changes in the effective reaction temperatures. Conditions where little effect of heating rate is expected are clarified through the definition of the critical heating rate in section 5.1. Based on this concept, the possibility of the formation of solid residue by secondary reactions on the external surfaces of coal particle was examined as a hypothesis to explain the observed differences in weight loss between the crucible runs and the free fall runs with the alumina collector. The insensitivity of volatile yield on bed depth led to the conclusion that the observed differences in weight loss were too large to be explained by the secondary reactions on the external surface of the coal particles.

The possibility of physical beakup or ejection of 'metaplast' as a mechanism to enhance the volatile yields under the rapid heating conditions was then examined in relation to the changes in the elemental composition in char during the devolatilization. Such mechanism appears

to be unlikely due to the good recovery of ash particles and the observed behavior of nitrogen in char.

The commonly used hypothesis that rapid escape of the volatile matter under rapid heating conditions decreases the secondary char forming reactions resulting in larger overall volatile yield was examined, based on a simple model describing the competition of the secondary reaction with the transport process. For lignite, which undergoes little apparent physical changes during devolatilization, the model appeared to contradict experimental observations as a consequence of the strong temperature dependence of the assumed secondary reactions relative to that of mass transfer process. For bituminous coal, uncertainty in the interpretation of the model remained due to the significant changes in the physical structure, but the model, as it is, was judged to be inadequate to explain the observed temperature dependence of the volatile yield.

In view of these fact and the experimental evidence on the important roles of hydrogen rich groups the following mechanism could be considered.

At relatively low temperatures mainly aliphatic and hydroaromatic bonds break to produce hydrogen rich volatiles. The remaining aromatic lamella condense to form larger noninvolatile units and the aromatic hydrogen is removed slowly. Further heating of such material to high temperatures may produce more radicals, but the loss of hydrogen rich groups in the early stage reduces the formation of small volatile species.

At high temperatures the rates of various bond reactions tend to overlap each other because of the similarity of the frequency

factors. Therefore, when coal 'molecules' are heated rapidly to high temperatures, large number of radicals are formed in the presence of hydrogen rich groups, hence preventing condensation or polymerization reactions leading to a solid residue.

Although the transport mechanisms contribute to increases in the volatile yield, the above mechanisms assume that the dominant factor is due to changes with temperature of the governing chemical reactions.

CHAPTER VI

KINETICS OF DEVOLATILIZATION6.1 First Order Arrhenius Parameters

Most of the kinetic parameters on the devolatilization of coal derived in the past were based on a first order reaction with respect to the remaining volatile matter. The rate equation is typically expressed by

$$\frac{dV}{dt} = k \cdot (V_{\infty} - V) \quad (6.1)$$

$$k = B e^{-\frac{E}{RT}} \quad (6.2)$$

Although the physical significance of the rate parameters obtained by such model is questionable, it provided a reasonably good correlation of the data for relatively narrow experimental ranges. Comparison of the first order rate parameters, however, show wide variations among different coals and also among different experimental conditions. In Fig. 1.3, some of the rate parameters obtained by different investigators are plotted. Since the present study extended the temperature range to a regime in which no kinetic parameters were available, it is of interest to compare the results on a common ground. Determination of the devolatilization rates, k , from Eq. (6.1) requires knowledge of the asymptotic values of the volatile matter evolved from the particle, V_{∞} , which depend on the temperature of devolatilization and other experimental conditions as observed in the experiments. Opinions may differ on whether different asymptotic value or a common value should be used. Based on the underlying concept of the single overall reaction that coal

'molecules' decompose to produce volatile matter and char with certain stoichiometric ratio, a constant value of 70% for V_{∞} was used in this study. The rates were determined by differentiating the weight loss-time curves and evaluating the rate constant at the instantaneous temperature of that point [calculated through the simplified model to predict the particle temperature (chapter 3)]. Since the data were considerably scattered, differentiations based on the actual data points would introduce significant scatters in the data. In view of the wide variations in the measured rates for different coals (Fig. 1.3), which showed more than two order of magnitude differences at the same temperature for some coals, it suffices to obtain approximate rates by graphically differentiating the smoothed weight loss-time curves. Such a method may give accuracies within about 20% of the determined rates. From Figs. 4.1 and 4.2, slopes of the smoothed weight loss-time curves at every 10% weight loss were taken. At high temperature and short residence times, considerably uncertainty exists on the temperatures at which the data should be associated. Therefore most of the data in the transient time of heating were discarded in order to avoid possible errors in the estimated temperature time histories of the coal particles. Also important is the sensitivity of Eq. (6.1) on the value of V_{∞} when the volatile yield is close to the asymptotic value. Therefore weight losses only up to 50% were used in the determination of the rates. Figures 6.1 and 6.2 show the results. Considerable scatter exists, but a clear trend is seen. The rate parameters based on the apparent trend

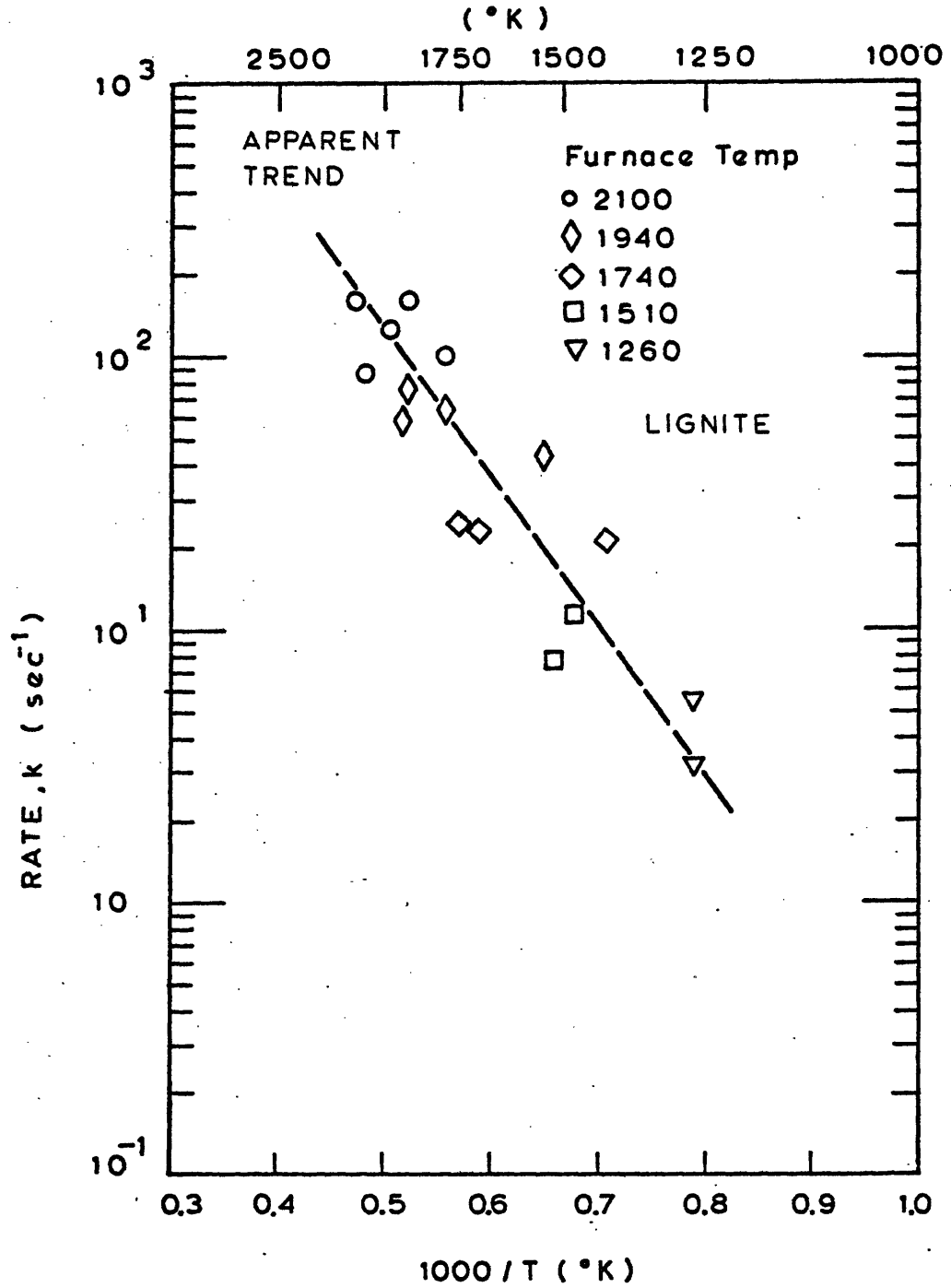


FIG. 6.1 FIRST ORDER ARRHENIUS PLOT FOR WEIGHT LOSS. MONTANA LIGNITE.

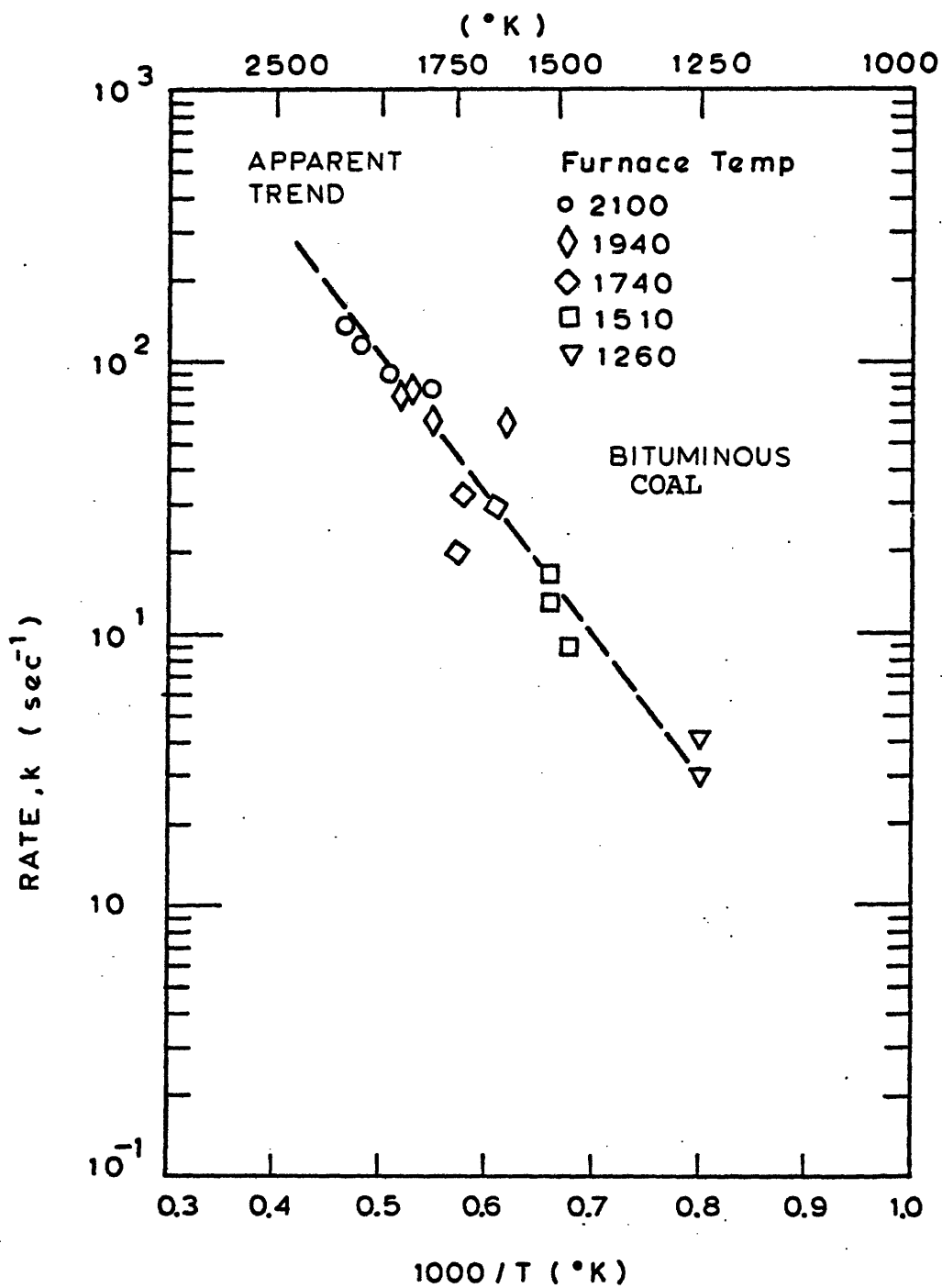


FIG. 6.2 FIRST ORDER ARRHENIUS PLOT FOR WEIGHT LOSS. PITTSBURGH SEAM BITUMINOUS COAL.

are

$$E \sim 25 \text{ Kcal/mole} \quad (6.3)$$

$$B \sim 6.6 \times 10^4 \text{ sec}^{-1} \quad (6.4)$$

The same method can be applied to the major elements in coal by using the retention-time curves (Figs. 4.18 and 4.19). Since the number of data points was only 3 to 5 at each temperature, slopes were evaluated only at middle data points. As the asymptotic values of retention, 40% was assumed for carbon and 0% for hydrogen and oxygen. Figures 6.3 and 6.4 show the results. The numbers beside the data points indicate the percent retentions for the data points. The rate parameters based on the apparent trends of carbon and hydrogen were very close to those for the overall weight. The "activation energy" for oxygen appeared to be somewhat lower than those for carbon and hydrogen, but it may well be within the scatter of data as the method employed in calculating the rates was relatively crude. Hence, the rate parameters obtained for the overall weight loss may be considered to be representative for all the elements. The same rate for different elements is not surprising. Since the elements are bonded together in many different ways in the structure of coal, ruptures of bonds produce volatile species with certain compositions of the elements, which may give nearly constant rates for each element on the overall average.

6.2 Comparison With Previous Results

The rates obtained in this study are shown in 6.5 together with the rates obtained under various conditions in the past. The source of the

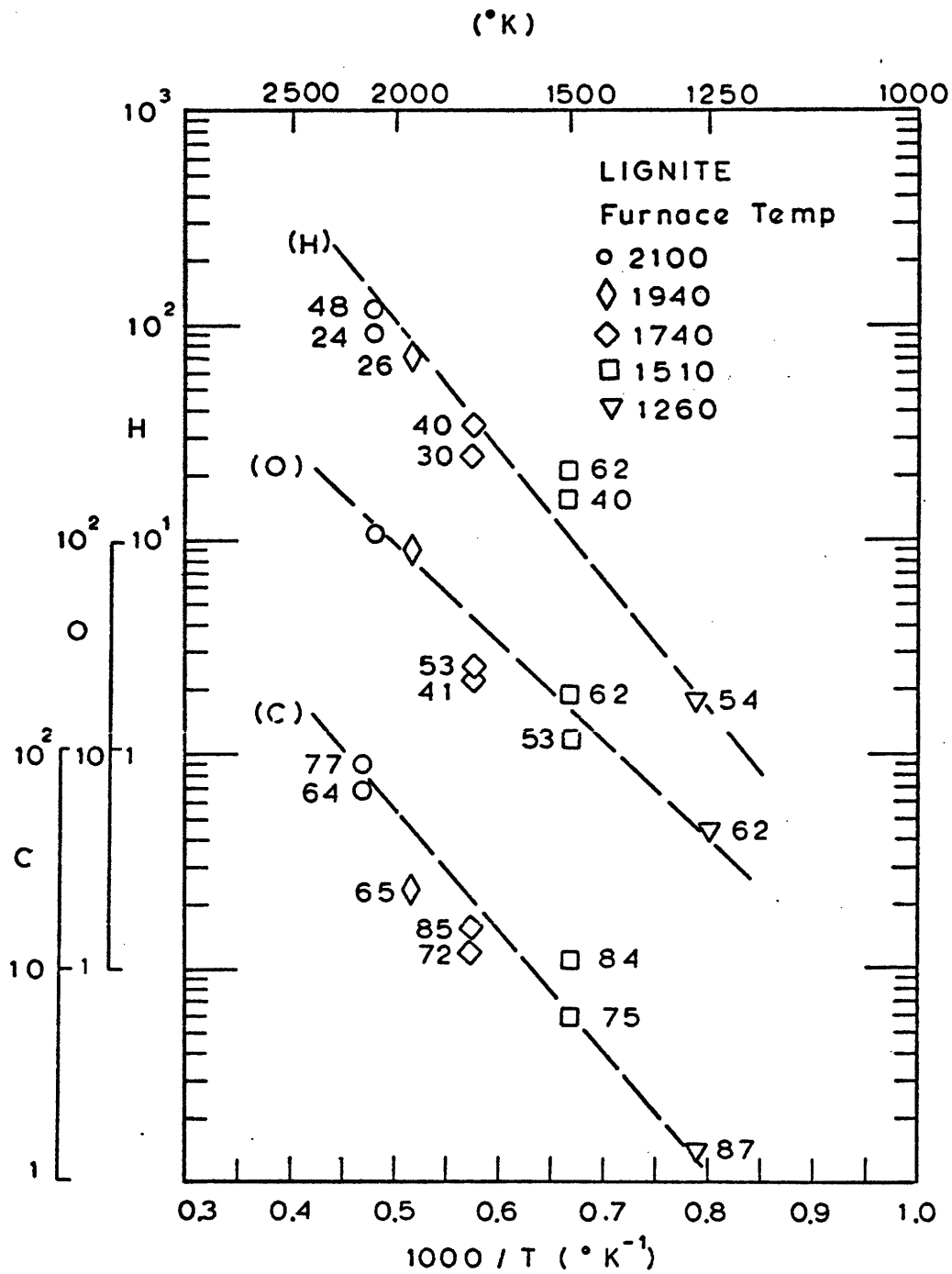


FIG. 6.3 FIRST ORDER ARRHENIUS PLOT FOR RETENTION OF C, H, O. MONTANA LIGNITE.

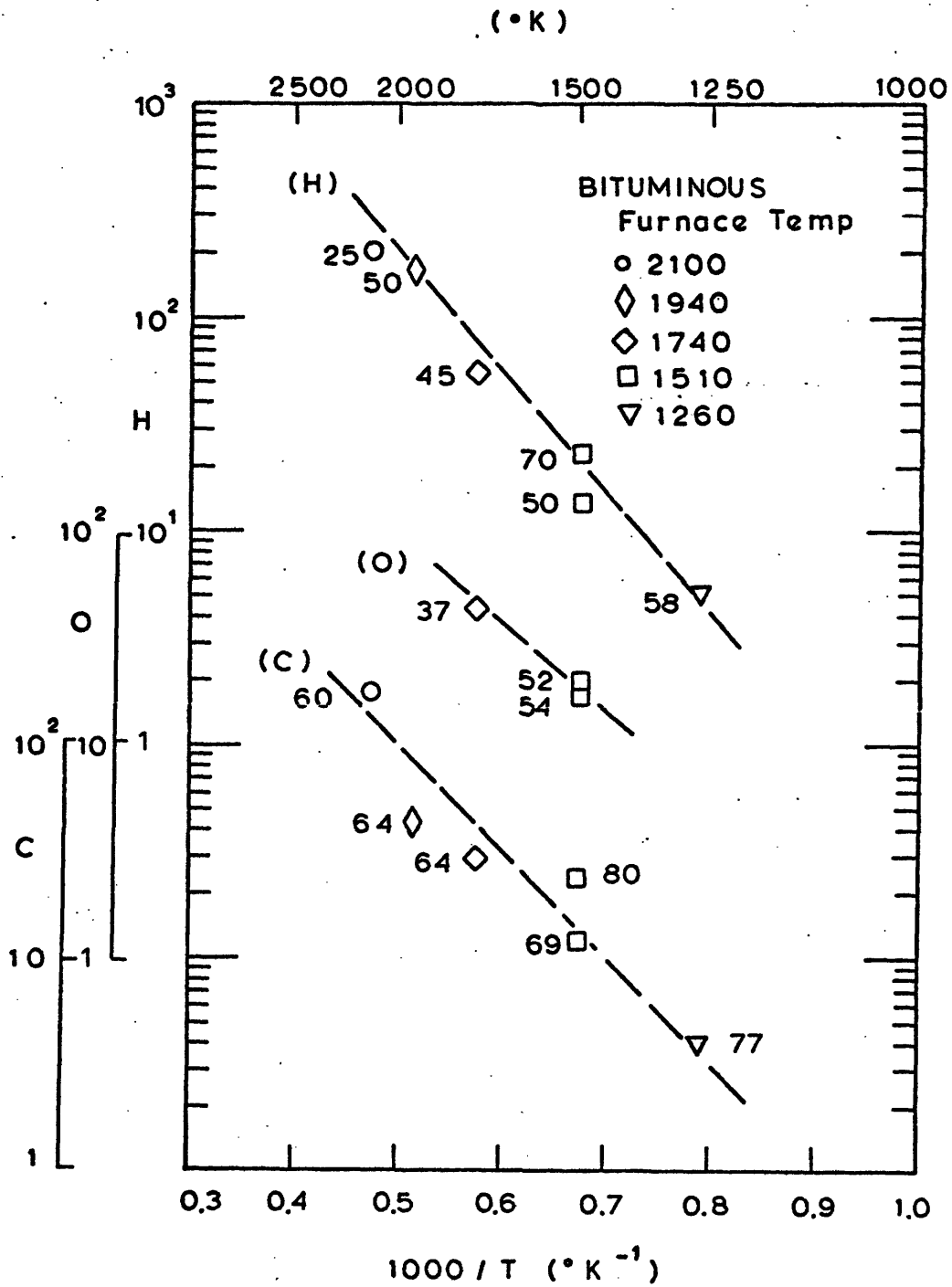


FIG. 6.4 FIRST ORDER ARRHENIUS PLOT FOR RETENTION OF C, H, O. PITTSBURGH SEAM BITUMINOUS COAL.

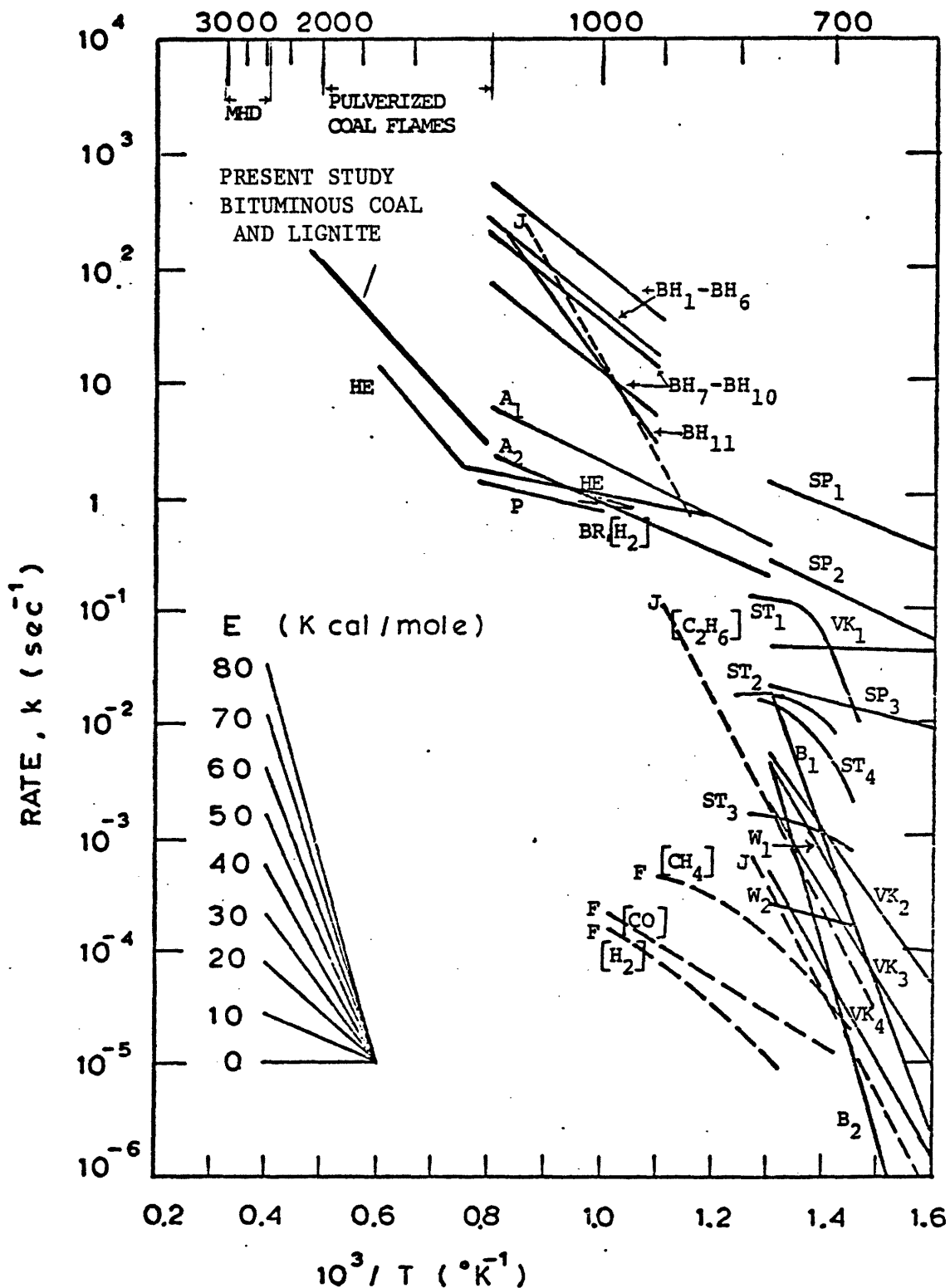


FIG. 6.5 COMPARISON OF DEVOLATILIZATION RATE CONSTANTS

data are tabulated in Table 1.1. The present results appeared to fit the overall trend, although large variation of rates exists especially at low temperatures. Since the data in figure 6.5 include a wide range of coals and various experimental conditions, effects of these factors on the rates have to be accounted for.

Figure 6.6 shows the variation of the rates for different coals under the same experimental conditions. Van Krevelan et al. (1951) obtained the rates by a thermogravimetric method by heating coals in a static bed at a constant rate of 2°C/min. The rates applies only to the authors 'primary' decomposition and the weight losses by the 'secondary degasification' process were compensated. For the bituminous coals, the differences were within about one and half order of magnitude, being higher for the coals with large volatile contents. The rate of devolatilization of the brown coal was about two to four orders of magnitude higher than those for the bituminous coals. Bazioch and Hawksby (1970) measured the devolatilization rates of eleven different coals in a flow furnace similar to the one used in this study. They observed a difference of about one and half order of magnitude for their coals, with the highest values found for the cases of the swelling bituminous coals. Since the volatile matter contents were higher for the weakly swelling coals, the relation of the rates to the volatile matter contents is opposite to that observed by Van Krevelen. From these two cases, it is clear that differences in coal alone, in the bituminous range, can cause one and half order of magnitude differences in the rate of devolatilization, and as large as four order of magnitude differences

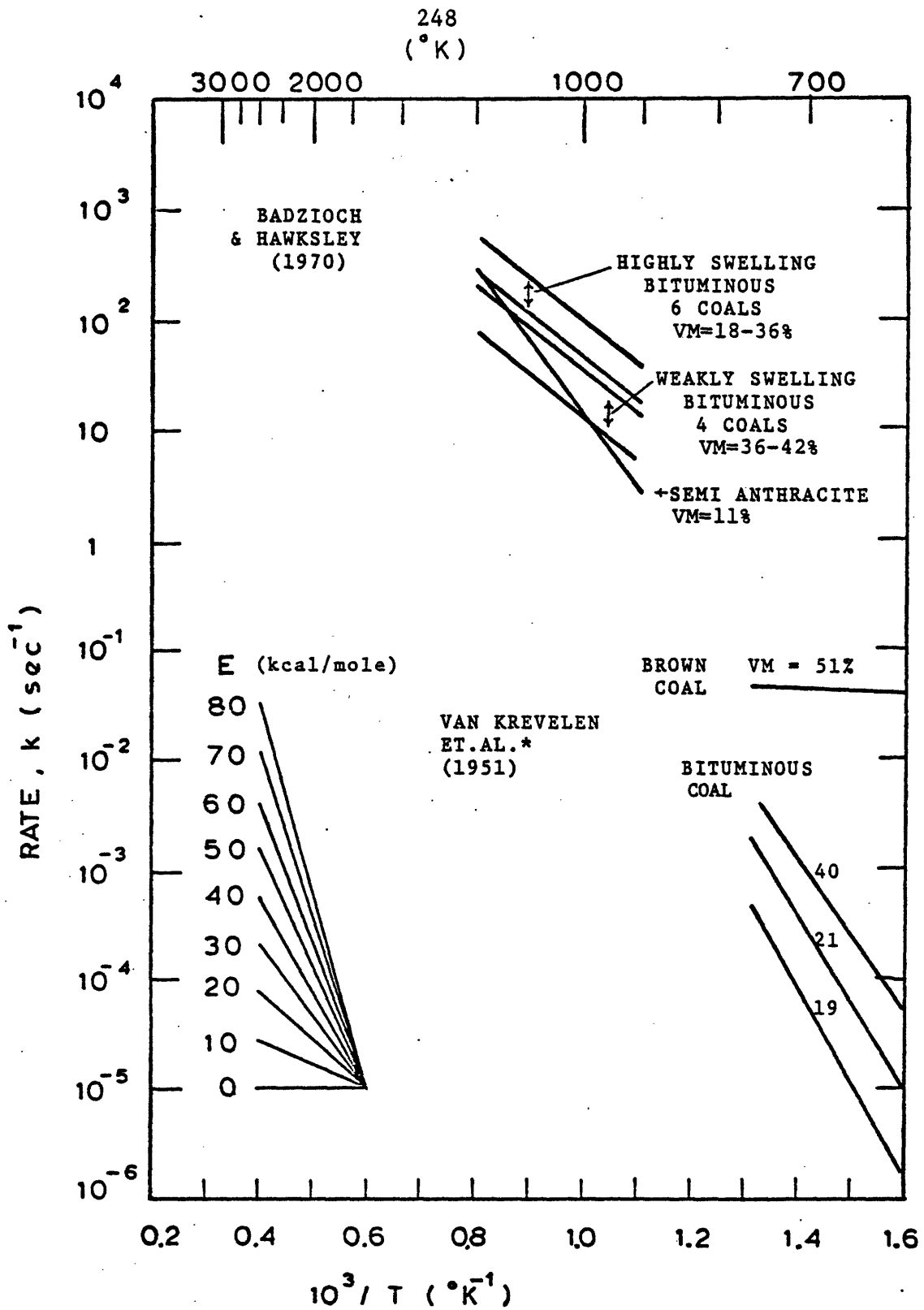


FIGURE 6.6 VARIATION OF DEVOLATILIZATION RATE CONSTANTS FOR DIFFERENT COALS

*Numerical Results modified by Jüntgen and Van Heek (1970)

could be explained if the coal differs widely in rank (e.g., brown coal vs low volatile bituminous coal).

Figure 6.7 shows variation of the rates for different stages of devolatilization under same experimental conditions for a give coal. Shapatina measured the weight loss by dropping coal particles in a vertical furnace and keeping the collected particles at a constant temperature for a certain period of time. Stone's method involved the rapid introduction of large amount of coal into a fluidized sand bed and samplings of the char/sample mixture every 15 seconds. In both cases, weight losses were determined from the volatile matter content of char, a method which tends to underestimate the weight loss because of the possible enhancement of volatile matter. Although the divisions of the devolatilization by the arbitrary reaction times are questionable, these results demonstrate wide variations of rates depending on the stage of devolatilization. Similar trends were observed in the present study. The rates in the laminar flow experiment (the reaction time 0 - 200 msec) were about one to two order of magnitude larger than those in the free fall experiments (about 1 sec with the bronze collector and about 10 min with the alumina collector). From these observations differences in the data reduction appeared to cause as much as two order of magnitude differences in the rates. If a single rate is applied to these cases the rates are expected to become close to the average value. It should be noted that the rate for the brown coal obtained by Van Krevelen lies between the last two zones of the Shapatina's rates for his brown coal.

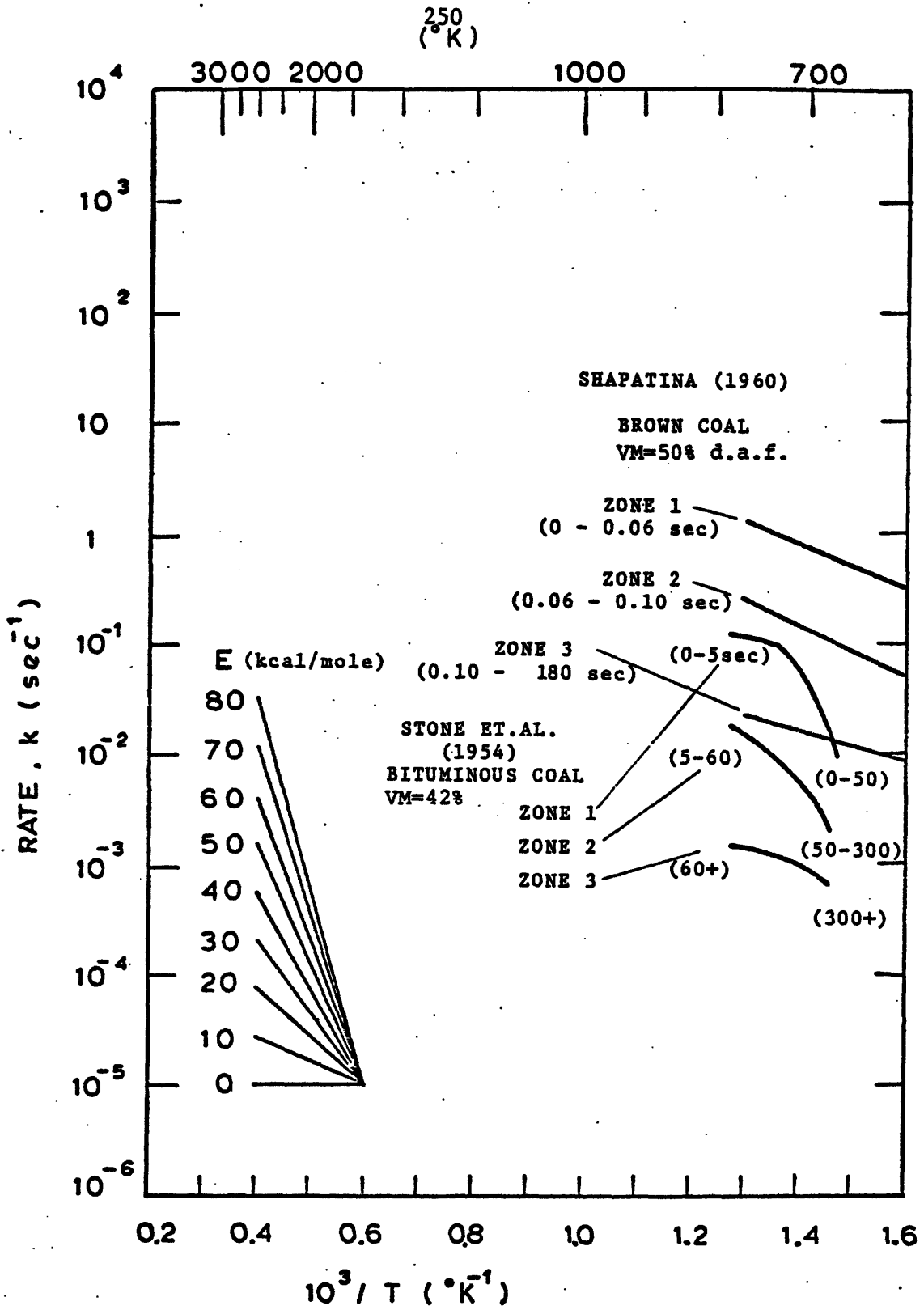


FIGURE 6.7 VARIATION OF DEVOLATILIZATION RATE CONSTANTS FOR DIFFERENT STAGES OF DEVOLATILIZATION.

By discarding the rates for the brown coals and for gases and retaining the rates of "zone 2" for Stone, Fig. 6.8 was obtained. Considering the differences in coal, a reasonable trend is now observed. By limiting the data, further more, to Pittsburgh Seam high volatile bituminous coals, figure 6.9 shows good agreements among different experimental conditions: present results from the flow furnace in argon atmosphere, Howard and Essenghing's in a pulverized coal flame, Anthony's by an electrically heated wire screen and Stone's et al. in a fluidized sand bed. Since the assumed asymptotic volatile yields were larger for the present study, use of a common value may increase the slope of the overall trend, but good agreements will be maintained in anycase.

6.3 Comparison With The Rates Of Decomposition Of Pure Hydrocarbons

Figure 6.10 shows comparison of the rates of devolatilization of coal with those for the decomposition of pure hydrocarbons. Virk et al. (1974) reported the first order rate parameters for decomposition of various aromatic compounds. The rates for benzene and anthracene are shown in the figure. Formations of two benzyl radicals from dibenzyl, and naphthal methylene radical atomic hydrogen from methyl naphthaline and methyl radicals from ethane are chosen as they may represent some of the typical aliphatic bond ruptures which could occur during the pyrolysis of coal. As seen from the figure, the rates of decomposition of these pure compounds and those for the overall volatile yields appeared to be in the same ranges. Considering the possible numerous reactions during

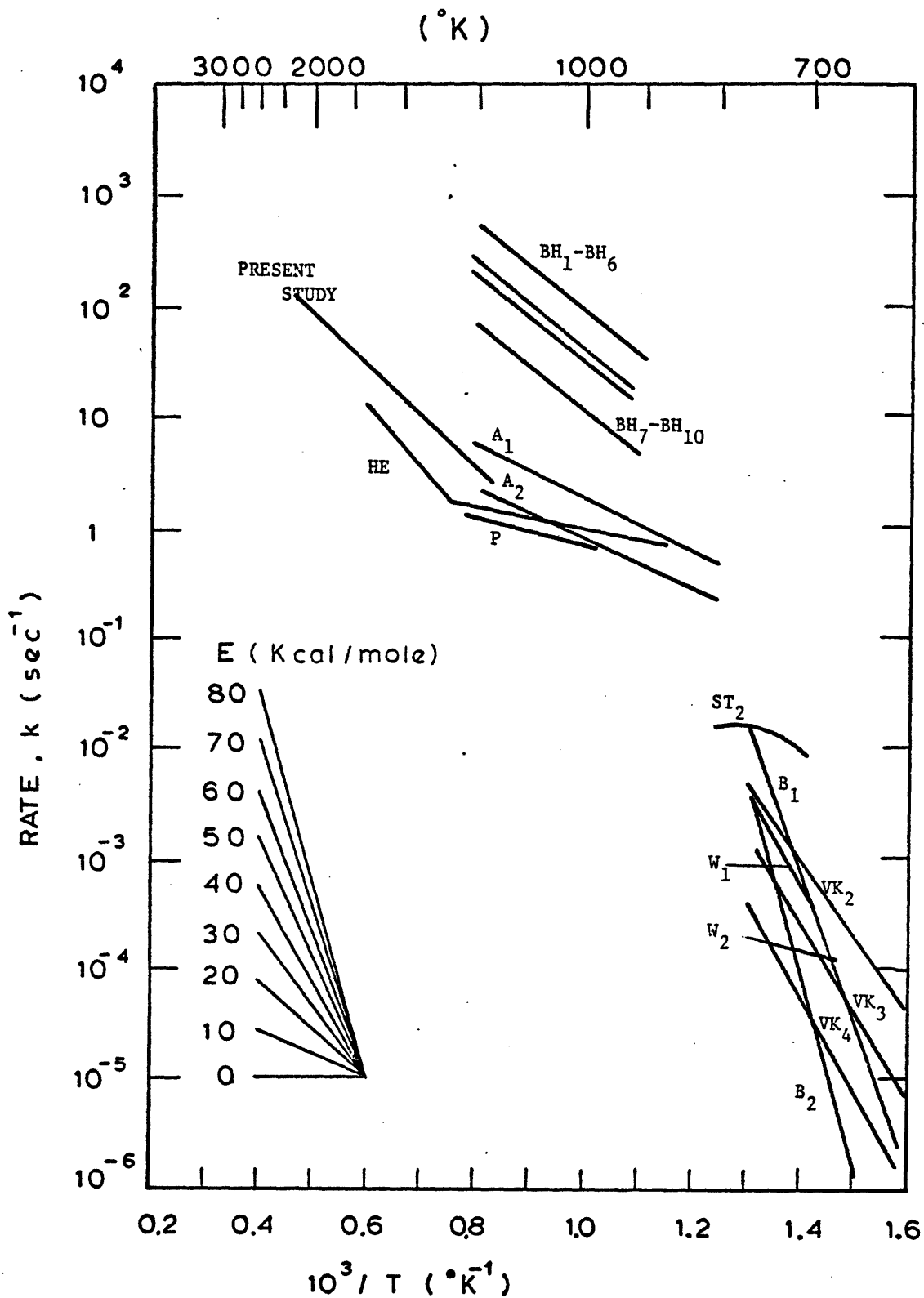


FIG. 6.8 COMPARISON OF DEVOLATILIZATION RATE CONSTANTS

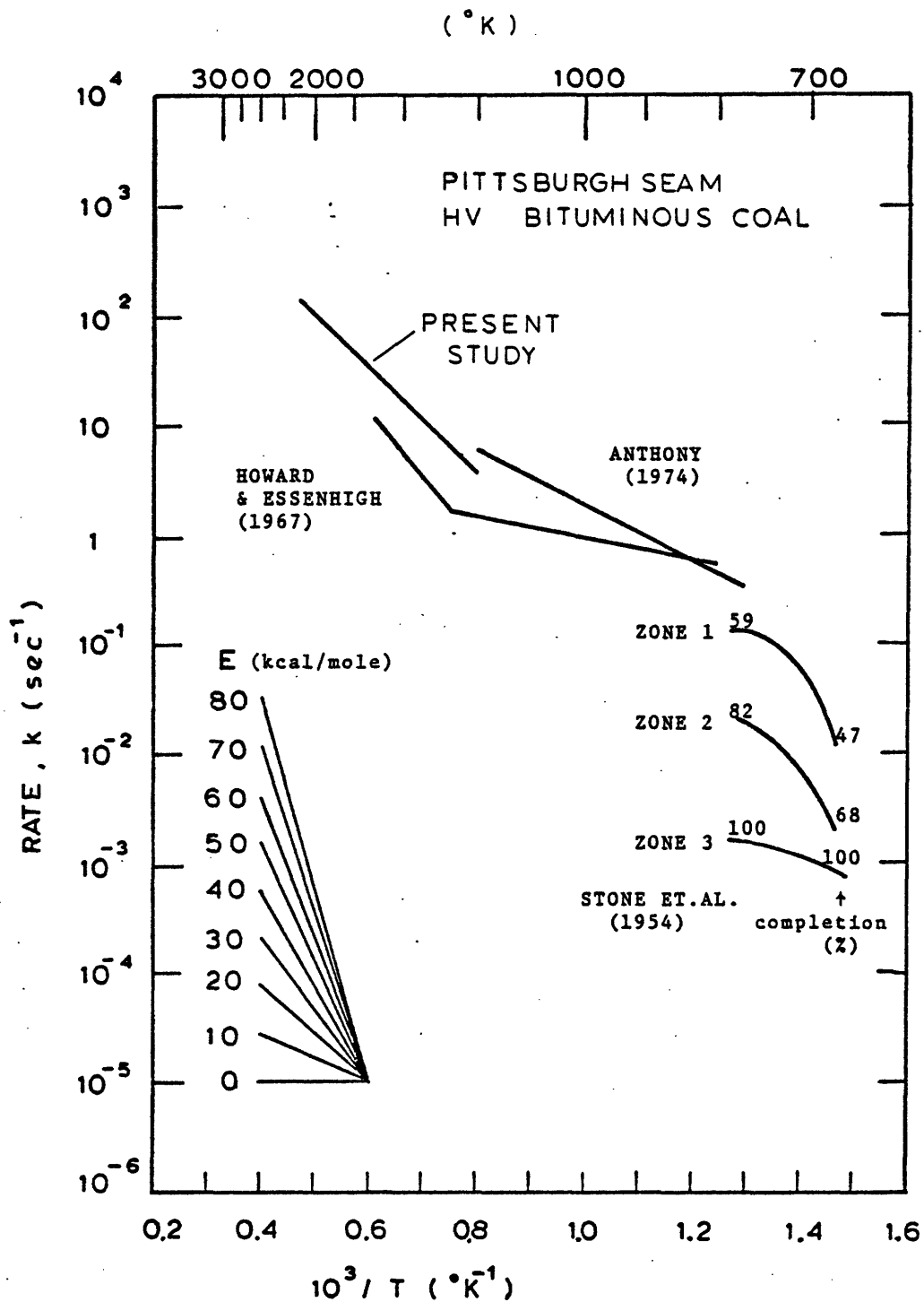


FIGURE 6.9 COMPARISON OF DEVOLATILIZATION RATE CONSTANTS FOR PITTSBURGH SEAM HV BITUMINOUS COAL.

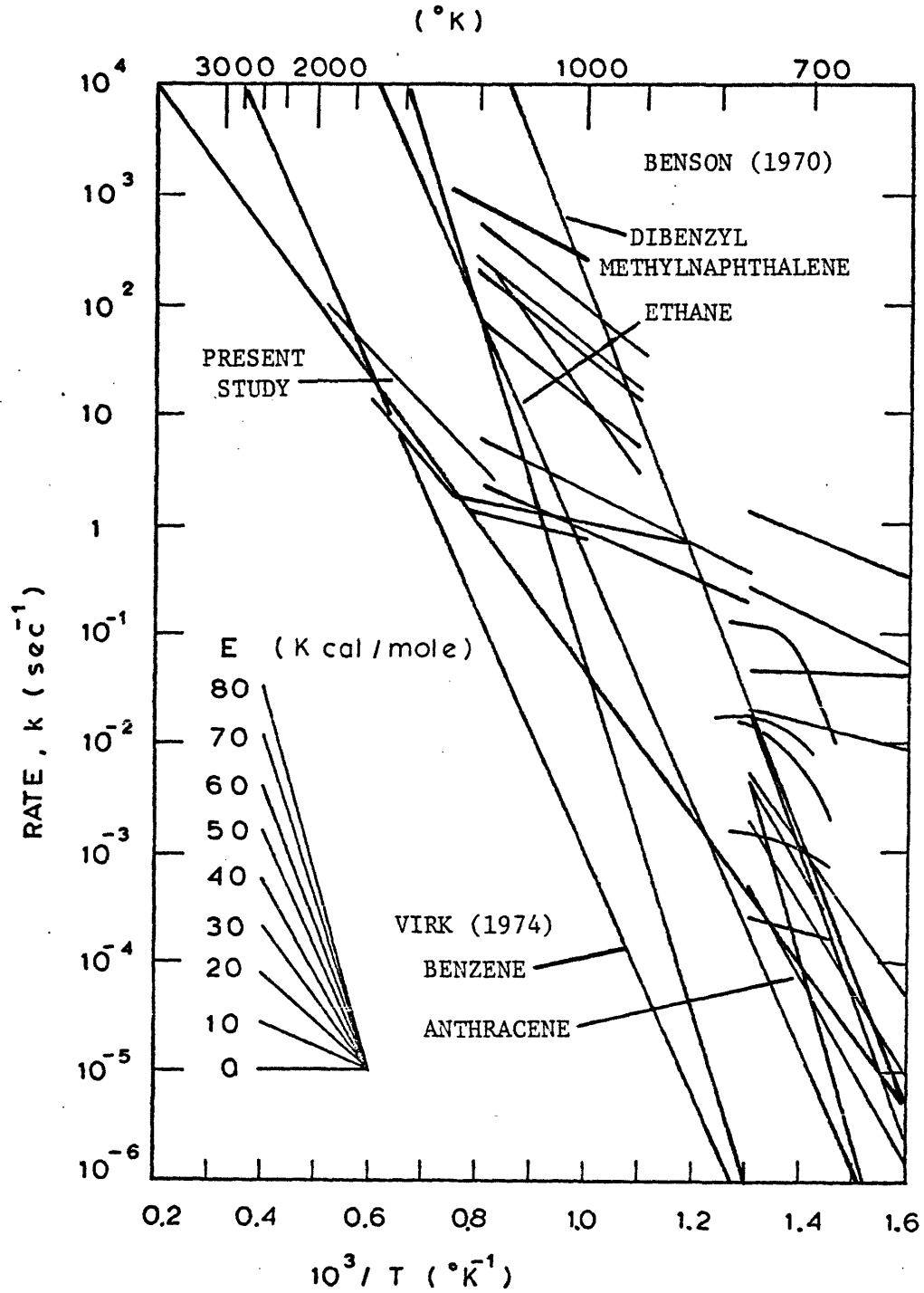


FIG. 6.10 COMPARISON OF FIRST ORDER DEVOLATILIZATION RATES WITH THOSE FOR DECOMPOSITION OF PURE HYDROCARBONS.

the decomposition of the complex coal structures, we may conclude that the observed rates for the devolatilization of coal are consistent with those for pure organic compounds. However, most of the activation energies for devolatilization are much lower than those for the pure compounds. The apparent low activation energies led some of the investigators to postulate physically rate controlled mechanisms such as pore diffusion (Berkowitz, 1960). Alternative explanation was presented by Jüntgen and Van Heek (1970), who demonstrated that eight parallel first order reactions with a common frequency factor of 10^{15} min^{-1} and activation energies ranging from 48 to 62 Kcal/mole can be closely approximated by a single reaction with a low activation energy of 20 Kcal/mole and a frequency factor of 10^4 min^{-1} . In order to examine the relation of the "true" activation energies and the apparent one under different experimental conditions, hypothetical three first order "true" reactions with a common frequency factor of $1.67 \times 10^{-13} \text{ sec}^{-1}$ and activation energies 46, 50 and 54 Kcal/mole are considered. Each reaction is assumed to contribute 10% volatile yield. Under isothermal experiments such as Stone's, the overall rate decreases with time because the faster reactions are completed initially. This is shown in figure 6.11 at three different temperatures with broken lines. Several calculated points were shown with the reaction times and weight losses. By comparing the hypothetical case with Stone's results (Fig. 6.7), the observed apparent low activation energies and decreases of the rates with the progress of devolatilization can be clearly understood. In Stone's experiment, different asymptotic volatile yields

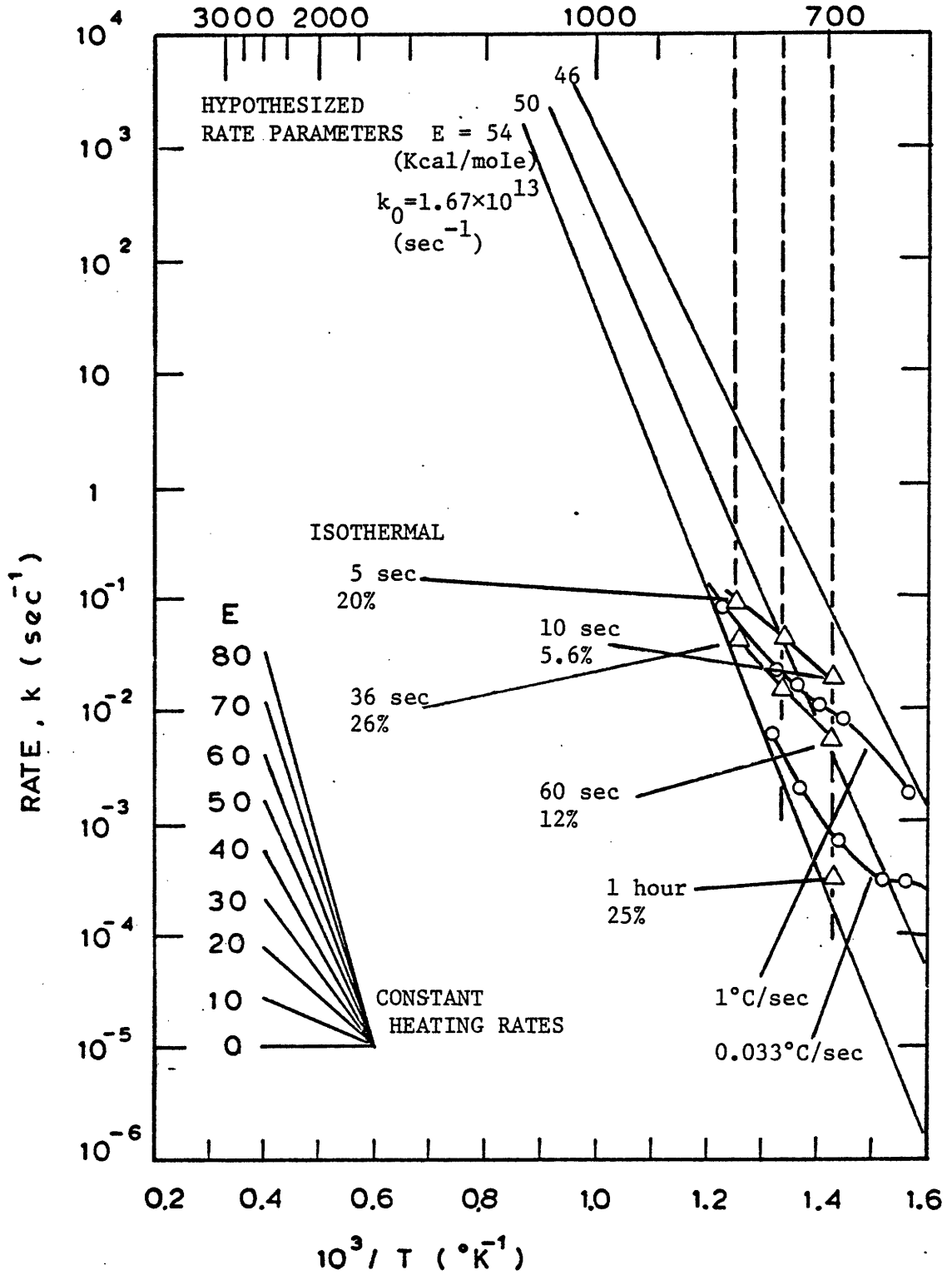


FIG. 6.11 APPARENT FIRST ORDER RATES APPROXIMATED FOR HYPOTHETICAL THREE FIRST ORDER PARALLEL REACTIONS.

were used at different temperatures, while in the hypothetical case a constant value of 30% volatile yield was assumed. If smaller asymptotic values are used for lower temperatures in the hypothetical case, the apparent activation energies become even lower. It should be noted that at 700°K, a 25% weight loss was obtained in 1 hour, while it took only 36 sec at 800°C to reach 26% weight loss. This explains why the asymptotic values of volatile yields depend on temperature within limited reaction times.

Simulations of constant heating conditions are also shown in the figure. Under these conditions apparent activation energies tend to be larger than those in the isothermal conditions. This might be the reason why Van Krevelen's values were closer to the typical rates for organic compounds.

In view of the above discussions, some of the observed wide discrepancies in the apparent activation energies appeared to be due to the different methods in the data reduction. From the examples shown in Fig. 6.11, it can be understood that if the rates at a given level of weight loss are connected under different temperatures in the isothermal case, an activation energy closer to the 'true' values can be obtained (e.g., 26% at 800°K and 25% at 700°K). This concept was applied in the present study. Figures 6.12 and 6.13 show the results. In spite of the limited number of data, the results for the lignite appeared to indicate faster rates at small weight losses. The apparent activation energy become about 45 Kcal/mole, which is considered to be closer to the 'true' values. The results for the bituminous coal, however, did not show an

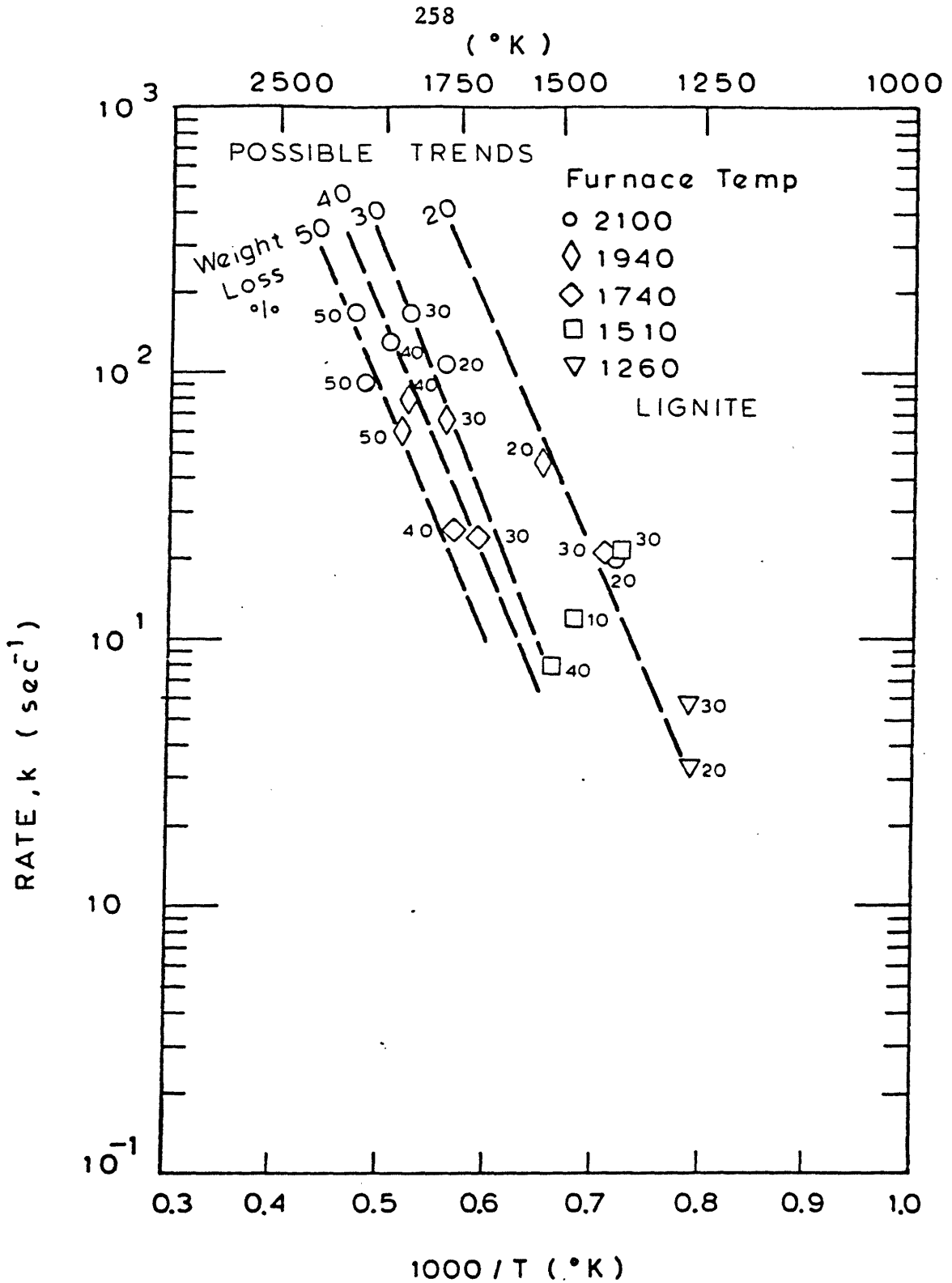


FIG. 6.12 FIRST ORDER ARRHENIUS RATES EVALUATED AT SAME WEIGHT LOSS LEVELS. MONTANA LIGNITE.

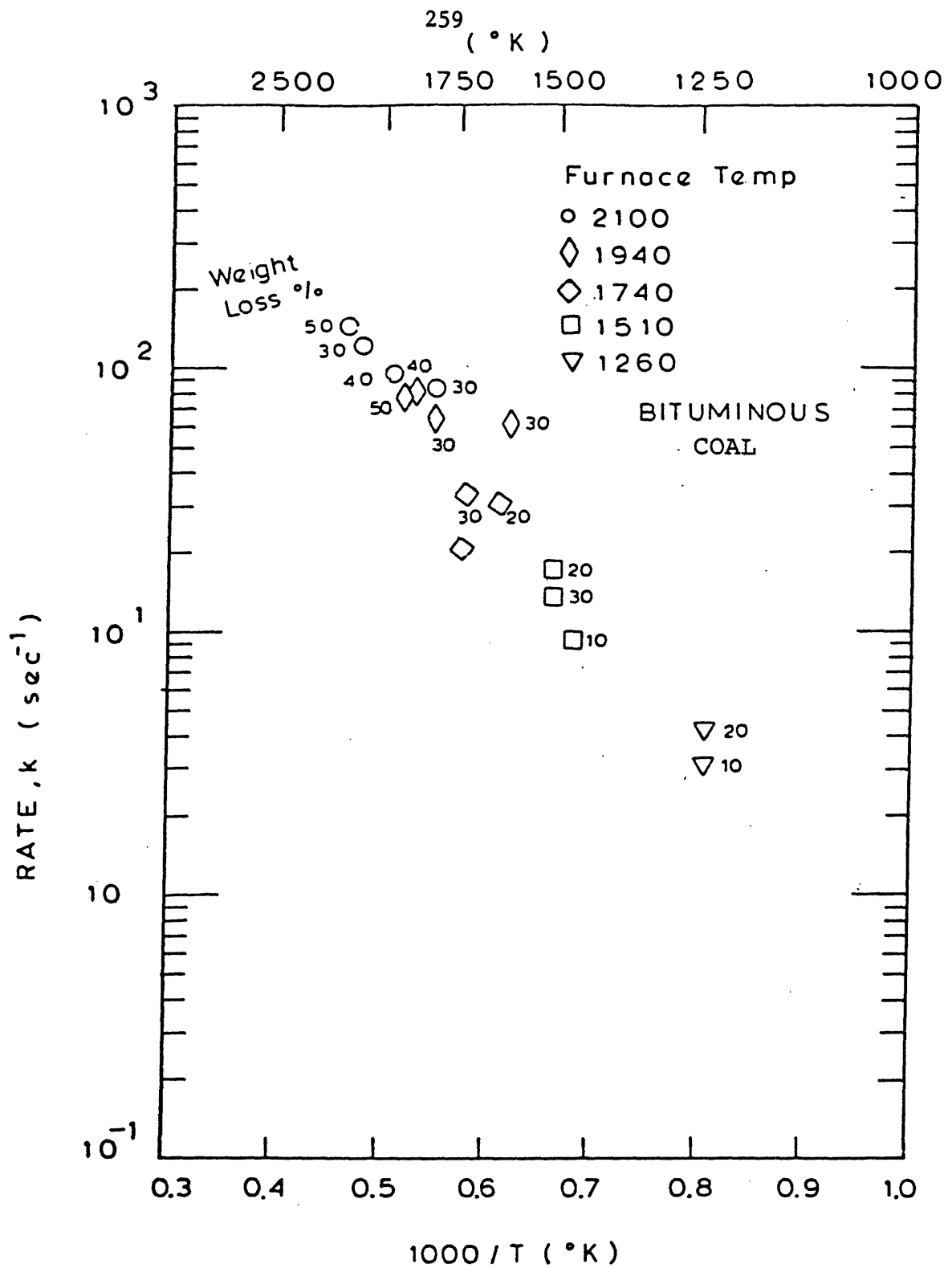


FIG. 6.13 FIRST ORDER ARRHENIUS RATES EVALUATED AT SAME WEIGHT LOSS LEVELS. PITTSBURGH SEAM BITUMINOUS COAL.

obvious trend, which may be due to the limited number of data.

In summary, the results of the present work agreed well with previous works, and the observed rates appeared to be consistent with the experimental and theoretical values of pure organic compounds. The apparent low activation energies and the wide differences between different experimental methods appeared to be explained by the existence of many reactions during the pyrolysis of complicated coal structures.

CHAPTER VII

DEVOLATILIZATION MODELS

Many models have been developed to describe different aspects of the devolatilization behaviors. They include the simple model with a simple overall reaction to models with many reactions, some of which were discussed in section 1.2.3. Although descriptive models based on the true chemical and physical structure of coal are desired, they are quite complex and tend to incur many uncertainties due to the lack of sufficient knowledge on the structure and the mechanism of devolatilization of coal. For engineering applications simple models with minimum number of parameters are preferred, which very often limit the applicability of the models to the ranges of conditions used to derive the constants in the model. As such, the proper selection of a model depending on the specific needs is important for practical purposes. Table 7.1 summarizes some of the possible kinetic models for engineering applications. Most of the models developed in the past are some variations of these different schemes. The consecutive reactions developed by Van Krevelen and his co-workers (1956) may be compared with reactions (7.3). Secondary char forming reactions may be modeled by reactions (7.4). Since the number of adjustable constants in the models based on some overall behaviors of devolatilization is proportional to the number of reactions proposed, only those with two reactions or statistical models are listed. Models based on the single overall reaction of the type (7.1) have been

TABLE 7.1 (cont.d)

II. Structural Models

1. Reactions based on product species.
2. Reactions based on original structure.

C, C₁, C₂, C_iCoal

V, V₁, V₂, V_iVolatile Matter

R, R₁, R₂, R_iResidue (char)

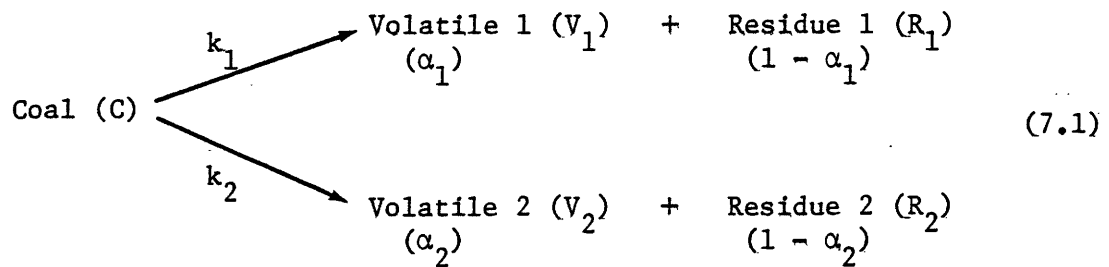
successfully applied to experimental ranges where the asymptotic yields of volatile matter are approximately constant. In the high temperature conditions investigated in this study, however, significant differences in the asymptotic weight loss were observed. Hence some corrections for the asymptotic yields are necessary if the single reaction model is used. The problem of the same asymptotic value of weight loss is mathematically inherent to all models which do not have certain competitive mechanisms. For example, a two-parallel reaction model (7.2) may explain the larger yields at high temperatures by postulating that one of the reaction, assigned a high activation energy, becomes important only at high temperatures. But it is clear that such a model predicts the same final yield regardless of temperature if sufficient reaction time is given. Within a reasonable reaction time, however, such models might still adequately correlate the data. Comparison of the results of the free fall experiment with alumina crucibles among different furnace temperatures, however, showed different ultimate yields within a time scale of about 10 minutes. More distinct differences were seen in the data between the crucible runs and the free fall runs. For the same final temperatures and similar reaction times, significant differences in weight losses were observed (Figs. 4.3 and 4.5). Hence use of such models appeared to be limited to relatively short times such as the laminar flow conditions.

Models which predict different final yields, therefore, must contain certain competing mechanisms. Competition between volatile escape and a secondary char forming reaction (Anthony, 1974), or between different reactions leading to different volatile yields (Reidelbach & Summerfield,

1975; Kobayashi, 1972) are some of the possible models. Difficulties in predicting larger yields at high temperatures in the secondary char forming reaction scheme were discussed in some depth in section 5.4. Since Reidelbach's model contains ten different reactions, practical applications of the model are difficult because of the number of the parameters involved. Therefore, competing reaction models may be applied to the present results. With the limitations of the number of parameters, two competing reactions (7.5) or multiple competing reactions with statistical distributions of rate parameters may be considered. These schemes involve four parameters; an activation energy and a frequency factor for each reaction for the former and average activation energy and frequency factor and parameter relating the distribution functions for the latter. The advantage of the statistical model can be seen in the fact that devolatilization does involve many reactions with different levels of energy requirements, and such model is expected to give reasonable values of activation energies compared with those for pure organic substances, as discussed in chapter 6. On the other hand, the model with two reactions has an advantage of simplicity, and at relatively low temperature it reduces to a single reaction. Therefore available rate parameters obtained at relatively low temperature assuming a single overall reaction could be used. Since the two competing reactions model has been used successfully (Kobayashi, 1972, Stickler et al., 1974), it is selected for the present purpose. It should be emphasized, however, that these phenomenological models are considered as tools in correlating data and not much physical significance could be attached to the parameters

obtained. In this sense efforts in describing each devolatilization product by a set of chemical reactions (Jüntgen and Van Heek, 1970, 1969, 1968, Hanbaba et al., 1968), or in deducing the rates parameters from the structures of coal are evaluated. But engineering applications of these results are rather cumbersome.

The model is based on the following reaction scheme,



where α_1 and α_2 are mass stoichiometric coefficients, and k_1 and k_2 denote Arrhenius type reaction rates.

$$k_1 = B_1 e^{-\frac{E_1}{RT}} \tag{7.2}$$

$$k_2 = B_2 e^{-\frac{E_2}{RT}} \tag{7.3}$$

At relatively low temperatures, the first reaction is assumed to be dominant leading to the asymptotic volatile yield of α_1 . At high temperatures the second reaction becomes faster than the first one because of the assumed high activation energy, resulting in larger volatile yields. Therefore the volatile yield under a specific condition is determined through the integrated effects of the two reactions. The rate equations are described by the following relations.

$$\frac{dm_{V_2}}{dt} = -\alpha_1 k_1 \frac{dm_c}{dt} \quad (7.4)$$

$$\frac{dm_{V_2}}{dt} = -\alpha_2 k_2 \frac{dm_c}{dt} \quad (7.5)$$

where m denotes dry-ash-free mass of each "species" specified by the subscripts. Integration of above equations results in the following expression for the overall weight loss, ΔW .

$$\Delta W = \frac{m_{V_1} + m_{V_2}}{m_{c,0}} = \int_0^t (\alpha_1 k_1 + \alpha_2 k_2) e^{-\int_0^t (k_1 + k_2) dt} dt \quad (7.6)$$

where $m_{c,0}$ is the original d.a.f. mass of coal. Under isothermal conditions, equation (7.6) can be integrated to give,

$$\Delta W = \frac{\alpha_1 k_1 + \alpha_2 k_2}{k_1 + k_2} (1 - e^{-(k_1 + k_2)t}) \quad (7.7)$$

The asymptotic values of weight loss under isothermal conditions are

$$\Delta W = \frac{\alpha_1 k_1 + \alpha_2 k_2}{k_1 + k_2} \quad (7.8)$$

From Equation (7.8) it can be seen that the asymptotic weight losses are weighted averages of α_1 and α_2 .

Under the present experimental conditions, the temperature-time histories of coal particles in the laminar flow experiment were calculated based on a simplified flow model described in chapter 3. Therefore numerical integration of Eq. (7.6) is possible. Methods for the evaluation of the kinetic parameter were discussed elsewhere (Stickler, et al., 1974; Kobayashi, 1972). α_1 and α_2 are the asymptotic values of weight loss at a relative low temperature and at a very high temperature respectively. Hence, $\alpha_2 = 1$ may be assigned, as the complete weight loss is expected at extremely high temperatures. α_1 may be approximate by the volatile matter or by a characteristic volatile yield at temperatures where the second reaction is negligible. Figures 7.1 and 7.2 show the capability of the model in correlating the data. The same parameters were used for both coals. Although the parameters are not the optimal values, good agreements between the calculated values and the experimental values are evident. One of the advantages of the present model is that the competing reactions reduce to a single reaction when the second reaction is much slower than the first one. Therefore kinetic parameters obtained under relatively low temperatures assuming a single overall reaction can be utilized for the first reaction. Figure 7.3 shows calculated results using the first order parameters obtained by Anthony (1974) for a Pittsburgh seam bituminous coal from the same

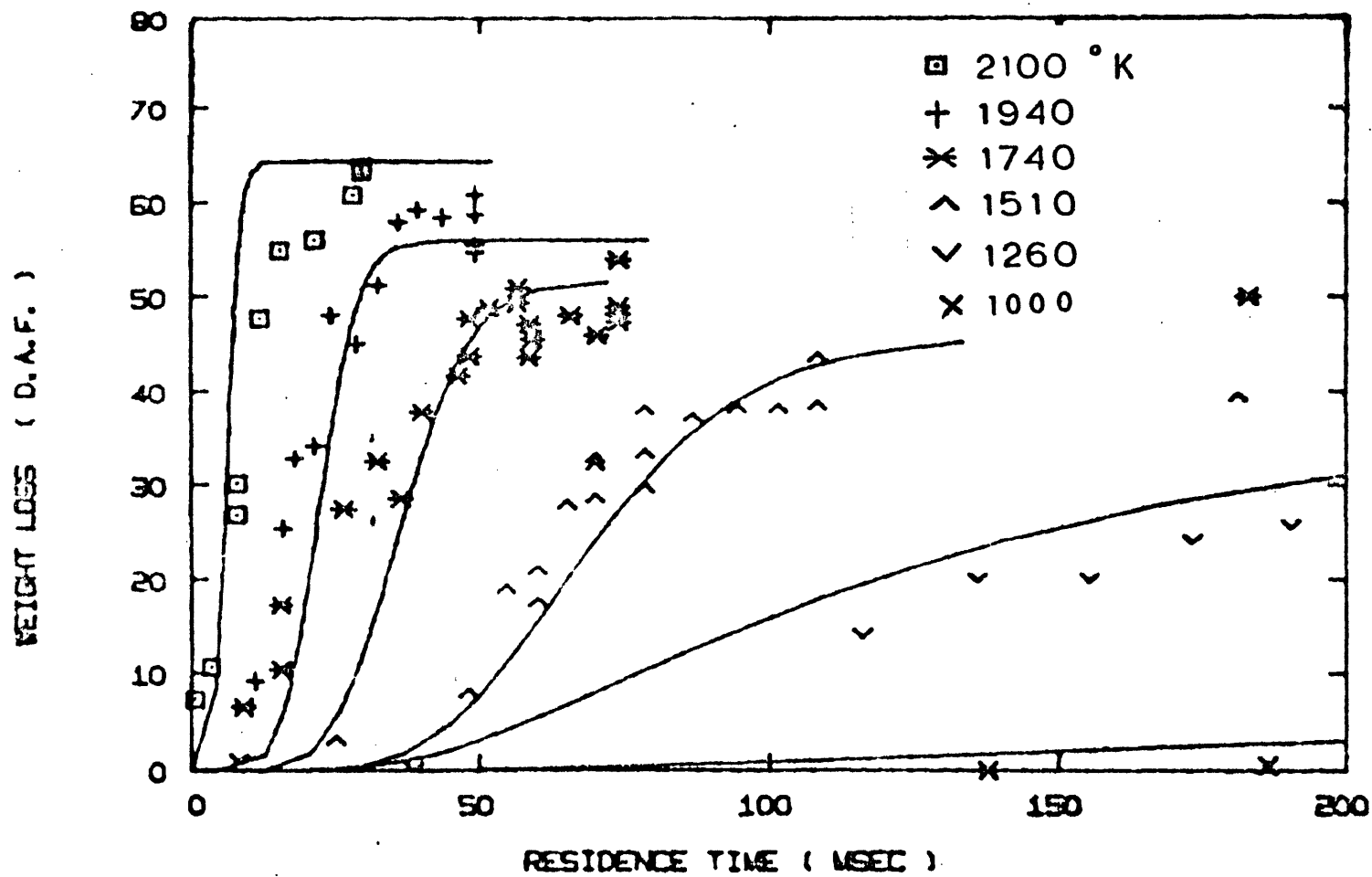


FIG. 7.1 COMPARISON OF MODEL CURVE FIT WITH EXPERIMENTAL DATA FOR MONTANA LIGNITE

$$\begin{array}{lll}
 \alpha_1 = 0.3 & E_1 = 25 \text{ Kcal/mole} & B_1 = 2 \times 10^5 \text{ sec}^{-1} \\
 \alpha_2 = 1.0 & E_2 = 40 \text{ Kcal/mole} & B_2 = 1.3 \times 10^7 \text{ sec}^{-1}
 \end{array}$$

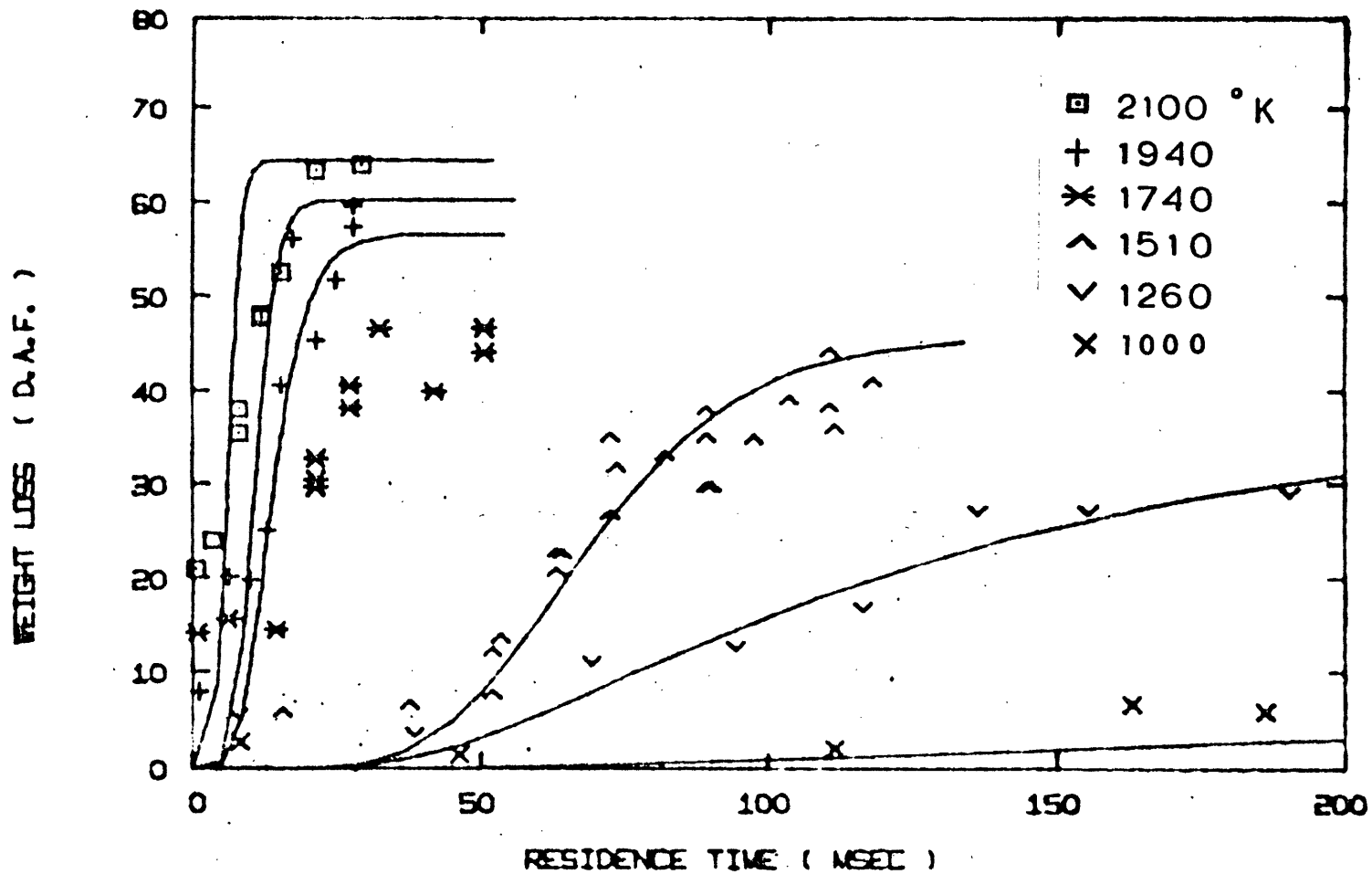


FIG. 7.2 COMPARISON OF MODEL CURVE FIT WITH EXPERIMENTAL DATA FOR PITTSBURGH SEAM BITUMINOUS COAL

$$\begin{aligned} \alpha_1 &= 0.3 & E_1 &= 25 \text{ Kcal/mole} & B_1 &= 2 \times 10^5 \text{ sec}^{-1} \\ \alpha_2 &= 1.0 & E_2 &= 40 \text{ Kcal/mole} & B_2 &= 1.3 \times 10^7 \text{ sec}^{-1} \end{aligned}$$

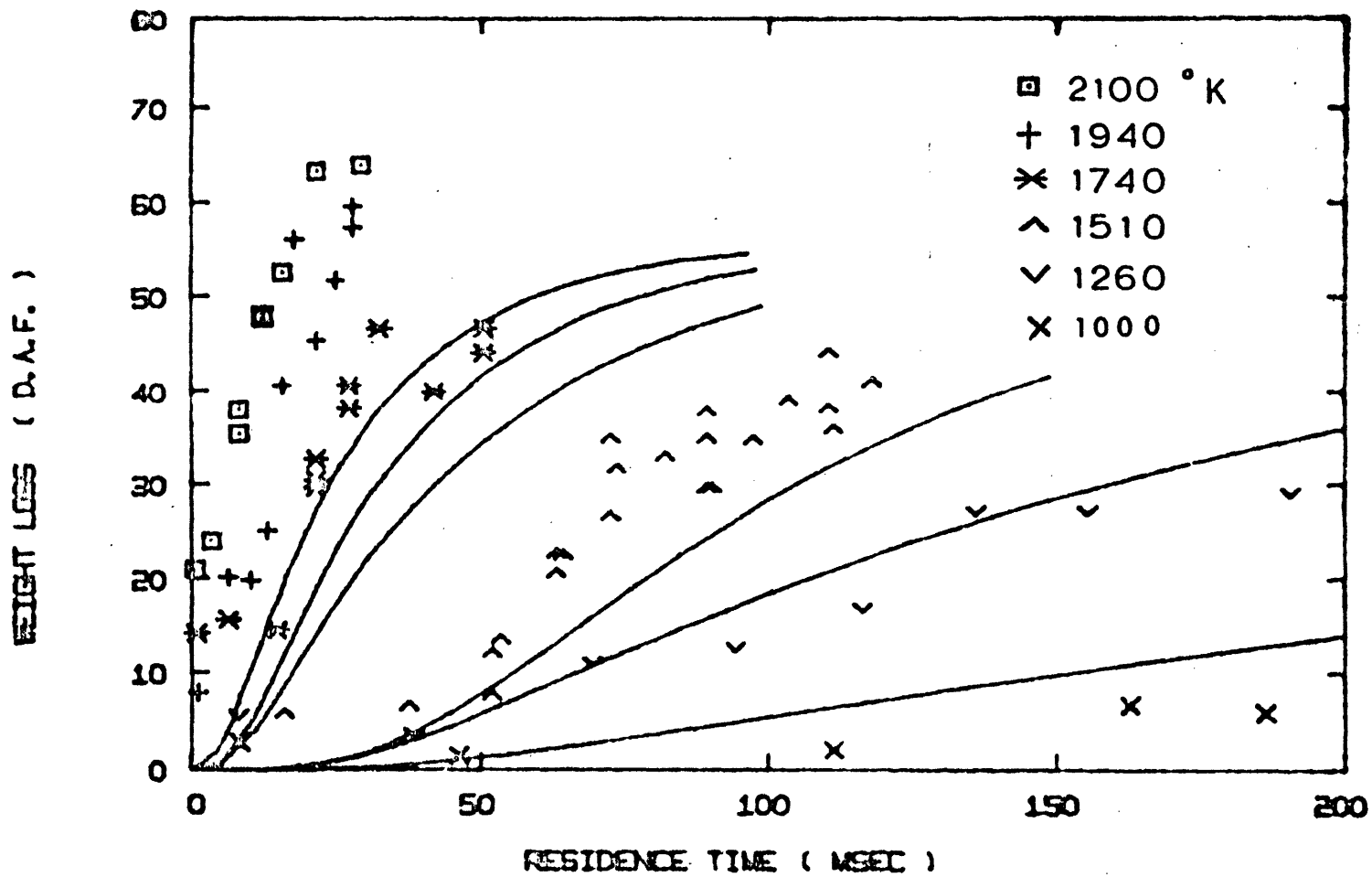


FIG. 7.3 COMPARISON OF A SINGLE OVERALL REACTION MODEL WITH EXPERIMENTAL RESULTS

$$\alpha_1 = 0.56 \quad E_1 = 11.8 \text{ Kcal/mole} \quad B_1 = 706 \text{ sec}^{-1}$$

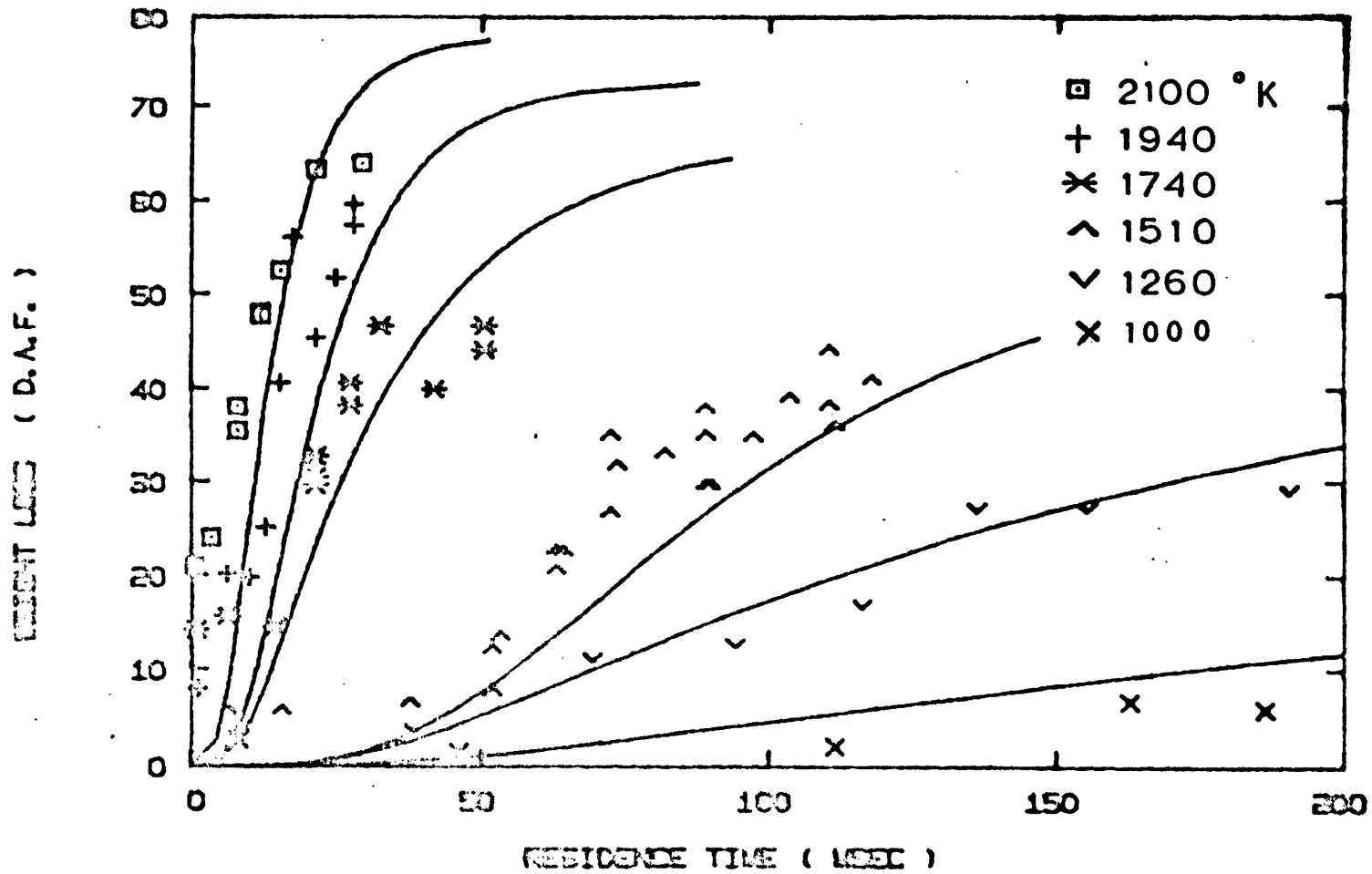


FIG. 7.4 COMPARISON OF MODEL CURVE FIT WITH EXPERIMENTAL DATA FOR PITTSBURGH SEAM BITUMINOUS COAL

$$\begin{array}{lll}
 \alpha_1 = 0.46 & E_1 = 11.8 \text{ Kcal/mole} & B_1 = 706 \text{ sec}^{-1} \\
 \alpha_2 = 1.0 & E_2 = 30 \text{ Kcal/mole} & B_2 = 10^5 \text{ sec}^{-1}
 \end{array}$$

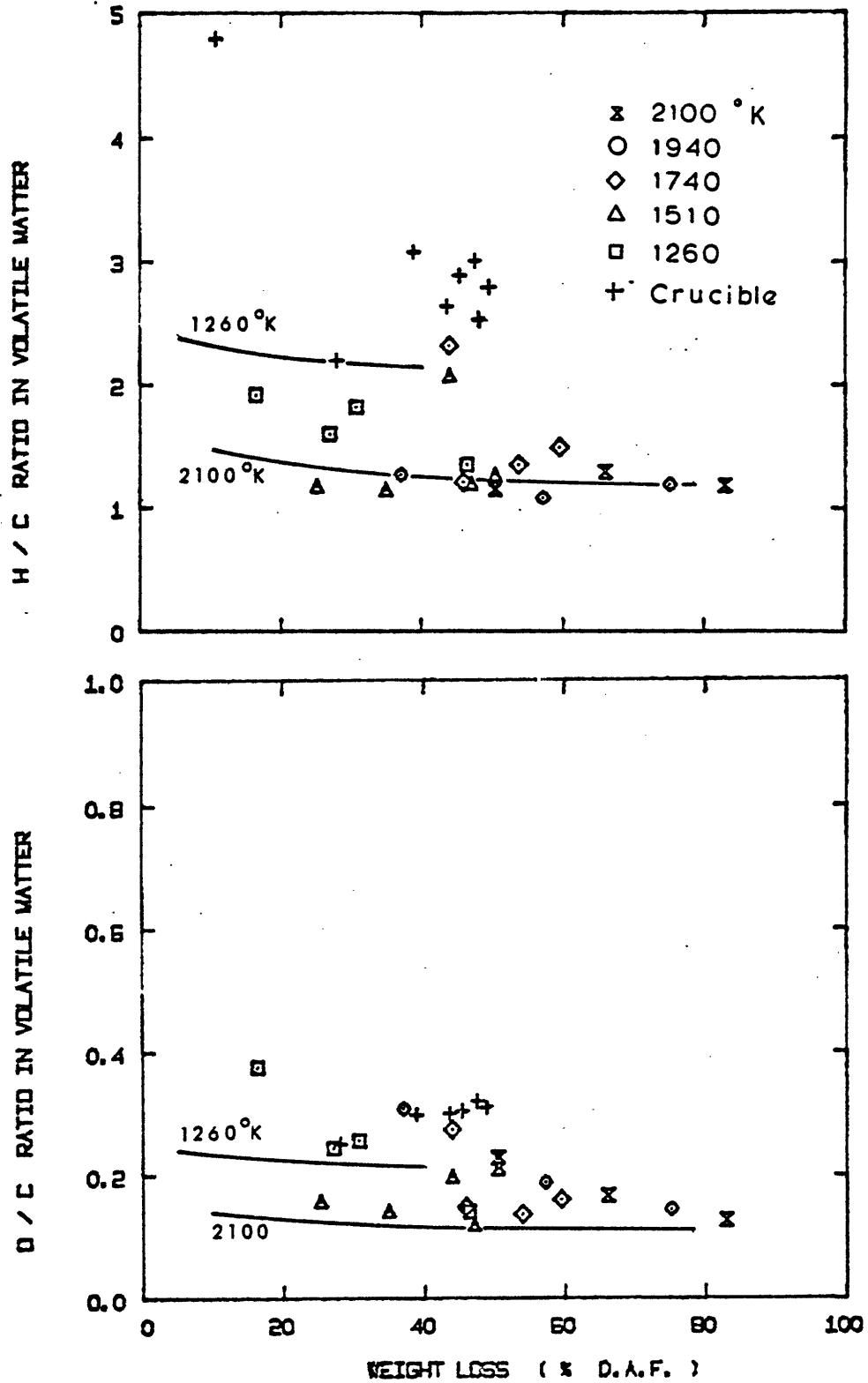


FIG. 7.5 COMPARISON OF CALCULATED H/C AND O/C RATIOS WITH EXPERIMENTAL DATA FOR PITTSBURGH SEAM BITUMINOUS COAL

In summary, the capability of the model to predict the devolatilization behavior for the wide range of experimental conditions were clearly demonstrated. As such, engineering applications of the model can be considered quite adequate. For example, predictions of both weight losses and atomic ratios of the volatile matter may enable calculation of equilibrium gas temperatures in pulverized coal flames. However, care has to be taken on the physical significance of the rate parameters obtained by the model. Although the two overall reactions could be interpreted as representative of condensation reactions forming non-volatile residue at relatively low temperatures versus extensive bond ruptures at high temperatures, they should be considered as empirical equations for correlating the wide ranges of data.

CHAPTER VIII

CONCLUSIONS

The major contributions of the thesis were to derive data on volatile yields and kinetics of devolatilization of coal at high temperatures. The major conclusions on each of these are summarized below. In addition, some conclusions are drawn on novel aspects of the experimental methodology employed in this thesis.

A. Volatile Yields

1. Significant enhancements in volatile yield occurs at high temperatures under rapid heating conditions. The Montana lignite used in this study yields 63 percent (d.a.f.) volatile matter at 2100°K in 30 msec, and the Pittsburgh seam bituminous coal under the same condition gives an apparent yield of 63 percent. In addition, the bituminous coal is found to yield appreciable amounts of condensed material, allowance for which would augment the volatile yield by possibly as much as 20 percent.

By contrast to the rapid heating of coal in dispersed flow, the slow heating of coal in crucibles to temperatures above about 1200°K does not increase the volatile yield appreciably. Changes in bed depth in the crucibles from about 100 particle layers (about 1 gm sample) to about 1 particle layer (about 10 mg) had no discernible effect on weight loss for lignite, and resulted in a slight increase (about 2 percent of the D.A.F. weight of the original coal) for bituminous coal.

2. Analysis of the chars showed that, at a given weight loss, more carbon, less hydrogen and less oxygen are retained in the crucible runs

than in the laminar flow runs.

3. It was postulated that the rapid heating increases the volatile yield by increasing the "effective devolatilization temperature."

It should be noted, however, that when coal particles are heated to a certain final temperature, there exists a critical heating rate above which no effect of heating rate is observed, providing an explanation for the disagreement in the literature on the effect of heating rates on volatile yields.

4. The simple models based on a competition between secondary char formation reactions and escape of the potentially char forming species (section 5.4) are judged to be inadequate for explaining the enhanced volatile yields at high temperatures under rapid heating conditions.

B. Kinetics of Devolatilization

1. The first order Arrhenius rate parameters for the overall weight loss assuming a constant potential yield of 70 percent (d.a.f.) are approximately 25 Kcal/mole for the activation energy and $6.6 \times 10^4 \text{ sec}^{-1}$ for the frequency factor for both coals. The first order rates agree well with the previous results, especially for those with Pittsburgh seam high volatile bituminous coals.

2. The rate of devolatilization decreases with extent of reaction. The rate of evolution of volatile matter in initial 200 msec is about one order of magnitude faster than that in the next 1 second period, and about three orders of magnitude faster than that in the next 10 minute periods.

3. A model based on two competing reactions was found to adequately correlate the experimental results on pyrolysis for a wide range of conditions.

C. Experimental Methodology

The use of ash as a tracer for determining volatile yields was critically evaluated. It was shown that the use of ash as a tracer in determining the weight loss could cause significant errors even at temperatures below that of the ASTM ash test. Ash losses greater than 50 percent occur when the coals are heated at 2100°K for 10 minutes.

Methods of estimating the amount of condensed material formed by use of ash were developed and demonstrated to be useful.

APPENDIX A

CHARACTERISTIC HEAT TRANSFER TIMES OF PARTICLES

In order to assess the relative importance of the various heat transfer processes of particles, characteristic heating times of gas phase conduction, radiation from hot surfaces, and conduction inside the particle are calculated.

Characteristic Heat Transfer Time of Gas Phase Conduction, t_c

Assuming that the temperature inside the particle is uniform, the energy balance equation can be expressed as

$$m_p \cdot C \cdot \frac{dT_p}{dt} = \frac{Nu \cdot \lambda_g \cdot s_p}{d} (T_g - T_p) \quad (A.1)$$

where m_p , s_p , T_p and d are mass, surface area, temperature and diameter of the particle. Upon integration, with the initial condition $T = T_o$ at $t = 0$ the temperature of the particle is

$$\frac{T_p - T_o}{T_g - T_o} = 1 - e^{-\frac{Nu \cdot \lambda_g \cdot s_p}{m_p \cdot C \cdot d} \cdot t} \quad (A.2)$$

The characteristic time may be defined

$$t_c = \frac{m_p \cdot C \cdot d}{Nu \cdot \lambda_g \cdot s_p} \quad (A.3)$$

For a spherical particle with density, ρ_p , Eq. (A.3) reduces to

$$t_c = \frac{\rho_p \cdot C \cdot d^2}{6 \cdot Nu \cdot \lambda_g} \quad (A.4)$$

Though $Nu = 2$ is well established for a spherical particle in an infinite stagnant media, evaluation of Nusselt number under non-ideal conditions

requires special treatments.

Characteristic Heat Transfer Time of Radiation, t_r

The energy balance equation can be written as

$$m_p C \frac{dT}{dt} = s_p \cdot \epsilon_p \cdot \sigma \cdot (T_w^4 - T^4) \quad (\text{A.5})$$

Upon integration, Eq. (A.5) gives

$$t = \frac{m_p C}{2\epsilon_p T_w s_p T_w^3} \left[\frac{1}{2} \log\left(\frac{T_w - T_o}{T_w - T} \cdot \frac{T_w + T}{T_w + T_o}\right) + \tan^{-1} \frac{\frac{T}{T_w} - \frac{T_o}{T_w}}{1 + \frac{T}{T_w} \cdot \frac{T_o}{T_w}} \right] \quad (\text{A.6})$$

The characteristic time may be defined as the time when the temperature becomes

$$\frac{T - T_o}{T_w - T_o} = 1 - e^{-1} = 0.632 \quad (\text{A.7})$$

Under this definition Eq. (A.6) becomes

$$t_r = \frac{m_p C}{2\epsilon_p \cdot \sigma \cdot s_p \cdot T_w^3} \cdot f\left(\frac{T_o}{T_w}\right) \quad (\text{A.8})$$

where $f(T_o/T_w)$ is the quantity in the bracket in Eq. (A.6), and it depends weakly on T_o/T_w . [$f(T_o/T_w) = 0.47, 0.42, 0.24$, for $T_o/T_w = 0.1, 0.2, 0.4$, respectively.] For a spherical particle Eq. (A.8) reduces to

$$t_r = \frac{\rho_p d C}{12\epsilon_p \sigma T_w^3} \cdot f\left(\frac{T_o}{T_w}\right) \quad (\text{A.9})$$

Characteristic Conduction Time Inside a Particle

When the surface of a spherical particle of radius a , whose initial temperature is homogeneously T_0 , is brought to temperature T_∞ at $t = 0$, the temperature at radius r is expressed as (Carslaw and Jaeger, 1959)

$$\frac{T - T_0}{T_\infty - T_0} = \frac{a}{r} \sum_{n=0}^{\infty} \left\{ \operatorname{erfc} \frac{(2n+1)a+r}{2(D_T t)^{1/2}} - \operatorname{erfc} \frac{(2n+1)a-r}{2(D_T t)^{1/2}} \right\} \quad (\text{A.10})$$

where $D_T = \frac{\lambda_p}{\rho_p C}$ = thermal diffusivity. Using Eq. (A.7) at the center of the sphere ($r = 0$), the characteristic conduction time can be defined

$$t_{c,p} = \frac{\rho_p C d_p^2}{20 \lambda_p} \quad (\text{A.11})$$

where λ_p is the thermal conductivity of the particle. Under high temperature rapid heating conditions, rapid ejection of volatile matter might change the apparent thermal conductivity significantly. A simplified analysis, however, indicated that the effects of "abrasion" is negligible even under very high rates of devolatilization.

In Fig. A.1 these three characteristics are plotted as a function of the particle size. The values of the properties used in the calculations are as follows.

$$C = 0.25 \text{ cal/gm } ^\circ\text{K}$$

$$\rho_p = 1.25 \text{ gm/cm}^3$$

$$\lambda_g = 1.02 \times 10^{-4} \text{ cal/cm sec } ^\circ\text{K (argon at } 1000^\circ\text{K)}$$

$$\epsilon_p = 0.9$$

$$\text{Nu} = 2$$

$$\lambda_p = 3.0 \times 10^{-3} \text{ cal/cm sec } ^\circ\text{K}$$

For pulverized coal particles ($d < 200 \mu\text{m}$), internal conduction is fast ($t_{c,p} \ll t_c, t_r$). Hence the particles can be treated as spatially isothermal. Radiation becomes dominant for larger particles ($\sim 100 \mu\text{m}$), especially at high temperatures.

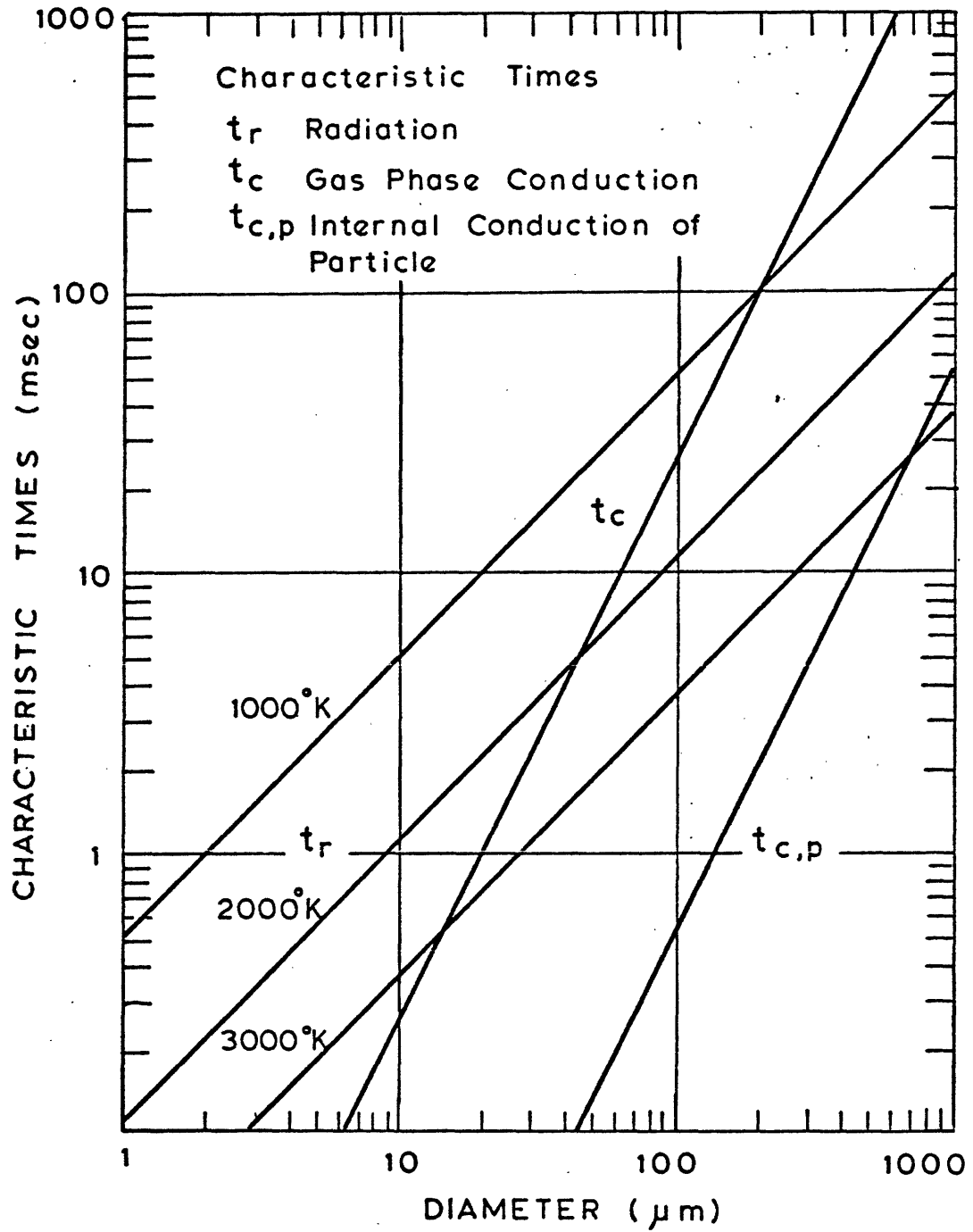


FIG. A.1 CHARACTERISTIC HEAT TRANSFER TIMES TO A PARTICLE

RESULTS OF LAMINAR FLOW EXPERIMENT

Tables B.1 and B.2 summarize the experimental result for the lignite and the bituminous coal, respectively. The following values were used in calculating the dry-ash-free weight loss.

<u>Coal</u>	<u>Moisture</u> (% wet coal)	<u>Ash</u> (% dry coal)
Montana Lignite	14.79 (LF100-LF240)	9.36
	14.09 (LF241-LF310)	
Pittsburgh Bituminous	1.98 (LF100-LF240)	10.89
	2.06 (LF241-LF310)	

The residence times of the coal particle calculated by the simplified flow field model described in chapter 3 were corrected for the acceleration caused by the high suction rate and by the converging section of the collector. As illustrated in figure B.1, the stream lines in the main flow converge into the collector due to the suction. Higher suction rates have a greater influence in the upstream section. As a first approximation, the influence may be assumed to be restricted to the conical section indicated in the broken lines, which was constructed by extending the converging section of the filter. The height of the section, l , can be determined by applying the condition that the mass flow across the area is the same as the suction rate. Upon integration of the mass conservation equation, the following formulas were obtained for the correction of the residence time.

$$\Delta t = \frac{\sqrt{3} (r_1 - r_o)}{U_m} - \frac{r_1}{\sqrt{3} U_m} \left\{ 1 - \left(\frac{r_o}{r_1} \right)^3 \right\} \quad (B.1)$$

$$r_1 = \sqrt{\frac{\dot{m}_{vac}}{\pi \cdot \rho_m U_m}} \quad (B.2)$$

where Δt : decrease in residence time by acceleration
 \dot{m}_{vac} : mass flow rate of suction
 ρ_m : density of main stream
 U_m : velocity of main stream

Actual calculations were made through a Fortran subroutine LFLOW, which is listed in Appendix J.

For bituminous coal, some of weight losses calculated by using ash as a tracer are consistently negative, and also some of ash loss figures are consistently negative. The reason for this is the preferential loss of soot from the filter as discussed in chapter 4.

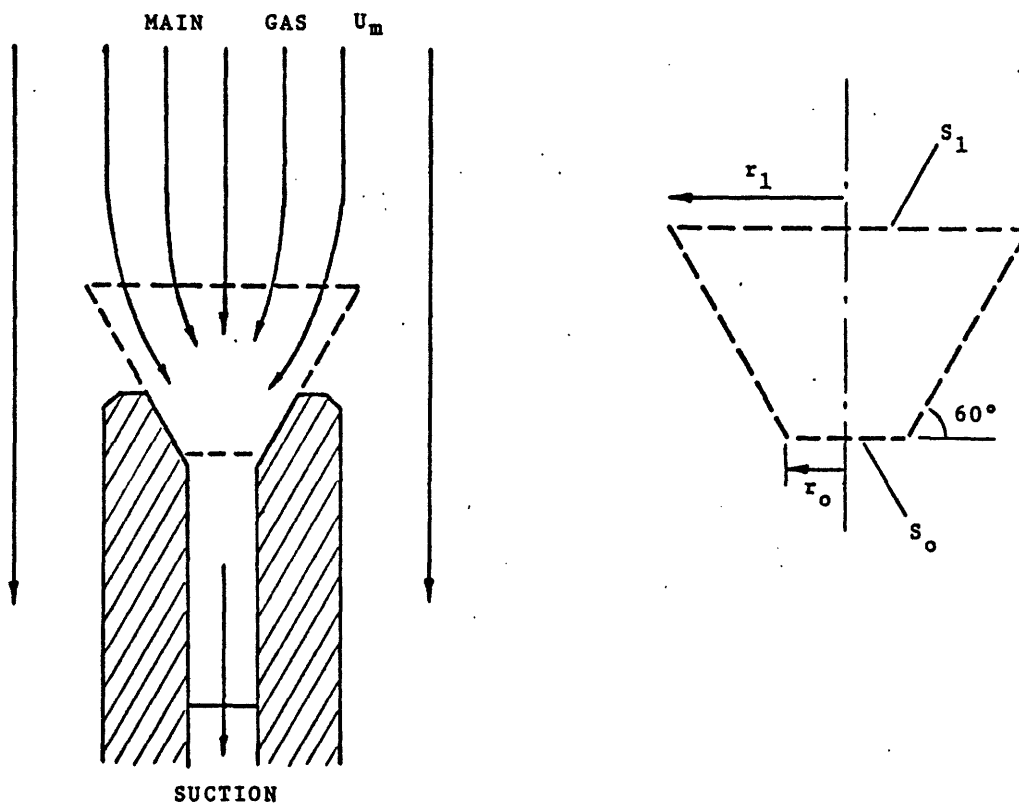


Figure B.1 Illustration for residence time correction

TABLE B.1 RESULTS OF LAMINAR FLOW EXPERIMENT,
MONTANA LIGNITE

RUN NO	COAL SIZE (MICRON)	TEMP (K)	RESIDENCE TIME (MSEC)	FEED RATE (GM/MIN)	WEIGHT LOSS	WFIGHT LOSS ASH TR.	ASH LOSS RS.ASH	ASH IN CHAR	DISTANCE (CM)
LF 234	LIG 27-67	1000.	46.4	0.019	-0.6	-12.8	10.0	8.4	2.5
LF 233	LIG 27-67	1000.	81.8	0.054	-0.7	4.6	-5.0	9.8	5.1
LF 232	LIG 27-67	1000.	111.4	0.109	-1.5	-3.5	1.8	9.1	7.6
LF 231	LIG 27-67	1000.	138.1	0.184	-0.0	-5.1	4.4	8.9	10.2
LF 230	LIG 27-67	1000.	162.8	0.198	-3.2	-5.0	1.6	9.0	12.7
LF 229	LIG 27-67	1000.	162.8	0.189	-0.9	2.9	-3.6	9.6	12.7
LF 228	LIG 27-67	1000.	186.2	0.151	0.5	-5.3	5.0	8.9	15.2
LF 227	LIG 27-67	1000.	208.6	0.206	-6.7	-1.8	-4.3	9.2	17.8
LF 226	LIG 27-67	1000.	230.1	0.087	0.6	-0.4	0.9	9.3	20.3
LF 225	LIG 27-67	1000.	250.8	0.200	-3.8	-0.2	-3.3	9.3	22.9
LF 177	LIG 27-67	1260.	8.0	0.112	0.8	0.0	0.7	9.4	0.0
LF 178	LIG 27-67	1260.	38.6	0.480	-0.1	-3.8	3.3	9.0	2.3
LF 179	LIG 27-67	1260.	69.6	0.195	-1.0	-10.1	7.5	8.6	4.8
LF 181	LIG 27-67	1260.	116.3	0.265	14.0	10.1	3.9	10.3GL	9.9
LF 182	LIG 27-67	1260.	136.5	0.180	20.0	12.9	7.2	10.6GL	12.4
LF 183	LIG 27-67	1260.	155.5	0.284	19.9	17.2	2.8	11.1	15.0
LF 184	LIG 27-67	1260.	173.5	0.228	23.8	21.8	2.2	11.7	17.5
LF 185	LIG 27-67	1260.	190.8	0.201	25.5	19.7	6.4	11.4	20.1
LF 186	LIG 27-67	1260.	207.5	0.252	24.9	23.5	1.6	11.9GL	22.6
LF 187	LIG 27-67	1260.	223.7	0.289	22.1	22.8	-0.9	11.8	25.1

- * Weight Loss (% d.a.f.)
- * Ash Loss (% of ASTM ash in raw coal)
- * Ash in Char (% of ash in char)
- * GL (ash analyzed at Galibraith Laboratory, Inc.,
Knoxville, Tennessee)

TABLE B.1 (cont'd) RESULTS OF LAMINAR FLOW EXPERIMENT
MONTANA LIGNITE

RUN NO	COAL SIZE (MICRON)	TEMP (K)	RESIDENCE TIME (MSEC)	FEED RATE (GM/MIN)	WEIGHT LOSS	WEIGHT LOSS ASH TR.	ASH LOSS BS.ASH	ASH IN CHAR	DISTANCE (CM)	
LF 142	LIG	27-67	1510.	25.1	0.154	3.5	4.6	-1.0	9.8	1.3
LF 112	LIG	27-67	1510.	48.0	0.153	8.6	1.0	7.0	9.4	3.8
LF 141	LIG	27-67	1510.	54.5	0.150	19.5	2.6	15.8	9.6	5.1
LF 111	LIG	27-67	1510.	60.1	0.159	18.0	12.2	6.0	10.5	6.4
LF 102	LIG	27-67	1510.	60.1	0.206	21.6	14.4	7.5	13.8	6.4
LF 143	LIG	27-67	1510.	65.3	0.152	28.5	27.6	1.2	12.5	7.6
LF 103	LIG	27-67	1510.	70.0	0.172	33.4	31.6	2.4	13.1	8.9
LF 105	LIG	27-67	1510.	70.0	0.169	29.2	20.2	9.9	11.5	8.9
LF 140	LIG	27-67	1510.	70.0	0.182	32.7	29.4	4.1	12.8	8.9
LF 104	LIG	27-67	1510.	78.8	0.217	30.4	23.7	7.7	11.9	11.4
LF 106	LIG	27-67	1510.	78.8	0.167	34.0	29.5	5.5	12.8	11.4
LF 139	LIG	27-67	1510.	78.8	0.160	38.7	31.1	9.6	13.0	11.4
LF 107	LIG	27-67	1510.	86.9	0.137	37.8	27.7	12.2	12.5	14.0
LF 108	LIG	27-67	1510.	94.5	0.156	38.9	31.7	9.1	13.1	16.5
LF 109	LIG	27-67	1510.	101.8	0.152	38.7	33.1	7.3	13.4	19.1
LF 110	LIG	27-67	1510.	108.7	0.141	39.2	30.8	10.5	13.0	21.6
LF 138	LIG	27-67	1510.	108.7	0.199	44.2	31.3	16.4	13.1	21.6
LF 146	LIG	27-67	1510.	181.6	0.128	39.8	36.7	4.3	14.0	12.7
LF 145	LIG	27-67	1510.	293.3	0.087	39.3	37.1	3.0	14.1GL	25.7

TABLE B.1 (cont'd) RESULTS OF LAMINAR FLOW EXPERIMENT,
MONTANA LIGNITE

RUN NO	COAL SIZE (MICRON)	TEMP (K)	RESIDENCE TIME (MSEC)	FEED RATE (GM/MIN)	WEIGHT LOSS	WEIGHT LOSS ASH TR.	ASH LOSS BS.ASH	ASH IN CHAR	DISTANCE (CM)
LF 126	LIG 27-67	1740.	9.2	0.148	6.5	-11.0	14.5	8.5	0.0
LF 152	LIG 27-67	1740.	15.8	0.151	17.3	-17.2	27.0	8.1GL	1.3
LF 154	LIG 27-67	1740.	15.8	0.155	10.5				1.3
LF 124	LIG 27-67	1740.	26.8	0.141	27.7	15.1	13.2	10.8	2.5
LF 123	LIG 27-67	1740.	32.3	0.149	32.8	16.6	17.3	11.0	3.8
LF 122	LIG 27-67	1740.	36.4	0.229	28.7	22.4	7.2	11.7	5.1
LF 119	LIG 27-67	1740.	40.0	0.129	37.9	29.4	10.5	12.8	6.4
LF 118	LIG 27-67	1740.	46.2	0.137	41.8				8.9
LF 174	LIG 27-67	1740.	48.5	0.243	43.9	36.4	10.1	14.0	9.9
LF 175	LIG 27-67	1740.	48.5	0.158	47.8	34.5	17.5	13.6	9.9
LF 151	LIG 27-67	1740.	51.6	0.215	48.9	30.0	23.6	12.8	11.4
LF 150	LIG 27-67	1740.	56.7	0.200	51.2	31.2	25.2	13.1	14.0
LF 153	LIG 27-67	1740.	56.7	0.164	49.6	35.1	19.3	13.7	14.0
LF 172	LIG 27-67	1740.	58.6	0.200	43.7	39.5	5.8	14.6	15.0
LF 173	LIG 27-67	1740.	58.6	0.197	47.3	36.2	15.0	13.9	15.0
LF 116	LIG 27-67	1740.	59.1	0.170	45.6	33.6	15.6	13.5	15.2
LF 115	LIG 27-67	1740.	65.9	0.152	48.1	36.3	16.0	13.9	19.1
LF 114	LIG 27-67	1740.	70.2	0.152	46.1	35.5	14.2	13.8	21.6
LF 168	LIG 27-67	1740.	74.0	0.175	49.1	42.5	9.8	15.2	23.9
LF 169	LIG 27-67	1740.	74.0	0.257	54.1	40.4	19.6	14.8	23.9
LF 170	LIG 27-67	1740.	74.0	0.222	47.5	42.4	7.6	15.2	23.9
LF 171	LIG 27-67	1740.	74.0	0.200	48.3	40.3	11.4	14.8	23.9
LF 176	LIG 27-67	1740.	183.2	0.201	50.1	39.0	15.5	14.5	15.0

TABLE B.1 (cont'd) RESULTS OF LAMINAR FLOW EXPERIMENT,
MONTANA LIGNITE

RUN NO	COAL SIZE (MICRON)	TEMP (K)	RESIDENCE TIME (MSEC)	FEED RATE (GM/MIN)	WEIGHT LOSS	WEIGHT LOSS ASH TR.	ASH LOSS BS.ASH	ASH IN CHAR	DISTANCE (CM)
LF 134	LIG 27-67	1940.	11.2	0.156	9.3	-6.3	13.3	8.9	1.3
LF 166	LIG 27-67	1940.	16.0	0.113	25.4	2.8	21.1	9.6GL	2.0
LF 133	LIG 27-67	1940.	18.0	0.199	33.0	11.2	21.9	10.4	2.5
LF 132	LIG 27-67	1940.	21.5	0.111	34.2	28.0	7.6	12.5	3.8
LF 131	LIG 27-67	1940.	24.2	0.295	48.3	33.8	18.9	13.5GL	5.1
LF 165	LIG 27-67	1940.	28.7	0.197	45.2	34.2	14.4	13.6	7.6
LF 164	LIG 27-67	1940.	32.5	0.140	51.4	36.6	20.1	14.0	14.2
LF 163	LIG 27-67	1940.	35.9	0.110	58.1	34.2	31.4	13.6	12.7
LF 135	LIG 27-67	1940.	39.1	0.131	59.4				15.2
LF 128	LIG 27-67	1940.	43.5	0.200	58.6	37.3	29.2	14.1	19.1
LF 136	LIG 27-67	1940.	49.2	0.142	60.9	34.0	35.3	13.5	24.1
LF 137	LIG 27-67	1940.	49.2	0.233	55.8	36.3	26.3	14.0	24.1
LF 162	LIG 27-67	1940.	49.2	0.087	58.8	28.4	37.2	12.6GL	24.1
LF 167	LIG 27-67	1940.	49.2	0.164	55.0				24.1
*LF 305	LIG 27-67	2100.	0.6	0.130	7.5	-2.8	9.1	9.1	0.0
LF 304	LIG 27-67	2100.	3.4	0.067	10.7	-14.5	20.2	8.3	2.0
LF 303	LIG 27-67	2100.	8.1	0.085	30.4	-5.7	31.1	8.9GL	4.6
LF 306	LIG 27-67	2100.	8.1	0.166	27.0	-7.2	29.1	8.8	4.6
LF 302	LIG 27-67	2100.	12.0	0.110	47.9	46.6	2.0	16.2GL	7.1
LF 301	LIG 27-67	2100.	15.5	0.123	55.0				9.7
LF 299	LIG 27-67	2100.	21.6	0.375	56.2	34.0	29.1	13.5	14.7
LF 300	LIG 27-67	2100.	28.2	0.321	61.0	38.5	31.3	14.4	21.1
LF 298	LIG 27-67	2100.	29.5	0.097	63.9				22.4
LF 307	LIG 27-67	2100.	29.5	0.166	63.5	47.0	26.0	16.3GL	22.4

TABLE B.2 RESULTS OF LAMINAR FLOW EXPERIMENT,
PITTSBURGH SEAM BITUMINOUS COAL

RUN NO	COAL SIZE (MICRON)	TEMP (K)	RESIDENCE TIME (MSEC)	FEED RATE (GM/MIN)	WEIGHT LOSS	WFIGHT LOSS ASH TR.	ASH LOSS BS.ASH	ASH IN CHAR	DISTANCE (CM)	
LF 224	BIT	27-90	1000.	9.0	0.218	2.8	-25.4	20.5	8.9	0.0
*LF 223	BIT	27-90	1000.	46.4	0.234	1.6	-18.9	15.6	9.3	2.5
*LF 222	BIT	27-90	1000.	81.8	0.153	-1.2	-20.9	14.8	9.2	5.1
LF 221	BIT	27-90	1000.	111.4	0.182	2.1	-14.9	13.4	9.6	7.6
LF 219	BIT	27-90	1000.	162.8	0.119	6.7	-20.4	20.4	9.2	12.7
LF 218	BIT	27-90	1000.	186.2	0.132	6.0	-15.3	16.7	9.6	15.2
LF 217	BIT	27-90	1000.	208.6	0.066	8.5	-17.5	20.0	9.4	17.8
LF 216	BIT	27-90	1000.	230.1	0.102	8.9	-12.1	16.9	9.8	20.3
LF 215	BIT	27-90	1000.	250.8	0.063	6.9				22.9
LF 199	BIT	27-90	1260.	8.0	0.110	5.3	-12.9	14.6	9.8	0.0
LF 198	BIT	27-90	1260.	38.6	0.115	3.4	-19.0	17.1	9.3	2.3
LF 197	BIT	27-90	1260.	69.6	0.118	10.9	19.5	-9.3	13.2	4.8
LF 196	BIT	27-90	1260.	94.4	0.102	12.5				7.4
LF 195	BIT	27-90	1260.	116.3	0.100	16.7	26.4	-11.3	14.2	9.9
LF 194	BIT	27-90	1260.	136.5	0.078	26.9	28.5	-1.9	14.6GL	12.4
LF 193	BIT	27-90	1260.	155.5	0.166	26.9	24.5	2.7	13.9	15.0
LF 191	BIT	27-90	1260.	190.8	0.162	28.9	30.2	-1.6	14.9GL	20.1
LF 188	BIT	27-90	1260.	207.5	0.161	27.0	32.5	-6.9	15.3	22.6
LF 189	BIT	27-90	1260.	207.5	0.134	33.0	37.0	-5.3	16.3	22.6

* Weight Loss (% d.a.f.)
 * Ash Loss (% of ASTM ash in raw coal)
 * Ash in Char (% of ash in char)
 * GL (ash analyzed at Galibraith Laboratory, Inc.,
 Knoxville, Tennessee)

TABLE B.2 (cont'd) RESULTS OF LAMINAR FLOW EXPERIMENT,
PITTSBURGH SEAM BITUMINOUS COAL

RUN NO	COAL SIZE (MICRON)	TEMP (K)	RESIDENCE TIME (MSEC)	FEED RATE (GM/MIN)	WEIGHT LOSS	WEIGHT LOSS ASH TR.	ASH LOSS BS.ASH	ASH IN CHAR	DISTANCE (CM)
LF 211	RIT 27-90	1510.	15.7	0.089	6.3	-1.6	6.9	10.7	0.0
LF 210	RIT 27-90	1510.	37.7	0.090	7.1	-14.1	16.7	9.7	2.3
LF 246	RIT 27-90	1510.	52.0	0.173	8.1	-1.0	8.0	10.8	4.6
LF 247	RIT 27-90	1510.	52.0	0.193	12.7				4.6
LF 209	RIT 27-90	1510.	53.3	0.134	14.2	11.2	2.9	12.1GL	4.8
LF 244	RIT 27-90	1510.	63.3	0.150	21.2	19.0	2.4	13.1	7.1
LF 245	RIT 27-90	1510.	63.3	0.176	23.3	16.0	7.6	12.7	7.1
LF 208	RIT 27-90	1510.	64.3	0.151	23.2				7.4
LF 242	RIT 27-90	1510.	72.7	0.141	35.5	34.0	2.0	15.6	9.7
LF 243	RIT 27-90	1510.	72.7	0.134	27.2	25.2	2.3	14.0	9.7
LF 207	RIT 27-90	1510.	73.6	0.098	32.5	30.2	2.8	14.9GL	9.9
LF 206	RIT 27-90	1510.	82.1	0.100	33.7	40.8	-10.0	17.1	12.4
LF 248	RIT 27-90	1510.	89.2	0.012	38.4	54.5	-27.9	21.2	14.7
LF 253	RIT 27-90	1510.	89.2	0.086	35.6	48.3	-19.8	19.1	14.7
LF 255	RIT 27-90	1510.	89.2	0.111	30.4	41.7	-16.1	17.3	14.7
LF 205	RIT 27-90	1510.	90.0	0.104	30.4	40.3	-13.8	17.0	15.0
LF 204	RIT 27-90	1510.	97.5	0.162	35.4	41.7	-8.8	17.3	17.5
LF 240	RIT 27-90	1510.	103.9	0.101	39.6	45.7	-9.2	18.4	19.8
LF 238	RIT 27-90	1510.	110.8	0.136	38.8	47.6	-13.7	18.9	22.4
LF 239	RIT 27-90	1510.	110.8	0.090	44.7	50.5	-9.4	19.8	22.4
LF 201	RIT 27-90	1510.	111.5	0.093	36.6	49.9	-21.3	19.6GL	22.6
LF 200	RIT 27-90	1510.	118.1	0.076	41.5	50.3	-14.3	19.8	25.1

TABLE B.2 (cont'd) RESULTS OF LAMINAR FLOW EXPERIMENT,
PITTSBURGH SEAM BITUMINOUS COAL

RUN NO	COAL SIZE (MICRON)	TEMP (K)	RESIDENCE TIME (MSEC)	FEED RATE (GM/MIN)	WEIGHT LOSS	WEIGHT LOSS ASH TR.	ASH LOSS RS.ASH	ASH IN CHAR	DISTANCE (CM)	
LF 278	BIT	27-90	1740.	0.9	0.059	14.3			0.0	
LF 276	BIT	27-90	1740.	6.4	0.138	15.8	-14.9	24.1	9.6	2.0
LF 275	BIT	27-90	1740.	14.7	0.133	14.6	-18.9	25.6	9.3	4.6
LF 274	BIT	27-90	1740.	21.5	0.122	32.8	35.8	-3.9	16.0GL	7.1
LF 279	BIT	27-90	1740.	21.5	0.131	29.8				7.1
LF 284	BIT	27-90	1740.	21.5	0.145	30.5				7.1
LF 273	BIT	27-90	1740.	27.3	0.123	38.3	44.7	-9.4	18.1GL	9.7
LF 280	BIT	27-90	1740.	27.3	0.121	40.7				9.7
LF 272	BIT	27-90	1740.	32.6	0.143	46.7	59.1	-23.2	23.0	12.2
LF 271	BIT	27-90	1740.	42.1	0.144	40.1	46.8	-10.3	18.7	17.3
LF 270	BIT	27-90	1740.	50.7	0.129	46.7				22.4
LF 282	BIT	27-90	1740.	50.7	0.124	44.1	52.6	-14.2	20.5GL	22.4

TABLE B.2 (cont'd) RESULTS OF LAMINAR FLOW EXPERIMENT,
PITTSBURGH SEAM BITUMINOUS COAL

RUN NO	COAL SIZE (MICRON)	TEMP (K)	RESIDENCE TIME (MSEC)	FEED RATE (GM/MIN)	WEIGHT LOSS	WEIGHT LOSS ASH TR.	ASH LOSS RS.ASH	ASH IN CHAR	DISTANCE (CM)
LF 265	BIT 27-90	1940.	1.2	0.084	8.0	-21.7	22.2	9.1	0.0
LF 264	BIT 27-90	1940.	6.4	0.150	20.3	-3.5	20.6	10.6	2.0
LF 266	BIT 27-90	1940.	10.0	0.108	19.9				3.3
LF 263	BIT 27-90	1940.	12.9	0.126	25.1	57.9	-60.4	22.5GL	4.6
LF 267	BIT 27-90	1940.	15.4	0.120	40.8	61.5	-40.9	24.1GL	5.8
*LF 262	BIT 27-90	1940.	17.5	0.126	56.1	45.4	16.1	18.3	7.1
*LF 268	BIT 27-90	1940.	21.4	0.116	45.5				9.7
LF 269	BIT 27-90	1940.	24.9	0.127	52.0				12.2
LF 260	BIT 27-90	1940.	28.1	0.114	57.4				14.7
LF 261	BIT 27-90	1940.	28.1	0.110	59.7	60.4	-1.4	23.6GL	14.7
LF 295	BIT 27-90	2100.	0.6	0.126	21.0	-21.0	31.5	9.2	0.0
LF 294	BIT 27-90	2100.	3.4	0.104	24.1	-10.6	28.3	9.9	2.0
LF 293	BIT 27-90	2100.	8.1	0.103	35.6	47.2	-17.9	18.8GL	4.6
LF 296	BIT 27-90	2100.	8.1	0.105	38.1				4.6
LF 291	BIT 27-90	2100.	12.0	0.079	47.9	53.5	-9.5	20.8GL	7.1
LF 292	BIT 27-90	2100.	12.0	0.110	48.2				7.1
LF 288	BIT 27-90	2100.	15.5	0.111	52.7	52.0	1.3	20.3	9.7
LF 286	BIT 27-90	2100.	21.6	0.101	63.3	72.0	-21.7	30.4GL	14.7
LF 285	BIT 27-90	2100.	29.5	0.126	64.1				22.4

RESULTS OF FREE FALL EXPERIMENTS

Tables C.1 to C.3 summarize the results of alumina collector runs. Table C.1 shows the results from pretreated coals, which should be considered as a special case. Reduction of the data was carried out by using a Fortran subroutine FREEF developed for this purpose (see Appendix J for the listings). The following moisture and ash values were used in the calculation of dry-ash-free weight loss.

		<u>Moisture (%)</u>
Montana Lignite	FF 500's	0.0
	other runs	14.09
Pittsburgh Bituminous	FF 500's	0.0
	other runs	2.06

The results of bronze collector runs are summarized in table C.4. Estimation of soot collected in the bronze disk is based on the following analysis.

TABLE C.1 RESULTS OF FREE FALL EXPERIMENT WITH ALUMINA COLLECTOR
 SAMPLE PREDRIED AT 105 C FOR 2 TO 48 HOURS

RUN NO	COAL SIZE (MICRON)	TEMP (K)	COAL WEIGHT (GM)	W. LS	W. LS	W. LS	W. LS	W. LS	ASH LS	THR.CR	FEED	
				APP.	ASH TR	ASH TR	THR.CR	THR.CR	RS.ASH	BS.CL	RATE	
				(1)	(2)	(3)	(4)	(5)	(6)	(7)	(GM/MIN)	
FF 503	RIT	27-90	930.	0.8739	39.7	39.9	42.2	42.7	42.8	-0.4	3.1	0.075
FF 504	RIT	27-90	940.	0.8178	36.5	37.4	39.7	38.9	39.0	-1.2	2.4	0.080
FF 502	RIT	27-90	950.	0.7467	41.3	41.8	44.2	44.1	44.1	-0.7	2.7	0.067
FF 510	RIT	27-90	1100.	0.8794	40.2	39.8	45.5	45.9	45.9	0.6	5.7	0.068
FF 509	RIT	27-90	1100.	0.8410	38.7	40.0	44.9	43.7	43.9	-1.8	5.0	0.093
FF 511	RIT	27-90	1290.	1.0276	50.1	48.4	52.1	53.6	53.3	2.7	3.5	0.233
FF 512	RIT	27-90	1290.	0.8927	44.7	44.0	49.7	50.3	50.1	1.1	5.5	0.105
FF 517	RIT	27-90	1460.				48.9					
FF 505	LIG	27-67	930.	0.5863	33.8	38.1	37.4	33.8	34.4	-6.0	0.0	0.065
FF 506	LIG	27-67	930.	0.8992	35.0	39.8	40.5	35.8	36.5	-6.8	0.8	0.064
FF 507	LIG	27-67	1100.	0.8945	43.7	45.4	45.3	44.0	44.3	-2.6	0.3	0.112
FF 508	LIG	27-67	1100.	0.7192	42.0	45.4	45.6	42.5	43.0	-5.3	0.5	0.060
FF 513	LIG	27-67	1300.	0.8011	47.2	47.0	48.7	49.0	48.9	0.3	1.8	0.100
FF 514	LIG	27-67	1300.	0.9688	48.0	49.5	49.3	48.1	48.3	-2.5	0.1	0.084
FF 516	LIG	27-67	1460.	0.9171	55.8	46.0	43.1	55.8	54.2	15.2	0.0	0.108
FF 515	LIG	27-67	1470.	0.9100	57.7	47.5	45.1	57.7	56.0	16.2	0.0	0.101

296

- (1) APPARENT WEIGHT LOSS (% D.A.F.)
- (2) WEIGHT LOSS BY ASH TRACER METHOD (% D.A.F.)
- (3) WEIGHT LOSS BY ASH TRACER METHOD COMPENSATED FOR THERMAL CRACKING (% D.A.F.)
- (4) WEIGHT LOSS, COMPENSATED FOR THERMAL CRACKING (% D.A.F.)
- (5) WEIGHT LOSS, COMPENSATED FOR THERMAL CRACKING AND ASH LOSS (% D.A.F.)
- (6) ASH LOSS, PERCENT OF ORIGINAL ASH
- (7) DEPOSIT ON CRUCIBLE WALL BY THERMAL CRACKING, PERCENT OF ORIGINAL COAL

TABLE C.2 RESULTS OF FREE FALL EXPERIMENT WITH ALUMINA COLLECTOR,
MONTANA LIGNITE

RUN NO	COAL SIZE (MICRON)	TEMP (K)	COAL WEIGHT (GM)	W. LS APP.	W. LS ASH TR	W. LS ASH TF THR.CF	W. LS THR.CR	W. LS THR.CR ASH LS	ASH LS BS.ASH	THR.CR BS.CL	FEED RATE (GM/MIN)
				(1)	(2)	(3)	(4)	(5)	(6)	(7)	
FF 703	LIG 27-67	920.	0.9940	47.8	41.2	41.7	48.3	47.3	9.6	0.5	0.105
FF 702	LIG 27-67	930.	0.9979	47.9	40.2	42.0	49.7	48.5	11.0	1.8	0.143
*FF 602	LIG 27-67	1020.	1.0062	48.4	47.7	46.6	49.4	49.3	1.2	1.0	0.101
FF 706	LIG 27-67	1070.	0.9966	54.2	44.9	46.0	54.7	53.3	14.3	0.5	0.112
FF 707	LIG 27-67	1070.	1.0024	52.2	42.4	46.7	54.4	52.9	14.4	2.3	0.172
FF 608	LIG 27-67	1110.	1.1316	53.9	46.4	47.3	54.2	53.0	11.7	0.4	0.151
FF 609	LIG 27-67	1110.	1.0313	53.0	48.3	48.4	53.3	52.5	7.6	0.2	0.088
FF 708	LIG 27-67	1270.	1.0103	61.2	57.7	54.2	61.2	60.5	6.5	0.0	0.104
FF 709	LIG 27-67	1280.	1.0047	61.4	54.1	54.8	62.0	60.6	13.0	0.6	0.105
FF 613	LIG 27-67	1290.	1.0225	63.4	48.3	50.4	65.1	62.5	24.3	1.7	0.157
FF 612	LIG 27-67	1300.	0.9951	61.5	49.4	51.0	63.5	61.4	19.8	2.0	0.133
FF 712	LIG 27-67	1470.	1.0012	66.0	49.9	51.7	67.0	64.3	26.7	1.0	0.078
FF 710	LIG 27-67	1480.			55.2	45.9					
FF 713	LIG 27-67	1480.			58.2	50.0					
FF 711	LIG 27-67	1490.			54.3	48.3					
FF 725	LIG 27-67	1560.			50.2	47.8					
FF 617	LIG 27-67	1570.			52.3	46.5					
FF 618	LIG 27-67	1600.			57.1						

297

(1) - (7) refer to Table C.1

TABLE C.3 RESULTS OF FREE FALL EXPERIMENT WITH ALUMINA COLLECTOR,
PITTSBURGH SEAM BITUMINOUS COAL

RUN NO	COAL SIZE (MICRON)	TEMP (K)	COAL WEIGHT (GM)	W. LS	W. LS	W. LS	W. LS	W. LS	ASH LS	THR.CR	FEED	
				APP.	ASH TR	ASH TR	THR.CR	THR.CR	RS.ASH	RS.CL	RATE (GM/MIN)	
				(1)	(2)	(3)	(4)	(5)	(6)	(7)		
FF 715	RIT	27-90	890.			53.2						
FF 704	RIT	27-90	920.			52.7						
FF 705	RIT	27-90	950.			50.3						
*FF 601	RIT	27-90	1010.			54.7						
*FF 605	RIT	27-90	1010.	1.0557	56.4	50.5	52.6	58.1	57.0	9.6	1.7	0.097
*FF 701	RIT	27-90	1010.	0.7541	51.2	44.4	49.1	54.9	53.7	10.0	3.7	0.127
*FF 606	RIT	27-90	1020.			50.8						
FF 718	RIT	27-90	1050.	0.9994	47.4	45.6	53.0	54.6	54.2	2.7	7.2	0.098
FF 719	RIT	27-90	1060.	0.9997	49.4	44.4	54.3	58.3	57.4	7.3	8.9	0.176
FF 720	RIT	27-90	1060.	0.9992	47.6	43.4	55.5	58.8	58.1	6.1	11.3	0.144
FF 610	RIT	27-90	1110.	0.9345	52.2	45.6	50.8	57.1	55.9	10.0	4.8	0.208
FF 611	RIT	27-90	1110.	1.1710	53.6	48.4	51.2	57.1	56.1	8.1	3.5	0.213
FF 616	RIT	27-90	1280.	0.9987	51.7	50.6	56.7	57.4	57.2	1.7	5.7	0.133
FF 721	RIT	27-90	1280.	0.9961	58.2	56.3	59.0	60.6	60.2	3.3	2.4	0.122
FF 722	RIT	27-90	1280.	1.0019	57.3	52.4	58.7	62.9	61.9	8.1	5.6	0.125
FF 614	RIT	27-90	1290.	0.9658	52.7	50.0	58.4	60.5	60.0	4.2	7.8	0.161
FF 723	RIT	27-90	1570.			44.6	51.1					
FF 620	RIT	27-90	1590.			56.2	47.3					
FF 724	RIT	27-90	1600.			49.4	56.5					

298

(1) - (7) refer to Table C.1

Estimation of Char and Condensed Material in Bronze Collector

Figure C-1 shows the distribution of char and condensed material on the bronze collector schematically. Char and condensed material formed a bell shape near the center of the collector. The height was about 1 inch and the diameter was about 1.5 inches. Most of the char particles were concentrated in the center and almost no char particles were found near the perimeter of the round collector. From these observations, the following assumptions were made:

- (1) Both char and condensed material have normal distributions with the peak at the center of the collector.
- (2) The standard deviations of char and condensed material are 0.5 inch and 0.75 inch respectively.
- (3) The condensed material has no ash.

Ash analyses are performed for two samples from a bronze collector, one taken from the center zone (zone A) and the other from the periphery zone (zone B). r_A and r_B specify these zones. The following relations hold between ash concentration in the char, f_A , ash concentration in the material from the central zone, $f_{A,A}$, and ash concentration in the material from the peripheral zone, $f_{A,B}$.

$$f_A \cdot \Phi(r_A/\tau_1) \cdot M_1 = f_{A,A} \cdot \left\{ \Phi(r_A/\tau_1) \cdot M_1 + \Phi(r_A/\tau_2) \cdot M_2 \right\} \quad (C-1)$$

$$f_A \cdot \left\{ \Phi(r_D/\tau_1) - \Phi(r_B/\tau_1) \right\} \cdot M_1$$

$$= f_{A,B} \cdot \left[\left\{ \Phi(r_D/\tau_1) - \Phi(r_B/\tau_1) \right\} \cdot M_1 + \left\{ \Phi(r_D/\tau_2) - \Phi(r_B/\tau_2) \right\} \cdot M_2 \right] \quad (C-2)$$

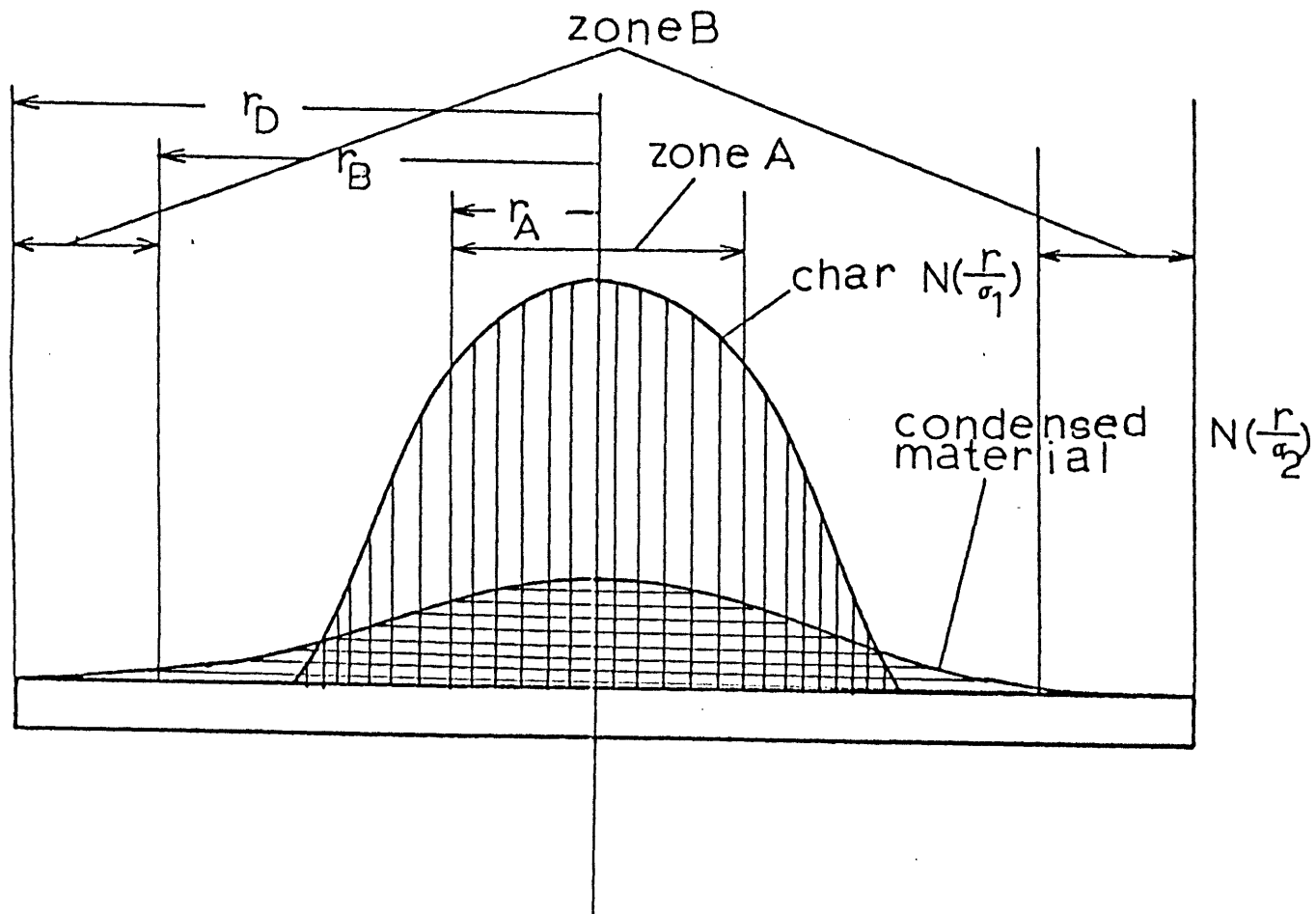


Figure C -1 Schematic diagram of the distributions of char and condensed material in the bronze filter

Where M_1 : weight of char

M_2 : weight of condensed material

τ_1 : standard deviation of char

τ_2 : standard deviation of condensed material

$$\Phi(r) = 1 - e^{-\frac{1}{2}r^2}$$

From Equations (C-1) and (C-2), the following expressions are obtained.

$$f_A = K \cdot f_{A,A} + (1-K) \cdot f_{A,B} \quad (C-3)$$

$$K = \frac{\Phi(r_A/\tau_1) \cdot \left\{ \Phi(r_D/\tau_2) - \Phi(r_B/\tau_2) \right\}}{\Phi(r_A/\tau_1) \left\{ \Phi(r_D/\tau_2) - \Phi(r_B/\tau_2) \right\} - \Phi(r_A/\tau_2) \left\{ \Phi(r_D/\tau_1) - \Phi(r_B/\tau_1) \right\}} \quad (C-4)$$

Since $f_{A,A}$ and $f_{A,B}$ are experimentally measured values, ash concentration in char, f_A , can be calculated from these equations. Weight loss can be calculated by the ash tracer method using f_A .

Table C.4 Measured Weight Loss in Free Fall Experiment with Bronze Collector (D.A.F.)

RUN NO.	COAL SIZE (MICRON)	TEMP. (K)	RESID. TIME (SEC)	FEED RATE (G/MIN)	W. LOSS APP.	W. LOSS ASH TR.	ASH IN CHAR	ASH CENTER	ASH PERIPH.	W. LOSS EST.
			(1)		(2)	(3)	(4)	(5)	(6)	(7)
FF 809	BIT 38-45	1490	1.5	0.156	37.8			21.4	4.8	61.8
FF 810	BIT 38-45	1490	1.5	0.130	30.7			23.0	5.9	65.1
FF 811	BIT 38-45	1490	1.5	0.143	32.4			22.7	5.9	64.5
FF 815	BIT 38-45	1490	0.7	0.139	39.0			22.1	6.7	62.8
FF 818	BIT 38-45	1490	0.5	0.047	35.2			21.8	4.4	62.8
FF 805	BIT 38-45	1830	1.2	0.125	35.6	43.1	17.7			
FF 806	BIT 38-45	1830	1.2	0.127	33.2			19.1	9.5	63.7
FF 807	BIT 38-45	1830	1.2	0.209	39.2			19.0	11.5	60.9
FF 804	BIT 38-45	1830	0.6	0.116	34.4	41.6	17.3			
FF 812	LIG 38-45	1490	1.5	0.188	45.0	43.8	15.5			
FF 813	LIG 38-45	1490	1.5	0.194	47.3	44.2	15.6			
FF 814	LIG 38-45	1490	0.7	0.134	44.9			16.2	14.7	44.5
FF 816	LIG 38-45	1490	0.5	0.108	45.8			14.9	14.3	39.3
FF 801	LIG 38-45	1830	1.2	0.101	59.0	58.7	20.0			
FF 808	LIG 38-45	1830	1.2	0.174	66.3	62.4	21.6			
FF 802	LIG 38-45	1830	0.6	0.218	54.9	54.9	18.6			
FF 803	LIG 38-45	1830	0.6	0.208	54.6	53.6	18.2			

302

Table C.4 Continued Next Page . . .

Table C.4 (Continued)

- (1) Estimated residence time of particle in the center zone (6 inches) of the furnace
- (2) Apparent weight loss
- (3) Ash tracer weight loss
- (4) Ash concentration in char
- (5) Ash concentration in the center zone of the collector ($d_A = 1.5$ inches for FF 806, FF807,
 $d_A = 0.5$ inches for the rest)
- (6) Ash concentration in the periphery zone of the collector ($d_B = 1.5$ inches for FF 806, FF 807,
 $d_B = 2.5$ inches for the rest)
- (7) Estimated weight loss compensated for the "condensed" material

RESULTS OF CRUCIBLE EXPERIMENTS

Tables D.1 to D.5 summarize the results of the crucible experiments. Run numbers with asterisk (*) in Tables D.1 to D.3 refer to the following note

CR103	nickel alloy crucible
CR110, CR116	platinum crucible
CR240, CR242	30 minutes at peak temperature
CR241, CR243	1 hour at peak temperature
CR226, CR234	platinum crucible
CR264	heated to peak temperature in 1.5 hours
CR277	char recycled from CR265
CR278	" " " CR266
CR281	" " " CR267
CR282	" " " CR268
CR400's	graphite crucibles

Run numbers with asterisks in Tables D.4 and D.5 are runs carried out with shallow alumina cylindrical crucibles. The temperatures reported for the runs with graphite crucibles (CR 400'S) refer to the furnace temperatures.

TABLE D.1 RESULTS OF CRUCIBLE EXPERIMENT,
SAMPLE PREDRIED AT 105 C FOR 2 TO 48 HOURS

RUN NO	COAL SIZE (MICRON)	TEMP (K)	COAL WEIGHT (GM)	W. LS	W. LS	W. LS	W. LS	W. LS	ASH LS	THR.CR
				APP.	ASH TR	ASH TR	THR.CR	THR.CR	BS.ASH	BS.CL
				(1)	(2)	(3)	(4)	(5)	(6)	(7)
CR 106	LIG	27-67	930.	1.1668	40.3	35.2			6.8	
CR 107	LIG	27-67	930.	0.8385	39.8	35.1			6.3	
CR 109	LIG	27-67	1090.	0.8704	43.2	38.9			6.1	
*CR 110	LIG	27-67	1090.	0.8025	44.0	40.9			4.4	
CR 111	LIG	27-67	1090.	0.8391	44.2	40.7			5.0	
CR 114	LIG	27-67	1330.	0.9991	45.7	41.3			6.3	
CR 115	LIG	27-67	1330.	1.4575	45.4	40.3			7.3	
CR 118	LIG	27-67	1580.	0.9666	48.5	41.1			10.7	
CR 119	LIG	27-67	1580.	0.9380	48.5	41.6			10.0	
CR 122	LIG	27-67	1760.	1.0702	49.3	36.3			17.6	
CR 123	LIG	27-67	1760.	1.0474	49.2	37.1			16.6	
CR 101	BIT	27-90	930.	0.8052	34.5	32.8			2.2	
CR 102	BIT	27-90	930.	0.6721	34.9	34.2			0.9	
*CR 103	BIT	27-90	930.	0.8782	35.6	34.5			1.4	
CR 112	BIT	27-90	1090.	0.8417	37.4	36.0			1.9	
CR 113	BIT	27-90	1090.	0.7149	37.8	36.2			2.1	
CR 117	BIT	27-90	1330.	0.9758	39.8	38.3			2.0	
*CR 116	BIT	27-90	1370.	1.0392	40.7	40.1			0.9	
CR 120	BIT	27-90	1580.	0.9421	46.4	19.4			29.0	
CR 121	BIT	27-90	1580.	0.9822	45.9	26.7			22.4	
CR 124	BIT	27-90	1760.	0.8337	47.7	29.1			22.4	
CR 125	BIT	27-90	1760.	1.0203	48.3	30.7			21.5	

(1) - (7) refer to Table C.1

TABLE D.2 RESULTS OF CRUCIBLE EXPERIMENT,
MONTANA LIGNITE

RUN NO	COAL SIZE (MICRON)	TFMP (K)	COAL WEIGHT (GM)	W. LS APP. (1)	W. LS ASH TR (2)	W. LS ASH TP THR.CP (3)	W. LS THR.CR (4)	W. LS THR.CP ASH LS (5)	ASH LS BS.ASH (6)	THR.CR BS.CL (7)
*CR 303	LIG 27-67	610.	2.5850	13.5						
*CR 305	LIG 27-67	610.	2.0556	14.1						
*CR 309	LIG 27-67	720.	2.5960	25.9						
*CR 308	LIG 27-67	740.	3.4930	28.7						
*CR 242	LIG 27-67	730.	1.0395	27.4	22.5	22.4	27.4	26.8	5.6	-0.1
*CR 243	LIG 27-67	730.	1.0710	29.1	21.3	21.3	29.1	28.2	8.7	0.0
*CR 264	LIG 27-67	740.	1.0591	28.5	25.6	25.6	28.6	28.2	3.5	0.0
*CR 265	LIG 27-67	740.	1.0223	27.7	23.2	22.9	27.7	27.2	5.3	-0.2
CR 258	LIG 27-67	830.	1.0754	35.2	31.2	31.1	35.2	34.6	5.0	-0.0
CR 259	LIG 27-67	830.	1.0482	34.4	30.0	30.0	34.4	33.8	5.5	-0.0
CR 247	LIG 27-67	940.	1.0603	41.8	35.4	35.4	41.8	40.9	8.6	0.0
CR 267	LIG 27-67	950.	1.0081	41.0	38.5	38.5	41.0	40.6	3.4	-0.0
CR 279	LIG 27-67	950.	1.0097	41.2	38.3	38.4	41.3	40.8	4.0	0.0
CR 246	LIG 27-67	950.	1.0377	42.0	36.5	36.5	42.1	41.3	7.5	0.0
CR 202	LIG 27-67	1110.	1.0137	44.2	40.7	40.5	44.2	43.7	5.1	-0.2
CR 204	LIG 27-67	1130.	1.0020	44.1	41.4	41.1	44.1	43.7	3.9	-0.3

(1) - (7) refer to Table C.1

TABLE D.2 (cont'd) RESULTS OF CRUCIBLE EXPERIMENT,
MONTANA LIGNITE

RUN NO	COAL SIZE (MICRON)	TEMP (K)	COAL WEIGHT (GM)	W. LS	W. LS	W. LS	W. LS	W. LS	ASH LS	THR.CR
				APP.	ASH TR	ASH TR	THR.CR	THR.CR	RS.ASH	BS.CL
				(1)	(2)	(3)	(4)	(5)	(6)	(7)
CR 283	LIG	27-67	1.0062	44.4	40.5	40.6	44.5	43.9	5.6	0.1
CR 284	LIG	27-67	1.0048	44.3	41.0	40.8	44.3	43.8	4.7	-0.2
*CR 277	LIG	27-67	0.6674	44.1	41.4	41.4	44.1	43.7	3.9	0.0
*CR 281	LIG	27-67	0.7132	45.2	41.5	41.5	45.2	44.6	5.4	0.0
CR 219	LIG	27-67	0.9733	44.9	40.5	40.6	45.0	44.3	6.3	0.0
CR 220	LIG	27-67	1.1080	45.0	41.3	41.4	45.1	44.5	5.4	0.1
CR 231	LIG	27-67	1.0128	46.6	41.1	41.1	46.6	45.8	8.0	-0.0
CR 233	LIG	27-67	0.9985	47.2	42.3	42.6	47.6	46.8	7.3	0.4
*CR 234	LIG	27-67	1.0534	46.8	41.4	41.2	46.8	46.0	7.8	-0.2
CR 238	LIG	27-67	1.0020	48.3	41.7	41.9	48.4	47.5	9.6	0.2
CR 239	LIG	27-67	1.0010	48.3	41.2	40.9	48.3	47.2	10.3	-0.2
*CR 289	LIG	27-67	1.0102	48.5	39.4	34.3	48.5	47.2	12.9	-4.4
CR 262	LIG	27-67	1.0198	49.9	38.1	33.2	49.9	48.2	16.4	-4.0
CR 263	LIG	27-67	1.0778	49.5	38.4	35.0	49.5	47.9	15.5	-2.9
CR 404	LIG	27-67	0.4828	52.0	23.7				32.7	
CR 405	LIG	27-67	0.4962	51.9	33.4				24.1	
CR 409	LIG	27-67	0.3962	55.2	-97.1				73.4	
CR 410	LIG	27-67	0.4993	55.0	-93.6				72.9	

(1) - (7) refer to Table C.1

TABLE D.3 RESULTS OF CRUCIBLE EXPERIMENT,
EFFECTS OF BED DEPTH, MONTANA LIGNITE

RUN NO	COAL SIZE (MICRON)	TEMP (K)	COAL WEIGHT (GM)	W. LS	W. LS	W. LS	W. LS	W. LS	ASH LS	THR.CR
				APP.	ASH TR	ASH TR	THR.CR	THR.CR	PS.ASH	BS.CL
				(1)	(2)	(3)	(4)	(5)	(6)	(7)
CR 220	LIG	27-67	1.1080	45.0	41.3	41.4	45.1	44.5	5.4	0.1
CR 283	LIG	27-67	1.0062	44.4	40.5	40.6	44.5	43.9	5.6	0.1
CR 284	LIG	27-67	1.0048	44.3	41.0	40.8	44.3	43.8	4.7	-0.2
CR 219	LIG	27-67	0.9733	44.9	40.5	40.6	45.0	44.3	6.3	0.0
CR 222	LIG	27-67	0.1396	43.1	40.7	40.6	43.1	42.7	3.4	-0.1
CR 224	LIG	27-67	0.0646	42.8	37.8	38.0	43.0	42.3	6.9	0.2
CR 225	LIG	27-67	0.0565	40.9	38.3	39.9	42.5	42.1	3.7	1.6
*CR 254	LIG	27-67	0.0318	43.7	44.8	45.2	44.1	44.3	-1.7	0.4
*CR 270	LIG	27-67	0.0214	40.7	36.1	37.4	41.9	41.3	6.2	1.2
*CR 272	LIG	27-67	0.0199	40.0	44.1	47.8	43.9	44.5	-6.2	3.9
*CR 252	LIG	27-67	0.0173	45.0	54.8	52.2	45.0	46.8	-17.6	-3.0
*CR 253	LIG	27-67	0.0171	48.0	42.8	41.2	48.0	47.2	7.6	-1.5
*CR 269	LIG	27-67	0.0138	37.7	37.1	38.0	38.7	38.6	0.9	0.9
*CR 271	LIG	27-67	0.0111	49.0	41.9	36.7	49.0	47.9	10.4	-4.6
*CR 255	LIG	27-67	0.0105	49.2	53.0	46.1	49.2	49.9	-6.6	-7.3

(1) - (7) refer to Table C.1

TABLE D.4 RESULTS OF CRUCIBLE EXPERIMENT,
PITTSBURGH SEAM BITUMINOUS COAL.

RUN NO	COAL SIZE (MICRON)	TEMP (K)	COAL WEIGHT (GM)	W. LS APP.	W. LS ASH TR	W. LS ASH TR THR.CP	W. LS THR.CR	W. LS THR.CP ASH LS	ASH LS RS.ASH	THR.CR BS.CL
				(1)	(2)	(3)	(4)	(5)	(6)	(7)
*CR 301	BIT	27-90	540. 2.3967	2.9						
*CR 304	BIT	27-90	610. 2.5698	10.7						
*CR 302	BIT	27-90	620. 2.7934	7.6						
*CR 307	BIT	27-90	740. 3.1913	28.1	27.2				1.2	
*CR 240	BIT	27-90	730. 1.0617	26.5	25.8	26.4	27.1	27.0	0.9	0.6
*CR 241	BIT	27-90	730. 1.0549	28.1	26.2	26.4	28.4	28.1	2.3	0.3
*CR 266	BIT	27-90	740. 1.0114	26.7	25.3	25.2	26.7	26.5	1.7	-0.1
CR 256	BIT	27-90	830. 1.0151	33.4	33.3	33.4	33.4	33.4	0.0	0.1
CR 257	BIT	27-90	830. 1.0071	34.3	33.0	33.0	34.3	34.1	1.6	-0.0
CR 244	BIT	27-90	950. 1.0678	39.8	39.0	39.4	40.2	40.1	1.1	0.4
CR 245	BIT	27-90	950. 1.1099	40.3	37.8	38.1	40.6	40.2	3.4	0.2
CR 262	BIT	27-90	950. 1.0466	39.5	39.5	39.6	39.7	39.7	0.1	0.2
CR 280	BIT	27-90	950. 1.0034	39.8	40.0	40.0	39.8	39.8	-0.3	0.0
CR 201	BIT	27-90	1110. 1.0034	41.1	41.2	42.1	42.0	42.0	-0.2	0.9
CR 203	BIT	27-90	1110. 3.0025	41.6	42.5	43.3	42.3	42.5	-1.4	0.7
CR 205	BIT	27-90	1120. 0.9006	41.3	40.4	41.9	42.8	42.6	1.3	1.4

(1) - (7) refer to Table C.1

TABLE D.4 (cont'd) RESULTS OF CRUCIBLE EXPERIMENT,
PITTSBURGH SEAM BITUMINOUS COAL

RUN NO	COAL SIZE (MICRON)	TEMP (K)	COAL WEIGHT (GM)	W. LS	W. LS	W. LS	W. LS	W. LS	ASH LS	THR.CR	
				APP.	ASH TR	ASH TR	THR.CR	THR.CR	RS.ASH	BS.CL	
				(1)	(2)	(3)	(4)	(5)	(6)	(7)	
*CR 278	BIT	27-90	1220.	0.6391	38.5	36.7	36.8	38.5	38.2	2.3	0.0
*CR 282	BIT	27-90	1220.	0.6782	42.8	42.4	42.4	42.8	42.7	0.5	0.0
CR 285	BIT	27-90	1220.	1.0243	42.6	42.7	43.2	43.1	43.1	-0.2	0.5
CR 286	BIT	27-90	1220.	1.0068	42.9	41.9	43.0	43.9	43.8	1.3	1.0
CR 206	BIT	27-90	1230.	1.2212	42.0	41.9	43.1	43.2	43.2	0.2	1.2
CR 207	BIT	27-90	1230.	2.2859	42.7	42.4	43.3	43.6	43.5	0.4	0.9
CR 229	BIT	27-90	1310.	1.0672	41.4	40.1	43.1	44.4	44.2	1.8	3.0
CR 230	BIT	27-90	1310.	0.9598	42.0	41.0	43.7	44.6	44.5	1.3	2.7
CR 227	BIT	27-90	1320.	0.9879	41.7	41.4	44.3	44.6	44.5	0.4	2.9
CR 228	BIT	27-90	1320.	1.2396	42.4	41.7	44.4	44.6	44.5	0.9	2.3
*CR 226	BIT	27-90	1330.	1.0511	43.4	43.5	43.8	43.7	43.7	-0.1	0.3
CR 236	BIT	27-90	1570.	0.9819	42.1	37.4	41.9	46.4	45.6	6.4	4.3
CR 235	BIT	27-90	1580.	1.0166	43.4	37.5	38.9	44.7	43.7	7.9	1.3
CR 237	BIT	27-90	1580.	1.0135	42.9	38.6	42.2	46.3	45.6	5.8	3.4
*CR 288	BIT	27-90	1580.	1.0015	45.9	36.1	33.9	45.9	44.4	12.9	-2.0
CR 260	BIT	27-90	1740.	1.0273	46.8	29.1	32.4	49.0	46.4	21.3	2.3
CR 261	BIT	27-90	1740.	1.0040	48.0	29.8	31.9	49.6	46.9	22.1	1.6
CR 407	BIT	27-90	2000.	0.5553	55.9	16.7				41.1	
CR 408	BIT	27-90	2000.	0.5338	53.1	19.0				36.6	
CR 414	BIT	27-90	2100.	0.4450	53.8	10.7				42.5	
CR 415	BIT	27-90	2100.	0.4563	53.8	12.2				41.6	

(1) - (7) refer to Table C.1

TABLE D.5 RESULTS OF CRUCIBLE EXPERIMENT,
EFFECTS OF BED DEPTH, PITTSBURGH SEAM
BITUMINOUS COAL

RUN NO	COAL SIZE (MICRON)	TEMP (K)	COAL WEIGHT (GM)	W. LS	W. LS	W. LS	W. LS	W. LS	ASH LS	THR.CR	
				APP.	ASH TR	ASH TR	THR.CR	THR.CR	PS.ASH	BS.CL	
				(1)	(2)	(3)	(4)	(5)	(6)	(7)	
CR 207	BIT	27-90	1230.	2.2859	42.7	42.4	43.3	43.6	43.5	0.4	0.9
CR 206	BIT	27-90	1230.	1.2212	42.0	41.9	43.1	43.2	43.2	0.2	1.2
CR 285	BIT	27-90	1220.	1.0243	42.6	42.7	43.2	43.1	43.1	-0.2	0.5
CR 286	BIT	27-90	1220.	1.0068	42.9	41.9	43.0	43.9	43.8	1.3	1.0
CR 208	BIT	27-90	1230.	0.5076	41.4	41.1	42.8	43.0	43.0	0.4	1.6
CR 209	BIT	27-90	1230.	0.1719	39.7	40.7	42.3	41.3	41.4	-1.5	1.6
CR 214	BIT	27-90	1240.	0.0667	36.7	36.2	42.7	43.2	43.1	0.7	6.5
CR 211	BIT	27-90	1240.	0.0665	37.3	35.7	42.1	43.6	43.3	2.1	6.3
CR 216	BIT	27-90	1240.	0.0549	36.1	37.1	41.1	40.2	40.3	-1.3	4.1
CR 215	BIT	27-90	1240.	0.0259	34.9	37.5	48.5	46.3	46.7	-3.5	11.4
CR 212	BIT	27-90	1220.	0.0250	38.5	42.4	51.1	47.6	48.3	-5.7	9.2
CR 217	BIT	27-90	1230.	0.0224	36.1	40.4	46.0	42.0	42.7	-6.1	5.9
CR 213	BIT	27-90	1210.	0.0218	39.2	45.3	47.9	42.1	43.2	-9.1	2.8
*CR 249	BIT	27-90	1220.	0.0285	45.9	45.0	45.4	46.3	46.1	1.3	0.4
*CR 272	BIT	27-90	1220.	0.0246	44.2	54.7	55.5	45.1	47.4	-18.2	0.9
*CR 250	BIT	27-90	1220.	0.0213	48.2	58.8	57.0	48.2	50.6	-19.8	-2.2
*CR 275	BIT	27-90	1220.	0.0192	43.0	44.7	45.3	43.6	43.9	-2.5	0.6
*CR 276	BIT	27-90	1220.	0.0163	52.5	54.5	53.2	52.5	52.9	-3.5	-1.4
*CR 248	BIT	27-90	1220.	0.0146	41.6	47.5	50.4	44.7	45.8	-9.2	3.1
*CR 274	BIT	27-90	1220.	0.0115	42.5	40.9	43.0	44.5	44.2	2.2	2.0

(1) - (7) refer to Table C.1

RESULTS OF ULTIMATE ANALYSIS OF CHAR

Table E.1 and E.2 summarize the elemental compositions of the char samples obtained from different experiments. Weights of the chars (% of dry coal) were those measured experimentally. The details of each run can be found in Appendices B, C, and D. Table E.3 shows the results of the bituminous coal in laminar flow runs calculated from the estimated weight losses compensated for soot formation. The method for the compensation is discussed in section 4.1.2. In the main text, the values of the elemental composition of bituminous coal are based on table E.3. Figures E.1, E.2, and E.3 show retentions of the elements versus weight losses, and elemental ratios in volatile matter versus weight losses for the bituminous coal, using the apparent weight losses (table E.2). Corresponding figures based on the corrected weight losses (table E.3) are figures 4.23, 4.29, and 4.31 respectively.

TABLE E.1. RESULTS OF ULTIMATE ANALYSIS OF CHAR, MONTANA LIGNITE

RUN NO	COAL SIZE (MICRON)	TEMP (K)	TIME (MSEC)	WEIGHT (%)	C	H	N	S	O	ASH	
LF 181	LIG 27-67	1260.	0.115E 03	CHAR	87.4	57.2	3.2	0.9	1.4	15.6	9.0
				ATOMIC RATIO		1.00	0.67	0.01	0.01	0.20	
				RETENSION		0.90	0.56	1.09	1.43	0.77	0.99
				VOLATILE	12.6	6.1	2.5	-0.1	-0.5	4.6	0.1
				ATOMIC RATIO		1.00	4.94	-0.01	-0.03	0.56	
LF 182	LIG 27-67	1260.	0.135E 03	CHAR	82.0	55.4	3.1	0.9	1.5	12.5	8.7
				ATOMIC RATIO		1.00	0.67	0.01	0.01	0.17	
				RETENSION		0.87	0.54	1.09	1.53	0.62	0.97
				VOLATILE	18.0	7.9	2.6	-0.1	-0.5	7.6	0.3
				ATOMIC RATIO		1.00	3.94	-0.01	-0.02	0.72	
LF 186	LIG 27-67	1260.	0.205E 03	CHAR	77.4	53.3	2.7	0.9	1.2	10.2	9.2
				ATOMIC RATIO		1.00	0.60	0.01	0.01	0.14	
				RETENSION		0.84	0.47	1.03	1.21	0.51	1.02
				VOLATILE	22.6	10.1	3.0	-0.0	-0.2	9.9	-0.1
				ATOMIC RATIO		1.00	3.63	-0.00	-0.01	0.74	
LF 112	LIG 27-67	1510.	0.515E 02	CHAR	92.3	55.5	4.3	0.9	0.9	21.9	8.7
				ATOMIC RATIO		1.00	0.94	0.01	0.01	0.30	
				RETENSION		0.88	0.76	1.06	0.92	1.09	0.96
				VOLATILE	7.7	7.8	1.4	-0.0	0.1	-1.8	0.4
				ATOMIC RATIO		1.00	2.12	-0.01	0.00	-0.17	
LF 111	LIG 27-67	1510.	0.653E 02	CHAR	83.7	53.5	3.6	0.8	0.3	17.2	10.2
				ATOMIC RATIO		1.00	0.80	0.01	0.00	0.24	
				RETENSION		0.84	0.62	0.96	0.31	0.85	1.13
				VOLATILE	16.3	9.8	2.2	0.0	0.7	2.9	-1.2
				ATOMIC RATIO		1.00	2.65	0.00	0.03	0.23	

TABLE E.1. (continued)

RUN NO	COAL SIZE (MICRON)	TEMP (K)	TIME (MSEC)	WEIGHT (%)		C	H	N	S	O	ASH	
LF 105	LIG	27-67	1510.	0.762E 02	CHAR	73.7	48.4	2.6	0.8	0.4	12.5	10.2
					ATOMIC RATIO		1.00	0.65	0.01	0.00	0.19	
					RETENSION		0.76	0.46	0.96	0.45	0.62	1.13
					VOLATILE	26.3	14.9	3.1	0.0	0.5	7.6	-1.1
					ATOMIC RATIO	1.00	2.49	0.00	0.01	0.38		
LF 106	LIG	27-67	1510.	0.856E 02	CHAR	69.3	47.5	2.3	0.8	0.5	10.6	8.5
					ATOMIC RATIO		1.00	0.57	0.01	0.00	0.17	
					RETENSION		0.75	0.40	0.92	0.48	0.53	0.94
					VOLATILE	30.7	15.9	3.5	0.1	0.5	9.5	0.5
					ATOMIC RATIO	1.00	2.62	0.00	0.01	0.45		
LF 109	LIG	27-67	1510.	0.109E 03	CHAR	64.9	44.6	1.6	0.7	0.4	8.6	9.0
					ATOMIC RATIO		1.00	0.42	0.01	0.00	0.15	
					RETENSION		0.70	0.27	0.83	0.41	0.43	1.00
					VOLATILE	35.1	18.7	4.2	0.1	0.6	11.5	-0.0
					ATOMIC RATIO	1.00	2.67	0.01	0.01	0.46		
LF 145	LIG	27-67	1510.	0.285E 03	CHAR	64.5	48.7	1.4	0.8	0.4	4.2	9.1
					ATOMIC RATIO		1.00	0.34	0.01	0.00	0.06	
					RETENSION		0.77	0.24	0.92	0.38	0.21	1.01
					VOLATILE	35.5	14.6	4.3	0.1	0.6	16.0	-0.1
					ATOMIC RATIO	1.00	3.57	0.00	0.02	0.82		
LF 152	LIG	27-67	1740.	0.153E 02	CHAR	84.3	53.7	4.0	1.0	0.5	18.4	6.8
					ATOMIC RATIO		1.00	0.90	0.02	0.00	0.26	
					RETENSION		0.85	0.70	1.15	0.48	0.91	0.75
					VOLATILE	15.7	9.6	1.7	-0.1	0.5	1.7	2.3
					ATOMIC RATIO	1.00	2.12	-0.01	0.02	0.13		

TABLE E.1. (continued)

RUN NO	COAL SIZE (MICRON)	TEMP (K)	TIME (MSEC)		WEIGHT (%)	C	H	N	S	O	ASH	
LF 123	LIG	27-67	1740.	0.354E 02	CHAR	70.4	48.3	2.3	0.9	0.5	10.6	7.7
					ATOMIC RATIO		1.00	0.57	0.02	0.00	0.17	
					RETENSION		0.76	0.40	1.14	0.47	0.53	0.86
					VOLATILE	29.6	15.0	3.4	-0.1	0.5	9.5	1.3
					ATOMIC RATIO	1.00	2.75	-0.01	0.01	0.47		
LF 119	LIG	27-67	1740.	0.447E 02	CHAR	65.6	45.6	1.9	0.7	0.3	8.3	9.0
					ATOMIC RATIO		1.00	0.49	0.01	0.00	0.14	
					RETENSION		0.72	0.32	0.80	0.27	0.41	0.99
					VOLATILE	34.4	17.7	3.9	0.2	0.7	11.8	0.1
					ATOMIC RATIO	1.00	2.62	0.01	0.01	0.50		
LF 118	LIG	27-67	1740.	0.518E 02	CHAR	62.1	36.4	3.2	0.8	0.4	6.8	14.5
					ATOMIC RATIO		1.00	1.07	0.02	0.00	0.14	
					RETENSION		0.58	0.57	0.94	0.44	0.34	1.60
					VOLATILE	37.9	26.9	2.5	0.1	0.5	13.3	-5.4
					ATOMIC RATIO	1.00	1.11	0.00	0.01	0.37		
LF 114	LIG	27-67	1740.	0.773E 02	CHAR	58.2	40.6	1.5	0.6	0.4	8.6	6.5
					ATOMIC RATIO		1.00	0.44	0.01	0.00	0.16	
					RETENSION		0.64	0.26	0.76	0.41	0.43	0.72
					VOLATILE	41.8	22.7	4.2	0.2	0.6	11.5	2.5
					ATOMIC RATIO	1.00	2.23	0.01	0.01	0.38		
LF 166	LIG	27-67	1940.	0.168E 02	CHAR	77.0	52.2	3.1	0.9	0.5	12.9	7.4
					ATOMIC RATIO		1.00	0.72	0.01	0.00	0.19	
					RETENSION		0.82	0.55	1.06	0.51	0.64	0.82
					VOLATILE	23.0	11.1	2.6	-0.0	0.5	7.2	1.6
					ATOMIC RATIO	1.00	2.77	-0.00	0.02	0.49		

TABLE E.1. (continued)

RUN NO	COAL SIZE (MICRON)	TEMP (K)	TIME (MSEC)	WEIGHT (%)		C	H	N	S	O	ASH	
LF 298	LIG	27-67	2100.	0.301E 02	CHAR	42.4	28.8	0.1	0.4	0.2	6.0	6.9
					ATOMIC RATIO		1.00	0.05	0.01	0.00	0.16	
					RETENSION		0.46	0.02	0.44	0.17	0.30	0.76
					VOLATILE	57.6	34.5	5.6	0.5	0.8	14.1	2.2
					ATOMIC RATIO	1.00	1.95	0.01	0.01	0.31		
FF 900	LIG	27-67	1000.	0.100E 04	CHAR	77.2	51.4	2.6	0.8	0.5	13.1	8.9
					ATOMIC RATIO		1.00	0.60	0.01	0.00	0.19	
					RETENSION		0.81	0.45	0.92	0.55	0.65	0.98
					VOLATILE	22.8	12.0	3.2	0.1	0.4	7.1	0.1
					ATOMIC RATIO	1.00	3.17	0.00	0.01	0.44		
FF 957	LIG	27-67	1250.	0.100E 04	CHAR	63.6	46.9	1.7	0.7	0.4	5.2	8.7
					ATOMIC RATIO		1.00	0.42	0.01	0.00	0.08	
					RETENSION		0.74	0.29	0.85	0.39	0.26	0.96
					VOLATILE	36.4	16.4	4.1	0.1	0.6	14.9	0.3
					ATOMIC RATIO	1.00	2.98	0.01	0.01	0.68		
FF 930	LIG	27-67	1500.	0.100E 04	CHAR	62.8	45.6	1.3	0.7	0.4	0.6	14.2
					ATOMIC RATIO		1.00	0.35	0.01	0.00	0.01	
					RETENSION		0.72	0.23	0.80	0.37	0.03	1.57
					VOLATILE	37.2	17.7	4.4	0.2	0.6	19.5	-5.2
					ATOMIC RATIO	1.00	2.99	0.01	0.01	0.83		
FF 940	LIG	27-67	1750.	0.100E 04	CHAR	45.1	34.0	0.3	0.3	0.6	0.8	9.0
					ATOMIC RATIO		1.00	0.10	0.01	0.01	0.02	
					RETENSION		0.54	0.05	0.38	0.67	0.04	1.00
					VOLATILE	54.9	29.3	5.4	0.5	0.3	19.3	0.0
					ATOMIC RATIO	1.00	2.22	0.02	0.00	0.49		

TABLE E.1. (continued)

RIIN NO	COAL SIZE (MICRON)	TEMP (K)	TIME (MSEC)	WEIGHT (%)	C	H	N	S	O	ASH		
FF 515	LIG	27-67	1750.	0.600E 06	CHAR	41.9	36.0	0.0	0.2	0.8	0.0	6.1
					ATOMIC RATIO		1.00	0.01	0.01	0.01	0.00	
					RETENSION		0.57	0.00	0.27	0.78	0.00	0.67
					VOLATILE	58.1	27.3	5.7	0.6	0.2	20.1	3.0
				ATOMIC RATIO		1.00	2.50	0.02	0.00	0.55		
CR 305	LIG	27-67	610.	0.720E 07	CHAR	87.3	58.6	3.6	0.9	0.7	14.6	8.9
					ATOMIC RATIO		1.00	0.74	0.01	0.00	0.19	
					RETENSION		0.93	0.64	1.12	0.72	0.73	0.98
					VOLATILE	12.7	4.7	2.1	-0.1	0.3	5.5	0.2
				ATOMIC RATIO		1.00	5.28	-0.02	0.02	0.88		
CR 309	LIG	27-67	720.	0.540E 07	CHAR	76.6	53.2	2.6	0.9	1.5	9.7	8.8
					ATOMIC RATIO		1.00	0.59	0.01	0.01	0.14	
					RETENSION		0.84	0.46	1.07	1.53	0.48	0.97
					VOLATILE	23.4	10.1	3.1	-0.1	-0.5	10.5	0.3
				ATOMIC RATIO		1.00	3.70	-0.00	-0.02	0.78		
CR 264	LIG	27-67	740.	0.360E 07	CHAR	74.5	52.4	2.3	0.9	0.4	10.3	8.2
					ATOMIC RATIO		1.00	0.54	0.02	0.00	0.15	
					RETENSION		0.83	0.41	1.11	0.37	0.51	0.91
					VOLATILE	25.5	10.9	3.4	-0.1	0.6	9.9	0.8
				ATOMIC RATIO		1.00	3.70	-0.01	0.02	0.68		
PA 101	LIG	27-67	1220.	0.420E 06	CHAR	58.9	47.0	0.5	0.6	0.5	6.9	3.4
					ATOMIC RATIO		1.00	0.14	0.01	0.00	0.11	
					RETENSION		0.74	0.10	0.72	0.53	0.34	0.38
					VOLATILE	41.1	16.3	5.2	0.2	0.5	13.3	5.6
				ATOMIC RATIO		1.00	3.80	0.01	0.01	0.61		

TABLE E.1. (continued)

RUN NO	COAL SIZE (MICRON)	TEMP (K)	TIME (MSEC)	WEIGHT (%)		C	H	N	S	O	ASH	
CR 277	LIG	27-67	1220.	0.600E 06	CHAR	60.4	49.1	0.8	0.7	0.5	1.5	8.3
					ATOMIC RATIO		1.00	0.20	0.01	0.00	0.02	
					RETENSION		0.78	0.15	0.79	0.56	0.08	0.92
					VOLATILE		39.6	14.2	4.9	0.2	0.4	18.6
ATOMIC RATIO	1.00	4.13	0.01	0.01	0.98							
CR 284	LIG	27-67	1220.	0.600E 06	CHAR	60.4	49.1	0.7	0.6	0.6	1.7	7.7
					ATOMIC RATIO		1.00	0.18	0.01	0.00	0.03	
					RETENSION		0.78	0.13	0.74	0.60	0.08	0.85
					VOLATILE		39.6	14.2	5.0	0.2	0.4	18.4
ATOMIC RATIO	1.00	4.20	0.01	0.01	0.97							
CR 238	LIG	27-67	1580.	0.300E 06	CHAR	56.3	47.7	0.4	0.2	0.5	0.1	7.5
					ATOMIC RATIO		1.00	0.10	0.00	0.00	0.00	
					RETENSION		0.75	0.07	0.23	0.47	0.00	0.83
					VOLATILE		43.7	15.7	5.3	0.6	0.5	20.1
ATOMIC RATIO	1.00	4.07	0.03	0.01	0.96							
CR 122	LIG	27-67	1760.	0.300E 06	CHAR	55.3	49.1	0.0	0.1	0.5	0.0	7.3
					ATOMIC RATIO		1.00	0.01	0.00	0.00	0.00	
					RETENSION		0.78	0.01	0.08	0.55	0.00	0.81
					VOLATILE		44.7	14.2	5.7	0.8	0.4	20.1
ATOMIC RATIO	1.00	4.80	0.05	0.01	1.06							
CR 411	LIG	27-67	2250.	0.300E 06	CHAR	50.1	48.7	0.0	0.0	0.3	1.0	0.0
					ATOMIC RATIO		1.00	0.00	0.00	0.00	0.02	
					RETENSION		0.77	0.00	0.00	0.31	0.05	0.00
					VOLATILE		49.9	14.6	5.7	0.8	0.7	19.1
ATOMIC RATIO	1.00	4.71	0.05	0.02	0.99							

TABLE E.2. RESULTS OF ULTIMATE ANALYSIS OF CHAR, PITTSBURGH BITUMINOUS COAL
(BASED ON APPARENT WEIGHT LOSS)

RUN NO	COAL SIZE (MICRON)	TEMP (K)	TIME (MSEC)	WEIGHT (%)		C	H	N	S	O	ASH	
LF 196	BIT	27-90	1260.	0.936E 02	CHAR	88.9	63.7	4.0	1.3	3.7	4.8	9.9
					ATOMIC RATIO		1.00	0.75	0.02	0.02	0.06	
					RETENSION		0.92	0.78	1.20	0.74	0.55	0.91
					VOLATILE	11.1	5.7	1.1	-0.2	1.3	3.9	0.9
					ATOMIC RATIO		1.00	2.43	-0.03	0.08	0.51	
LF 194	BIT	27-90	1260.	0.135E 03	CHAR	65.0	45.5	2.6	0.9	3.6	3.0	9.3
					ATOMIC RATIO		1.00	0.67	0.02	0.03	0.05	
					RETENSION		0.66	0.50	0.87	0.74	0.34	0.86
					VOLATILE	35.0	23.8	2.6	0.1	1.3	5.8	1.5
					ATOMIC RATIO		1.00	1.30	0.00	0.02	0.18	
LF 191	BIT	27-90	1260.	0.189E 03	CHAR	74.4	52.4	2.5	1.0	2.9	4.4	11.1
					ATOMIC RATIO		1.00	0.58	0.02	0.02	0.06	
					RETENSION		0.76	0.49	0.91	0.59	0.50	1.03
					VOLATILE	25.6	17.0	2.6	0.1	2.0	4.3	-0.3
					ATOMIC RATIO		1.00	1.85	0.00	0.04	0.19	
LF 209	BIT	27-90	1510.	0.575E 02	CHAR	87.4	62.3	4.2	1.3	2.8	6.5	9.0
					ATOMIC RATIO		1.00	0.82	0.02	0.02	0.08	
					RETENSION		0.90	0.82	1.26	0.57	0.74	0.84
					VOLATILE	12.6	7.1	0.9	-0.3	2.1	2.3	1.8
					ATOMIC RATIO		1.00	1.54	-0.03	0.11	0.24	
LF 208	BIT	27-90	1510.	0.699E 02	CHAR	79.4	55.4	3.6	1.1	3.8	5.4	9.6
					ATOMIC RATIO		1.00	0.77	0.02	0.03	0.07	
					RETENSION		0.80	0.70	1.05	0.77	0.62	0.89
					VOLATILE	20.6	14.0	1.6	-0.1	1.2	3.3	1.2
					ATOMIC RATIO		1.00	1.35	-0.00	0.03	0.18	

TABLE E.2 (continued)

RUN NO	COAL SIZE (MICRON)	TEMP (K)	TIME (MSEC)	WEIGHT (%)		C	H	N	S	O	ASH	
LF 207	BIT	27-90	1510.	0.800E 02	CHAR	71.1	48.0	2.6	1.1	3.9	4.7	10.6
					ATOMIC RATIO		1.00	0.65	0.02	0.03	0.07	
					RETENSION		0.69	0.50	1.05	0.79	0.54	0.98
					VOLATILE		28.9	21.4	2.5	-0.1	1.0	4.0
ATOMIC RATIO	1.00	1.43	0.00	0.02	0.14							
LF 201	BIT	27-90	1510.	0.119E 03	CHAR	67.5	47.3	2.3	1.0	3.4	0.1	13.2
					ATOMIC RATIO		1.00	0.58	0.02	0.03	0.00	
					RETENSION		0.68	0.45	0.98	0.69	0.01	1.23
					VOLATILE		32.5	22.1	2.8	0.0	1.5	8.6
ATOMIC RATIO	1.00	1.55	0.00	0.03	0.29							
LF 274	BIT	27-90	1740.	0.240E 02	CHAR	72.1	49.9	2.8	1.0	3.1	3.8	11.5
					ATOMIC RATIO		1.00	0.67	0.02	0.02	0.06	
					RETENSION		0.72	0.54	0.97	0.63	0.43	1.07
					VOLATILE		27.9	19.5	2.4	0.0	1.8	5.0
ATOMIC RATIO	1.00	1.46	0.00	0.04	0.19							
LF 273	BIT	27-90	1740.	0.303E 02	CHAR	64.8	44.2	1.7	1.0	3.1	3.2	11.7
					ATOMIC RATIO		1.00	0.45	0.02	0.03	0.05	
					RETENSION		0.64	0.32	0.91	0.63	0.37	1.08
					VOLATILE		35.2	25.2	3.5	0.1	1.8	5.5
ATOMIC RATIO	1.00	1.66	0.00	0.03	0.16							
LF 282	BIT	27-90	1740.	0.547E 02	CHAR	59.5	42.1	0.8	0.9	2.3	1.2	12.2
					ATOMIC RATIO		1.00	0.24	0.02	0.02	0.02	
					RETENSION		0.61	0.16	0.81	0.47	0.14	1.13
					VOLATILE		40.5	27.3	4.3	0.2	2.6	7.5
ATOMIC RATIO	1.00	1.90	0.01	0.04	0.21							

TABLE E.2. (continued)

RUN NO	COAL SIZE (MICRON)	TEMP (K)	TIME (MSEC)	WEIGHT (%)	C	H	N	S	O	ASH		
LF 286	BIT	27-90	2100.	0.215E 02	CHAR	42.7	28.4	0.0	0.4	0.5	0.0	13.3
					ATOMIC RATIO		1.00	0.00	0.01	0.01	0.00	
					RETENSION		0.41	0.00	0.39	0.10	0.00	1.24
					VOLATILE	57.3	40.9	5.1	0.7	4.4	8.7	-2.6
				ATOMIC RATIO		1.00	1.51	0.01	0.04	0.16		
FF 950	BIT	27-90	1000.	0.100E 04	CHAR	74.9	51.2	2.9	0.8	3.1	6.8	10.0
					ATOMIC RATIO		1.00	0.69	0.01	0.02	0.10	
					RETENSION		0.74	0.57	0.77	0.64	0.78	0.92
					VOLATILE	25.1	18.2	2.2	0.2	1.8	1.9	0.8
				ATOMIC RATIO		1.00	1.46	0.01	0.04	0.08		
FF 958	BIT	27-90	1250.	0.100E 04	CHAR	72.6	52.2	2.5	1.0	3.0	2.9	11.0
					ATOMIC RATIO		1.00	0.58	0.02	0.02	0.04	
					RETENSION		0.75	0.49	0.89	0.62	0.33	1.02
					VOLATILE	27.4	17.2	2.6	0.1	1.9	5.9	-0.2
				ATOMIC RATIO		1.00	1.82	0.01	0.04	0.26		
FF 910	BIT	27-90	1500.	0.100E 04	CHAR	60.8	45.5	1.0	0.6	2.0	2.4	9.2
					ATOMIC RATIO		1.00	0.27	0.01	0.02	0.04	
					RETENSION		0.66	0.20	0.56	0.40	0.28	0.86
					VOLATILE	39.2	23.8	4.1	0.5	3.0	6.3	1.5
				ATOMIC RATIO		1.00	2.08	0.02	0.05	0.20		
FF 920	BIT	27-90	1750.	0.100E 04	CHAR	60.8	46.6	0.7	0.6	1.9	0.4	10.3
					ATOMIC RATIO		1.00	0.19	0.01	0.02	0.01	
					RETENSION		0.67	0.15	0.52	0.39	0.05	0.96
					VOLATILE	39.2	22.8	4.4	0.5	3.0	8.3	0.5
				ATOMIC RATIO		1.00	2.32	0.02	0.05	0.27		

TABLE E.2. (continued)

RUN NO	COAL SIZE (MICRON)	TEMP (K)	TIME (MSEC)	WEIGHT (%)	C	H	N	S	O	ASH		
FF 806	BIT	27-90	1830.	0.100E 04	CHAR	70.4	55.6	0.3	0.5	2.8	0.4	10.7
					ATOMIC RATIO		1.00	0.06	0.01	0.02	0.01	
					RETENSION		0.80	0.05	0.51	0.58	0.05	0.99
					VOLATILE	29.6	13.7	4.9	0.5	2.1	8.3	0.1
					ATOMIC RATIO		1.00	4.27	0.03	0.06	0.45	
FF 806	BIT	27-90	1830.	0.100E 04	CHAR	70.4	61.1	0.2	0.6	2.8	0.1	5.6
					ATOMIC RATIO		1.00	0.04	0.01	0.02	0.00	
					RETENSION		0.88	0.04	0.53	0.56	0.01	0.52
					VOLATILE	29.6	8.2	4.9	0.5	2.2	8.6	5.2
					ATOMIC RATIO		1.00	7.21	0.05	0.10	0.79	
FF 512	BIT	27-90	1500.	0.600E 06	CHAR	54.5	42.3	0.0	0.4	2.1	0.0	10.1
					ATOMIC RATIO		1.00	0.00	0.01	0.02	0.00	
					RETENSION		0.61	0.00	0.41	0.42	0.00	0.93
					VOLATILE	45.5	27.0	5.1	0.6	2.9	8.7	0.7
					ATOMIC RATIO		1.00	2.28	0.02	0.04	0.24	
CR 304	BIT	27-90	610.	0.456E 08	CHAR	90.5	66.3	3.9	1.2	4.5	4.0	10.6
					ATOMIC RATIO		1.00	0.71	0.02	0.03	0.05	
					RETENSION		0.96	0.76	1.11	0.92	0.46	0.98
					VOLATILE	9.5	3.1	1.2	0.1	0.4	4.7	0.2
					ATOMIC RATIO		1.00	4.80	0.03	0.05	1.15	
CR 307	BIT	27-90	740.	0.720E 08	CHAR	75.0	54.3	2.4	1.0	3.1	3.7	10.5
					ATOMIC RATIO		1.00	0.53	0.02	0.02	0.05	
					RETENSION		0.78	0.46	0.96	0.63	0.42	0.97
					VOLATILE	25.0	15.1	2.8	0.0	1.8	5.0	0.3
					ATOMIC RATIO		1.00	2.20	0.00	0.05	0.25	

TABLE E.2. (continued)

RUN NO	COAL SIZE (MICRON)	TEMP (K)	TIME (MSEC)		WEIGHT (%)	C	H	N	S	O	ASH	
CP 124	RIT	27-90	1760.	0.300E 06	CHAR	57.5	48.9	0.0	0.1	1.1	0.0	8.9
					ATOMIC RATIO		1.00	0.00	0.00	0.01	0.00	
					RETENSION		0.71	0.00	0.11	0.22	0.00	0.82
					VOLATILE	42.5	20.4	5.1	0.9	3.9	8.7	1.9
					ATOMIC RATIO		1.00	3.01	0.04	0.07	0.32	
CP 413	BIT	27-90	2250.	0.300E 06	CHAR	52.1	48.3	0.3	0.0	1.0	0.0	2.6
					ATOMIC RATIO		1.00	0.06	0.00	0.01	0.00	
					RETENSION		0.70	0.05	0.00	0.19	0.00	0.24
					VOLATILE	47.9	21.0	4.9	1.1	4.0	8.7	8.2
					ATOMIC RATIO		1.00	2.79	0.04	0.07	0.31	

TABLE E.3. RESULTS OF ULTIMATE ANALYSIS, PITTSBURGH BITUMINOUS COAL
(BASED ON WEIGHT LOSS CORRECTED FOR SOOT)

RUN NO	COAL SIZE (MICRON)	TEMP (K)	TIME (MSEC)	WEIGHT (%)	C	H	N	S	O	ASH		
LF 196	BIT	27-90	1260.	0.936E 02	CHAR	85.5	61.2	3.8	1.2	3.5	4.7	9.5
					ATOMIC RATIO		1.00	0.75	0.02	0.02	0.06	
					RETENSION		0.88	0.75	1.15	0.71	0.53	0.88
					VOLATILE	14.5	8.1	1.3	-0.2	1.4	4.1	1.3
					ATOMIC RATIO		1.00	1.92	-0.02	0.07	0.38	
LF 194	BIT	27-90	1260.	0.135E 03	CHAR	76.0	53.2	3.0	1.1	4.2	3.5	10.8
					ATOMIC RATIO		1.00	0.67	0.02	0.03	0.05	
					RETENSION		0.77	0.58	1.02	0.86	0.40	1.01
					VOLATILE	24.0	16.1	2.2	-0.0	0.7	5.3	-0.1
					ATOMIC RATIO		1.00	1.60	-0.00	0.02	0.24	
LF 191	BIT	27-90	1260.	0.189E 03	CHAR	58.6	41.2	2.0	0.8	2.3	3.5	8.8
					ATOMIC RATIO		1.00	0.58	0.02	0.02	0.06	
					RETENSION		0.59	0.39	0.72	0.47	0.40	0.81
					VOLATILE	41.4	28.1	3.2	0.3	2.6	5.3	2.0
					ATOMIC RATIO		1.00	1.35	0.01	0.04	0.14	
LF 209	BIT	27-90	1510.	0.575E 02	CHAR	77.5	55.2	3.8	1.2	2.5	5.7	8.0
					ATOMIC RATIO		1.00	0.82	0.02	0.02	0.08	
					RETENSION		0.80	0.73	1.12	0.50	0.66	0.74
					VOLATILE	22.5	14.1	1.4	-0.1	2.5	3.0	2.8
					ATOMIC RATIO		1.00	1.18	-0.01	0.07	0.16	
LF 208	BIT	27-90	1510.	0.699E 02	CHAR	69.0	48.1	3.1	1.0	3.3	4.7	8.3
					ATOMIC RATIO		1.00	0.77	0.02	0.03	0.07	
					RETENSION		0.69	0.60	0.92	0.67	0.54	0.77
					VOLATILE	31.0	21.2	2.0	0.1	1.6	4.0	2.5
					ATOMIC RATIO		1.00	1.15	0.00	0.03	0.14	

327

TABLE E.3. (continued)

RUN NO	COAL SIZE (MICRON)	TEMP (K)	TIME (MSEC)	WEIGHT (%)		C	H	N	S	O	ASH
LF 263	BIT 27-90	1940.	0.150E 02	CHAR	67.0	48.1	2.9	1.0	2.0	0.0	13.0
				ATOMIC RATIO		1.00	0.72	0.02	0.02	0.00	
				RETENSION		0.69	0.56	0.93	0.41	0.00	1.21
				VOLATILE	33.0	21.3	2.2	0.1	2.9	8.7	-2.2
				ATOMIC RATIO		1.00	1.27	0.00	0.05	0.31	
LF 267	BIT 27-90	1940.	0.179E 02	CHAR	49.0	34.7	2.0	0.6	1.2	0.0	11.8
				ATOMIC RATIO		1.00	0.70	0.02	0.01	0.00	
				RETENSION		0.50	0.39	0.58	0.25	0.00	1.10
				VOLATILE	51.0	34.7	3.1	0.5	3.7	8.7	-1.0
				ATOMIC RATIO		1.00	1.08	0.01	0.04	0.19	
LF 260	BIT 27-90	1940.	0.320E 02	CHAR	33.0	23.7	0.6	0.4	1.4	0.0	7.8
				ATOMIC RATIO		1.00	0.31	0.01	0.02	0.00	
				RETENSION		0.34	0.12	0.35	0.28	0.00	0.72
				VOLATILE	67.0	45.6	4.5	0.7	3.6	8.7	3.0
				ATOMIC RATIO		1.00	1.19	0.01	0.03	0.14	
LF 293	BIT 27-90	2100.	0.720E 01	CHAR	55.0	40.6	2.4	0.7	1.9	0.0	10.3
				ATOMIC RATIO		1.00	0.70	0.02	0.02	0.00	
				RETENSION		0.59	0.46	0.67	0.39	0.00	0.96
				VOLATILE	45.0	28.7	2.8	0.4	3.0	8.7	0.5
				ATOMIC RATIO		1.00	1.15	0.01	0.04	0.23	
LF 291	BIT 27-90	2100.	0.104E 02	CHAR	41.0	29.9	0.9	0.5	1.8	0.0	8.6
				ATOMIC RATIO		1.00	0.37	0.01	0.02	0.00	
				RETENSION		0.43	0.18	0.43	0.36	0.00	0.79
				VOLATILE	59.0	39.4	4.2	0.6	3.2	8.7	2.2
				ATOMIC RATIO		1.00	1.29	0.01	0.03	0.17	

TABLE E.3. (continued)

RUN NO	COAL SIZE (MICRON)	TEMP (K)	TIME (MSEC)	WEIGHT (%)	C	H	N	S	O	ASH	
LF 286	RIT 27-90	2100.	0.215E 02	CHAR	26.0	17.3	0.0	0.3	0.3	0.0	8.1
				ATOMIC RATIO	1.00	0.00	0.01	0.01	0.00		
				RETENSION	0.25	0.00	0.24	0.06	0.00	0.75	
				VOLATILE	74.0	52.0	5.1	0.8	4.6	8.7	2.7
				ATOMIC RATIO	1.00	1.18	0.01	0.03	0.13		

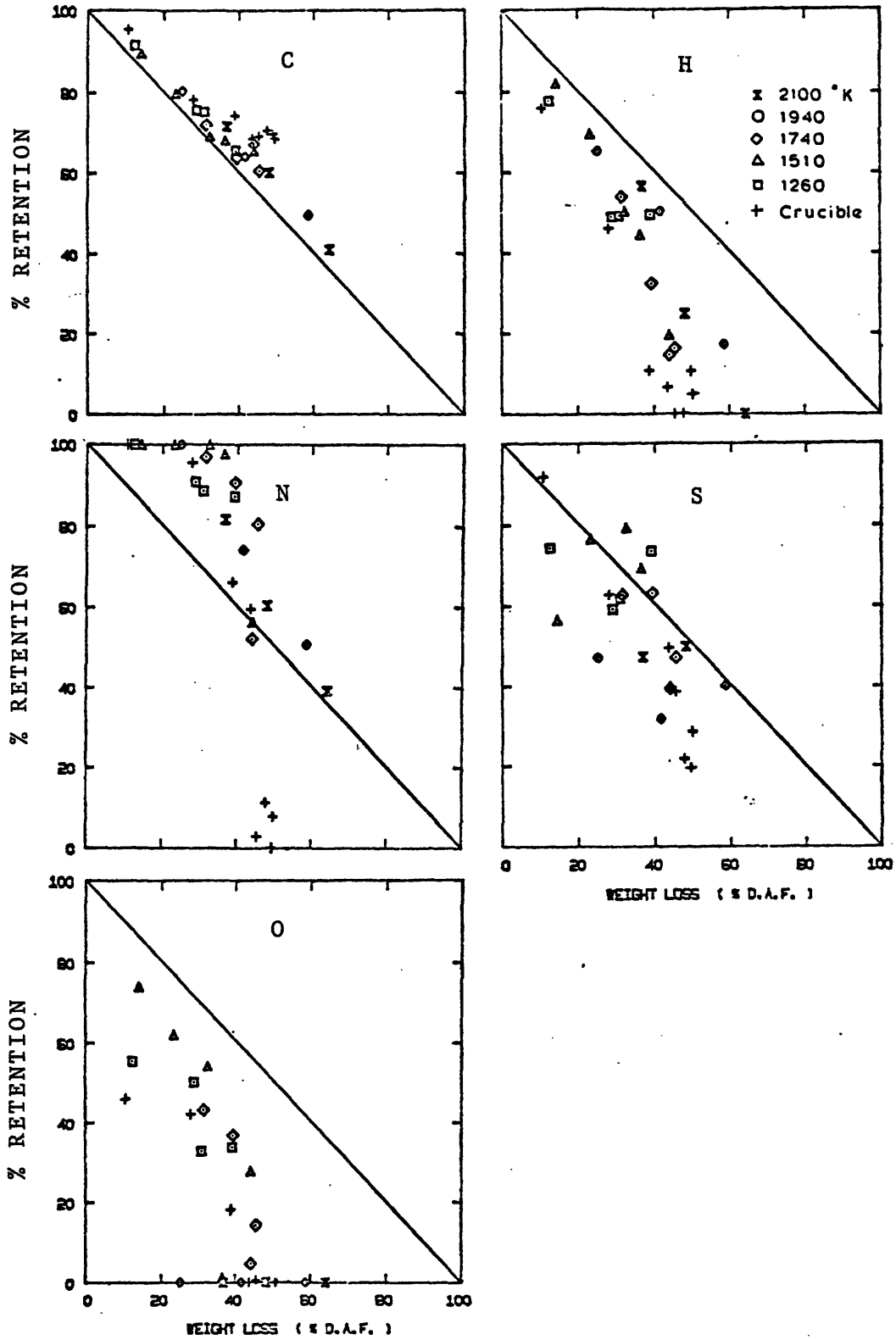


FIGURE E.1. ELEMENTS RETAINED IN CHAR AT DIFFERENT WEIGHT LOSSES
PITTSBURGH SEAM BITUMINOUS COAL
(APPARENT WEIGHT LOSS)

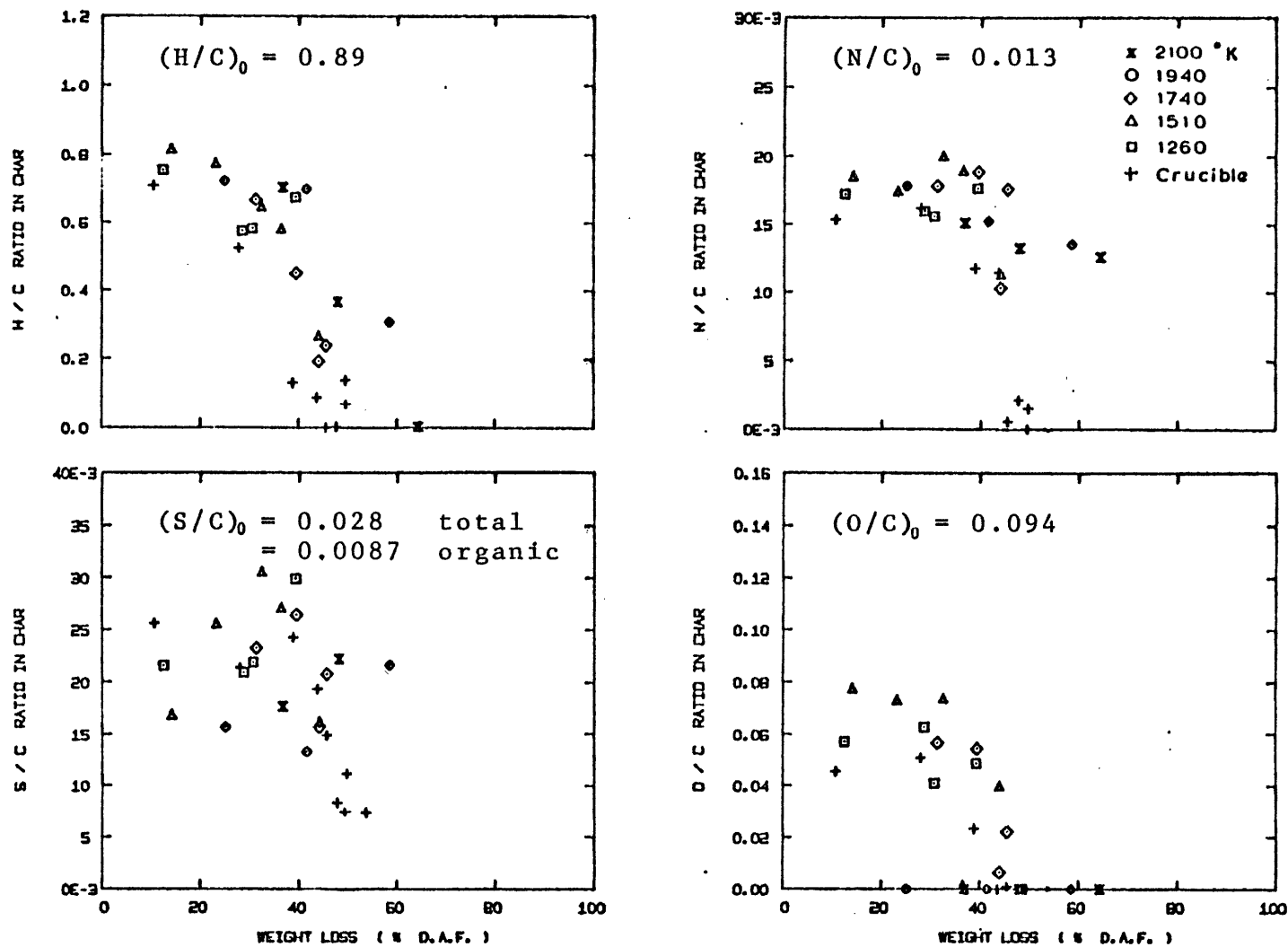


FIGURE E.2 CHANGES IN ELEMENTAL RATIOS IN CHAR WITH WEIGHT LOSS, PITTSBURGH SEAM BITUMINOUS COAL (APPARENT WEIGHT LOSS)

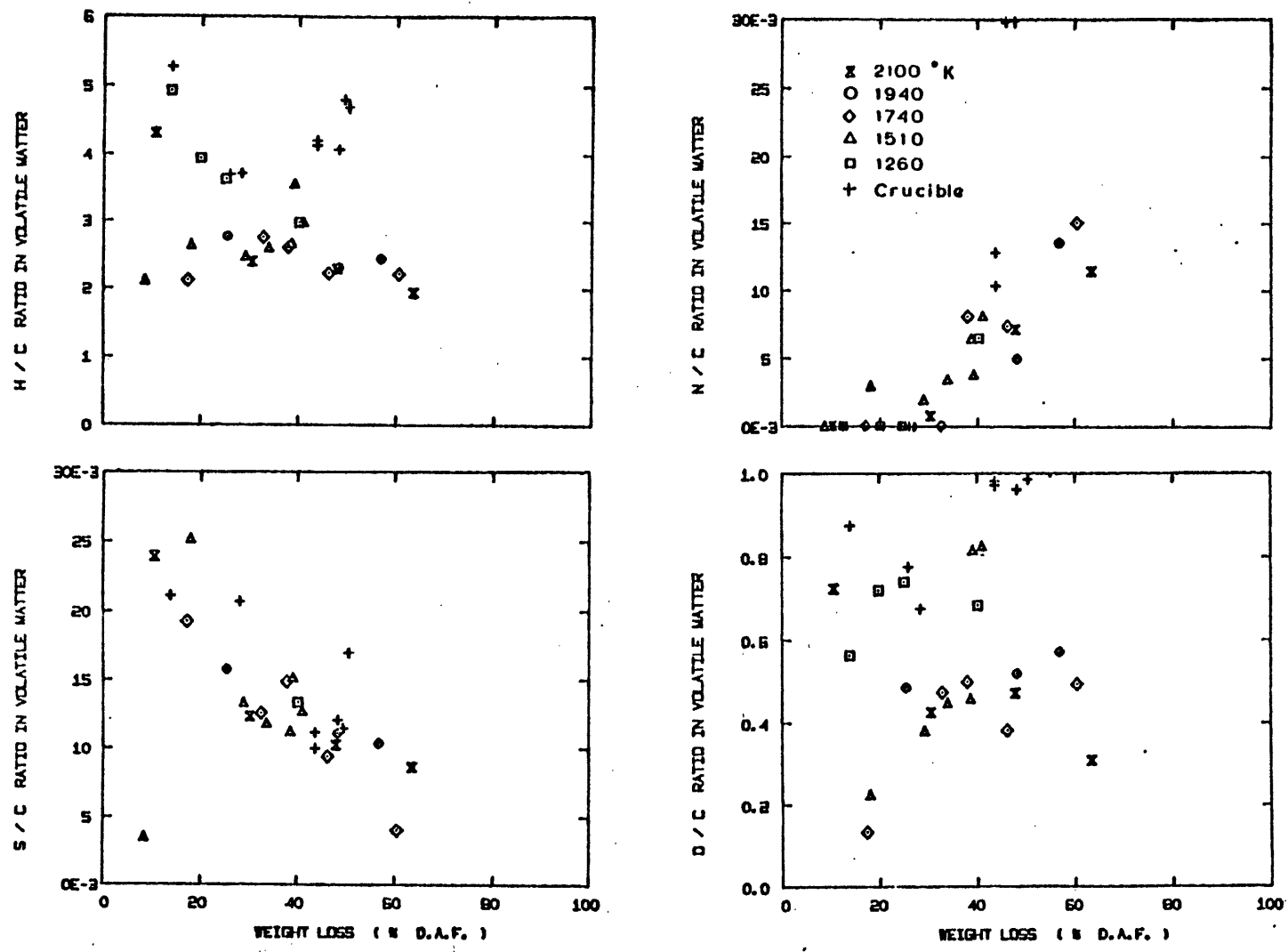


FIGURE E.3 CHANGES IN ELEMENTAL RATIOS IN VOLATILE MATTER WITH WEIGHT LOSS PITTSBURGH SEAM BITUMINOUS COAL (APPARENT WEIGHT LOSS)

APPENDIX F

PARTICLE VELOCITIES MEASURED BY A LASER DOPPLER ANEMOMETER

Table F.1 summarizes the particle velocities measured by the laser doppler anemometer (Chapter 3) under different conditions. Each particle velocity listed in the table is the average of 50 to 200 particle velocities which were sampled randomly for a time span of several minutes. Most of the velocity distributions were close to the Normal distributions. Main gas velocities and carrier gas velocities are the average velocities evaluated at the furnace temperatures.

TABLE F.1 PARTICLE VELOCITIES MEASURED BY LASER DOPPLER ANEMOMETER

RUN NO	COAL SIZE (MICRON)	TEMP	MAIN VELOCITY (M/SEC)	CARRIER VELOCITY (M/SEC)	DISTANCE (CM)	PARTICLE VELOCITY (M/SEC)	STANDARD DEVIATION (M/SEC)
PV 1	LIG 38-45	1500.	2.87	0.24	5.08	2.237	0.682
PV 2	LIG 38-45	1550.	4.96	0.77	5.08	2.855	0.269
PV 3	ALM 75-90	1500.	0.00	0.03	5.08	0.156	0.071
PV 4	LIG 38-45	1500.	0.00	0.03	5.08	0.126	0.067
PV 5	LIG 38-45	1500.	0.00	0.24	5.08	0.129	0.036
PV 6	LIG 38-45	1500.	0.00	0.03	5.08	0.156	0.072
PV 7	LIG 38-45	1500.	0.69	0.24	5.08	0.906	0.047
PV 8	LIG 38-45	1500.	0.04	0.03	5.08	0.219	0.101
PV 9	LIG 75-90	1500.	0.04	0.03	5.08	0.216	0.049
PV 10	LIG 75-90	1500.	0.09	0.03	5.08	0.357	0.045
PV 11	LIG 75-90	1500.	0.09	0.03	5.08	0.266	0.050
PV 12	LIG 75-90	1500.	0.20	0.04	5.08	0.701	0.080
PV 13	LIG 38-45	1500.	0.20	0.03	5.08	0.458	0.073
PV 14	LIG 38-45	1500.	0.20	0.11	5.08	0.485	0.068
PV 15	LIG 38-45	1500.	0.20	0.37	5.08	0.526	0.073
PV 16	LIG 38-45	1500.	0.09	0.03	5.08	0.399	0.140
PV 17	ALM 75-90	1500.	0.04	0.03	5.08	0.580	0.062
PV 18	ALM 75-90	1500.	0.09	0.03	5.08	0.696	0.103
PV 19	LIG 75-90	1500.	2.87	0.24	5.08	2.055	0.085
PV 20	LIG 75-90	1500.	2.87	0.72	5.08	1.846	0.062
PV 21	LIG 38-45	1500.	2.87	0.24	5.08	1.873	0.095
PV 22	LIG 38-45	1500.	2.87	0.24	2.54	1.251	0.080
PV 23	LIG 38-45	1500.	2.87	0.72	2.54	1.258	0.046
PV 24	LIG 38-45	1500.	2.87	1.49	2.54	1.690	0.080
PV 25	LIG 38-45	1500.	2.87	0.24	1.27	0.692	0.052

TABLE F.1 PARTICLE VELOCITIES MEASURED BY LASER DOPPLER ANEMOMETER (cont'd)

RUN NO	CELL	SIZE	TEMP	MAIN VELOCITY (M/SEC)	CARRIER VELOCITY (M/SEC)	DISTANCE (CM)	PARTICLE VELOCITY (M/SEC)	STANDARD DEVIATION (M/SEC)
	(NOTION)							
PV 26	LIG	32-45	1200.	2.87	0.72	1.27	0.944	0.064
PV 27	LIG	32-45	1200.	2.87	0.24	0.63	0.347	0.028
PV 28	LIG	32-45	1200.	2.87	0.72	0.63	0.688	0.162
PV 29	LIG	32-45	1200.	0.04	0.03	0.63	0.273	0.085
PV 30	LIG	32-45	1200.	0.04	0.11	0.63	0.308	0.061
PV 31	LIG	32-45	1200.	0.04	0.03	1.27	0.265	0.085
PV 32	LIG	32-45	1200.	0.04	0.11	1.27	0.370	0.116
PV 33	LIG	32-45	1200.	0.04	0.37	1.27	0.421	0.050
PV 34	LIG	32-45	1200.	0.04	0.03	2.54	0.291	0.068
PV 35	LIG	32-45	1200.	0.04	0.11	2.54	0.331	0.064
PV 36	LIG	32-45	1200.	0.04	0.37	2.54	0.360	0.068
PV 37	LIG	32-45	1200.	0.04	0.03	5.08	0.178	0.063
PV 38	LIG	32-45	1200.	0.04	0.11	5.08	0.161	0.044
PV 39	LIG	32-45	1200.	0.04	0.37	5.08	0.366	0.091
PV 40	LIG	32-45	1200.	0.04	0.03	7.62	0.171	0.053
PV 41	LIG	32-45	1200.	0.04	0.11	7.62	0.178	0.036
PV 42	LIG	32-45	1200.	0.04	0.37	7.62	0.238	0.039
PV 43	LIG	32-45	1250.	0.80	0.21	7.62	1.064	0.168
PV 44	LIG	32-45	1250.	0.80	0.21	5.08	0.876	0.190
PV 45	LIG	32-45	1250.	0.80	0.21	2.54	0.659	0.109
PV 46	LIG	32-45	1250.	0.80	0.21	0.63	0.310	0.057
PV 47	LIG	32-45	1250.	0.80	0.21	1.27	0.571	0.072
PV 48	LIG	32-45	1250.	0.80	0.21	0.33	0.166	0.049
PV 49	LIG	32-45	1250.	0.80	0.21	0.00	0.319	0.133
PV 50	LIG	32-45	1250.	0.80	0.52	0.00	0.280	0.167

TABLE F.1 PARTICLE VELOCITIES MEASURED BY LASER DOPPLER ANEMOMETER (cont'd)

RUN NO	COAL SIZE (MICRON)	TEMP	MAIN VELOCITY (M/SEC)	CARRIER VELOCITY (M/SEC)	DISTANCE (CM)	PARTICLE VELOCITY (M/SEC)	STANDARD DEVIATION (M/SEC)
PV 51	L10 38-45	1550.	0.80	0.31	0.00	0.512	0.265
PV 52	L10 38-45	1550.	0.80	0.16	0.00	0.240	0.151
PV 53	L10 38-45	1550.	0.80	0.03	0.00	0.223	0.128
PV 54	L10 38-45	1550.	0.80	0.15	0.00	0.289	0.107
PV 55	L10 38-45	1550.	0.80	0.21	0.00	0.359	0.101
PV 56	L10 38-45	1550.	0.80	0.31	0.00	0.528	0.230
PV 57	L10 38-45	1550.	0.80	0.52	0.00	0.797	0.260
PV 58	L10 38-45	1550.	0.80	0.95	0.00	1.392	0.282
PV 59	L10 38-45	1550.	0.80	0.03	5.08	0.178	0.075
PV 60	L10 38-45	1550.	0.84	0.03	5.08	0.175	0.089
PV 61	L10 38-45	1550.	4.96	0.52	0.00	0.565	0.151
PV 62	L10 38-45	1550.	4.96	0.52	0.63	0.645	0.059
PV 63	L10 38-45	1550.	4.96	0.52	1.27	0.983	0.041
PV 64	L10 38-45	1550.	4.96	0.52	2.54	1.782	0.098
PV 65	L10 38-45	1550.	4.96	0.52	5.08	3.103	0.130
PV 66	L10 38-45	1550.	4.96	0.52	7.62	0.211	0.202
PV 67	L10 38-45	1550.	4.96	0.52	5.08	3.080	0.120
PV 68	L10 38-45	1550.	4.96	0.52	5.08	3.095	0.209
PV 69	L10 38-45	1560.	0.84	0.03	5.08	0.208	0.022
PV 70	L10 38-45	1560.	0.84	0.11	5.08	0.231	0.023
PV 71	L10 38-45	1560.	0.84	0.03	2.54	0.251	0.030
PV 72	L10 38-45	1560.	0.84	0.11	2.54	0.277	0.027
PV 73	L10 38-45	1560.	0.84	0.03	1.27	0.382	0.054
PV 74	L10 38-45	1560.	0.84	0.11	1.27	0.407	0.023
PV 75	L10 38-45	1560.	0.84	0.37	1.27	0.481	0.035

APPENDIX G

PHYSICAL CHANGES OF COAL DURING DEVOLATILIZATION

Coal undergoes considerable physical changes upon heating. Of the two coals used in this study, the Pittsburgh Seam bituminous coal is a highly swelling coking coal and hence marked changes in size occurred during the rapid heating conditions. Montana lignite showed little change in size. Some of the preliminary results of changes in size for the bituminous coal are described below, based on studies with a scanning electron microscope (SEM). The average particle size, \bar{x} , and the standard deviation, σ , are obtained by counting different size particles in SEM photographs using a Zeiss semi-automatic particle size analyzer.

Figure G.1 shows developments of bubbles in the early stage of devolatilization. Softening of coal coupled with internal evolution of volatile matter is considered to be responsible for the bubbles. Formation of many bubbles from a single particle is apparent from the last picture in the figure. The weight loss at this stage is less than 10 percent (d.a.f.)* and particle sizes are close to the original size.

Figure G.2 shows swelling and void development with the progress of devolatilization at 1500°K. Open pores become apparent after about 15 percent of the coal weight is lost, and the swelling appears to be completed at about 23 percent weight loss. A large number of open pores for a single particle indicates that the swelling behavior is not similar to the expansion of a hollow sphere followed by ejections of volatile matter from a few holes. Since the asymptotic weight loss at the

* Weight losses shown in the figure are apparent values and some particle losses (less than 5 percent) are included in the values.

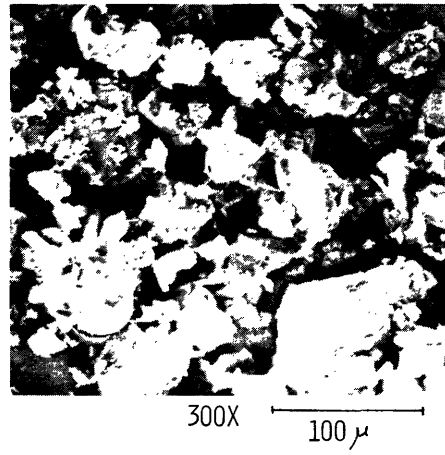
temperature is about 56 percent, about 60 percent of the volatile matter is evolved after the particles reach the maximum size. In the last picture many broken particles are seen, but it is not clear whether the broken particles were produced physically when char samples were removed from the bronze filter by a spatula, by evolution of volatile matter, or by rapid quenching with the water jets.

Figure G.3 shows a close-up of a char particle which was almost completely devolatilized in the free fall experiment with an alumina collector at 1250°K (estimated weight loss about 58 percent). The surface shows clear evidence that the particle has experienced a plastic stage during the devolatilization. The picture at the bottom right shows a close-up of one of the holes. The inside wall appears to be similar to the outside wall.

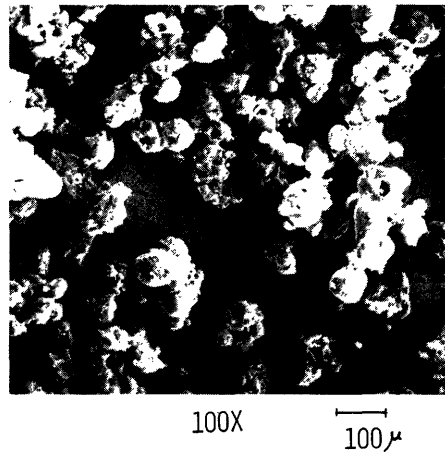
Figure G.4 shows a photomicrograph of polished sections of the chars for both bituminous coal and lignite. The hollow structure of bituminous char and porous structure of lignite can be seen.

Figure G.5 shows chars from the alumina collector at four different temperatures. At 1000°C most of the particles are close to spherical and each particle has a relatively small number of holes. Irregularity of the shape of the particles and the number of holes appeared to increase with the increases in temperature. Each char particle in the picture does not necessarily correspond to a single coal particle. Coagulation of several particles is evident in some of the pictures, and close-up pictures of those particles are shown in Fig. G.6.

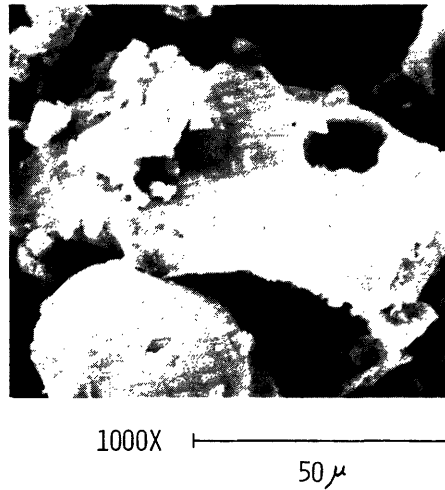
BUBBLE DEVELOPMENT, PITTSBURGH SEAM #8 BITUMINOUS COAL



$T = 1000^{\circ}\text{K}$
 $t = 155 \text{ ms}$
 $WL = 7\% \text{ D.A.F.}$
 $\bar{X} = 48.7 \mu\text{M}$
 $\sigma = 20.3 \mu\text{M}$



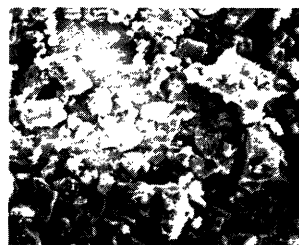
$T = 1000^{\circ}\text{K}$
 $t = 244 \text{ ms}$
 $WL = 9\% \text{ D.A.F.}$
 $\bar{X} = 113.4 \mu\text{M}$
 $\sigma = 44.7 \mu\text{M}$



$T = 1250^{\circ}\text{K}$
 $t = 69.2 \text{ ms}$
 $WL = 10.9\% \text{ D.A.F.}$
 $\bar{X} = 70.5 \mu\text{M}$
 $\sigma = 29.4 \mu\text{M}$

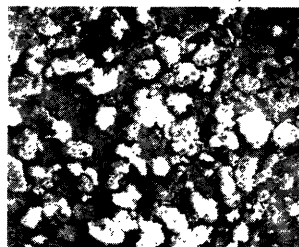
FIG. G.1

VOID DEVELOPMENT WITH TIME
 PITTSBURGH SEAM #8 BITUMINOUS COAL
 FURNACE TEMPERATURE 1500°K



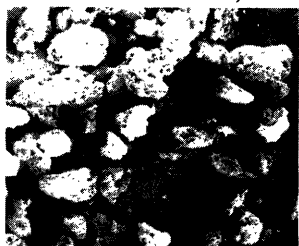
300X μ

$t = 38$ ms
 WL = 7.1% D.A.F.
 $\bar{X} = 46.6 \mu\text{M}$
 $\sigma = 17.8 \mu\text{M}$



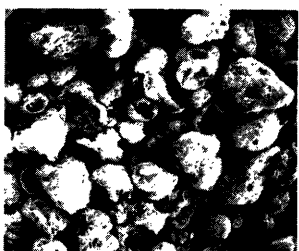
30X μ

$t = 51$ ms
 WL = 14.2% D.A.F.
 $\bar{X} = 276.9 \mu\text{M}$
 $\sigma = 53 \mu\text{M}$



30X

$t = 63$ ms
 WL = 23.2 D.A.F.
 $\bar{X} = 457.2 \mu\text{M}$
 $\sigma = 153.8 \mu$



30X

$t = 81$ ms
 WL = 33.7 D.A.F.
 $\bar{X} = 404.0 \mu\text{M}$
 $\sigma = 114.6 \mu\text{M}$

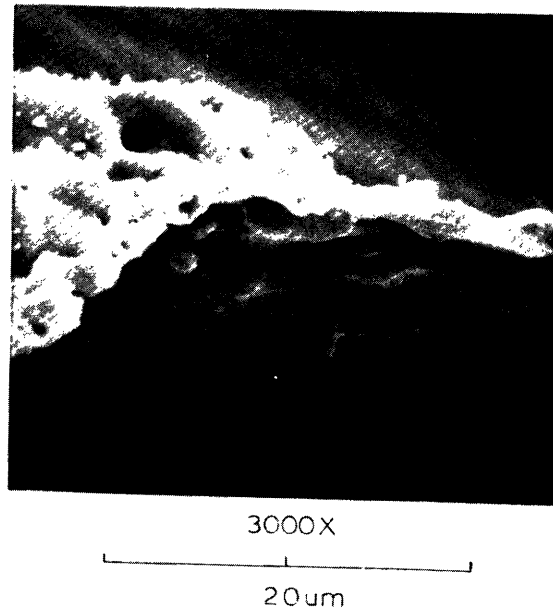
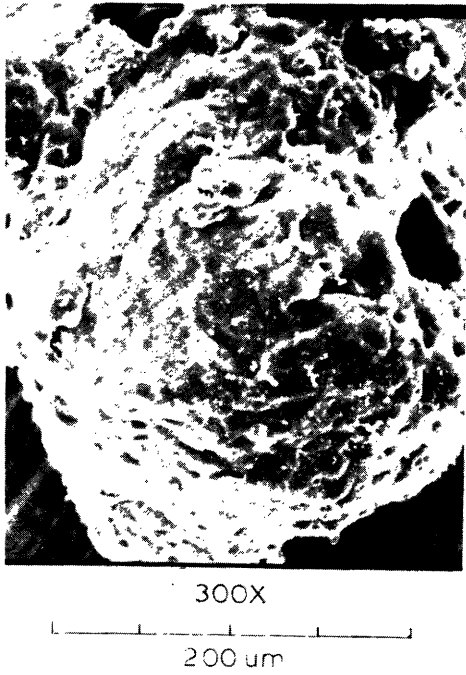
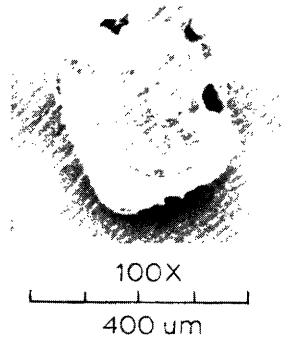


30X

$t = 113$ ms
 WL = 36.6% D.A.F.
 $\bar{X} = 253.9 \mu\text{M}$
 $\sigma = 75.3 \mu\text{M}$

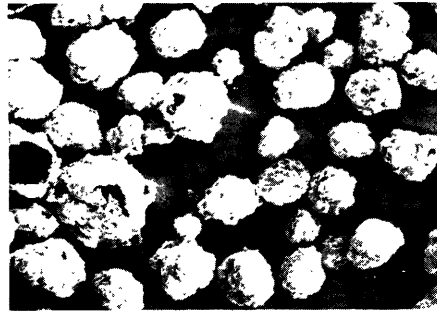
FIG. G.2

DEVOLATILIZED BITUMINOUS COAL 1250 K

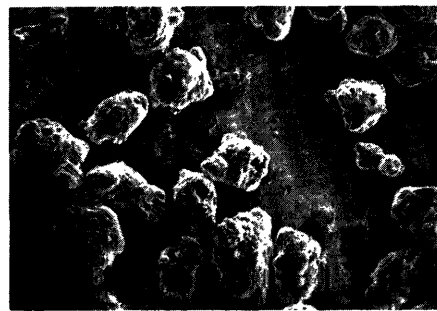


Electronmicrographs of a devolatilized bituminous coal particle

VOID DEVELOPMENT WITH TEMPERATURE
 PITTSBURGH SEAM #8 BITUMINOUS COAL, FREE FALL TO CUP (ASYMPTOTIC)

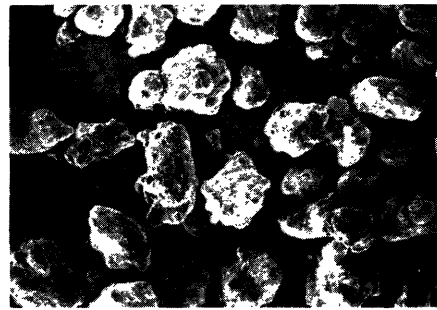


$T = 1000^{\circ}\text{K}$
 $WL = 53.1 \text{ D.A.F.}$
 $\bar{X} = 521.2 \mu\text{M}$
 $\sigma = 173.3 \mu\text{M}$

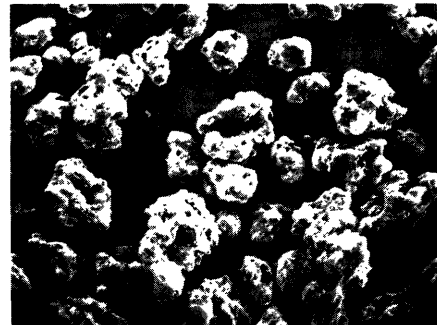


$T = 1250^{\circ}\text{K}$
 $WL = 54.2 \text{ D.A.F.}$
 $\bar{X} = 523.6 \mu\text{M}$
 $\sigma = 108.4 \mu\text{M}$

30X 100 μ



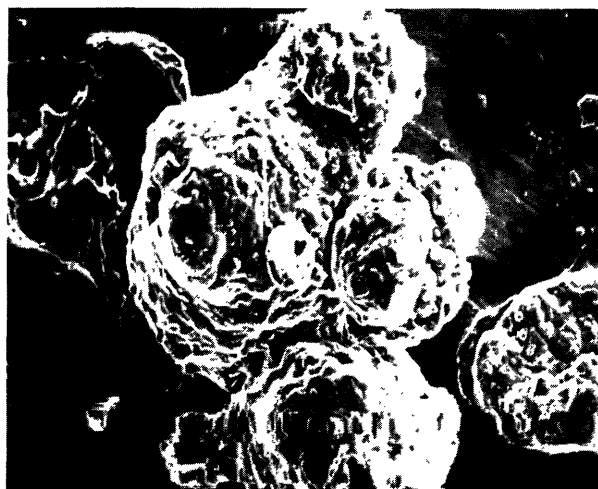
$T = 1500^{\circ}\text{K}$
 $WL = 59.0 \text{ D.A.F.}$
 $\bar{X} = 489.5 \mu\text{M}$
 $\sigma = 138.6 \mu\text{M}$



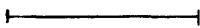
$T = 1750^{\circ}\text{K}$
 $WL = 63.0 \text{ D.A.F.}$
 $\bar{X} = 566.7 \mu\text{M}$
 $\sigma = 145.3 \mu\text{M}$

FIG. G.5

AGGLOMERATION, PITTSBURGH SEAM #8 BITUMINOUS COAL



$T = 1250^{\circ}\text{K}$
 $WL = 54.2 \text{ D.A.F.}$
 $\bar{X} = 523.6 \mu\text{M}$
 $\sigma = 108.4 \mu\text{M}$

100X 
300 μ



$T = 1500^{\circ}\text{K}$
 $WL = 59.0 \text{ D.A.F.}$
 $\bar{X} = 489.5 \mu\text{M}$
 $\sigma = 138.6 \mu\text{M}$

FIG. G.6

APPENDIX H

ENHANCED VOLATILE YIELD UNDER RAPID HEATING CONDITIONS

Tables H.1 to H.10 summarize enhanced volatile yields reported by different researchers. Symbols used in the tables are defined as follows.

$$R = \frac{\Delta W}{V_o} \quad (\text{H.1})$$

$$f'_E = \frac{\Delta W + V_R(1 - \Delta W)}{V_o} \quad (\text{H.2})$$

$$Q = \frac{\Delta W}{V_o(1 - D)} \quad (\text{H.3})$$

$$D = \frac{V_R(1 - \Delta W)}{V_o} \quad (\text{H.4})$$

where

ΔW = weight loss by devolatilization (d.a.f.)

V_o = proximate volatile matter of coal (d.a.f.)

V_R = proximate volatile matter of char

D = fraction of original volatile matter remaining in char (d.a.f.)

Interpretations of the enhancement factors, R , f'_E and Q are discussed in section 1.2.1.

TABLE H.1 WEIGHT LOSS OF VARIOUS COALS IN A LAMINAR FLOW FURNACE
Badzioch and Hawksley (1970)

Coal ⁽¹⁾ Rank	Particle ⁽²⁾ Size (μ)	VM (%d.a.f.)	ΔW	D ⁽³⁾	Q	R	f' _E
902	20	37.9		0.14	1.32	1.32	1.27
	40	42.0		0.14	1.30	1.12	1.28
	60	40.6		0.14	1.36	1.17	1.31
902	20	36.4		0.14	1.28	1.10	1.24
802	22	37.8		0.14	1.31	1.13	1.27
802	27	36.1		0.14	1.51	1.30	1.44
602	26	34.3		0.08	1.66	1.53	1.61
601	22	35.3		0.11	1.68	1.50	1.61
401	25	34.4		0.10	1.43	1.29	1.39
301 b	25	25.2		0.13	1.72	1.50	1.63
301 a	18	22.7		0.17	1.72	1.43	1.60
	62	23.4		0.17	1.58	1.31	1.48
203	27	17.7		0.22	1.83	1.42	1.64

(1) NCB coal rank code number

(2) Median diameter

(3) Fraction of original volatile matter remaining in char (d.a.f.)
evaluated at 950°C from the reported empirical equation.

Atmosphere: Nitrogen
Furnace temperature: up to 1270°K
Residence time: 30 to 110 msec
Heating rate: 25,000-50,000 °K/sec

TABLE H.2 WEIGHT LOSS OF COALS AT DIFFERENT TEMPERATURES
IN A LAMINAR FLOW FURNACE
Kimber and Gray (1967-a, 1967-b)

Coal Rank	Particle Size (μ) ⁽²⁾	Reactor Temp. ($^{\circ}$ K)	Reaction Time (msec)	Δ W (%d.a.f.)	D	Q	R	f'_E
902	30	1050	70	12	.76	1.30	0.31	1.07
	30		100	39			1.02	
	30	1370	75	48	.21	1.55	1.24	1.46
	30		110	48			1.24	
	53	1620	75	45			1.12	
	30		18	50			1.31	
	53	1720	18	40			1.00	
	30		55	60			.10	1.75
	53	1920	15	65			1.62	
	30		45	71			.5	1.95
	30 [†]	2170	90	72			1.87	
	53		45	69			.2	1.75
	802	22	1770 [*]				1.6 [*]	
102	24	2370 [*]	25	10~14		~2.0 [*]		

[†] Char recycled

^{*} Read from Fig. 3 (Kimber and Gray, 1967-b)

(1) NCB coal rank code number

(2) Median diameter

Rank	Size (μ)	VM (%d.a.f.)
902	30	38.3
	53	40.0
802	22	
102	24	7.5

Atmosphere: Argon

Heating rate: $10^5 - 10^6$ $^{\circ}$ K/sec

TABLE H.3 WEIGHT LOSS OF AN ELKOL COAL IN A TRANSPORT REACTOR
Eddinger, et al. (1966)

Run No.	Furnace Temp. (°K)	ΔW^* (%d.a.f.)	V_R^{**} (%d.a.f.)	D	Q	R	f'_E
88	1370	52.4	16.3	.19	1.51	1.22	1.41
97	1570	46.9	5.9	.08	1.19	1.10	1.17
80	1370	45.0	21.5	.28	1.45	1.05	1.33
81	1370	42.0	23.0	.32	1.44	.98	1.30

Proximate volatile matter of coal: 42.8% d.a.f.

Particle size: 100- x 200-mesh cut (75-150 micron)

Atmosphere: Helium

Estimated gas and particle temperature:

900 ~ 1060°K (furnace temp. 1370°K)

1030 ~ 1250°K (furnace temp. 1570°K)

Residence time: 10 - 40 msec

Heating rate: Larger than 2500°K/sec

Run No's 88, 97: Reactor tube length 8 in.

Run No's 80, 81: Reactor tube length 4 in., gas preheated to 720°K

* Weight loss not corrected for vapor-cracked carbon
(5 - 16 wt% reported for similar cases)

** Proximate volatile matter of char.

TABLE H.4 WEIGHT LOSS OF A HIGH-VOLATILE A BITUMINOUS COAL
IN AN ARGON PLASMA
Graves, et al. (1966)

Run No.	Average* Plasma Temp. (°K)	ΔW (%d.a.f.)	V_R (%d.a.f.)	D	Q	R	f'_E
38	5100	26.4	17.4	.47	1.10	.71	1.06
41	7600	37.1**	10.2	.27	1.21	1.00	1.18
40	9100	54.7**	12.3	.33	1.73	1.47	1.62

Proximate volatile matter of coal: 37.2% d.a.f.

Particle size: -325 mesh (-45 micron)

Atmosphere: Argon

* Coal particle temperature is much lower than average plasma temperature

** Possible loss of fine particles through filter indicated.

TABLE H.5 WEIGHT LOSS OF VARIOUS COALS IN A HYDROGEN PLASMA
Stickler, et al. (1974)

Coal	VM (%)	ΔW %	V %R	D	Q	R	f'_E
Williams	41.4	71.7	16.3	.39	1.96	1.73	1.84
Corbin	38.8	62.0	11.8	.30	1.81	1.60	1.71
Seacoal	38.0	62.6	14.0	.37	1.91	1.64	1.79
Pitts Seam	37.7	65.0	11.2	.30	1.92	1.72	1.83
River King	37.7	56.6	15.4	.41	1.82	1.50	1.68
Old Ben	37.4	49.5	17.3	.46	1.73	1.32	1.56
Robena	36.2	58.5	21.0	.58	2.13	1.62	1.86
Power Mine	32.7	43.8	23.1	.71	2.22	1.34	1.74

Atmosphere: Hydrogen

TABLE H.6 WEIGHT LOSS OF A HIGH-VOLATILE B UTAH COAL
 IN AN ENTRAINED FLOW REACTOR
 WITH HYDROGEN-OXIGEN COMBUSTION GASES
 Coates, et al. (1974)

Run No.	Reactor Temp. (°K)	ΔW^* (%d.a.f.)	D	Q	R	f'_E
5-8-4	1058	31.4				0.80
5-8-2	1227	59.8				1.54
5-8-1	1341	62.5				1.60
6-9-4	1347	64.4				1.65
7-31-1	1454	62.2				1.60
8-23-1	1318	56.6				1.45

Proximate volatile matter of coal: 39.0% d.a.f.

Particle size: -200 mesh (-75 micron)

Residence time: 10 to 300 msec

Atmosphere: Hydrogen-oxygen combustion gases

* Weight loss calculated using ash as a tracer

TABLE H.7 WEIGHT LOSS OF VARIOUS COALS BY PULSE-HEATING
IN A WIRE-SCREEN HEATING ELEMENT
Mentser, et al. (1974)

Coal Rank	Temp. (°K)	VM (%d.a.f.)	ΔW (%d.a.f.)	D	Q	R	$f \frac{R}{E}$
lvb	1170	16.9	18.7			1.10	
	1420*		21.0*			1.25	
mvb	1020	25.5	31.1			1.22	
	1370*		36.0*			1.42	
hvAb	970	35.7	48.8			1.36	
	1420*		43.0*			1.23	
hvcb	1070	48.4	56.4			1.16	
	1420*		47.0*			.98	
Sub A	1170	37.9	42.6			1.13	
	1420*		55.0*			1.46	

Particle size: 44-53 micron

Heating rate: 8250°K/sec

Atmosphere: Vacuum (10^{-3} torr)

Reaction time: 65 to 155 msec pulse time plus cooling time

* Numbers from Figs. 1 and 2, Mentser et al. (1974)

TABLE H.8 WEIGHT LOSS BY AN ELECTRICALLY HEATED WIRE SCREEN
 UNDER VARIOUS ATMOSPHERES
 Anthony (1974)

Coal Rank	VM (%d.a.f.)	Pressure (atm)	Atmosphere	ΔW	D	Q	R	f'_E
hvAb	46.2	10^{-3}	Helium	61			1.32	
		1		56			1.21	
		69		42			.91	
		1	Hydrogen	56			1.21	
		10		57			1.23	
		69		67			1.45	
Lignite	46.2	10^{-3}	Helium	42			.91	
		1		42			.91	
		69		42			.91	
		1	Hydrogen	42			.91	
		13		48			1.04	
		69		63			1.36	

Maximum temperature: About 1300°K

Heating rates: Up to 10^4 °K/sec

Reaction time: Up to 20 sec

Particle size: 53-83 micron

TABLE H.9 WEIGHT LOSS OF VARIOUS COALS BY MICROSAMPLE STRIP FURNACE
Rau and Robertson (1966)

Coal	Rank	VM (%dry)	ΔW^* (%dry)	D	Q	R	f'_E
Elkel	Sub B	40.7	45-51			1.10-1.25	
Federal	hvAb	37.7	45-50			1.19-1.33	
Kopperston	hvAb	31.6	22-42			.70-1.33	
Colver	m vb	25.3	13-26			.51-1.03	
Orient	hvBb	44.0	40-45			.90-1.02	

Temperatures: 1200-1500°K

Heating rate: About 400-600°K/sec

Coal size: 1-2 mg piece

* From Figs. 3 to 7, Rau and Robertson (1966)

TABLE H.10 WEIGHT LOSS OF VARIOUS COAL IN AN ELECTRICALLY HEATED
WIRE SCREEN
Loison and Chauvin (1964)

Coal	VM (%d.a.f.)	ΔW (%d.a.f.)	D	Q	R	f'_E
Maigre Oignies	10.0	10.0			1.00	
Bergmannsglück	21.0	25.3			1.30	
Emma	22.6	27.1			1.25	
Lens-Levin	29.2	31.9			1.09	
Flenus de Bruay	32.9	41.6			1.18	
Wendel III	36.7	37.4			1.02	
Faulquemont	38.6	38.9			1.01	

Maximum temperature: 1320°K

Particle size: 50-80 micron

Heating rate: 1500°K/sec

Reaction time: Heating time plus about 4 sec for cooling

Atmosphere: Nitrogen

COAL CHARACTERIZATION

(prepared by J. H. Pohl, 1976)

Coals differ widely depending on geological age, geographical location, geological conditions. Major differences may be found in coal composition even between different positions in a particular coal seam. Classifications developed to differentiate between different coals have been based on rank, physical appearance, elemental analysis and functional group analysis.

Rank is a gross measure of properties such as heat of combustion, carbon content, agglomerating and agglutinating tendencies of coals with definitions differing between countries. The classification accepted in the U.S.A. is summarized in Table I-1.

Different petrographic constituents in coal have different optical properties and form a basis for a classification based on reflectivity (Tschemler and de Ruiter, 1963). In order of increasing reflectances, the major constituents are exinite, vitrinite, micronite and fusinite.

Because of ease of utilization, rank, sometimes supplemented by elemental analysis, has been the classification adopted by industry for providing a measure of those properties that determine the end use of coal. Research workers have been seeking a more fundamental measure of coal behaviour and limited success has been achieved using petrographic analysis. Functional form analysis provides a more fundamental measure of coal structure but its use is qualified by the difficulty of the measurements, which usually require solvation of the coal with possible

TABLE I-1ASTM COAL RANK

ASTM - D388-19 (1973)

Percent Fixed Carbon on Dry Mineral Matter Free Basis

	<u>>98 Meta-Anthracite</u>	
	<u>92-98 Anthracite</u>	
	<u>86-92 Semi-Anthracite</u>	
Percent F.C. ---	-----	Non-Agglomerating
		Agglomerating
	<u>78-86 Low Volatile Bituminous</u>	
	<u>69-78 Medium Volatile Bituminous</u>	
	<u><69 High Volatile or Subbituminous</u>	

High Volatile or Subbituminous

Heating Value on Moist Mineral Matter Free Basis

	<u>>14K H-V-A-Bituminous</u>	
	<u>13-14K H-V-B-Bituminous</u>	
	<u>10.5-13K H-V-C-Bituminous</u>	Either Non-
Heating Value	-----	Agglomerating or
(BTU/lb) ---		Non Weathering
	<u>10.5-11.5K Subbituminous A</u>	Weathering and
	<u>9.5-10.5K Subbituminous B</u>	Agglomerating
	<u>8.3-9.5K Subbituminous C</u>	
	<u>6.3-8.3K Lignite A</u>	
	<u><6.3K Lignite B</u>	

modification of the coal structure.

It is the long-range objective of fundamental coal studies to correlate the behaviour of coals with a classification scheme, preferably simple. For the current study, a lignite and a bituminous coal, which differ widely in many properties, have been selected. The characterization of these, incomplete because of time and financial constraints, is given below.

I-1.0 Montana Lignite

The Montana lignite was chosen as an example of certain low rank, low sulfur, non-caking western coal which could be strip mined. These coals are likely to find future use as raw material for gasifiers and possibly as fuel for local power generation. The reserves of lignites in the United States represent approximately 6×10^4 quadrillion BTU; or almost 30% of the ultimate United States Coal reserves.

I-1.1 Visual Appearance of Montana Lignite

Scanning electron micrographs of the Montana lignite used in these studies are shown in figure 2:9 . The lignite has been ground and classified to nominally 38-43 microns. The low magnification micrograph shows many small particles have escaped mechanical size classification and a few large, irregularly shaped particles are also present in the supposed narrowly-sized fraction. The micrographs at higher magnification show the particle surface is relatively smooth, has few visible macropores, and has ash particles on the order of several microns

physically held on the surface.

The photomicrographs of polished sections under oil immersion are shown in figure 2.10. The micrographs show that the coal particles are not uniform in internal macropore area or in reflectance. Four different levels of reflectance have been identified in the polished section slides. Most particles appeared to be composed of only one petrographic element although occasionally one particle will contain as many as three different elements.

The top micrograph in figure 2.10 shows three particles of different reflectances. The whitish particle on the right side of the micrograph is tentatively identified as micronite; the highly reflective fusinite particles are very rare in lignites and are not evident in the samples; the dull, barely visible particle just to the left of the micronite particle has been identified as exinite; and the particle below and to the left of the exinite particle has been identified as vitrinite. The top micrograph shows some macropore structure in the vitrinite and exinite, but most of the macropore structure is in the medium reflective micronite. The macropores appear either in micronite in the form of circular voids as large as ten microns in diameter or as dendritic like structures with stem diameters on the order of several microns. Fewer pores are visible in vitrinite and exinite; these pores are either irregular shaped voids on the order of 5-10 microns in diameter, or relatively straight fissures, about one micron in diameter.

I-1.2 Size Distribution

The Montana lignite was received as $\frac{1}{8}$ inch particles. These particles were ground in a ball mill and separated through roto-taped Tyler screens. Most of this study was conducted with the 38-43 micron size range, although some data were taken using the 74-88 micron size range. These two size ranges were chosen as being representative of coal fed to a pulverized coal flame.

The electron micrograph in figure 2.9 shows that the closely sized fraction had a number of undersized particles and a few oversized particles, shown more quantitatively by the particle size distribution in figures 2.13 and 2.14. The cumulative mass distribution was fitted with the Rosin-Rammler (1939) distribution function, as for example in figure 2.13. Scanning electron micrographs of lignite particles were counted on a Zeiss particle counter and Rosin-Rammler parameters were developed using a least square fit of the particle frequency. The mean particle diameter derived from the Rosin-Rammler distribution was 52.3 microns. The Rosin-Rammler derived curve is compared in figure 2.14 with the original data. The original data gave a mean particle size distribution of 47.6 microns and a standard deviation of 15.2 microns. The fit of the data is considered satisfactory, in spite of the differences in calculated and measured frequency at large particle diameters, because the size interval is small and relatively few oversized particles are present.

I-1.3 Surface Area

Numerous measurements of surface areas of raw coal and processed coals have been reported. Spencer and Bond (1966), however, have questioned the use of adsorption isotherms to derive absolute surface areas of microporous solids. Van Krevelen (1961) showed that the areas determined by conventional adsorption methods at liquid nitrogen temperatures are two orders of magnitude lower than values derived from adsorption at room temperature or values derived from methanol heat of wetting data. The diffusion process appears to have an activation energy of about 4 kcal/g-mole. The activated diffusion process accounts for the low values of surface area obtained at low temperature, because the adsorbate cannot penetrate completely into the microstructure of coal in a reasonable period of time at low temperatures.

Marsh (1965) has reviewed the various methods of determining surface area and concluded that adsorption of CO₂ near room temperature gives the most reasonable values for surface areas of coal and cokes. Typical surface areas for coals with less than 85% carbon (dmmf) are in the range of 200 m²/g. Adsorption of inert gases at 77⁰K gives values on the order of 2 m²/g. Adsorption of krypton at 77⁰K for the lignite used in this study gave a surface area of 2 m²/g when analyzed using the Dubinin-Polanyi equation and 1.2 m²/g when analyzed using the BET equation. These values are not representative of the total surface area but are considered to be representative of that fraction.

of the surface area contained in pores with diameters greater than about 12 Å. (See Van Krevelen, Marsh, Gan, et al., 1972, and Tingey and Morrey, 1973.)

Surface areas from CO₂ adsorption at room temperature are not yet available for the coals used in this study. The surface area might be expected to be about 183 m²/g as measured by Nsakala et al. (1975) for a North Dakota lignite with a daf carbon content of 71%. This value is slightly lower but in reasonable agreement with the surface areas found by Gan et al. (1972) of 225-308 m²/g for North American lignites containing between 63 and 72% carbon. Swann et al. report a value the CO₂ adsorption area of Australian Yallourn brown coal of 290 m²/g comparable to that of American lignites.

The integrated particle size distribution curve yields a superficial surface area of 0.11 m²/g. This value is 20 times smaller than the krypton adsorption area and 2000 times smaller than the normal CO₂ areas for lignites.

I-1.4 Proximate Analysis

Proximate analysis - moisture, volatile matter and ash content - were performed at three independent laboratories with similar results. The proximate analysis is reported in Table 2.3 along with other information for the two coals used in this study. The volatile matter was approximately 36.2%, the equilibrium moisture content was close to 13.6%, and the ash was 7.8% on an as received basis. The lignite was treated as a sparking coal.

I-1.5 Heat of Combustion

Rank classification of coal, below 69% daf carbon content, is based on the heating value and the agglomerating and agglutinating properties of the coal. The heating value is the high heating value of the coal (water as a liquid) on moist mineral free basis. The mineral matter is usually calculated based on the ash and sulfur content of the coal by empirical equations, most frequently the Parr formula, but is best obtained by use of low-temperature ashing.

The heat of combustion was measured on a dry sample of the Montana lignite and corrected to a moist mineral free basis using the mineral matter determined by low temperature ashing and either the equilibrium moisture content or the moisture content found by Paulson et al (1972), for samples from the same mine. The heating values are in reasonable agreement with heating values previously calculated using the Dulong formula. The measured heating value is reported in Table 2.3 as 8809 BTU/lb with equilibrium moisture content and 7346 BTU/lb with mine moisture; the latter value classifies the coal used in this study as lignite-A.

I-1.6 Elemental Analysis

Ultimate analysis of the coals used in this study were performed at the Galbraith Laboratories, Inc., Knoxville, Tennessee and are reported in Table 2.3 on an as received basis and in Table 2.4 on several common bases. Sulfur form

analysis is also reported in Table 2.3.

The Montana lignite contained 73.3% carbon on a dry mineral matter free basis, 0.83% nitrogen and 0.98% sulfur on a dry basis. Approximately 65% of the sulfur is organic sulfur. Oxygen was determined by difference so is not considered very accurate. Oxygen is determined by subtracting ash and all other elements from 100%. This procedure can lead to rather substantial errors in the oxygen concentration because mineral matter changes weight when sulfides and carbonates react during ashing. The procedure gives 22% too high an oxygen concentration for the Montana lignite.

I-1.7 Ash Analysis

The mineral elements of ash (Table I-2) were determined by atomic absorption of the metallic elements, reported as if the elements are in their natural oxidation state.

The principal components of mineral matter in coals are SiO_2 and Al_2O_3 associated with. The ash from a Montana lignite contained 27% silica and 16% alumina. The ash also had high concentrations of calcium (28% as CaO), magnesium (9% as MgO), and a large amount of sulfur (13.5% as SO_3). Iron and phosphorus are the only other significant elements; Fe_2O_3 accounts for 3.4% of the ash and P_2O_5 accounts for 1%. Titanium, potassium, and sodium are the remaining major elements in the lignite ash.

TABLE I-2ASH CHARACTERIZATION *

Wt. % on ignited basis	Montana Lignite-A	Pittsburgh Seam #8 High Volatile Bituminous-A
Ash Air	7.84	10.55
P ₂ O ₅	1.02	0.30
SiO ₂	26.80	37.52
Fe ₂ O ₃	3.41	29.34
Al ₂ O ₃	16.41	19.15
TiO ₂	0.50	0.57
CaO	28.44	4.65
MgO	9.02	0.73
SO ₃	13.45	4.10
K ₂ O	0.35	1.29
Na ₂ O	0.27	0.38

* Analysis by Galbraith Laboratories, Inc., Knoxville, Tennessee and Padia (1976).

I-1.8 Functional Group Analysis

No functional group analysis was performed on the coals used in this study, nor has a functional group analysis of the lignite used in this study been found in the literature. Tingey and Morrey have compiled average functional group analysis for various rank coals from literature values. Values for the functional group composition for a lignite of 70.6% carbon will be used for comparison purposes until direct measurements become available.

Tingey and Morrey's functional group distribution is shown in Table I-3. A lignite can be expected to have an average ring size of about 2-4, 27% of the carbon will be aliphatic carbon and 65% of the hydrogen will be attached to aliphatic carbons. About half of the carbon in such small ring systems is peripheral carbon. The aliphatic hydrogen is mostly attached to aliphatic carbon that is attached either to α or β position to an aromatic ring; hydroxyl hydrogen accounts for only about 5% of the hydrogen.

Oxygen concentration and distribution are not included in the functional group summary presented by Tingey and Morrey. Oxygen concentrations can be estimated by difference, after allowance for a concentration of nitrogen and sulfur of about 2%. The oxygen concentration obtained by difference is about 20%, which is a high but reasonable value for an American lignite. Hydroxyl oxygen may then account for a third of the oxygen present with most of the remaining oxygen present as carbonyl oxygen. These results are consistent with generalized analysis reported by Dryden (1963).

TABLE I-3FUNCTIONAL GROUP ANALYSIS OF A LIGNITE

From Tingey and Morrey (1973)
and Dryden (1963)

	Hydrogen Distribution % of total H	Carbon Distribution % of total C	Oxygen Distribution % of total O
Total daf	4.74	70.6	~22.
Average Ring Sizes	-	2-4	-
Aromatic	30.7	73.2	-
Monoring	16.4	27.6	-
Condensed Ring	14.3	45.6	-
Peripheral C	-	51.7	-
Interior C	-	21.5	-
Aliphatic	64.7	26.8	-
Methylene Bridges	14.0	5.63	-
α CH _x	25.7	12.0	-
β CH _x	23.7	9.2	-
Hydroxyl	4.6	-	~36.
Carbonyl	-	-	~45.
Carboxyl	-	-	~19.

I-2.0 Pittsburgh Seam #8 Bituminous Coal

The Pittsburgh bituminous coal was chosen as an example of highly swelling and caking eastern coals used in coking operations or in utility boilers. United States reserves of bituminous coal represent about 46% of total coal reserves or approximately 9.6×10^4 quadrillion BTUs.

I-2.1 Visual Appearance of Pittsburgh Bituminous Coal

The bituminous coal was ground and classified in the same manner as the lignite. Scanning electron micrographs of the classified bituminous coal are shown in figure 2.11. The electron micrograph at low magnification shows, as for lignite, irregular shaped particles and poor classification. There are more fines present in the bituminous coal than in the lignite, and this is thought to be because the bituminous coal has much lower equilibrium moisture content and exhibits more pronounced static attraction. The bituminous coal, when viewed under higher magnification, appears to have a hard, smooth surface with some visible fracture patterns. The lignite had very few macropores but the bituminous coal appears to be almost entirely free of such large external openings. A few micron-size ash particles were observed clinging to the bituminous coal particle surface.

Polished surfaces of bituminous coal, shown in Figure 2.12 viewed under cedar oil exhibit similar petrographic elements to those observed earlier for lignite. The predominance of

a low reflecting element, most likely vitrinite, and two elements that reflect more light are seen in the top micrograph. The larger and darker of the two highly reflecting elements appears similar to the element identified as micronite in the lignite; the smaller highly reflective element appears to be a rare fusanite element. The macropore structure of the micronite elements appears to be less pronounced than was found for the lignite, but the lower reflective elements in bituminous coal appear to have greater macropore structure than the lignite. As in the lignite, most particles are petrographically pure, although several petrographic forms are occasionally observed; for example, three different reflectivities are evident in one particle in the bottom micrograph.

I-2.2 Particle Size Distribution

Mass particle size distributions, calculated in the same manner as for the lignite, gave a poorer fit of the data for bituminous coal than for lignite, even though more than three times as many particles were counted. The fit of cumulative particle mass by the Rosin-Rammler distribution function is shown in figure 2.15. The mass average particle size determined from the cumulative distribution is 64.9 microns, while average particle diameter determined from the raw data is 57.5 microns and the standard deviation is 22.2 microns. The average particle size determined from both methods is larger than the maximum screen size of 43 microns. A 43 micron opening could allow a particle with a maximum dimension in at least one direction

of about 60 microns to pass. Narrow particles with two dimensions less than the maximum size opening could pass through the screen with a very large size in one dimension. Electron micrographs were checked and a few odd shaped particles appeared in the pictures. A few large particles can skew a mass average distribution to much higher mass average particle sizes. Another possibility that cannot be completely eliminated, but which could account for the large particles present in the classified sample is rents or enlarged holes in the screens. The original data and the derived Rosin-Rammler distribution curve are shown in figure 2.16. The agreement is considered satisfactory with the reservations previously mentioned in the section on lignite distribution.

I-2.3 Surface Area

Surface areas, determined using krypton adsorption, are as in the case of lignite significantly below the true surface area, representing only pores with restrictions greater than about 12 Å. Calculations of the surface area from krypton adsorption data at 77°K using the Dubinin-Polanyi equation gave 2.1 m²/g, the BET equation gave 1.25 m²/g. Gan et al (1972) measured the CO₂ adsorption area for a Pittsburgh seam bituminous coal with 82.4% carbon (dmmf) and found a surface area of 141 m²/g. This value is consistent with the value of about 150 m²/g obtained from neon adsorption at 298°K for a coal with 83% C (Dryden, 1963).

I-2.4 Proximate Analysis

Proximate analyses for the bituminous coal of this study is reported on an as received basis in Table 2.3. The Pittsburgh seam #8 bituminous coal has a low equilibrium moisture content of about 2.2%. This value is taken to be representative of mine samples.

I-2.5 Heat of Combustion

The heat of combustion of the Pittsburgh Seam #8 bituminous coal, determined in the same way as that of lignite, is 14,377 BTU/lb on a moist mineral matter free basis. This value is consistent with other values reported for Pittsburgh seam coals and classifies this coal as a high volatile A bituminous coal.

I-2.6 Elemental Analysis

Elemental analysis of the bituminous coal and sulfur form analysis are presented in Table 2.3 on an as received basis, and in Table 2.5 on other commonly used bases. The bituminous coal has 1.04% nitrogen and a high sulfur content of 4.55% on an as received basis. The major portion of the sulfur is pyritic (2.29%) but the organic sulfur is much higher (1.58%) than that of ordinary plant materials. The carbon content is 82.27% on a dry mineral matter free basis.

I-2.7 Ash Analysis

The ash composition of the two coals are compared in Table I-2. The bituminous coal has a higher ash content than lignite,

about 10.5 weight percent versus about 7.8 percent. A very large portion of the bituminous coal's ash is composed of iron compounds, mostly present as pyrites (Padia, 1976). The high pyrites content of the mineral matter accounts for the major portion of the sulfur content of the bituminous coal. Iron, calculated as ferric oxide accounts for 30% by weight of the ash compared with 38% for silica and 19% for alumina. Calcium, residual sulfur trioxide and potassium are the only other constituents of consequence in bituminous ash.

I-2.8 Functional Group Analysis

Functional group analysis has not as yet been performed on the bituminous coal sample of this study. A partial functional group analysis has been reported in the literature on a vitrain concentrated sample of a Pittsburgh Seam bituminous coal. Heredy and Fugassi (1966) investigated a benzene extract for hydrogen distribution by proton NMR for a vitrain concentrate from the same mine (Ireland) as the bituminous coal used in this study. Their results showed that 16.3% of the hydrogen was substituted on condensed aromatic rings, 14.7% of the hydrogen was attached to either monocyclic aromatic rings or phenolic oxygen; 69% of the hydrogen was attached to aliphatic carbons, 29.6% to α carbons and 39.4% to β carbons. These figures agree only fairly with the figures reported in Table I-4 and have not been considered in constructing Table I-4 since the benzene extract accounted for only about 10% of the total coal.

Retcofsky and Friedel (1970) have also investigated functional group distribution of a vitrain rich sample of the coal from a Pittsburgh seam bituminous coal. Their findings are consistent with the results of Tingey and Morrey reported in Table 2.8. Retcofsky and Friedel studied high resolution proton NMR of pyridine and carbon disulfide coal extracts. The pyridine extract contained 21.4% of the coal and had an elemental analysis close to that of the whole coal; the carbon disulfide extract contained only 2.5% of the coal and had significantly higher carbon and hydrogen contents and lower oxygen content than the original coal. Aromatic carbon accounted for 73% of the carbon in the pyridine extract, 35% of the hydrogen was aromatic, the α aliphatic hydrogen accounted for 26% and β^+ hydrogen accounted for 36% of the total hydrogen. Hydroxyl hydrogen accounted for only 3% of the total hydrogen. The values derived from the carbon disulfide extract were similar although a higher percentage of aliphatic compounds seem to be present in the carbon disulfide extract.

The average ring size of a high volatile bituminous coal with 83% carbon content may be 5-8; the distribution of the carbon may be about 70% aromatic, 30% aliphatic, with only 6% of the carbon in methylene bridges; the distribution of the hydrogen may be 20% aromatic, 75% aliphatic and about 5% in the phenolic OH; the oxygen may be split equally between hydroxyl and carbonyl oxygen with negligible amounts in carboxyl and ether groups.

TABLE I-4

FUNCTIONAL GROUP ANALYSIS OF
A HIGH VOLATILE BITUMINOUS COAL

From Tingey and Morrey, (1973)
and Dryden, (1963)

	Hydrogen Distribution % of total H	Carbon Distribution % of total C	Oxygen Distribution % of total O
Total daf	5.57	82.4	~9.
Average Ring Size	-	5-8	-
Aromatic	19.6	70.5	-
Monoring	11.2	21.1	-
Condensed Ring	8.4	49.4	-
Peripheral C	-	37.1	-
Interior C	-	33.4	-
Aliphatic	75.7	29.5	-
Methylene Bridges	5.3	2.1	-
α CH _x	36.0	13.2	-
β^+ CH _x	37.8	14.1	-
Hydroxyl	4.7	-	45.
Carbonyl	-	-	55.
Carboxyl	-	-	0.

I-3 Physical Properties of Coal

Estimates of some of the physical properties of coal have been used in this study. These values are not very accurate and have been used only for crude calculations. The values of interest are specific gravity, thermal conductivity, and specific heat. The interpretation of these values for a substance such as coal that is very heterogenous and changes both chemically and physically when mildly heated is questionable. Even when no changes occur in the coal the values are uncertain because of difficulties in accounting for the strong effects of coal rank, mineral matter content and moisture content.

Average values of the physical properties needed have been taken from McCabe and Boley (1945), Badzioch et al (1964) and Kirov (1965). Specific gravity is usually between 1.3 and 1.35 for coals. Specific gravity will increase roughly 0.01 unit for a percent increase in ash content. Thermal conductivity of raw coals below 400°C varies from 5×10^{-4} to 8×10^{-4} cal/g-cm-sec-K. Above about 300-400°C, where carbonization reactions begin, the thermal conductivity rises rapidly until at 900°C (the maximum temperature in Badzioch et al's study) it has a value of about 60×10^{-4} cal/g-cm-sec-K. This high value in all probability represents conductive heat transfer augmented by radiative transfer through pores and convective transfer by volatile products flowing through cracks and pores. The latter two effects are difficult to separate from the former experimentally. The thermal conductivity of the particle is needed for calculating the rate of temperature rise in the

particle. Since the resistance to heat transfer by conduction within the particle is negligible relative to the external resistance, uncertainty in the value of the thermal conductivity is of little significance.

Measurements of specific heat will also be affected by the heterogenous nature of coal and by the physical and chemical changes of the coal during heating. The specific heat of raw coal increases with increasing volatile matter and increasing moisture content and decreases with increasing ash content. The specific heat of raw coals with less than 10% volatile matter (d.a.f.) will be between 0.2 and 0.25 cal/g-K, while coals with volatile matter (d.a.f.) between 10 and 50% will have specific heats between 0.25 and 0.35 cal/g-K. Coals with volatile matter in the range of 40% (d.a.f.) will have specific heats around 0.3 cal/g-K.

Char residuals (based on weight of raw coal) could have a maximum specific heat of 0.42 cal/g-K at 320°C for a char from a coal with 50% d.a.f. volatile matter. The specific heat of chars produced from coals with volatile matter (d.a.f.) greater than 30% have a specific heat maximum in the region of rapid devolatilization, the temperature of which region increases with heating rate. The specific heat then decreases towards an asymptotic value, which for moderate heating rates may occur at temperatures above 1100°C. For a given heating rate, the position of the specific heat maximum is displaced towards higher temperatures as the volatile matter of the coal decreases. Chars produced from coals with d.a.f. volatile

matter in the range of 30-40% would be expected to have a specific heat value of about 0.33 cal/g-K based on the weight of the raw coal.

APPENDIX J

LISTINGS OF COMPUTER PROGRAMS AND DATA CARDS

FORTTRAN SUBROUTINE's used in the present study are as follows.

LFLOW	Data reduction for the laminar flow experiment
QUDFU	Quadratic curve fit used in LFLOW
QUDFT	Quadratic curve fit used in LFLOW
FREEF	Data reduction for the free/fall experiment with alumina crucibles
CRUCI	Data reduction for thr crucible experiment
EQSIM	Predicts the velocity and temperature of coal particles in the furnace. EQSIM is called in a main line program DYSYS, which is a general program to solve nonlinear first order simultaneous equations developed at the Department of Mechanical Engineering, M.I.T.
BLAYER	Calculates the boundary layer thickness on the injector surface. BLAYER is called in EQSIM.
INPPR	Prints out the inputs used in two competing reaction models.
COMPT	Calculates weight loss and others by using two competing reaction models.
GETB2	Finds an optimal value for the second frequency factor B_2 in two competing reaction models.
ERRRS	Calculates the standard deviation of the errors between the data and the results of simulation by two competing reaction models.
PICTR	Special plotting subroutine available at the Department of Mechanical Engineering, M.I.T.

Numbers in the data cards are explained as follows.

LAMINAR FLOW

- (1) Code for experiment
- (2) Run number
- (3) Type of coal: 11 lignite, 21 bituminous coal.
- (4) Furnace temperature ($^{\circ}$ K)
- (5) Main gas flow rate (ℓ /sec)
- (6) Distance of the collector from the feeder (inch)
- (7) Weight of coal fed (undried, gram)
- (8) Weight of char collected (dried, gram)
- (9) Weight of char used in ash analysis.
If the number is 0.1000, ash was analyzed in Galibraith Laboratory Inc., and the weight is assumed to be 0.1000 gm for calculation purpose (ash concentration in char was known).
- (10) Weight of ash after the ash analysis
- (11) Feed time (minutes . seconds)
- (12) Suction rate (ℓ /sec)

Free Fall Experiment

- (1) Code for experiment
- (2) Run number
- (3) Type of coal: 11 lignite, 21 bituminous coal.
- (4) Maximum temperature recorded by the thermocouple (°C)
- (5) Weight of coal fed (gram).
If this column is 0.0000, the weight is unknown (some particle loss was evident).
- (6) Weight of char collected (gram)
- (7) Weight of char (gram) used in the ash analysis
- (8) Weight of solid deposit (gram) in the collector wall and char remaining in the collector analyzed for ash content.
- (9) Weight of char recovered from the collector (gram)
- (10) Weight of ash from char (7)
- (11) Weight of ash from solid deposit and char (8)
- (12) Feed time (minutes . seconds)

Crucible Experiment

- (1) Code for experiment
- (2) Run number
- (3) Type of coal: 11 lignite, 21 bituminous coal.
- (4) Maximum temperature recorded by the thermocouple (°C)
- (5) Weight of coal (gram)
- (6) Weight of char (gram)
- (7) Weight of char used in the ash analysis (gram)
- (8) Weight of ash from char (7) (gram)
- (9) Weight of solid deposit on the crucible wall and char remaining in the crucible (gram)
- (10) Weight of ash from solid deposit and char (9)
- (11) Comments: 0 typical experimental conditions,
1 special experimental conditions.

LFLOW - 1 -

```

SUBROUTINE LFLOW(CFH20,CDAF,NDATA,APLOT)
C   COAL DEVOLATILIZATION IN A LAMINAR FLOW FURNACE
  INTEGER SMIN,SMAX
  DIMENSION APLOT(10,100)
  DIMENSION DIST(60),VEL(60),PTIME(60)
  NREAD=8
  NWRT=5
  SMIN=27
  KCONT=0
  READ(NREAD,177) NDATP
171  FORMAT(I2)
  READ(NREAD,277) (DIST(I), I=1,NDATP)
  READ(NREAD,277) (VEL(I), I=1,NDATP)
  READ(NREAD,277) (PTIME(I), I=1,NDATP)
270  FORMAT(10X,14F5.2)
271  FORMAT(10X,14F5.1)
  READ(NREAD,117) CLAB1,CLAB2
110  FORMAT(2A3)
  DO 11 I=1,NDATA
  READ(NREAD,107) RCODE,NORUN,IDC,TMAXF,FLOW,POSIT,WCOAL,CHAR
  +      ,CHRCR,ASHCR,TFEED,VACFL,NOTE
100  FORMAT(A2,I4,I3,F6.7,F5.2,F4.1,F7.4,F6.2,F5.2,I3)
  IF(IDC=1) 30,51,30
  30  IF(IDC=2) 20,52,29
  29  CONTINUE
  IF(IDC=11) 41,41,42
  41  FASH0=.0936
  SMAX=-67
  CLAB=CLAB1
  IF(NORUN=240) 51,52,52
  51  FH20=.01479
  GO TO 43
  52  FH20=.01409
  GO TO 43
  42  FASH0=.01089
  SMAX=-90
  CLAB=CLAB2
  IF(NORUN=240) 53,54,54
  53  FH20=.0198
  GO TO 43
  54  FH20=.02224
  43  CONTINUE
  FH20=CFH20*CFH0
C.....ASH FRACTION IN DRY BASIS
  DAF=1.-FASH0*CDAF
C.....APPARENT VOLATILE YIELD
  FAPVL=1.-CLAB/WCOAL/(1.-FH20)
  FAPVL=FAPVL/DAF
  FAPVL=FAPVL*100.
  POSIT=POSIT+2.54
  CALL QUANT(POSIT,XVEL ,DIST,VEL ,NDATP,KCONT)
  DIST0=0.28*2.54
  XDIST=POSIT+DIST0

```


LFLOW - 3 -

```
APLOT(2,I)=WCAL  
APLOT(3,I)=FAVL  
APLOT(4,I)=FVAT  
( APLOT(5,I)=RTIME  
  APLOT(8,I)=FALS  
  APLOT(10,I)=FRAT  
11 CONTINUE  
  RETURN  
  END
```

QUDFU

```

SUBROUTINE QUDFU(XDIS, XTEMP, DIST, TEMP, NDATP, KCONT)
  DIMENSION A(60), R(60), C(60)
  DIMENSION DIST(60), TEMP(60)
  IF(KCONT) 111, 111, 112
111 CONTINUE
  NNN=NDATP-5
  DO 4 M=1, NNN
    J=M+1
    K=M+2
    R=TEMP(M)-TEMP(K)
    S=(TEMP(M)-TEMP(J))/(DIST(M)**2-DIST(J)**2)
    T=DIST(M)**2-DIST(K)**2
    U=DIST(M)-DIST(K)
    V=DIST(M)+DIST(J)
C.....DETERMINE CONSTANTS FOR QUADRATIC EQUATION.
    B(M)=(R-S*T)/(U-T/V)
    A(M)=S-D(M)/V
    4 C(M)=TEMP(M)-A(M)*DIST(M)**2-R(M)*DIST(M)
112 CONTINUE
    M=1
9    IF(XDIS=DIST(M)) 5, 6, 7
7    IF(M=NNN) 10, 70, 8
10   M=M+1
    GO TO 9
8    WRITE(NWRIT, 70)
75   FORMAT(' YOU BLEW IT CHARLIE!')
    GO TO 1000
6    TEMPX=TEMP(M)
    GO TO 50
5    IF(M=1) 8, 70, 71
70   NY=M
    GO TO 72
71   NY=M-1
72   XTEMP=A(NY)*XDIS**2+B(NY)*XDIS+C(NY)
50   CONTINUE
1000 RETURN
    END

```

QU

QUDEF

```

SUBROUTINE QUDEF(XDIS,XTEMP,DIST,TEMP,NDATP,KCONT)
DIMENSION A(60),R(60),C(60)
DIMENSION DIST(60),TEMP(60)
IF(KCONT) 111,111,112
111 CONTINUE
NNN=NDATP-2
DO 4 M=1,NNN
J=M+1
K=M+2
R=TEMP(M)-TEMP(K)
S=(TEMP(M)-TEMP(J))/(DIST(M)**2-DIST(J)**2)
T=DIST(M)**2-DIST(K)**2
U=DIST(M)-DIST(K)
V=DIST(M)+DIST(K)
C.....DTERMINE CONSTANTS FOR QUADRATIC EQUATION.
B(M)=(R-S*T)/(U-T/V)
A(M)=S-B(M)/V
4 C(M)=TEMP(M)-A(M)*DIST(M)**2-B(M)*DIST(M)
112 CONTINUE
M=1
9 IF(XDIS=DIST(M)) 5,6,7
7 IF(M=NNN) 10,70,8
10 M=M+1
GO TO 9
8 WRITE(NWRIT,70)
75 FORMAT(' YOU BLEW IT CHARLIE')
GO TO 1000
6 TEMPX=TEMP(M)
GO TO 50
5 IF(M=1) 8,70,71
70 NY=M
GO TO 72
71 NY=M-1
72 XTEMP=A(NY)*XDIS**2+B(NY)*XDIS+C(NY)
50 CONTINUE
1000 RETURN
END

```

FREEF - 1 -

```

SUBROUTINE FREEF(CFH20,CDAF,NDATA,APLOT)
  DIMENSION APLDT(10,100)
C   FREE FALLING COAL PARTICLE DEVOLATILIZATION
  INTEGER SMIN,SMAX
  NREAD=8
  NWRITE=6
  READ(NREAD,110) CLAB1,CLAB2
110  FORMAT(2A3)
  SMIN=27
  WRITE(NWRITE,200)
200  FORMAT(1H,10Y,
+      'IRIN NO COAL SIZE TEMP COAL W. LS W. LS W. LS
+      W. LS W. LS ASH LS THR.CF FEED' /
+      ',37X,WEIGHT APP. ASH TR ASH TR THR.CR THR.CF BS.ASH', ' PS.C
+      L RATE' / ,22X, '(MICRON) (K) (GM)',17X, 'THR.CF ASH LS',
+      +15X, '(GM/MIN)' /)
  WRITE(NWRITE,201)
201  FORMAT(1H,45X, '(1) (2) (3) (4) (5) (6) (7)' /)
  DO 11 I=1,NDATA
  READ(NREAD,100) PCODE,NORUN,IDC,TMAXF,WCOAL,CHAR,CHRCR,CHRCP,CHRSR
+      ,ASHCR,ASHCF,TFEED,NOTE
100  FORMAT(A2,I4,I3,F6.0,7F7.0,F6.0,I3)
  TMAXF=TMAXF+273.
  IF (IDC=1) 30,31,30
30  IF (IDC=2) 29,32,29
29  CONTINUE
  XI=FIX(TFEED)
  FEEDT=XI+(TFEED-XI)/.60
  IF (IDC=11) 41,41,42
41  FASH0=0.0936
  SMAX=-67
  CLAB=CLAB1
  IF (NORUN=700) 51,52,52
51  FH20=0.1223
  GO TO 43
52  FH20=0.1400
  GO TO 43
42  FASH0=0.1089
  SMAX=-90
  CLAB=CLAB2
  IF (NORUN=700) 53,54,54
53  FH20=0.0198
  GO TO 43
54  FH20=0.0206
43  CONTINUE
  FH20=FM20*CFH20
C.....ASH FRACTION IN DRY BASIS
  DAF=1.-FASH0*CDAF
  IF (WCOAL=0.0001) 46,46,45
45  CONTINUE
C.....APPARENT VOLATILE YIELD
  FAPVL=1.-CHAR/WCOAL/(1.-FH20)
  FAPVL=FAPVL/DAF

```

FREEF - 2 -

```

      FAR1=ASHCR/CH5CR
      ASH=ASHCR*CHRP/CHRCR+ASHCP
C.....ASH FRACTION IN CHAR
      FAP=ASH/CHAR
C.....VOLATILE YIELD BY ASH TRACER
      FVAT=1.-FASH0/FAR
      FVAT=FVAT/DAF
      FVATT=1.-FASH2/FAR1
      FVATT=FVATT/DAF
      ASHLS=WCOAL*(1.-FH20)*FASH0-ASH
      FALSC=ASHLS/WFOAL/DAF/(1.-FH20)
      FALS=ASHLS/FACH0/WCOAL/(1.-FH20)
C.....DEPOSITE BY THERMAL CRACKING
      XTC=CHRCR-ASHCP/FAR1
      IF(XTC) 61,62,62
61 XTC=0.
62 CONTINUE
      FTC=XTC/WCOAL/DAF/(1.-FH20)
C.....VOLATILE YIELD COMPENSATED FOR THERMAL CRACKING
      FVT=1.-((CHAR-XTC)/WCOAL)/(1.-FH20)
      FVT=FVT/DAF
C.....VOLATILE YIELD COMPENSATED FOR THERMAL CRACKING AND ASH LOSS
      FVTAL=1.-((CHAR-XTC+ASHLS)/WCOAL)/(1.-FH20)
      FVTAL=FVTAL/DAF
      FAPVL=FAPV1*100.
      FVAT=FVAT*100.
      FVATT=FVATT*100.
      FVT=FVT*100.
      FVTAL=FVTAL*100.
      FALS=FALS*100.
      FTC=FTC*100.
      FDRAT=WCOAL/FEEDT
      WRITE(NWRIT,320) RCODE,NORUN,CLAB ,SMIN,SMAX,TMAXF,WCOAL,FAPVL,
+
+           FVAT,FVATT,FVT,FVTAL,FALS,           FTC,FDRAT
300 FORMAT(1H ,10X
+           ,A2,I4,2X,A3,I4,I3,F7.0,F7.4,7F7.1,F7.3)
      IF(NOTE) 10,10,12
46 IF(CHRCR=0.00001) 50,47,47
47 IF(CHRCP=0.00001) 48,49,49
48 FAR1=ASHCR/CH5CR
      FVATT=1.-FASH2/FAR1
      FVATT=FVATT/DAF
      FVATT=FVATT*100.
      WRITE(NWRIT,375) RCODE,NORUN,CLAB ,SMIN,SMAX,TMAXF           ,FVATT
315 FORMAT(1H ,10X
+           ,A2,I4,2X,A3,I4,I3,F7.0,21X,F7.1)
      IF(NOTE) 10,10,12
49 FAR1=ASHCR/CH5CR
      ASH=ASHCR+ASHCP
      CHAR=CHRCR+CH5CP
      FAP=ASH/CHAR
      FVAT=1.-FACH0/FAR
      FVATT=1.-FASH2/FAR1

```

FREEF - 3 -

```

      FVAT=FVAT/DAF
      FVATT=FVATT/DAF
      FVAT=FVAT*100.
      FVATT=FVATT*100.
      WRITE(NWRIT,35) RCODE,NORUN,CLAB ,SMIN,SMAX,TMAXF,FVAT,FVATT
325  FORMAT(1H ,10X
      +      ,A2,I4,2X,A3,I4,I3,F7.0,14X,F7.1,F7.1)
      IF(NOTE) 10,10,12
50  FAR2=ASHCP/CHSCP
      FVAT=1.-FASHQ/FAR2
      FVAT=FVAT/DAF
      FVAT=FVAT*100.
      WRITE(NWRIT,35) RCODE,NORUN,CLAB ,SMIN,SMAX,TMAXF,FVAT
335  FORMAT(1H ,10X
      +      ,A2,I4,2X,A3,I4,I3,F7.0,14X,F7.1)
      IF(NOTE) 10,10,12
31  WRITE(NWRIT,401)
401  FORMAT(1H ,' ')
      GO TO 10
32  WRITE(NWRIT,402)
402  FORMAT(1H0,' ')
12  WRITE(NWRIT,501)
501  FORMAT(1H+,9X,'*')
10  CONTINUE
      APLOT(1,I)=TMAXF
      APLOT(2,I)=WCHAL
      APLOT(3,I)=FASVL
      APLOT(4,I)=FVAT
      APLOT(5,I)=FVATT
      APLOT(6,I)=FVT
      APLOT(7,I)=FVVAL
      APLOT(8,I)=FAS
      APLOT(9,I)=FTC
      APLOT(10,I)=FRRAT
11  CONTINUE
      RETURN
      END

```

CRUCI - 1 -

```

SUBROUTINE CRUCI(CFH20,CDAF,NDATA,APLOT)
C   COAL DEVOLATILIZATION IN A CRUCIBLE
  DIMENSION APLNT(10,100)
  INTEGER SMIN,CMAX
  NWRIT=5
  NREAD=8
  READ(NREAD,110) CLAB1,CLAB2
110  FORMAT(2A3)
  SMIN=27
  WRITE(NWRIT,200)
200  FORMAT(1H,10Y,
+       'RIN NO COAL SIZE TEMP COAL W. LS W. LS W. LS
+       W. LS W. LS ASH LS THR.CP /
+       ,37X,'WEIGHT APP. ASH TR ASH TR THR.CR THR.CP BS.ASH', ' BS.C
+       L',
+       ,22X,'(MICRON) (K) (GM)',17X,'THR.CR ASH LS',15X,/)
  WRITE(NWRIT,201)
201  FORMAT(1H,45Y,'(1) (2) (3) (4) (5) (6) (7)')
  DO 11 I=1,NDATA
  READ(NREAD,100) RCODE,NORUN,IDC,TMAXF,WCOAL,CHAR,CHRCR,ASHCR
+       ,CHR2,ASH2,NOTE
100  FORMAT(A2,I4,I3,F6.0,6F7.0,I3)
  TMAXF=TMAXF+273.
  IF(IDC=1) 30,51,30
  30  IF(IDC=2) 29,52,29
  29  CONTINUE
  IF(IDC=11) 41,41,42
  41  FASH0=0.0926
  SMAX=-67
  CLAB=CLAB1
  IF(NORUN=200) 81,82,82
  81  FH20=0.0
  GO TO 43
  82  CONTINUE
  IF(NORUN=240) 51,52,52
  51  FH20=0.1223
  GO TO 43
  52  FH20=0.1409
  GO TO 43
  42  FASH0=0.1089
  SMAX=-90
  CLAB=CLAB2
  IF(NORUN=200) 83,84,84
  83  FH20=0.0
  GO TO 43
  84  CONTINUE
  IF(NORUN=240) 53,54,54
  53  FH20=0.2198
  GO TO 43
  54  FH20=0.0206
  43  CONTINUE
  FH20=FM20*CFH20
C.....ASH FRACTION IN DRY BASIS

```

CRUCI - 2 -

```

      DAF=1.-FASH2/*DAF
C..... APPARENT VOLATILE YIELD
      FAPVL=1.-CHAR/WCOAL/(1.-FH20)
      FAPVL=FAPVL/DAF
      FAPVL=FAPVL*100.
      IF (CHR2=0.00001) 71,71,70
71 IF (CHRCR=0.00001) 73,73,72
70 CONTINUE
      ASH=ASHCR+ASH2*(CHAR-CHRCR)/CHP2
C..... ASH FRACTION IN CHAR
      FAR=ASH/CHAR
C..... VOLATILE YIELD BY ASH TRACER
      FVAT=1.-FASH0/FAR
      FVAT=FVAT/DAF
      FAR2=ASH2/CHR2
      FVAT2=1.-FASH2/FAR2
      FVAT2=FVAT2/DAF
      ASHLS=WCOAL*(1.-FH20)*FASH0-ASH
      FALS=ASHLS/WCOAL/DAF/(1.-FH20)
      FALS=ASHLS/FASH0/WCOAL/(1.-FH20)
C..... DEPOSITE BY THERMAL CRACKING
      XTC=CHRCR-ASH2/FAR2
      FTC=XTC/WCOAL/DAF/(1.-FH20)
      IF (XTC) 61,62,62
61 XTC=0.
62 CONTINUE
C..... VOLATILE YIELD COMPENSATED FOR THERMAL CRACKING
      FVT=1.-((CHAR-XTC)/WCOAL)/(1.-FH20)
      FVT=FVT/DAF
C..... VOLATILE YIELD COMPENSATED FOR THERMAL CRACKING AND ASH LOSS
      FVTAL=1.-((CHAR-XTC+ASHLS)/WCOAL)/(1.-FH20)
      FVTAL=FVTAL/DAF
      FVAT=FVAT*100.
      FVAT2=FVAT2*100.
      FVT=FVT*100.
      FVTAL=FVTAL*100.
      FALS=FALS*100.
      FTC=FTC*100.
      WRITE(NWRITE,300) RCODE,NORUN,CLAB,SMIN,SMAX,TMAXF,WCOAL,FAPVL,
+
+          FVAT,FVAT2,FVT,FVTAL,FALS,      FTC
300 FORMAT(1H,10X
+          ,A2,I4,2X,A3,I4,I3,F7.0,F7.4,7F7.1)
      GO TO 112
72 CONTINUE
      ASH=ASHCR+ASH2/CHRCR
      FAR=ASH/CHAR
      FVAT=1.-FASH0/FAR
      FVAT=FVAT/DAF
      ASHLS=WCOAL*(1.-FH20)*FASH0-ASH
      FALS=ASHLS/WCOAL/DAF/(1.-FH20)
      FALS=ASHLS/FASH0/WCOAL/(1.-FH20)
      XTC=0.
      FVTAL=1.-((CHAR-XTC+ASHLS)/WCOAL)/(1.-FH20)

```

CRUCI - 3 -

```

      FVTAL=FVTAL/D1F
      FVAT=FVAT*100.
      FALS=FALS*100.
      WRITE(NWRIT,301) RCODE,NORUN,CLAB ,SMIN,SMAX,TMAXF,WCOAL,FAPVL,
+
301  FORMAT(1H ,10Y
+
      ,A2,I4,2X,A3,I4,I3,F7.0,F7.4,2F7.1,21X,F7.1)
      GO TO 112
      73  CONTINUE
      WRITE(NWRIT,302) RCODE,NORUN,CLAB ,SMIN,SMAX,TMAXF,WCOAL,FAPVL
302  FORMAT(1H ,10Y
+
      ,A2,I4,2X,A3,I4,I3,F7.0,F7.4,F7.1)
112  CONTINUE
      IF(NOTE)10,10,12
      12  WRITE(NWRIT,501)
501  FORMAT(1H+,9X,'*')
      GO TO 10
      31  WRITE(NWRIT,401)
401  FORMAT(1H ,' ')
      GO TO 10
      32  WRITE(NWRIT,402)
402  FORMAT(1H0,' ')
10   CONTINUE
      APLOT(1,I)=TMAXF
      APLOT(2,I)=WCOAL
      APLOT(3,I)=FAPVL
      APLOT(4,I)=FVAT
      APLOT(5,I)=FVATT
      APLOT(6,I)=FVATT
      APLOT(6,I)=FVT
      APLOT(7,I)=FVTAL
      APLOT(8,I)=FALS
      APLOT(9,I)=FTC
11   CONTINUE
      RETURN
      END

```

EQSIM - 1 -

```

      SUBROUTINE FQSIM
C.....PARTICLE VELOCITY SIMULATION
C      T IS DISTANCE
C.....Y(1) IS CENTER VELOCITY
C.....Y(2) IS CENTER TEMPERATURE
C.....Y(3) IS BOUNDARY VELOCITY
C.....Y(4) IS BOUNDARY TEMPERATURE
C.....Y(5) IS RESIDENCE TIME OF PARTICLE
C.....Y(6) IS MAIN GAS VELOCITY
C.....Y(7) IS NONDIMENSIONAL CENTER VELOCITY
C.....Y(8) IS NONDIMENSIONAL BOUNDARY VELOCITY
C.....Y(9) IS NONDIMENSIONAL MAIN GAS VELOCITY
C.....Y(10) IS NONDIMENSIONAL CENTER TEMPERATURE
C.....Y(11) IS NONDIMENSIONAL BOUNDARY TEMPERATURE
      REAL NDIST
      DIMENSION EVEL(12), EDIST(12)
      DIMENSION APLAT(12,100), XSCL(4), XLAB(56)
      COMMON T, DT, Y(20), F(20), STIME, FTIME, NEWDT, IFWRT,
*          IPR, IFO, ICN, TNEXT, PNEXT, TBACK
      DATA NREAD, NWRIT / 8, 5 /
      DATA DMAIN, FORAT / 5.28, 2.15 /
      IF(NEWDT) 100,300,200
100  CONTINUE
      READ(NREAD,407) TEMPG,VMAIN,VCARR,VPART, C, NDATA
401  FORMAT(6F10.0)
      C=4.5
      RTE=3.1416
      EMISS=1.0
      SIGMA=.365E-15
      CAPR=0.3
      CAPC=3.125
      DENCPC=1.3
      RP=0.302
      TG4=TEMPG*.4
      CF1=C
      CF2=C
      CE1=3.*C
      CE2=3.*C
      FPOSI=2.54
      GRAV=980.
      XMPAR=FORAT/6.*
      DENC2=0.00162
      EF=2.*SIGMA+EMISS/DENCPC/RP*XMPAR
      VISC=1.0004*(TEMPG/300.)**1.5/(TEMPG+167.)*0.0467
      DENC3=0.001621302./TEMPG
      TCONG =4.71E-15*(TEMPG/300.)**0.65
      REYVM=DENC3*VMAIN*DMAIN/VISC
      PRATI=VISC *C/PG/TCONG
      CALL BLAYER(UAV,TAV,RR,VMAIN,TEMPG)
      Y(3)=UAV
      Y(4)=TAV
      DELTE=RR-0.235
      RC=0.36

```


EQSIM - 2 -

```

SC=PIE*PC*PC
SP=PIE*PR*PR ISC
DRQ(ND)=P.*PR
WRITE(NWRIT,5-1)
501 FORMAT(1H1,200,'SIMULATION OF FLOW FIELD'////11X,'INPUT VARIIVLES'
+//)
DCENT=2.*Rc
WRITE(NWRIT,5-2) TEMPG,VMAIN,VCAPP,VPART,DCENT
502 FORMAT(1H ,120,'TEMPERATURE (K)',T50,F5.0/11X,
+'MAIN GAS VELOCITY (CM/SEC)',T50,F5.0/11X,
+'CARRIER GAS VELOCITY (CM/SEC)',T50,F5.0/11X,
+'PARTICLE INITIAL VELOCITY (CM/SEC)',T50,F5.0/11X,
+'DIAMETER OF CENTER STREAM (CM)',T50,F4.2)
WRITE(NWRIT,5-3) FDRAT,REYNN,PRANT,DELTA,DBOUND, C
503 FORMAT(1H ,120,'COAL FEED RATE (GM/MIN)',T50,F4.2/11X,
+'MAIN FLOW REYNOLDS NUMBER',T50,F5.0/11X,
+'MAIN FLOW PRANTLE NUMBER',T50,F5.3/11X,
+'THERMAL DISPLACEMENT THICKNESS',T50,F5.3/11X
+'BOUNDARY LAYER DIAMETER',T50,F5.3/11X,
+'CONSTANT',T50,F5.2)
200 CONTINUE
IF (T.GE. 5.0) DT=0.2
NDIST=(T+FRST)/DMAIN/REYNN*400.
IF (NDIST.LE. 6. ) UMAIN=VMAIN*( 1. + 0.34*NDIST**0.45)
IF (NDIST.GT. 6. ) UMAIN=VMAIN*( 2. -3.48/NDIST**1.47)
TEMPC=Y(2)
TEMPB=Y(4)
TEMP1=(TEMPB+TEMPC)/2.
TEMP2=(TEMPB+TEMPG)/2.
VIS1 = 1.98*(TEMP1/300.)**1.5/(TEMP1+167.)*0.0467
VIS2 = 1.98*(TEMP2/300.)**1.5/(TEMP2+167.)*0.0467
TCOINC=4.74E-05*(TEMP1/300.)**0.65
TCONMA=4.74E-05*(TEMP2/300.)**0.65
DENC=DFENCA*300./Y(2)
DENCB=DFENCB*300./Y(4)
DVMAX=2.*VMAIN
DTMAX=TEMPG-300.
Y(6)=UMAIN
Y(7)=(Y(1) )/DVMAX
Y(8)=(Y(3) )/DVMAX
Y(9)=(Y(6) )/DVMAX
Y(10)=(Y(2)-300.)/DTMAX
Y(11)=(Y(4)-300.)/DTMAX
300 CONTINUE
XMC0=SC*DENC
XMC0=SP*DENCB
XMC=XMC0*Y(1)
XMC=XMC0*Y(3)
A1=VMC00+XMC
A2=0.
A3=CAPP,XMCAR,XMC*CAPG*(Y(2)+Y(4))/Y(2)/2.
A4=XMC0,CAG*,Y(2)+Y(4))/2.
A5=XMC

```

EQSIM - 3 -

```

A6=0.
A7=XMC*(Y(3)-Y(1))/V(1)
A8=-XMC*(Y(3)-Y(1))/Y(2)
A9=XMB-CAPG*(V(4)+TEMPG)/Y(4)/2.
A10=XMR+CAPG*(Y(4)-TEMPG)/2.
A11=XMC*CAPG*(Y(2)-TEMPG)/Y(2)/2. *(-1.)
A12=XMR+CAPG*(Y(2)-TEMPG)/2.
FVBC=PIE*VIS1*CF1*(Y(3)-Y(1))
FVBR=PIE*VIS2*CF2*(Y(6)-Y(3))
FGBC=SC*GRAV*(DENCB-DENCG)
FGBR=S1*GRAV*(DENCB-DENCG)
FG=XMR*P/Y(1)*GRAV
SCBC=PIE*TCONGC*CE1*(Y(4)-Y(2))
SCBR=PIE*TCONGR*CE2*(TEMPG-Y(4))
EE=FE/Y(1)*(T04-Y(2)**4)
FF=FVBR-FVBC+FGBR
FC=FVBC+FG+FGBC
EB=ECMB-ECBC
EC=ECBC+EB
F(1)=FC/A1
F(2)=(FC-A4*F(1))/A3
F(3)=(EB+A7*F(1)+A8*F(2))/A5
F(4)=(-A10*F(3)-A11*F(2)-A12*F(1)+EB)/A9
F(5)=1./Y(1) *1000.
RETURN
END

```

BLAYER

```

SUBROUTINE BLAYER(UAV,TAV,FB,UM,TM )
  FX(P)=SIN(PIE/2.*(R-RC))
  GX(P)=1./(TA1+TA2*SIN(PIE/2.*(R-RC)))
  TA1=300./TM
  TA2=1.-TA1
  PIE=3.1416
  VISC=1.980*(TG /370.)*1.5/(TM +167.)*0.0467
  DENCG=0.20162/300./TM
  REYNX=DENCG*U.*2.54/VISC
  DELTA=2.54/SQRT(REYNX)*5.
  DELTA=0.238+DELTA
  RC=0.238/DELTA
  NDIV=100
  DR=(1.-RC)/FLRAT(NDIV)
  R=RC
  XM=0.
  XW=0.
  NN=NDIV-1
  DO 10 I=1,NN
    R=R+DR
    XW=XW+R*FX(R)+GX(R)
    XM=XM+R*FX(R)+GX(R)
10 CONTINUE
  XM=DR*(XM*2.+EX(1.)*FX(1.)*GX(1.))
  XW=DR*(XW*2.+EX(1.)*GX(1.))
  YE=4./PIE*(EX(1.)*(2./PIE-1.+RC)+1.-COS(PIE/2.*(1.-RC)))
  TAV=300./TM
  DENCAV=1./TAV
  REP=(XW-1.-DENCAV*(YE-1.))/(DENCAV-1.)
  RP=SQRT(RP)
  UAV=(YE-1.+RP/RR)/(RB*RB-RC*RC)
  UAV=UAV*UM
  TAV=TAV*TM
  RP=RP*DELTA
  RETURN
END

```

```

SUBROUTINE INPPR(XNUSS,TCONG,DENCL,CPC,DIA,ALFA1,ALFA2,E1,E2,B1,
+             R2,TCHC,TCHM)
  NWRIT=5
  WRITE(NWRIT,5016)
2016 FORMAT(1H,1V,VALUES OF THE PROPERTIES USED IN THE MODEL'////)
  WRITE(NWRIT,5011) XNUSS
2011 FORMAT(1H,20V,'NUSSLET NUMBER='F6.3)
  WRITE(NWRIT,5012) TCONG
2012 FORMAT(1H,20V,'THERMAL CONDUCTIVITY OF GAS   TCONG='E11.4'(CAL/S
1EC CM K)')
  WRITE(NWRIT,5013) DENCL
2013 FORMAT(1H,20V,'DENSITY OF COAL   DENCL='F7.4'(G/CM**3)')
  WRITE(NWRIT,5014) CPC
2014 FORMAT(1H,20V,'SPECIFIC HEAT OF COAL'F6.3'(CAL/GM K)')
  WRITE(NWRIT,5015) DIA
2015 FORMAT(1H,20V,'DIAMETER OF COAL='F10.6'(CM)')
C
C   PRINTING THE INPUT VARIABLES
  WRITE(NWRIT,5027)
2027 FORMAT(1H,1V,INPUT VARIABLES'////)
  WRITE(NWRIT,5021) ALFA1
  WRITE(NWRIT,5031) ALFA2
2021 FORMAT(1H,20V,'ALFA1='F7.4)
2031 FORMAT(1H,20V,'ALFA2='F7.4)
  WRITE(NWRIT,5023) E1
  WRITE(NWRIT,5033) E2
2023 FORMAT(1H,20V,'ACTIVATION ENERGY   E1='F10.0'(CAL/GM MOL)')
2033 FORMAT(1H,20V,'ACTIVATION ENERGY   E2='F10.0'(CAL/GM MOL)')
  WRITE(NWRIT,5025) B1
  WRITE(NWRIT,5035) B2
2025 FORMAT(1H,20V,'FREQUENCY FACTOR   B1='E11.4'(1/SEC)')
2035 FORMAT(1H,20V,'FREQUENCY FACTOR   B2='E11.4'(1/SEC)')
  WRITE(NWRIT,5027) TCHC
2027 FORMAT(1H,20V,'CHARACTERISTIC COAL CONDUCTION TIME   TCHC1='E11.4'
1(SEC)')
  WRITE(NWRIT,5028) TCHM
2028 FORMAT(1H,20V,'CHARACTERISTIC MIXING TIME   TCHM='E11.4'(SEC)')
  RETURN
  END

```

COMPT - 1 -

```

SUBROUTINE COMPT(E1 ,R1,ALFA1,E2 ,B2,ALFA2,DT,TCHC,TCHM,
+           TEMPX,FTIME,ITERN,XTIME,XWTL,XTEMP,
+           XRAT1,XRAT2,XUBCL,XRES1,XRES2)
DIMENSION XTIME(200),XWTL(200),XTEMP(200)
DIMENSION XRAT1(200),XRAT2(200),XUBCL(200),XRES1(200),XRES2(200)
C   INITIAL VALUES
E1BYR=E1/1.984
E2BYR=E2/1.984
TCHDI =TCHM-TCHC
C1=TCHC/TCHDI
C2=TCHM/TCHDI
TIME=-DT
TEMP0=300.
RATE1=R1*EXP(-E1BYR/TEMP0)
RATE2=R2*EXP(-E2BYR/TEMP0)
RTIT1=0.0
RTIT2=0.0
WTL=0.0
ITERN =0
NM=2
EXX=0.0
EXX1=0.
EXX2=0.
RES1=0.
RES2=0.
C   INTEGRATION USING TRAPEZOIDAL RULE
50 TIME=TIME+DT
ITERN =ITERN +1
AA1=TIME/TCHC
AA2=TIME/TCHM
IF(AA1.GE.100.)AA1=100.
IF(AA2.GE.100.)AA2=100.
TEMP=TEMP0+(TEMPX -TEMP0)*(1.+C1*EXP(- AA1
1-C2*EXP(- AA2
))
RAT10=RATE1
RAT20=RATE2
RATE1=R1*EXP(-E1BYR/TEMP)
RATE2=R2*EXP(-E2BYR/TEMP)
RTIT1=RTIT1+0.5*(RAT10 +RATE1)*DT
RTIT2=RTIT2+0.5*(RAT20 +RATE2)*DT
IF(RTIT2 .GE.100.) RTIT2 =100.
IF(RTIT1 .GE.100.) RTIT1 =100.
ERTI1=EXP(-RTIT1)
ERTI2=EXP(-RTIT2)
UBCL=ERTI1*ERTI2
EXX0=EXX
EXX10=EXX1
EXX20=EXX2
EXX1=UBCL*RATE1
EXX2=UBCL*RATE2
EXX=EXX1*ALFA1+EXX2*ALFA2
RES1=RES1+0.5*(EXX10+EXX1)*DT*(1.-ALFA1)
RES2=RES2+0.5*(EXX20+EXX2)*DT*(1.-ALFA2)

```

```
WTLS=WTLS+0.5*(FXX0+EXX)*DT
IF(0.5*(EXX0+EXX)*DT.LT.0.0020)DT=DT*2.
IF(0.5*(EXX0+EXX)*DT.GT.0.010)DT=DT*0.5
IF(TIME.LT.0.05 .AND. DT.GT.0.002)DT=0.002
IF(NN=2) 30,40,40
40 NN=0
I=JTERN/2+1
XTIME(I)=TIME
XTEMP(I)=TEMP
XPAT1(I)=RATE1
XPAT2(I)=RATE2
XUBCL(I)=UBCL
XWTLS(I)=WTLS
XRES1(I)=RES1
XRES2(I)=RES2
30 NN=NN+1
IF(JTERN=100) 49,49,1010
49 IF(TIME=FTIME) 50,50,1010
1010 RETURN
END
```

```

SUBROUTINE GETB2(ERRW,B2,NE2,B2NEW)
  ERRW1=ERRW
  B21=B2
  IF(NE2-1) 410,410,420
410  ERRW2=ERRW
  ERRW3=ERRW
  B22=B2
  B23=B2
420  IF(ERRW1=ERRW2) 200,201,201
201  IF(ERRW2=ERRW3) 210,220,220
200  ERFCAR=ERRW2
  B2CAR=B22
  ERRW2=ERRW1
  ERRW1=ERFCAR
  B22=B21
  B21=B2CAR
  GO TO 201
210  ERFCAR=ERRW3
  B2CAR=B23
  ERRW3=ERRW2
  B23=B22
  ERFCAR=ERFCAR
  B22=B2CAR
  IF(ERRW1=ERRW3) 205,205,220
205  ERRW2=ERRW1
  B22=B21
  ERRW1=ERFCAR
  B21=B2CAR
220  IF(ERRW1) 230,230,221
221  IF(ERRW3) 222,240,240
222  IF(ERRW2) 223,223,224
223  B2NEW=B21+(B23-B21)*ERRW1/(ERRW1-ERRW2)
  ERRW3=ERRW1
  B23=B21
  GO TO 1020
224  B2NEW=B22+(B23-B22)*ERRW2/(ERRW2-ERRW3)
  GO TO 1020
230  B2NEW=0.1*B21
  ERRW3=ERRW1
  B23=B21
  GO TO 1020
240  B2NEW=10.*B23
1020  RETURN
  END

```

```

SUBROUTINE FRORS(TIME,WTLS,NOPT,ETIME,EWTLS,NDATA,XDIF1,XDIF2,
+             STD,TEMP,CWTLS,CTEMP)
+ DIMENSION TIME(200),WTLS(200),ETIME(50),EWTLS(50)
+ DIMENSION CWTLS(50),CTEMP(50),TEMP(200)
XDIF1=0.2
XDIF2=0.
MM=1
DO 10 I=1,NDATA
NN=MM
DO 20 J=NN,NOPT
IF (TIME(J)-ETIME(I)) 20,21,21
21 MM=J
GO TO 30
20 CONTINUE
30 XWTLS=WTLS(MM-1)+(WTLS(MM)-WTLS(MM-1))*(ETIME(I)-TIME(MM-1))
+   /(TIME(J)-TIME(MM-1))
+ XTEMP=TEMP(MM-1)+(TEMP(MM)-TEMP(MM-1))*(ETIME(I)-TIME(MM-1))
+   /(TIME(J)-TIME(MM-1))
CWTLS(I)=XWTLS
CTEMP(I)=XTEMP
DIF=EWTLS(I)-WTLS
XDIF1=XDIF1+DIF
XDIF2=XDIF2+DIF*DIF
10 CONTINUE
STD=SQRT(XDIF2/FLOAT(NDATA))
RETURN
END

```


MAIN - 1 - (TWO COMPETING REACTION MODEL)

```

INTFGFR SMIN,SMAX
DIMENSION TIME(200),WTLS(200),TEMP(200),RATE1(200),RATE2(200)
DIMENSION LIPC(200),RES1(200),RES2(200),HRYC(200),ORYC(200)
DIMENSION NOPUN(50),ETIME(50),FDRAT(50),EWTLS(50),TMAXF(6)
DIMENSION ANOSUN(6,50),XETIME(6,50),XFDRAT(6,50),XEWTLS(6,50)
DIMENSION PLOT(12,50),APLOT(12,203),NPA(6),NFB(6)
DIMENSION XTEMPX(6),XFTIME(6),NNDATA(6),XTMIX(6)
DIMENSION XSCL(4),XLAB(56)
DIMENSION TESWL(6),TESTM(6)
DIMENSION CWTIS(50),CTEMP(50)
DATA XMISS, TONG, DENCL, CPC / 2.0, 0.000129, 1.25, 0.25 /
DATA TEMPO / 3.0 /
DATA TESTM / 0.058, 0.018, 0.018, 0.025, 0.025 /
DATA TESWL / 0.25, 0.21, 0.31, 0.34, 0.34 /
DATA CC, HC, OC / 0.83, 0.062, 0.12 /
DATA CP1, HR1, OR1 / 0.96, 0.016, 0.026 /
DATA CR2, HR2, OR2 / 1.00, 0.00, 0.00 /
DI = 0.0001
NPTYES=1
NPF2=1
NNPF2=1
NPEAD=R
NPFIT=5
LOOK=1
MOVE=0
ISCL=-2
BTIME=0.0
IA=12
NOPLI=0
READ(NRFAD,185) (XLAB(I),I=1,20)
182 FORMAT(20A4)
READ(NRFAD,195) (XSCL(I),I=1,4)
192 FORMAT(4F10.0)
READ(NRFAD,185) (XLAB(I),I=21,56)
183 FORMAT(40A2)
NSPAC=2
C.....READING THE EXPERIMENTAL RESULTS
NCASE=6
DO 35 I=1,NCASE
  READ (NREAD,250) XTEMPX(I),XFTIME(I),NNDATA(I),XTMIX(I)
220 FORMAT(2F10.0,1I0,F10.0)
  NDATA=NNDATA(I)
  READ(NRFAD,285) (RCODE,NNOPUN(I,K),CLAB,SMIN,SMAX,
+                 TMAXF(I),XETIME(I,K),XFDRAT(I,K),XEWTLS(I,K),
+                 K=1,NDATA)
880 FORMAT( A2,I4,2X,A3,I4,I3,F7.0,F7.1,F9.3,F7.1)
  35 CONTINUE
  NNN=4
  DO 1400 IIT=1,NNN
    LSPFL=1004
    READ(NRFAD,204) ALFA1,B1,E1,ALFA2,B2,E2,TMIX,DT
200 FORMAT(F10.0,F10.3,F10.0,F10.2,E10.3,F10.0,F10.0,F10.0)
    DO 16 I=1,NCASE

```

```

FTIME=XFTIME(I)
NDATA=NDATA(I)
TEMP=XTEMP(I)
TMIX=XTMIX(I)
C
C   DEFINING THE CONSTANTS
TCHM=TMIX
TCHC=DIA*DIA*DENCL*CPC/XNUSS/TCONG/6.
C
C   PRINTING THE PROPERTIES USED IN THE MODEL
IF(NNB2.GE.2) GO TO 500
IF(I.GE.2) GO TO 500
WRITE(NWRIT,2010)
2010 FORMAT(1H,///,40X,'TWO COMPETING REACTION MODEL'////)
CALL      JN6PR(XNUSS,TCONG,DENCL,CPC,DIA,ALFA1,ALFA2,E1,E2,R1,
+           B2,TCHC,TCHM)
IF(NOB2.GT.0) GO TO 500
C
C   TEST R2 IN ORDER TO GET SATISFACTORY
C   WEIGHT LOSS AT T=1750 K AND TIME=18 MSEC
C
WRITE(NWRIT,2000)
2000 FORMAT(///,1H,'FINDING THE OPTIMAL VALUE FOR R2'////)
TCHC=DIA*DIA*DENCL*CPC/XNUSS/TCONG/6.
NR2=0
TTEMP=2100.
TWLS=0.63
TTIME=2.025
TTCHM=0.0031
300 NR2=NR2+1
IF(NR2=20) 250,250,1111
250 CONTINUE
C
C   CALCULATING WEIGHT LOSS
CALL      COJPT(E1,R1,ALFA1,E2,B2,ALFA2,DT,TCHC,TTCHM,
+           TTEMP,TTIME,ITERN,TIME,WLTS,TEMP,
+           RATE1,RATE2,URCL,RES1,RES2)
IF(ITERN=1000) 260,260,1111
260 ITERN=ITERN/2
WRITE(NWRIT,2001) NR2,B2,WLTS(ITERN),TIME(ITERN)
2001 FORMAT(1H,13,3X,'B2='E11.4,10X,'WEIGHT LOSS='F7.4,10X,'TIME='F7.4
1)
ERRW=TWLS-WLTS(ITERN)
IF(FRRW=0.01) 61,61,400
61 IF(ERRW=0.01) 400,500,500
C
C   DETERMINE THE OPTIMAL VALUE FOR R2
400 CALL GETR2(ERRW,R2,NR2,B2NEW)
B2=B2NEW
DT=0.0002
GO TO 300
500 CONTINUE
C

```

```

C      R2 WAS CHOSEN
C      CALCULATING WEIGHT LOSS
      DT=0.0002
      CALL      COOPT(E1 ,B1,ALFA1,E2 ,B2,ALFA2,DT,TCHC,TCHM,
+            TEMP,FTIME,ITERN, TIME, WTLS, TEMP,
+            RATE1,RATE2,URCL,RES1,RES2)
      ITERN=ITERN/2
C.....PRINTING OUT THE CALCULATED RESULTS
      WRITE(NWRIT,1,7) TMAXF(I)
107  FORMAT(1H0,'TEMPERATURE='F7.0)
      IF(WRTYES.GT. 0.0)
+WRITE(NWRIT,1,8)
108  FORMAT(///,110,'TIME      WEIGHT LOSS  TEMPERATURE  REAC. RATE 1',
+ ' REAC. RATE 2  UNREACTED COAL  RESIDUE 1  RESIDUE 2  H/C  C/C'
+//11X)
+ '(MSEC)      ( G. A. F. )',T37,'( K )      (PER SEC)',T63,
+ '(PER SFC)')//)
      DO 22 J=1,ITERN
      TIME(J)=TIME(1)*100.
      WTLS(J)=WTLS(1)*100.
      URCL(J)=URCL(1)*100.
      RES1(J)=RES1(1)*100.
      RES2(J)=RES2(1)*100.
      CCP=URCL(J)*C1+RES1(J)*CR1+RES2(J)*CR2
      HCR=URCL(J)*H1+RES1(J)*HR1+RES2(J)*HR2
      OCR=URCL(J)*O1+RES1(J)*OR1+RES2(J)*OR2
      HBYC(J)=HCR/C1R*12.
      ORYC(J)=OCR/C1R*12./16.
20  CONTINUE
      IF(NOPT.EQ. 7) GO TO 23
      J=0
      DO 22 JJJ=1,ITERN,2
      J=J+1
      APLCT(I,J)=TIME(JJJ)
      APJNT(I+6,J)=WTLS(JJJ)
22  CONTINUE
      NP2(I)=NDATA
      NP4(I)=J
23  CONTINUE
      ITERN=ITERN-2
      IF(WRTYES.GT. 0.0)
+WRITE(NWRIT,1,1) (TIME(J), WTLS(J), TEMP(J),
+RATE1(J),RATE2(J),URCL(J),RES1(J),RES2(J),HBYC(J),ORYC(J),
+ J=1,ITERN,NSPAC )
101  FORMAT(1H ,100,'F5.1,F11.2,F13.0,E16.4,E14.4,F11.2,F14.2,F11.2,F10.
+3,F6.3)
      NOPT=ITERN
      DO 37 KK=1,NDATA
      ETIME(KK)=XFTIME(I,KK)
      EWTLS(KK)=XFWTLS(I,KK)
      ENOPLN(KK)=XNOPLN(I,KK)
      EFRAT(KK)=XFRAT(I,KK)
37  CONTINUE

```

```

CALL FRFRS(TIME,WTLS,NOPT,ETIME,EWTLS,NDATA,XDIF1,XDIF2,
+         STD,TEMP,CWTLS,CTEMP)
+ IF(WRTYES.GT.0.0)
+WRITE(NWRIT,270)
210 FORMAT(1H ,//,11X,
+         'RIN NO COAL SIZE TEMP RESIDENCE FEED WEIGHT WEI
+GHT PARTICLE'
+         /,37X,TIME RATE LOSS LOSS TEMP/
+ ,22X,'(MICRON) (K) (MSEC) (GM/MIN) (MFS) (CALC) (K)')
+ IF(WRTYES.GT.0.0)
+WRITE(NWRIT,301)(RCODE,NORIN(M),CLAB,SMIN,SMAX,TMAXF(I),
+         ETIME(M),FRAT(M),EWTLS(M),CWTLS(M),CTEMP(M),
+         M=1,NDATA)
301 FORMAT(1H ,10X
+         ,A2,I4,2X,A3,I4,I3,F7.0,F7.1,F9.3,F7.1,F8.1,F10.0)
+ WRITE(NWRIT ,5110) XDIF1
2110 FORMAT(1H0, //,1X, 'TOTAL SUM OF ERRORS='F10.5)
+ WRITE(NWRIT ,5111) XDIF2
2111 FORMAT(1H0, //,40X, 'TOTAL SUM OF SQUARE ERRORS='F10.5)
+ WRITE(NWRIT ,5112) STD
2112 FORMAT(1H0, //,40X, 'STANDARD DEVIATION='F10.5)
+ IF(NOPLT.EQ.7) GO TO 10
KPLOT=0
K=I+KPLOT
DO 30 J=1,NDATA
BPLOT(K,J)=FWTLS(J)
BPLOT(K+6,J)=ETIME(J)
30 CONTINUE
10 CONTINUE
+ IF(NOPLT.EQ.7) GO TO 1000
PAUSE
DO 40 I=1,NCAVE
K=I+KPLOT
NPTS=NPR(I)
NVAR=-2**(K-7)-2**(K+5)
NX=K+6
CALL PICTR(BPLOT,IA,XLAB,XSCL,NVAR,NPTS,NX,MOVE,LABEL,ISCL,
+         FT,ME,LOOK)
+ LABEL=10
NPTS=NPA(I)
NVAR=-2**(I-7)-2**(I+5)
NX=I
CALL PICTR(BPLOT,IA,XLAB,XSCL,NVAR,NPTS,NX,MOVE,LABEL,ISCL,
+         FT,ME,LOOK)
+ LABEL=1000
40 CONTINUE
1000 CONTINUE
PAUSE
1111 CALL EXIT
END

```

DATA CARDS

LAMINAR FLOW - 1 -

(1)	(2)	(3)	(4)	(5)	(6)	(7)	(8)	(9)	(10)	(11)	(12)
LF	234	11	1222.	0.49	1.0	0.1421	0.1217	0.0489	0.0041	7.33	0.25
LF	233	11	1222.	0.49	2.0	0.1302	0.1116	0.0563	0.0055	2.24	0.25
LF	232	11	1222.	0.49	3.0	0.2301	0.1987	0.0540	0.0049	2.07	0.25
LF	231	11	1222.	0.49	4.0	0.2269	0.1934	0.0514	0.0046	1.14	0.25
LF	230	11	1222.	0.49	5.0	0.2177	0.1928	0.0536	0.0048	1.06	0.25
LF	229	11	1222.	0.49	5.0	0.3470	0.2982	0.0593	0.0057	1.50	0.25
LF	228	11	1222.	0.49	6.0	0.3655	0.3101	0.0683	0.0061	2.25	0.25
LF	227	11	1222.	0.49	7.0	0.3299	0.2981	0.0630	0.0058	1.36	0.25
LF	226	11	1222.	0.49	8.0	0.4214	0.3574	0.1104	0.0103	4.52	0.25
LF	225	11	1222.	0.49	9.0	0.4005	0.3531	0.0685	0.0064	2.00	0.25
LF	177	11	1262.	0.49	0.0	0.2455	0.2076	0.0566	0.0053	2.12	0.25
LF	178	11	1262.	0.49	0.0	0.2321	0.1979	0.0652	0.0059	0.29	0.25
LF	179	11	1262.	0.49	1.0	0.5108	0.4393	0.0793	0.0068	2.37	0.25
LF	181	11	1262.	0.49	3.0	0.4285	0.3182	0.1020	0.0103	1.37	0.25
LF	182	11	1262.	0.49	4.0	0.5572	0.3889	0.1000	0.0126	3.06	0.25
LF	183	11	1260.	0.49	5.0	0.4787	0.3344	0.0649	0.0072	1.41	0.25
LF	184	11	1260.	0.49	6.0	0.5544	0.3704	0.0497	0.0058	2.26	0.25
LF	185	11	1260.	0.49	7.0	0.6188	0.4054	0.0500	0.0057	3.05	0.25
LF	186	11	1260.	0.49	8.0	0.7152	0.4717	0.1000	0.0119	2.50	0.25
LF	187	11	1260.	0.49	9.0	0.4910	0.3347	0.0449	0.0053	1.42	0.25
LF	142	11	1510.	1.16	0.5	0.6038	0.4981	0.1106	0.0108	3.55	0.54
LF	112	11	1510.	1.16	1.5	0.7023	0.5519	0.1504	0.0142	4.36	0.54
LF	141	11	1510.	1.16	2.0	0.5251	0.3682	0.0407	0.0039	3.30	0.54
LF	111	11	1510.	1.16	2.5	0.6979	0.4974	0.1350	0.0142	4.23	0.54
LF	102	11	1510.	1.16	2.5	0.4126	0.2828	0.1978	0.0213	2.00	0.54
LF	143	11	1510.	1.16	3.0	0.6377	0.4928	0.0625	0.0078	4.11	0.54
LF	103	11	1510.	1.16	3.5	0.5413	0.3214	0.0961	0.0126	3.09	0.54
LF	105	11	1510.	1.16	3.5	0.6486	0.4064	0.1544	0.0177	3.50	0.54
LF	144	11	1510.	1.16	3.5	1.0225	0.6128	0.1928	0.0246	5.38	0.54
LF	104	11	1510.	1.16	4.5	0.5713	0.3527	0.0780	0.0093	2.38	0.54
LF	106	11	1510.	1.16	4.5	0.7385	0.4355	0.1022	0.0128	4.26	0.54
LF	130	11	1510.	1.16	4.5	0.7943	0.4395	0.0852	0.0111	4.57	0.54
LF	107	11	1510.	1.16	5.5	0.6713	0.3760	0.1080	0.0135	4.55	0.54
LF	108	11	1510.	1.16	6.5	0.3055	0.4446	0.1058	0.0139	5.09	0.54
LF	109	11	1510.	1.16	7.5	0.6896	0.3814	0.1129	0.0151	4.33	0.54
LF	110	11	1510.	1.16	8.5	0.7556	0.4153	0.0955	0.0124	5.21	0.54
LF	138	11	1510.	1.16	8.5	0.9527	0.4863	0.0536	0.0070	4.47	0.54
LF	146	11	1510.	0.28	5.0	1.0105	0.5503	0.1591	0.0223	7.52	0.28
LF	145	11	1510.	0.28	10.1	0.5120	0.2810	0.1000	0.0141	5.53	0.28
LF	126	11	1740.	1.71	0.0	0.2370	0.1900	0.1316	0.0112	1.36	0.86
LF	152	11	1740.	1.71	0.5	0.4478	0.3217	0.1000	0.0081	2.58	0.86

DATA CARDS LAMINAR FLOW - 2 -

(1)	(2)	(3)	(4)	(5)	(6)	(7)	(8)	(9)	(10)	(11)	(12)
LF	154	11	1740.	1.71	0.5	0.3355	0.2527	0.0000	0.0000	2.10	0.86
LF	124	11	1740.	1.71	1.0	0.4678	0.2942	0.0876	0.0095	3.16	0.86
LF	123	11	1740.	1.71	1.5	0.9446	0.5656	0.1634	0.0120	6.20	0.86
LF	122	11	1740.	1.71	2.0	0.9535	0.6008	0.2290	0.0269	4.10	0.86
LF	119	11	1740.	1.71	2.5	0.7668	0.4229	0.1214	0.0155	5.57	0.86
LF	118	11	1740.	1.71	3.0	0.7485	0.3960	0.0000	0.0000	5.29	0.86
LF	174	11	1740.	1.71	3.9	0.3600	0.1848	0.0322	0.0045	1.29	0.86
LF	175	11	1740.	1.71	3.9	0.2638	0.1273	0.0521	0.0071	1.40	0.86
LF	151	11	1740.	1.71	4.5	0.2724	0.1292	0.0467	0.0060	1.16	0.86
LF	150	11	1740.	1.71	5.0	0.2037	0.0931	0.0314	0.0041	1.01	0.86
LF	153	11	1740.	1.71	5.5	0.2187	0.1026	0.0255	0.0035	1.20	0.86
LF	172	11	1740.	1.71	5.9	0.2968	0.1528	0.0569	0.0083	1.29	0.86
LF	173	11	1740.	1.71	5.9	0.3148	0.1533	0.0280	0.0039	1.36	0.86
LF	116	11	1740.	1.71	6.0	0.2974	0.1486	0.1010	0.0136	1.45	0.86
LF	115	11	1740.	1.71	7.0	0.3275	0.1573	0.0581	0.0081	2.09	0.86
LF	114	11	1740.	1.71	8.0	0.7702	0.3819	0.0956	0.0132	5.05	0.86
LF	163	11	1740.	1.71	9.0	0.1751	0.0828	0.0092	0.0014	1.00	0.86
LF	169	11	1740.	1.71	9.0	0.1974	0.0857	0.0176	0.0026	0.46	0.86
LF	170	11	1740.	1.71	9.0	0.3885	0.1885	0.0487	0.0074	1.45	0.86
LF	171	11	1740.	1.71	9.0	0.2994	0.1434	0.0427	0.0063	1.30	0.86
LF	176	11	1740.	0.28	5.9	0.2249	0.1047	0.0221	0.0032	1.07	0.28
LF	134	11	1940.	2.50	0.5	0.3541	0.2764	0.2304	0.0204	2.16	0.83
LF	166	11	1940.	2.50	2.0	0.4797	0.3145	0.1000	0.0096	4.14	0.83
LF	133	11	1940.	2.50	1.0	0.5298	0.3165	0.1054	0.0114	2.40	0.83
LF	132	11	1940.	2.50	1.5	0.3684	0.2165	0.1411	0.0177	3.20	0.83
LF	131	11	1940.	2.50	2.0	0.4914	0.2355	0.1000	0.0135	1.40	0.83
LF	165	11	1940.	2.50	3.0	0.2392	0.1204	0.0339	0.0046	1.13	0.83
LF	164	11	1940.	2.50	4.0	0.2547	0.1159	0.0364	0.0051	1.49	0.83
LF	163	11	1940.	2.50	5.0	0.2879	0.1161	0.0295	0.0040	2.37	0.83
LF	135	11	1940.	2.50	6.0	0.3496	0.1376	0.0000	0.0000	2.40	0.83
LF	138	11	1940.	2.50	7.0	0.2198	0.0878	0.0594	0.0084	1.06	0.83
LF	136	11	1940.	2.50	9.0	0.3778	0.1441	0.0739	0.0100	2.40	0.83
LF	137	11	1940.	2.50	9.0	0.2449	0.1032	0.0645	0.0090	1.03	0.83
LF	162	11	1940.	2.50	9.0	0.2037	0.0810	0.1000	0.0126	2.20	0.83
LF	167	11	1940.	2.50	9.0	0.2247	0.0961	0.0000	0.0000	1.22	0.83
LF	205	11	2100.	2.50	0.0	0.1411	0.1130	0.0263	0.0024	1.05	0.83
LF	204	11	2100.	2.50	0.8	0.3059	0.2372	0.0133	0.0011	4.36	0.83
LF	203	11	2100.	2.50	1.8	0.1598	0.0995	0.1000	0.0089	1.53	0.83
LF	206	11	2100.	2.50	1.8	0.1413	0.0917	0.0330	0.0029	0.51	0.83
LF	202	11	2100.	2.50	2.8	0.1554	0.0756	0.1000	0.0162	1.25	0.83
LF	201	11	2100.	2.50	3.8	0.1881	0.0810	0.0000	0.0000	1.32	0.83
LF	209	11	2100.	2.50	5.8	0.1438	0.0606	0.0227	0.0028	0.23	0.83

DATA CARDS LAMINAR FLOW - 3 -

(1)	(2)	(3)	(4)	(5)	(6)	(7)	(8)	(9)	(10)	(11)	(12)
LF	200	11	2100.	2.50	8.3	0.1552	0.0596	0.0146	0.0021	0.29	0.83
LF	208	11	2100.	2.50	8.8	0.1095	0.0396	0.0000	0.0000	1.08	0.83
LF	207	11	2100.	2.50	8.8	0.1551	0.0566	0.1000	0.0163	0.56	0.83
LF	224	21	1000.	0.49	0.0	0.2074	0.1983	0.0259	0.0023	0.57	0.25
LF	223	21	1000.	0.49	1.0	0.2618	0.2530	0.0676	0.0063	1.07	0.25
LF	222	21	1000.	0.49	2.0	0.4628	0.4584	0.1089	0.0100	3.01	0.25
LF	221	21	1000.	0.49	3.0	0.3674	0.3534	0.1103	0.0106	2.01	0.25
LF	219	21	1000.	0.49	5.0	0.4164	0.3837	0.0727	0.0067	3.30	0.25
LF	218	21	1000.	0.49	6.0	0.4509	0.4184	0.0918	0.0088	3.25	0.25
LF	217	21	1000.	0.49	7.0	0.4655	0.4217	0.0467	0.0044	7.03	0.25
LF	216	21	1000.	0.49	8.0	0.4122	0.3720	0.0702	0.0069	4.02	0.25
LF	215	21	1000.	0.49	9.0	0.3108	0.2859	0.0000	0.0000	4.58	0.25
LF	199	21	1260.	0.49	0.0	0.5363	0.5007	0.0973	0.0095	4.53	0.25
LF	198	21	1260.	0.49	0.9	0.5592	0.5314	0.0623	0.0058	4.53	0.25
LF	197	21	1260.	0.49	1.9	0.2700	0.2390	0.0478	0.0063	2.17	0.25
LF	196	21	1260.	0.49	2.9	0.1894	0.1649	0.0000	0.0000	1.51	0.25
LF	195	21	1260.	0.49	3.9	0.1970	0.1643	0.0379	0.0054	1.58	0.25
LF	194	21	1260.	0.49	4.9	0.2614	0.1947	0.1000	0.0146	3.22	0.25
LF	193	21	1260.	0.49	5.9	0.2351	0.1752	0.0323	0.0045	1.25	0.25
LF	191	21	1260.	0.49	7.9	0.2424	0.1765	0.1000	0.0149	1.30	0.25
LF	188	21	1260.	0.49	8.9	0.2811	0.2092	0.0274	0.0042	1.45	0.25
LF	186	21	1260.	0.49	8.9	0.2626	0.1816	0.0203	0.0033	1.58	0.25
LF	211	21	1510.	1.16	0.0	0.1762	0.1630	0.0298	0.0032	1.59	0.54
LF	210	21	1510.	1.16	0.9	0.1424	0.1308	0.0403	0.0039	1.35	0.54
LF	246	21	1510.	1.16	1.8	0.1818	0.1652	0.0491	0.0053	1.03	0.54
LF	247	21	1510.	1.16	1.8	0.1544	0.1341	0.0000	0.0000	0.48	0.54
LF	209	21	1510.	1.16	1.9	0.1607	0.1376	0.1000	0.0121	1.12	0.54
LF	244	21	1510.	1.16	2.8	0.1652	0.1312	0.0435	0.0057	1.06	0.54
LF	245	21	1510.	1.16	2.8	0.1993	0.1547	0.0370	0.0047	1.08	0.54
LF	208	21	1510.	1.16	2.9	0.1533	0.1192	0.0000	0.0000	1.01	0.54
LF	242	21	1510.	1.16	3.8	0.1031	0.0690	0.0301	0.0047	0.44	0.54
LF	243	21	1510.	1.16	3.8	0.1879	0.1394	0.0292	0.0041	1.24	0.54
LF	207	21	1510.	1.16	3.9	0.2083	0.1451	0.1000	0.0149	2.07	0.54
LF	206	21	1510.	1.16	4.9	0.2031	0.1393	0.0368	0.0063	2.02	0.54
LF	248	21	1510.	1.16	5.8	0.1869	0.1204	0.0411	0.0027	15.23	0.54
LF	253	21	1510.	1.16	5.8	0.1854	0.1239	0.0293	0.0056	2.10	0.54
LF	255	21	1510.	1.16	5.8	0.1627	0.1162	0.0592	0.0087	1.28	0.54
LF	205	21	1510.	1.16	5.9	0.2094	0.1497	0.0353	0.0060	2.01	0.54
LF	204	21	1510.	1.16	6.9	0.1755	0.1177	0.0254	0.0044	1.05	0.54
LF	240	21	1510.	1.16	7.9	0.1384	0.0877	0.0185	0.0034	1.22	0.54
LF	238	21	1510.	1.16	8.8	0.1364	0.0875	0.0185	0.0035	1.00	0.54

DATA CARDS

LAMINAR FLOW

- 4 -

(1)	(2)	(3)	(4)	(5)	(6)	(7)	(8)	(9)	(10)	(11)	(12)
LF	239	21	1510.	1.16	8.2	0.1486	0.0277	0.0389	0.0077	1.39	0.54
LF	291	21	1510.	1.16	8.3	0.1977	0.1306	0.1000	0.0196	2.08	0.54
LF	200	21	1510.	1.16	9.9	0.2467	0.1524	0.0400	0.0079	3.16	0.54
LF	278	21	1740.	1.71	0.0	0.0965	0.0825	0.0000	0.0000	1.38	0.86
LF	276	21	1740.	1.71	0.2	0.0688	0.0579	0.0208	0.0020	0.30	0.86
LF	275	21	1740.	1.71	1.2	0.0641	0.0546	0.0236	0.0022	0.29	0.86
LF	274	21	1740.	1.71	2.2	0.0508	0.0352	0.1000	0.0160	0.25	0.86
LF	279	21	1740.	1.71	2.2	0.0591	0.0425	0.0000	0.0000	0.27	0.86
LF	284	21	1740.	1.71	2.2	0.0460	0.0328	0.0000	0.0000	0.19	0.86
LF	273	21	1740.	1.71	3.2	0.0552	0.0356	0.1000	0.0181	0.27	0.86
LF	280	21	1740.	1.71	3.2	0.0442	0.0276	0.0000	0.0000	0.22	0.86
LF	272	21	1740.	1.71	4.2	0.0642	0.0367	0.0087	0.0020	0.27	0.86
LF	271	21	1740.	1.71	6.2	0.0910	0.0573	0.0091	0.0017	0.38	0.86
LF	270	21	1740.	1.71	8.2	0.1226	0.0701	0.0000	0.0000	0.57	0.86
LF	282	21	1740.	1.71	8.2	0.0599	0.0356	0.1000	0.0205	0.29	0.86
LF	265	21	1940.	2.52	0.2	0.1431	0.1301	0.0526	0.0048	1.42	0.83
LF	264	21	1940.	2.52	0.9	0.0476	0.0382	0.0161	0.0017	0.19	0.83
LF	266	21	1940.	2.52	1.2	0.0705	0.0568	0.0000	0.0000	0.39	0.83
LF	263	21	1940.	2.52	1.8	0.0832	0.0637	0.1000	0.0225	0.40	0.83
LF	267	21	1940.	2.52	2.2	0.0542	0.0338	0.1000	0.0241	0.27	0.83
LF	262	21	1940.	2.52	2.2	0.1052	0.0515	0.0175	0.0032	0.50	0.83
LF	268	21	1940.	2.52	3.2	0.0464	0.0270	0.0000	0.0000	0.24	0.83
LF	269	21	1940.	2.52	4.2	0.0445	0.0234	0.0000	0.0000	0.21	0.83
LF	260	21	1940.	2.52	5.2	0.1142	0.0546	0.0000	0.0000	1.00	0.83
LF	261	21	1940.	2.52	5.2	0.0840	0.0385	0.1000	0.0236	0.46	0.83
LF	295	21	2100.	2.52	0.0	0.0628	0.0500	0.0229	0.0021	0.30	0.83
LF	294	21	2100.	2.52	0.9	0.0641	0.0493	0.0191	0.0019	0.37	0.83
LF	293	21	2100.	2.52	1.2	0.0707	0.0473	0.1000	0.0188	0.41	0.83
LF	296	21	2100.	2.52	1.2	0.0645	0.0417	0.0000	0.0000	0.37	0.83
LF	291	21	2100.	2.52	2.2	0.0999	0.0561	0.1000	0.0208	1.16	0.83
LF	292	21	2100.	2.52	2.2	0.0806	0.0450	0.0000	0.0000	0.44	0.83
LF	288	21	2100.	2.52	3.2	0.1354	0.0703	0.0212	0.0043	1.13	0.83
LF	286	21	2100.	2.52	5.2	0.1047	0.0447	0.1000	0.0304	1.02	0.83
LF	285	21	2100.	2.52	8.2	0.0545	0.0229	0.0000	0.0000	0.26	0.83

DATA CARDS

FREE FALL - 1 -

(1)	(2)	(3)	(4)	(5)	(6)	(7)	(8)	(9)	(10)	(11)	(12)	
FF	703	11	647.	0.9940	0.4937	0.2239	0.0189	0.4730	0.0337	0.0011	9.30	0
FF	702	11	657.	0.9979	0.4949	0.3045	0.0183	0.4679	0.0460	0.0007	7.00	0
FF	602	11	747.	1.0062	0.4956	0.3536	0.0081	0.5042	0.0573	0.0020	10.00	1
FF	706	11	707.	0.9956	0.4356	0.3321	0.0278	0.4844	0.0533	0.0038	8.55	0
FF	707	11	707.	1.0024	0.4548	0.2413	0.0473	0.3956	0.0424	0.0048	5.50	0
FF	608	11	837.	1.1316	0.5282	0.3125	0.0283	0.4759	0.0512	0.0041	7.30	0
FF	609	11	837.	1.0313	0.4701	0.2406	0.0163	0.4553	0.0401	0.0024	11.45	0
FF	708	11	997.	1.0113	0.3866	0.1765	0.0414	0.3450	0.0325	0.0124	9.45	0
FF	700	11	1007.	1.0047	0.3829	0.1964	0.0347	0.3482	0.0365	0.0056	9.35	0
FF	613	11	1017.	1.0225	0.3819	0.3351	0.0409	0.3418	0.0577	0.0047	6.30	0
FF	612	11	1027.	0.9951	0.3866	0.3460	0.0365	0.3562	0.0602	0.0036	7.30	0
FF	712	11	1107.	1.0012	0.3455	0.1419	0.0685	0.2743	0.0250	0.0107	12.50	0
FF	710	11	1207.	0.9900	0.0000	0.1484	0.0582	0.0000	0.0238	0.0149	0.00	0
FF	713	11	1207.	0.0000	0.0000	0.0654	0.1212	0.0000	0.0112	0.0258	0.00	0
FF	711	11	1217.	0.0000	0.0000	0.0967	0.1056	0.0000	0.0161	0.0212	0.00	0
FF	725	11	1287.	0.0000	0.0000	0.0823	0.0307	0.0000	0.0136	0.0058	0.00	0
FF	617	11	1297.	0.0000	0.0000	0.1780	0.0474	0.0000	0.0288	0.0113	0.00	0
FF	618	11	1327.	0.0000	0.0000	0.0000	0.0165	0.0000	0.0000	0.0032	0.00	0
FF	715	21	617.	0.0000	0.0000	0.0667	0.0000	0.0000	0.0138	0.0000	0.00	0
FF	704	21	647.	0.2000	0.0000	0.1520	0.0000	0.0000	0.0312	0.0000	0.00	0
FF	705	21	677.	0.0000	0.0000	0.2108	0.0000	0.0000	0.0416	0.0000	0.00	0
FF	601	21	737.	0.0000	0.0000	0.1412	0.0000	0.0000	0.0300	0.0000	0.00	1
FF	605	21	737.	1.0557	0.5147	0.2881	0.0510	0.4617	0.0591	0.0272	10.50	1
FF	701	21	737.	0.7541	0.4015	0.1291	0.0724	0.3258	0.0250	0.0093	5.57	1
FF	606	21	747.	0.0000	0.0000	0.1678	0.0000	0.0000	0.0334	0.0000	0.00	1
FF	718	21	777.	0.9994	0.5657	0.3136	0.0720	0.4935	0.0647	0.0219	10.15	0
FF	719	21	797.	0.9997	0.5481	0.2433	0.1140	0.4326	0.0513	0.0076	5.40	0
FF	720	21	787.	0.9992	0.5639	0.1396	0.1657	0.3970	0.0301	0.0145	6.55	0
FF	610	21	837.	0.9345	0.4896	0.2044	0.0742	0.4162	0.0407	0.0069	4.30	0
FF	611	21	837.	1.1710	0.5998	0.1828	0.0790	0.5300	0.0366	0.0067	5.30	0
FF	616	21	1007.	0.9937	0.5281	0.2356	0.0837	0.4419	0.0519	0.0074	7.30	0
FF	721	21	1007.	0.9961	0.4698	0.3361	0.0362	0.4319	0.0772	0.0035	8.10	0
FF	722	21	1007.	1.0019	0.4805	0.2164	0.1181	0.3615	0.0494	0.0157	8.00	0
FF	614	21	1017.	0.9658	0.5023	0.1695	0.1750	0.3255	0.0385	0.0248	6.00	0
FF	723	21	1297.	0.0000	0.0000	0.1891	0.0987	0.0000	0.0378	0.0142	0.00	0
FF	620	21	1317.	0.0000	0.0000	0.0866	0.0231	0.0000	0.0163	0.0078	0.00	0
FF	724	21	1327.	0.0000	0.0000	0.0762	0.0508	0.0000	0.0167	0.0080	0.00	0
FF	503	21	657.	0.8730	0.5535	0.5182	0.0395	0.5107	0.0905	0.0029	11.40	0
FF	504	21	667.	0.8178	0.5412	0.1643	0.0358	0.5057	0.0277	0.0031	10.10	0
FF	502	21	677.	0.7467	0.4625	0.4308	0.0235	0.4412	0.0790	0.0010	11.10	0
FF	510	21	837.	0.8734	0.5536	0.3795	0.0495	0.5033	0.0695	0.0011	13.00	0
FF	509	21	827.	0.8410	0.5401	0.0953	0.0367	0.5034	0.0173	0.0000	9.00	0

DATA CARDS

FREE FALL - 2 -

(1)	(2)	(3)	(4)	(5)	(6)	(7)	(8)	(9)	(10)	(11)	(12)	
FF	511	21	1017.	0.0276	0.5573	0.2255	0.0600	0.4961	0.0458	0.0060	4.25	0
FF	512	21	1017.	0.8927	0.5261	0.2188	0.0829	0.4419	0.0428	0.0078	8.30	0
FF	517	21	1157.	0.0000	0.0000	0.0922	0.0700	0.0000	0.0178	0.0000	0.00	0
FF	505	11	657.	0.5863	0.3571	0.2083	0.0734	0.3547	0.0295	0.0008	9.00	0
FF	506	11	657.	0.8932	0.5389	0.3416	0.0056	0.5338	0.0505	0.0000	14.00	0
FF	507	11	827.	0.6945	0.4739	0.2457	0.0147	0.4623	0.0390	0.0020	8.00	0
FF	508	11	827.	0.7192	0.3910	0.2324	0.0147	0.3778	0.0371	0.0019	12.00	0
FF	513	11	1027.	0.8011	0.4024	0.2340	0.0364	0.3666	0.0392	0.0042	8.00	0
FF	514	11	1027.	0.9628	0.4802	0.2935	0.0513	0.4310	0.0497	0.0086	11.30	0
FF	516	11	1197.	0.9171	0.3979	0.2212	0.0544	0.3423	0.0340	0.0113	8.30	0
FF	515	11	1197.	0.9170	0.3810	0.2165	0.0494	0.3297	0.0343	0.0104	9.00	0

DATA CARDS

411

CRUCIBLE - 1 -

(1)	(2)	(3)	(4)	(5)	(6)	(7)	(8)	(9)	(10)	(11)
CF	203	11	337.	2.5850	1.0484	0.0000	0.0000	0.0000	0.0000	1
CF	205	11	337.	2.0556	1.5406	0.2025	0.0229	0.0000	0.0000	1
CF	209	11	447.	2.5960	1.7070	0.2218	0.0269	0.0000	0.0000	1
CF	208	11	467.	3.4930	2.2213	0.1565	0.0198	0.0000	0.0000	1
CF	242	11	457.	1.0395	0.6711	0.0023	0.0004	0.2368	0.0278	1
CF	243	11	457.	1.0710	0.6778	0.0002	0.0000	0.3922	0.0455	1
CF	264	11	467.	1.0591	0.6746	0.0002	0.0000	0.2798	0.0341	1
CF	265	11	467.	1.0223	0.6574	0.0025	0.0005	0.2082	0.0246	1
CF	258	11	557.	1.0754	0.6295	0.0020	0.0003	0.6234	0.0813	0
CF	259	11	557.	1.0482	0.6196	0.0021	0.0003	0.6163	0.0792	0
CF	247	11	667.	1.0633	0.5660	0.0001	0.0000	0.2671	0.0368	0
CF	267	11	677.	1.0081	0.5446	0.0012	0.0002	0.2846	0.0409	0
CF	279	11	677.	1.0097	0.5432	0.0008	0.0001	0.1582	0.0227	0
CF	246	11	677.	1.0377	0.5518	0.0001	0.0000	0.2245	0.0314	0
CF	202	11	837.	1.0137	0.5329	0.0028	0.0007	0.3444	0.0509	0
CF	204	11	857.	1.0020	0.5280	0.0030	0.0008	0.3414	0.0509	0
CF	283	11	947.	1.0062	0.5162	0.0038	0.0005	0.2945	0.0436	0
CF	284	11	947.	1.0048	0.5170	0.0028	0.0006	0.2673	0.0397	0
CF	277	11	947.	0.6674	0.3441	0.0001	0.0000	0.1328	0.0199	1
CF	281	11	947.	0.7132	0.3618	0.0001	0.0000	0.2147	0.0322	1
CF	219	11	957.	0.9733	0.5063	0.0024	0.0003	0.2702	0.0400	0
CF	220	11	957.	1.1080	0.5757	0.0012	0.0001	0.3432	0.0514	0
CF	231	11	1037.	1.0128	0.5131	0.0019	0.0003	0.2339	0.0349	0
CF	233	11	1037.	0.9985	0.5015	0.0048	0.0003	0.2281	0.0348	0
CF	234	11	1077.	1.0534	0.5325	0.0013	0.0004	0.5307	0.0793	1
CF	238	11	1307.	1.0020	0.4948	0.0055	0.0006	0.2937	0.0443	0
CF	239	11	1307.	1.0010	0.4939	0.0058	0.0011	0.2977	0.0443	0
CF	289	11	1307.	1.0102	0.4862	0.0181	0.0072	0.2585	0.0351	1
CF	262	11	1467.	1.0198	0.4797	0.0134	0.0061	0.2322	0.0311	0
CF	263	11	1467.	1.0778	0.5102	0.0110	0.0048	0.3850	0.0528	0
CF	404	11	1727.	0.4828	0.2192	0.2156	0.0257	0.0000	0.0000	0
CF	405	11	1727.	0.4962	0.2257	0.2236	0.0300	0.0000	0.0000	0
CF	409	11	1827.	0.3962	0.1700	0.1687	0.0084	0.0000	0.0000	0
CF	410	11	1827.	0.4993	0.2152	0.2153	0.0100	0.0000	0.0000	0
CF	220	11	957.	1.1080	0.5757	0.0012	0.0001	0.3432	0.0514	0
CF	283	11	947.	1.0062	0.5162	0.0038	0.0005	0.2945	0.0436	0
CF	284	11	947.	1.0048	0.5170	0.0028	0.0006	0.2673	0.0397	0
CF	219	11	957.	0.9733	0.5063	0.0024	0.0003	0.2702	0.0400	0
CF	222	11	957.	0.1396	0.0747	0.0006	0.0001	0.0729	0.0108	0
CF	224	11	957.	0.0644	0.0347	0.0001	0.0000	0.0343	0.0049	0
CF	225	11	967.	0.0565	0.0312	0.0007	0.0000	0.0307	0.0045	0
CF	254	11	947.	0.0318	0.0165	0.0001	0.0000	0.0164	0.0026	1
CF	270	11	947.	0.0214	0.0116	0.0002	0.0000	0.0113	0.0016	1
CF	272	11	947.	0.0199	0.0109	0.0006	0.0000	0.0123	0.0017	1

DATA CARDS

CRUCIBLE

- 2 -

(1)	(2)	(3)	(4)	(5)	(6)	(7)	(8)	(9)	(10)	(11)
CP	252	11	947.	0.0173	0.00288-0.00004	0.00000	0.00090	0.0016		1
CP	253	11	947.	0.0171	0.00283-0.00002	0.00000	0.00087	0.0013		1
CP	260	11	947.	0.0138	0.00278	0.00001	0.00000	0.0077	0.0011	1
CP	271	11	947.	0.0111	0.00253-0.00004	0.00000	0.00057	0.0008		1
CR	255	11	947.	0.0105	0.00250-0.00006	0.00000	0.00056	0.0009		1
CP	261	21	247.	2.3967	2.2276	0.1220	0.0134	0.0000	0.0000	1
CP	264	21	327.	2.5698	2.2773	0.1441	0.0166	0.0000	0.0000	1
CP	262	21	347.	2.7934	2.5497	0.0000	0.0000	0.0000	0.0000	1
CP	277	21	467.	3.1913	2.3417	0.1907	0.0274	0.0000	0.0000	1
CR	240	21	457.	1.0617	0.7942	0.0096	0.0006	0.4616	0.0657	1
CR	241	21	457.	1.0549	0.7743	0.0124	0.0014	0.4064	0.0579	1
CP	266	21	467.	1.0114	0.7546	0.0098	0.0015	0.2628	0.0369	1
CR	256	21	557.	1.0151	0.6987	0.0382	0.0058	0.6461	0.1002	0
CP	257	21	557.	1.0071	0.6851	0.0272	0.0042	0.6395	0.0987	0
CP	244	21	677.	1.0678	0.6748	0.0098	0.0010	0.2979	0.0500	0
CP	245	21	677.	1.1099	0.6962	0.0071	0.0008	0.3288	0.0542	0
CP	263	21	677.	1.0466	0.6641	0.0270	0.0043	0.3505	0.0590	0
CP	280	21	677.	1.0034	0.6344	0.0126	0.0021	0.1867	0.0316	0
CR	271	21	237.	1.0034	0.6233	0.0109	0.0006	0.6102	0.1063	0
CR	202	21	227.	3.0025	1.8530	0.0370	0.0031	1.0486	0.1858	0
CR	205	21	247.	0.9006	0.5575	0.0146	0.0006	0.2544	0.0442	0
CR	278	21	947.	0.6391	0.4114	0.0001	0.0000	0.2643	0.0428	1
CP	282	21	947.	0.6782	0.4111	0.0001	0.0000	0.2593	0.0454	1
CR	285	21	947.	1.0243	0.6227	0.0372	0.0058	0.3446	0.0610	0
CP	286	21	947.	1.0068	0.6092	0.0289	0.0035	0.2504	0.0442	0
CP	206	21	957.	1.2212	0.7485	0.0167	0.0007	0.3319	0.0587	0
CR	227	21	957.	2.2859	1.3879	0.0325	0.0027	0.7913	0.1403	0
CR	229	21	1037.	1.0672	0.6605	0.0473	0.0034	0.3347	0.0592	0
CP	220	21	1037.	0.9598	0.5889	0.0280	0.0010	0.3704	0.0661	0
CP	227	21	1047.	0.9879	0.6084	0.0374	0.0023	0.2958	0.0532	0
CP	228	21	1047.	1.2396	0.7564	0.0328	0.0015	0.2937	0.0526	0
CP	226	21	1057.	1.0511	0.6316	0.0100	0.0013	0.6203	0.1108	1
CP	236	21	1297.	0.9819	0.6010	0.0504	0.0024	0.3203	0.0557	0
CP	235	21	1307.	1.0166	0.6111	0.0330	0.0036	0.3553	0.0592	0
CP	237	21	1307.	1.0135	0.6135	0.0557	0.0045	0.3356	0.0586	0
CP	288	21	1327.	1.0015	0.5794	0.0540	0.0111	0.3141	0.0490	1
CP	264	21	1467.	1.0273	0.5868	0.0341	0.0021	0.2423	0.0369	0
CP	261	21	1467.	1.0040	0.5626	0.0298	0.0024	0.3044	0.0463	0
CR	427	21	1727.	0.5553	0.2729	0.2642	0.0338	0.0000	0.0000	0
CR	428	21	1727.	0.5338	0.2754	0.2678	0.0351	0.0000	0.0000	0
CR	414	21	1827.	0.4450	0.2267	0.2185	0.0263	0.0000	0.0000	0
CR	415	21	1827.	0.4563	0.2328	0.2235	0.0273	0.0000	0.0000	0
CP	267	21	957.	2.2859	1.3879	0.0325	0.0027	0.7913	0.1403	0

DATA CARDS

CRUCIBLE - 3 -

(1)	(2)	(3)	(4)	(5)	(6)	(7)	(8)	(9)	(10)	(11)
CR	206	21	957.	1.2212	0.7485	0.0167	0.0007	0.3319	0.0587	0
CR	285	21	947.	1.0243	0.6227	0.0372	0.0058	0.3446	0.0610	0
CR	286	21	947.	1.0268	0.6092	0.0289	0.0035	0.2504	0.0442	0
CR	208	21	957.	0.5076	0.3142	0.0090	0.0003	0.1478	0.0260	0
CR	220	21	957.	0.1719	0.1089	0.0058	0.0006	0.1030	0.0180	0
CR	214	21	967.	0.0667	0.0440	0.0049	0.0002	0.0387	0.0068	0
CR	211	21	967.	0.0665	0.0435	0.0088	0.0009	0.0350	0.0061	0
CR	216	21	967.	0.0549	0.0365	0.0037	0.0003	0.0326	0.0056	0
CR	215	21	967.	0.0259	0.0175	0.0031	0.0001	0.0146	0.0028	0
CR	212	21	947.	0.0250	0.0161	0.0080	0.0012	0.0085	0.0017	0
CR	217	21	957.	0.0224	0.0149	0.0017	0.0001	0.0130	0.0024	0
CR	213	21	937.	0.0218	0.0139	0.0037	0.0006	0.0100	0.0019	0
CR	249	21	947.	0.0285	0.0165	0.0001	0.0000	0.0164	0.0030	1
CR	273	21	947.	0.0246	0.0146	0.0002	0.0000	0.0144	0.0031	1
CR	250	21	947.	0.0213	0.0119	0.0004	0.0000	0.0122	0.0027	1
CR	275	21	947.	0.0192	0.0116	0.0001	0.0000	0.0115	0.0021	1
CR	276	21	947.	0.0163	0.0085	0.0002	0.0000	0.0087	0.0018	1
CR	248	21	947.	0.0146	0.0090	0.0004	0.0000	0.0086	0.0017	1
CR	274	21	947.	0.0115	0.0070	0.0002	0.0000	0.0068	0.0012	1
CR	106	11	657.	1.1668	0.7410	0.7410	0.1018	0.0000	0.0000	0
CR	107	11	657.	0.8385	0.5357	0.5357	0.0735	0.0000	0.0000	0
CR	109	11	817.	0.8704	0.5292	0.5292	0.0765	0.0000	0.0000	0
CR	110	11	817.	0.8025	0.4828	0.4828	0.0718	0.0000	0.0000	1
CR	111	11	817.	0.8391	0.5032	0.5032	0.0746	0.0000	0.0000	0
CR	114	11	1057.	0.9991	0.5854	0.5854	0.0876	0.0000	0.0000	0
CR	115	11	1057.	1.4575	0.8583	0.4688	0.0691	0.0000	0.0000	0
CR	118	11	1307.	0.9666	0.5419	0.2662	0.0397	0.0000	0.0000	0
CR	119	11	1307.	0.9380	0.5255	0.3160	0.0475	0.0000	0.0000	0
CR	122	11	1487.	1.0702	0.5919	0.5888	0.0821	0.0000	0.0000	0
CR	123	11	1487.	1.0474	0.5804	0.5804	0.0818	0.0000	0.0000	0
CR	101	21	657.	0.8052	0.5579	0.5579	0.0858	0.0000	0.0000	0
CR	122	21	657.	0.6721	0.4631	0.4631	0.0725	0.0000	0.0000	0
CR	103	21	657.	0.8782	0.5997	0.5997	0.0943	0.0000	0.0000	1
CR	112	21	817.	0.8417	0.5610	0.5610	0.0899	0.0000	0.0000	0
CR	113	21	817.	0.7149	0.4743	0.4743	0.0762	0.0000	0.0000	0
CR	117	21	1057.	0.9758	0.6294	0.6294	0.1041	0.0000	0.0000	0
CR	116	21	1057.	1.0392	0.6621	0.6621	0.1127	0.0000	0.0000	1
CR	120	21	1307.	0.9421	0.5529	0.5413	0.0713	0.0000	0.0000	0
CR	121	21	1307.	0.9822	0.5807	0.5369	0.0767	0.0000	0.0000	0
CR	124	21	1487.	0.8337	0.4793	0.4712	0.0693	0.0000	0.0000	0
CR	125	21	1487.	1.0203	0.5815	0.5815	0.0872	0.0000	0.0000	0

REFERENCES

- Anthony, D. B., Howard, J. B., Hottel, H. C., and Meissner, H. P., "Rapid Devolatilization and Hydrogasification of Bituminous Coal," 170th National Meeting, Amer. Chem. Soc., Chicago, Aug. (1975)
- Anthony, D. B., et al., "Rapid Devolatilization of Pulverized Coal," Proc. 15th Internat. Symp. on Combustion, The Combustion Institute, Pittsburgh, 1303 (1975)
- Anthony, D. B., "Rapid Devolatilization and Hydrogasification of Puvrized Coal," Sc.D. Thesis, Dept. Chem. Engr., M.I.T., Jan. (1974)
- Badzioch, S., and Hawksley, P.G.W., "Kinetics of Thermal Decomposition of Pulverized Coal Particles," Ind. Eng. Chem. Process Design Develop., 9, 82, Aug. (1970)
- Badzioch, S., Sainsbury, R. B., and Hawksley, P.G.W., BCURA Member's Information Circular, No. 340 (1968)
- Badzioch, S., "Thermal Decomposition," BCURA Monthly Bulletin, 31, 4, 193 (1967)
- Badzioch, S., Gregory, D. R., and Field, M. A., "Investigation of the Temperature Variation of the Thermal Conductivity and Thermal Diffusion of Coal," Fuel, 43,
- Badzioch, S., "Rapid and Controlled Decomposition of Coal," BCURA Monthly Bulletin, 35, 8, 285 (1961)
- Benson, S., Thermochemical Kinetics, John Wiley & Sons, N.Y. (1968)
- Benson, S. W., and O'Neal, H. E., "Kinetic Data on Gas Phase Unimolecular Reactions," NSRDS-NBS, 21 (1970)
- Berkowitz, N., "Mechanism of Coal Pyrolysis, I," Fuel, 39, 47 (1960)
- Berkowitz, N., and Den Hertog, W., "Mechanisms of Coal Pyrolysis, V," Fuel, 41, 507 (1962)
- Billington, A. H., Dryden, I.G.C., and Napier, D. H., BCURA Bulletin, 16, 258 (1952)
- Bond, R. L., Ladner, W. R., and Wheatley, R., " ESR of Rapidly Heated Coals," Fuel, 47, 213 (1968)

- Bond, R. L., Ladner, W. R., and McCornell, G.I.T., "Reaction of Coal under Conditions of High Energy Input and High Temperature," Coal Science, Advances in Chemistry Services, 55, Amer. Chem. Soc. (1966)
- Bond, R. L., et al., "Production of Acetylen from Coal using a Plasma Jet," Nature, 200, p. 1313, Dec. (1963)
- Boyer, M.S.F., Compt. Rend. Assoc. Tech. de l'Indus. du gaz en France Congres, 653 (1952) as reported by Yellow, P. C., BCURA, Monthly Bulletin, 29, 285 (1965)
- Brown, J. K., "The Infrared Spectra of Coals," J. Chem. Soc., London, p. 744 (1955)
- Brown, J. K., "Infrared Studies of Carbonized Coals," J. Chem. Soc., London, p. 752 (1955)
- Carslaw, H. S., and Jaegger, J. C., Conduction of Heat in Solids, 2nd Ed., Oxford University Press (1959)
- Chakrabartty, S. K., and Berkowitz, N., "Studies on the Structure of Coals. 3. Some Inferences About Skeletal Structures," Fuel, 53, 240 (1974)
- Chakrabartty, S. K., and Kretschmer, H. O., "Studies on the Structure of Coals. 2. The Valence State of Carbon in Coal," Fuel, 53, 132 (1974)
- Chakrabartty, S. K., and Kretschmer, H. O., "Studies on the Structure of Coals. Part 1. The Nature of Aliphatic Groups," Fuel, 51, 160 (1972)
- Cheong, P. H., Oka, H., and Gavalas, G. R., "Modeling and Experimental Studies of Coal Pyrolysis," NSF Workshop on Fundamental Organic Chemistry of Coal, Knoxville, TN, July (1975)
- Chermin, H.A.G., and Van Krevelen, D. W., "Chemical Structure and Properties of Coal XVII - A Mathematical Model of Coal Pyrolysis," Fuel, 36, 85 (1957)

- Chukhanov, Z. F., Izv. Akad. SSSR, Otd Tekh, Nauk, 8, 7 (1954), quoted by Yellow (1965) and Jones (1964)
- Coates, R. L., Chen, L. L., and Pope, B. J., "Coal Devolatilization in a Low Pressure, Low Residence Time Entrained Flow Reactor," Coal Gasification, Chap.7, Advances in Chemistry Series No. 131 (L. G. Massey, ed.) Amer. Chem. Soc. (1974)
- Den Hertog, W., and Berkowitz, N., "Mechanisms of Coal Pyrolysis II," Fuel, 39, 125 (1960)
- Dryden, I.G.C., "Chemical Constitution and Reactions of Coal," Chemistry of Coal Utilization, Supplementary Vol., p. 232 (H. H. Lowry, ed.) John Wiley & Sons, N.Y. (1963)
- Dryden, I.G.C., and Joy, W. K., "Some Chemical Factors Governing the Plastic Softening of Coals on Heating," Fuel, 40, p. 473 (1961)
- Dryden, I.G.C., "Chemistry of Coal and its Relation to Coal Carbonization," J. Inst. Fuel, 30, 193 (1957)
- Eddinger, R. T., Friedman, L. D., and Rau, E., "Devolatilization of Coal in a Transport Reactor," Fuel, 45, 245 (1966)

- Field, M. A., Gill, D. W., Morgan, B. B., and Hawksley, P. G. W.,
"Combustion of Pulverized Coal," BCURA, Chenly and Sons Ltd., London.
(1967)
- Fuchs, W., and Sandhoff, A. G., "Theory of Coal Pyrolysis," Ind. Eng. Chem., 34, 587 (1942)
- Fitzgerald, D., and Van Krevelen, D. W., "Chemical Structure and Properties of Coal XXI - The Kinetics of Coal Carbonization," Fuel, 38, p17 (1959)
- Fitzgerald, D., "Kinetic Study of Coal Carbonization in the Plastic Zone," Fuel, 35, p178 (1956)
- Gan, H., Nandi, S. P., and Walker, Jr., P. L., "Nature of the Porosity in American Coals," Fuel, 51, 272 (1972)
- Gannon, R. E., Stickler, D. B., and Kobayashi, H., "Coal Processing Employing Rapid Devolatilization Reactions in an MHD Power Cycle," 14th Symposium, Engineering Aspects of Magnetohydrodynamics, Tullahoma, Tennessee (1974)
- Given, P. H., "The Distribution of Hydrogen in Coals and its Relation to Coal Structure," Fuel, 39, 147 (1960)
- Ghosh, G., Banerjee, A., and Mazumdar, B. K., "Skeletal Structure of Coal," Fuel, 54, p294 (1975)
- Granger, A. F., and Ladner, W. R., "The Flash Heating of Pulverized Coal," Fuel, 49, 17 (1970)
- Graves, R. D., et al., "Reaction of Coal in a Plasma Jet," Ind. Eng. Chem. Process Design and Develop., 5, No.1, 59, (1966)
- Gray, D., Cogoli, J. G., and Essenhigh, R. H., "Problems in Pulverized Coal and Char Combustion," Chap. 6, "Coal Gasification," Advances in Chemistry Series No. 131, (Massey, L. G., editor) ACS 1974, Washington D.C.
- Gregory, D. R., and Littlejohn, R. F., "A Survey of Numerical Data on the Thermal Decomposition of Coal," BCURA Monthly Bulletin, 29 (6), 173 (1965)

- Hanbaba, P., Jüntgen, H., and Peters, W., "Nicht-isotherme Reaktionskinetik der Kohlenpyrolyse, Teil II: Erweiterung der Theorie der Gasabspaltung und Experimentelle Bestätigung an Steinkohlen," Brennstoff-Chem., 49, 368 (1968)
- Heredy, L. A., and Fugassi, P., "Pheranthrene Extraction of Bituminous Coal," in Coal Science Advances in Chemistry Series, 55, p. 448 ACS, Washington, D.C. (1966)
- Hottel, H. C., and Howard, J. B., "An Agenda for Energy" Technology Review, January 1972
- Heywood, J. B., et al., "Open Cycle MHD Power Generation," Pergamon Press. (1969)
- Hottel, H. C., and Howard, J. B., "New Energy Technology," M.I.T. Press, Cambridge, Mass. (1971)
- Howard, H. C., "Pyrolytic Reactions of Coal," Chemistry of Coal Utilization, Supplementary Vol., Chap. 9, John Wiley & Sons, New York, 1963
- Howard, J. B., and Essenhigh, R. H., "The Mechanism of Ignition of Pulverized Coal," Comb. & Flame, 9, p.337. (1965)
- Howard, J. B., and Essenhigh, R. H., "Pyrolysis of Coal Particles in Pulverized Fuel Flames," Ind. Eng. Chem. Process Design Develop., 6, 74 (1967)
- Jones, J. F., Schmid, M. R., and Eddinger, R. T., "Fluidized Bed Pyrolysis of Coal," Chem. Eng. Progr., 60(6), 69 (1964)
- Jones, W. I., "The Thermal Decomposition of Coal," Fuel, 37, p.3 (1964)
- Jüntgen, H., and Van Heek, K. H., "Reaktionabläufe unter Nicht-isothermen Bedingungen," "Fortschritte der Chemischen Forschung," Vol. 13, pp. 601-699, Springer-Verlag, Berlin (1970)
- Jüntgen, H., and Van Heek, K. H., "Fortschritte der Forschung auf dem Gebiet der Steinkohlenpyrolyse," Brennstoff-Chemie, 50, 172 (1969)
- Jüntgen, H., and Van Heek, K. H., "Gas Release from Coal as a Function of the Rate of Heating," Fuel, 47, 103 (1968)
- Karn, F. S., Friedel, R. A., and Sharkey, Jrl, A. G., "Mechanism of Gas Flow Through Coal," Fuel, 54, p279 (1975)

- Karn, F. S., Sharkey, Jr., A. G., Logar, A. F., and Friedel, R. A., "Coal Investigations Using Laser Irradiations," Bureau of Mines Rept. of Inv. 7328, 32. (1970)
- Karn, F. S., Friedel, R. A., and Sharkey, Jr., A. G., "Studies of the Solid and Gaseous Products from Laser Pyrolysis of Coal," Private Communication. (1972)
- Karn, F. S., and Singer, J. M., "Photographic Study of Laser Irradiation of Coal and Graphite," Fuel, 47, 235. (1968)
- Karn, F. S., et al., "Distribution of Gaseous Products from Laser Pyrolysis of Coal of Various Rank," Carbon, 5, pp. 25-32. (1967)
- Kawa, W., "Reaction of Coal in Argon and Argon Hydrogen Plasmas," Rept. of Inv., U.S. Bureau of Mines, 6829
- Kimber, G. M., and Gray, M. D., "Rapid Decomposition of Small Coal Particles," Comb. & Flame, 11, 360. (1967a)
- Kimber, G. M., and Gray, M. D., "Measurements of Thermal Decomposition of Low and High Rank Non-Swelling Coals at MHD Temperatures," BCURA Document, No. MHD 32. (January, 1967b)
- Kirov, N. Y., "Specific Heats and Total Heat Contents of Coals and Related Materials at Elevated Temperatures," The British Coal Utilization Research Association, Monthly Bulletin, 29(2), February-March, Part I (1965)
- Kobayashi, H., "Rapid Decomposition Mechanism of Pulverized Coal Particles," M.S. Thesis, Aero and Astro, Mass. Institute of Technology, Sept.(1972)
- Langhaar, H. L., ASME Trans. vol. 64, 1942
- Landolt, R. G., "Oxidation of coal models, Reaction of aromatic compounds with sodium hypochlorite," Fuel, 54, 299 (1975)
- Lewellen, P. C., "Product Decomposition effects in coal pyrolysis," M.S. Thesis, Chem. Engr., Mass. Institute of Technology, Sept. (1975)
- Littlejohn, R. F., "Mineral Matter and Ash Distribution in 'As-Fired' Samples of Pulverized Fuels," J. Inst. Fuel, 59 (Feb. 1966)
- Loison, R., and Chauvin, F., "Pyrolyse Rapide Du Charbon," Chem. Ind. (Paris), 91, 269 (1964) (Reviewed by Badzioch, S., BCURA Monthly Bulletin, 31. 1967)
- Louis, J. F., et al., "Open Cycle Coal Burning MHD Power Generation," A Report of the MHD Power Generation Study Group M.I.T. (1971)

- Lowry, H. H., ed., Chemistry of Coal Utilization, Vols. 1, 2, and Supplementary Vol., John Wiley & Sons, NY (1963)
- Marsh, H., "The Determination of Surface Areas of Coals - Some Physico-chemical Considerations," Fuel, 253 (1965)
- Mazumdar, B. K., and Chatterjee, N. N., "Mechanism of Coal Pyrolysis in Relation to Industrial Practice," Fuel, 52, 11 (1973)
- Mazumdar, B. K., et al., Advances in Chemistry, Series 55, Coal Science, p. 475 (1966)
- McCabe, L. C., and Boley, C. C., "Physical Properties of Coals," Chemistry of Coal Utilization (H. H. Lowry, ed.) p. 310, John Wiley & Sons, NY (1945)
- McMath, H. C., Lumpkin, R. E., and Sass, A., "Production of Gas from Western Sub-bituminous Coals by the Garrett Flash Pyrolysis Process," 66th A.I.C.H.E. Meeting, Nov. 9/1973)
- Mentser, M., et al., "Devolatilization of Coal by Rapid Heating," Coal Gasification, Chap. I, Advances in Chemistry Series No. 131 (L. G. Massey, ed.), Amer. Chem. Soc. (1974)
- Mills, A. F., James, R. K., and Antoniuk, D., "Analysis of Coal Particles Undergoing Rapid Pyrolysis," Internat. Center for Heat and Mass Transfer, Internat. Seminar: Future Energy Production - Heat and Mass Transfer Problems, Dubrovnik, Aug. (1975)
- Moseley, F., and Paterson, D., "The Rapid High-Temperature High-Pressure Hydrogenation of Bituminous Coal," Fuel, 40, 523 (1967)
- Moseley, F., and Paterson D., "The Rapid High-Temperature Hydrogenation of Coal Chars. Part II: Hydrogen Pressure up to 1000 Atmospheres," Fuel, 38, 378 (1965)
- Moseley, F., and Paterson, D., "The Rapid High-Temperature Hydrogenation of Coal Chars. Part I: Hydrogen Pressure up to 100 Atmospheres," Fuel, 38, 13 (1965)
- Nail, R. F., Meadows, D. L., and Stanley-Miller, J., "The Transition to Coal," Technology Review, Oct (1975)
- Netson, E. T., Worrall, J., and Walker Jr., P. L., "Kinetics of Volatile Matter Release from Pennsylvania Anthracites," Coal Science, Advances in Chemistry Series, 55, Amer. Chem. Soc. (1966)
- Nettleton, M. A., and Stiring, R., "The Influence of Additives on the Burning of Clouds of Coal Particles in Shocked Gases," Comb. and Flame, 22, 407 (1974)

- Nettleton, M. A., and Stiring, R., "The Combustion of Clouds of Coal Particles in Shock-Heated Mixtures of Oxygen and Nitrogen," Proc. Roy. Soc. Lond. A., 322, 207-221. (1971)
- Nettleton, M. A. and Stiring, R., "The Ignition of Clouds of Particles in Shock-Heated Oxygen," Proc. Roy. Soc. Lond. A., 300, 622 (1967)
- Nsakala, N., Essenhigh, R. H., and Walker Jr., P. L., "Rapid and Slow Devolatilizations of North Dakota Lignite CPSO(-246)," OCR Quarterly Progress Report, Penn. State, May 22, (1975).
- Orning, A. A. and Greifer, "Infra-red Spectrum of the Solid Distillate from High Vacuum Pyrolysis of a Bituminous Coal," Fuel, 35, 381 (1956)
- Padia, A. S., "The Behavior of Ash in Pulverized Coal Under Simulated Combustion Conditions," ScD. Thesis, Massachusetts Institute of Technology, Dept. of Chemical Engineering, Cambridge, Mass. (1976)
- Paulson, L. E., Beckering, W., and Fowkes, W., "Separation and Identification of Minerals from Northern Great Plains Province Lignite," Fuel, 51, 224 (1972)
- Perry, R. H., Chilton, C. H., and Kirkpatrick, S. D., "Perry's Chemical Engineers' Handbook," 4th Ed., McGraw-Hill, New York (1963)
- Peters, W. and Bertling, H., "Kinetics of the Rapid Degasification of Coals," Fuel, 44, 267 (1962)
- Portal, C., and Tan, D., "The Effect of Heating Rate on the Devolatilization of Coal," S.B. Thesis, Massachusetts Institute of Technology, (1974)
- Pohl, J. H., "Fate of Fuel Nitrogen," Sc.D. Thesis, Massachusetts Institute of Technology, April (1976)
- Rau, E., and Robertson J. A., "The Use of the Microsample Strip Furnace in Coal Research," Fuel, 45, p. 73 (1966)
- Reidelbach, H. and Summerfield, M., "Kinetic Model for Coal Pyrolysis Optimization," Amer. Chem. Soc., Div. Fuel Chem., 20, 1, 161 (1975)
- Retcofsky, H. L., and Friedel, R. A., "Spectra of Coals and Coal Extracts: Proton Magnetic Resonance Spectra of Pyridine and Carbon Disulfide Extracts," Spectrometry of Fuels, (R. A. Friedel, ed.), p. 70, Plenum Press, New York (1970)

- Rosin, P. and Rammler, E., "The Laws Governing the Fineness of Powdered Coal," J. Inst. Fuel, 1, 29 (1933)
- Sass, A., "The Garrett Research and Development Process for the Conversion of Coal into Liquid Fuels," 65th Annual AIChE Meeting, New York, New York, November 30 1972
- Shapatina, E. A., V. V. Kalyuzhnyi, and Z. F. Chukhanov, Technological Utilization of Fuel for Energy, 1-Thermal Treatment of Fuels, 1960 [reviewed by Badzioch, S., BCURA Monthly Bulletin, 25, 285 (1961)]
- Sharkey Jr., A. G., Shultz, J. L., and Friedel, R. A., "Gases from Flash and Laser Irradiation of Coal," Coal Science, Advances in Chemistry Series, 55, Amer. Chem. Soc., 643-647 (1966)
- Shultz, J. L., et al., "Gases from Laser Irradiation of Coal," Carbon, 5, 57-59 (1967)
- Sklyar, M. G., Shustikov, V. I. and Virozub, I. V., "Investigation of the Kinetics of Thermal Decomposition of Coals," International Chem. Eng., 9, 595 (1969)
- Soo, S. L., "Pipe Flow of Suspensions," Appli. Sci. Res., 21, 1, 68 (1969)
- Spencer, D. H. T. and R. L. Bond, "The Determination and Use of Specific Surface Values for Coals," Coal Science, Advances in Chemistry Series, 55, 724, ACS, Washington, D.C. (1966)
- Stone, H. N., Bachelor, J. D. and Johnstone, H. F., "Low Temperature Carbonization Rates in a Fluidized Bed," Ind. Eng. Chem., 46, 274 (1954)
- Stickler, D. B., Gannon, R. E. and Kobayashi, H., "Rapid Devolatilization Modeling of Coal," Technical Meeting, the Eastern Section of the Combustion Institute, Nov. (1974)
- Swann, D. D., Allardice, D. J., and Evans, D. G., "Low Temperature Oxidation of Brown Coal. 1. Changes in Internal Surface Due to Oxidation," Fuel, 53, 85 (1974)
- Tingey, G. L. and Morrey, J. R., "Coal Structure and Reactivity," Battelle Energy Program Report, Pacific Northwest Lab., Richland, Washington (1973)
- Tschamler, H. and de Ruiter, "Physical Properties of Coals," (H. H. Lowry, ed.) Chemistry of Coal Utilization, Supplementary Volume, John Wiley & Sons, Inc., New York (1963)

- Van Heek, K. H., Juntgen, H., and Peters, W., "Nichtisotherme Reaktionskinetik der Kohlenpyrolyse," Brennstoff Chemie, 48, 163 (1967)
- Van Krevelen, D. W., Coal, Elsevier Publishing Co., Amsterdam (1961)
- Van Krevelen, D. W., Huntjens, F. J., and Dormans, J. N. M., "Chemical Structure and Properties of Coal XVI," Fuel, 35, 462 (1956)
- Van Krevelen, D. W., Van Heerden, C., and Huntjens, F. J., "Physico-chemical Aspects of the Pyrolysis of Coal and Related Organic Compounds," Fuel, 30, 253 (1951) (Numerical results modified by Juntgen and Van Heek, 1970)
- Virk, P. S., Chambers, L. E., and Woebcke, H. N., "Thermal Hydrogasification of Aromatic Compound," Coal Gasification, Ch. 14, (L. G. Massey, Ed.) 237, Advances in Chemistry Series 131, ACS, Washington, D.C. (1974)
- Von Fredersdorff, C. G., and Elliott, M. S., "Coal Gasification in Chemistry of Coal Utilization," Supplementary Vol., (H. H. Lowry, Ed.) John Wiley and Sons, New York (1963)
- Wiser, W. H., Hill, G. R., and Kertamus, N. J., "Kinetic Study of the Pyrolysis of a High-Volatile Bituminous Coal," Ind. Eng. Chem. Process Design Develop., 6, 133 (1967)
- Woodburn, E. T., Everson, R. C. and Kirk, A. R. M., "Thermal Decomposition and Hydrogenation of Coal Dust in a Shock Tube," Fuel, 53, 38 (1974)
- Yellow, P. C., "Kinetics of the Thermal Decomposition of Coal," BCURA Monthly Bulletin, 29, 9, 285 (1965)
- Zielinski, E., "The Evolution of Volatile Matter from Pulverized Coal Particles," Fuel, 46, 329 (1967)

BIOGRAPHICAL NOTE

The author, Hisashi Kobayashi, was born on December 5, 1946, in Hokkaido, Japan. He attended Toyama High School in Tokyo, and then joined the University of Tokyo. He was awarded the degree of Kōgaku-shi (Bachelor of Engineering) in Aeronautics in April 1970. He married the former Miyako Kojima in May 1971.

The author was awarded a Murata Scholarship for Foreign Studies, which enabled him to study at the Massachusetts Institute of Technology in September 1971. He received the degree of Master of Science in the Department of Aeronautics and Astronautics in September 1972, and the degree of Mechanical Engineer in the Department of Mechanical Engineering in May 1975. He is the author of three technical publications.

At the present time, he has accepted an appointment as Research Engineer at Union Carbide Corporation, Tarrytown, New York, to begin in June 1976.



Room 14-0551
77 Massachusetts Avenue
Cambridge, MA 02139
Ph: 617.253.5668 Fax: 617.253.1690
Email: docs@mit.edu
<http://libraries.mit.edu/docs>

DISCLAIMER OF QUALITY

Due to the condition of the original material, there are unavoidable flaws in this reproduction. We have made every effort possible to provide you with the best copy available. If you are dissatisfied with this product and find it unusable, please contact Document Services as soon as possible.

Thank you.

Some pages in the original document contain pictures, graphics, or text that is illegible.